

TABLE OF CONTENTS

Summary of Section 6, Seismic Risk Analysis

Purpose:

Section 6 assesses the probability of levee failures in the Delta under seismic events.

Methods of Analysis:

The seismic hazard assessment of the Delta (Section 6.1) uses a probabilistic seismic hazard analysis (PSHA), which is a standard practice in the engineering seismology/earthquake engineering community. However, in a departure from standard PSHAs, which assume a time-independent Poissonian process, time-dependent hazard is calculated from the major Bay Area faults using the range of models that were considered by the Working Group on California Earthquake Probabilities. The products of the PSHA include hazard-consistent, site-specific acceleration response spectra at selected levee sites distributed throughout the Delta area.

For the levee vulnerability analysis (Section 6.2), the conditional probability of levee failures is calculated for each levee vulnerability class. The analysis identified the seismic failure modes and defined levee vulnerability classes. Several thousand borings and laboratory tests describing subsurface conditions of the Delta levees were reviewed to characterize the hundreds of miles of levees and foundations.

Main Findings:

Section 6.3 summarizes the findings of the seismic vulnerability analysis. Some of the key conclusions are as follows:

- Levees composed of liquefiable fill are likely to undergo extensive damage as a result of a moderate to large earthquake in the region.
- Levees founded on liquefiable foundations are expected to experience large deformations (in excess of 10 feet) under a moderate to large earthquake in the region.
- At Suisun Marsh, the earthquake-induced deformations under strong shaking are large as a result of deep, very soft clay deposits forming at the levee foundation.

TABLE OF CONTENTS

Section 1	Seismic Risk Analysis.....	6-1
6.1	Evaluation of Seismic Hazard.....	6-1
6.1.1	Introduction.....	6-1
6.1.2	Seismic Hazard	6-2
6.1.3	Seismic Source Characterization	6-3
6.1.4	Ground Motion Attenuation.....	6-4
6.1.5	Individual Site Hazard Results.....	6-5
6.1.6	Source, Magnitude and Distance Deaggregation.....	6-6
6.2	Levee Seismic Vulnerability.....	6-6
6.2.1	Introduction.....	6-6
6.2.2	Seismic Failure Modes.....	6-7
6.2.3	Definition of Vulnerability Classes	6-7
6.2.4	Uncertainty in Assigning Vulnerability Class	6-9
6.2.5	Methodology for Developing Seismic Fragility Functions	6-10
6.2.6	Evaluation of Levee Response Functions	6-10
6.2.7	Conditional Probability of Failure Functions	6-27
6.2.8	Evaluation of Seismic Fragility Functions.....	6-29
6.2.9	Sensitivity Analysis of the Geographic Extent (Length Effect) of the Vulnerability Classes.....	6-35
6.3	Summary of Findings.....	6-36

Tables

6-1	Bay Area Time-Independent Seismic Source Parameters
6-2	Bay Area Time-Dependent Seismic Source Parameters
6-3	Mean Expert Weights for Probability Models Applied to the SFBR Fault Systems (Table 5.5, WGCEP 2003)
6-4	Empirical Model Factors
6-5	Ground Motions with a 2% Exceedance Probability in 50 Years (2,500-Year Return Period)
6-6	Vulnerability Class Details for Seismic Fragility
6-7	Dynamic Soil Parameters Selected for Analysis
6-8	Calculated FLAC Deformations – Idealized Sections Liquefiable
6-9	Stability Analysis Results – Non-Liquefiable Sand Layer
6-10a	Calculated Newmark Deformations – Idealized Sections Non-Liquefiable
6-10b	Calculated Newmark Deformations – Suisun Marsh Non-Liquefiable
6-11	Distribution of Probability of Failure – Sample Results

TABLE OF CONTENTS

Figures

- 6-1 Faults in the San Francisco Bay Region
- 6-2 Active Faults in the Site Region
- 6-3 Time-Dependent Probabilities for the San Andreas Rupture Scenarios for 2005
- 6-4 Time-Dependent Probabilities for the San Andreas Rupture Scenarios for 2050
- 6-5 Time-Dependent Probabilities for the San Andreas Rupture Scenarios for 2100
- 6-6 Time-Dependent Probabilities for the San Andreas Rupture Scenarios for 2200
- 6-7 Time-Dependent Seismic Hazard Curves for Mean Peak Horizontal Acceleration for Clifton Court for 2005
- 6-8 Time-Dependent Seismic Hazard Curves for Mean Peak Horizontal Acceleration for Delta Cross Channel for 2005
- 6-9 Time-Dependent Seismic Hazard Curves for Mean Peak Horizontal Acceleration for Montezuma Slough for 2005
- 6-10 Time-Dependent Seismic Hazard Curves for Mean Peak Horizontal Acceleration for Sacramento for 2005
- 6-11 Time-Dependent Seismic Hazard Curves for Mean Peak Horizontal Acceleration for Sherman Island for 2005
- 6-12 Time-Dependent Seismic Hazard Curves for Mean Peak Horizontal Acceleration for Stockton for 2005
- 6-13a Seismic Source Contributions to Mean Peak Horizontal Acceleration Time-Dependent Hazard for Clifton Court for 2005
- 6-13b Seismic Source Contributions to 1.0 Sec Horizontal Spectral Acceleration Time-Dependent Hazard for Clifton Court for 2005
- 6-14a Seismic Source Contributions to Mean Peak Horizontal Acceleration Time-Dependent Hazard for Delta Cross Channel for 2005
- 6-14b Seismic Source Contributions to 1.0 Sec Horizontal Spectral Acceleration Time-Dependent Hazard for Delta Cross Channel for 2005
- 6-15a Seismic Source Contributions to Mean Peak Horizontal Acceleration Time-Dependent Hazard for Montezuma Slough for 2005
- 6-15b Seismic Source Contributions to 1.0 Sec Horizontal Spectral Acceleration Time-Dependent Hazard for Montezuma Slough for 2005
- 6-16a Seismic Source Contributions to Mean Peak Horizontal Acceleration Time-Dependent Hazard for Sacramento for 2005
- 6-16b Seismic Source Contributions to 1.0 Sec Horizontal Spectral Acceleration Time-Dependent Hazard for Sacramento for 2005
- 6-17a Seismic Source Contributions to Mean Peak Horizontal Acceleration Time-Dependent Hazard for Sherman Island for 2005

TABLE OF CONTENTS

6-17b	Seismic Source Contributions to 1.0 Sec Horizontal Spectral Acceleration Time-Dependent Hazard for Sherman Island for 2005
6-18a	Seismic Source Contributions to Mean Peak Horizontal Acceleration Time-Dependent Hazard for Stockton for 2005
6-18b	Seismic Source Contributions to 1.0 Sec Horizontal Spectral Acceleration Time-Dependent Hazard for Stockton for 2005
6-19	PGA Hazard for a 100-Year Return Period
6-20	PGA Hazard for a 500-Year Return Period
6-21	Comparison of Ground Motions from Other Studies; Potential Stiff Soil/Rock Earthquake Motions for a 100-year Earthquake
6-22	Magnitude and Distance Contributions to the Mean Peak Horizontal Acceleration Hazard for Clifton Court for 2005
6-23	Magnitude and Distance Contributions to the Mean Peak Horizontal Acceleration Hazard for Delta Cross Channel for 2005
6-24	Magnitude and Distance Contributions to the Mean Peak Horizontal Acceleration Hazard for Montezuma Slough for 2005
6-25	Magnitude and Distance Contributions to the Mean Peak Horizontal Acceleration Hazard for Sacramento for 2005
6-26	Magnitude and Distance Contributions to the Mean Peak Horizontal Acceleration Hazard for Sherman Island for 2005
6-27	Magnitude and Distance Contributions to the Mean Peak Horizontal Acceleration Hazard for Stockton for 2005
6-28	Levee Slumping Histories Earthquake Damage During Jan 17, 1995, Kobe Earthquake at Kobe, Japan
6-29	Levee Slumping Histories Schematic Diagram of Levee Failure During Jan 17, 1995, Kobe Earthquake at Kobe, Japan
6-30	Levee Slumping Histories Earthquake Damage During May 18, 1940 Imperial Valley Earthquake
6-31	Levee Slumping Histories Earthquake Damage During October 18, 1989 Loma Prieta Earthquake (Moss Landing)
6-32	Dam Slumping Histories Earthquake Damage During February 11, 1971 San Fernando Earthquake (Van Norman Dam)
6-33	Schematic Diagram of Levee Slumping and Proposed Emergency Repair Method
6-34	Thickness of Organic Materials
6-35	Corrected Blow Count, $(N1)_{60-cs}$ Distribution for Foundation Sand
6-36	Type of Levee Materials
6-37a	Spatial Distribution of Vulnerability Classes

TABLE OF CONTENTS

6-37b	Percentage of Levee Length with Seismic Vulnerability Classes 1 Through 4
6-37c	Seismic Vulnerability Groups
6-38	Approach to Calculate Seismic Fragility Functions
6-39	Target Response Spectra for M 5.5 @ 20km, M 6.5 @ 20km, and M 7.5 @ 75km
6-40	Spectrally Matched Time History for M 5.5 Event for 1991 Sierra Madre Earthquake at Station USGS 4734, 360 deg Component
6-41	Spectrally Matched Time History for M 5.5 Event for 1991 Sierra Madre Earthquake at Station USGS 4734, 270 deg Component
6-42	Spectrally Matched Time History for M 6.5 Event for 1987 Superstition Hills Earthquake at Station Wildlife Liquefaction Array, 090 deg Component
6-43	Spectrally Matched Time History for M 6.5 Event for 1987 Superstition Hills Earthquake at Station Wildlife Liquefaction Array, 360 deg Component
6-44	Spectrally Matched Time History for M 7.5 Event for 1992 Landers Earthquake at Station Hemet Fire Station, 000 deg Component
6-45	Spectrally Matched Time History for M 7.5 Event for 1992 Landers Earthquake at Station Hemet Fire Station, 090 deg Component
6-46	Comparison of Response Spectra for M 5.5 Event
6-47	Comparison of Response Spectra for M 6.5 Event
6-48	Comparison of Response Spectra for M 7.5 Event
6-49	Calculated Displacements for Validation QUAD4M vs. FLAC Steep Slope Water Side Slope 5 Feet of Peat
6-50	Strain Compatible Strength Peat vs. Mineral Soil
6-51	P-Q Plot at 5% Shear Strain for Peat Total Stress
6-52	P'-Q Plot at 5% Shear Strain for Peat Effective Stress
6-53	$(N1)_{60-cs}$ Distribution for Foundation Sand with $(N1)_{60-cs} < 20$
6-54	$(N1)_{60-cs}$ Distribution for Levee Sand with $(N1)_{60-cs} < 20$
6-55a	Typical vs. Profile Sherman Island
6-55b	Typical vs. Profile Mandeville Island
6-55c	Typical vs. Profile Little Vince Island
6-55d	Typical vs. Profile Bacon Island
6-55e	Typical vs. Profile Clifton Court
6-55f	Typical vs. Profile Twitchell Island
6-55g	Typical vs. Profile Montezuma Slough
6-56a	G/G_{max} Curves for Peat (Wehling et al. 2001)
6-56b	Damping Curves for Peat (Wehling et al. 2001)
6-57	Modulus and Damping Curves used in Dynamic Analysis
6-58	Bradford Island – Station 169+00 Stability Analysis – Long Term
6-59	Holland Island – Station 156+00 Stability Analysis – Long Term
6-60a	Sherman Island – Station 650+00 Stability Analysis – Long Term
6-60b	Sherman Island – Station 650+00 Stability Analysis – Seismic

TABLE OF CONTENTS

6-61	Finite Element Model for Seismic Analysis Sherman Island – Station 650+00
6-62	Calculated Newmark Displacements Sherman Island – Sta. 650+00 35 Feet of Peat
6-63	Calculated FLAC Displacements Sherman Island – Sta. 650+00 35 Feet of Peat
6-64a	Undrained Residual Shear Strength and Probabilistic Liquefaction Triggering Correlation
6-64b	r_d vs. Depth and Reference PGA vs. Peak Crest Acceleration Relationships (Tadaihiro et al. 2007)
6-65	FLAC Finite Element Model for Seismic Analysis Idealized Section – No Peat
6-66	FLAC Finite Element Model for Seismic Analysis Idealized Section – 5 ft Peat
6-67	FLAC Finite Element Model for Seismic Analysis Idealized Section – 15 ft Peat
6-68	FLAC Finite Element Model for Seismic Analysis Idealized Section – 25 ft Peat
6-69	CSR Time History at Liquefiable Sand Layer Idealized Section – 5 ft Peat Input Motion M 5.5 H1, 0.2g
6-70	Pore Pressure Time History at Liquefiable Sand Layer Idealized Section – 5 ft Peat Input Motion M 5.5 H1, 0.2g
6-71	CSR Time History at Liquefiable Sand Layer Idealized Section – 5 ft Peat Input Motion M 6.5 H1, 0.2g
6-72	Pore Pressure Time History at Liquefiable Sand Layer Idealized Section – 5 ft Peat Input Motion M 6.5 H1, 0.2g
6-73	CSR Time History at Liquefiable Sand Layer Idealized Section – 5 ft Peat Input Motion M 7.5 H1, 0.2g
6-74	Pore Pressure Time History at Liquefiable Sand Layer Idealized Section – 5 ft Peat Input Motion M 7.5 H1, 0.2g
6-75	CSR Time History at Liquefiable Sand Layer Idealized Section – 15 ft Peat Input Motion M 5.5 H1, 0.2g
6-76	Pore Pressure Time History at Liquefiable Sand Layer Idealized Section – 15 ft Peat Input Motion M 5.5 H1, 0.2g
6-77	CSR Time History at Liquefiable Sand Layer Idealized Section – 15 ft Peat Input Motion M 6.5 H1, 0.2g
6-78	Pore Pressure Time History at Liquefiable Sand Layer Idealized Section – 15 ft Peat Input Motion M 6.5 H1, 0.2g
6-79	CSR Time History at Liquefiable Sand Layer Idealized Section – 15 ft Peat Input Motion M 7.5 H1, 0.2g
6-80	Pore Pressure Time History at Liquefiable Sand Layer Idealized Section – 15 ft Peat Input Motion M 7.5 H1, 0.2g
6-81	CSR Time History at Liquefiable Sand Layer Idealized Section – 25 ft Peat Input Motion M 5.5 H1, 0.2g
6-82	Pore Pressure Time History at Liquefiable Sand Layer Idealized Section – 25 ft Peat Input Motion M 5.5 H1, 0.2g

TABLE OF CONTENTS

6-83	CSR Time History at Liquefiable Sand Layer Idealized Section – 25 ft Peat Input Motion M 6.5 H1, 0.2g
6-84	Pore Pressure Time History at Liquefiable Sand Layer Idealized Section – 25 ft Peat Input Motion M 6.5 H1, 0.2g
6-85	CSR Time History at Liquefiable Sand Layer Idealized Section – 25 ft Peat Input Motion M 7.5 H1, 0.2g
6-86	Pore Pressure Time History at Liquefiable Sand Layer Idealized Section – 25 ft Peat Input Motion M 7.5 H1, 0.2g
6-87	Displacement Contours Idealized Section – 5 ft Peat Input Motion M 5.5 H1, 0.2g
6-88	Displacement Contours Idealized Section – 5 ft Peat Input Motion M 6.5 H1, 0.2g
6-89	Displacement Contours Idealized Section – 5 ft Peat Input Motion M 7.5 H1, 0.2g
6-90	Displacement Contours Idealized Section – 15 ft Peat Input Motion M 5.5 H1, 0.2g
6-91	Displacement Contours Idealized Section – 15 ft Peat Input Motion M 6.5 H1, 0.2g
6-92	Displacement Contours Idealized Section – 15 ft Peat Input Motion M 7.5 H1, 0.2g
6-93	Displacement Contours Idealized Section – 25 ft Peat Input Motion M 5.5 H1, 0.2g
6-94	Displacement Contours Idealized Section – 25 ft Peat Input Motion M 6.5 H1, 0.2g
6-95	Displacement Contours Idealized Section – 25 ft Peat Input Motion M 7.5 H1, 0.2g
6-96	Calculated FLAC Displacements Idealized Section with Liquefiable Foundation Sand Layer 5 Feet of Peat
6-97	Calculated FLAC Displacements Idealized Section with Liquefiable Foundation Sand Layer 15 Feet of Peat
6-98	Calculated FLAC Displacements Idealized Section with Liquefiable Foundation Sand Layer 25 Feet of Peat
6-99	FLAC Deformed Mesh for Post Seismic Static Slumping Analysis Residual Strength of Embankment 230 psf
6-100	Idealized Section Stability Analysis – Seismic No Peat
6-101	Idealized Section Stability Analysis – Seismic 5 Feet of Peat
6-102	Idealized Section Stability Analysis – Seismic 15 Feet of Peat
6-103	Idealized Section Stability Analysis – Seismic 25 Feet of Peat
6-104	Idealized Section Stability Analysis – Seismic Suisun Marsh
6-105	Finite Element Model for Seismic Analysis Idealized Section – No Peat
6-106	Finite Element Model for Seismic Analysis Idealized Section – 5 ft. Peat
6-107	Finite Element Model for Seismic Analysis Idealized Section – 15 ft. Peat
6-108	Finite Element Model for Seismic Analysis Idealized Section – 25 ft. Peat
6-109	Finite Element Model for Seismic Analysis Suisun Marsh Section

TABLE OF CONTENTS

6-110	Horizontal Acceleration Time Histories Along Free Field Column: Island Side (Input Motion: M 7.5 Horizontal-1 PGA 0.20g) Idealized Section – No Peat
6-111	Horizontal Acceleration Time Histories Along the Center Line of Levee (M 7.5 Horizontal-1 PGA 0.20g) Idealized Section – No Peat
6-112	Horizontal Acceleration Time Histories Along Free Field Column: Water Side (Input Motion: M 7.5 Horizontal-1 PGA 0.20g) Idealized Section – No Peat
6-113	Horizontal Acceleration Time Histories Along Free Field Column: Island Side (Input Motion: M 7.5 Horizontal-1 PGA 0.20g) Idealized Section – 5 Feet of Peat
6-114	Horizontal Acceleration Time Histories Along the Center Line of Levee (M 7.5 Horizontal-1 PGA 0.20g) Idealized Section – 5 Feet of Peat
6-115	Horizontal Acceleration Time Histories Along Free Field Column: Water Side (Input Motion: M 7.5 Horizontal-1 PGA 0.20g) Idealized Section – 15 Feet of Peat
6-116	Horizontal Acceleration Time Histories Along Free Field Column: Island Side (Input Motion: M 7.5 Horizontal-1 PGA 0.20g) Idealized Section – 15 Feet of Peat
6-117	Horizontal Acceleration Time Histories Along the Center Line of Levee (M 7.5 Horizontal-1 PGA 0.20g) Idealized Section – 15 Feet of Peat
6-118	Horizontal Acceleration Time Histories Along Free Field Column: Water Side (Input Motion: M 7.5 Horizontal-1 PGA 0.20g) Idealized Section – 15 Feet of Peat
6-119	Horizontal Acceleration Time Histories Along Free Field Column: Island Side (Input Motion: M 7.5 Horizontal-1 PGA 0.20 g) Idealized Section – 25 Feet of Peat
6-120	Horizontal Acceleration Time Histories Along the Center Line of Levee (M 7.5 Horizontal-1 PGA 0.20g) Idealized Section – 25 Feet of Peat
6-121	Horizontal Acceleration Time Histories Along Free Field Column: Water Side (Input Motion: M 7.5 Horizontal-1 PGA 0.20g) Idealized Section – 25 Feet of Peat
6-122	Horizontal Acceleration Time Histories Along Free Field Column: Island Side (Input Motion: M 7.5 Horizontal-1 PGA 0.20g) Suisun Marsh Section
6-123	Horizontal Acceleration Time Histories Along the Center Line of Levee (M 7.5 Horizontal-1 PGA 0.20g) Suisun Marsh Section
6-124	Horizontal Acceleration Time Histories Along Free Field Column: Water Side (Input Motion: M 7.5 Horizontal-1 PGA 0.20g) Suisun Marsh Section
6-125	Calculated Newmark Displacements M 7.5 Horizontal #1 Time History, 0.2 g PGA Idealized Section 15 Feet of Peat
6-126	Calculated Newmark Displacements Idealized Section No Peat
6-127	Calculated Newmark Displacements Idealized Section 5 Feet of Peat
6-128	Calculated Newmark Displacements Idealized Section 15 Feet of Peat
6-129	Calculated Newmark Displacements Idealized Section 25 Feet of Peat
6-130	Calculated Newmark Displacements Idealized Section Suisun Marsh

TABLE OF CONTENTS

6-131	Calculated Newmark Displacements Idealized Section with Steep Water Side Slope No Peat
6-132	Calculated Newmark Displacements Idealized Section with Steep Water Side Slope 5 ft Peat
6-133	Calculated Newmark Displacements Idealized Section with Steep Water Side Slope 15 ft Peat
6-134	Calculated Newmark Displacements Idealized Section with Steep Water Side Slope 25 ft Peat
6-135	Probability of Failure vs. $D_v/Ini-FB$ (Vertical Displacement/Initial Freeboard)
6-136	Flowchart of Key Steps in Monte Carlo Simulation
6-137a	Estimated Failure Probability at 16%, 50%, and 84% Confidence Levels for $M=6.5$ and $IFB = 2$ ft for Vulnerability Classes 1, 2, 3 and 4
6-137b	Estimated Failure Probability at 16%, 50%, and 84% Confidence Levels for $M=6.5$ and $IFB=2$ feet for Vulnerability Classes 5, 6, 7 and 8
6-137c	Estimated Failure Probability at 16%, 50%, and 84% Confidence Levels for $M=6.5$ and $IFB=2$ feet for Vulnerability Classes 9, 10, 11, and 12
6-137d	Estimated Failure Probability at 16%, 50%, and 84% Confidence Levels for $M=6.5$ and $IFB=2$ feet for Vulnerability Classes 13, 14, 15, and 16
6-137e	Estimated Failure Probability at 16%, 50%, and 84% Confidence Levels for $M=6.5$ and $IFB=2$ feet for Vulnerability Classes 17, 18, 19, and 20
6-137f	Estimated Failure Probability at 16%, 50%, and 84% Confidence Levels for $M=6.5$ and $IFB=2$ feet for Vulnerability Classes 21 and 22
6-138a	Sensitivity of Island Fragility Curve to the Vulnerability Class Assignment of Levee Reaches: Union Island, $M=5$
6-138b	Sensitivity of Island Fragility Curve to the Vulnerability Class Assignment of Levee Reaches: Union Island, $M=6$
6-138c	Sensitivity of Island Fragility Curve to the Vulnerability Class Assignment of Levee Reaches: Union Island, $M=7$

Appendices

6A	Step-by-Step Hand Calculation for a Selected Vulnerability Class (VC 10), Magnitude (M 6.5), and Freeboard (2 feet)
----	--

This section presents the framework for the seismic risk analysis of levee failures and discusses the results of this analysis. The first step in evaluating the seismic risk of the Delta and Suisun Marsh levees is to assess the seismic hazard of the site. The input from seismic hazard analysis is then used for evaluating the seismic vulnerability of levees. The effects of earthquakes may be the most significant natural hazard that can impact the Delta and the Suisun Marsh levees. These levees face an increasing risk of damage and failure from a moderate to large earthquake in the San Francisco Bay region, as shown later in this section.

The Working Group on California Earthquake Probabilities (WGCEP) (2003) estimated that the probability of large earthquakes (magnitude $[M] \geq 6.7$) in the region is increasing with time. In 2002, the Working Group assessed the probability of such an earthquake in the succeeding 30-year period as 62 percent, and this value will increase with time. The Seismology Technical Memorandum (TM) (URS/JBA 2007a) presents a detailed analysis of the expected ground motions and their probabilities for the various seismic sources affecting the project area. The Levee Vulnerability TM (URS/JBA 2008c) presents the detailed calculations and the analysis results of the expected levee system performance under these seismic events.

6.1 EVALUATION OF SEISMIC HAZARD

6.1.1 Introduction

The seismic hazard of the project site was evaluated using a probabilistic seismic hazard analysis (PSHA), which is a standard practice in the engineering seismology/earthquake engineering community (McGuire 2004). The PSHA methodology allows for the explicit consideration of epistemic uncertainties and inclusion of the range of possible conditions in the seismic hazard model, including seismic source characterization and ground motion estimation. Uncertainties in models and parameters are incorporated into the hazard analysis through the use of logic trees.

A key assumption of the standard PSHA model is that earthquake occurrences can be modeled as a Poisson process. The occurrence of ground motions at the site in excess of a specified level is also a Poisson process, if (1) the occurrence of earthquakes is a Poisson process, and (2) the probability that any one event will result in ground motions at the site in excess of a specified level is independent of the occurrence of other events.

In a departure from standard PSHAs, which assume a time-independent Poissonian process, time-dependent hazard was calculated from the major Bay Area faults using the range of models that were considered by the WGCEP. (Note, the models considered by WGCEP [2003] do not result in a 100 percent time-dependent hazard.) The seismic hazard is calculated at selected times over the next 200 years. In this study, the seismic analysis team calculated the time-independent hazard in the Delta for the purposes of comparison.

The seismic hazard analysis generates probabilities of occurrence of all plausible earthquake events (defined by their locations, magnitudes, and ground motions). These are used to develop assessments of risk (defined as the annual probability of seismically induced levee failure) at selected times over the next 200 years. The products of the PSHA include hazard-consistent site-specific acceleration response spectra at selected levee sites distributed throughout the Delta area.

The products developed in this study included the following elements of seismic risk analysis:

- The annual probabilities of occurrence at selected times over the next 200 years (i.e., 2005, 2050, 2100, and 2200) of plausible earthquake events, defined by their location, magnitude, and ground motion amplitude, for all seismic sources that could impact the Delta.
- The likelihood of multiple/simultaneous levee failures during individual scenario earthquakes (includes the correlation in ground motions that occurs during an event).
- Time-dependent seismic hazard results for six sites in the Delta in the years of 2005, 2050, 2100, and 2200 (Figures 6-1 and 6-2). The results include the following elements:
 - fractile hazard curves for all ground motion measures the 5th, 15th, 50th (median), 85th, and 95th percentiles, and the mean;
 - M-D (magnitude-distance) deaggregated hazard results for all ground motion measures for 0.01, 0.001, 0.002 and 0.0004 annual probabilities of exceedance
 - mean hazard curves for each seismic source for each ground motion measure.

The seismic hazard results are defined for a stiff soil condition.

- Probabilistic ground shaking hazard maps for 2 percent and 10 percent probabilities of exceedance in 50 years (2,475 and 475 year return periods, respectively) for peak horizontal acceleration and 0.2 and 1.0 sec spectral accelerations (SAs), and an outcropping stiff soil site condition.

6.1.2 Seismic Hazard

In their analyses to assess earthquake probabilities along the major faults in the San Francisco Bay Area, the WGCEP (2003) used several models, including non-Poissonian models that are time-dependent (i.e., they account for the size and time of the last earthquake). In this study, the probabilities of occurrence for all significant and plausible earthquake scenarios for each seismic source at specified times over the next 200 years are required for the risk analysis, which mandates heavy reliance on the results of WGCEP (2003). For many seismic sources, insufficient information exists to assess time-dependent probabilities of occurrence and they were treated in a Poissonian manner.

Seismic source characterization is concerned with three fundamental elements: (1) the identification, location and geometry of significant sources of earthquakes; (2) the maximum size of the earthquakes associated with these sources; and (3) the rate at which they occur. In this study, the dates of past earthquakes on specific faults are also required in addition to the frequency of occurrence. The source parameters for the significant faults in the site region (Figure 6-1) are characterized for input into the hazard analyses. Both areal source zones and Gaussian smoothing of the historical seismicity are used in the PSHA to account for the hazard from background earthquakes.

The fundamental seismic source characterization came from the work done by the U.S. Geological Survey (USGS) Working Group on Northern California Earthquake Potential (WGNCEP 1996), the USGS Working Group on California Earthquake Probabilities (WGCEP 2003) and the CGS's seismic source model used in the USGS National Hazard Maps (Cao et al.

2003). This characterization was updated and revised based on recent research. Table 6-1 describes the final seismic source model used in the time-independent PSHA calculations.

The basic inputs required for the PSHA and the risk analysis are the seismic source model and the ground motion attenuation relations or more accurately ground motion predictive equations.

The Seismology Technical Memorandum (URS/JBA 2007a) includes detailed descriptions of the faults in the area.

The seismic hazard calculations were made using the computer program HAZ38 developed by Norm Abrahamson. An earlier version of this program HAZ36 was validated as part of Pacific Gas and Electric Company's submittal to the Nuclear Regulatory Committee and the new features resulting in HAZ38 were validated as part of ongoing URS Corporation (URS) work for the U.S. Department of Energy.

6.1.3 Seismic Source Characterization

The time-dependent hazard calculations are based on WGCEP (2003). The source characterization and the time-dependent earthquake probability models were used directly with computer codes obtained from the USGS to obtain rates of characteristic events for the seven major faults in the San Francisco Bay Area considered by WGCEP (2003): San Andreas, Hayward/Rodger's Creek, Calaveras, Concord/Green Valley, San Gregorio, Greenville, and Mt. Diablo referred to as the San Francisco Bay Region (SFBR) model faults. All other faults considered in the hazard analysis were modeled only with a time-independent probability model due to the lack of data to characterize time dependence for these faults.

The SFBR model consists of many rupture sources (i.e., a single fault segment or combination of two or more adjacent segments that produce an earthquake). For instance, the Greenville source has three rupture sources: southern segment (GS), northern segment (GN), and unsegmented (GS+GN). A rupture scenario is a combination of rupture sources that describes complete failure of the entire fault (e.g., the Greenville fault has three scenarios: GN and GS rupture independently, GN+GS, and a floating rupture along GN+GS). Fault rupture models are the weighted combinations of the fault-rupture scenarios. These weights were determined by each expert considering what would be the frequency (percentage) of each rupture scenario if the entire length of the fault failed completely 100 times. These weights are adjusted slightly to account for moment balancing. The rupture scenarios and adjusted model weights provide the long-term mean rate of occurrence of each rupture source for each of the characterized faults. The WGCEP (2003) approach described above differs from the logic tree characterization used in typical time-independent hazard analyses. Rupture scenarios in the WGCEP (2003) model are treated as an aleatory variable. The experts were asked to consider the distribution of the rupture scenarios for each fault. Logic trees characterize rupture scenarios as epistemic uncertainty, with each rupture scenario given a weight representing the expert's estimation of how likely it is the actual rupture scenario. The rupture sources and their characteristics are shown in Table 6-2. The experts referred to in this section are the members of the Working Group on California Earthquake Probabilities. Their names and affiliations are listed in the report in the section titled "Working Group Participants" (WGCEP 2003) and is too long to list in this report.

The time-dependent hazard is calculated using the range of earthquake probability models that were considered by WGCEP (2003), which considered five probability models that take into

account date of last rupture, post-1906 seismicity rates, and slip in the 1906 earthquake. One of the models in the suite is the Poisson model, which yields time-independent probabilities. Therefore, the results using the WGCEP (2003) model are not 100 percent time-dependent. The five probability models (Poisson, Empirical, Brownian Passage Time [BPT], BPT-step, and Time-Predictable) as described by the WGCEP (2003) are alternative methods for calculating earthquake probabilities. WGCEP (2003) applied weights to these five models for each of the seven major faults it considered (Table 6-3). The five probability models and their weights along with the source characterization were used to compute the rates of characteristic events on each rupture source, which would then be used in the hazard analysis. Rupture probabilities were calculated for 1-year exposure windows using starting dates of 2005, 2055, 2105, and 2205. The following modifications to the WGCEP (2003) inputs were made.

The program for computing the time-predictable probabilities for the San Andreas rupture scenarios was obtained from Dr. William Ellsworth of the USGS. The inputs to this program were modified to change the exposure time to 1 year and to compute results for the four starting times. Figures 6-3 through 6-6 show the program output plots for each case.

The Empirical Model of Reasenberget al. (2003) was used to obtain the scale factors to modify the long-term rate. WGCEP (2003) used Reasenberget al. (2003) models A through F as shown in WGCEP (2003, Table 5.1) and assigned weights of 0.1, 0.5, and 0.4 to the minimum, average, and maximum scale factor, respectively. The values listed in Table 6-4 were obtained by using the values for models A through D listed in the WGCEP (2003, Table 5.1) and scaling the linear models E and F from WGCEP (2003, Figure 5.6),

The only modifications made for the Poisson, BPT and BPT-step model inputs were to change the exposure time to 1 year and to compute results for the four starting times (2005, 2050, 2100, and 2200).

6.1.4 Ground Motion Attenuation

To characterize the attenuation of ground motions in the PSHA, empirical attenuation relationships appropriate for the western U.S., particularly coastal California were used. All relationships provide the attenuation of peak ground acceleration (PGA) and SAs at 5 percent damping.

New attenuation relations developed as part of the Next Generation of Attenuation (NGA) Project sponsored by the Pacific Earthquake Engineering Research Center Lifelines Program have been released to the public in 2007. These new attenuation relationships have a substantially better scientific basis than current relationships because they are developed through the efforts of five selected attenuation relationship development teams working in a highly interactive process with other researchers who have: (1) developed an expanded and improved database of strong ground motion recordings and supporting information on the causative earthquakes, the source-to-site travel path characteristics, and the site and structure conditions at ground motion recording stations; (2) conducted research to provide improved understanding of the effects of various parameters and effects on ground motions that are used to constrain attenuation models; and (3) developed improved statistical methods to develop attenuation relationships including uncertainty quantification. Review of the NGA relationships indicate that, in general, ground motions particularly at short-periods (e.g., peak acceleration) are significantly reduced particularly for very large magnitudes ($M \geq 7.5$) compared to current relationships.

At this time, only the relationships by Chiou and Youngs, Campbell and Bozorgnia, and Boore and Atkinson are available (see Pacific Earthquake Engineering Research's NGA web site) and these were used in the PSHA. The relationships were reviewed and weighted equally in the PSHA. Intra-event and inter-event aleatory uncertainties for each attenuation relationship are required for the risk analysis. The basin depth beneath the Delta ($Z_{2.5}$) was assumed to be 5 kilometers (km) based on Brocher (2005).

For the Cascadia subduction zone megathrust, the relationships by Youngs et al. (1997), Atkinson and Boore (2003), and Gregor et al. (written communication, 2007) were used with equal weights.

A geologic site condition needs to be defined where the hazard will be calculated. Often this condition has been parameterized as a generic condition such as rock or soil or more recently the average shear-wave velocity (V_S) in the top 100 feet (V_{S30}) of the stiff reference site. In this analysis, the hazard will be defined for a stiff soil site condition characterized by an average V_{S30} of 1,000 ft/sec. The fragility estimates for the levees are referenced to these ground motions. All of the NGA relationships use V_{S30} as an input.

6.1.5 Individual Site Hazard Results

The results of the time-dependent PSHA of the six locations in the Delta are presented in terms of ground motion as a function of annual exceedance probability. This probability is the reciprocal of the average return period. Figures 6-7 to 6-12 show the mean, median, 5th, 15th, 85th, and 95th percentile hazard curves for PGA for 2005 at the six sites. These fractiles indicate the range of uncertainties about the mean hazard. A return period of 2,500 years has a factor of 50 percent difference between the 5th and 95th percentile values at the Montezuma Slough. The probabilistic PGA and 1.0 sec horizontal SA are listed in Table 6-5 for a return period of 2,500 years for the year 2005 as well as 2050, 2100, and 2200. The PGA values range from 0.30 g in Sacramento, which is the most eastern site on the edge of the Delta faults to 0.74 g at Montezuma Slough. The latter site is located adjacent to the Pittsburg-Kirby Hills fault.

The contributions of the various seismic sources to the mean PGA and 1 sec SA hazards in 2005 are shown on Figures 6-13a to 6-18a and Figures 6-13b to 6-18b, respectively. The controlling seismic source varies from site to site but the Southern Midland fault and Northern Midland zone are a major contributor to several sites within the Delta at a return period of 2,500 years. At long-period ground motions (e.g., 1.0 sec SA), the Southern Midland and the Cascadia subduction zone are contributing significantly to the hazard in 2005. The San Andreas fault becomes a major contributor, at long periods, due to it approaching a 1906-type rupture.

The PGA contour maps for 100, and 500-year return periods are shown on Figures 6-19 through 6-20. The calculated PGAs for a 200-year return period for the six sites are compared in Figure 6-21 to the 1992 "Seismic Stability of Delta Levees" by the Department of Water Resources (DWR) and the 2000 "Seismic Vulnerability of the Sacramento-San Joaquin Delta Levees" by the California Bay-Delta Authority Program (CALFED) (2000b). The three studies show that the results are relatively similar. The slight differences can be attributed to the new attenuation relationships and the time-dependant models. The DWR 1992 and the CALFED 2000 studies used time-independent Poissonian model.

6.1.6 Source, Magnitude and Distance Deaggregation

Figures 6-22 to 6-27 illustrate the contributions by events for the deaggregated mean PGA hazard by magnitude and distance bins in 2005. At the 2,500-year return period, the PGA hazard is controlled by nearby events (< 20 km) in the **M** 6 to 7 range. For Sacramento and Stockton, the hazard is relatively low and more distant events are contributing. At long period, > 1.0 sec SA, the pattern is similar but the contribution from **M** ~8.0 San Andreas earthquakes is quite apparent.

6.2 LEVEE SEISMIC VULNERABILITY

6.2.1 Introduction

This section describes the development of the seismic vulnerability of the Delta and Suisun Marsh levees. Historically, there have been 165 Delta and Suisun Marsh flood-induced levee failures leading to island inundations since 1900. No reports could be found to indicate that seismic shaking had ever induced significant damage. However, the lack of historical damage is not a reliable indicator that Delta levees are not vulnerable to earthquake shaking. Furthermore, the present-day Delta levees, at their current size, have not been significantly tested by moderate to high seismic shaking.

The largest earthquakes experienced in recent history in the region include the 1906 Great San Francisco Earthquake and the 1989 Loma Prieta Earthquake. The 1906 earthquake occurred while the levees were in their early stages of construction. They were much smaller than they are today, and were not representative of the current configuration. The epicenter of the 1989 Loma Prieta earthquake was too distant and registered levels of shaking in the Delta too small to cause perceptible damage to the levees. Nonetheless, the Delta Risk Management Strategy (DRMS) seismic analysis team performed a special simulation analysis of the 1906 Great San Francisco Earthquake to evaluate the potential effects of this event on the current levees. The results of this simulation are presented later in this section.

In addition to the simulation of these largest regional earthquakes, recent smaller and closer earthquakes were also evaluated. They include: the 1980 Livermore Earthquake (**M** 5.8) and the 1984 Morgan Hill Earthquake (**M** 6.2). Except for the 1906 earthquake, which would have caused deformations of some of the weakest levees, the other earthquakes were either too small or too distant to cause any significant damage to the Delta levees. These results are consistent with the seismic vulnerability prediction model developed for this study.

The analyses and assessments presented in this technical memorandum are based on available information. No investigations, or further research to fill data gaps, were part of this study. As described in Section 2 of the Levee Vulnerability TM (URS/JBA 2008c), several thousands of borings and laboratory tests describing subsurface conditions of the Delta levees were reviewed to characterize the hundreds of miles of levees and foundations. The data from these borings were also digitized and entered into a database to support the geographic information system (GIS) mapping needs for the various analyses.

6.2.2 Seismic Failure Modes

The earthquake-induced levee deformations can result either in liquefaction-induced flow slides, inertia-induced seismic deformation in non-liquefiable case, or a combination of the two. The potential seismically induced modes of failure include: overtopping as a result of crest slumping and settlement, internal piping and erosion caused earthquake-induced differential deformations, sliding blocks and lateral spreading resulting in transverse cracking, and exacerbation of existing seepage problems due to deformations and cracking.

Unlike the flood-induced failures (conventional breaches; see Section 7), the seismically induced levee failures tend to extend for thousands of feet if not miles. The seismic analysis team reviewed past performances of levees/dams under seismic loading to identify potential seismically induced modes of failure. The review included:

1. During the 1995 Kobe Earthquake, many levees slumped as a result of ground shaking. Figure 6-28 shows a picture of one of these slumped levees. The damage extends as far as the eye can see. Figure 6-29 shows a reconstruction and interpretation of the damage resulting from liquefaction-induced failure.
2. During the 1940 Imperial Valley Earthquake, the irrigation canal levees experienced extensive and continuous slumping as far as the eye can see as shown on Figure 6-30. The mark on the white post in the figure indicated that the levee crest slumped by about 7 feet.
3. During the 1989 Loma Prieta Earthquake, levees in Moss Landing breached as a result of liquefaction-induced slumping and lateral spreading as shown on Figure 6-31.
4. During the 1971 San Fernando Earthquake, Van Norman Dam experienced extensive damage. Figure 6-32 shows that the upstream shell and crest of the dam failed as a result of liquefaction-induced slide.

Most of these historical observations show that, the earthquake-induced deformations result in a much extended damage (thousands of feet) than the breach failures associated with flood or sunny-day failures (few hundred feet). A discussion on the flood-related levee breaches is presented in the Levee Vulnerability TM (URS/JBA 2008c). Even if some levees do not breach during the earthquake, the miles of damaged levees can fail during the succeeding wet season, if they are not repaired immediately. To estimate the cost associated with repairing levees damaged by an earthquake, a typical slumped levee cross section was developed based on review of the patterns of historical levees damages by earthquakes. Figure 6-33 shows a schematic illustration of a slumped levee. The emergency repair consists of raising the levee, removing portion of the slumped levee materials on the landside, and reconstructing the levee. Figure 6-33 shows the proposed emergency repair, which includes rock placement on the waterside slope (slope of 3 horizontal to 1 vertical [3H:1V]), reconstructing the levee crest, and landside slope. The berm on the landside will be constructed at much flatter slope (6H:1V) than the original levee (i.e., pre-earthquake levee).

6.2.3 Definition of Vulnerability Classes

Because of the large area covered by the Delta and Suisun Marsh and the extensive variability of the levee and foundations conditions, the study area was divided into a number of “similar”

zones. For the purpose of this analysis, these similar zones are referred to as levee Vulnerability Classes (VCs). Two vulnerability classes are defined similarly if they yield the same probability of failure when subjected to same seismic shaking. The description of the vulnerability classes follows.

The factors that would differentiate the performance of these classes will include the subsurface profile, the levee fill conditions and geometry, past performance, and maintenance history. The use of GIS mapping was very instrumental in allowing spatial display of subsurface conditions and discretization into desired zones. Examples of these displays include the thickness of peat throughout the Delta as shown in Figure 6-34, and the distribution of foundation sand blow counts and levee fill description as shown in Figures 6-35 and 6-36, respectively. Specifically, the VCs were defined using the following factors:

- The equivalent clean sand blow count $[(N1)_{60-cs}]$ of levee fill – The standard penetration test (SPT) blow counts and the equivalent cone penetration test blow counts were considered only for levees designated as sandy levees (details of this levee designation are presented in Section 2 of the Levee Vulnerability TM [URS/JBA 2008c]). $(N1)_{60-cs}$ values were grouped into two intervals: less than 20 and greater than 20. Only two groups were defined for the levee sand: potentially liquefiable or not. It was assumed that because of the sloping condition of the levees and the low confining stresses, any saturated sand with blow count below 20 has potential to liquefy and may result in flow failure. The potential liquefaction of the levee fill was evaluated probabilistically with $(N1)_{60-cs}$ and the cyclic stress ratios (CSR) considered as random variables.
- The equivalent clean sand SPT blow count $(N1)_{60-cs}$ of the foundation sand – The $(N1)_{60-cs}$ were considered in the levee reaches that have loose foundation sands and silts. The $(N1)_{60-cs}$ were grouped into four intervals: 0–5, 5–10, 10–20, and greater than 20. The probability of liquefaction of the saturated sands in the levee foundation is dependent on the blow count, the effective overburden stresses. The post-liquefaction residual strength is estimated from the corrected blow counts $(N1)_{60-cs}$. Both the corrected blow count and the post-liquefaction residual strength are treated as random variables.
- The thicknesses of the peat/organic deposits – The peat and organic deposits were divided into four depth intervals representing the variation of the peat thickness (in feet) within the Delta region: no peat, 0.5–10, 10–20, and greater than 20.
- The waterside levee slope – The waterside slopes show steep cuts in places, and hence were defined by two broad groups representing the variability in the waterside slope of the levee: steep (steeper than 1.5H:1V) and non-steep (flatter than 1.5H:1V).

For the purpose of this study, we defined 64 ($2 \times 4 \times 4 \times 2$) vulnerability classes. Further examination of these classes indicated that although different classes have distinctly different properties, they yielded similar deformations under seismic loading. Such cases include classes with liquefiable foundation and levee fill and classes with only liquefiable levee fill. The liquefaction of the levee fill generally controls the deformation regardless of whether the foundation or the waterside slope is liquefiable. As a result of the screening of the performance of the vulnerability classes, only 22 classes remained in the Delta and two classes in the Suisun Marsh (Table 6-6). The following paragraphs discuss the justification for the selection of the 22 classes.

- If a levee reach had liquefiable levee fill with $(N1)_{60-cs}$ less than 20, the seismic behavior of that levee reach would not be controlled by the liquefaction potential of the foundation sand and the levee geometry. Nonetheless, the liquefaction probability of the foundation sand is considered for the full range of $(N1)_{60-cs}$. This screening resulted in a total of only 4 classes [$(N1)_{60-cs}$ as opposed to a possible 32 classes ($1 \times 2 \times 4 \times 4$). These four classes were numbered from VC 1 to VC 4, as shown in Table 6-6.
- If a levee had non-liquefiable fill (no sand or $(N1)_{60-cs}$ greater than 20) and foundation had liquefiable sand (i.e., $(N1)_{60-cs}$ less than 20), the seismic behavior of the levee would not be controlled by the levee geometry. This screening resulted in a total of 12 classes (4×3) as opposed to 24 classes ($3 \times 2 \times 4$). Furthermore, in the case of shallow foundation sand (no peat), the levee deformation is insensitive to the blow count in the liquefiable foundation sand. This reduces further the number of classes by 2, resulting in a total of 10 vulnerability classes. These 10 classes were numbered from VC 5 to VC 14, as shown in Table 6-6.
- Finally, if a class had non-liquefiable levee fill and non-liquefiable foundation sand, then only the levee geometry (steep or non steep) and the thickness of peat would influence the seismic behavior of the levee. The resulting 8 classes were numbered from VC 15 to VC 22, as shown in Table 6-6.

The following list summarizes the development of the 22 vulnerability classes.

Liquefiable Levee Fill	Liquefiable Foundation	Presence of Peat in Foundation	Waterside Slope	No. of VCs
1 (Yes)	1 (Yes)	4	NC	$1 \times 4 = 4$
1 (No)	3 (Yes)	3	NC	$3 \times 3 = 9$
		1 (No peat)	NC	1
	1 (No)	4	2	$4 \times 2 = 8$
Total VCs				22

Note: NC = not considered, or not appropriate. See Table 6-6 for definition of VC.

The levees in Suisun Marsh were divided into two VCs mainly based on presence or absence of potentially liquefiable levee and foundation sands. Table 6-6 also lists classes VC 23 and VC 24 considered for Suisun Marsh. Figure 6-37a shows the spatial distribution of the VCs for the study region. Figure 6-37b shows the percentage of levee length accounted for by the weakest classes (vulnerability classes 1 through 4) for each island. Figure 6-37c illustrates how the 24 levee VCs may be arranged into three general groups. The High Vulnerability Group is the group of VCs having a probability of failure that is greater than 50 percent under 0.3g PGA. The Medium Vulnerability Group is the group of VCs having a probability of failure that is 50 percent to 20 percent under 0.3g PGA. The Low Vulnerability Group is the group of VCs whose probability of failure is less than 20 percent under 0.3g PGA.

6.2.4 Uncertainty in Assigning Vulnerability Class

The spatial variation of the peat thickness and the blow counts $(N1)_{60-cs}$ of the levee fill and foundation were used to develop the vulnerability classes in the geographic space forming the study area. This distribution was considered to be deterministic. However, the variation of these factors within each class was considered to be random. For example, there was little uncertainty

that the peat thickness would fall outside, say, 0 and 5 feet for a given vulnerability class, but within that interval the peat thickness was treated as a random variable. Similarly, the range of blow counts within a given class was treated as random variable. Other random variables included the material properties, the ground motions, and the post-liquefaction residual shear strength. Finally, the liquefaction occurrence was treated probabilistically. The random variables considered in this evaluation are further explained in the following sections.

6.2.5 Methodology for Developing Seismic Fragility Functions

The development of the seismic fragility functions followed the method illustrated in Figure 6-38 for each vulnerability class. The first step involved the evaluation of *levee response functions*, which estimate the horizontal deformations as a function of the magnitude and peak ground acceleration for the reference site (see Figure 6-38, diagram a). The seismic deformations were evaluated using generalized geotechnical models as discussed in the Section titled Analysis Methods below.

The second step involved the development of the *conditional probability of failure functions*, which relate the conditional probability of a levee breach to the loss of freeboard (see Figure 6-38, diagram b). This step relied solely on expert elicitation. The range of expert elicitation was used to quantify the epistemic uncertainty in the assessed probability of failure. The potential seismic modes of failure included the following:

- Overtopping as a result of crest slumping and settlement
- Internal piping and erosion caused by earthquake-induced differential deformations
- Sliding blocks and lateral spreading resulting in transverse cracking
- Exacerbation of existing seepage problems due to deformation and cracking

The third and last step involved the development of the *levee fragility functions*, which relate the probability of failure to the ground motions and earthquake magnitudes for each VC (see Figure 6-38, diagram c). This step combines the levee response functions with the conditional probability of failure functions, using Monte Carlo simulations, to generate the fragility functions. Sections 6.2.6 through 6.2.8 describe in detail each of the above three steps, respectively.

6.2.6 Evaluation of Levee Response Functions

The evaluation of levee response functions requires the estimation of seismic-induced levee and foundation deformations for each vulnerability class. The seismic-induced levee deformations can result from liquefaction-induced flow slides, inertia-induced seismic deformation in a non-liquefiable case, or a combination of the two. Two-dimensional effects were considered in the seismic deformation analysis to account for the interaction between the levee and foundation soil (upper foundation soil above the reference stiff half space).

6.2.6.1 Ground Motions

The evaluation of levee response function requires the development of ground motions for the study area. The levee response was calculated in terms of the seismic deformation of the levee

for a given event. The earthquake event is represented by a given magnitude and acceleration response spectrum (ARS) calculated at a reference site. The PGA associated with each ARS is often used as a proxy for the ARS in the remainder of this section.

The ARS were generated for a reference site with an average shear wave velocity profile V_{S-30} of about 1,000 feet per second (feet/sec). The reference site ARS are the calculated ground motions at an outcropping stiff reference site, with an average shear wave velocity of 1,000 feet/sec. In most of the Delta this reference site underlies the upper loose sand and soft organic deposits. A review of the site geology indicates that the bedrock within the Delta study area is at a depth of 400 feet or greater below ground surface. Overlying the bedrock are dense and stiff sand and clay deposits, with an average shear wave velocity equal to or greater than 1,100 feet/sec (reference site). The stiff and dense deposits are in turn overlaid by the more recent deltaic loose and soft sediments and organic layers, which are about 100 feet thick in the central-western Delta.

Three magnitudes were considered, **M 5.5**, **M 6.5**, and **M 7.5**, to represent small-to-medium local earthquakes and medium-to-large earthquakes in the region. For each magnitude, mean response spectra and ranges around the mean spectra were generated using the new generation attenuation relationships. The same relationships were used in the Seismology TM (URS/JBA 2007a). The response spectra were then scaled up and down to generate a suite of values to represent the various distances from the sources to different parts of the Delta and Suisun Marsh.

Figure 6-39 shows the 5 percent-damped mean response spectra corresponding to the selected three earthquake magnitudes. These response spectra represent free-field motions for the outcropping reference stiff soil site condition mentioned above.

6.2.6.2 Development of Time Histories for Dynamic Analyses

To perform the dynamic response analyses of the levee and foundation system, earthquake acceleration time histories were developed as input to the numerical models. Recorded motions from past earthquakes were selected to match the magnitudes and distances used for the analysis. The selected records were: the **M 5.5** 1991 Sierra Madre earthquake recorded at Station USGS 4734, the **M 6.5** 1987 Superstition Hills earthquake recorded at the Wildlife station, and the 1992 **M 7.3** Landers earthquake, recorded at Hemet fire station. The site conditions at these stations are classified as stiff soils. The record from the 1992 Landers earthquake was selected to represent the **M 7.5** events on the San Andreas and Hayward faults. The 1991 Sierra Madre and 1987 and the Superstition Hills earthquakes were selected to represent the **M 5.5** and **M 6.5** seismic events on the local seismic sources, respectively.

The selected acceleration time histories were spectrally matched to the response spectra (**M 7.5**, **M 6.5**, and **M 5.5** events) using the method proposed by Lilhanand and Tseng (1988) and modified by Abrahamson (1993). The plots of the acceleration, velocity and displacement time histories of the spectrally matched motions are presented in Figures 6-40 through 6-45. The 5 percent damped response spectra for the modified motions are shown in Figures 6-46 through 6-48 along with the smooth target spectra.

The modified time histories were then scaled to PGAs of 0.05g, 0.1g, 0.2g, 0.3g, 0.4g, and 0.5g for each earthquake magnitude to cover the range of possible ground shaking levels for the entire study area.

6.2.6.3 Uncertainties in Ground Motions

The seismic fragility functions are calculated as conditional probabilities of failure given the probability of the seismic events. The probabilities of the seismic events are calculated in the Seismology TM (URS/JBA 2007a). The PSHA methodology allows for the explicit consideration of aleatory and epistemic uncertainties associated with the seismic sources and ground motions. The shapes of the response spectra generated from natural time histories are random and irregular. The aleatory and epistemic uncertainties in the estimated spectral accelerations at different periods due to multiple acceleration time histories for an event with the same magnitude and same distance are captured in the PSHA. Since the levee fragility was assessed conditional on a given event, these uncertainties are not considered in the levee fragility analysis. Otherwise, these uncertainties would be double-counted. The levee fragility analysis did incorporate the aleatory uncertainty due to the fact that the recurrence of the same earthquake event with the same time history at a given location would not produce the same levee deformation.

To simplify the numerical analysis for estimating levee deformations, the selected acceleration time histories of past earthquakes were spectrally matched to the response spectra. Smoothed response spectra were developed and used in the numerical deformation analysis. To incorporate the effects of different PGAs and spectral accelerations, the smoothed response spectra were scaled up or down to cover the range of interest. This assumes that the response spectra at different periods are perfectly correlated. That is, if the PGA (i.e., the response spectrum at zero period) increases, the response spectrum at any other period would also increase proportionately. Both the use of smoothed response spectra and its scaling with PGA are common practice.

In reality, the response spectra would show a jagged pattern and the correlation of the response spectra at different periods would be less than perfect. However, the expected uncertainty in the estimated deformation due to these two factors is much smaller than the uncertainty due to multiple time histories for recurrence of events, and the latter uncertainty is properly captured in the analysis.

6.2.6.4 Seismic Deformation Analysis Methods

The seismic deformation of the levees was evaluated using the following two approaches.

The first approach consisted of estimating the dynamic response analysis using the two-dimensional equivalent-linear finite element method using the computer program QUAD4M (Hudson et al. 1994). The seismic-induced inertial deformations were then calculated using the Newmark sliding block procedure. This procedure requires input parameters such as the average acceleration within a potential sliding mass and the associated yield acceleration for that potential sliding mass. QUAD4M calculates the average acceleration within a potential sliding mass given an input acceleration time history. The yield acceleration (K_y) value associated with each potential sliding mass, defined as the horizontal acceleration that results in a pseudo-static factor of safety of 1.0, was computed using a limit-equilibrium slope stability analysis (UTEXAS3 [Wright 1992]). This approach was mainly used for the non-liquefaction-susceptible cases (i.e., for VCs 15 through 22).

In the second approach, the earthquake-induced levee deformations were directly calculated using a time-domain nonlinear analyses with the computer program FLAC, Version 5.0 (Itasca

2005) coupled with an empirical pore-pressure generation scheme (Dawson et al. 2001). This second approach was mainly used for liquefaction-susceptible cases (i.e., for VCs 1 through 14).

These analyses were performed for the best estimate mean values and for the full range of distribution around the mean for the random variables contributing to the levee responses as discussed in the following sections.

6.2.6.4.1 VCs 1 through 5

VCs 1 through 5 have either potentially liquefiable levee fill and/or liquefiable foundation materials. When the levee fill or when both the levee fill and foundation materials are susceptible to liquefaction, the earthquake-induced deformations tend to be very large and may cause the computer programs to not converge. Typically, large strains are not well accounted for in numerical codes, and when excessive deformations take place, the computer programs will not converge on the solution. To mitigate these conditions (when the runs do not converge), a simplified use of the FLAC model was considered to capture the “post-liquefaction static slumping.” In this simplified method, the levee fill was first modeled using the pre-liquefied shear strength values, then in a quasi-static fashion, these strength values were reduced in a step-wise function to the post-liquefactions residual shear strength values. Most of the calculated “post-liquefaction static slumps” for these cases showed large deformations leading to levee breaches, and therefore the calculations of the inertial deformation were not necessary.

6.2.6.4.2 VCs 6 through 14

By definition, VCs 6 through 14 have non-liquefiable levee fill but potentially liquefiable foundation materials. For these classes, a time domain fully coupled non-linear analysis was performed using the computer program FLAC. Soil behavior was simulated by a Mohr-Coulomb, elastic/perfectly plastic model. For the liquefiable foundation layer, this model was coupled with an empirical pore pressure generation scheme. Pore pressure is generated in response to shear stress cycles, following the cyclic-stress approach of H.B. Seed (Seed 1979). However, unlike the standard cyclic-stress approach, pore pressure is generated incrementally during shaking. Thus, pore-pressure generation is fully integrated with the dynamic effective stress analysis.

In the current analyses, pore pressures are updated continuously for each element in response to shear stress cycles. As pore pressures increase, the effective stresses decrease and a state of liquefaction is approached for frictional materials. As the available shear strength of the material decreases, increments of permanent deformation are accumulated. The simultaneous coupling of pore-pressure generation with the stress analysis results in a more realistic dynamic response of the model. Specifically, the plastic strains generated as a result of increased pore pressures significantly contribute to the internal damping of the modeled earth structure.

6.2.6.4.3 VCs 15 through 22

VCs 15 through 22 have non-liquefiable materials in both the levee and foundation. The seismic deformations of these levees were estimated using the first approach, QUAD4M-K_y-Newmark. A limited number of runs were performed to compare the results of the first approach, QUAD4M-Newmark, to the second approach, using the FLAC method. The results of these comparison runs showed a reasonable agreement between the two approaches. Results from one

of these comparison runs are presented in Figure 6-49. This run was performed for a **M** 7.5 event with a range of PGAs between 0.1g and 0.5g. The first approach was used for the multiple runs because it offers more ease in its use and the ability to produce multiple runs in a shorter time frame.

QUAD4M Analysis. QUAD4M uses an equivalent linear procedure (Seed and Idriss 1970) to model the nonlinear behavior of soils. The softening of the soil stiffness is represented by shear modulus reduction (G/G_{\max}) and damping ratios (ξ) versus shear strain curves. QUAD4M also incorporates a compliant base (energy-transmitting base), which can be used to model the elastic half-space. This program was used to calculate shear stresses and acceleration time histories within the levee and foundation for a given seismic event. This program was also used to calculate the average acceleration time histories of potential sliding masses.

Calculation of Yield Acceleration K_y . The limit-equilibrium slope stability program UTEXAS3 was used to calculate the K_y associated with each potential slip surface. The computer program UTEXAS3 is capable of performing two stage computations to simulate seismic loading conditions. To perform two-stage computations, both effective (S-envelope) and total (R-envelope) strength envelopes need to be defined for fine-grained soils. Two-stage stability computations consist of two complete sets of stability calculations; of which the first step is performed to calculate the long-term steady-state stresses along the potential sliding mass, and the second step is performed to compute the factor of safety for the undrained loading due to earthquake event. The seismic coefficient representing the earthquake load is applied and a pseudo-static factor of safety is calculated. The seismic coefficient that results in a pseudo-static factor of safety of 1.0 is referred to as K_y .

Newmark Sliding Block. Seismic-induced permanent deformations of the embankment slopes were estimated using the Newmark Double Integration Method (Newmark 1965). The Newmark Double Integration Method is based on the concept that deformations of an embankment will result from incremental sliding during the short periods when earthquake inertia forces in the critical slide mass exceed the available resisting forces. This method involves the calculation of the displacement (deformation) increment of a critical slide mass at each time step using the average horizontal acceleration (k_{ave}) and K_y calculated for the slide mass. The displacement increment is calculated by double integrating the difference between k_{ave} and k_y values acting on the slide mass. The estimated permanent deformation of the slide mass is then taken as the sum of the displacement increments at the end of ground shaking.

6.2.6.4.4 VCs 23 and 24

The analysis method used to calculate the response of VC 23 was the same as that used for VCs 15 through 22. There is no levee reach in the Suisun Marsh area that belongs to VC 24 (see Figure 6-37a); therefore, no analysis was performed for this class.

6.2.6.5 Material Properties and Characterization

The main engineering properties required for the evaluation of levee response function include shear wave velocities, unit weights, drained and undrained shear strength parameters (c' , ϕ' , c , ϕ), residual undrained strength (S_r), shear modulus reduction (G/G_{\max} vs. γ) and damping ratios (ξ vs. γ) as a function of shear strain for the levee embankment and foundation materials. In the

following subsections, the raw data and the characterization of the engineering properties and their statistical distributions are presented.

Several geotechnical and environmental studies have been performed in the Delta. A list of these past studies and the compilation and interpretation of the data are presented in Section 2.0 of the Levee Vulnerability TM (URS/JBA 2008c). These studies included several field investigations and laboratory tests dating back to 1950s (early data developed for the salinity control projects). The field investigations included exploratory borings, cone penetration tests, and down-hole geophysical surveys.

The laboratory test results pertaining to seismic analysis were reviewed to develop both static and dynamic properties. The aleatory uncertainties associated with the dynamic properties of the levee and foundation soils (e.g., modulus reduction and damping as a function of shear strain, shear wave velocity, c , ϕ , S_u , unit weight) were considered in the seismic analyses as described in Section 6.2.5.8.

The available shear strength test data for the peat/organic soils consisting mainly of unconsolidated undrained (UU) and consolidated undrained (CU) triaxial strengths are compiled in Appendix B of the Levee Vulnerability TM (URS/JBA 2008c). These test data showed progressive increase in deviator stress as axial strain increased, often resulting in large strain levels as high as 15 percent before failure is reached. Shear strength data suggest that large strains are needed to cause shear failure in peat and peaty soils. The levee fill materials generally behave more like mineral soils (reaching peak shear strength at about 4 to 6 percent strain) compared to foundation peat and organic marsh deposits. During large induced strain in the foundation (i.e., due to seismic loading), the levee embankments may experience cracking and differential displacement while the foundation peat is still undergoing larger deformation but not reaching its ultimate shear strength. This will result in strong strain incompatibility as shown in Figure 6-50. Because the levee embankment may reach failure earlier, while the peat foundation is still below the failure state, it was estimated that the shear strength of peat/organic soils at 5 percent strain or less would represent the “apparent” strength threshold for use in these analyses or a strain compatible with the failure strain of the mineral soils.

6.2.6.5.1 Static Strength Data for Peat/Organic Deposits

The mean principal stress versus maximum shear stress for each of the tests was plotted for both total stress and effective stress at the 5 percent strain level. This is referred to as a p-q plot. The best linear fit of the total stress p-q data has an intercept of 130 pounds per square foot (psf) and a slope angle of 18 degrees (Figure 6-51). This corresponds to a Mohr-Coulomb envelope with cohesion intercept (c) of 140 psf and a slope angle (ϕ) of 19 degrees. In a similar manner for the effective stresses, the best linear fit of p' -q data has an intercept (c') of 205 psf and a slope angle (ϕ') of 30 degrees (Figure 6-52). This corresponds to a Mohr-Coulomb envelope with a cohesion intercept of 250 psf and a slope angle of 35 degrees.

6.2.6.5.2 Post-Liquefaction Residual Strength for Saturated Cohesionless Soils

The liquefaction of loose saturated sandy and silty materials in the foundation and levees will result in substantial loss of strength (post-liquefaction residual shear strength) as a result of increasing pore pressure. The residual shear strength values were estimated using the relationships by Seed and Harder (1990). For a given $(N1)_{60-cs}$, this relationship provides a range

of possible residual shear strength values. The range of S_r was used as an aleatory uncertainty. A discussion of the treatment of this uncertainty is presented in Section 6.2.7.

The $(N1)_{60-cs}$ value was selected from the data distribution developed for both levee fill and foundation materials in the study area. Figures 6-53 and 6-54 show the data distribution of the $(N1)_{60-cs}$ values of the foundation and levee sand materials, respectively, within the Delta. Cone penetration test data obtained within the top 20 feet through the levee fill were also digitized and converted to equivalent SPT blow counts (Figure 6-54) using the procedure proposed by Boulanger and Idriss (2004). Review of the blow count data indicates that about 75 percent of the blow counts collected in the upper loose foundation sands are less than 20 and 95 percent of the blow counts collected in the levee sand fill are below 20.

6.2.6.5.3 Shear Wave Velocity and Maximum Shear Modulus (V_s , G_{max})

DWR conducted shear (V_s) and body (V_p) wave velocity measurements of levee and foundation materials in at least five locations, extending about 100 to 120 feet below the crest of the levees. Most of these velocity measurements were conducted during the installation of downhole array of accelerometers at Sherman Island, Clifton Court Forebay, Staten Island, and Montezuma slough. Although there is significant variability throughout the Delta, the data suggests that the shear wave velocity (V_s) is less than 100 feet/sec for the free field peat, and over 200 feet/sec for peat confined under the levees. The shear wave velocity profiles tend to increase with depth, reaching values of about 1,100 to 1,200 feet/sec in the lower dense sand and stiff clay stratum located 100 to 120 feet below the levee crests. Representative shear wave velocity profiles are shown in Figures 6-55a through 6-55g. The shear wave velocity profiles along with the boring data were used to identify the stiff soil layer used as the reference site for the ground motion calculations.

Depending on the location of the near-surface soft deposits (peat and organic marsh deposits), the relationships between maximum shear modulus, over-consolidation ratio and effective pressure proposed by Wehling (2001) for peat were used to evaluate the dependency of the shear modulus (or shear wave velocity) on the effective vertical stresses. This relationship is expressed in the following equation:

$$\frac{G_{max}}{Pa} = 75.7 \left[\frac{\sigma'_{1c}}{Pa} \right]^{0.87} OCR^{0.65}$$

where Pa and σ'_{1c} are the atmospheric and effective vertical pressures, respectively.

6.2.6.5.4 Modulus Reduction and Damping Ratio (G/G_{max} , ζ)

The variations of shear modulus and damping with shear strain for the various soil profiles were represented by modulus reduction and damping relationships. The modulus reduction relationship with shear strain corresponds to the variation of normalized secant shear modulus, G/G_{max} , with strain.

G/G_{max} and damping curves were obtained from UC Davis (Wehling et al. 2001) for the peat/organic soils as shown in Figures 6-56a and 6-56b. The series of curves, along with their distribution around the mean, were used in the statistical model to generate mean and standard deviations for the probabilistic seismic deformation analysis.

The shear modulus reduction curves (G/G_{\max}) and damping curves of Seed and Idriss (1970) and Vucetic and Dobry (1991) were applied for the sandy soils (embankment fill and alluvium) and clay, respectively. The selected dynamic soil properties used for the response analyses are summarized in Table 6-7. Plots of the selected G/G_{\max} and damping vs. shear strain relationships are presented in Figure 6-57.

The sensitivity of the seismic deformation of the levees to the range of values of the shear modulus and damping curves indicated a second order effect compared to the other soil parameters discussed in this section.

The variation of the soil parameters for the other deposits (non-peat and non-liquefiable deposits), such as the stiff clays and dense sands, also produces second order effects on the levee and foundation seismic deformations and hence their best-estimate properties were used deterministically.

6.2.6.6 Calibration Analysis

Very often data collected in the field and tests performed in the laboratories do not represent fully the levee and foundation conditions, particularly when dealing with hundreds of miles of levees across varying geologic and soil conditions. It was desirable to perform a calibration of the soil parameters using the best-estimate values from the data sets compiled for the Delta and discussed above. The calibration was performed at sites with known geotechnical issues (i.e., failed or cracked levees due to slope instability of steep levee slopes that are still stable). The objective of the calibration was to run stability analyses with the best-estimate values compiled for those known cases, and compare the results to the field observations. When applicable, the material properties were then adjusted to match the field observations. Based on discussions with the local geotechnical engineers and maintenance agencies, two sites were identified as prime candidates. The site at Bradford Island is experiencing tension crack and vertical offset at the levee crest, while the site at Holland Tract is experiencing erosion resulting in over-steepened waterside slope. The calibration analysis and results are discussed below.

6.2.6.6.1 Bradford Island Station 169+00

Stability-induced cracking was reported at the Station 169+00 in Bradford Island. Figure 6-58 shows the approximate location of this site, located at the midpoint of the northern boundary of the island along with the known geometry, subsurface information, water level, and piezometric line. The local District engineer reported that the cracking resulted from placement of approximately 2 feet of fill on the levee crest in the late 2002. No fill was placed on the slopes. Cracking was first observed in 2005 with some vertical and horizontal offsets in the crest. It appears that the crest movement has been gradually increasing since 2005. A vertical offset in the range of 6 to 12 inches was observed in the summer of 2006. Some horizontal offsets have also occurred. The movement of the crest may be attributed to the consolidation of soft foundation materials such as peat/organic and soft clays resulting from additional weight of the new fill and creeping of the peat/organic soils under sustained shear stresses.

An analysis cross section was developed at this location based on available topographical and subsurface data. Since cracking was observed at this location, it was assumed that this levee section is at best marginally stable. A static factor of safety of 1.1 to 1.15 was considered to represent appropriately the observed condition. The stability of the levees was analyzed using the

limit equilibrium method based on Spencer's procedure as coded in the computer program UTEXAS3. UTEXAS3 was used to compute factors of safety using circular slip surfaces.

The slope stability analysis was first performed using the best-estimate shear strength parameters for the peat/organic soils from previous laboratory tests. Subsequently, the shear strength was adjusted until it yielded a factor of safety of about 1.13, as shown in Figure 6-58.

6.2.6.6.2 Holland Tract Station 60+00

The waterside slope at this location is very steep and therefore this section was selected for testing the reasonableness of the calibrated shear strength parameters of peat/organic soils. The results of the slope stability analysis for this section are presented in Figure 6-59. The calibrated peat strength parameters for Bradford Island above produce a factor of safety of 1.0 for Holland Tract.

Back calculation performed by Hultgren-Tillis Engineers (2003) for Holland Island at Station 60+00 indicated that for waterside factor of safety of about 1.0, the effective cohesion and friction angle were 100 psf and 28 degrees, respectively. These are reasonably similar to the 120 psf and 28 degrees estimated in the calibration described above. The results of this analysis is shown in Figure 6-59. These "calibrated" strength parameters were then used for the rest of the stability analyses for this project.

6.2.6.6.3 Back Calculations from Four Island Levee Failures

M.W. Driller (1990) investigated the failures of island levees in the Delta and Suisun Marsh from 1950 to 1982, and performed back calculations for four slope failures of Delta levees to estimate the strength parameters of the peat/organic deposits. The four island were Tyler Island, Twitchell Island, Webb Tract, and McDonald Tract. The back-calculated strength parameters were developed for a range of coupled cohesions with effective friction angles. For a cohesion of 140 psf, the results yielded friction angles ranging from 11.5 to 16 degrees compared to an effective cohesion of 140 psf and a friction angle of 18 degrees used in this analysis.

6.2.6.6.4 Further Comparisons and Verifications

The purpose of this comparison and verification section was to compare the outcome of the levee stability analyses to those levees where other previous studies have been completed recently. There were a number of studies performed by others in Sherman Island in the recent past (DWR 1993; GEI 1996; URS 2000; Hultgren-Tillis Engineers [HTE] 2003). It should be noted that the slope stability analyses for DRMS 2007 and GEI (1996) were conducted for the same station. For the remaining three other references (URS 2000; HTE 2003; DWR 1993) the slope stability analyses were performed by the DRMS seismic analysis team at the same location using the material properties developed by those studies. The comparison analysis was performed for a cross section at station 650+00 in Sherman Island (south side of the island). At that location the peat layer forming the foundation exceeds 40 feet in thickness. As shown in Figures 6-60a and 6-60b, the long-term factors of safety for the best-estimate material parameters are equal to 1.29 and 1.60, and the corresponding yield accelerations are 0.05 and 0.07 for the landside and waterside slopes, respectively. The results are generally consistent with the other previous studies of Sherman Island, as shown below.

Studies	Landside Factor of Safety	Comments
This Study (URS/JBA 2008h)	FS = 1.29	
GEI (1996)	FS = 1.20	
Hultgren-Tillis Engineers (2003)	FS = 1.49	Calculated for this study*
DWR (1992)	FS = 1.24	Calculated for this study*
URS (2000)	FS = 1.21	Calculated for this study*

*Indicates results calculated in this study using their material properties.

Seismic deformation analysis was also conducted for the same cross-section. The analysis was performed for three earthquake magnitudes (**M** 5.5, **M** 6.5, and **M** 7.5) and a range of reference site peak ground accelerations ranging from 0.1 to 0.5 g. The dynamic analysis was conducted using both FLAC and QUAD4M-Newmark type procedures. The finite element mesh is illustrated in Figure 6-61. The results of the dynamic analysis indicate that the two methods, QUAD4M-Newmark and FLAC, produce generally similar results, as shown in Figures 6-62 and 6-63, respectively. The results further indicate that under large earthquake shaking, the south levee of Sherman Island could undergo 5 feet or more of horizontal deformation.

6.2.6.7 Simulation of Levee Response to Past Earthquakes

On January 24, 1980, an earthquake of magnitude **M** 5.8 occurred near Livermore, about 18 km south of the Delta. A recording station maintained by the California Department of Mines and Geology (CDMG-67070) at Antioch located at a site with a $V_{S-30} = 338.5$ m/sec recorded a PGA of 0.0355g.

On March 24, 1984, an earthquake of magnitude **M** 6.19 occurred in Morgan Hill on Calaveras Faults about 80 km south of the Delta. No recording station at or near the Delta was reported. However, a recording station maintained by the California Department of Mines and Geology CDMG-56012 at Los Banos (80 km south east) located at a site with a $V_{S-30} = 271.4$ m/sec recorded a PGA of 0.0560g.

These events were the closest and strongest recorded earthquakes near the Delta in recent history (since the beginning of strong motion instrumentation). There were no observations of damage reported in the Delta following these events. Similar observations are also drawn by applying the recorded PGA values and associated magnitudes to the calculated levee deformation functions and fragility function presented in this section. Generally, we estimate no damage or insignificant damage for PGAs equal to or less than 0.05g.

A simulation of the 1906 Great San Francisco Earthquake (**M** 8.0) was conducted to estimate the mean PGA at the western portion of the Delta. The calculated mean PGA was obtained using the four new attenuation relationships for the reference site and assigning equal weight to each. The attenuation relationships used were the same ones used in the PSHA. The calculated PGA near Sherman Island (west of the Delta) was equal to 0.11g. Applying this calculated PGA and the associated magnitude to the calculated fragility functions yielded minor to moderate damage to the levees and foundations should a repeat of the 1906 earthquake occur today. The expected earthquake-induced deformations ranged from negligible to 3 feet depending on the levee vulnerability classes and its location in the Delta. The expected probabilities of failure calculated

in the risk model predict on average 0.004 to 0.23 probability of failure for and M-8 on the San Andreas fault.

Key observations and model predictions from the above simulations are summarized in the table below.

Earthquake Event	Observations	Model Prediction
M 5.8 Livermore EQ (1980)	No damage observed	No damage calculated
M 6.19 Morgan Hill EQ (1984)	No damage observed	No damage calculated
M 8.0 San Francisco EQ (1906)	Levees were much smaller and no post-earthquake eyewitness reports exist	Expected levee deformation, for today's levees, ranges from 0 to 3 feet and the conditional probability of levee failure ranges from 0 to 23%.

The model results were also compared to other sites where earthquake-induced liquefaction caused damage to levees. Two case histories are used in this comparison. They include the 1995 M 6.9 Kobe Japan earthquake and the levee failure along the Pajaro River in Watsonville, California, after the 1989 M 6.7 Loma Prieta Earthquake.

The Kobe earthquake generated peak ground accelerations in excess of 0.5g at the levee site shown in Figure 6-28. Figure 6-29 shows a vertical deformation (vertical slump) of about 15 feet (4.6 meters) for the flood wall and 10.5 feet (3.3 meters) for the crest road. The levee was about 21 feet in height (to the top of the crest road). The calculated deformation for a levee in the Delta with liquefiable sand in the foundation (Figure 6-96, below) is in excess of 10 feet for a PGA equal to or greater than 0.5g. This estimated value from Figure 6-96 was interpolated between the curves for magnitudes 6.5 and 7.5. The probability of failure predicted from the fragility functions (Figure 6-137a, below) for class 1 (no peat) shows a probability of failure ranging approximately from 70 to 100 percent.

A similar comparison was performed for the Pajaro River levee failure in 1989. The estimated earthquake PGA at the site was about 0.33g. Sand boils were reported in many sites along the river banks (USACE 1989). The levee was about 6 feet in height. The field damage survey showed tension cracks 18 inches wide at the crest of the levee with one foot vertical offset. The calculated deformation for a levee in the Delta with liquefiable sand in the foundation (Figure 6-96) is about 4 feet for a PGA equal to 0.33g. This estimated value, from Figure 6-96, is for a 20-foot tall levee as opposed to the 6-foot tall levee along the Pajaro River. The probability of failure predicted from the fragility functions (Figure 6-137a) for class 1 (no peat) shows a probability of failure ranging approximately from 58 to 88 percent.

After the calibration analysis at Bradford Island and Holland Tract, and the comparison with other studies for Sherman Island, and the verification against past earthquakes, then the analysis of the typical/idealized cross-sections representing the range of the VCs was initiated.

6.2.6.8 Selection of Random Variables and Estimation of Their Statistical Distribution

Several parameters contribute to the seismic response of levees and their foundation. Some are primary and have first order contribution to the response functions and others are secondary and have insignificant contribution to the response of the levees response functions. Several potential

material parameters were evaluated by performing sensitivity analyses. The material properties whose variations showed relatively little effects on levee deformation were treated deterministically with best point estimate values. The material properties whose variations showed significant effects on the levee deformation were treated as random variables and their probability distribution functions were calculated based on the statistical analysis of the available data. These probability distributions quantify the aleatory uncertainty in the materials properties.

A lognormal distribution was assumed for each random input variable because it is a commonly accepted probability distribution of soil properties and the shape of this distribution provides a reasonable fit to the distribution of field data. A lognormal distribution is completely defined by two statistical parameters: the median and the logarithmic standard deviation.

For VCs 1 through 14, the random variables:

(N₁)_{60-cs} and residual shear strength (Sr) of the liquefiable levee fill and foundation sand were treated as random variables. The (N₁)_{60-cs} and Sr are based on correlation relationships proposed by Seed and Harder (1990) as shown in Figure 6-64a(1).

Liquefaction potential of levee fill and foundation sand was treated as a probability distribution. The probability of liquefaction was assessed using the procedure proposed by Seed et al. (2003) as shown in Figure 6-64a(2).

Peat thickness was treated as a random variable within each selected interval, as discussed in Section 6.2.3.

The deterministic parameters included:

Levee geometry within the ranges of “steep” or “not steep” groups as defined earlier.

Water level in the slough and rivers was considered at mean higher high water (MHHW) level. It was assumed that the probability of both flood and seismic events happening at the same time was very low and will not have significant contribution to the total hazard. The mean higher high water level typically occurs few times a month (average of the two weeks highs) and is more likely to occur during or immediately after the earthquake event. The piezometric line through the embankment for the MHHW is also considered deterministically.

For VCs 15 through 22 the random variables included:

Cohesion and friction angle of peat/organic deposits were treated as random variables. The available p-q data of peat (as discussed in Section 6.4.3) were utilized to calculate the standard deviations in cohesion and friction angle of peat/organic deposits.

Peat thickness was treated as a random variable within each selected interval, as discussed in Section 6.2.3.

The deterministic parameters included:

Levee geometry - variation in the waterside slope was considered to have some impact in the seismic deformation. Analyses were considered using two levee geometries: with steep and non-steep waterside slopes. All other dimensions of the levee such as widths and landsides slope were found to have insignificant effects on the calculated seismic deformations, for the range of data compiled.

Water level in the slough and rivers - Water level was considered at MHHW as explained above. The piezometric line through the embankment for the MHHW is also considered deterministically.

Variation of modulus reduction and damping with shear strain - for the ranges of data shown on Figure 6-56a and 6-56b. These parameters were found to have a second order effects on the seismic deformation of the levees for the range of the statistical data.

Soil properties of other soils (i.e., other than peat and organic deposits) - Since the seismic behavior of the Delta levees are mainly controlled by the liquefaction of levee fill and/or foundation materials and the peat/organic soils, the variation of the material properties for the stiff clays and dense sands have no significant effects on the levee responses to seismic loading. Therefore, soil properties of these dense and stiff materials were treated deterministically using the best-estimate values.

Unit weights of peat and loose sands - The unit weights of the loose fill, the loose foundation sand, and the peat were treated deterministically using the best-estimate values.

6.2.6.9 Analyses and Results

6.2.6.9.1 Analysis and Results for VCs 1 through 14

Probability of Liquefaction Analysis

For those VCs with liquefiable fill or foundation (VCs 1 through 14), seismic displacement was calculated under both liquefaction and no-liquefaction scenarios. The probability of liquefaction of either the fill or the foundation was assessed using the procedure recommended in Seed et al. (2003). The following are key steps involved in the calculation of probability of liquefaction.

Step 1: Simulate levee soil properties

For each simulation trial, the following soil properties were simulated: fill $(N1)_{60}$ foundation $(N1)_{60}$ and peat thickness. The probability distribution for each of these soil properties was characterized based on a statistical analysis of available field data over the Delta. Each distribution was assumed to be lognormal and was defined in terms of the mean and standard deviation of the natural logarithm of the variable. These parameters are shown in the following list:

Soil Property	Mean	Standard Deviation
Fill (N1) ₆₀	6.5	1.65
Foundation (N1) ₆₀	14.4	2.27
Peat Thickness (ft)	Varies with Thickness Intervals	2.09

The simulated value of each soil property was constrained to lie within the applicable range for each vulnerability class. For example, for VC 2, the fill (N1)₆₀ was constrained to be less than or equal to 20 and peat thickness was constrained to be between 0.1 and 10 feet. Note for VC 1, peat thickness was defined to be 0 and no simulation of peat thickness was necessary for this class.

Step 2: Select a particular combination of earthquake magnitude, M, and reference peak ground acceleration, PGA

Different combinations of three earthquake magnitudes (M 5.5, M 6.5, and M 7.5) and 21 PGA values (0.05g, and 0.1g to 2.0g in increments of 0.1g) were considered in this analysis. The subsequent steps were repeated for each M and PGA combination.

Step 3: Calculate probabilities of fill and foundation liquefaction.

The following equation recommended in Seed et al. (2003) was used to calculate the probability of liquefaction:

$$P_L(N_{1,60}, CSR, M, \sigma'_v, FC) = \Phi \left[\frac{\left((N1)_{60} \cdot (1 + 0.004 \cdot FC) - 13.32 \cdot \ln(CSR) - 29.53 \cdot \ln(M) - 3.70 \cdot \ln(\sigma'_v) + 0.05 \cdot FC + 44.97 \right)}{2.70} \right] \quad (1)$$

where

- P_L = the probability of liquefaction in decimals (i.e., 0.3, 0.4, etc.)
- $(N1)_{60}$ = fill (N1)₆₀ or foundation (N1)₆₀
- CSR = cyclic stress ratio
- M = earthquake magnitude
- σ'_v = effective overburden stress
- FC = fines content
- Φ = the standard cumulative normal distribution

The use of this equation requires estimates of CSR, effective overburden stress (σ'_v), and fines content (FC). The values of these variables were obtained as follows:

Cyclic Stress Ratio

The CSR values for the probability of liquefaction were calculated using the results from a study performed by Kishida et al. (2007). As part of this study, two analysis cross sections were

developed to represent general conditions at Sherman Island (peat thickness about 30 feet) and Bacon Island (peat thickness about 15 feet) and were analyzed using the computer program, QUAD4M. Two hundred and sixty four ground motions were used as input motions for the dynamic analysis. These ground motions had the following characteristics:

- PGA ranged from 0.004 g to 1.78 g
- Moment magnitude (M_w) from 4.3 to 7.9
- Seismic distance from 1.1 km to 296 km

The ratio between the crest acceleration and the acceleration within the levee fill was estimated to be about 1.0 based on analyses conducted by URS (QUAD4M and FLAC) and Kishida et al (2007). The peak crest acceleration was multiplied by the reduction factor r_d and a σ_v/σ_v' approximated to 1.0 to estimate the CSR.

Fill CSR was calculated for different earthquake time histories for each of three peat thickness: 0 feet, 15 feet, and 25 feet. Two separate regression equations were developed to estimate the natural logarithm of fill CSR – one for peat thickness of 0 feet and the other for peat thickness greater than 0 feet. These regression equations are as follows:

For peat thickness = 0 feet

$$\ln(CSR) = -2.35 + 0.213 \cdot M + 0.783 \cdot \ln(PGA) \tag{2}$$

(RMSE = 0.327)

where

CSR = cyclic stress ratio

M = earthquake magnitude

PGA = reference peak ground acceleration in g

For peat thickness > 0 feet

$$\ln(CSR) = -2.14 + 0.268 \cdot M + 0.743 \cdot \ln(PGA) - 0.0379 \cdot peat \tag{3}$$

(RMSE = 0.351)

where

CSR = cyclic stress ratio

M = earthquake magnitude

PGA = reference peak ground acceleration in g

$peat$ = peat thickness in feet

The root mean square error (RMSE) in each regression equation was assumed to be the logarithmic standard deviation of CSR for given values of M, PGA, and peat thickness. A lognormal distribution was assumed for fill CSR with a mean of natural logarithm of CSR calculated from Equation (2) or (3) and logarithmic standard deviation equal to the RMSE.

For the foundation loose sand, the acceleration within the foundation was estimated from Figures 6-64b(1) and 6-64b(2) given values of M , PGA , and peat thickness. The regression relationships shown in Figure 6-64b(2) were developed based on review of several analysis results by URS (Quad4M and FLAC analyses) and Kishida et al. (2007).

The equation used to calculate the CSR for foundation sand is as follows:

$$CSR = 0.65 \cdot r_d \cdot (a_{max}/g) \cdot (\sigma_v/\sigma_v')$$
(4)

Fines Content

Based on available gradation data, empirical probability distributions were defined for the fill and foundation FC. These distributions are shown in the table below.

Fines Content Category	Fines Content, FC (%)	% of Total
FC Fill C1	5	22.6
FC Fill C2	8	3.52
FC Fill C3	15	39.2
FC Fill C4	25	6.03
FC Fill C5	35	28.6
FC Foundation C1	5	4.8
FC Foundation C2	8	1.8
FC Foundation C3	15	87.5
FC Foundation C4	25	0.5
FC Foundation C5	35	5.3

Step 4: Simulate liquefaction outcome

Using the probability of fill liquefaction estimated from Equation (1), a binary variable was simulated with an outcome of either liquefaction or no liquefaction of the fill. A similar binary variable was simulated for the foundation liquefaction. If $(N1)_{60}$ of either the fill or foundation was greater than 20, the probability of liquefaction was assumed to be negligible. The two binary variables defined four possible liquefaction outcomes, as follows:

- Outcome 1: Both fill and foundation liquefy.
- Outcome 2: Fill liquefies, but foundation does not.
- Outcome 3: Fill does not liquefy, but foundation does.
- Outcome 4: Neither fill nor foundation liquefies.

For each simulation trial, one and only one of the four outcomes is generated.

6.2.6.10 Deformation Analysis

Liquefaction of Foundation Material

The FLAC meshes developed to model the four idealized sections are shown in Figures 6-65 through 6-68. For illustration purposes, the time history of the CSR and the pore pressure ratio in the liquefiable sand layer are shown in Figures 6-69 through 6-86 for the low (**M** 5.5), moderate (**M** 6.5), and large (**M** 7.5) earthquakes and a reference peak ground acceleration of 0.2g.

The seismic-induced post-liquefaction deformation contours are shown in Figures 6-87 through 6-95. As shown in these figures, the analyses results for this case show high excess pore pressure and therefore high strength degradation in the liquefiable sand layer resulting in excessive deformations (8 to 10 feet). The mean total displacements are summarized in Table 6-8 and shown in Figures 6-96 through 6-98. It should be noted that for the section with no peat, the deformations are very large and the computer model could not converge, indicating flow failures beyond 10 feet.

Liquefaction of Levee Fill

For the case of the potentially liquefiable levee fill, the computer program FLAC was utilized. It was noted however, that in this case again, the deformation were very large (beyond 10 feet) and hence the non-linear time-domain analysis could not converge because of the excessive deformations. A simplified approach using the post-liquefaction static-slumping method (discussed earlier) was used as a substitute, recognizing that it does not represent the inertia-induced deformations. An example of the pre- and post static slump deformation is illustrated in Figure 6-99 showing 10 feet of vertical slump for a levee fill with residual strength of 230 psf. Below 230 psf residual strength, the computer program did not converge, indicating deformations in excess of 10 feet.

Non-liquefiable Levee Foundation and Fill (VCs 14 through 22)

The static stability analyses for long-term conditions were performed for five idealized cross sections with peat thickness of 0, 5 feet, 15 feet, 25 feet, and a section representing Suisun Marsh. The results are summarized in Table 6-9, and the cross sections with the most critical slip surfaces and factors of safety are shown in Figures 6-100 through 6-104. The results of these analyses indicate that the yield acceleration decreases as the peat thickness increases. For Suisun Marsh, the yield accelerations range from 0.03 to 0.09g. For the Delta levees, the yield accelerations range from as low as 0.05g for peat thicker than 40 feet (Sherman Island) and as high as 0.24g in places, where peat is not present.

The seismic deformation analyses were performed using the QUAD4M-K_y-Newmark method as discussed earlier. These analyses were performed for the mean estimates of soil properties for all five idealized cross-sections. Two levee geometries were considered for these analyses depending on the VC, steep and non-steep waterside slope.

The finite element meshes for the five idealized cross sections with non-steep waterside slopes are shown in Figures 6-105 through 6-109. The acceleration time histories recorded from the base of the mesh to the crest of the levee or the free field surface are presented in Figures 6-110 through 6-124. Figure 6-125 presents a typical displacement time history from the Newmark sliding block analysis. The results of the deformation analyses for the five idealized sections are

presented in Figures 6-126 through 6-130. The calculated displacements range from a fraction of an inch for the cross-section with no peat and no liquefaction, to several feet (up to 14 feet) for Suisun Marsh and the liquefiable fill cases. The results are also summarized in Tables 6-10a and 6-10b for Delta and Suisun Marsh levees, respectively. These calculated displacements correspond to horizontal translations of the center of mass of each sliding block. The corresponding vertical displacements were obtained from relationships between horizontal and vertical deformations obtained from the FLAC analysis. Generally, a ratio of 1H to 1/2 V displacement was observed in the cases evaluated. This ratio was discussed and approved by the experts elicited for the development of the *conditional probability of failure functions* (see Section 6.2.7)

The results of the calculated levee deformation for levees with the steep waterside slope are presented in Figures 6-131 through 6-134.

6.2.7 Conditional Probability of Failure Functions

The development of the conditional probability of levee failure given earthquake-induced deformations was solely based on expert elicitation. The group of experts selected for the levee vulnerability have either a long standing work experience with levees in the Delta and/or are known to have performed research and published technical subject matters related to the performance of the Delta levees. The following experts were convened to offer expert opinion:

- Professor Ray Seed (UC Berkeley)
- Dr. Leslie Harder (DWR)
- Mr. Michael Driller (DWR)
- Dr. Ulrich Luscher (Consultant)
- Dr. Faiz Makdisi (Geomatrix)
- Mr. Michael Ramsbotham (USACE)
- Mr. Gilbert Cosio (MBK Engineers)
- Mr. Kevin Tellis (Hultgren-Tillis)
- Mr. Edward Hultgren (Hultgren-Tillis)
- Dr. Said Salah-Mars (URS - Facilitator)

First a scope of the expert elicitation was presented to the panel of experts. The scope consisted mainly of introducing the experts to the development methodology of the entire levee fragility task, which includes the three steps forming the methodology as described in Section 6.2.3.

These three steps are as follows:

1. The development of the *levee response functions*
2. The development of the *conditional probability of failure functions*
3. The development of the *levee fragility functions*

The second part of the scope consisted of eliciting expert opinion and recommendations on the development of the *conditional probability of failure functions*, given their involvement as TAC

members in the levee seismic vulnerability and their understanding of the entire methodology for the development of the levee fragility functions.

For a period of few months, the experts participated and developed a full understanding of the process behind the development of the levee response and the levee fragility methodology.

Based on the understanding of the entire task, the experts were then asked to develop their own (individual) recommendations on the shapes of the *conditional probability of failure functions*, given the knowledge and the understanding of the entire process. Specific questions were asked of the experts such as:

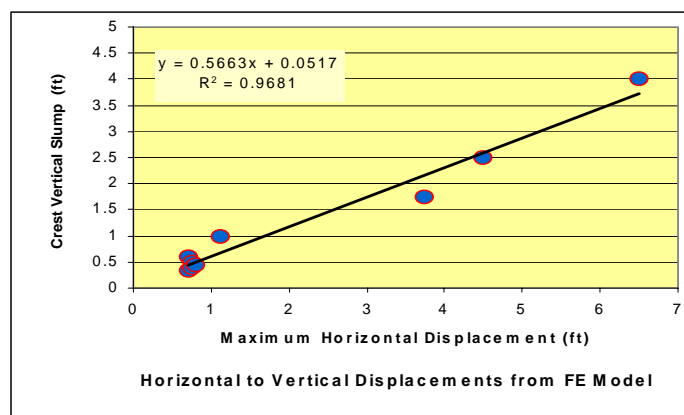
- Should the functions be developed assuming human intervention or not?
- What is a simple and reasonable relationship between vertical deformation and horizontal deformation?
- What is the proper abscissa parameter that should be used for the conditional probability of failure functions?

These questions were discussed among the experts and resolved before they developed their recommendations.

The experts submitted their recommendations on both issues: (1) developing the shapes of the conditional probability functions and (2) answering the specific questions. The experts convened in a meeting where their recommendations were shared and discussed. During this meeting the experts were able to present their thoughts on their recommendations and listened to other experts' opinions and justifications.

After the shared session the experts were given an option to revisit their recommendations in light of the discussion and knowledge exchanged during the shared session. The experts then resubmitted their recommendations, which were then processed by the seismic analysis team, giving equal weight to each of the recommendations. The mean and distribution around the mean are shown in Figure 6-135, relating the conditional probability of failure to the relative loss of freeboard (i.e., ratio of vertical deformation over initial freeboard) assuming normal flood fight efforts during emergency response. These curves represent the epistemic uncertainty associated with the expected failure (levee breach) given earthquake-induced levee permanent vertical deformations. In addition to the loss of freeboard leading to overtopping, the failure mechanisms and their uncertainties consider also the likelihood of post-deformation cracking leading to internal erosion and piping.

On the issue of the vertical to horizontal deformation the consensus was to use a factor of about two to represent the horizontal to vertical deformation for a sliding mass on the side slopes of the levees. The data obtained from the finite element deformation mesh was reviewed and used in this recommendation, as shown in the figure. Although the calculated deformations using finite elements provide both vertical and



horizontal deformations (they were used for the liquefaction cases), the bulk of the runs were performed using QUAD4-M and Newmark analyses, which provide horizontal deformation only.

6.2.8 Evaluation of Seismic Fragility Functions

The objectives of this analysis were to assess the (conditional) probability of levee failure due to displacement under different seismic events and to quantify the uncertainty in the assessed failure probability. The Monte Carlo simulation method was used to assess the probability of levee failure under different combinations of earthquake magnitude and reference peak ground acceleration. The failure probability was assessed separately for the different levee VCs that were defined based on levee geometry and soil properties. Section 6.2.3 describes the definition of the different VCs and the random variables for each vulnerability class.

The Monte Carlo simulation method involved defining the probability distribution of each random variable based on a statistical analysis of available data and simulating a value of the variable by randomly sampling from its probability distribution. The commercial software Crystal Ball® was used to simulate values of random variables from their defined probability distributions. These simulated values were used to calculate levee displacement under different seismic events.

Conditional probability of failure as a function of seismic deformation was previously developed using expert opinion as discussed in the previous section. These conditional probability functions were combined with the simulated seismic displacement to assess the probability of levee failure under different combinations of earthquake magnitude and reference PGA.

6.2.8.1 Step-by-Step Procedure

Figure 6-136 shows a flowchart of the key steps of the simulation procedure. These steps are described below. The first four steps have already been discussed in the previous sections. They represented the simulation of the levee soil properties, the selection of M and PGA combinations, the calculation of probabilities of liquefaction for levee fill and foundation materials, and the simulation of their outcome. The following paragraphs describe the remaining steps.

Step 5: For the given liquefaction outcome, simulate levee horizontal displacement.

The procedures to estimate levee horizontal displacement for each of the four liquefaction outcomes are described below.

Displacement under Outcome 1: Both fill and foundation liquefy

For this outcome, displacement was assumed to be the sum of two components – one due to fill liquefaction alone and the other due to foundation liquefaction alone. These two components of displacement were simulated using the following procedures.

Displacement due to Fill Liquefaction Alone

Assuming liquefied fill, the residual undrained shear strength, S_r , was first simulated. A regression equation was developed to estimate the mean S_r (in psf) as a function of fill $(N1)_{60-cs}$ using the curve provided in Seed and Harder (1990) Figure 6-64a(1). This equation is as follows:

$$S_r = 11.8 + 2.82 \cdot ((N1)_{60-cs})^2 \tag{5}$$

where

S_r = the residual undrained shear strength in psf

$(N1)_{60-cs}$ = fill $N_{1-60-cs}$

The upper-bound curve in the above reference showed an increase of about 200 psf above the mean curve over the full range of fill $(N1)_{60-cs}$. This upper bound was taken to be the 95th percentile curve (i.e., 95 percent of S_r values would be at or below this upper-bound). The spread around the mean curve, as shown in the above reference, was symmetric, suggesting that a normal distribution would be appropriate. Assuming a normal distribution for S_r at any given value of fill $(N1)_{60-cs}$, the difference between the 95th percentile and mean would be equal to $1.645 \times$ standard deviation. Using this relationship, the standard deviation of S_r was estimated to be $(200/1.645=)$ 121.6 psf.

A value of S_r was simulated assuming a normal distribution with the mean value from Equation (5) and a standard deviation of 121.6 psf. This value of S_r was used next to define a distribution of horizontal displacement, D_H . Using results of seismic displacement analysis under liquefied fill and the resulting S_r , a regression equation was developed to estimate the natural logarithm of D_H as a function of S_r for the case of liquefied fill. This equation is as follows:

$$\ln(D_H) = 3.26 + 0.00404 \cdot S_r - 0.0000369 \cdot S_r^2 \tag{6}$$

$(RMSE = 0.172)$

where

D_H = horizontal displacement in feet

S_r = the residual undrained shear strength in psf

The RMSE of this regression equation was 0.172 feet. A value of D_H was simulated assuming a lognormal distribution with the natural logarithmic mean calculated from Equation (6) and a natural logarithmic standard deviation of 0.172.

Displacement due to Liquefied Foundation Alone

Levee displacement was estimated for different combinations of **M**, **PGA**, peat thickness, and foundation $(N1)_{60-cs}$ under the condition of liquefied foundation. Using the results of this analysis, the following regression equation was developed:

$$\ln(D_H) = -5.89 + 0.916 \cdot M + 7.02 \cdot PGA - 0.0163 \cdot peat - 0.127 \cdot (N1)_{60-cs} \quad (7)$$

(RMSE = 0.650)

where

D_H = horizontal displacement in feet

M = earthquake magnitude

PGA = reference peak ground acceleration in g

$peat$ = peat thickness in feet

$(N1)_{60-cs}$ = foundation $(N1)_{60-cs}$

Displacement under Outcome 2: Fill Liquefies, but Foundation Does Not

For this outcome, the overall displacement was again assumed to be the sum of two components: one due to fill liquefaction alone and the other due to the movement of non-liquefied foundation alone. The first component was simulated using the same procedure as in Outcome 1. For the second component, displacements estimated for a non-liquefied foundation were used to develop a regression equation. The displacement analysis showed that the soil strength parameters c and ϕ influenced the estimated displacements when the levee profile included a peat layer. Therefore, two separate regression equations were derived – one for zero peat thickness and one for non-zero peat thickness. These two regression equations are as follows:

For peat thickness = 0 feet

$$\ln(D_H) = -9.69 + 0.794 \cdot M + 4.04 \cdot PGA + 1.69 \cdot waterside \quad (8)$$

(RMSE = 0.630)

where

D_H = horizontal displacement in feet

M = earthquake magnitude

PGA = reference peak ground acceleration in g

$waterside$ = waterside levee slope indicator (0 = non-steep; 1 = steep)

The variable “waterside levee slope indicator” in Equation (8) was defined to be 1 for a steep slope (defined as steeper than 1.5H:1V) and 0 for a non-steep slope. This variable was assumed to be deterministic; that is, the slope was assumed to be known for individual levee reaches. Note that the slope indicator is used only for VCs 15 through 22. For VCs 1 through 14, the fill or foundation was susceptible to liquefaction and the influence of the levee slope was assessed to be negligible. Consequently, the slope indicator was not used to define VCs 1 through 14. For these vulnerability classes, the slope indicator was set equal to its prevalent value of 0 (i.e., non-steep slope).

For peat thickness > 0 feet

$$\ln(D_H) = -7.86 + 1.19 \cdot M + 7.81 \cdot PGA + 0.0464 \cdot peat - 0.0115 \cdot c - 0.128 \cdot \phi + 0.962 \cdot waterside \tag{9}$$

(RMSE = 0.595)

where

D_H = horizontal displacement in feet

M = earthquake magnitude

PGA = reference peak ground acceleration in g

$peat$ = peat thickness in feet

c = soil strength parameter, c , in psf

ϕ = soil strength parameter in degrees

$waterside$ = waterside levee slope indicator (0 = non-steep; 1 = steep)

The parameter c was assumed to be lognormally distributed with the mean and standard deviation of natural logarithm of c of 4.79 and 0.336, respectively. The friction angle ϕ was assumed to be lognormally distributed with the mean and standard deviation of natural logarithm of ϕ of 3.33 and 0.0677, respectively. The parameters c and ϕ were assumed to be probabilistically independent. The same distributions were assumed to apply to all Delta levees.

Displacement under Outcome 3: Fill Does Not Liquefy, but Foundation Does

For this outcome, displacement was estimated using the procedure described under *Displacement due to Liquefied Foundation Alone* for Outcome 1.

Displacement under Outcome 4: Neither Fill nor Foundation Liquefies

For this outcome, displacement was estimated using the procedure described under Outcome 2.

Step 6: Calculate the probability of failure for given values of initial freeboard at different confidence levels.

At the end of Step 5, a simulated value of D_H was generated for each selected (M , PGA) combination. The vertical displacement was assessed to be 50 percent of the horizontal displacement. For different values of initial freeboard (IFB), the following ratio, R , was calculated:

$$R = (\text{vertical displacement} / IFB) = (0.5 \times D_H / IFB) \tag{10}$$

Levee fragility curves were previously developed using expert opinion. The development of these curves was described in Section 6.2.4. The variability of input from different experts represents epistemic uncertainty. The assessments of multiple experts were used to calculate the median (i.e., 50th percentile) and 84th percentile of the failure probability, p_f , for different values of R . Using these two percentiles, the mean of natural logarithm of p_f for a given R was calculated as natural logarithm of median p_f , and the standard deviation of natural logarithm of p_f was calculated as natural logarithm of (84th percentile of p_f / median p_f). Regression equations

were developed to estimate mean and standard deviation of natural logarithm of p_f as a function of R . These equations were as follows:

$$m(\ln p_f) = \ln \left(\frac{e^{(8.97 \cdot R - 5.67)}}{1 + e^{(8.97 \cdot R - 5.67)}} \right) \tag{11}$$

$$s(\ln p_f) = -1.28 \cdot R + 1.16 \tag{12}$$

where

$m(\ln p_f)$ = mean of logarithm of probability of failure

$s(\ln p_f)$ = standard deviation of logarithm of probability of failure

R = ratio of vertical displacement divided by *IFB*

For each R , the mean and standard deviation of natural logarithm of p_f were calculated from Equations (11) and (12), respectively. Using these two parameters and assuming a normal distribution for natural logarithm of p_f , one hundred values of p_f were calculated for confidence levels in increments of 1 percent starting from 0.5 percent to 99.5 percent. The following equation was used to calculate p_f for a specified confidence level of $p\%$:

$$p_f(p\%) = e^{(m(\ln p_f) + z_{p\%} \times s(\ln p_f))} \tag{13}$$

where

$p_f(p\%)$ = probability of failure at confidence level of $p\%$

$m(\ln p_f)$ = mean of logarithm of probability of failure

$z_{p\%}$ = standard normal variable corresponding to a cumulative probability of $p\%$

$s(\ln p_f)$ = standard deviation of logarithm of probability of failure

This process divides the continuous distribution of p_f into a discrete distribution of one hundred values and each value has a probability of occurrence of 1 percent. This probability distribution of p_f captures the epistemic uncertainty defined by the variability in the expert input.

This process was repeated for each of different values of *IFB* in the range of 0 feet to 20 feet.

Step 7: Repeat Steps 3 through 6 for different combinations of M and PGA.

Steps 3 through 6 were repeated for different combinations of **M** and **PGA**. Thus, for a given simulation trial, the completion of Step 7 generated values of p_f for different *IFB* values for each combination of **M** and **PGA**.

Step 8: Repeat Steps 1 through 7 for a specified number of simulation trials.

For this analysis, 500 simulation trials were performed. At the completion of this step, 500 simulated values of p_f were generated at each of 100 confidence levels for each *IFB* value for each combination of **M** and **PGA**.

Step 9: Calculate the overall failure probability at different confidence levels for each (M, PGA, IFB) combination.

The overall probability of failure at each specified confidence level for each combination of (M, PGA, IFB) was calculated by integrating over the entire probability distribution of D_H , as follows:

$$P[\text{failure} | M, PGA, IFB] = \sum_i P[\text{failure} | D_{H_i}, IFB] \times P[D_{H_i} | M, PGA] \tag{14}$$

The probability distribution of D_H was defined based on the 500 simulated values for each (M, PGA) combination. Because each of the 500 simulated D_H values occurs with an equal probability (of 1 in 500), the overall failure probability from Equation (14) for a given confidence level is the average of the corresponding 500 values of p_f calculated at that confidence level.

The model developed by Seed et al. (2003) was used as the primary model to assess the probability of liquefaction. However, other published models (Liao et al. 1988; Liao and Lum 1998; Youd and Noble 1997; Toprak et al. 1999) provide somewhat different assessments of liquefaction probability for given values of $(N1)_{60}$ and CSR. The range of the liquefaction probability from the Seed model and other published models represents the epistemic uncertainty in the liquefaction probability. An analysis of the results from the different models suggested a coefficient of variation of about 28 percent around the liquefaction probability assessed from the Seed model. The analysis of levee response showed that the levee failure probability varied in proportion to the change in the liquefaction probability. Therefore, an epistemic uncertainty of 28 percent in the assessed failure probability was set to reflect the range of published research on liquefaction probability.

A hand calculation on a selected vulnerability class (VC 10) for one magnitude, three PGAs, and one water level is presented in Appendix 6A. The hand calculation is provided to illustrate the steps of the development of a fragility function using the mean values to carry the calculation to the end by hand and without being too cumbersome by adding the uncertainties around the mean.

6.2.8.2 Results of Analysis of Failure Frequencies for Different Vulnerability Classes

The calculated fragility functions included a total of 22 classes, 3 magnitudes, 21 PGAs, 20 water levels, and 100 fractiles (0 to 100 confidence levels). The total number of data points amounted to 2,772,000. The digital file in the format presented in Table 6-11 was prepared as input into the risk calculation model.

A limited sample of fragility functions is shown in Figures 6-137a through 6-137f. These figures show the assessed failure probability for 16 percent, 50 percent, and 84 percent confidence levels for **M** 6-1/2 and 2 feet of freeboard.

We discuss here the interpretation of the results for the first four vulnerability classes (VC 1 through VC 4) shown in Figure 6-137a. The difference between VC 2, VC 3, and VC 4 is explained by the difference in the relative contribution of the probability of liquefaction of the

fill versus the probability of no liquefaction of the fill. The probability of failure is the weighted sum of the probability of deformation multiplied by the probability of liquefaction or no liquefaction. The CSR is the primary factor that controls the probability of liquefaction. The higher CSR results in higher probability of liquefaction of the fill, and consequently the lower probability of no liquefaction. The CSR is related to the site amplification shown in Figure 6-64b(2). The higher crest acceleration results in higher CSR. Because the probability of failure is directly related to the calculated displacement, which in turn is related to the probability of liquefaction, then the fragility curves with the higher CSR would yield higher probability of failure for a given magnitude and reference PGA. This explains why the probability of failure for VC 2 is higher than that of VC 3, which in turn is higher than VC 4.

VC 1 is somewhat different and cannot be readily compared to VC 2, VC 3, and VC 4 because it represents a different site condition. VC 1 represents sites with no peat, that have some soft clay deposits in the foundation below the loose foundation sand.

6.2.9 Sensitivity Analysis of the Geographic Extent (Length Effect) of the Vulnerability Classes

Although there is a large number of existing subsurface exploratory borings, they did not provide full coverage of all Delta levees equally, were rather irregular, and lacked a high resolution in many locations. In many places the ends of a vulnerability class were not well defined and could vary by a few hundred feet because of the widely spaced boring locations.

One of the instructions given in comments by the Levee Seismic Vulnerability Review Panel (SRP) was to evaluate the sensitivity of the length effects of the various VCs around any given island or tract, and determine whether the uncertainty associated with the geographic extent of the VCs should be considered in the analysis.

At the request of the SRP, and before modifying the previous fragility functions, a series of test cases was performed by varying the occurrence VCs within a given island. Union Island was selected as the test case. On Union Island there are 13 reaches in the model, 11 of which are assigned to VCs 1 to 5. The other two are assigned to VCs 15 and 19.

The sensitivity analysis included the following variations:

1. Base Case: As modeled in the DRMS study
2. Test Case 1: Five reaches are in VCs 1–5, one reach in VC 19, and seven reaches in VC 15
3. Test Case 2: Five reaches are in VCs 1–5, seven reaches in VC 19, and one reach in VC 15
4. Test Case 3: One reach in VCs 1–5, six reaches in VC 15, and six reaches in VC 19

The results of the sensitivity analysis indicate that the probability of the island failure is generally controlled by the “weakest link” regardless of its length. There is relatively little change in the median PGA fragility value among the cases analyzed.

The results are shown in Figures 6-138a through 6-138c for earthquakes of magnitudes **M** 5, **M** 6, and **M** 7, respectively. In each figure the fragility curves for the individual VCs are shown along with the island fragility curves for each test case.

6.3 SUMMARY OF FINDINGS

The material properties controlling the behavior of the levees under static and seismic loading were developed from previous studies and laboratory tests. The stability models were further calibrated against past performance (static failures in the Delta) and compared to other studies. The calibrated properties are generally in good agreement with other geotechnical studies of the Delta levees.

- Past earthquakes were re-simulated in the seismic vulnerability of Delta levee model. These past earthquakes included the 1980 Livermore (M 5.8) earthquake, the 1984 Morgan Hill (M 6.19) earthquake, and the 1906 San Francisco (M 8.0) earthquake. The simulations of these earthquakes were performed to find the mean estimate of the ground motion for a stiff reference site. The results indicate that negligible to no deformations are calculated for the Livermore and the Morgan Hill earthquakes, which is consistent with the observations. For the Great 1906 San Francisco Earthquake, the calculations indicate that small to moderate damage would have occurred if the levees were at today's configuration during the 1906 event.
- The earthquake ground motions were compared to the 1992 DWR study and to the 2000 CALFED study (DWR 1992; CALFED 2000b). The results for the 200-year return period event were found to be very similar. The 200-year event is being considered as the design earthquake for the seismic upgrade of the Delta levees.
- The vulnerability classes 1 through 4 are the most vulnerable levees to seismic loading. These include islands with liquefiable levee fill, and peat/organic soil deposits and potentially liquefiable sand deposits in the foundation. Such islands include but are not limited to Sherman, Brannan-Andrus, Twitchel, Webb, Venice, Bouldin, and many others. The majority of the islands have at least one levee reach in vulnerability classes 1 to 4, as shown in Figure 6-37b.
- The sensitivity analysis showed that the weakest vulnerability class within an island levee generally controls the performance of that island, per the "weakest link" principle.
- Seismic site response in the Delta is quite complex due to the highly variable younger alluvial deposits, organic marsh deposits, and levee fill condition. Studies conducted on this topic have produced a promising generalized methodology for estimating site response in the Delta (Kishida et al. 2007). However, other studies such as the work conducted under DRMS, which looked at a limited number of sites and a limited number of earthquake time histories, showed higher site amplification when comparing the maximum crest acceleration to the reference PGA. We adopted the results from the published studies by Kishida et al. (2007) since other studies are still in progress. The use of the site response from Kishida et al. (2007) may not appear to be conservative compared to other work, but when comparing reference PGA to acceleration within the foundation loose sand or at the base of the levee, these differences become much smaller.

Assuming 2 feet of freeboard:

- The median probabilities of failure for classes 1 to 4 (liquefiable fill and peat in the foundation) range from 5 percent to 28 percent at a reference PGA of 0.10g and from 70 percent to 90 percent for a reference PGA of 0.5g.

- The median probabilities of failure for classes with no liquefiable foundation sand and no liquefiable levee fill increase with peat thickness under the levee. When peat is absent, generally the probabilities of failure are small (less than 22 percent) for the largest ground motions of 0.5g. However, the probabilities of failure at the locations of the thickest peat (more than 25 feet) range from 30 percent to 60 percent for a PGA of 0.5g.
- Where waterside slopes are steeper than 1.5H:1V, the assessed probabilities of failure tend to be larger for the same vulnerability classes. For example the steep waterside slope VC 18 shows a two-times-higher probability of failure when compared to the non-steep waterside slope VC 22.

General seismic performance observations:

- At Suisun Marsh, the earthquake-induced deformations under strong shaking are large as a result of deep, very soft clay deposits forming at the levee foundation.
- The areas most prone to liquefaction potential are in the northern region and the southeastern region of the Delta. The central and western regions of the Delta and Suisun Marsh show discontinuous areas of moderate to low liquefaction potential.
- Levees composed of liquefiable fill are likely to undergo extensive damage as a result of a moderate to large earthquake in the region.
- Levees founded on liquefiable foundations are expected to experience large deformations (in excess of 10 feet) under a moderate to large earthquake in the region.

Tables

Table 6-1 Bay Area Time-Independent Seismic Source Parameters

Fault Name	Probability of Activity ¹	Rupture Scenario ²	Segment Name	Rupture Length ³	Width ⁴	Dip ⁵	Direction of Dip ⁶	Sense of Slip ⁷	Magnitude ⁸	Slip Rate ⁹	Notes
San Andreas (Northern and Central)	1.0	Unsegmented (0.5)	1906	473	13 ± 3	90	N/A	SS	7.9	24 ± 3	Characterization based on WGCEP (2003). Unsegmented rupture scenario is a repeat of the 1906 M 7.9 San Francisco earthquake.
		Two Segments (0.2)	Offshore + North Coast	326	11 ± 2	90	N/A	SS	7.7	24 ± 3	
			Peninsula + Santa Cruz Mountains	147	13 ± 2	90	N/A	SS	7.4	17 ± 4	
		Three Segments (0.1)	Offshore + North Coast	326	11 ± 2	90	N/A	SS	7.7	24 ± 3	
			Peninsula	85	13 ± 2	90	N/A	SS	7.2	17 ± 4	
			Santa Cruz Mountains	62	15 ± 2	90	N/A	SS	7.0	17 ± 4	
		Floating Earthquake (0.2)	N/A	N/A	13 ± 3	90	N/A	SS	6.9	24 ± 3	
Calaveras	1.0	Unsegmented (0.05)	Northern + Central + Southern Calaveras	123	11 ± 2	90	N/A	SS	6.9	4 (0.2) 6 (0.4) 15 (0.3) 20 (0.1)	Characterization of WGCEP (2003) modified by recent paleoseismic data of Kelson (written communication, 2006).
		Two Segments (0.05)	Northern Calaveras	45	13 ± 2	90	N/A	SS	6.8	6 ± 2	
			South + Central Calaveras	78	11 ± 2	90	N/A	SS	6.4	15 ± 3	
		Three Segments (0.3)	Northern Calaveras	45	13 ± 2	90	N/A	SS	6.8	6 ± 2	
			Central Calaveras	59	11 ± 2	90	N/A	SS	6.2	15 ± 3	
			Southern Calaveras	19	11 ± 2	90	N/A	SS	5.8	15 ± 3	
		Segment + Floating Earthquake (0.5)	Northern Calaveras	45	13 ± 2	90	N/A	SS	6.8	6 ± 2	
			Floating Earthquake on Central + South Calaveras	N/A	11 ± 2	90	N/A	SS	6.2	15 ± 3	
		Floating Earthquake (0.1)	N/A	N/A	11 ± 2	90	N/A	SS	6.2	4 (0.2) 6 (0.4) 15 (0.3) 20 (0.1)	
		Concord – Green Valley	1.0	Unsegmented (0.35)	N/A	56	14 ± 2	90	N/A	SS	
Three Segments (0.1)	Concord			20	16 ± 2	90	N/A	SS	6.25	4 ± 2	
	Southern Green Valley			22	14 ± 2	90	N/A	SS	6.25	5 ± 3	
	Northern Green Valley			14	14 ± 2	90	N/A	SS	6.0	5 ± 3	
Two Segments (0.15)	Concord			20	16 ± 2	90	N/A	SS	6.25	4 ± 2	
	Green Valley			36	14 ± 2	90	N/A	SS	6.5	5 ± 3	
Two Segments (0.15)	Concord + Southern Green Valley			42	14 ± 2	90	N/A	SS	6.6	5 ± 3	
	Northern Green Valley			14	14 ± 2	90	N/A	SS	6.0	5 ± 3	
Floating Earthquake (0.25)	N/A	N/A	14 ± 2	90	N/A	SS	6.2	5 ± 3			
Greenville	1.0	Unsegmented (0.4)	N/A	58	15 ± 3	90	N/A	SS	6.9	2 (0.2) 4 (0.6) 6 (0.2)	Characterization based on paleoseismic data from Sawyer and Unruh (2002). and T.L. Sawyer (personal communication, 2006).
		Floating (0.6)	N/A	N/A	15 ± 3	90	N/A	SS	6.5	2 (0.2) 4 (0.6) 6 (0.2)	

Table 6-1 Bay Area Time-Independent Seismic Source Parameters

Fault Name	Probability of Activity ¹	Rupture Scenario ²	Segment Name	Rupture Length ³	Width ⁴	Dip ⁵	Direction of Dip ⁶	Sense of Slip ⁷	Magnitude ⁸	Slip Rate ⁹	Notes
Hayward – Rodgers Creek	1.0	Unsegmented (0.05)	Hayward + Rodgers Creek	151	12 ± 2	90	N/A	SS	7.3	9 ± 2	Characterization based on WGCEP (2003) model.
		Two Segment (A) (0.1)	North Hayward + Rodgers Creek	98	12 ± 2	90	N/A	SS	7.1	9 ± 2	
			Southern Hayward	53	12 ± 2	90	N/A	SS	6.7	9 ± 2	
		Two Segment (B) (0.3)	Rodgers Creek	63	12 ± 2	90	N/A	SS	7.0	9 ± 2	
			Hayward	88	12 ± 2	90	N/A	SS	6.9	9 ± 2	
		Three Segment (0.5)	Rodgers Creek	63	12 ± 2	90	N/A	SS	7.0	9 ± 2	
			North Hayward	35	12 ± 2	90	N/A	SS	6.5	9 ± 2	
Southern Hayward	53		12 ± 2	90	N/A	SS	6.7	9 ± 2			
Floating Earthquake (0.05)	N/A	N/A	12 ± 2	90	N/A	SS	6.9	9 ± 2			
Mt Diablo	1.0	Unsegmented (0.5)	N/A	31	17 ± 2	30 (0.2) 45 (0.6) 50 (0.2)	NE	R	6.7	1 (0.2) 3 (0.6) 5 (0.2)	Characterization from Unruh (2006). Fault tip inferred to approach within 5 km (0.5) to 1 km (0.5) of the surface based on restorable cross section, and on map-scale relationships between surface faults and fold axis.
		Segmented (0.5)	Mt. Diablo North	12	17 ± 2	30 (0.2) 45 (0.6) 50 (0.2)	NE	R	6.3	1 (0.2) 3 (0.6) 5 (0.2)	North: Fault tip inferred to approach within 4 km (0.5) to 2 km (0.5) of the surface based on model in restorable cross section.
			Mt. Diablo South	19	17 ± 2	30 (0.2) 45 (0.6) 50 (0.2)	NE	R	6.6	1 (0.2) 3 (0.6) 5 (0.2)	South: Fault tip inferred to approach within 5 km (0.5) to 1 km (0.5) of the surface based on model in restorable cross section, and map-scale relationships between surface faults and fold axis.
San Gregorio	1.0	Unsegmented (0.35)	Northern + Southern San Gregorio	176	13 ± 2	90	N/A	SS	7.5	1 (0.1) 3 (0.4) 7 (0.4) 10 (0.1)	Characterization based on WGCEP (2003) model.
		Segmented (0.35)	Northern San Gregorio	110	13 ± 2	90	N/A	SS	7.2	7 ± 3	
			Southern San Gregorio	66	12 ± 2	90	N/A	SS	7.0	3 ± 2	
		Floating Earthquake (0.3)	N/A	N/A	13 ± 2	90	N/A	SS	6.9	1 (0.1) 3 (0.4) 7 (0.4) 10 (0.1)	
Briones (zone)	1.0	N/A	N/A	23	15 ± 3	90	N/A	SS	6.5	0.5 (0.2) 1.0 (0.6) 2.0 (0.2)	Characterization from Unruh (2006).
Collayomi	1.0	Unsegmented (1.0)	N/A	29	10	90	N/A	SS	6.5	0.6 ± 0.3	Cao et al. (2003)
Cordelia	1.0	Unsegmented (1.0)	N/A	19	15 ± 3	90	N/A	SS	6.6	0.05 (0.4) 0.6 (0.5) 1.0 (0.1)	Characterization based on paleoseismic data from Harlan Tait & Associates (1994).
CRSB North of Delta	1.0	Multisegment (0.1)	Mysterious Ridge	35	13 ± 2	25 ± 5	W	R	6.7	1.0 (0.7) 3.5 (0.3)	Characterization revised from WGNCEP (1996) using data from O’Connell et al. (2001). Fault tip of Mysterious Ridge, Trout Creek, and Gordon Valley at depths of 7, 9, and 8 km, respectively. Segment lengths have an uncertainty of ± 5 km.
			Trout Creek + Gordon Valley	38	13 ± 2	25 ± 10	W	R	6.8	0.5 (0.3) 1.25 (0.6) 2.0 (0.1)	
		Segmented (0.9)	Mysterious Ridge	35	13 ± 2	25 ± 5	W	R	6.7	1.0 (0.7) 3.5 (0.3)	
			Trout Creek	20	13 ± 2	20 ± 5	W	R	6.5	0.5 (0.3) 1.25 (0.6) 2.0 (0.1)	

Table 6-1 Bay Area Time-Independent Seismic Source Parameters

Fault Name	Probability of Activity ¹	Rupture Scenario ²	Segment Name	Rupture Length ³	Width ⁴	Dip ⁵	Direction of Dip ⁶	Sense of Slip ⁷	Magnitude ⁸	Slip Rate ⁹	Notes
CRSB North of Delta (cont'd.)			Gordon Valley	18	13 ± 2	30 ± 5	W	R	6.4	0.5 (0.3) 1.25 (0.6) 2.0 (0.1)	
Cull Canyon-Lafayette-Reliz Valley	1.0	Unsegmented (1.0)	N/A	25	12 ± 3	90°	N/A	SS	6.6	0.5 (0.2) 1.0 (0.6) 3.0 (0.2)	Characterization from Unruh and Kelson (2002) and Unruh (2006).
Foothill Thrust System	0.6	Floating Earthquake (1.0)	N/A	N/A	15 ± 3	60	SW	R	6.25 (0.3) 6.5 (0.3) 6.75 (0.3) 7.0 (0.1)	0.2 (0.2) 0.5 (0.6) 0.8 (0.2)	Simplified characterization based on WGCEP (2003) subgroup and recent studies as summarized in Kennedy et al. (2005). Incorporates Berrocal, Shannon-Monte Vista, Stanford, and Cascade faults. Although evidence of Holocene and latest Pleistocene fold deformation along this fault zone is clear (Hitchcock and Kelson 1999; Bullard et al. 2004), the fault is assigned a Probability of Activity of 0.6 to address the uncertainty as to whether the fault is an independent seismic source capable of generating moderate to large magnitude earthquakes. The seismogenic potential of the range front thrust faults is not well known. Aseismic slip (Bürgmann et al. 1994) and coseismic slip during large magnitude events on the San Andreas fault system fault, such as occurred during the 1989 Loma Prieta earthquake (Haugerud and Ellen 1990) may account for some or all of the local San Andreas fault-normal contraction, precluding the need for independent large magnitude events on the compressive structures. (Angell et al. 1997; Hitchcock and Kelson 1999).
Hunting Creek-Berryessa	1.0	Unsegmented (1.0)	N/A	60	12	90	N/A	SS	6.9	6 ± 3	Cao et al. (2003)
Las Trampas	0.5	Unsegmented	N/A	12	14 ± 3	45° 60° 75°	SW	R	6.2	0.5 (0.2) 1.0 (0.6) 3.0 (0.2)	Characterization from Unruh and Kelson (2002) and Unruh (personal communication, 2006).
Los Medanos Fold and Thrust Belt	1.0	Unsegmented (0.2)	N/A	15	17 ± 2	30 (0.2) 45 (0.2) 60 (0.6)	NE	R	6.5	0.3 (0.3) 0.5 (0.4) 0.7 (0.3)	Characterization based on Unruh and Hector (1999) and the Thrust Fault Subgroup of the 1999 Working Group. Roe thrust: fault tip inferred to lie between 0 km and 1 km depth based on analysis of gas well data.
		Segmented (0.8)	Roe Island	5	5 ± 2	30 (0.2) 45 (0.2) 60 (0.6)	NE	R	5.8	0.3 (0.3) 0.5 (0.4) 0.7 (0.3)	Roe thrust: fault tip inferred to lie between 0 km and 1 km depth based on analysis of gas well data.
			Los Medanos	10	10 ± 2	30 (0.2) 45 (0.6) 60 (0.2)	NE	R	6.0	0.3 (0.3) 0.5 (0.4) 0.7 (0.3)	Los Medanos thrust: fault tip inferred to lie between 1 km and 2 km depth based on analysis of gas well data and construction of geologic cross sections.
Maacama-Garberville	1.0	Unsegmented (1.0)	N/A	182	12	90	N/A	SS	7.4	9.0 ± 2.0	Cao et al. (2003)
Midway/ Black Butte	1.0	Floating Earthquake (1.0)	N/A	31	15 ± 3	70 ± 10	W	RO	6.25 (0.2) 6.5 (0.4) 6.75 (0.4)	0.1 (0.3) 0.5 (0.4) 1.0 (0.3)	The Black Butte fault is a documented late Quaternary-active reverse (oblique?) fault (Sowers et al. 1992) that appears to be related to the late Cenozoic dextral Midway fault by a short left-restraining bend. Limited data are available on slip rate and rupture behavior. The slip rate estimate is based on uplift of middle to early Pleistocene pediment surface across the Black Butte fault (Sowers et al. 1992) and an inferred H:V ratio for the components of slip of ≤ 3:1.
Monterey Bay-Tularcitos	1.0	Unsegmented (1.0)	N/A	84	14	90	N/A	SS	7.1	0.5 ± 0.4	Cao et al. (2003)

Table 6-1 Bay Area Time-Independent Seismic Source Parameters

Fault Name	Probability of Activity ¹	Rupture Scenario ²	Segment Name	Rupture Length ³	Width ⁴	Dip ⁵	Direction of Dip ⁶	Sense of Slip ⁷	Magnitude ⁸	Slip Rate ⁹	Notes
Montezuma Hills (zone)	0.5	Floating Earthquake (1.0)	N/A	N/A	15 ± 5	70	W	RO	6.0 (0.3) 6.25 (0.4) 6.5 (0.3)	0.05 (0.3) 0.25 (0.4) 0.5 (0.3)	The Montezuma Hills source zone is considered as a possible independent source of seismicity based on the following: 1) the topographic and structural gradient of the hills is to the northeast, which is contrary to what would be expected if the hills were being uplifted in the hanging wall of the Midland fault; 2) the topography dies out west of the subsurface trace of the Midland fault, rather than extending up to the fault; 3) the Montezuma hills are spatially associated with the Antioch and Sherman Island faults, as well as some anomalous topography near the town of Oakley south of the Sacramento River. Alternatively, the uplift of this region is secondary tectonic deformation related to movement in the hanging wall of the Midland fault or transfer of slip from the Vernalis/West Tracy faults to the Pittsburg/Kirby Hills fault zone. Preferred orientation of modeled fault planes within zone (N20°W).
Mt Oso	0.7	Unsegmented (1.0)	N/A	25	15 ± 2	30 (0.3) 45 (0.4) 60 (0.3)	NE	R	6.9	0.5 (0.2) 1.5 (0.6) 2.5 (0.2)	Inferred thrust fault occupying the contractional stepover between the Ortigalita and Greenville faults. NE-dipping rupture geometry inferred from the SW-vergence of the Mt. Oso anticline and analogy to Mt. Diablo thrust (Unruh, Lettis and Associates, personal communication, 2006). Activity based on slip transfer from the northern Ortigalita to the southern Greenville. Fault tip at 5 km depth.
Northern Midland (zone)	1.0	Floating Earthquake (1.0)	N/A	N/A	15 ± 5	70	W	RO	6.0 (0.3) 6.25 (0.4) 6.5 (0.3)	0.1 (0.3) 0.5 (0.4) 1.0 (0.3)	Preferred orientation of modeled fault planes within zone (N30°W). North of Rio Vista, published data from gas exploration indicate that the Midland fault breaks into a zone of right-stepping en echelon fault traces. Anomalous, apparently uplifted Quaternary topography that appears to be associated with the stepover regions may be related to recent movement on a system of underlying oblique reverse faults in this zone. Tips of faults are inferred by CDOG (1982) to extend above the base of the Tertiary Markley Formation to depths of about 1.5 km, and possibly shallower. Minimum fault depth not constrained by data in CDOG (1982).
Orestimba	1.0	Unsegmented (1.0)	N/A	60	Tip 1 (0.5) 3 (0.5) Base 15 ± 3	30° (0.2) 45° (0.6) 60° (0.2)	W	R	6.7	0.2 (0.2) 0.4 (0.6) 0.6 (0.2)	Characterization based on Anderson and Piety (2001). Segment of Coast Range/Sierran block boundary(CRSB) (also referred to as the Coast Range/Central Valley fault system.). Anderson and Piety (2001) assign steeper dips (20 to 30°) to the Orestimba fault than considered in the CGS source model (Cao et al. 2003). The Thrust Subgroup of the 1999 Working Group, that provided input to WGCEP (2003), suggested a range of dip between 25° (similar to the Coalinga thrust fault) and 60° (predicted by Coulomb failure criteria).The steepness of the range along these segments from between approximately 36.5°N to 38°N suggests that the dip of the underlying structures is probably at the higher end of this range. Anderson and Piety (2001) provide estimates for the uplift rate along several segments based on the elevation of uplifted early (?) to middle Pleistocene pediment surfaces and late Pleistocene fluvial terraces (Sowars et al. 1992). These uplift rates are converted into slip rates using the range of fault dips assigned to each segment.

Table 6-1 Bay Area Time-Independent Seismic Source Parameters

Fault Name	Probability of Activity ¹	Rupture Scenario ²	Segment Name	Rupture Length ³	Width ⁴	Dip ⁵	Direction of Dip ⁶	Sense of Slip ⁷	Magnitude ⁸	Slip Rate ⁹	Notes
Ortigalita	1.0	Segmented (0.3)	Northern Ortigalita	40	15 ± 3	90	N/A	SS	6.9	0.5 (0.15) 0.35 (0.35) 2.5 (0.15)	Characterization revised from Cao et al. (2003) using recent mapping and paleoseismic data from Anderson and Piety (2001) to modify the lengths and slip rates for the north and south segments of the fault. They estimate a slip rate of 1.0-2.0 mm/yr for the northern section based on abundant geomorphic evidence for probable latest Pleistocene and Holocene displacement and, paleoseismic trench investigations that indicate that Quaternary deposits estimated to be between 10 ka and 25 ka, are right laterally offset between about 13 and 25 meters by the Cottonwood Arm segment of the Ortigalita fault. They note the southern segment appears much less active and accordingly, they assign a lower slip rate of 0.2 to 1.0 mm/yr to this segment.
			Southern Ortigalita	60	15 ± 3	90	N/A	SS	7.1	0.2 (0.2) 0.6 (0.6) 1.0 (0.2)	
Ortigalita (cont'd.)		Segmented + Floating Earthquake (0.7)	Northern Ortigalita	40	15 ± 3	90	N/A	SS	6.9	0.5 (0.15) 1.0 (0.35) 2.0 (0.35) 2.5 (0.15)	
			Floating Earthquake on Southern Ortigalita	60	15 ± 3	90	N/A	SS	6.6	0.2 (0.2) 0.6 (0.6) 1.0 (0.2)	
Pittsburgh-Kirby Hills	1.0	Unsegmented (0.4)	N/A	24	20 ± 5	90	N/A	SS	6.7	0.3 (0.4) 0.5 (0.4) 0.7 (0.2)	Characterization from the Thrust Fault Subgroup of the 1999 Working Group.
		Floating Earthquake (0.6)	N/A	N/A	20 ± 5	90	N/A	SS	6.3	0.3 (0.4) 0.5 (0.4) 0.7 (0.2)	
Potrero Hills	0.7	Unsegmented (1.0)	N/A	9	9 ± 2	40 ± 10	SW	R	5.75 (0.3) 6.0 (0.6) 6.25 (0.1)	0.1 (0.2) 0.3 (0.6) 0.6 (0.2)	Characterization based on Unruh and Hector (1999). Fault tip inferred to lie between 0 km and 1 km depth based on analysis of gas well data and construction of geologic cross sections. The fault is assigned a Probability of Activity of (0.7) based on geomorphic and physiographic evidence that slip is being transferred from the active Pittsburg Kirby Hills fault to Wragg Canyon and Hunting Creek-Berryessa fault zones to the north via the Potrero Hills fault.
Pt. Reyes	0.8	Unsegmented	N/A	47	12 ± 3	40 (0.2) 50 (0.6) 60 (0.2)	NE	R	7.0	0.05 (0.2) 0.3 (0.6) 0.5 (0.2)	Cao et al. (2003)
Quien Sabe	1.0	Unsegmented (1.0)	N/A	23	10	90	N/A	SS	6.4	0.1 (0.2) 1.0 (0.6) 2.0 (0.2)	Cao et al. (2003)
San Andreas (Southern)	1.0	Unsegmented (1.0)	N/A	312	12 ± 2	90	N/A	SS	7.8	28 (0.2) 33 (0.6) 38 (0.2)	Characterization from URS.
Sargent	0.8	Unsegmented (1.0)	Sargent	52	15 ± 3	80 ± 10	SW	RO	6.9	1.5 (0.3) 3.0 (0.4) 4.5 (0.3)	Characterization based on WGNCEP (1996). Geodetic measurements indicative of right slip across the southern Sargent fault (Prescott and Burford 1976), evidence for creep of about 3-4 mm/yr, as well as associated historical microseismicity suggest that the Sargent fault is an independent seismic source. The Sargent fault experienced triggered slip during the 1989 M _w 6.9 Loma Prieta earthquake (Aydin 1982). A Probability of Activity of less than 1.0 (0.9) considers that fault slip may occur coseismically as creep or during large magnitude events on the San Andreas fault.

Table 6-1 Bay Area Time-Independent Seismic Source Parameters

Fault Name	Probability of Activity ¹	Rupture Scenario ²	Segment Name	Rupture Length ³	Width ⁴	Dip ⁵	Direction of Dip ⁶	Sense of Slip ⁷	Magnitude ⁸	Slip Rate ⁹	Notes
Southeast Extension of Hayward (zone)	1.0	Unsegmented (1.0)	N/A	26	10	90	N/A	SS/RO	6.4	1.0 (0.2) 3.0 (0.6) 5.0 (0.2)	Characterization based on WGNCEP (1996), Graymer et al. (2006), and Fenton and Hitchcock (2001).
Southern Midland	0.8	Unsegmented (1.0)	N/A	26	15 ± 5	70	W	RO	6.6	0.1 (0.3) 0.5 (0.4) 1.0 (0.3)	Activity and rate is inferred from displacement of late Tertiary (and possibly early Pleistocene) strata in seismic reflection profiles (Weber-Band 1994) and apparent displacement of basal peat (Holocene) inferred from analysis of Atwater (1982) data (this study). Tip of fault is inferred by CDOG (1982) to extend above the base of the Tertiary Markley Formation to depths of about 1.5 km, and possibly shallower. Minimum fault depth not constrained by data in CDOG (1982).
Thornton Arch (zone)	0.2	Floating Earthquake (1.0)	N/A	N/A	15 ± 5	70	S (E-W strike)	RO	6.0 (0.3) 6.25 (0.4) 6.5 (0.3)	0.05 (0.3) 0.10 (0.4) 0.15 (0.3)	Possible localization of Quaternary uplift suggesting the presence of active blind fault(s) is inferred based on the deflection of the Mokelumne River north around an arch mapped in the subsurface from oil and gas exploration data (California Division of Oil and Gas 1982). EW strike - based on the orientation of the mapped arch.
Vernalis	0.8	Floating Earthquake (1.0)	N/A	46	15 ± 3	70 ± 10	W	RO	6.25 (0.2) 6.5 (0.4) 6.75 (0.4)	0.07 (0.3) 0.25 (0.4) 0.5 (0.3)	Quaternary activity of the Vernalis fault is inferred from the distribution of older Quaternary deposits (CDMG 1:25,000 San Jose quadrangle) that indicate differential uplift across the fault. Sterling (1992) describes stratigraphic and structural relationships imaged by seismic reflection data indicating “movement as recently as late Pliocene.” The slip rate is estimated to be comparable to the estimated rate for the West Tracy fault.
Verona/Williams Thrust System	1.0	Unsegmented (0.6)	N/A	22	21 ± 2	30 (0.1) 45 (0.6) 60 (0.3)	NE	R	6.7	0.1 (0.2) 0.7 (0.5) 1.4 (0.3)	In this model, the Verona/Williams fault is the near surface expression of a deeper east-to northeast-dipping blind thrust fault that underlies the Livermore Valley (Unruh and Sawyer 1997; Sawyer 1998). This model explains fault and fold deformation in the Livermore Valley (including the Los Positas fault, Livermore thrust and Springtown anticline) as secondary structures that either root into the deeper structure or are secondary structures in the hanging wall of the Verona/Williams thrust. These secondary structures are nonseismogenic and are not treated as independent seismic sources. The slip rate distribution is from Savy and Foxall (2002). Fault tip is estimated to be at a depth of 3 km (0.5) or 5 km (0.5).
		Segmented (0.4)	Verona	10	10	30 (0.2) 45 (0.4) 60 (0.4)	NE	R	6.2	0.1 (0.2) 0.7 (0.5) 1.4 (0.3)	Characterization of the fault is based on information summarized in Herd and Brabb (1980), Hart (1980 1981a,b), Jahns and Harding (1982), and source parameters developed by the Thrust Fault Subgroup of Working Group 1999 (WGCEP (2003) subgroup). The total length of the fault is approximately 7-9 km. Field observations and trenching described by Herd and Brabb (1980) provide evidence for late Quaternary surface-rupturing events on the fault. A 5.65-km-long-segment of the fault is included in an Alquist-Priolo zone (Hart 1980, 1981a,b). The slip rate distribution is from Savy and Foxall (2002). Fault tip is estimated to be at a depth of 3 km (0.5) or 5 km (0.5).
			Williams	13	13	30 (0.1) 45 (0.6) 60 (0.3)	NE	R	6.3	0.1 (0.2) 0.3 (0.6) 1.0 (0.2)	Characterization of the fault is based on the following. The total length of the fault is based on mapping by Dibblee (1980, 1981). Carpenter et al. (1984) show the fault as a southwest-vergent thrust fault. The DWR (1979) suggested the fault was active based on displacements observed in Plio-Pleistocene Livermore gravels in the Hetch-Hetchy tunnel and the occurrence of moderate seismicity adjacent to its trace. In the absence of any reported slip rate estimates, a rate of slip comparable to Verona fault is used. Fault tip is estimated to be at a depth of 3 km (0.5) or 5 km (0.5).

Table 6-1 Bay Area Time-Independent Seismic Source Parameters

Fault Name	Probability of Activity ¹	Rupture Scenario ²	Segment Name	Rupture Length ³	Width ⁴	Dip ⁵	Direction of Dip ⁶	Sense of Slip ⁷	Magnitude ⁸	Slip Rate ⁹	Notes
			Las Positas P(a) = 0.7	17.5	15 ± 3	90	N/A	SS	6.5	0.1 (0.2) 0.3 (0.6) 1.0 (0.2)	Characterization is based on information summarized by Carpenter et al. (1980,1984) as follows. The total length of ~17.5 km is based on geologic mapping and air photo interpretation. Movement on both southern and northern fault traces extends up into Holocene deposits: faulting may have occurred as recently as 500 to 1,000 years ago. The average slip rate for the north branch of the Las Positas fault zone is 0.4 mm/yr; the range of rates obtained from observed vertical offset and inferred horizontal-to-vertical ratios and age estimates is 0.02 to 0.9 mm/yr.
West Napa	1.0	Unsegmented (0.15)	St. Helena/Dry Creek + West Napa	52	15 ± 3	90	N/A	SS	6.9	1.0 (0.3) 2.0 (0.3) 3.0 (0.3) 4.0 (0.1)	Characterization is based on recent compilation and mapping of the West Napa fault by Hanson and Wesling (2006, 2007) and Clahan et al. (2006) conducted in support of the USGS Quaternary fault database for Northern California (Graymer et al. 2006). The slip rate for the West Napa is not well constrained, but was previously considered to be on the order of 1 mm/yr (1 ± 1 mm/yr, Cao et al. 2003). Several recent studies and observations suggest
		Floating Earthquake (0.35)	N/A	N/A	15 ± 3	90	N/A	SS	6.5	0.5 (0.1) 1.0 (0.3) 2.0 (0.3) 3.0 (0.2) 4/0 (0.1)	the slip rate is higher. These include: 1) more detailed mapping of the fault zone (Hanson and Wesling 2006, 2007) that shows that the fault is better expressed geomorphically than had been recognized previously with evidence for recent (< 600 to 700 years B. P.) displacement; 2) comparison of slip budgets between the regions north and south of Carquinez Strait suggests that a significant amount of slip is being transferred from the North Calaveras fault to the West Napa fault via the Cull Canyon/Laffette/Reliz Valley fault zone; and 3) a recent analysis of GPS data with the preferred model indicating a rate of 4 ± 3 mm/yr (d'Alessio et al. 2005).
		Segmented (0.15)	St. Helena/Dry Creek	24	15 ± 3	90	N/A	SS	6.6	1.0 (0.5) 2.0 (0.2) 3.0 (0.1)	
			West Napa	38	15 ± 3	90	N/A	SS	6.8	1.0 (0.5) 2.0 (0.2) 3.0 (0.1)	
		Segmented + Floating Earthquake (0.35)	Floating Earthquake on West Napa	N/A	15 ± 3	90	N/A	SS	6.4	1.0 (0.5) 2.0 (0.2) 3.0 (0.1)	
			St. Helena/Dry Creek	N/A	15 ± 3	90	N/A	SS	6.4	1.0 (0.5) 2.0 (0.2) 3.0 (0.1)	
		Floating Earthquake (0.9)	N/A	N/A	15 ± 5	70	W	RO	6.0 (0.3) 6.25 (0.4) 6.5 (0.3)	0.1 (0.3) 0.5 (0.4) 1.0 (0.3)	
West Tracy	0.9	Floating Earthquake (1.0)	N/A	30	15 ± 3	70 ± 10	W	RO	6.25 (0.2) 6.5 (0.4) 6.75 (0.4)	0.07 (0.3) 0.25 (0.4) 0.5 (0.3)	Quaternary activity of the West Tracy fault is inferred from the distribution of older Quaternary deposits (CDMG 1:25,000 San Jose quadrangle) that indicate differential uplift across the fault. Very limited data are available to estimate the rate of slip and recent fault behavior. The rate of reverse-oblique slip is inferred to be approximately half the rate estimated for the Midway/Black Butte fault zone. A lower bound of 0.07 mm/yr on the slip rate is estimated based on total vertical separation of about 800 feet (244 meters) of a basal Miocene unconformity across the fault as reported by Sterling (1992), and an assumed duration of deformation (active during the past ~3.5 Ma).
Wragg Canyon	0.7	Unsegmented (1.0)	N/A	17	15 ± 3	90	N/A	SS	6.5	0.1 (0.2) 0.3 (0.6) 0.5 (0.2)	Fault mapped by Sims et al. (1973) along Wragg Canyon; O'Connell et al. (2001) inferred that small earthquakes with strike-slip focal mechanisms are associated with the fault.
Zayante-Vergeles	1.0	Unsegmented (1.0)	N/A	58	12	70 ± 10	SW	R	6.9	0.1 ± 0.1	Cao et al. (2003); Dip information from USGS Quaternary Database

Table 6-2 Bay Area Time-Dependent Seismic Source Parameters

Fault Name	Probability of Activity ¹	Rupture Source ²	Segment Name	Rupture Length ³	Width ⁴	Dip ⁵	Direction of Dip ⁶	Sense of Slip ⁷	Magnitude ⁸	Year	Rate of Characteristic Event ⁹			Activity Rate		
											5%	5%	Mean	95%	Mean	95%
		SAS	Santa Cruz Mountains	62	15	90	N/A	SS	6.87 7.03 7.19	2005: 2050: 2100: 2200:	0.00E+00 0.00E+00 0.00E+00 0.00E+00	4.31E-04 2.19E-03 4.77E-03 7.37E-03	1.79E-03 8.26E-03 1.92E-02 3.02E-02	0.00E+00 0.00E+00 0.00E+00 0.00E+00	1.77E-03 9.01E-03 1.96E-02 3.03E-02	7.34E-03 3.39E-02 7.90E-02 1.24E-01
		SAP	Peninsula	85	13	90	N/A	SS	6.97 7.15 7.31	2005: 2050: 2100: 2200:	0.00E+00 0.00E+00 0.00E+00 0.00E+00	1.31E-03 2.61E-03 3.71E-03 4.44E-03	5.60E-03 9.56E-03 1.41E-02 1.64E-02	0.00E+00 0.00E+00 0.00E+00 0.00E+00	4.32E-03 8.63E-03 1.23E-02 1.47E-02	1.85E-02 3.16E-02 4.66E-02 5.43E-02
		SAN	North Coast	191	11	90	N/A	SS	7.30 7.45 7.59	2005: 2050: 2100: 2200:	0.00E+00 0.00E+00 0.00E+00 0.00E+00	2.12E-04 4.14E-04 6.07E-04 8.10E-04	9.31E-04 1.67E-03 2.25E-03 2.99E-03	0.00E+00 0.00E+00 0.00E+00 0.00E+00	1.15E-03 2.24E-03 3.29E-03 4.38E-03	5.04E-03 9.06E-03 1.22E-02 1.62E-02
		SAO	Offshore	135	11	90	N/A	SS	7.13 7.29 7.44	2005: 2050: 2100: 2200:	0.00E+00 0.00E+00 0.00E+00 0.00E+00	1.80E-04 4.04E-04 7.08E-04 1.16E-03	8.87E-04 1.70E-03 2.67E-03 4.33E-03	0.00E+00 0.00E+00 0.00E+00 0.00E+00	7.50E-04 1.69E-03 2.96E-03 4.83E-03	3.70E-03 7.10E-03 1.11E-02 1.81E-02
		SAS+SAP	Peninsula + Santa Cruz Mountains	147		90	N/A	SS	7.28 7.42 7.55	2005: 2050: 2100: 2200:	3.87E-05 1.46E-04 2.08E-04 2.46E-04	1.01E-03 2.06E-03 3.14E-03 4.09E-03	3.22E-03 5.83E-03 9.59E-03 1.28E-02	2.03E-04 7.68E-04 1.09E-03 1.29E-03	5.33E-03 1.08E-02 1.65E-02 2.15E-02	1.69E-02 3.06E-02 5.03E-02 6.69E-02
		SAN+SAO	Offshore + North Coast	326	11	90	N/A	SS	7.55 7.70 7.83	2005: 2050: 2100: 2200:	2.05E-05 2.82E-04 4.05E-04 4.87E-04	9.43E-04 1.65E-03 2.35E-03 3.17E-03	2.95E-03 4.50E-03 5.94E-03 7.99E-03	1.73E-04 2.38E-03 3.42E-03 4.11E-03	7.96E-03 1.40E-02 1.98E-02 2.67E-02	2.49E-02 3.80E-02 5.01E-02 6.74E-02
		SAS+SAP+SAN	North Coast + Peninsula + Santa Cruz Mountains	338	13 ± 3	90	N/A	SS	7.62 7.76 7.89	2005: 2050: 2100: 2200:	0.00E+00 0.00E+00 0.00E+00 0.00E+00	1.66E-05 2.71E-05 3.68E-05 4.64E-05	8.98E-05 1.10E-04 1.34E-04 1.58E-04	0.00E+00 0.00E+00 0.00E+00 0.00E+00	1.57E-04 2.56E-04 3.47E-04 4.38E-04	8.47E-04 1.04E-03 1.27E-03 1.49E-03
		SAP+SAN+SAO	Offshore + North Coast + Peninsula	411	11 ± 2	90	N/A	SS	7.67 7.82 7.97	2005: 2050: 2100: 2200:	0.00E+00 0.00E+00 0.00E+00 0.00E+00	4.43E-05 7.34E-05 1.01E-04 1.31E-04	2.82E-04 4.21E-04 4.99E-04 5.96E-04	0.00E+00 0.00E+00 0.00E+00 0.00E+00	4.84E-04 8.02E-04 1.10E-03 1.43E-03	3.08E-03 4.60E-03 5.46E-03 6.52E-03
		SAS+SAP+SAN+SAO	Offshore + North Coast + Peninsula + Santa Cruz Mountains (1906)	473	13 ± 2	90	N/A	SS	7.75 7.90 8.06	2005: 2050: 2100: 2200:	7.82E-05 5.97E-04 1.03E-03 1.31E-03	1.46E-03 2.30E-03 3.08E-03 3.94E-03	4.25E-03 6.16E-03 7.74E-03 9.02E-03	9.74E-04 7.44E-03 1.29E-02 1.64E-02	1.81E-02 2.86E-02 3.83E-02 4.90E-02	5.30E-02 7.66E-02 9.63E-02 1.12E-01
		Floating Earthquake	N/A	N/A	13 ± 3	90	N/A	SS	6.9	2005: 2050: 2100: 2200:	1.62E-04 1.99E-04 2.09E-04 2.12E-04	1.81E-03 3.72E-03 5.80E-03 8.03E-03	6.49E-03 1.32E-02 2.14E-02 3.12E-02	3.87E-04 4.76E-04 5.00E-04 5.07E-04	4.33E-03 8.89E-03 1.39E-02 1.92E-02	1.55E-02 3.16E-02 5.12E-02 7.45E-02

Table 6-2 Bay Area Time-Dependent Seismic Source Parameters

Fault Name	Probability of Activity ¹	Rupture Source ²	Segment Name	Rupture Length ³	Width ⁴	Dip ⁵	Direction of Dip ⁶	Sense of Slip ⁷	Magnitude ⁸	Year	Rate of Characteristic Event ⁹			Activity Rate		
											5%	5%	Mean	95%	Mean	95%
Hayward – Rodgers Creek	1.0	HS	Southern Hayward	53	12 ± 2	90	N/A	SS	6.42 6.67 6.90	2005:	8.66E-04	4.24E-03	1.08E-02	1.56E-03	7.63E-03	1.95E-02
										2050:	1.15E-03	5.13E-03	1.28E-02	2.06E-03	9.23E-03	2.31E-02
										2100:	1.28E-03	5.75E-03	1.48E-02	2.31E-03	1.04E-02	2.66E-02
										2200:	1.38E-03	6.41E-03	1.65E-02	2.49E-03	1.15E-02	2.96E-02
		HN	North Hayward	35	12 ± 2	90	N/A	SS	6.20 6.49 6.73	2005:	9.57E-04	5.17E-03	1.46E-02	1.44E-03	7.77E-03	2.19E-02
										2050:	1.05E-03	5.48E-03	1.54E-02	1.58E-03	8.25E-03	2.32E-02
										2100:	1.14E-03	5.75E-03	1.57E-02	1.72E-03	8.66E-03	2.37E-02
2200:	1.20E-03									6.06E-03	1.64E-02	1.81E-03	9.13E-03	2.47E-02		
HS+HN	Hayward	88	12 ± 2	90	N/A	SS	6.71 6.90 7.09	2005:	7.36E-04	3.38E-03	8.65E-03	1.72E-03	7.91E-03	2.03E-02		
								2050:	8.37E-04	3.88E-03	1.03E-02	1.96E-03	9.10E-03	2.42E-02		
								2100:	9.21E-04	4.26E-03	1.14E-02	2.16E-03	9.97E-03	2.66E-02		
								2200:	1.02E-03	4.67E-03	1.28E-02	2.38E-03	1.10E-02	3.01E-02		
RC	Rodgers Creek	63	12 ± 2	90	N/A	SS	6.83 6.98 7.14	2005:	1.56E-03	5.93E-03	1.44E-02	4.16E-03	1.58E-02	3.85E-02		
								2050:	1.72E-03	6.49E-03	1.71E-02	4.58E-03	1.73E-02	4.56E-02		
								2100:	1.89E-03	6.97E-03	1.88E-02	5.05E-03	1.86E-02	5.02E-02		
								2200:	2.23E-03	7.59E-03	2.07E-02	5.93E-03	2.02E-02	5.50E-02		
HN+RC	North Hayward + Rodgers Creek	98	12 ± 2	90	N/A	SS	6.96 7.11 7.27	2005:	4.10E-05	7.60E-04	2.34E-03	1.29E-04	2.38E-03	7.35E-03		
								2050:	4.49E-05	8.25E-04	2.53E-03	1.41E-04	2.59E-03	7.95E-03		
								2100:	4.91E-05	8.81E-04	2.78E-03	1.54E-04	2.76E-03	8.73E-03		
								2200:	4.91E-05	9.50E-04	2.97E-03	1.54E-04	2.98E-03	9.32E-03		
HS+HN+RC	Hayward + Rodgers Creek	151	12 ± 2	90	N/A	SS	7.11 7.26 7.40	2005:	6.14E-05	4.11E-04	1.11E-03	2.39E-04	1.60E-03	4.35E-03		
								2050:	6.76E-05	4.59E-04	1.32E-03	2.64E-04	1.79E-03	5.14E-03		
								2100:	7.33E-05	4.98E-04	1.43E-03	2.86E-04	1.94E-03	5.60E-03		
								2200:	7.95E-05	5.44E-04	1.63E-03	3.10E-04	2.12E-03	6.37E-03		
Floating Earthquake	N/A	N/A	12 ± 2	90	N/A	SS	6.90	2005:	1.02E-04	2.52E-04	4.80E-04	2.44E-04	6.02E-04	1.15E-03		
								2050:	1.09E-04	2.59E-04	4.85E-04	2.61E-04	6.20E-04	1.16E-03		
								2100:	1.19E-04	2.70E-04	4.94E-04	2.84E-04	6.45E-04	1.18E-03		
								2200:	1.35E-04	2.90E-04	5.46E-04	3.23E-04	6.94E-04	1.30E-03		
Calaveras	1.0	CS	Southern Calaveras	19	11 ± 2	90	N/A	SS	0.0 5.79 6.12	2005:	0.00E+00	1.17E-02	3.77E-02	0.00E+00	1.60E-02	5.15E-02
										2050:	0.00E+00	1.21E-02	4.03E-02	0.00E+00	1.66E-02	5.52E-02
										2100:	0.00E+00	1.25E-02	4.15E-02	0.00E+00	1.70E-02	5.68E-02
										2200:	0.00E+00	1.30E-02	4.24E-02	0.00E+00	1.78E-02	5.80E-02
		CC	Central Calaveras	59	11 ± 2	90	N/A	SS	5.79 6.23 6.61	2005:	8.25E-04	6.40E-03	1.80E-02	1.00E-03	7.78E-03	2.19E-02
										2050:	1.97E-03	8.52E-03	2.49E-02	2.40E-03	1.04E-02	3.03E-02
										2100:	2.10E-03	9.12E-03	2.63E-02	2.55E-03	1.11E-02	3.20E-02
										2200:	2.38E-03	9.57E-03	2.70E-02	2.90E-03	1.16E-02	3.29E-02
		CS+CC	South + Central Calaveras	78	11 ± 2	90	N/A	SS	5.93 6.36 6.68	2005:	0.00E+00	2.16E-03	7.92E-03	0.00E+00	2.85E-03	1.04E-02
										2050:	0.00E+00	2.74E-03	1.01E-02	0.00E+00	3.61E-03	1.33E-02
2100:	0.00E+00									2.94E-03	1.09E-02	0.00E+00	3.88E-03	1.44E-02		
2200:	0.00E+00									3.09E-03	1.14E-02	0.00E+00	4.08E-03	1.50E-02		
CN	Northern Calaveras	45	13 ± 2	90	N/A	SS	6.62 6.78 6.93	2005:	1.10E-03	5.14E-03	1.45E-02	2.28E-03	1.06E-02	3.00E-02		
								2050:	1.23E-03	5.50E-03	1.57E-02	2.54E-03	1.14E-02	3.26E-02		
								2100:	1.35E-03	5.82E-03	1.68E-02	2.79E-03	1.20E-02	3.48E-02		
								2200:	1.56E-03	6.26E-03	1.81E-02	3.23E-03	1.30E-02	3.74E-02		
CC+CN	Central + Northern Calaveras	104	13 ± 2	90	N/A	SS	6.72 6.91 7.08	2005:	0.00E+00	1.37E-04	1.00E-03	0.00E+00	3.24E-04	2.37E-03		
								2050:	0.00E+00	1.65E-04	1.14E-03	0.00E+00	3.91E-04	2.70E-03		
								2100:	0.00E+00	1.81E-04	1.28E-03	0.00E+00	4.28E-04	3.02E-03		
								2200:	0.00E+00	1.97E-04	1.36E-03	0.00E+00	4.67E-04	3.21E-03		

Table 6-2 Bay Area Time-Dependent Seismic Source Parameters

Fault Name	Probability of Activity ¹	Rupture Source ²	Segment Name	Rupture Length ³	Width ⁴	Dip ⁵	Direction of Dip ⁶	Sense of Slip ⁷	Magnitude ⁸	Year	Rate of Characteristic Event ⁹			Activity Rate		
											5%	5%	Mean	95%	Mean	95%
Calaveras (cont'd.)		CS+CC+CN	Northern + Central + Southern Calaveras	123	11 ± 2	90	N/A	SS	6.76 6.94 7.11	2005:	0.00E+00	8.05E-04	2.81E-03	0.00E+00	1.99E-03	6.96E-03
										2050:	0.00E+00	9.38E-04	3.40E-03	0.00E+00	2.32E-03	8.42E-03
										2100:	0.00E+00	1.00E-03	3.58E-03	0.00E+00	2.48E-03	8.85E-03
										2200:	0.00E+00	1.07E-03	3.71E-03	0.00E+00	2.65E-03	9.17E-03
		Floating Earthquake	N/A	N/A	11 ± 2	90	N/A	SS	6.2	2005:	6.17E-04	2.63E-03	6.66E-03	7.83E-04	3.34E-03	8.45E-03
										2050:	6.92E-04	2.73E-03	6.67E-03	8.78E-04	3.46E-03	8.47E-03
										2100:	7.43E-04	2.85E-03	6.88E-03	9.43E-04	3.62E-03	8.73E-03
										2200:	8.39E-04	3.11E-03	7.86E-03	1.06E-03	3.95E-03	9.98E-03
		Floating Earthquake on CS+CC	N/A	N/A	11 ± 2	90	N/A	SS	6.2	2005:	2.10E-03	1.04E-02	2.50E-02	2.66E-03	1.32E-02	3.17E-02
										2050:	2.22E-03	1.07E-02	2.51E-02	2.81E-03	1.36E-02	3.18E-02
										2100:	2.37E-03	1.13E-02	2.64E-02	3.00E-03	1.43E-02	3.35E-02
										2200:	2.55E-03	1.23E-02	2.88E-02	3.24E-03	1.56E-02	3.66E-02
Concord – Green Valley	1.0	CON	Concord	20	16 ± 2	90	N/A	SS	5.79 6.25 6.65	2005:	1.56E-04	1.88E-03	5.70E-03	1.91E-04	2.30E-03	6.97E-03
										2050:	2.02E-04	2.06E-03	6.03E-03	2.47E-04	2.51E-03	7.36E-03
										2100:	2.21E-04	2.21E-03	6.63E-03	2.70E-04	2.70E-03	8.10E-03
										2200:	2.66E-04	2.41E-03	7.06E-03	3.25E-04	2.94E-03	8.63E-03
		GVS	Southern Green Valley	22	14 ± 2	90	N/A	SS	5.81 6.24 6.60	2005:	6.22E-05	8.78E-04	2.85E-03	7.57E-05	1.07E-03	3.47E-03
										2050:	8.50E-05	9.57E-04	3.08E-03	1.03E-04	1.16E-03	3.75E-03
										2100:	9.77E-05	1.02E-03	3.20E-03	1.19E-04	1.25E-03	3.90E-03
										2200:	1.16E-04	1.11E-03	3.49E-03	1.41E-04	1.35E-03	4.25E-03
		CON+GVS	Concord + Southern Green Valley	42	14 ± 2	90	N/A	SS	6.20 6.58 6.87	2005:	2.78E-05	5.99E-04	2.00E-03	4.42E-05	9.54E-04	3.19E-03
										2050:	3.28E-05	6.52E-04	2.13E-03	5.23E-05	1.04E-03	3.40E-03
										2100:	4.30E-05	6.99E-04	2.29E-03	6.85E-05	1.11E-03	3.64E-03
										2200:	5.32E-05	7.60E-04	2.52E-03	8.47E-05	1.21E-03	4.01E-03
		GVN	Northern Green Valley	14	14 ± 2	90	N/A	SS	5.56 6.02 6.43	2005:	1.98E-04	2.36E-03	7.05E-03	2.17E-04	2.59E-03	7.74E-03
										2050:	2.33E-04	2.55E-03	7.56E-03	2.55E-04	2.80E-03	8.31E-03
										2100:	2.73E-04	2.71E-03	7.66E-03	3.00E-04	2.98E-03	8.41E-03
										2200:	3.14E-04	2.92E-03	8.23E-03	3.45E-04	3.21E-03	9.04E-03
		GVS+GVN	Green Valley	36	14 ± 2	90	N/A	SS	6.11 6.48 6.77	2005:	8.35E-05	1.20E-03	3.78E-03	1.22E-04	1.76E-03	5.53E-03
										2050:	1.03E-04	1.31E-03	4.23E-03	1.51E-04	1.92E-03	6.19E-03
										2100:	1.18E-04	1.40E-03	4.41E-03	1.72E-04	2.05E-03	6.44E-03
										2200:	1.39E-04	1.52E-03	4.81E-03	2.04E-04	2.22E-03	7.03E-03
		CON+GVS+GVN	Concord+Green Valley	56	14 ± 2	90	N/A	SS	6.42 6.71 6.95	2005:	2.53E-04	2.32E-03	7.37E-03	4.67E-04	4.27E-03	1.36E-02
										2050:	3.06E-04	2.57E-03	7.91E-03	5.64E-04	4.73E-03	1.46E-02
										2100:	3.70E-04	2.77E-03	8.24E-03	6.82E-04	5.11E-03	1.52E-02
										2200:	4.63E-04	3.05E-03	8.76E-03	8.54E-04	5.62E-03	1.62E-02
		Floating Earthquake	N/A	N/A	14 ± 2	90	N/A	SS	6.2	2005:	1.06E-04	2.40E-03	1.07E-02	1.36E-04	3.07E-03	1.37E-02
										2050:	1.18E-04	2.47E-03	1.08E-02	1.51E-04	3.16E-03	1.39E-02
										2100:	1.23E-04	2.56E-03	1.10E-02	1.57E-04	3.28E-03	1.41E-02
										2200:	1.32E-04	2.74E-03	1.13E-02	1.69E-04	3.51E-03	1.44E-02
San Gregorio	1.0	SGS	Southern San Gregorio	66	12 ± 2	90	N/A	SS	6.76 6.96 7.12	2005:	0.00E+00	8.17E-04	3.09E-03	0.00E+00	2.04E-03	7.71E-03
										2050:	0.00E+00	8.96E-04	3.33E-03	0.00E+00	2.24E-03	8.32E-03
										2100:	0.00E+00	9.75E-04	3.58E-03	0.00E+00	2.43E-03	8.94E-03
										2200:	0.00E+00	1.11E-03	3.83E-03	0.00E+00	2.77E-03	9.55E-03
		SGN	Northern San Gregorio	110	13 ± 2	90	N/A	SS	7.07 7.23 7.40	2005:	0.00E+00	1.41E-03	5.03E-03	0.00E+00	5.42E-03	1.93E-02
										2050:	0.00E+00	1.58E-03	5.45E-03	0.00E+00	6.06E-03	2.09E-02
										2100:	0.00E+00	1.73E-03	5.81E-03	0.00E+00	6.66E-03	2.23E-02
										2200:	0.00E+00	1.97E-03	6.23E-03	0.00E+00	7.58E-03	2.39E-02

Table 6-2 Bay Area Time-Dependent Seismic Source Parameters

Fault Name	Probability of Activity ¹	Rupture Source ²	Segment Name	Rupture Length ³	Width ⁴	Dip ⁵	Direction of Dip ⁶	Sense of Slip ⁷	Magnitude ⁸	Year	Rate of Characteristic Event ⁹			Activity Rate		
											5%	5%	Mean	95%	Mean	95%
San Gregorio (cont'd.)		SGS+SGN	Northern + Southern San Gregorio						7.30 7.44 7.58	2005: 2050: 2100: 2200:	0.00E+00 0.00E+00 0.00E+00 0.00E+00	9.22E-04 1.03E-03 1.15E-03 1.33E-03	2.93E-03 3.33E-03 3.52E-03 4.01E-03	0.00E+00 0.00E+00 0.00E+00 0.00E+00	4.94E-03 5.51E-03 6.16E-03 7.13E-03	1.57E-02 1.78E-02 1.89E-02 2.15E-02
		Floating Earthquake	N/A	N/A	13 ± 2	90	N/A	SS	6.9	2005: 2050: 2100: 2200:	3.05E-04 3.21E-04 3.34E-04 3.50E-04	7.23E-04 7.45E-04 7.76E-04 8.37E-04	1.23E-03 1.24E-03 1.25E-03 1.45E-03	7.35E-04 7.73E-04 8.04E-04 8.44E-04	1.74E-03 1.79E-03 1.87E-03 2.02E-03	2.96E-03 2.99E-03 3.02E-03 3.49E-03
Greenville	1.0	GS	Southern Greenville	24	15 ± 3	90	N/A	SS	6.40 6.60 6.78	2005: 2050: 2100: 2200:	3.26E-05 9.32E-05 1.91E-04 3.30E-04	1.08E-03 1.19E-03 1.31E-03 1.51E-03	2.80E-03 2.90E-03 3.08E-03 3.44E-03	5.46E-05 1.56E-04 3.20E-04 5.52E-04	1.81E-03 1.99E-03 2.19E-03 2.53E-03	4.69E-03 4.85E-03 5.16E-03 5.76E-03
		GN	Northern Greenville	27	15 ± 3	90	N/A	SS	6.45 6.66 6.84	2005: 2050: 2100: 2200:	1.16E-05 6.08E-05 1.39E-04 2.32E-04	1.03E-03 1.12E-03 1.23E-03 1.43E-03	2.82E-03 2.80E-03 3.14E-03 3.67E-03	2.06E-05 1.08E-04 2.46E-04 4.11E-04	1.82E-03 1.98E-03 2.18E-03 2.53E-03	4.99E-03 4.96E-03 5.57E-03 6.50E-03
		GS+GN	Southern+Northern Greenville	51	15 ± 3	90	N/A	SS	6.78 6.94 7.11	2005: 2050: 2100: 2200:	9.29E-05 1.16E-04 1.38E-04 1.75E-04	5.32E-04 5.79E-04 6.38E-04 7.40E-04	1.29E-03 1.36E-03 1.48E-03 1.71E-03	2.34E-04 2.93E-04 3.49E-04 4.42E-04	1.34E-03 1.46E-03 1.61E-03 1.87E-03	3.26E-03 3.43E-03 3.73E-03 4.31E-03
		Floating Earthquake	N/A	N/A	15 ± 3	90	N/A	SS	6.2	2005: 2050: 2100: 2200:	5.82E-05 6.17E-05 6.37E-05 6.55E-05	1.49E-04 1.54E-04 1.60E-04 1.72E-04	2.73E-04 2.74E-04 2.85E-04 3.20E-04	7.44E-05 7.89E-05 8.15E-05 8.38E-05	1.91E-04 1.96E-04 2.04E-04 2.20E-04	3.49E-04 3.50E-04 3.64E-04 4.10E-04
Mt Diablo	1.0	MTD	Mt. Diablo	31	17 ± 2	30 (0.2) 45 (0.6) 50 (0.2)	NE	R	6.48 6.65 6.83	2005: 2050: 2100: 2200:	3.97E-04 5.52E-04 6.16E-04 6.64E-04	2.71E-03 2.97E-03 3.23E-03 3.66E-03	6.72E-03 7.45E-03 7.89E-03 8.99E-03	7.07E-04 9.84E-04 1.10E-03 1.18E-03	4.84E-03 5.29E-03 5.75E-03 6.53E-03	1.20E-02 1.33E-02 1.41E-02 1.60E-02

Table 6-3 Mean Expert Weights for Probability Models Applied to the SFBR Fault Systems (Table 5.5, WGCEP 2003)

Fault System	Poisson	Empirical	BPT	BPT-step	Time-Predictable
San Andreas	0.100	0.181	0.154	0.231	0.335
Hayward/Rodger's Creek	0.123	0.285	0.131	0.462	—
Calaveras	0.227	0.315	0.142	0.315	—
Concord/Green Valley	0.246	0.277	0.123	0.354	—
San Gregorio	0.196	0.292	0.115	0.396	—
Greenville	0.231	0.288	0.131	0.350	—
Mt. Diablo Thrust	0.308	0.396	0.092	0.204	—

Table 6-4 Empirical Model Factors

Model	Extrapolated Annual Number of Events for Year:			
	2005	2055	2105	2205
A	0.014	0.014	0.014	0.014
B	0.016	0.016	0.016	0.016
C	0.011	0.011	0.011	0.011
D	0.020	0.020	0.020	0.020
E	0.016	0.018	0.020	0.025
F	0.018	0.026	0.034	0.050
Empirical Factors Based on Long Term Rate of 0.031				
Minimum	0.355	0.355	0.355	0.355
Average	0.512	0.567	0.622	0.733
Maximum	0.645	0.850	1.107	1.623

Table 6-5 Ground Motions with a 2% Exceedance Probability in 50 Years (2,500-Year Return Period)

Peak Ground Acceleration (g)

	TI	2005	2050	2100	2200
Sherman Island	0.64	0.64	0.64	0.64	0.65
Clifton Court	0.66	0.66	0.66	0.66	0.67
Montezuma Slough	0.75	0.74	0.74	0.74	0.75
Delta Cross Channel	0.38	0.37	0.37	0.37	0.37
Stockton	0.33	0.32	0.32	0.32	0.33
Sacramento	0.30	0.30	0.30	0.30	0.30

1.0 Sec Spectral Acceleration (g)

	TI	2005	2050	2100	2200
Sherman Island	0.77	0.77	0.78	0.79	0.80
Clifton Court	0.82	0.82	0.83	0.84	0.85
Montezuma Slough	0.91	0.90	0.90	0.91	0.93
Delta Cross Channel	0.48	0.48	0.49	0.49	0.50
Stockton	0.45	0.44	0.45	0.46	0.47
Sacramento	0.43	0.42	0.43	0.43	44

TI = Time-Independent

Table 6-6 Vulnerability Class Details for Seismic Fragility

Geographic Area	Vulnerability Class Index	Waterside Levee Slope	(N₁)_{60-cs} Fill	(N₁)_{60-cs} Foundation	Peat Thickness (ft)	Random Input Variables
Delta	1	Any	0-20	Any	0	(N ₁) _{60-cs} Fill, (N ₁) _{60-cs} Foundation, S _u
	2	Any	0-20	Any	0.1-10	(N ₁) _{60-cs} Fill, (N ₁) _{60-cs} Foundation, S _u , Peat Thickness
	3	Any	0-20	Any	10.1-20	(N ₁) _{60-cs} Fill, (N ₁) _{60-cs} Foundation, S _u , Peat Thickness
	4	Any	0-20	Any	>20	(N ₁) _{60-cs} Fill, (N ₁) _{60-cs} Foundation, S _u , Peat Thickness
	5	Any	>20	0-20	0	(N ₁) _{60-cs} Foundation
	6	Any	>20	0-5	0.1-10	(N ₁) _{60-cs} Foundation, Peat Thickness
	7	Any	>20	0-5	10.1-20	(N ₁) _{60-cs} Foundation, Peat Thickness
	8	Any	>20	0-5	>20	(N ₁) _{60-cs} Foundation, Peat Thickness
	9	Any	>20	5.1-10	0.1-10	(N ₁) _{60-cs} Foundation, Peat Thickness
	10	Any	>20	5.1-10	10.1-20	(N ₁) _{60-cs} Foundation, Peat Thickness
	11	Any	>20	5.1-10	>20	(N ₁) _{60-cs} Foundation, Peat Thickness
	12	Any	>20	10.1-20	0.1-10	(N ₁) _{60-cs} Foundation, Peat Thickness
	13	Any	>20	10.1-20	10.1-20	(N ₁) _{60-cs} Foundation, Peat Thickness
	14	Any	>20	10.1-20	>20	(N ₁) _{60-cs} Foundation, Peat Thickness
	15	Steep	>20	>20	0	
	16	Steep	>20	>20	0.1-10	c, φ, Peat Thickness
	17	Steep	>20	>20	10.1-20	c, φ, Peat Thickness
	18	Steep	>20	>20	>20	c, φ, Peat Thickness
	19	Non-Steep	>20	>20	0	
	20	Non-Steep	>20	>20	0.1-10	c, φ, Peat Thickness
	21	Non-Steep	>20	>20	10.1-20	c, φ, Peat Thickness
	22	Non-Steep	>20	>20	>20	c, φ, Peat Thickness

Table 6-6 Vulnerability Class Details for Seismic Fragility

Geographic Area	Vulnerability Class Index	Waterside Levee Slope	(N₁)_{60-cs} Fill	(N₁)_{60-cs} Foundation	Peat Thickness (ft)	Random Input Variables
Suisun Marsh	23	Any	>20	>20	Thin layer	c
	24	Any	<=20	<=20	Thin Layer	(N ₁) _{60-cs} Fill, (N ₁) _{60-cs} Foundation, S _u

Note: (N₁)_{60-cs} – corrected clean sand equivalent SPT blow count, c – cohesion, ϕ , - friction angle, S_u = Residual undrained shear strength

Table 6-7 Dynamic Soil Parameters Selected for Analysis

Description		Moist Unit Weight (pcf)	K_{2max}	Shear Wave Velocity (ft/sec)	Modulus and Damping Curves
Embankment Materials					
Sandy Fill		115	35	-	Sand ¹
Peat	- free-field	70	-	100	Peat ²
	- under embankment			300	Peat ³
Sand		125	65	-	Sand ¹
Bay Deposits		110		400	Clay ⁴
Clay		125	-	900	Clay ⁴

Note:

1. Relationships of Seed and Idriss (1970)
2. Relationships of Wehling et al (2001) for 12 kPa
3. Relationships of Wehling et al (2001) for 40 kPa
4. Relationships of Vucetic and Dobry (1991) for PI = 30

Table 6-8: Calculated FLAC Deformations – Idealized Sections Liquefiable

Earthquake Magnitude	PGA	Peat Thickness, ft	(N1-60), Foundation	Deformation, ft
5.5	0.05	5	11	0.1
			16	0.1
			6	0.1
5.5	0.1	5	11	0.2
			16	0.1
			6	0.5
5.5	0.2	5	11	0.6
			16	0.4
			6	1.5
5.5	0.3	5	11	2
			16	0.8
			6	4
5.5	0.4	5	11	3
			16	1
			6	6
5.5	0.5	5	11	3.5
			16	1.5
			6	8
6.5	0.05	5	11	0.1
			16	0.1
			6	0.1
6.5	0.1	5	11	0.2
			16	0.1
			6	1
6.5	0.2	5	11	1
			16	0.7
			6	3
6.5	0.3	5	11	2
			16	1.5
			6	6
6.5	0.4	5	11	3
			16	2
			6	8
6.5	0.5	5	11	4
			16	2.5
			6	10
7.5	0.05	5	11	0.4
			16	0.2
			6	2
7.5	0.1	5	11	3
			16	1.5
			6	7.5
7.5	0.2	5	11	6
			16	4
			6	10
7.5	0.3	5	11	10
			16	8
			6	>10

**Table 6-8: Calculated FLAC Deformations – Idealized Sections Liquefiable
cont.**

Earthquake Magnitude	PGA	Peat Thickness, ft	(N1-60), Foundation	Deformation, ft
7.5	0.4	5	11	>10
			16	>10
			6	>10
7.5	0.5	5	11	>10
			16	>10
			6	>10
5.5	0.05	15	11	0.1
			16	0.1
			6	0.1
5.5	0.1	15	11	0.1
			16	0.1
			6	0.2
5.5	0.2	15	11	0.6
			16	0.2
			6	1.5
5.5	0.3	15	11	1.3
			16	0.5
			6	3
5.5	0.4	15	11	1.8
			16	0.6
			6	4
5.5	0.5	15	11	2
			16	0.8
			6	5
6.5	0.05	15	11	0.1
			16	0.1
			6	0.1
6.5	0.1	15	11	0.1
			16	0.1
			6	0.4
6.5	0.2	15	11	0.7
			16	0.2
			6	1.8
6.5	0.3	15	11	1.5
			16	0.6
			6	3.5
6.5	0.4	15	11	2
			16	0.8
			6	5
6.5	0.5	15	11	2.5
			16	1.3
			6	6
7.5	0.05	15	11	0.4
			16	0.2
			6	1.8
7.5	0.1	15	11	2
			16	0.6
			6	5

Table 6-8: Calculated FLAC Deformations – Idealized Sections Liquefiable cont.				
Earthquake Magnitude	PGA	Peat Thickness, ft	(N1-60), Foundation	Deformation, ft
7.5	0.2	15	11	4
			16	2
			6	8
7.5	0.3	15	11	5
			16	4
			6	10
7.5	0.4	15	11	6
			16	5
			6	>10
7.5	0.5	15	11	8
			16	6
			6	>10
5.5	0.05	>25	11	0.1
			16	0.1
			6	0.1
5.5	0.1	>25	11	0.1
			16	0.1
			6	0.3
5.5	0.2	>25	11	0.7
			16	0.3
			6	1.5
5.5	0.3	>25	11	1.3
			16	0.6
			6	2.5
5.5	0.4	>25	11	1.5
			16	0.8
			6	3
5.5	0.5	>25	11	1.8
			16	1
			6	3.5
6.5	0.05	>25	11	0.1
			16	0.1
			6	0.1
6.5	0.1	>25	11	0.1
			16	0.1
			6	0.4
6.5	0.2	>25	11	0.8
			16	0.3
			6	1.8
6.5	0.3	>25	11	1.3
			16	0.6
			6	3
6.5	0.4	>25	11	1.8
			16	1
			6	3.5
6.5	0.5	>25	11	2.3
			16	1.5
			6	4.5

Table 6-8: Calculated FLAC Deformations – Idealized Sections Liquefiable cont.				
Earthquake Magnitude	PGA	Peat Thickness, ft	(N1-60), Foundation	Deformation, ft
7.5	0.05	>25	11	0.4
			16	0.2
			6	1.5
7.5	0.1	>25	11	1.8
			16	0.6
			6	3.5
7.5	0.2	>25	11	3.5
			16	2.5
			6	7
7.5	0.3	>25	11	4
			16	3
			6	10
7.5	0.4	>25	11	7.5
			16	6
			6	>10
7.5	0.5	>25	11	10
			16	8
			6	>10

Table 6-9 Stability Analysis Results – Non-Liquefiable Sand Layer

Section	Factor of Safety		Yield Acceleration, K_v	
	Landside	Waterside	Landside	Waterside
No Peat	1.79	1.85	0.24	0.19
5 feet Peat	1.57	2.02	0.16	0.16
15 feet Peat	1.39	1.79	0.11	0.11
>25 feet Peat	1.38	1.79	0.09	0.11
Suisun Marsh	1.77	1.15	0.09	0.03

Table 6-10a: Calculated Newmark Deformations – Idealized Sections Non Liquefiable

Waterside Levee Slope	Earthquake Magnitude	PGA	Peat Thickness, ft	C	phi	Deformation, ft
Non-Steep	5.5	0.05	0	120	28	<0.1
				120	29.96	<0.1
				120	26.17	<0.1
				168	28	<0.1
				85.71	28	<0.1
Non-Steep	5.5	0.1	0	120	28	<0.1
				120	29.96	<0.1
				120	26.17	<0.1
				168	28	<0.1
				85.71	28	<0.1
Non-Steep	5.5	0.2	0	120	28	<0.1
				120	29.96	<0.1
				120	26.17	<0.1
				168	28	<0.1
				85.71	28	<0.1
Non-Steep	5.5	0.3	0	120	28	<0.1
				120	29.96	<0.1
				120	26.17	<0.1
				168	28	<0.1
				85.71	28	<0.1
Non-Steep	5.5	0.4	0	120	28	<0.1
				120	29.96	<0.1
				120	26.17	<0.1
				168	28	<0.1
				85.71	28	<0.1
Non-Steep	5.5	0.5	0	120	28	<0.1
				120	29.96	<0.1
				120	26.17	<0.1
				168	28	<0.1
				85.71	28	<0.1
Non-Steep	6.5	0.05	0	120	28	<0.1
				120	29.96	<0.1
				120	26.17	<0.1
				168	28	<0.1
				85.71	28	<0.1
Non-Steep	6.5	0.1	0	120	28	<0.1
				120	29.96	<0.1
				120	26.17	<0.1
				168	28	<0.1
				85.71	28	<0.1

Table 6-10a: Calculated Newmark Deformations – Idealized Sections Non Liquefiable
Cont.

Waterside Levee Slope	Earthquake Magnitude	PGA	Peat Thickness, ft	C	phi	Deformation, ft
Non-Steep	6.5	0.2	0	120	28	<0.1
				120	29.96	<0.1
				120	26.17	<0.1
				168	28	<0.1
				85.71	28	<0.1
Non-Steep	6.5	0.3	0	120	28	<0.1
				120	29.96	<0.1
				120	26.17	<0.1
				168	28	<0.1
				85.71	28	<0.1
Non-Steep	6.5	0.4	0	120	28	<0.1
				120	29.96	<0.1
				120	26.17	<0.1
				168	28	<0.1
				85.71	28	<0.1
Non-Steep	6.5	0.5	0	120	28	<0.1
				120	29.96	<0.1
				120	26.17	<0.1
				168	28	<0.1
				85.71	28	<0.1
Non-Steep	7.5	0.05	0	120	28	<0.1
				120	29.96	<0.1
				120	26.17	<0.1
				168	28	<0.1
				85.71	28	<0.1
Non-Steep	7.5	0.1	0	120	28	<0.1
				120	29.96	<0.1
				120	26.17	<0.1
				168	28	<0.1
				85.71	28	<0.1
Non-Steep	7.5	0.2	0	120	28	<0.1
				120	29.96	<0.1
				120	26.17	<0.1
				168	28	<0.1
				85.71	28	<0.1
Non-Steep	7.5	0.3	0	120	28	<0.1
				120	29.96	<0.1
				120	26.17	<0.1
				168	28	<0.1
				85.71	28	<0.1

Table 6-10a: Calculated Newmark Deformations – Idealized Sections Non Liquefiable
Cont.

Waterside Levee Slope	Earthquake Magnitude	PGA	Peat Thickness, ft	C	phi	Deformation, ft
Non-Steep	7.5	0.4	0	120	28	<0.1
				120	29.96	<0.1
				120	26.17	<0.1
				168	28	<0.1
				85.71	28	<0.1
Non-Steep	7.5	0.5	0	120	28	0.11
				120	29.96	0.11
				120	26.17	0.11
				168	28	0.11
				85.71	28	0.11
Steep	5.5	0.05	0	120	28	<0.1
				120	29.96	<0.1
				120	26.17	<0.1
				168	28	<0.1
				85.71	28	<0.1
Steep	5.5	0.1	0	120	28	<0.1
				120	29.96	<0.1
				120	26.17	<0.1
				168	28	<0.1
				85.71	28	<0.1
Steep	5.5	0.2	0	120	28	<0.1
				120	29.96	<0.1
				120	26.17	<0.1
				168	28	<0.1
				85.71	28	<0.1
Steep	5.5	0.3	0	120	28	<0.1
				120	29.96	<0.1
				120	26.17	<0.1
				168	28	<0.1
				85.71	28	<0.1
Steep	5.5	0.4	0	120	28	<0.1
				120	29.96	<0.1
				120	26.17	<0.1
				168	28	<0.1
				85.71	28	<0.1
Steep	5.5	0.5	0	120	28	0.123
				120	29.96	0.123
				120	26.17	0.123
				168	28	0.123
				85.71	28	0.123

Table 6-10a: Calculated Newmark Deformations – Idealized Sections Non Liquefiable
Cont.

Waterside Levee Slope	Earthquake Magnitude	PGA	Peat Thickness, ft	C	phi	Deformation, ft
Steep	6.5	0.05	0	120	28	<0.1
				120	29.96	<0.1
				120	26.17	<0.1
				168	28	<0.1
				85.71	28	<0.1
Steep	6.5	0.1	0	120	28	<0.1
				120	29.96	<0.1
				120	26.17	<0.1
				168	28	<0.1
				85.71	28	<0.1
Steep	6.5	0.2	0	120	28	<0.1
				120	29.96	<0.1
				120	26.17	<0.1
				168	28	<0.1
				85.71	28	<0.1
Steep	6.5	0.3	0	120	28	0.141
				120	29.96	0.141
				120	26.17	0.141
				168	28	0.141
				85.71	28	0.141
Steep	6.5	0.4	0	120	28	0.32
				120	29.96	0.32
				120	26.17	0.32
				168	28	0.32
				85.71	28	0.32
Steep	6.5	0.5	0	120	28	0.678
				120	29.96	0.678
				120	26.17	0.678
				168	28	0.678
				85.71	28	0.678
Steep	7.5	0.05	0	120	28	<0.1
				120	29.96	<0.1
				120	26.17	<0.1
				168	28	<0.1
				85.71	28	<0.1
Steep	7.5	0.1	0	120	28	<0.1
				120	29.96	<0.1
				120	26.17	<0.1
				168	28	<0.1
				85.71	28	<0.1

Table 6-10a: Calculated Newmark Deformations – Idealized Sections Non Liquefiable
Cont.

Waterside Levee Slope	Earthquake Magnitude	PGA	Peat Thickness, ft	C	phi	Deformation, ft
Steep	7.5	0.2	0	120	28	<0.1
				120	29.96	<0.1
				120	26.17	<0.1
				168	28	<0.1
				85.71	28	<0.1
Steep	7.5	0.3	0	120	28	0.543
				120	29.96	0.543
				120	26.17	0.543
				168	28	0.543
				85.71	28	0.543
Steep	7.5	0.4	0	120	28	1.324
				120	29.96	1.324
				120	26.17	1.324
				168	28	1.324
				85.71	28	1.324
Steep	7.5	0.5	0	120	28	2.673
				120	29.96	2.673
				120	26.17	2.673
				168	28	2.673
				85.71	28	2.673
Non-Steep	5.5	0.05	5	120	28	<0.1
				120	29.96	<0.1
				120	26.17	<0.1
				168	28	<0.1
				85.71	28	<0.1
Non-Steep	5.5	0.1	5	120	28	<0.1
				120	29.96	<0.1
				120	26.17	<0.1
				168	28	<0.1
				85.71	28	<0.1
Non-Steep	5.5	0.2	5	120	28	<0.1
				120	29.96	<0.1
				120	26.17	<0.1
				168	28	<0.1
				85.71	28	<0.1
Non-Steep	5.5	0.3	5	120	28	<0.1
				120	29.96	<0.1
				120	26.17	<0.1
				168	28	<0.1
				85.71	28	<0.1

Table 6-10a: Calculated Newmark Deformations – Idealized Sections Non Liquefiable
Cont.

Waterside Levee Slope	Earthquake Magnitude	PGA	Peat Thickness, ft	C	phi	Deformation, ft
Non-Steep	5.5	0.4	5	120	28	<0.1
				120	29.96	<0.1
				120	26.17	<0.1
				168	28	<0.1
				85.71	28	<0.1
Non-Steep	5.5	0.5	5	120	28	<0.1
				120	29.96	<0.1
				120	26.17	<0.1
				168	28	<0.1
				85.71	28	<0.1
Non-Steep	6.5	0.05	5	120	28	<0.1
				120	29.96	<0.1
				120	26.17	<0.1
				168	28	<0.1
				85.71	28	<0.1
Non-Steep	6.5	0.1	5	120	28	<0.1
				120	29.96	<0.1
				120	26.17	<0.1
				168	28	<0.1
				85.71	28	<0.1
Non-Steep	6.5	0.2	5	120	28	<0.1
				120	29.96	<0.1
				120	26.17	<0.1
				168	28	<0.1
				85.71	28	<0.1
Non-Steep	6.5	0.3	5	120	28	<0.1
				120	29.96	<0.1
				120	26.17	<0.1
				168	28	<0.1
				85.71	28	<0.1
Non-Steep	6.5	0.4	5	120	28	<0.1
				120	29.96	<0.1
				120	26.17	0.11
				168	28	<0.1
				85.71	28	0.12
Non-Steep	6.5	0.5	5	120	28	0.16
				120	29.96	0.15
				120	26.17	0.21
				168	28	0.13
				85.71	28	0.22

Table 6-10a: Calculated Newmark Deformations – Idealized Sections Non Liquefiable
Cont.

Waterside Levee Slope	Earthquake Magnitude	PGA	Peat Thickness, ft	C	phi	Deformation, ft
Non-Steep	7.5	0.05	5	120	28	<0.1
				120	29.96	<0.1
				120	26.17	<0.1
				168	28	<0.1
				85.71	28	<0.1
Non-Steep	7.5	0.1	5	120	28	<0.1
				120	29.96	<0.1
				120	26.17	<0.1
				168	28	<0.1
				85.71	28	<0.1
Non-Steep	7.5	0.2	5	120	28	<0.1
				120	29.96	<0.1
				120	26.17	<0.1
				168	28	<0.1
				85.71	28	<0.1
Non-Steep	7.5	0.3	5	120	28	<0.1
				120	29.96	<0.1
				120	26.17	0.13
				168	28	<0.1
				85.71	28	0.14
Non-Steep	7.5	0.4	5	120	28	0.25
				120	29.96	0.22
				120	26.17	0.36
				168	28	0.16
				85.71	28	0.38
Non-Steep	7.5	0.5	5	120	28	0.61
				120	29.96	0.56
				120	26.17	0.86
				168	28	0.44
				85.71	28	0.91
Non-Steep	5.5	0.05	15	120	28	<0.1
				120	29.96	<0.1
				120	26.17	<0.1
				168	28	<0.1
				85.71	28	<0.1
Non-Steep	5.5	0.1	15	120	28	<0.1
				120	29.96	<0.1
				120	26.17	<0.1
				168	28	<0.1
				85.71	28	<0.1

Table 6-10a: Calculated Newmark Deformations – Idealized Sections Non Liquefiable
Cont.

Waterside Levee Slope	Earthquake Magnitude	PGA	Peat Thickness, ft	C	phi	Deformation, ft
Non-Steep	5.5	0.2	15	120	28	<0.1
				120	29.96	<0.1
				120	26.17	<0.1
				168	28	<0.1
				85.71	28	<0.1
Non-Steep	5.5	0.3	15	120	28	<0.1
				120	29.96	<0.1
				120	26.17	<0.1
				168	28	<0.1
				85.71	28	<0.1
Non-Steep	5.5	0.4	15	120	28	0.11
				120	29.96	<0.1
				120	26.17	0.16
				168	28	<0.1
				85.71	28	0.21
Non-Steep	5.5	0.5	15	120	28	0.19
				120	29.96	0.17
				120	26.17	0.27
				168	28	0.14
				85.71	28	0.34
Non-Steep	6.5	0.05	15	120	28	<0.1
				120	29.96	<0.1
				120	26.17	<0.1
				168	28	<0.1
				85.71	28	<0.1
Non-Steep	6.5	0.1	15	120	28	<0.1
				120	29.96	<0.1
				120	26.17	<0.1
				168	28	<0.1
				85.71	28	<0.1
Non-Steep	6.5	0.2	15	120	28	<0.1
				120	29.96	<0.1
				120	26.17	<0.1
				168	28	<0.1
				85.71	28	0.14
Non-Steep	6.5	0.3	15	120	28	0.21
				120	29.96	0.18
				120	26.17	0.34
				168	28	0.14
				85.71	28	0.49

Table 6-10a: Calculated Newmark Deformations – Idealized Sections Non Liquefiable
Cont.

Waterside Levee Slope	Earthquake Magnitude	PGA	Peat Thickness, ft	C	phi	Deformation, ft
Non-Steep	6.5	0.4	15	120	28	0.5
				120	29.96	0.42
				120	26.17	0.78
				168	28	0.3
				85.71	28	1.06
Non-Steep	6.5	0.5	15	120	28	0.98
				120	29.96	0.84
				120	26.17	1.39
				168	28	0.59
				85.71	28	1.77
Non-Steep	7.5	0.05	15	120	28	<0.1
				120	29.96	<0.1
				120	26.17	<0.1
				168	28	<0.1
				85.71	28	<0.1
Non-Steep	7.5	0.1	15	120	28	<0.1
				120	29.96	<0.1
				120	26.17	<0.1
				168	28	<0.1
				85.71	28	<0.1
Non-Steep	7.5	0.2	15	120	28	0.26
				120	29.96	0.19
				120	26.17	0.42
				168	28	0.13
				85.71	28	0.59
Non-Steep	7.5	0.3	15	120	28	1.03
				120	29.96	0.87
				120	26.17	1.47
				168	28	0.63
				85.71	28	1.9
Non-Steep	7.5	0.4	15	120	28	2.35
				120	29.96	2.07
				120	26.17	3.35
				168	28	1.54
				85.71	28	4.23
Non-Steep	7.5	0.5	15	120	28	5.17
				120	29.96	4.51
				120	26.17	6.81
				168	28	3.39
				85.71	28	8.2

Table 6-10a: Calculated Newmark Deformations – Idealized Sections Non Liquefiable
Cont.

Waterside Levee Slope	Earthquake Magnitude	PGA	Peat Thickness, ft	C	phi	Deformation, ft
Non-Steep	5.5	0.05	>25	120	28	<0.1
				120	29.96	<0.1
				120	26.17	<0.1
				168	28	<0.1
				85.71	28	<0.1
Non-Steep	5.5	0.1	>25	120	28	<0.1
				120	29.96	<0.1
				120	26.17	<0.1
				168	28	<0.1
				85.71	28	<0.1
Non-Steep	5.5	0.2	>25	120	28	<0.1
				120	29.96	<0.1
				120	26.17	<0.1
				168	28	<0.1
				85.71	28	<0.1
Non-Steep	5.5	0.3	>25	120	28	<0.1
				120	29.96	<0.1
				120	26.17	<0.1
				168	28	<0.1
				85.71	28	<0.1
Non-Steep	5.5	0.4	>25	120	28	0.13
				120	29.96	<0.1
				120	26.17	0.18
				168	28	<0.1
				85.71	28	0.22
Non-Steep	5.5	0.5	>25	120	28	0.2
				120	29.96	0.14
				120	26.17	0.26
				168	28	0.11
				85.71	28	0.31
Non-Steep	6.5	0.05	>25	120	28	<0.1
				120	29.96	<0.1
				120	26.17	<0.1
				168	28	<0.1
				85.71	28	<0.1
Non-Steep	6.5	0.1	>25	120	28	<0.1
				120	29.96	<0.1
				120	26.17	<0.1
				168	28	<0.1
				85.71	28	<0.1

Table 6-10a: Calculated Newmark Deformations – Idealized Sections Non Liquefiable
Cont.

Waterside Levee Slope	Earthquake Magnitude	PGA	Peat Thickness, ft	C	phi	Deformation, ft
Non-Steep	6.5	0.2	>25	120	28	<0.1
				120	29.96	<0.1
				120	26.17	<0.1
				168	28	<0.1
				85.71	28	0.14
Non-Steep	6.5	0.3	>25	120	28	0.24
				120	29.96	0.13
				120	26.17	0.37
				168	28	0.1
				85.71	28	0.5
Non-Steep	6.5	0.4	>25	120	28	0.49
				120	29.96	0.27
				120	26.17	0.76
				168	28	0.2
				85.71	28	1.01
Non-Steep	6.5	0.5	>25	120	28	0.98
				120	29.96	0.58
				120	26.17	1.38
				168	28	0.42
				85.71	28	1.68
Non-Steep	7.5	0.05	>25	120	28	<0.1
				120	29.96	<0.1
				120	26.17	<0.1
				168	28	<0.1
				85.71	28	<0.1
Non-Steep	7.5	0.1	>25	120	28	<0.1
				120	29.96	<0.1
				120	26.17	<0.1
				168	28	<0.1
				85.71	28	<0.1
Non-Steep	7.5	0.2	>25	120	28	0.25
				120	29.96	0.1
				120	26.17	0.43
				168	28	<0.1
				85.71	28	0.59
Non-Steep	7.5	0.3	>25	120	28	0.98
				120	29.96	0.47
				120	26.17	1.47
				168	28	0.33
				85.71	28	1.92

Table 6-10a: Calculated Newmark Deformations – Idealized Sections Non Liquefiable
Cont.

Waterside Levee Slope	Earthquake Magnitude	PGA	Peat Thickness, ft	C	phi	Deformation, ft
Non-Steep	7.5	0.4	>25	120	28	2.27
				120	29.96	1.14
				120	26.17	3.39
				168	28	0.82
				85.71	28	4.3
Non-Steep	7.5	0.5	>25	120	28	5.43
				120	29.96	3.07
				120	26.17	6.61
				168	28	2.32
				85.71	28	7.86
Steep	5.5	0.05	5	120	28	<0.1
				120	29.96	<0.1
				120	26.17	<0.1
				168	28	<0.1
				85.71	28	<0.1
Steep	5.5	0.1	5	120	28	<0.1
				120	29.96	<0.1
				120	26.17	<0.1
				168	28	<0.1
				85.71	28	<0.1
Steep	5.5	0.2	5	120	28	<0.1
				120	29.96	<0.1
				120	26.17	<0.1
				168	28	<0.1
				85.71	28	<0.1
Steep	5.5	0.3	5	120	28	<0.1
				120	29.96	<0.1
				120	26.17	<0.1
				168	28	<0.1
				85.71	28	0.111
Steep	5.5	0.4	5	120	28	0.121
				120	29.96	0.1
				120	26.17	0.148
				168	28	0.103
				85.71	28	0.205
Steep	5.5	0.5	5	120	28	0.216
				120	29.96	0.162
				120	26.17	0.278
				168	28	<0.1
				85.71	28	0.357

Table 6-10a: Calculated Newmark Deformations – Idealized Sections Non Liquefiable
Cont.

Waterside Levee Slope	Earthquake Magnitude	PGA	Peat Thickness, ft	C	phi	Deformation, ft
Steep	6.5	0.05	5	120	28	<0.1
				120	29.96	<0.1
				120	26.17	<0.1
				168	28	<0.1
				85.71	28	<0.1
Steep	6.5	0.1	5	120	28	<0.1
				120	29.96	<0.1
				120	26.17	<0.1
				168	28	<0.1
				85.71	28	<0.1
Steep	6.5	0.2	5	120	28	<0.1
				120	29.96	<0.1
				120	26.17	<0.1
				168	28	<0.1
				85.71	28	0.116
Steep	6.5	0.3	5	120	28	0.252
				120	29.96	0.188
				120	26.17	0.33
				168	28	<0.1
				85.71	28	0.42
Steep	6.5	0.4	5	120	28	0.458
				120	29.96	0.368
				120	26.17	0.614
				168	28	0.246
				85.71	28	0.834
Steep	6.5	0.5	5	120	28	1.013
				120	29.96	0.797
				120	26.17	1.31
				168	28	0.5425
				85.71	28	1.676
Steep	7.5	0.05	5	120	28	<0.1
				120	29.96	<0.1
				120	26.17	<0.1
				168	28	<0.1
				85.71	28	<0.1
Steep	7.5	0.1	5	120	28	<0.1
				120	29.96	<0.1
				120	26.17	<0.1
				168	28	<0.1
				85.71	28	<0.1

Table 6-10a: Calculated Newmark Deformations – Idealized Sections Non Liquefiable
Cont.

Waterside Levee Slope	Earthquake Magnitude	PGA	Peat Thickness, ft	C	phi	Deformation, ft
Steep	7.5	0.2	5	120	28	0.157
				120	29.96	<0.1
				120	26.17	0.257
				168	28	<0.1
				85.71	28	0.391
Steep	7.5	0.3	5	120	28	0.856
				120	29.96	0.662
				120	26.17	1.109
				168	28	0.3795
				85.71	28	1.425
Steep	7.5	0.4	5	120	28	1.915
				120	29.96	1.571
				120	26.17	2.358
				168	28	1.0365
				85.71	28	2.886
Steep	7.5	0.5	5	120	28	3.809
				120	29.96	3.193
				120	26.17	4.538
				168	28	2.318
				85.71	28	5.405
Steep	5.5	0.05	15	120	28	<0.1
				120	29.96	<0.1
				120	26.17	<0.1
				168	28	<0.1
				85.71	28	<0.1
Steep	5.5	0.1	15	120	28	<0.1
				120	29.96	<0.1
				120	26.17	<0.1
				168	28	<0.1
				85.71	28	<0.1
Steep	5.5	0.2	15	120	28	<0.1
				120	29.96	<0.1
				120	26.17	<0.1
				168	28	<0.1
				85.71	28	<0.1
Steep	5.5	0.3	15	120	28	0.119
				120	29.96	<0.1
				120	26.17	0.134
				168	28	<0.1
				85.71	28	0.184

Table 6-10a: Calculated Newmark Deformations – Idealized Sections Non Liquefiable
Cont.

Waterside Levee Slope	Earthquake Magnitude	PGA	Peat Thickness, ft	C	phi	Deformation, ft
Steep	5.5	0.4	15	120	28	0.28
				120	29.96	0.203
				120	26.17	0.326
				168	28	0.137
				85.71	28	0.408
Steep	5.5	0.5	15	120	28	0.491
				120	29.96	0.39
				120	26.17	0.568
				168	28	0.289
				85.71	28	0.679
Steep	6.5	0.05	15	120	28	<0.1
				120	29.96	<0.1
				120	26.17	<0.1
				168	28	<0.1
				85.71	28	<0.1
Steep	6.5	0.1	15	120	28	<0.1
				120	29.96	<0.1
				120	26.17	<0.1
				168	28	<0.1
				85.71	28	<0.1
Steep	6.5	0.2	15	120	28	0.111
				120	29.96	<0.1
				120	26.17	0.155
				168	28	<0.1
				85.71	28	0.214
Steep	6.5	0.3	15	120	28	0.453
				120	29.96	0.293
				120	26.17	0.554
				168	28	0.198
				85.71	28	0.756
Steep	6.5	0.4	15	120	28	1.25
				120	29.96	0.939
				120	26.17	1.492
				168	28	0.655
				85.71	28	1.855
Steep	6.5	0.5	15	120	28	2.33
				120	29.96	1.75
				120	26.17	2.532
				168	28	0.655
				85.71	28	3.021

Table 6-10a: Calculated Newmark Deformations – Idealized Sections Non Liquefiable
Cont.

Waterside Levee Slope	Earthquake Magnitude	PGA	Peat Thickness, ft	C	phi	Deformation, ft
Steep	7.5	0.05	15	120	28	<0.1
				120	29.96	<0.1
				120	26.17	<0.1
				168	28	<0.1
				85.71	28	<0.1
Steep	7.5	0.1	15	120	28	<0.1
				120	29.96	<0.1
				120	26.17	<0.1
				168	28	<0.1
				85.71	28	<0.1
Steep	7.5	0.2	15	120	28	0.463
				120	29.96	0.314
				120	26.17	0.593
				168	28	0.18
				85.71	28	0.799
Steep	7.5	0.3	15	120	28	1.806
				120	29.96	1.375
				120	26.17	2.1
				168	28	1.008
				85.71	28	2.586
Steep	7.5	0.4	15	120	28	4.554
				120	29.96	3.611
				120	26.17	5.148
				168	28	2.736
				85.71	28	6.111
Steep	7.5	0.5	15	120	28	8.294
				120	29.96	6.571
				120	26.17	8.976
				168	28	5.276
				85.71	28	10.492
Steep	5.5	0.05	>25	120	28	<0.1
				120	29.96	<0.1
				120	26.17	<0.1
				168	28	<0.1
				85.71	28	<0.1
Steep	5.5	0.1	>25	120	28	<0.1
				120	29.96	<0.1
				120	26.17	<0.1
				168	28	<0.1
				85.71	28	<0.1

Table 6-10a: Calculated Newmark Deformations – Idealized Sections Non Liquefiable
Cont.

Waterside Levee Slope	Earthquake Magnitude	PGA	Peat Thickness, ft	C	phi	Deformation, ft
Steep	5.5	0.2	>25	120	28	<0.1
				120	29.96	<0.1
				120	26.17	<0.1
				168	28	<0.1
				85.71	28	<0.1
Steep	5.5	0.3	>25	120	28	0.265
				120	29.96	0.135
				120	26.17	0.322
				168	28	0.105
				85.71	28	0.297
Steep	5.5	0.4	>25	120	28	0.4
				120	29.96	0.317
				120	26.17	0.495
				168	28	0.219
				85.71	28	0.611
Steep	5.5	0.5	>25	120	28	0.649
				120	29.96	0.536
				120	26.17	0.754
				168	28	0.412
				85.71	28	0.889
Steep	6.5	0.05	>25	120	28	<0.1
				120	29.96	<0.1
				120	26.17	<0.1
				168	28	<0.1
				85.71	28	<0.1
Steep	6.5	0.1	>25	120	28	<0.1
				120	29.96	<0.1
				120	26.17	<0.1
				168	28	<0.1
				85.71	28	<0.1
Steep	6.5	0.2	>25	120	28	0.162
				120	29.96	0.111
				120	26.17	0.222
				168	28	<0.1
				85.71	28	0.327
Steep	6.5	0.3	>25	120	28	0.96
				120	29.96	0.698
				120	26.17	1.154
				168	28	0.463
				85.71	28	1.458

Table 6-10a: Calculated Newmark Deformations – Idealized Sections Non Liquefiable
Cont.

Waterside Levee Slope	Earthquake Magnitude	PGA	Peat Thickness, ft	C	phi	Deformation, ft
Steep	6.5	0.4	>25	120	28	2.363
				120	29.96	1.804
				120	26.17	2.56
				168	28	1.363
				85.71	28	3.022
Steep	6.5	0.5	>25	120	28	3.568
				120	29.96	2.979
				120	26.17	4.06
				168	28	2.385
				85.71	28	4.744
Steep	7.5	0.05	>25	120	28	<0.1
				120	29.96	<0.1
				120	26.17	<0.1
				168	28	<0.1
				85.71	28	<0.1
Steep	7.5	0.1	>25	120	28	<0.1
				120	29.96	<0.1
				120	26.17	<0.1
				168	28	<0.1
				85.71	28	<0.1
Steep	7.5	0.2	>25	120	28	0.721
				120	29.96	0.549
				120	26.17	0.881
				168	28	0.38
				85.71	28	1.134
Steep	7.5	0.3	>25	120	28	3.375
				120	29.96	2.52
				120	26.17	3.642
				168	28	1.91
				85.71	28	4.41
Steep	7.5	0.4	>25	120	28	7.161
				120	29.96	5.876
				120	26.17	7.905
				168	28	4.696
				85.71	28	9.151
Steep	7.5	0.5	>25	120	28	15.102
				120	29.96	8.886
				120	26.17	16.608
				168	28	9.368
				85.71	28	16.593

Table 6-10b: Calculated Newmark Deformations – Suisun Marsh Non Liquefiable

Earthquake Magnitude	PGA	Bay Deposit Thickness, ft	C	Deformation, ft
5.5	0.05	40	120	0.003
			168	0
			85.71	>10
5.5	0.1	40	120	0.026
			168	0
			85.71	>10
5.5	0.2	40	120	0.208
			168	0
			85.71	>10
5.5	0.3	40	120	0.408
			168	0.015
			85.71	>10
5.5	0.4	40	120	0.746
			168	0.049
			85.71	>10
5.5	0.5	40	120	1.185
			168	0.096
			85.71	>10
6.5	0.05	40	120	0.008
			168	0
			85.71	>10
6.5	0.1	40	120	0.104
			168	0
			85.71	>10
6.5	0.2	40	120	0.593
			168	0.007
			85.71	>10
6.5	0.3	40	120	1.764
			168	0.049
			85.71	>10
6.5	0.4	40	120	3.28
			168	0.121
			85.71	>10
6.5	0.5	40	120	4.841
			168	0.276
			85.71	>10
7.5	0.05	40	120	0.016
			168	0
			85.71	>10
7.5	0.1	40	120	0.328
			168	0
			85.71	>10
7.5	0.2	40	120	2.19
			168	0.02
			85.71	>10
7.5	0.3	40	120	4.927
			168	0.135
			85.71	>10

Table 6-10b: Calculated Newmark Deformations – Suisun Marsh Non Liquefiable cont.

Earthquake Magnitude	PGA	Bay Deposit Thickness, ft	C	Deformation, ft
7.5	0.4	40	120	9.083
			168	0.483
			85.71	>10
7.5	0.5	40	120	13.989
			168	1.207
			85.71	>10

Table 6-11 Distribution of Probability of Failure – Sample Results

Vulnerability Class Index	Initial Freeboard (ft)	Earthquake Magnitude	Epistemic Cumulative % Prob.	Probability of Failure for Given Ground Motion Level											
				0.05	0.1	0.2	0.3	0.4	0.5	0.6	0.7	0.8	0.9	1	
1	4	5.5	50%	0.0034	0.0074	0.0663	0.2063	0.3368	0.5133	0.6075	0.6952	0.7166	0.7769	0.7975	
1	4	6.5	50%	0.0094	0.0660	0.3513	0.5945	0.7332	0.8022	0.8522	0.8710	0.8898	0.9045	0.9145	
1	4	7.5	50%	0.0775	0.3527	0.6696	0.8153	0.8641	0.8970	0.9171	0.9328	0.9457	0.9495	0.9564	
2	4	5.5	50%	0.0094	0.0333	0.2046	0.3828	0.5047	0.6439	0.7307	0.8027	0.8470	0.8979	0.9514	
2	4	6.5	50%	0.0532	0.2580	0.5790	0.7252	0.7915	0.8471	0.8928	0.9278	0.9602	0.9821	0.9907	
2	4	7.5	50%	0.3029	0.6069	0.7602	0.8322	0.8857	0.9320	0.9590	0.9770	0.9862	0.9939	0.9976	
3	4	5.5	50%	0.0034	0.0095	0.0768	0.2081	0.3415	0.4620	0.5498	0.6593	0.7679	0.8670	0.9416	
3	4	6.5	50%	0.0134	0.1246	0.3861	0.6163	0.7043	0.8132	0.8778	0.9140	0.9606	0.9871	0.9963	
3	4	7.5	50%	0.1322	0.4762	0.7133	0.8208	0.8709	0.9329	0.9578	0.9823	0.9945	0.9978	0.9987	
4	4	5.5	50%	0.0035	0.0035	0.0110	0.0477	0.0953	0.1766	0.2809	0.4717	0.6876	0.8457	0.9577	
4	4	6.5	50%	0.0065	0.0290	0.1305	0.2799	0.4022	0.5735	0.7483	0.8925	0.9586	0.9867	0.9974	
4	4	7.5	50%	0.0310	0.1476	0.4563	0.6297	0.8091	0.9037	0.9694	0.9920	0.9971	0.9987	0.9987	
5	4	5.5	50%	0.0034	0.0034	0.0038	0.0116	0.0582	0.1773	0.2975	0.4374	0.5324	0.5930	0.6649	
5	4	6.5	50%	0.0034	0.0049	0.0280	0.1392	0.3508	0.5561	0.7399	0.8270	0.8593	0.8935	0.9334	
5	4	7.5	50%	0.0061	0.0465	0.2408	0.4845	0.7317	0.8981	0.9358	0.9828	0.9868	0.9809	0.9951	
6	4	5.5	50%	0.0034	0.0036	0.0109	0.0683	0.3267	0.6635	0.8970	0.9609	0.9855	0.9811	0.9987	
6	4	6.5	50%	0.0067	0.0222	0.1760	0.4930	0.8316	0.9731	0.9904	0.9987	0.9987	0.9987	0.9987	
6	4	7.5	50%	0.0679	0.2855	0.6006	0.8975	0.9801	0.9985	0.9987	0.9987	0.9987	0.9987	0.9987	
7	4	5.5	50%	0.0034	0.0034	0.0077	0.0323	0.2092	0.4899	0.7545	0.8629	0.9229	0.9516	0.9918	
7	4	6.5	50%	0.0044	0.0089	0.1086	0.3854	0.7510	0.9302	0.9913	0.9972	0.9931	0.9987	0.9987	
7	4	7.5	50%	0.0321	0.1770	0.5491	0.8829	0.9788	0.9986	0.9987	0.9987	0.9987	0.9987	0.9987	
8	4	5.5	50%	0.0035	0.0036	0.0047	0.0123	0.0598	0.1858	0.3627	0.5245	0.7481	0.9012	0.9825	
8	4	6.5	50%	0.0044	0.0085	0.0346	0.1715	0.4540	0.6974	0.8714	0.9617	0.9854	0.9976	0.9968	
8	4	7.5	50%	0.0129	0.0506	0.3101	0.6677	0.8899	0.9774	0.9920	0.9975	0.9973	0.9987	0.9987	
9	4	5.5	50%	0.0034	0.0034	0.0045	0.0212	0.1121	0.3555	0.6524	0.8336	0.8889	0.9602	0.9750	
9	4	6.5	50%	0.0035	0.0059	0.0521	0.2383	0.5644	0.8914	0.9718	0.9900	0.9974	0.9987	0.9987	
9	4	7.5	50%	0.0129	0.0739	0.3396	0.7241	0.9347	0.9920	0.9968	0.9987	0.9987	0.9987	0.9987	
10	4	5.5	50%	0.0034	0.0034	0.0037	0.0081	0.0450	0.2189	0.4375	0.6194	0.7410	0.8701	0.9610	
10	4	6.5	50%	0.0035	0.0038	0.0269	0.1570	0.4135	0.7803	0.9312	0.9740	0.9922	0.9971	0.9987	
10	4	7.5	50%	0.0103	0.0429	0.2629	0.6295	0.9012	0.9809	0.9975	0.9974	0.9987	0.9987	0.9987	
11	4	5.5	50%	0.0035	0.0036	0.0040	0.0086	0.0222	0.0774	0.1827	0.3470	0.6350	0.8305	0.9423	

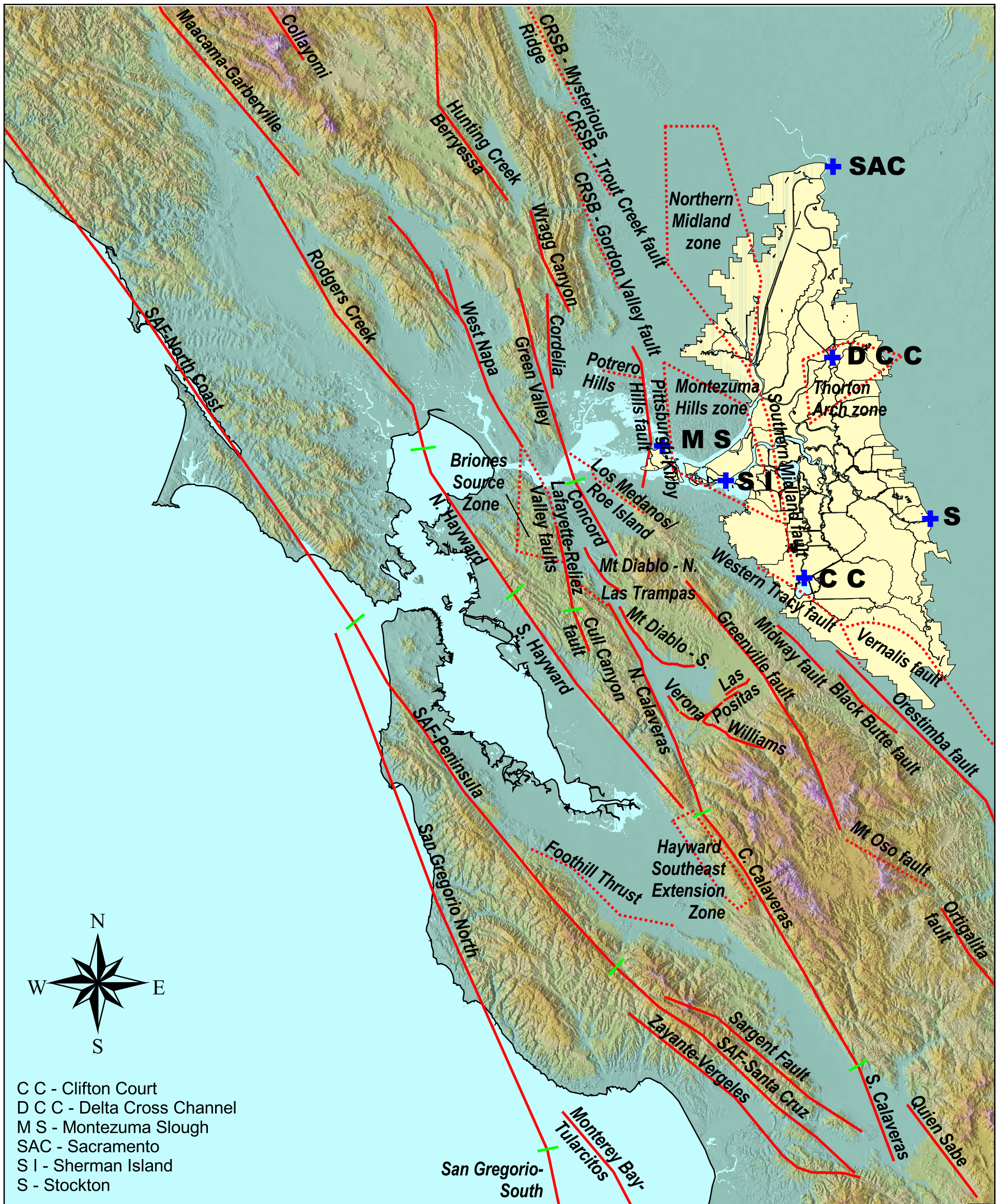
Table 6-11 Distribution of Probability of Failure – Sample Results

Vulnerability Class Index	Initial Freeboard (ft)	Earthquake Magnitude	Epistemic Cumulative % Prob.	Probability of Failure for Given Ground Motion Level											
				0.05	0.1	0.2	0.3	0.4	0.5	0.6	0.7	0.8	0.9	1	
11	4	6.5	50%	0.0046	0.0042	0.0162	0.0485	0.2272	0.4659	0.7381	0.8995	0.9683	0.9971	0.9982	
11	4	7.5	50%	0.0132	0.0233	0.1316	0.4035	0.7382	0.9333	0.9864	0.9966	0.9987	0.9987	0.9987	
12	4	5.5	50%	0.0034	0.0034	0.0035	0.0039	0.0152	0.0590	0.1584	0.3580	0.5319	0.7007	0.8558	
12	4	6.5	50%	0.0034	0.0037	0.0071	0.0342	0.1452	0.4302	0.6832	0.8736	0.9529	0.9859	0.9967	
12	4	7.5	50%	0.0050	0.0087	0.0680	0.2786	0.5777	0.8731	0.9787	0.9918	0.9986	0.9987	0.9987	
13	4	5.5	50%	0.0034	0.0034	0.0035	0.0037	0.0057	0.0238	0.0740	0.2007	0.3504	0.6346	0.8413	
13	4	6.5	50%	0.0035	0.0035	0.0040	0.0147	0.1049	0.2759	0.5082	0.7974	0.8981	0.9704	0.9922	
13	4	7.5	50%	0.0038	0.0069	0.0369	0.2080	0.5033	0.7599	0.9433	0.9831	0.9971	0.9987	0.9987	
14	4	5.5	50%	0.0035	0.0036	0.0060	0.0095	0.0161	0.0362	0.0788	0.2524	0.4606	0.7441	0.9324	
14	4	6.5	50%	0.0046	0.0080	0.0093	0.0253	0.0782	0.1898	0.4481	0.7049	0.9008	0.9819	0.9939	
14	4	7.5	50%	0.0125	0.0151	0.0504	0.1371	0.3734	0.6918	0.8984	0.9731	0.9961	0.9987	0.9987	
15	4	5.5	50%	0.0035	0.0036	0.0037	0.0038	0.0041	0.0045	0.0055	0.0071	0.0114	0.0259	0.0623	
15	4	6.5	50%	0.0037	0.0038	0.0041	0.0045	0.0056	0.0071	0.0115	0.0211	0.0571	0.1489	0.3041	
15	4	7.5	50%	0.0042	0.0045	0.0052	0.0073	0.0112	0.0263	0.0583	0.1584	0.2975	0.5151	0.7376	
16	4	5.5	50%	0.0034	0.0035	0.0035	0.0038	0.0042	0.0066	0.0212	0.1113	0.3167	0.6613	0.9024	
16	4	6.5	50%	0.0036	0.0036	0.0040	0.0049	0.0103	0.0522	0.1930	0.5283	0.8148	0.9541	0.9890	
16	4	7.5	50%	0.0040	0.0044	0.0061	0.0210	0.0951	0.3525	0.6984	0.8966	0.9757	0.9965	1.0000	
17	4	5.5	50%	0.0035	0.0035	0.0036	0.0040	0.0050	0.0086	0.0486	0.1712	0.5070	0.7933	0.9401	
17	4	6.5	50%	0.0036	0.0038	0.0043	0.0061	0.0172	0.0902	0.3419	0.6777	0.9031	0.9853	0.9947	
17	4	7.5	50%	0.0044	0.0053	0.0093	0.0468	0.2233	0.5279	0.7990	0.9513	0.9898	0.9991	0.9987	
18	4	5.5	50%	0.0038	0.0043	0.0070	0.0141	0.0433	0.0993	0.2524	0.4851	0.7651	0.9330	0.9876	
18	4	6.5	50%	0.0084	0.0150	0.0285	0.0696	0.1644	0.3348	0.6697	0.8724	0.9724	0.9900	0.9981	
18	4	7.5	50%	0.0303	0.0408	0.1030	0.2580	0.5049	0.7787	0.9319	0.9908	0.9982	1.0000	1.0000	
19	4	5.5	50%	0.0034	0.0034	0.0034	0.0035	0.0035	0.0036	0.0037	0.0038	0.0041	0.0044	0.0051	
19	4	6.5	50%	0.0034	0.0035	0.0035	0.0036	0.0036	0.0038	0.0040	0.0043	0.0051	0.0069	0.0116	
19	4	7.5	50%	0.0035	0.0036	0.0037	0.0038	0.0040	0.0044	0.0052	0.0067	0.0107	0.0242	0.0535	
20	4	5.5	50%	0.0034	0.0034	0.0034	0.0035	0.0037	0.0041	0.0058	0.0141	0.0535	0.2519	0.5906	
20	4	6.5	50%	0.0034	0.0035	0.0036	0.0039	0.0049	0.0070	0.0295	0.1385	0.4527	0.7409	0.9315	
20	4	7.5	50%	0.0036	0.0037	0.0042	0.0060	0.0153	0.0785	0.2666	0.5909	0.8593	0.9701	0.9911	
21	4	5.5	50%	0.0034	0.0034	0.0035	0.0036	0.0039	0.0045	0.0089	0.0276	0.1301	0.4268	0.7293	
21	4	6.5	50%	0.0035	0.0035	0.0037	0.0041	0.0059	0.0136	0.0719	0.2430	0.5918	0.8632	0.9660	

Table 6-11 Distribution of Probability of Failure – Sample Results

Vulnerability Class Index	Initial Freeboard (ft)	Earthquake Magnitude	Epistemic Cumulative % Prob.	Probability of Failure for Given Ground Motion Level										
				0.05	0.1	0.2	0.3	0.4	0.5	0.6	0.7	0.8	0.9	1
21	4	7.5	50%	0.0037	0.0039	0.0051	0.0081	0.0246	0.1493	0.4250	0.7480	0.9063	0.9878	0.9979
22	4	5.5	50%	0.0036	0.0040	0.0043	0.0092	0.0153	0.0311	0.0877	0.1975	0.4387	0.7207	0.9042
22	4	6.5	50%	0.0046	0.0075	0.0102	0.0270	0.0616	0.1336	0.3099	0.6109	0.8402	0.9541	0.9915
22	4	7.5	50%	0.0129	0.0188	0.0348	0.0894	0.2018	0.4418	0.7389	0.9137	0.9789	0.9970	1.0000
23	4	5.5	50%	0.0959	0.1221	0.1764	0.2526	0.3675	0.4375	0.5460	0.6306	0.7315	0.7899	0.8265
23	4	6.5	50%	0.1222	0.1588	0.2412	0.3299	0.4108	0.5116	0.6200	0.6994	0.7702	0.8038	0.8742
23	4	7.5	50%	0.1695	0.2013	0.3032	0.3873	0.5005	0.5891	0.6913	0.7363	0.8232	0.8588	0.8900

Figures



C C - Clifton Court
 D C C - Delta Cross Channel
 M S - Montezuma Slough
 SAC - Sacramento
 S I - Sherman Island
 S - Stockton

Legal Delta Boundary V. 2002-4
 Surficial faults used in the hazard analysis
 Blind faults used in the hazard analysis
 Bounds of delta islands
 CRSB - Coast Range Sierran Block
 SAF - San Andreas Fault

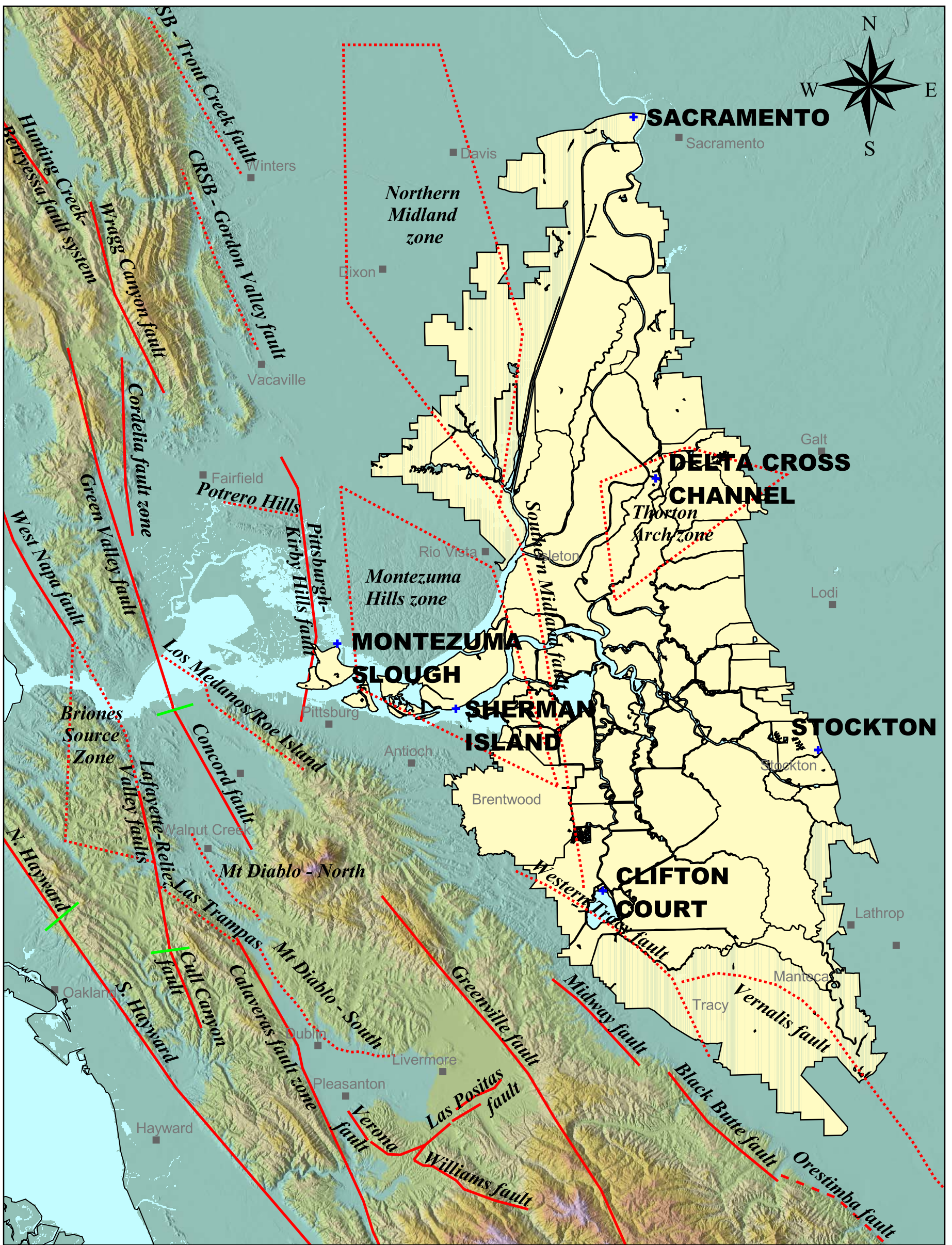
0 30 60 90 Kilometers
 0 20 40 60 Miles



Delta Risk Management
 Strategy, California
 Project No. 26815431

**FAULTS IN THE
 SAN FRANCISCO BAY REGION**

**Figure
 6-1**



-  Legal Delta Boundary V. 2002-4
-  Surficial faults used in the hazard analysis
-  Blind faults used in the hazard analysis
-  Bounds of delta islands
- CRSB - Coast Range Sierran Block

0 10 20 30 Miles

0 10 20 30 40 50 Kilometers

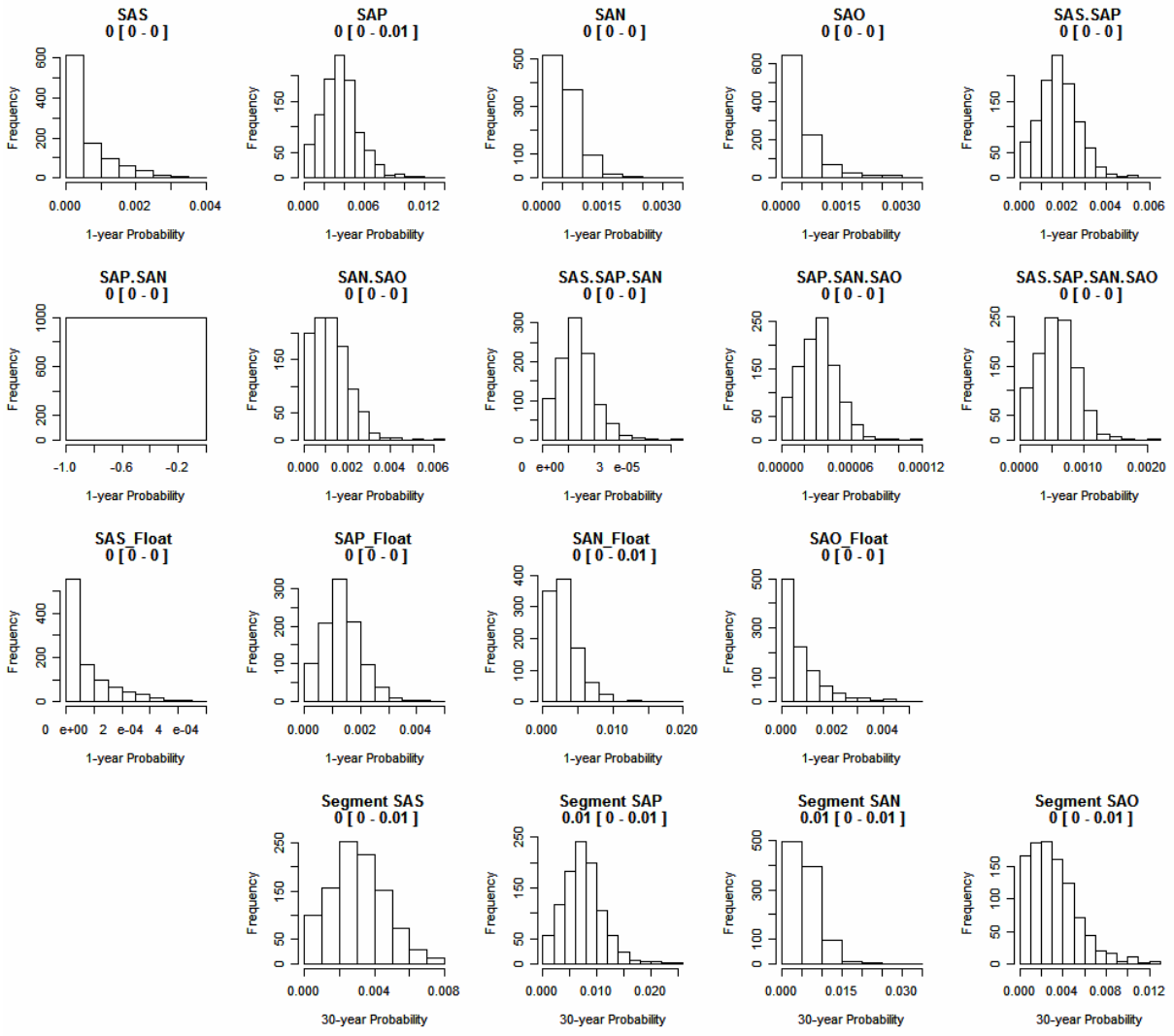


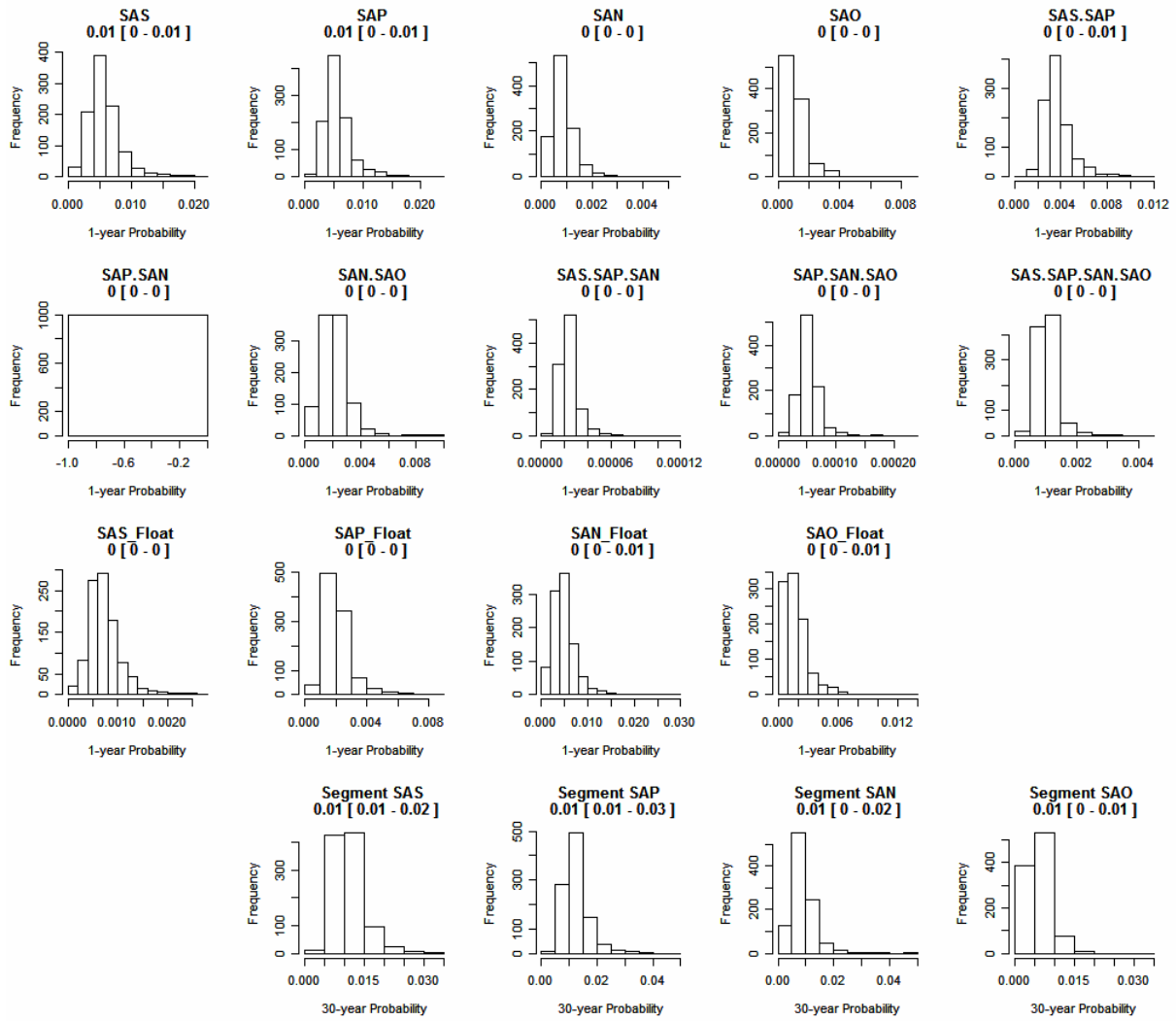
Delta Risk Management
Strategy, California

Project No. 26815431

ACTIVE FAULTS IN THE SITE REGION

Figure
6-2



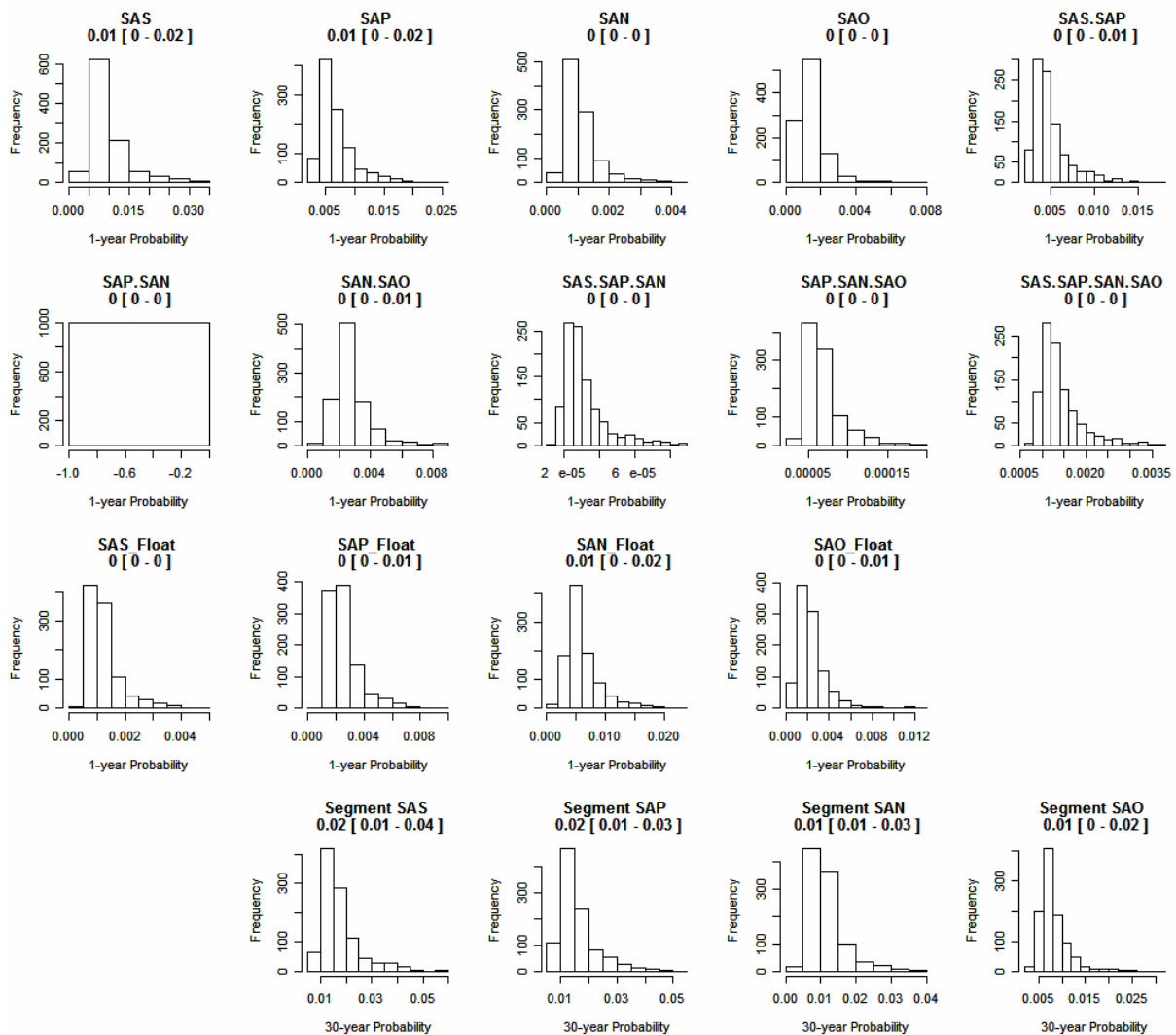


DELTA RISK
MANAGEMENT STRATEGY
California

Project No. 26815621

Time-Dependent Probabilites
for the San Andreas Rupture Scenarios for 2050

Figure
6-4

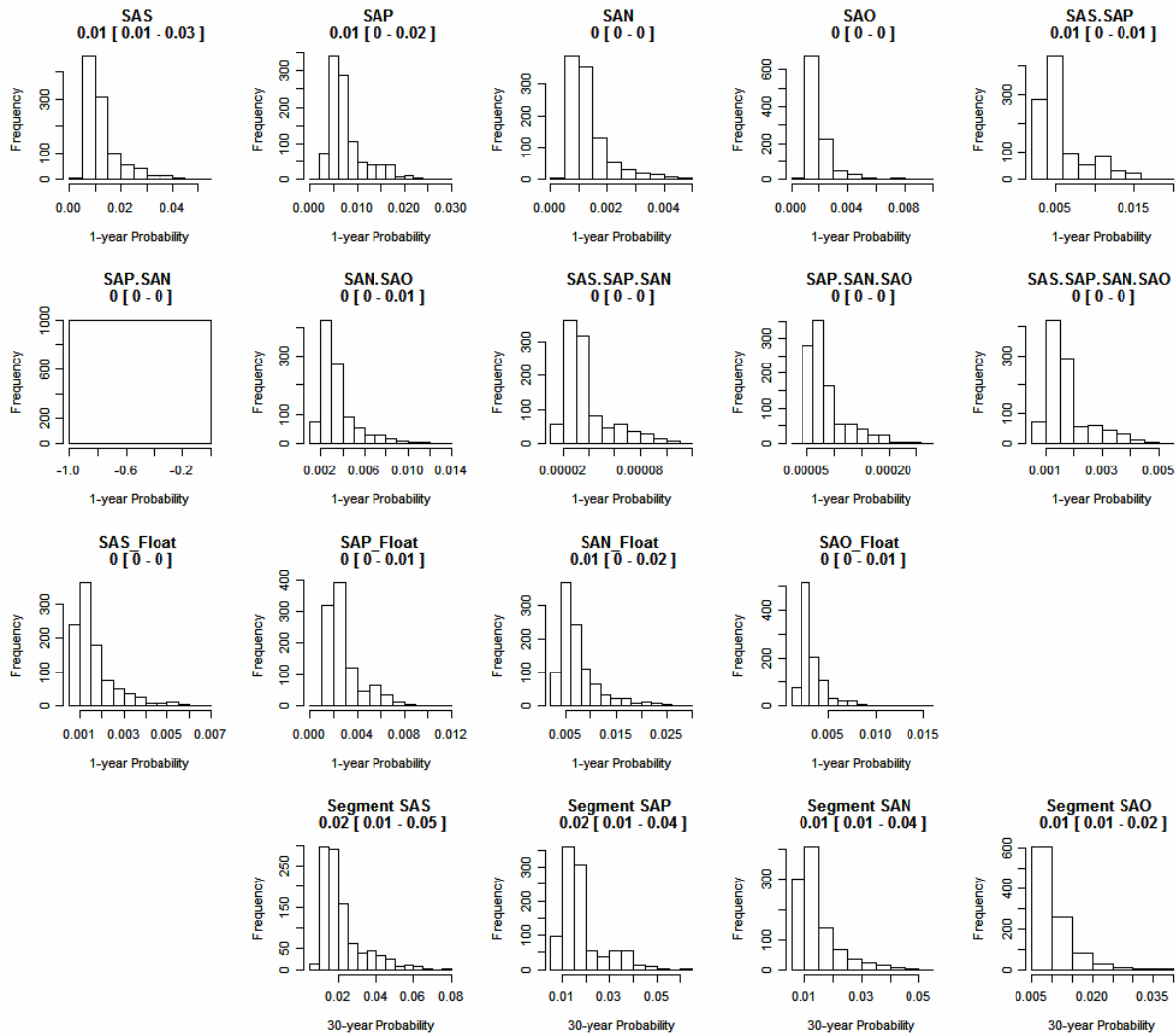


DELTA RISK
MANAGEMENT STRATEGY
California

Project No. 26815621

Time-Dependent Probabilities
for the San Andreas Rupture Scenarios for 2100

Figure
6-5

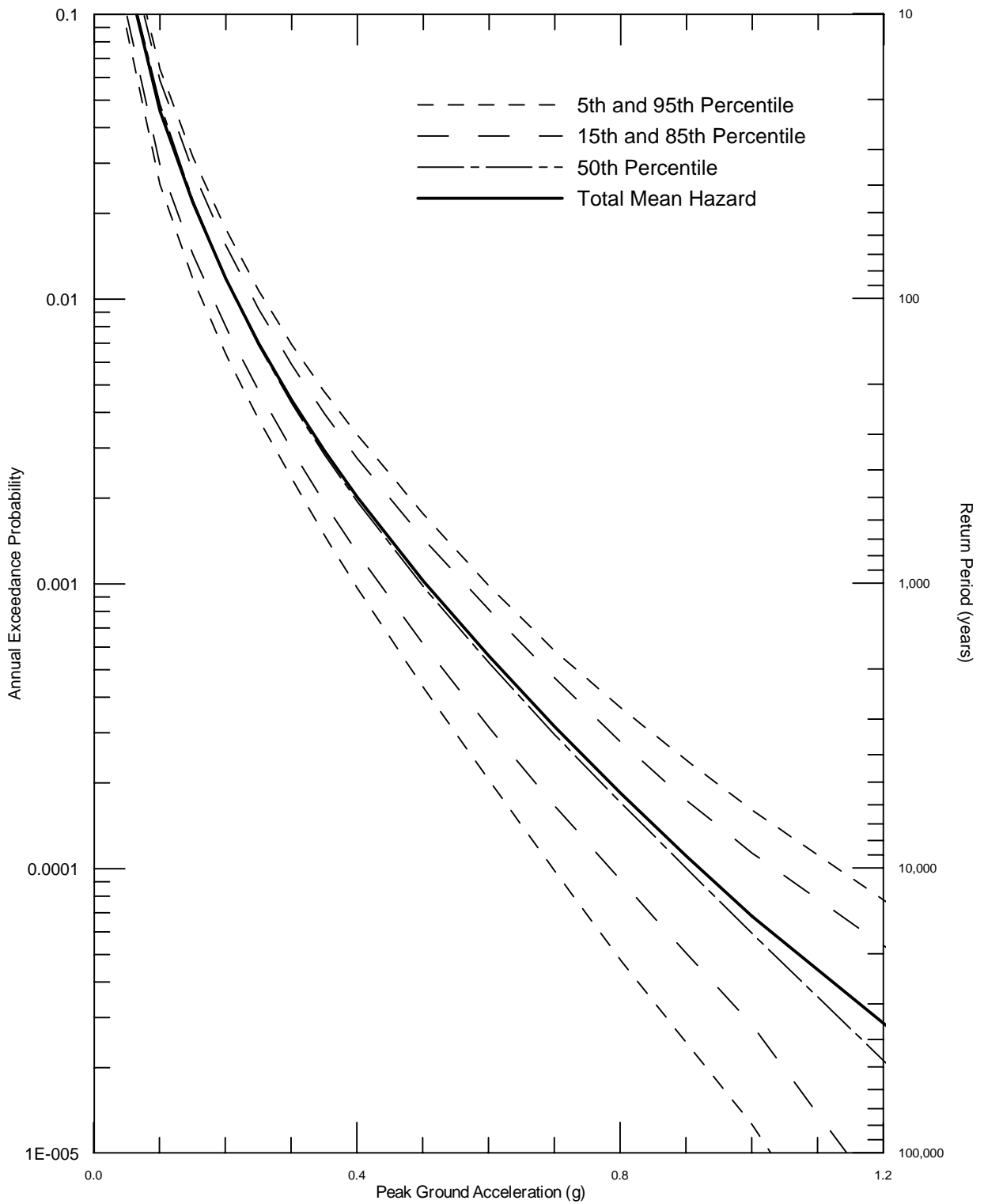


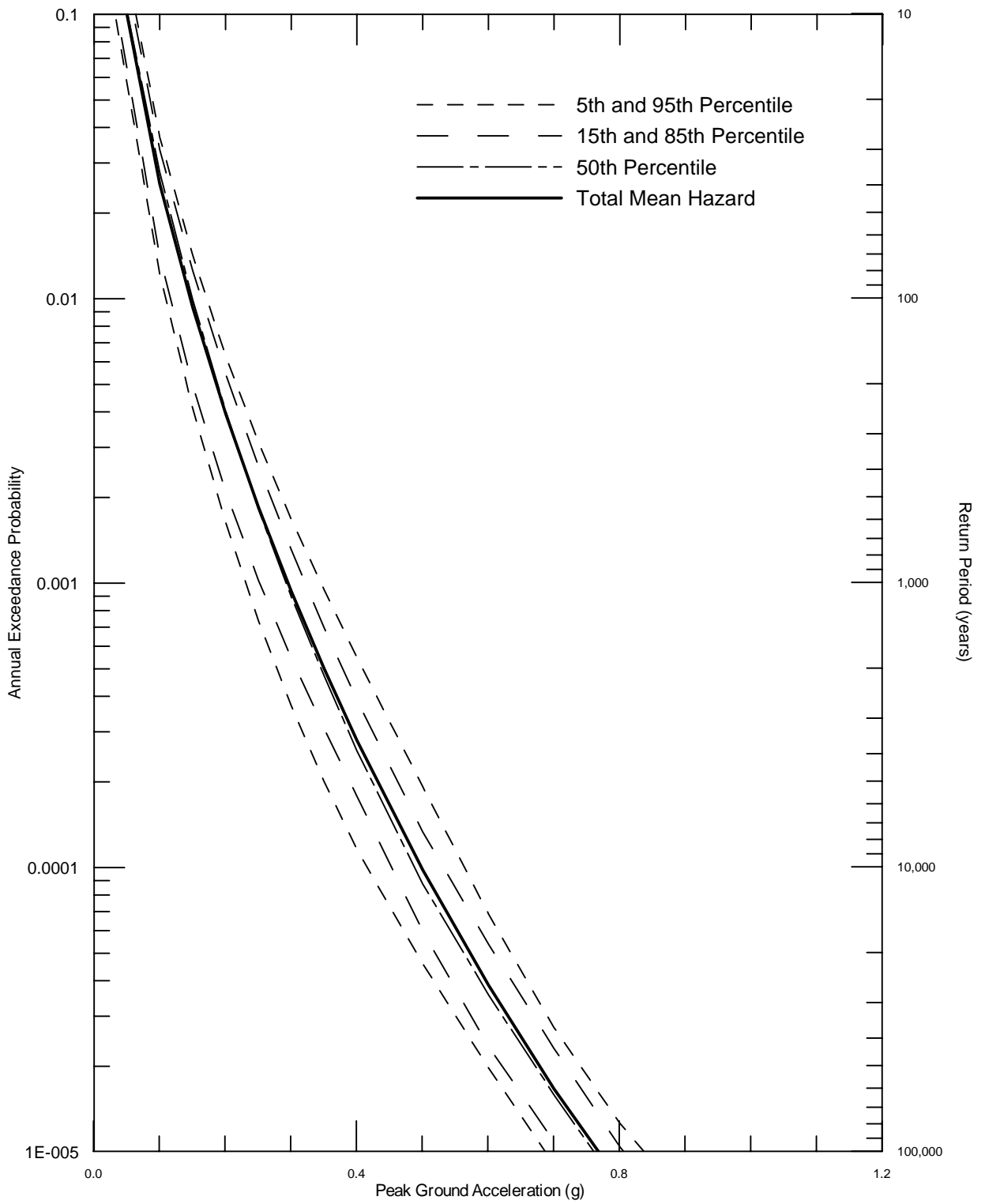
DELTA RISK
MANAGEMENT STRATEGY
California

Project No. 26815621

Time-Dependent Probabilities
for the San Andreas Rupture Scenarios for 2200

Figure
6-6



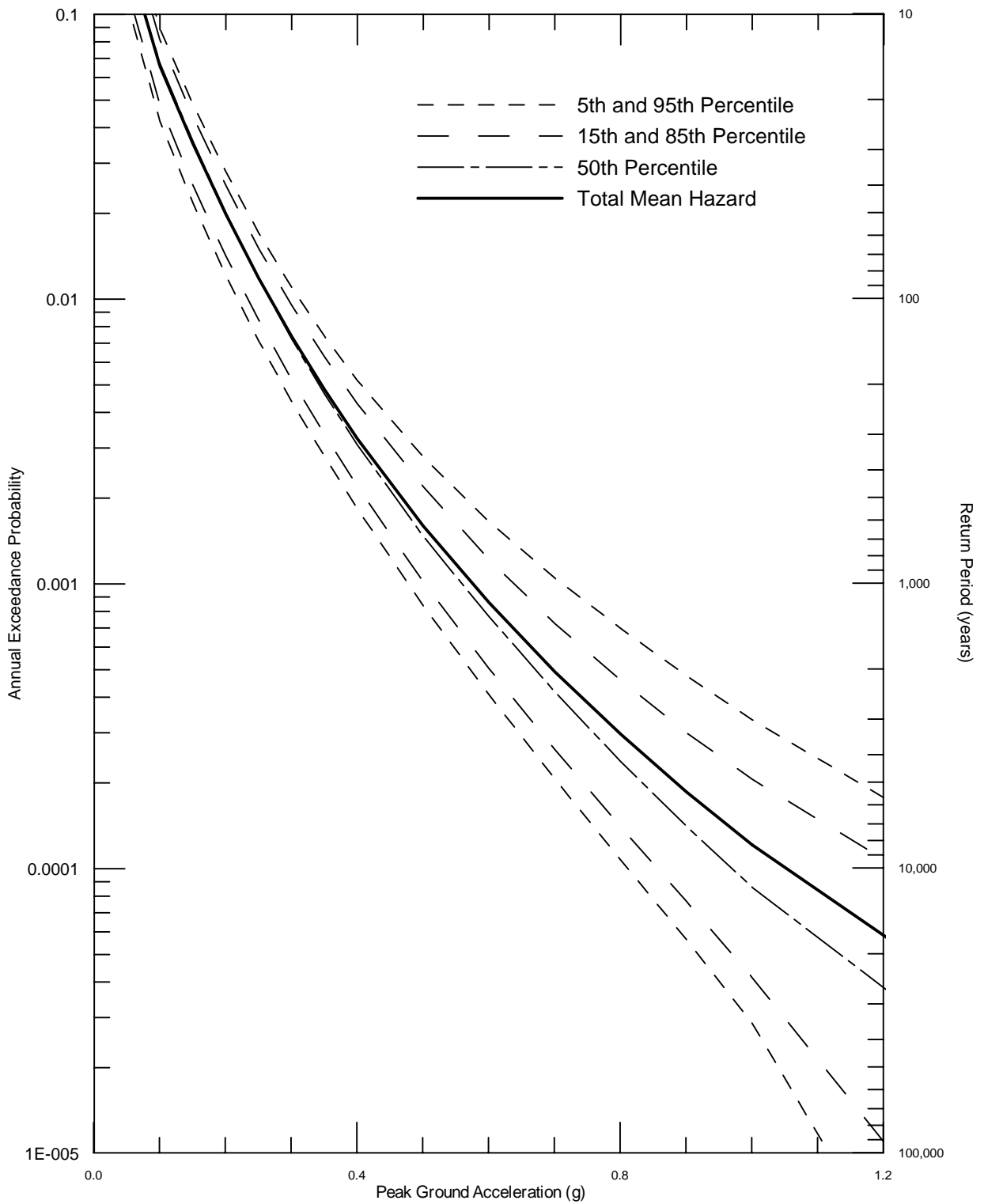


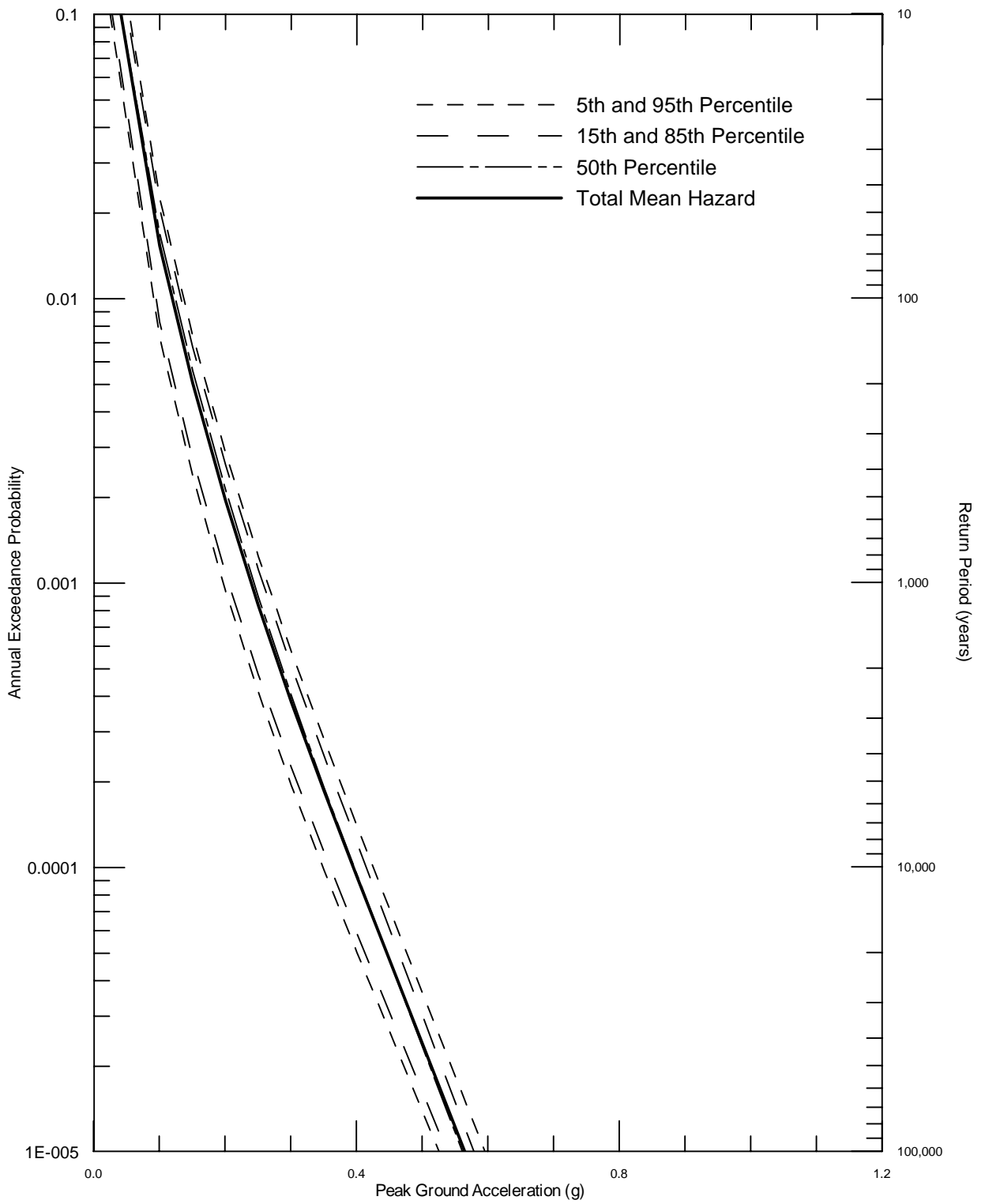
DELTA RISK
MANAGEMENT STRATEGY
CALIFORNIA

Project No. 26815900

TIME DEPENDENT SEISMIC HAZARD CURVES
FOR MEAN PEAK HORIZONTAL ACCELERATION
FOR DELTA CROSS CHANNEL FOR 2005

Figure
6-8



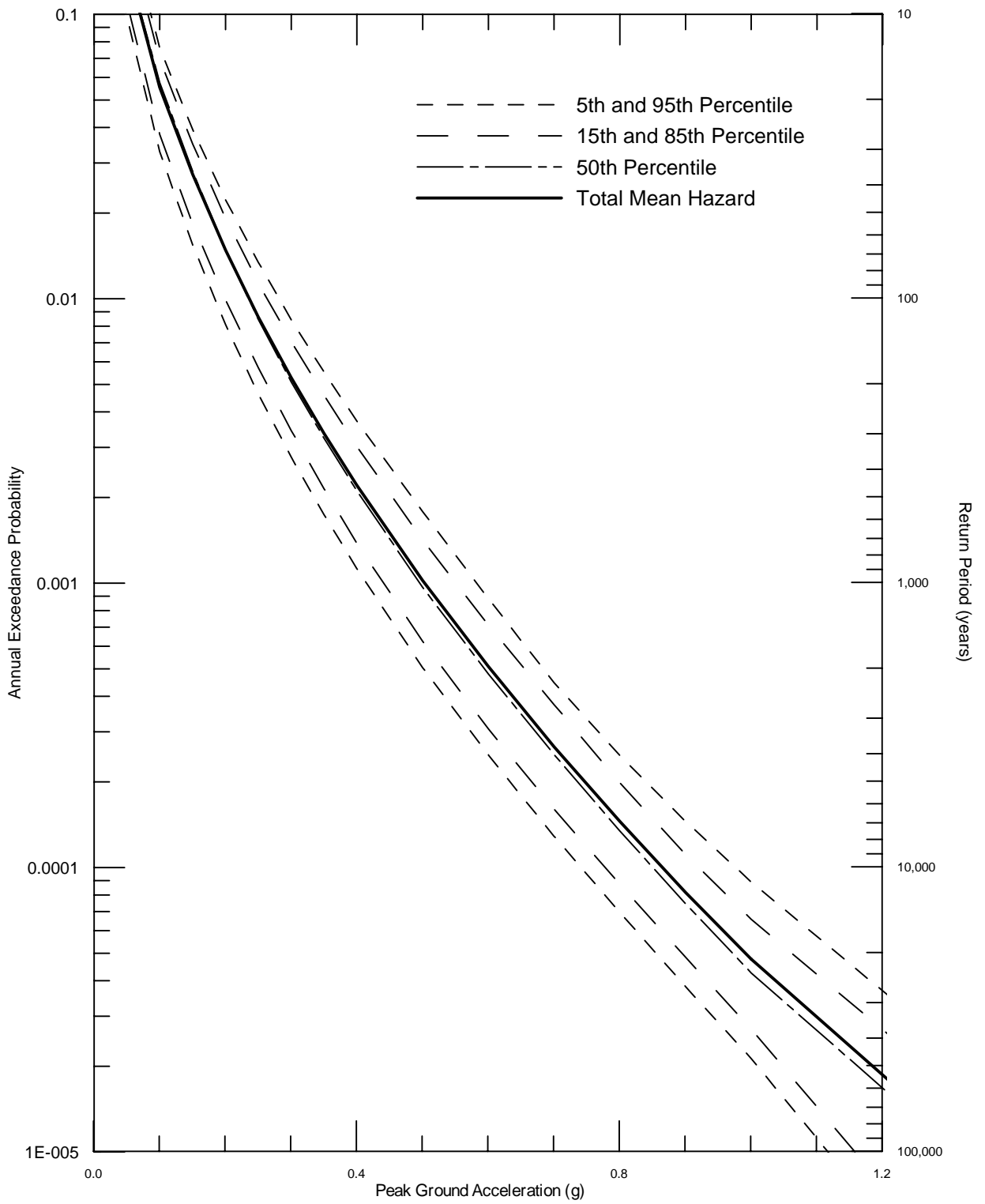


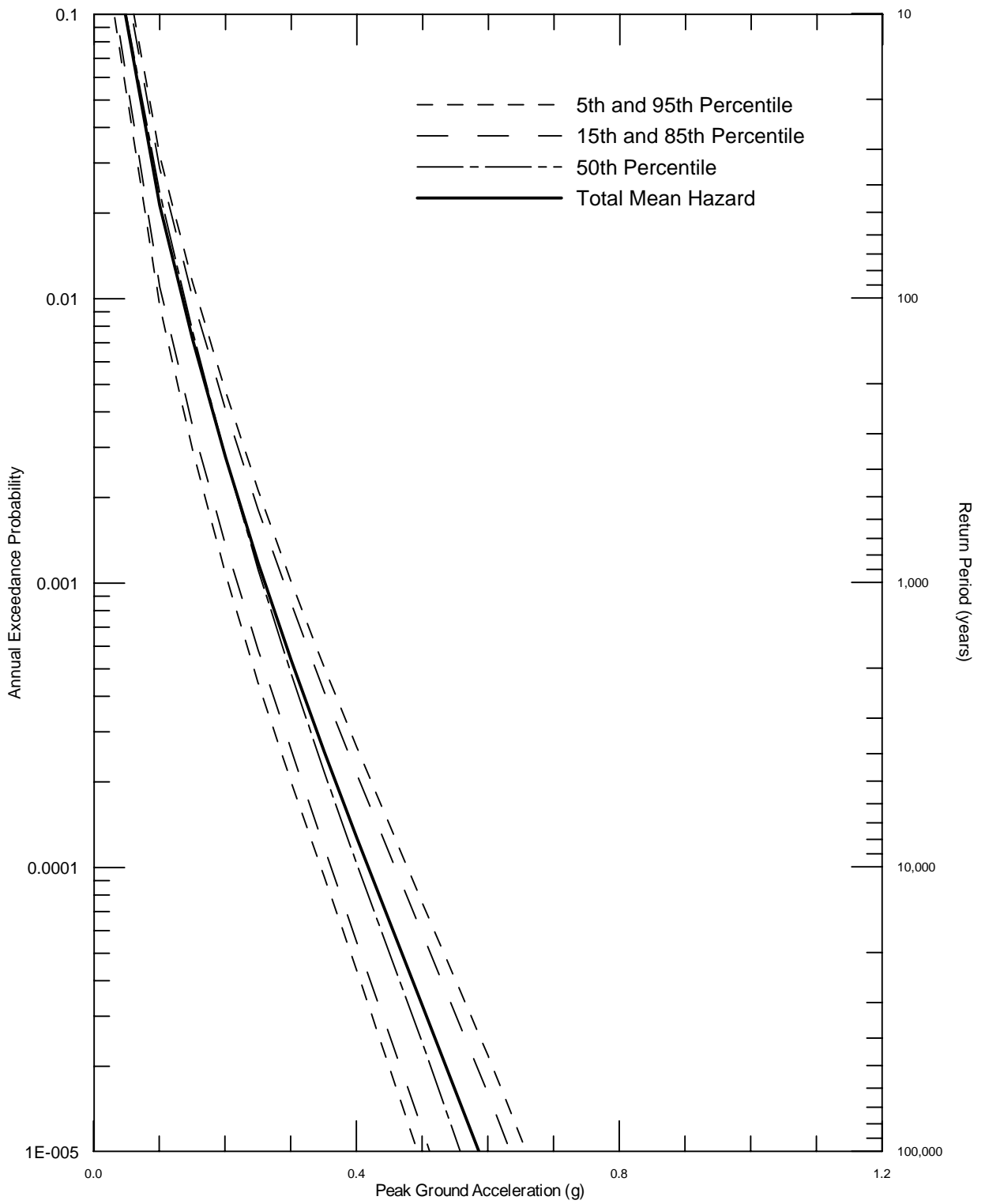
DELTA RISK
MANAGEMENT STRATEGY
CALIFORNIA

Project No. 26815900

TIME DEPENDENT SEISMIC HAZARD CURVES
FOR MEAN PEAK HORIZONTAL ACCELERATION
FOR SACRAMENTO FOR 2005

Figure
6-10



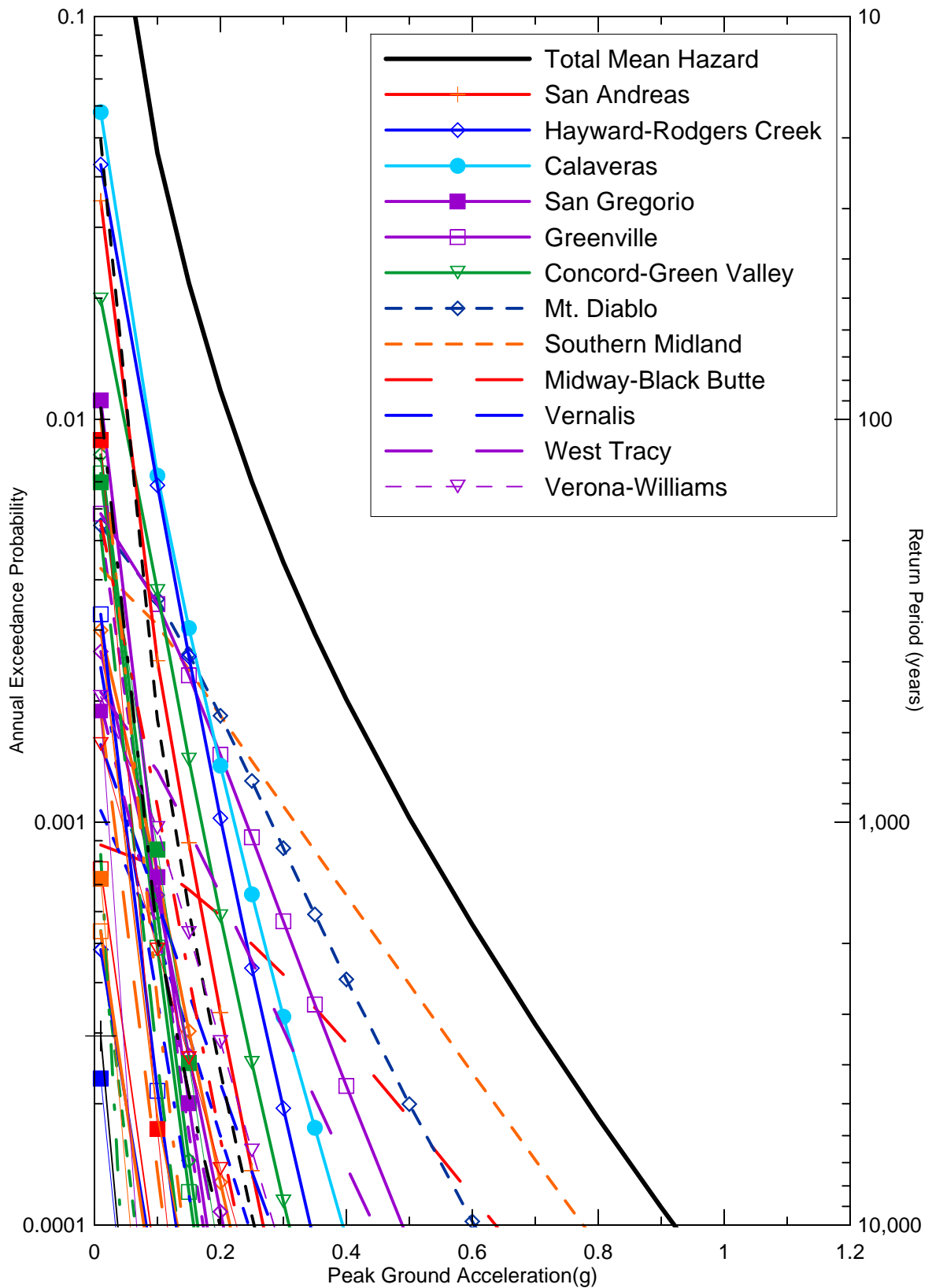


DELTA RISK
MANAGEMENT STRATEGY
CALIFORNIA

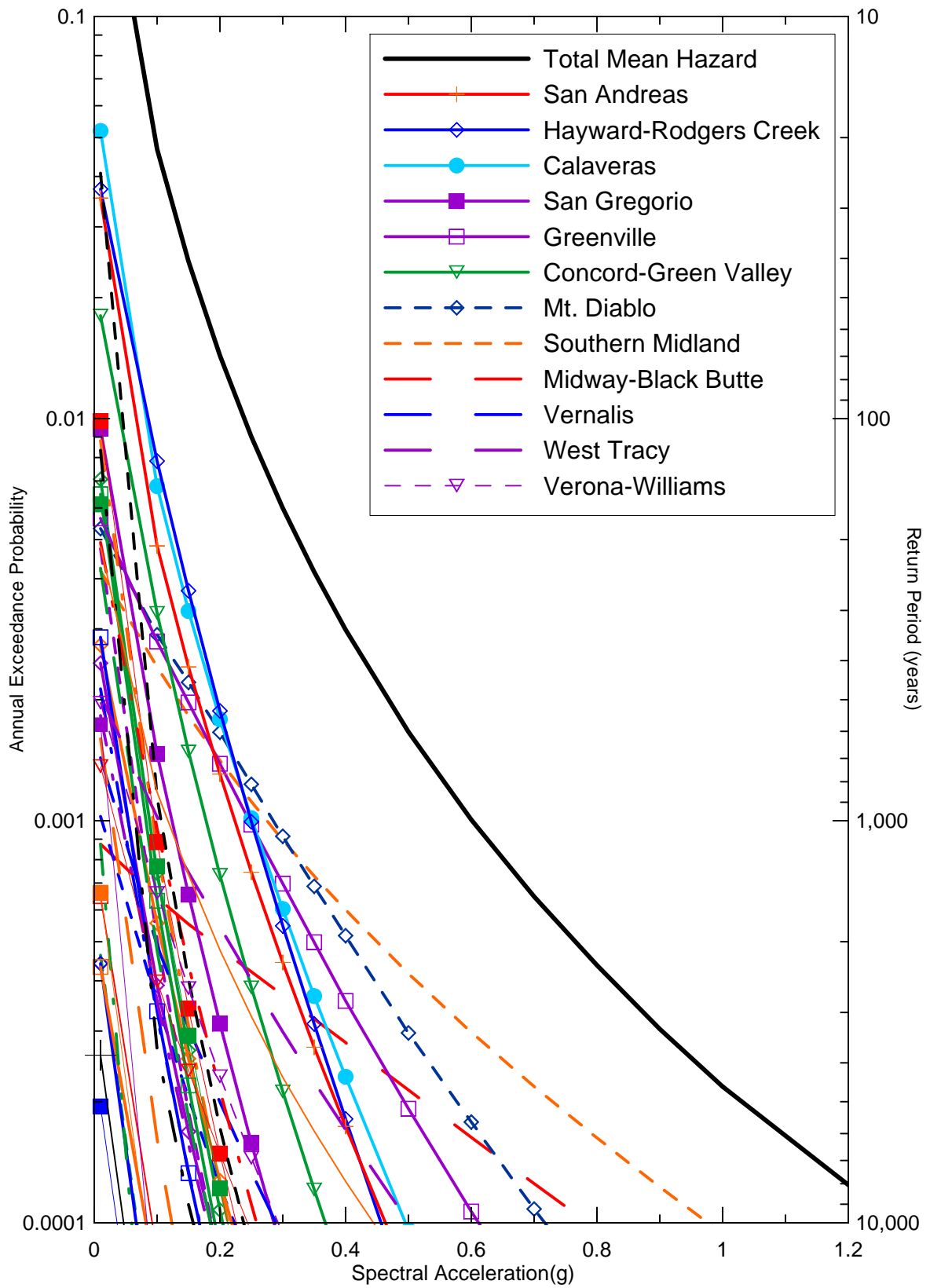
Project No. 26815900

TIME DEPENDENT SEISMIC HAZARD CURVES
FOR MEAN PEAK HORIZONTAL ACCELERATION
FOR STOCKTON FOR 2005

Figure
6-12



Delta Risk\figures\DR2-ppga-2005.grf



Delta Risk\figures\DR2-11-2005.grf

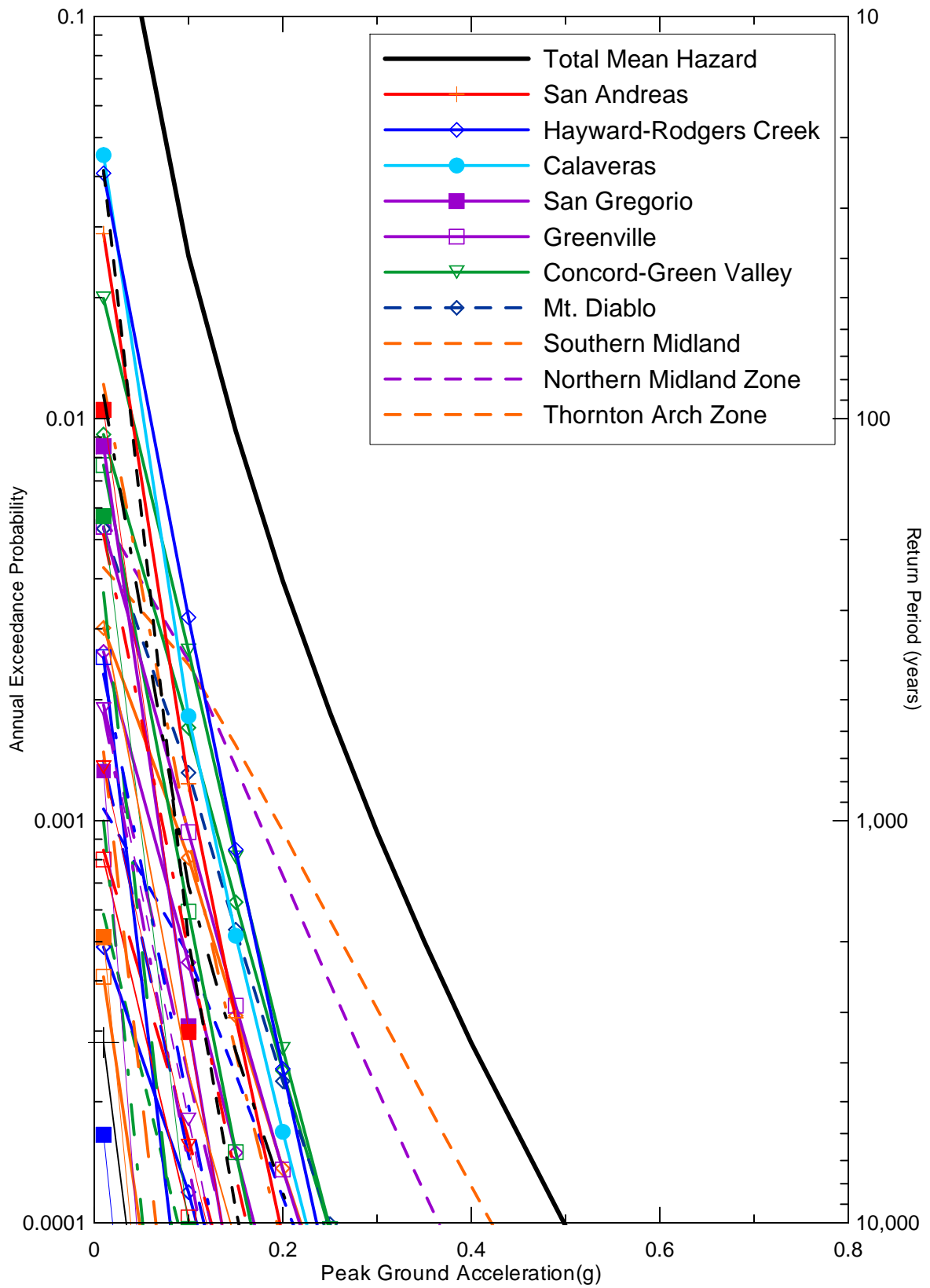


DELTA RISK
MANAGEMENT STRATEGY
CALIFORNIA

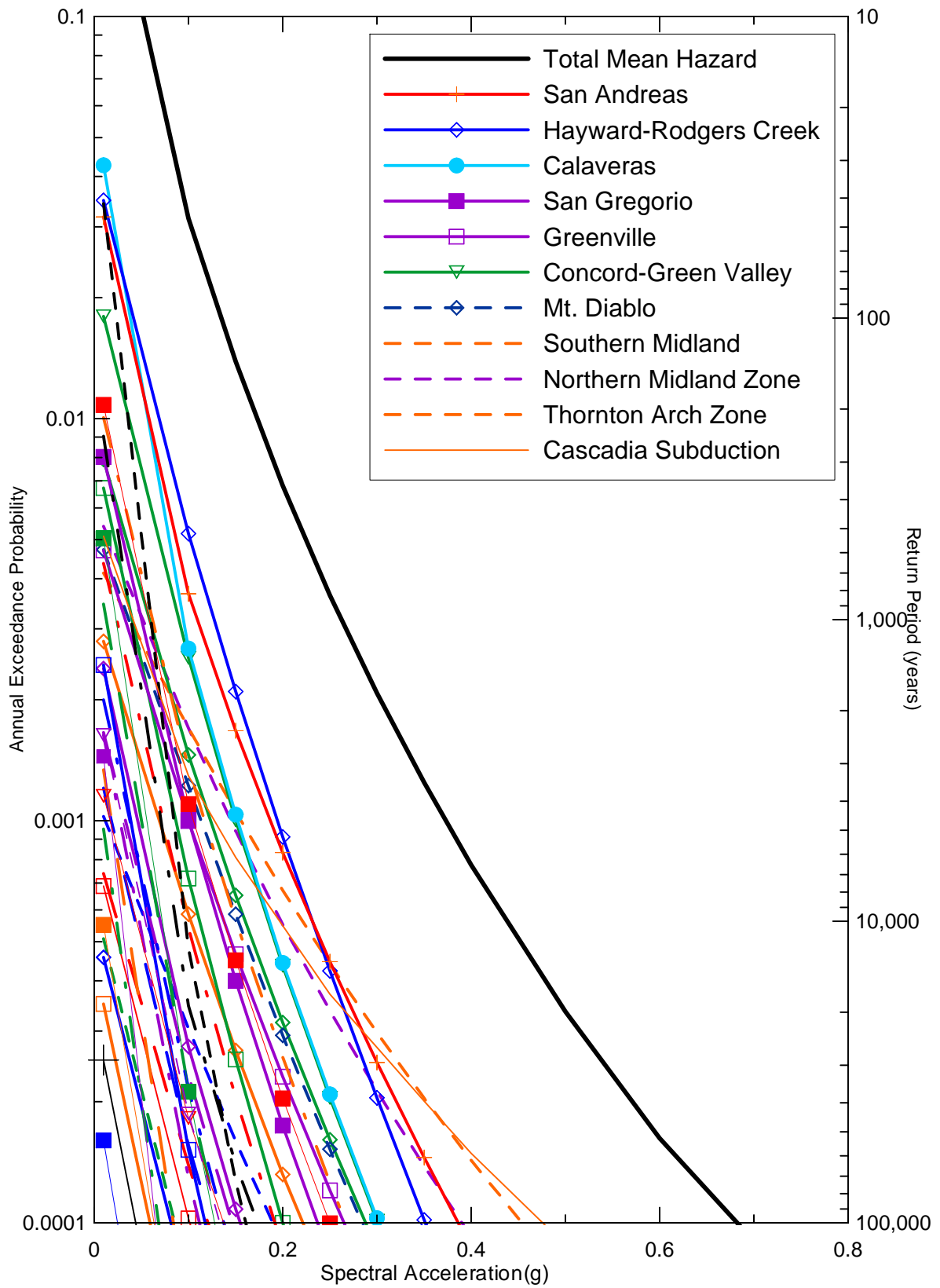
Project No. 26815900

SEISMIC SOURCE CONTRIBUTIONS TO 1.0 SEC
HORIZONTAL SPECTRAL ACCELERATION TIME-
DEPENDENT HAZARD FOR CLIFTON COURT
FOR 2005

Figure
6-13b



Delta Risk\figures\DR-4-pga-2005.grf



Delta Risk\figures\DR4-11-2005.grf

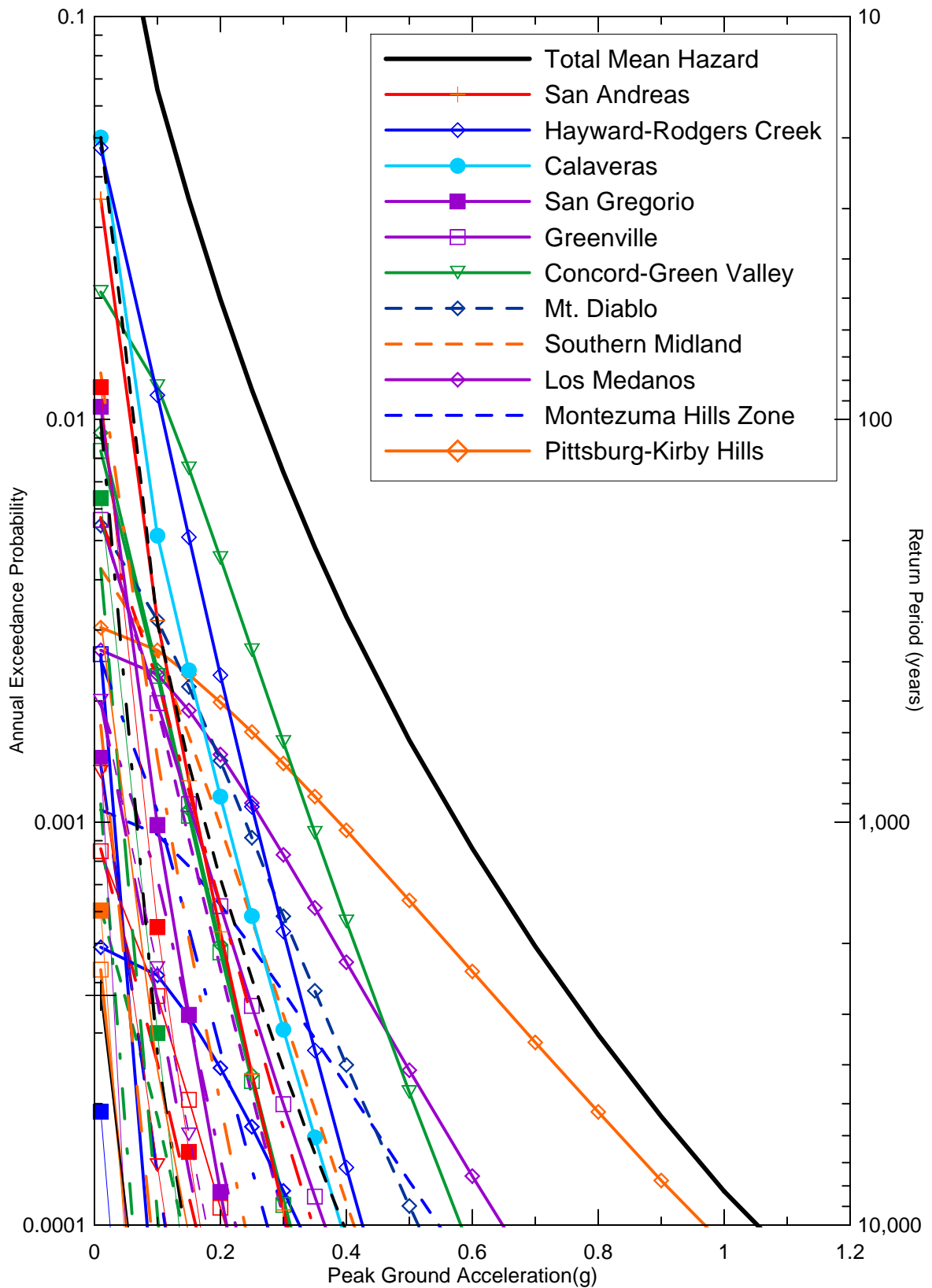


DELTA RISK
MANAGEMENT STRATEGY
CALIFORNIA

Project No. 26815900

SEISMIC SOURCE CONTRIBUTIONS TO 1.0 SEC
HORIZONTAL SPECTRAL ACCELERATION TIME-
DEPENDENT HAZARD FOR DELTA CROSS CHANNEL
FOR 2005

Figure
6-14b



Delta Risk\Figures\DR3-pga-2005.grf

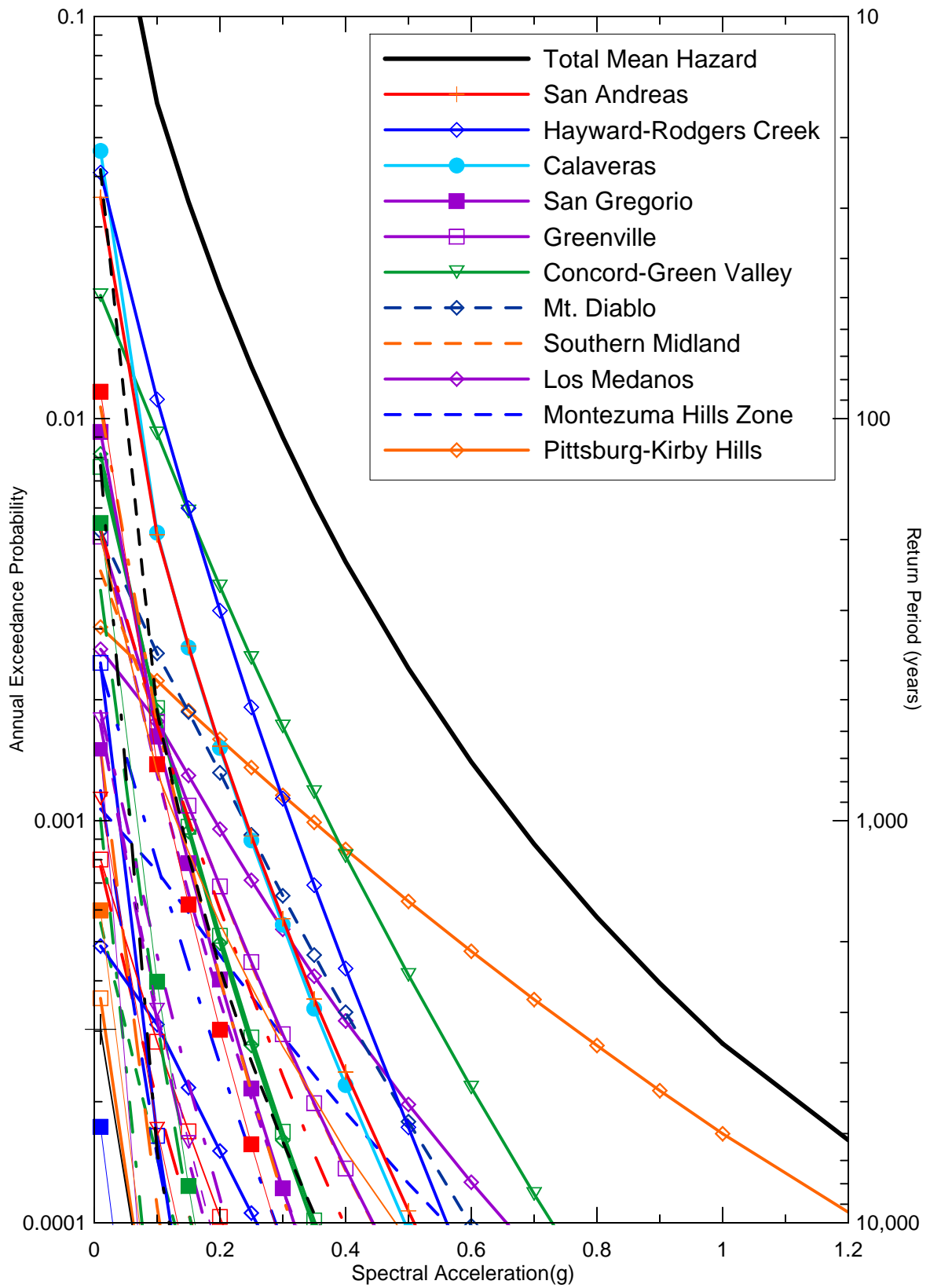


DELTA RISK
MANAGEMENT STRATEGY
CALIFORNIA

Project No. 26815900

SEISMIC SOURCE CONTRIBUTIONS TO MEAN
PEAK HORIZONTAL ACCELERATION TIME-
DEPENDENT HAZARD FOR MONTEZUMA SLOUGH
FOR 2005

Figure
6-15a



Delta Risk\figures\DR3-11-2005.grf

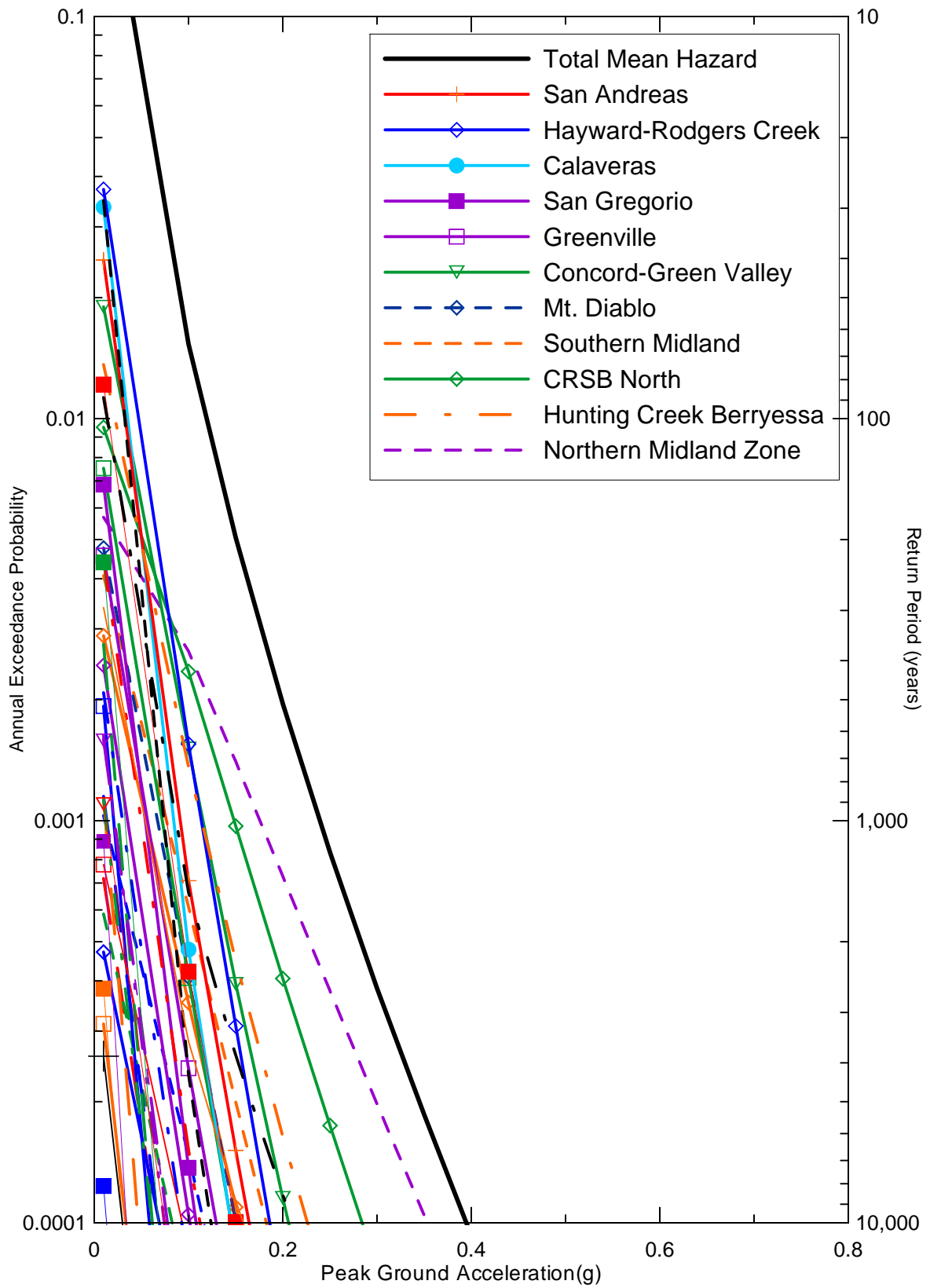


DELTA RISK
MANAGEMENT STRATEGY
CALIFORNIA

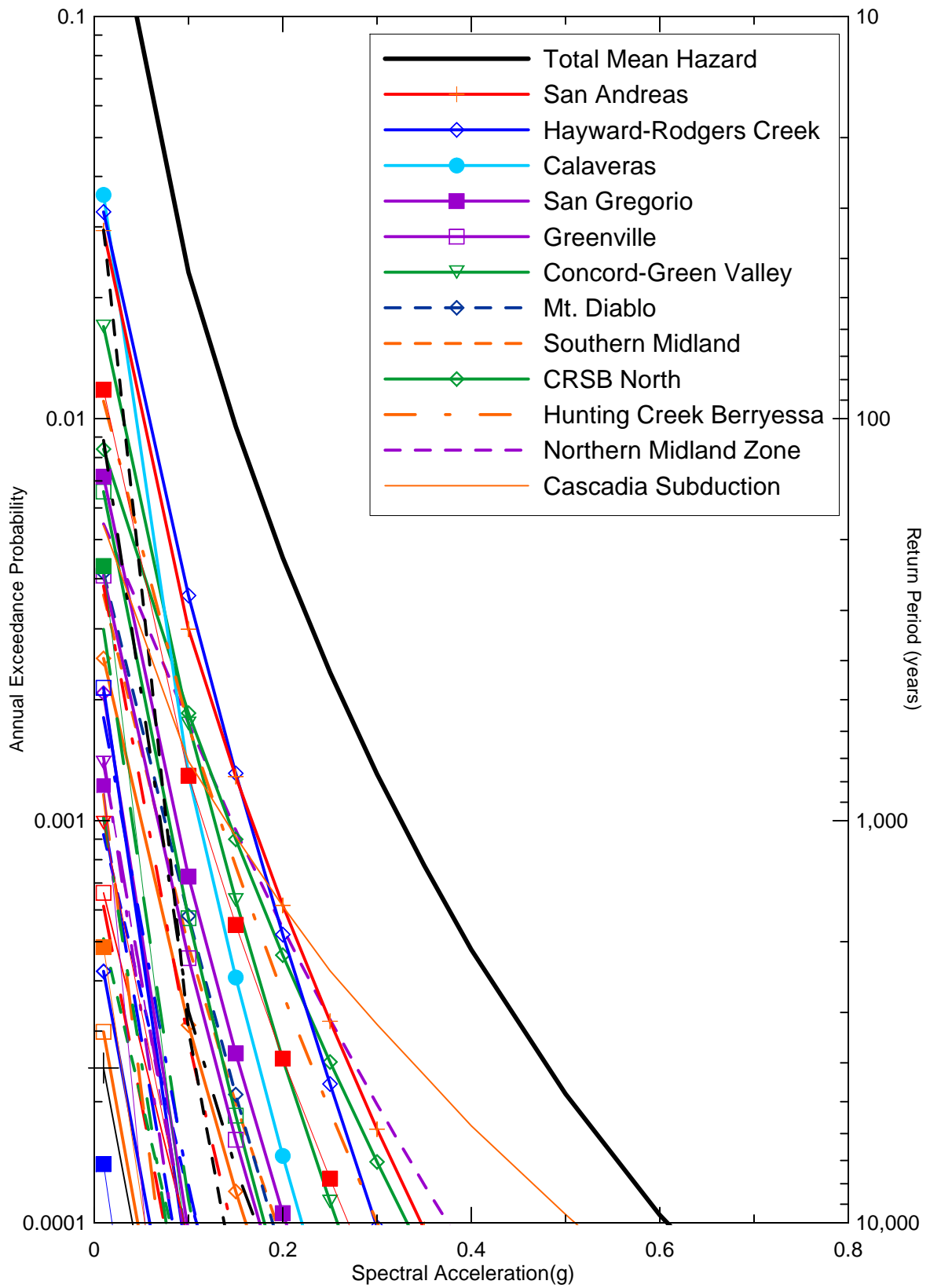
Project No. 26815900

SEISMIC SOURCE CONTRIBUTIONS TO 1.0 SEC
HORIZONTAL SPECTRAL ACCELERATION TIME-
DEPENDENT HAZARD FOR MONTEZUMA SLOUGH
FOR 2005

Figure
6-15b



Delta Risk\figures\DR6-pga-2005.grf



Delta Risk\figures\DR6-11-2005.grf

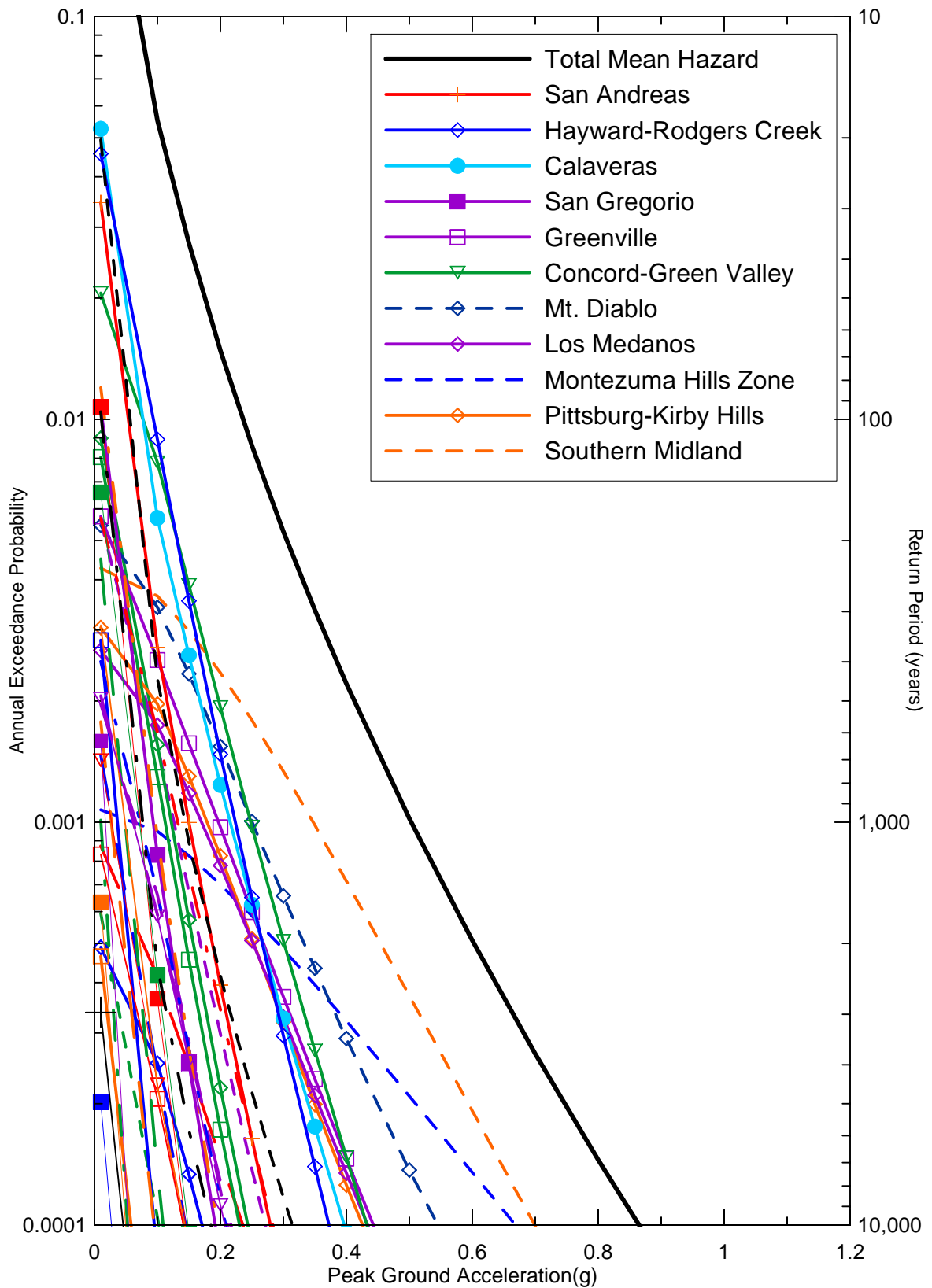


DELTA RISK
MANAGEMENT STRATEGY
CALIFORNIA

Project No. 26815900

SEISMIC SOURCE CONTRIBUTIONS TO 1.0 SEC
HORIZONTAL SPECTRAL ACCELERATION TIME-
DEPENDENT HAZARD FOR SACRAMENTO
FOR 2005

Figure
6-16b



Delta Risk\figures\DR1-ppga-2005.grf

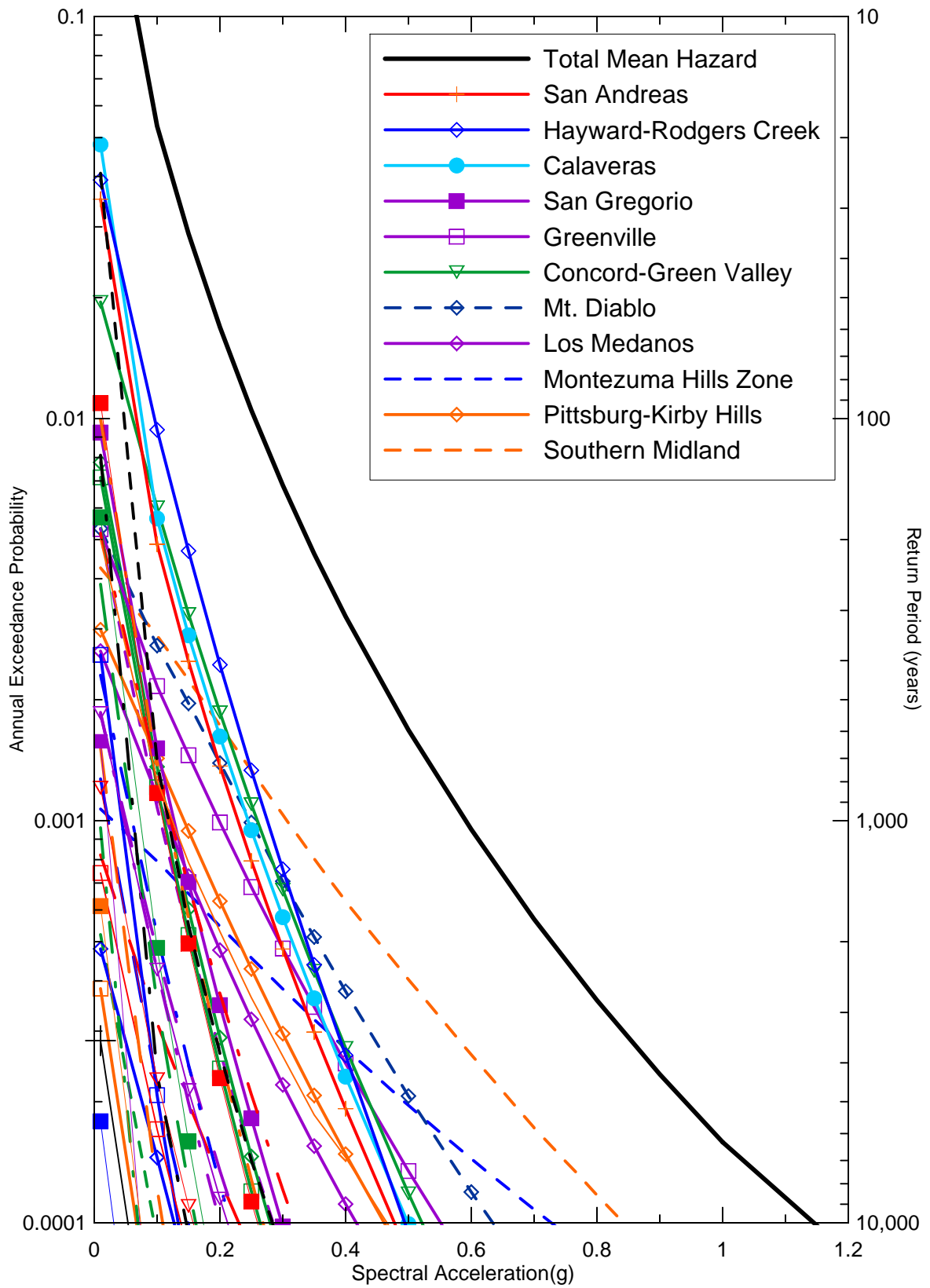


DELTA RISK
MANAGEMENT STRATEGY
CALIFORNIA

Project No. 26815900

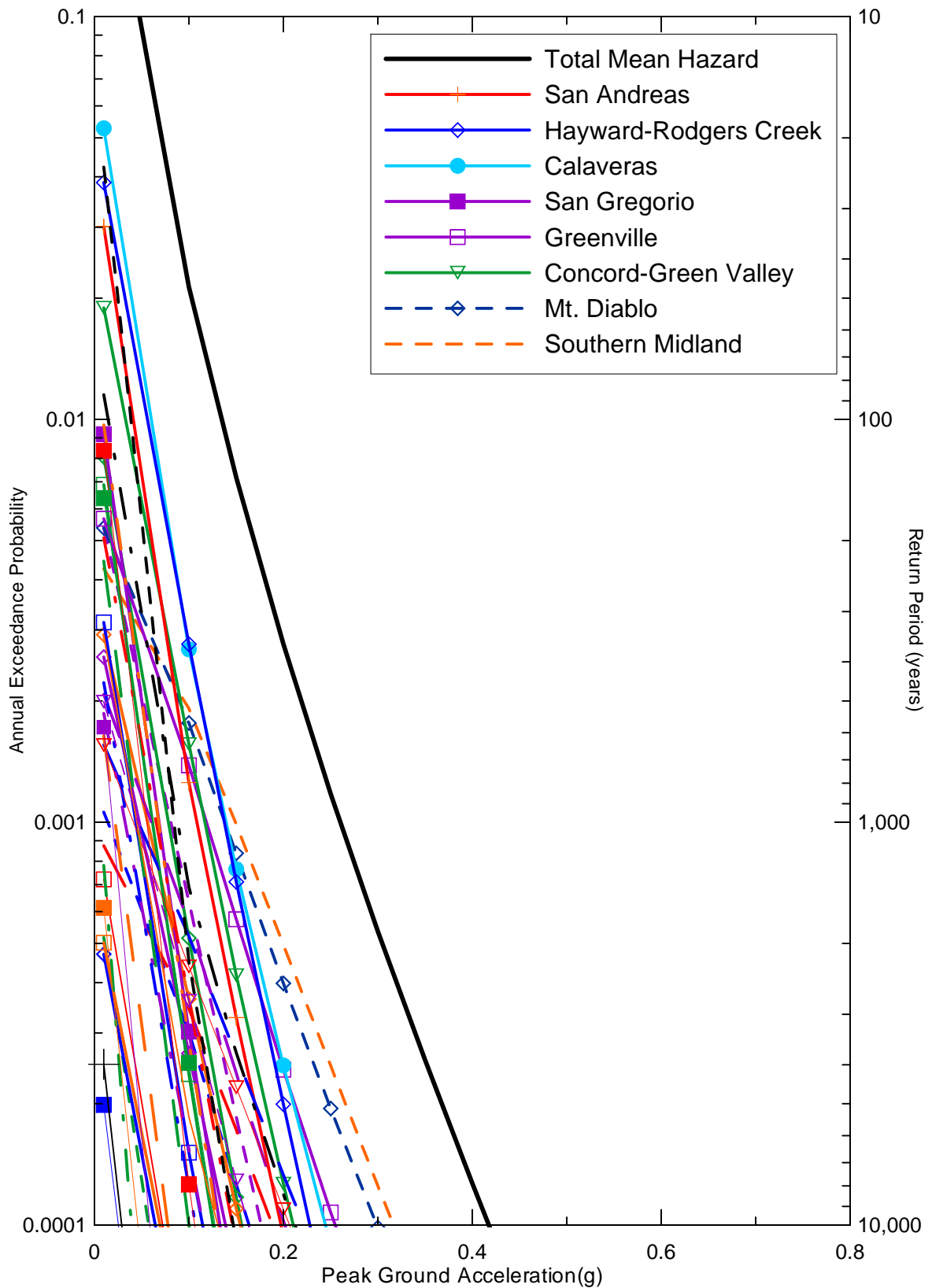
SEISMIC SOURCE CONTRIBUTIONS TO MEAN
PEAK HORIZONTAL ACCELERATION TIME-
DEPENDENT HAZARD FOR SHERMAN ISLAND
FOR 2005

Figure
6-17a



Delta Risk\figures\DR1-11-2005.grf

	<p>DELTA RISK MANAGEMENT STRATEGY CALIFORNIA</p>	<p>SEISMIC SOURCE CONTRIBUTIONS TO 1.0 SEC HORIZONTAL SPECTRAL ACCELERATION TIME- DEPENDENT HAZARD FOR SHERMAN ISLAND FOR 2005</p>	<p>Figure 6-17b</p>
<p>Project No. 26815900</p>			



Delta Risk\figures\DR5-pga-2005.grf

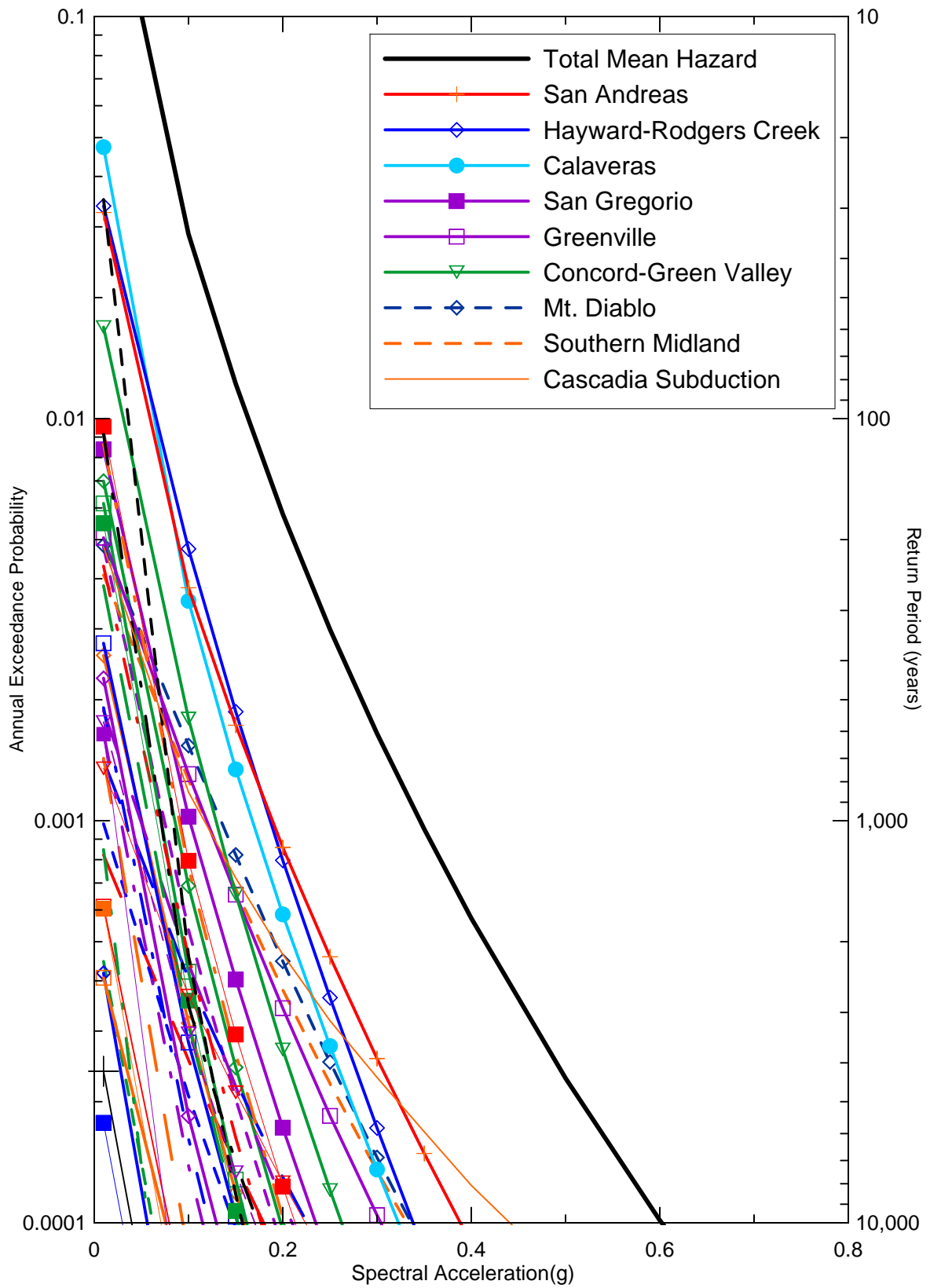


DELTA RISK
MANAGEMENT STRATEGY
CALIFORNIA

Project No. 26815900

SEISMIC SOURCE CONTRIBUTIONS TO MEAN
PEAK HORIZONTAL ACCELERATION TIME-
DEPENDENT HAZARD FOR STOCKTON
FOR 2005

Figure
6-18a



Delta Risk\figures\DR5-11-2005.grf

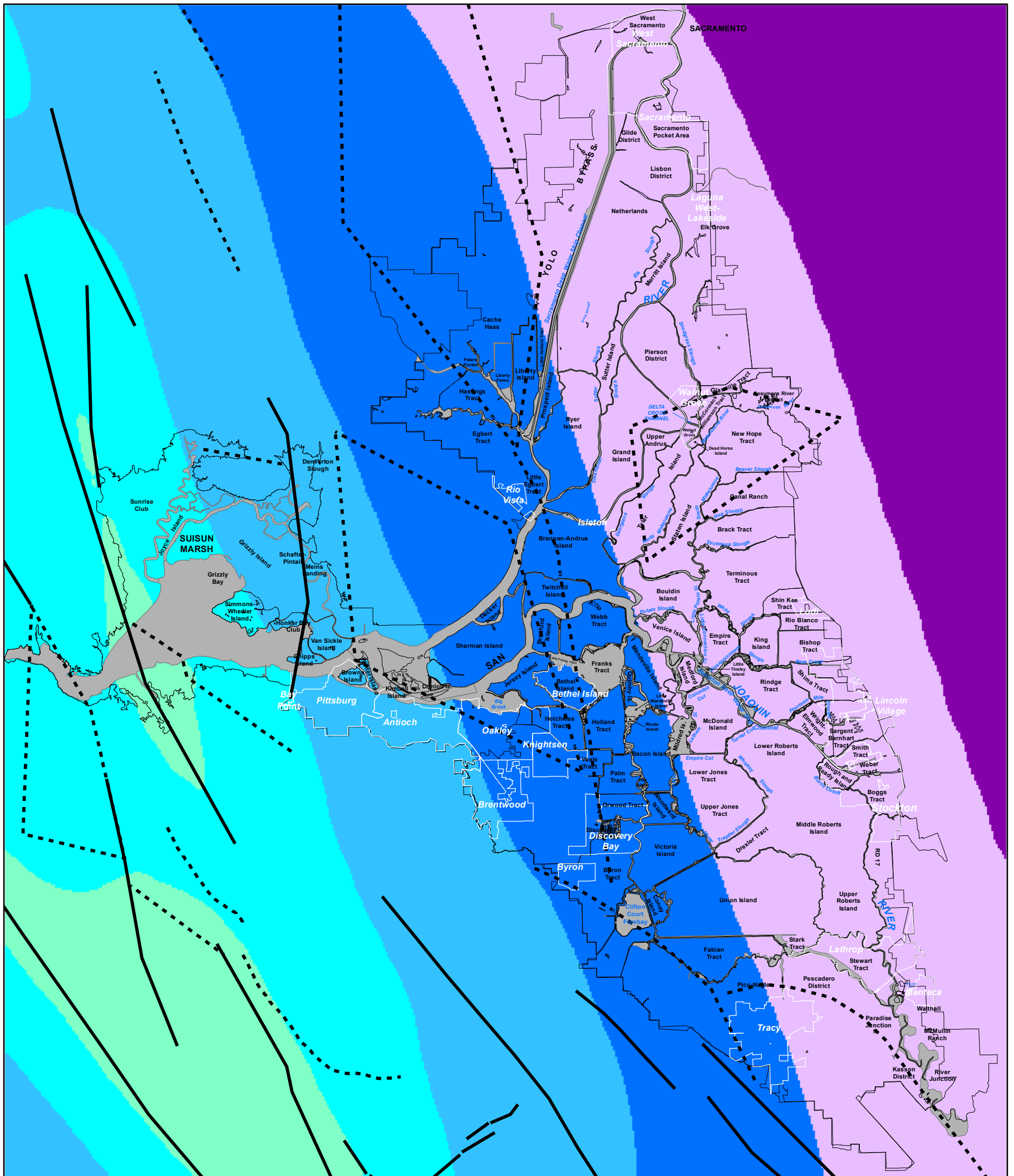


DELTA RISK
MANAGEMENT STRATEGY
CALIFORNIA

Project No. 26815900

SEISMIC SOURCE CONTRIBUTIONS TO 1.0 SEC
HORIZONTAL SPECTRAL ACCELERATION TIME-
DEPENDENT HAZARD FOR STOCKTON
FOR 2005

Figure
6-18b



Legend

Mapped Faults

— Surficial faults used in the hazard analysis

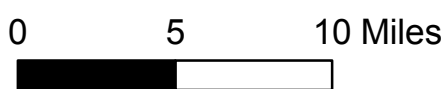
Blind Faults

- - - Blind faults used in the hazard analysis

□ Legal Delta and Suisun Marsh Boundary

PGA, 100 Year Return Period

0.00 - 0.10	0.36 - 0.40
0.11 - 0.15	0.41 - 0.45
0.16 - 0.20	0.46 - 0.50
0.21 - 0.25	0.51 - 0.55
0.26 - 0.30	0.56 - 0.60
0.31 - 0.35	0.61 - 0.65
	0.66 - 0.70

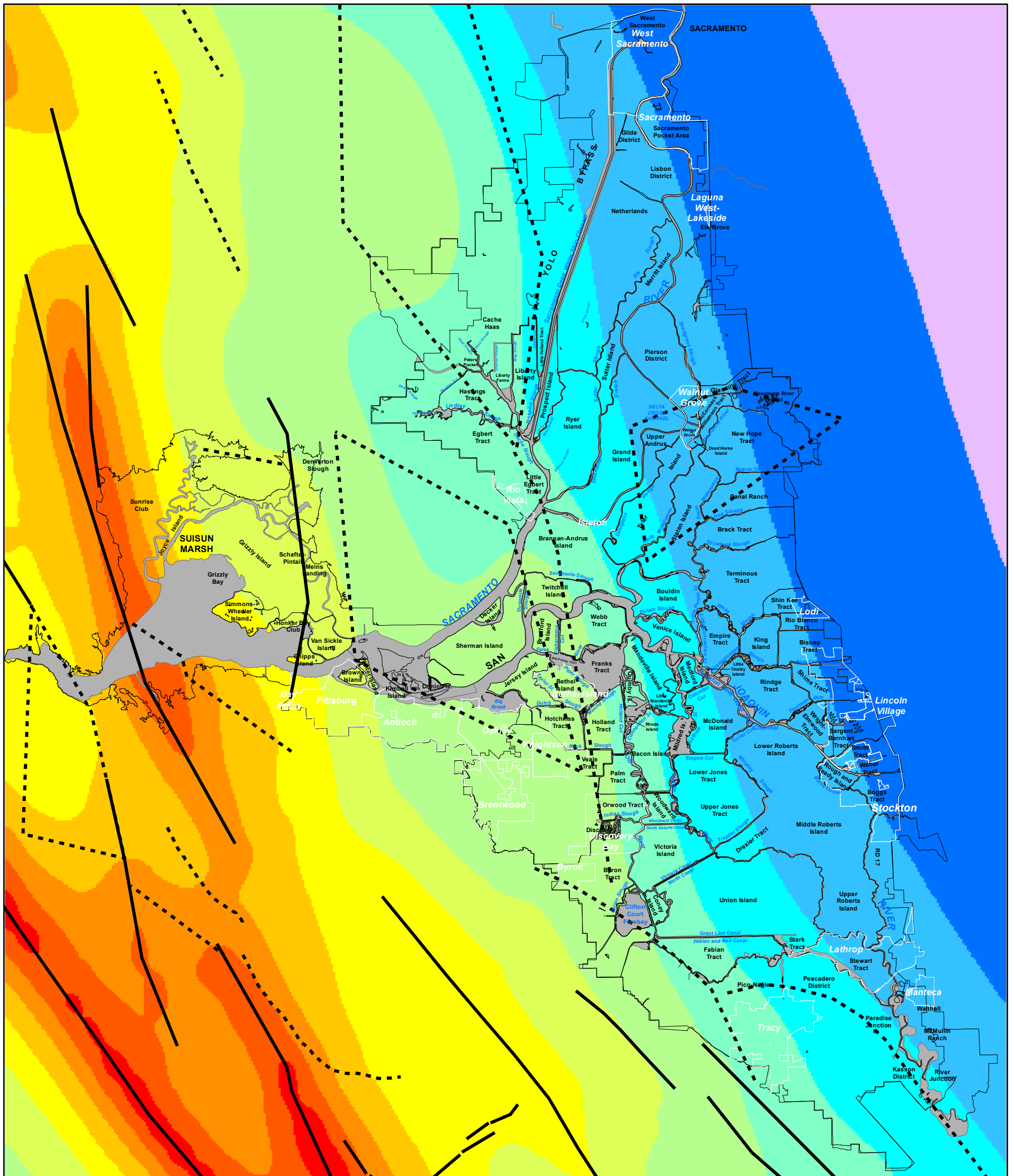


DRMS

26815431

PGA Hazard for a 100-Year Return Period

FIGURE 6-19



Legend

Mapped Faults

— Surficial faults used in the hazard analysis

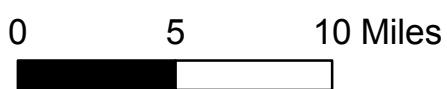
Blind Faults

- - - Blind faults used in the hazard analysis

□ Legal Delta and Suisun Marsh Boundary

PGA, 500 Year Return Period

0.00 - 0.10	0.36 - 0.40
0.11 - 0.15	0.41 - 0.45
0.16 - 0.20	0.46 - 0.50
0.21 - 0.25	0.51 - 0.55
0.26 - 0.30	0.56 - 0.60
0.31 - 0.35	0.61 - 0.65
	0.66 - 0.70

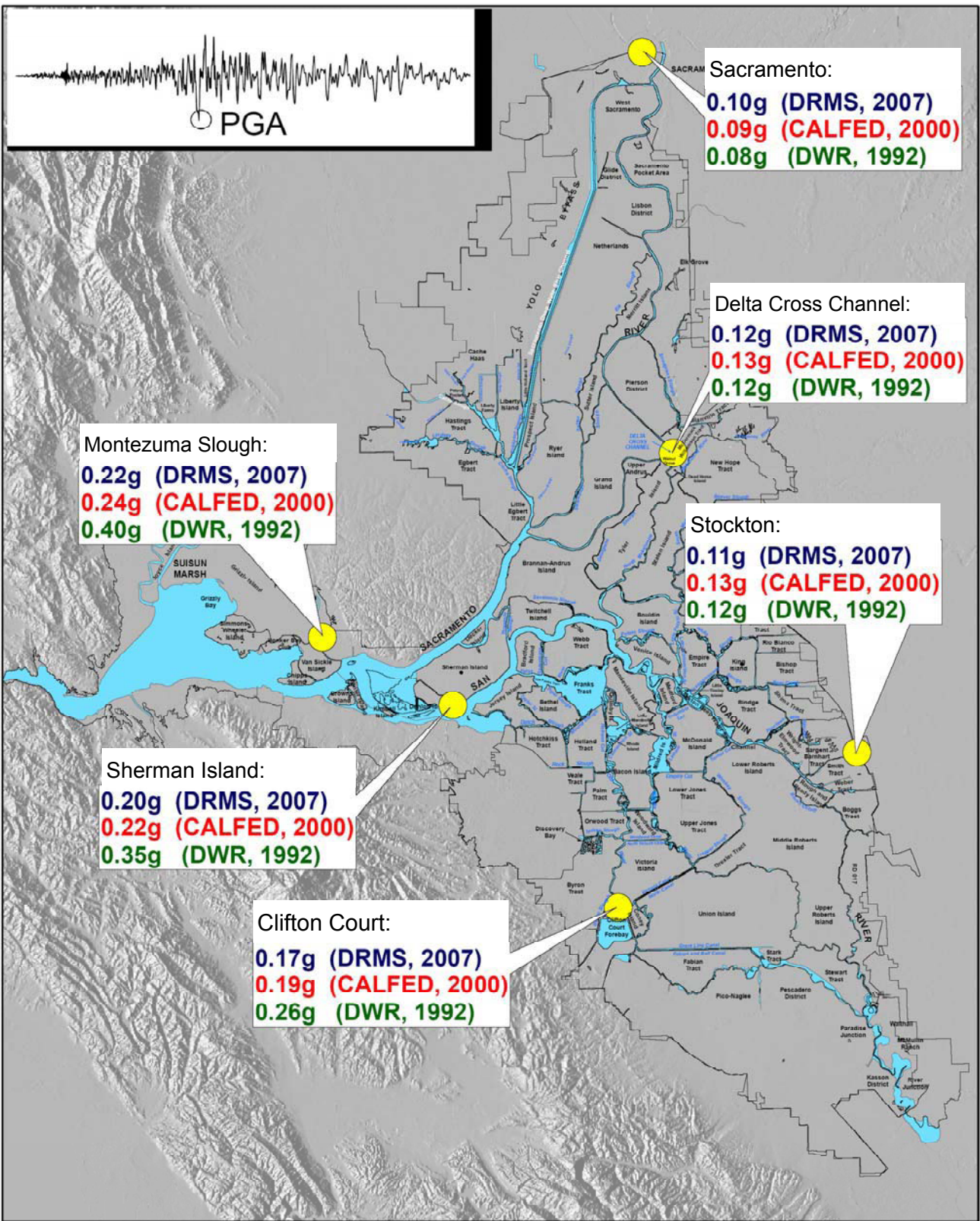


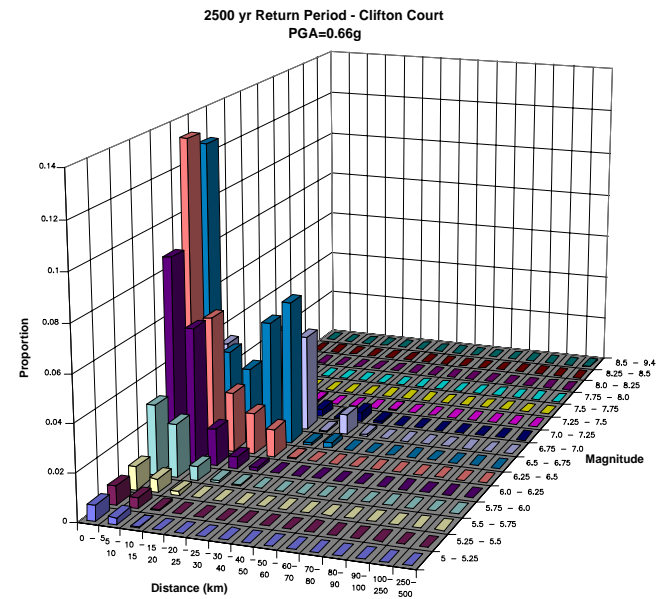
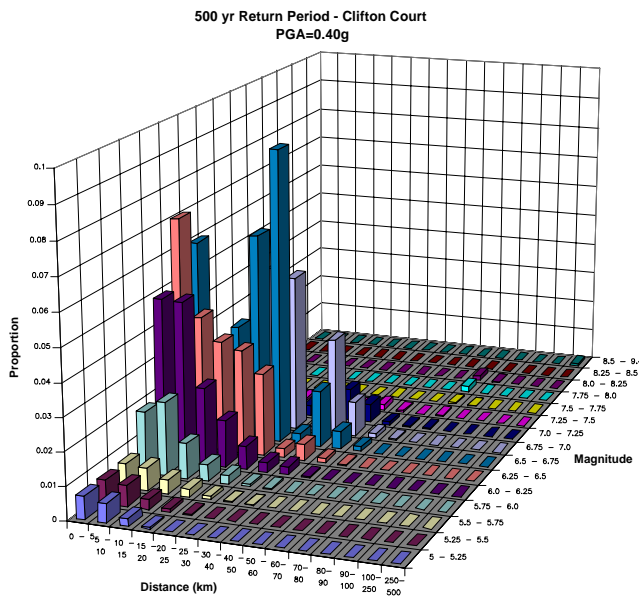
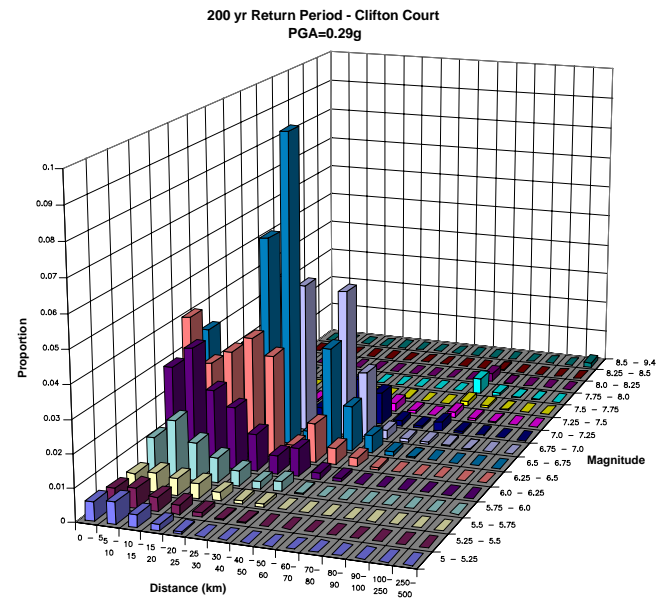
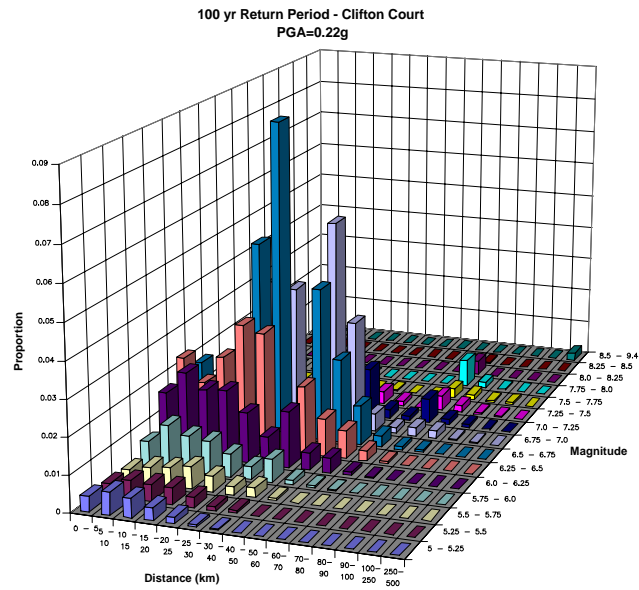
DRMS

26815431

PGA Hazard for a 500-Year Return Period

FIGURE 6-20



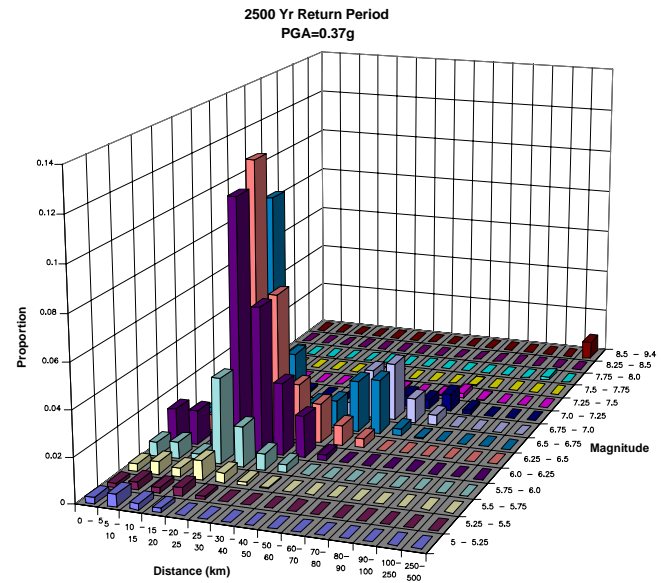
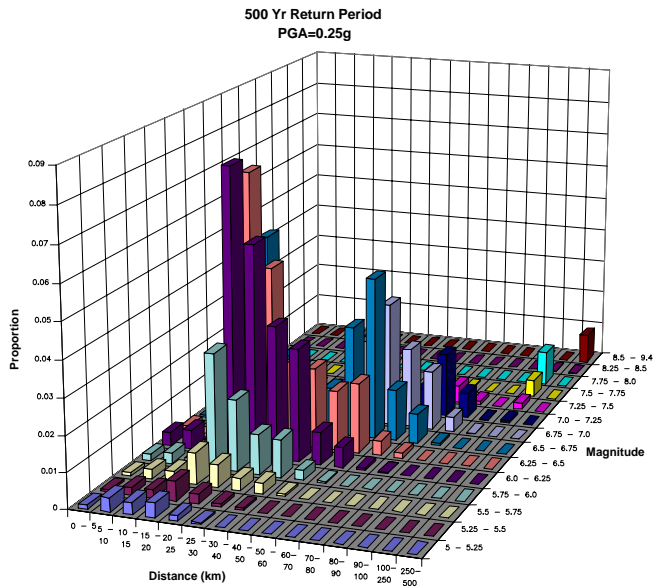
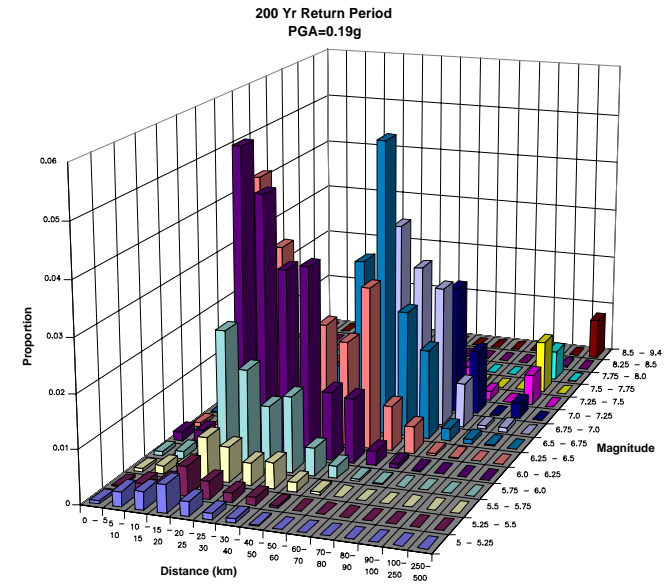
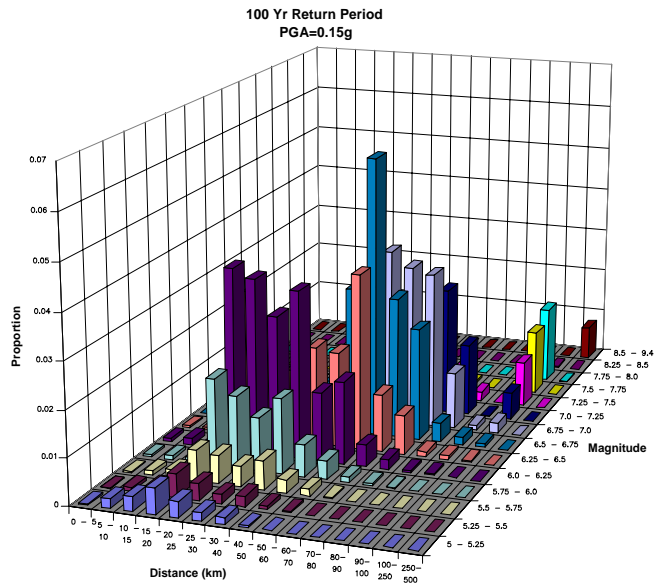


DELTA RISK MANAGEMENT STRATEGY
CALIFORNIA

PROJECT No. 26815621

MAGNITUDE AND DISTANCE CONTRIBUTIONS
TO THE MEAN PEAK HORIZONTAL
ACCELERATION HAZARD FOR
CLIFTON COURT FOR 2005

Figure
6-22

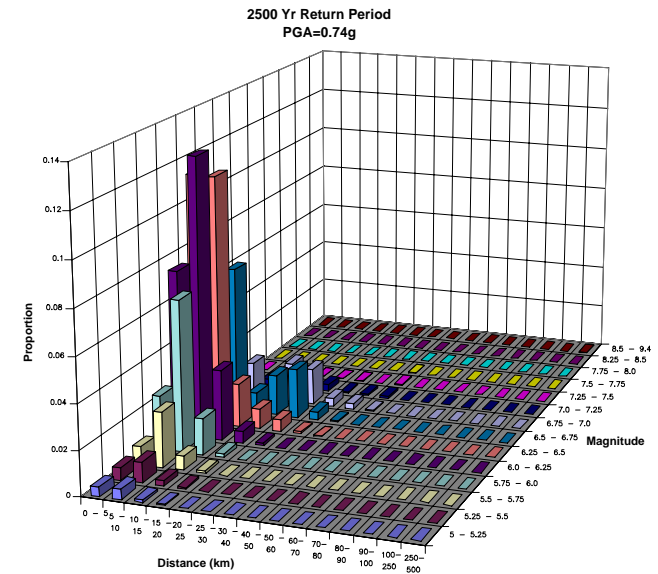
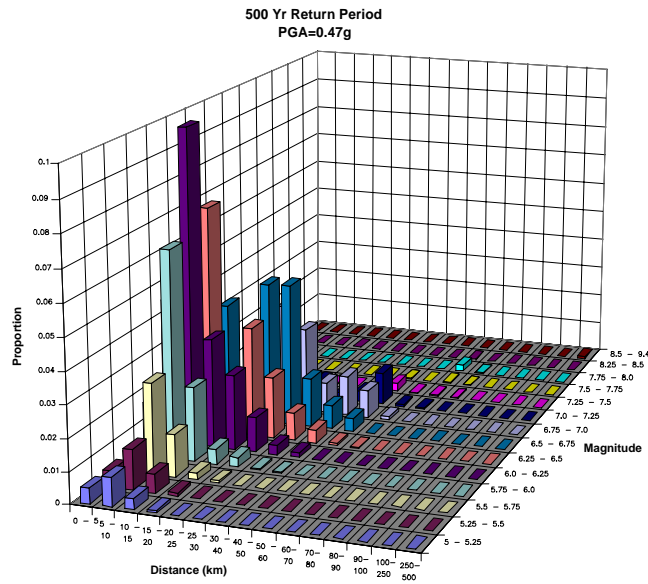
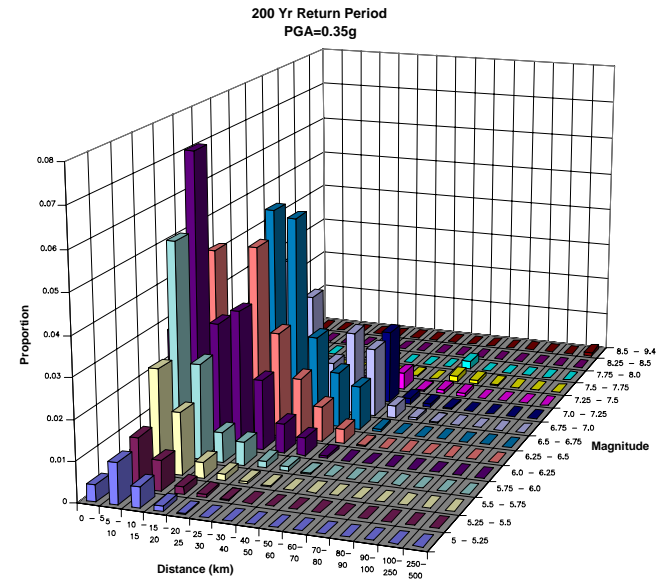
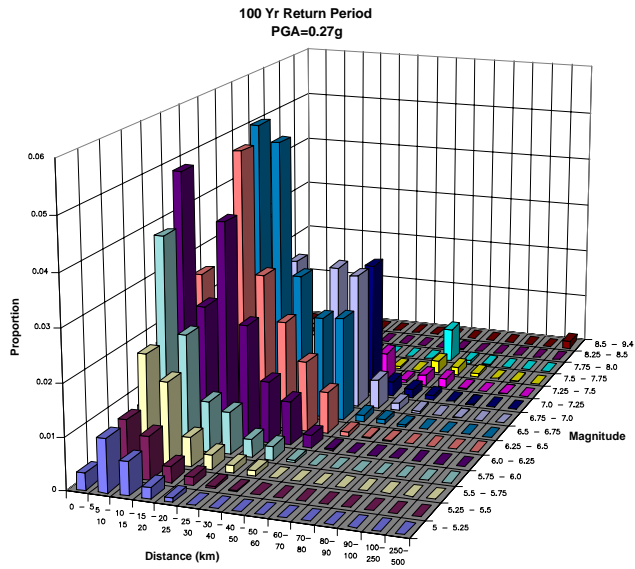


DELTA RISK MANAGEMENT STRATEGY
CALIFORNIA

PROJECT No. 26815621

MAGNITUDE AND DISTANCE CONTRIBUTIONS
TO THE MEAN PEAK HORIZONTAL
ACCELERATION HAZARD FOR
DELTA CROSS CHANNEL FOR 2005

Figure
6-23

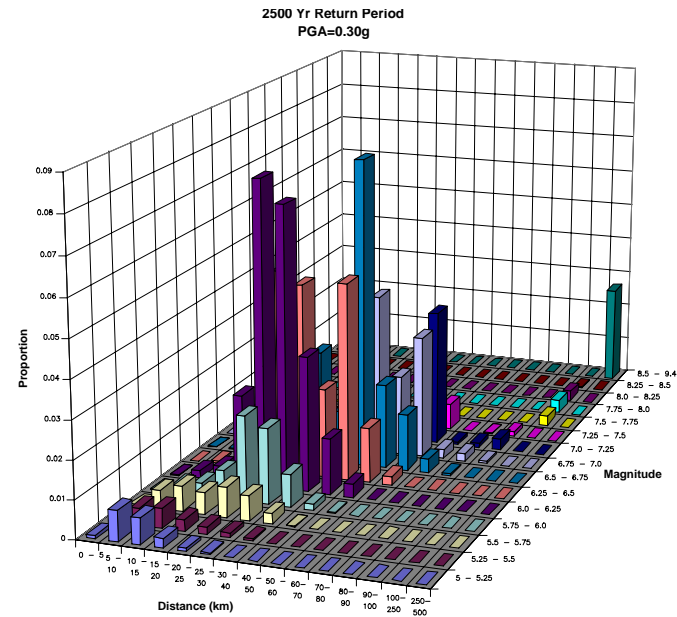
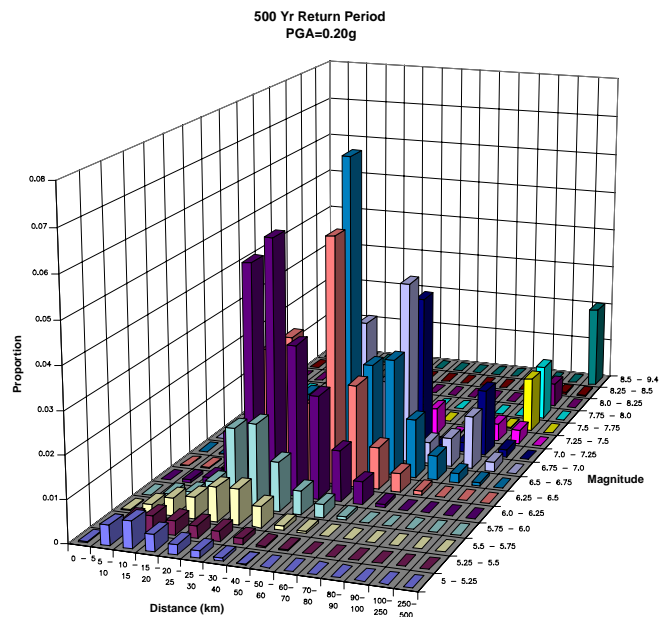
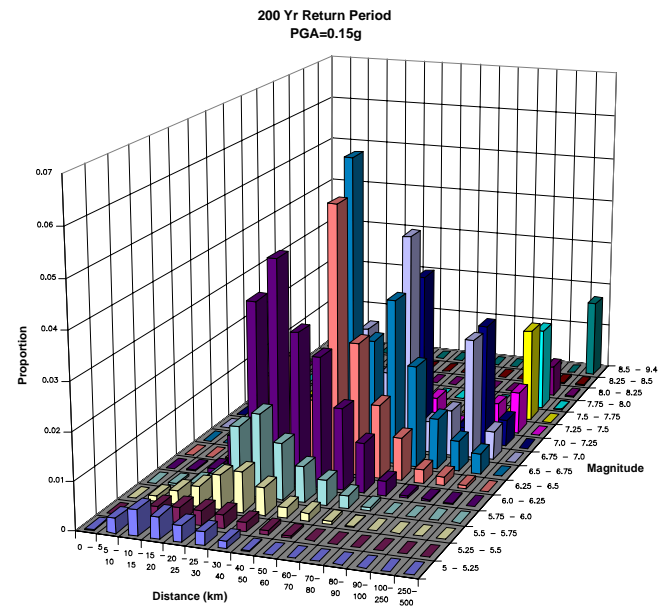
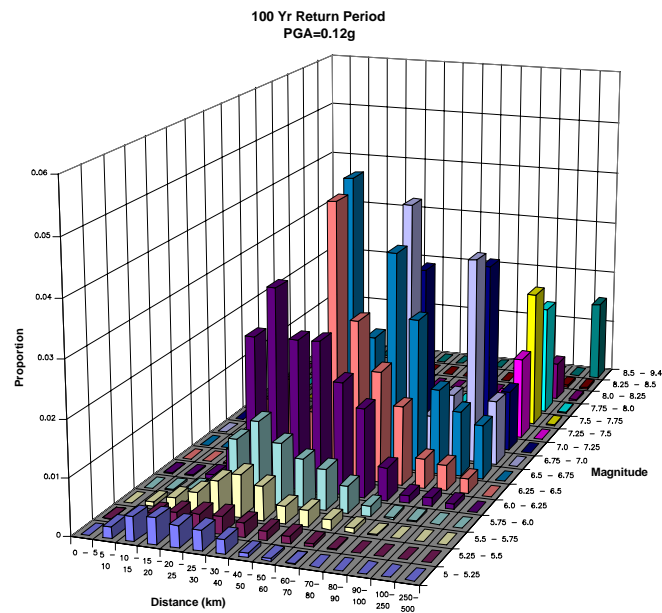


DELTA RISK MANAGEMENT STRATEGY
CALIFORNIA

PROJECT No. 26815621

MAGNITUDE AND DISTANCE CONTRIBUTIONS
TO THE MEAN PEAK HORIZONTAL
ACCELERATION HAZARD FOR
MONTEZUMA SLOUGH FOR 2005

Figure
6-24

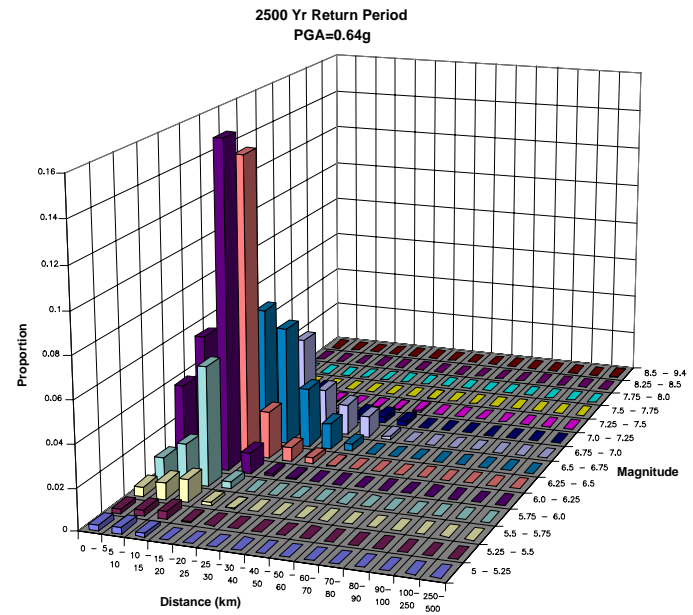
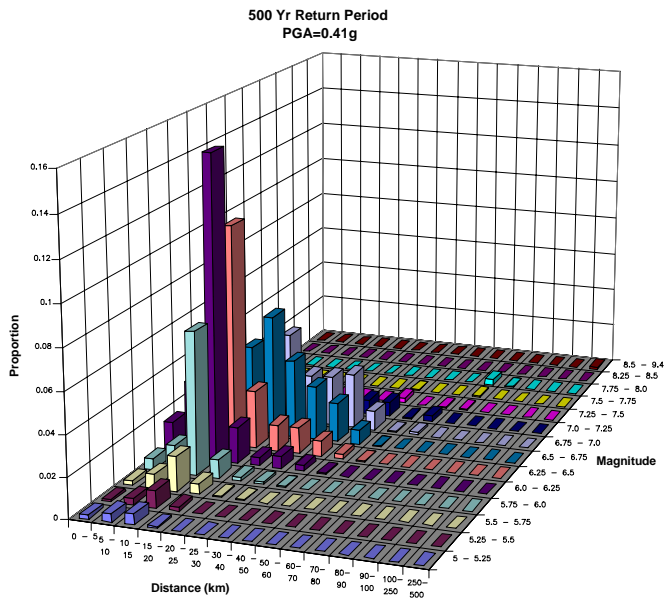
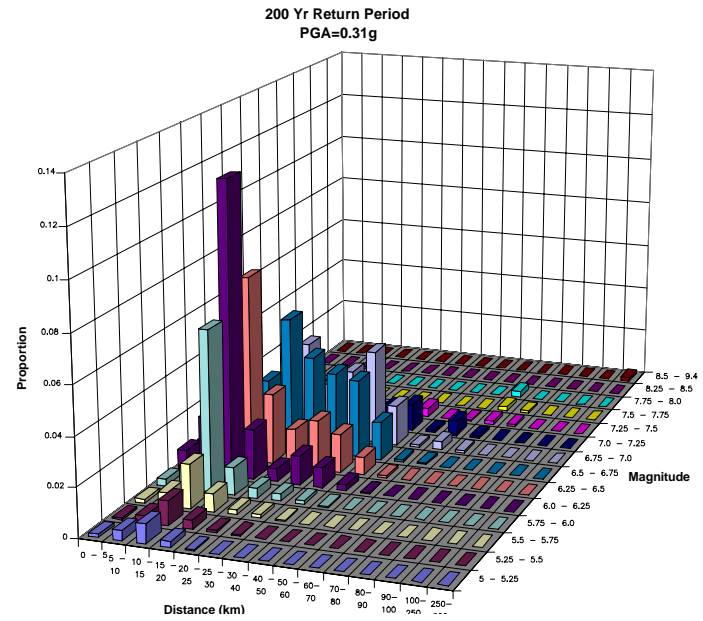
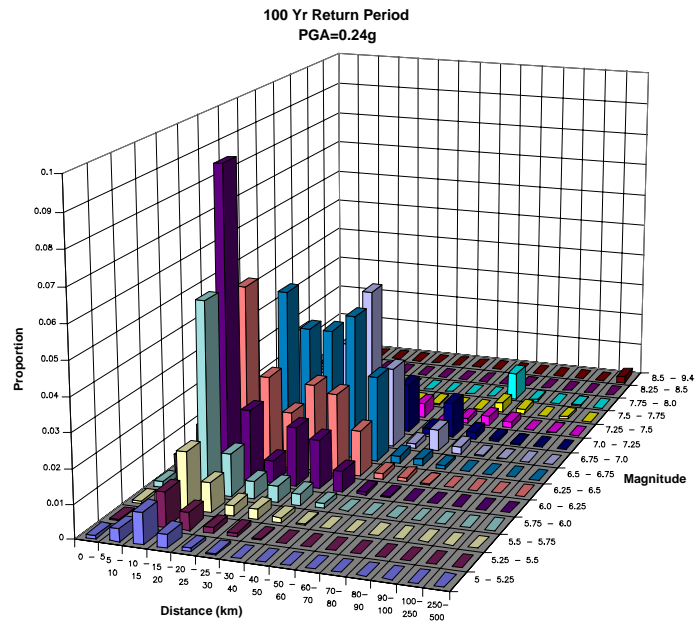


DELTA RISK MANAGEMENT STRATEGY
CALIFORNIA

PROJECT No. 26815621

MAGNITUDE AND DISTANCE CONTRIBUTIONS
TO THE MEAN PEAK HORIZONTAL
ACCELERATION HAZARD FOR
SACRAMENTO FOR 2005

Figure
6-25

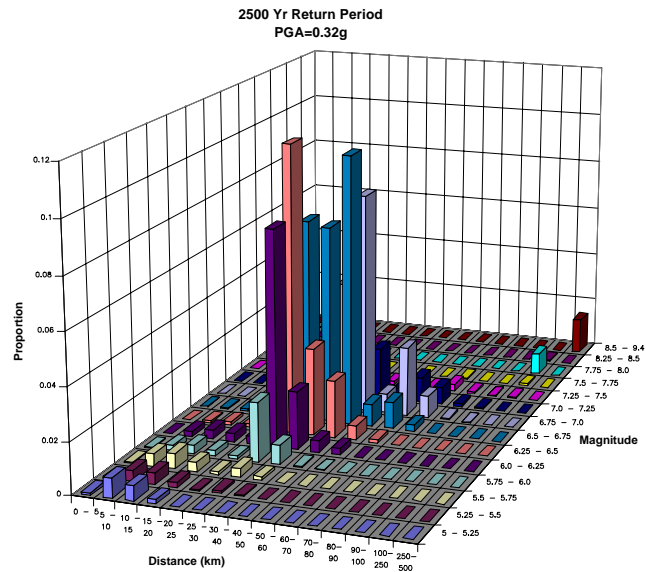
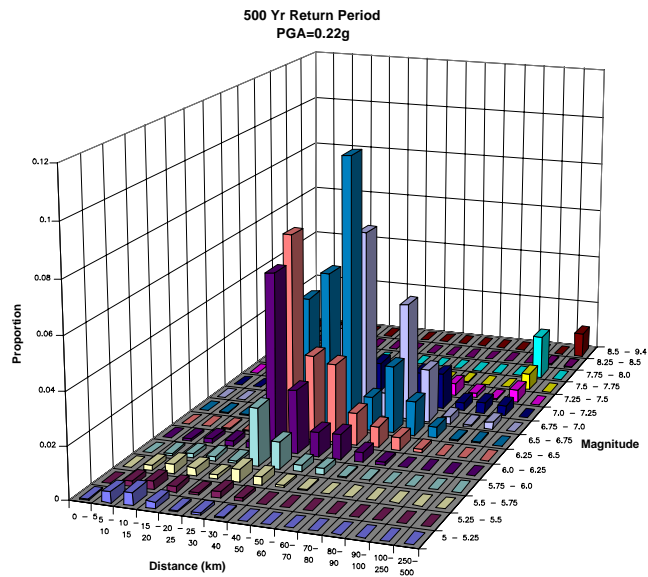
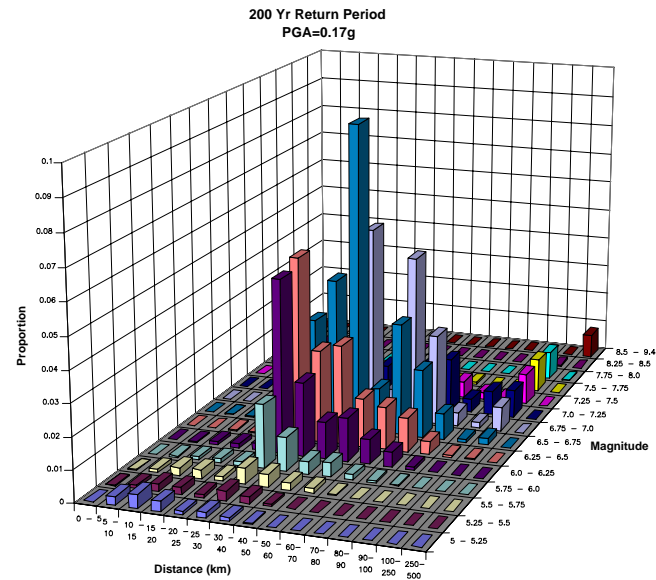
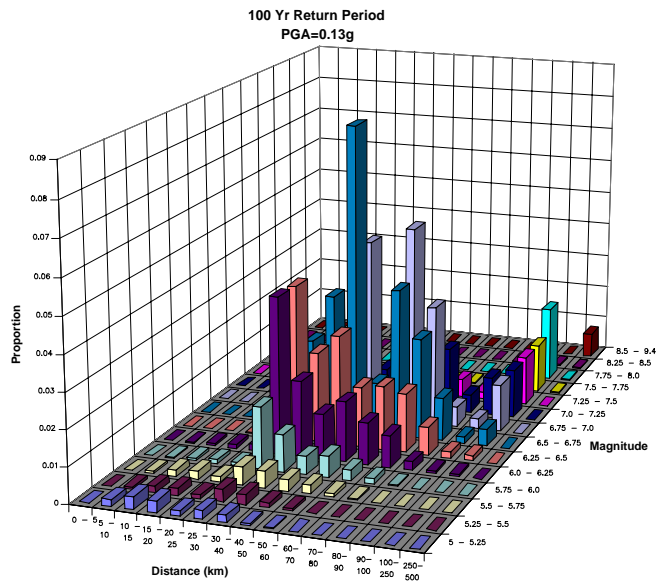


DELTA RISK MANAGEMENT STRATEGY
CALIFORNIA

PROJECT No. 26815621

MAGNITUDE AND DISTANCE CONTRIBUTIONS
TO THE MEAN PEAK HORIZONTAL
ACCELERATION HAZARD FOR
SHERMAN ISLAND FOR 2005

Figure
6-26



DELTA RISK MANAGEMENT STRATEGY
CALIFORNIA

PROJECT No. 26815621

MAGNITUDE AND DISTANCE CONTRIBUTIONS
TO THE MEAN PEAK HORIZONTAL
ACCELERATION HAZARD FOR
STOCKTON FOR 2005

Figure
6-27



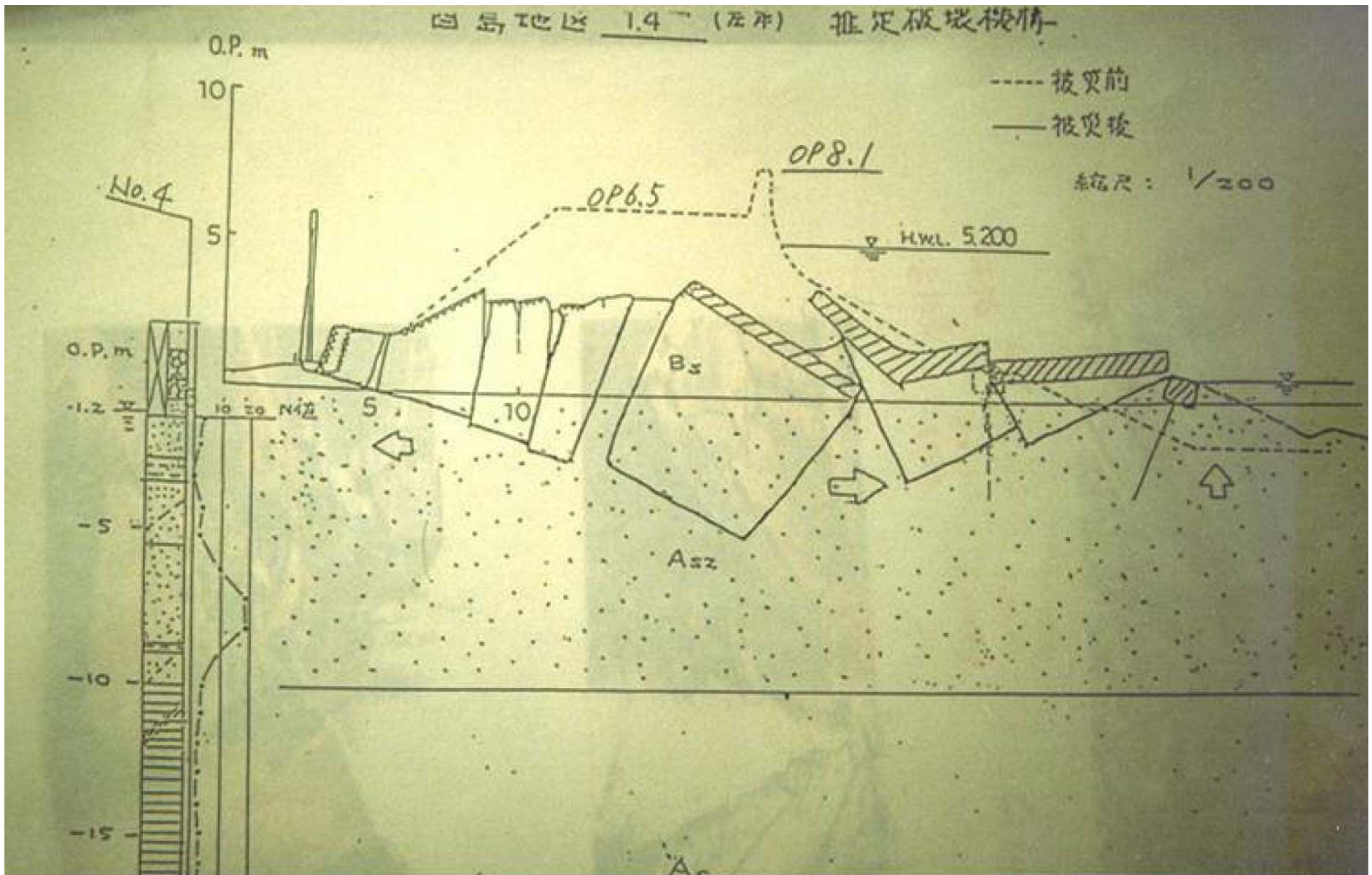
Delta Risk Management Strategy (DRMS)
Levee Fragility

URS

Project No. 26815621

Levee Slumping Histories
Earthquake Damage
During Jan 17, 1995 Kobe Earthquake
at Kobe, Japan

Figure
6-28



Delta Risk Management Strategy (DRMS)
Levee Fragility

URS

Project No. 26815621

Levee Slumping Histories
Schematic Diagram of Levee Failure
During Jan 17, 1995 Kobe Earthquake
at Kobe, Japan

Figure
6-29



Delta Risk Management Strategy (DRMS)
Levee Fragility



Project No. 26815621

Levee Slumping Histories
Earthquake Damage
During May 18, 1940
Imperial Valley Earthquake

Figure
6-30



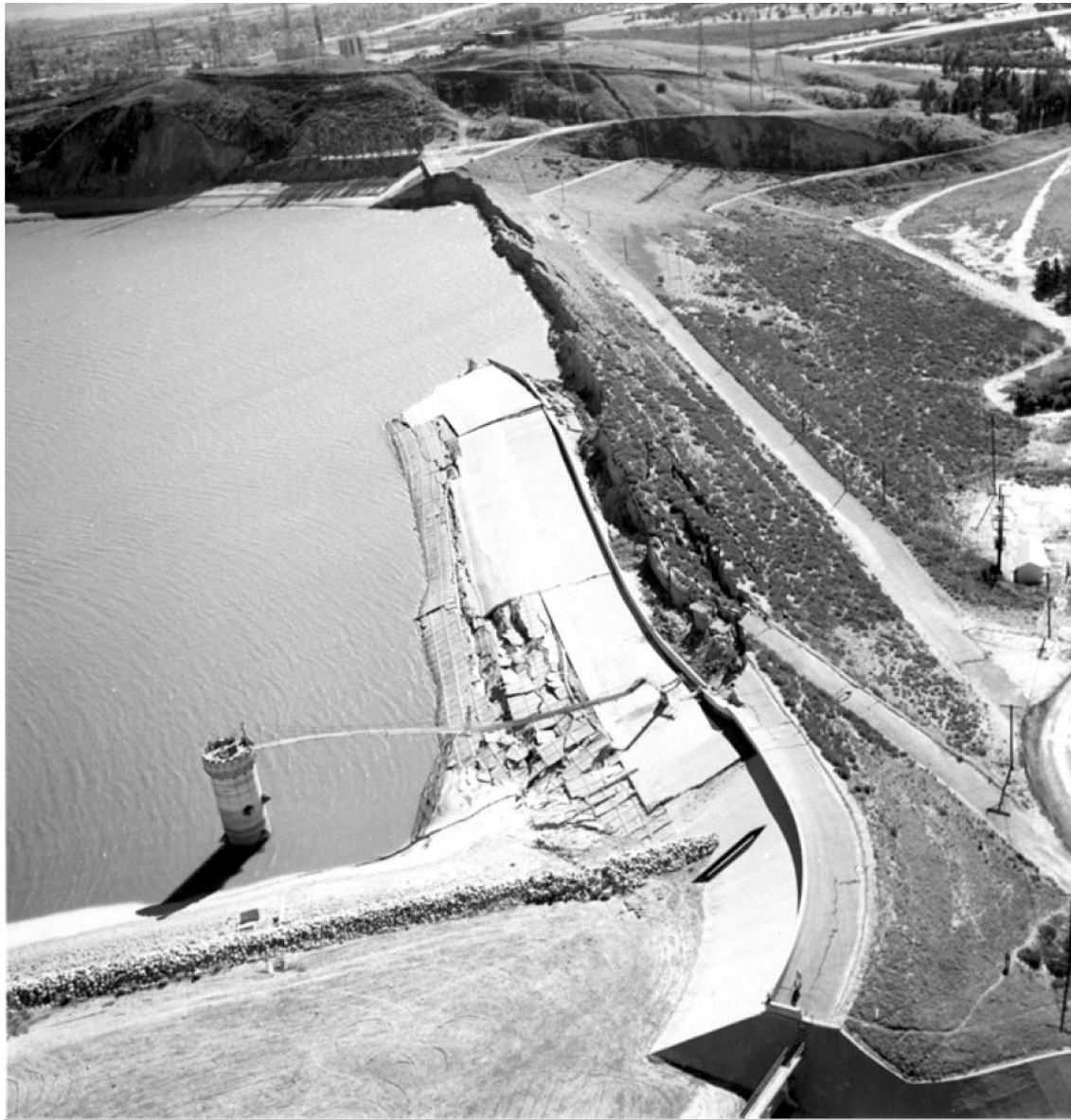
Delta Risk Management Strategy (DRMS)
Levee Fragility

URS

Project No. 26815621

Levee Slumping Histories
Earthquake Damage
During October 18, 1989
Loma Prieta Earthquake
(Moss Landing)

Figure
6-31



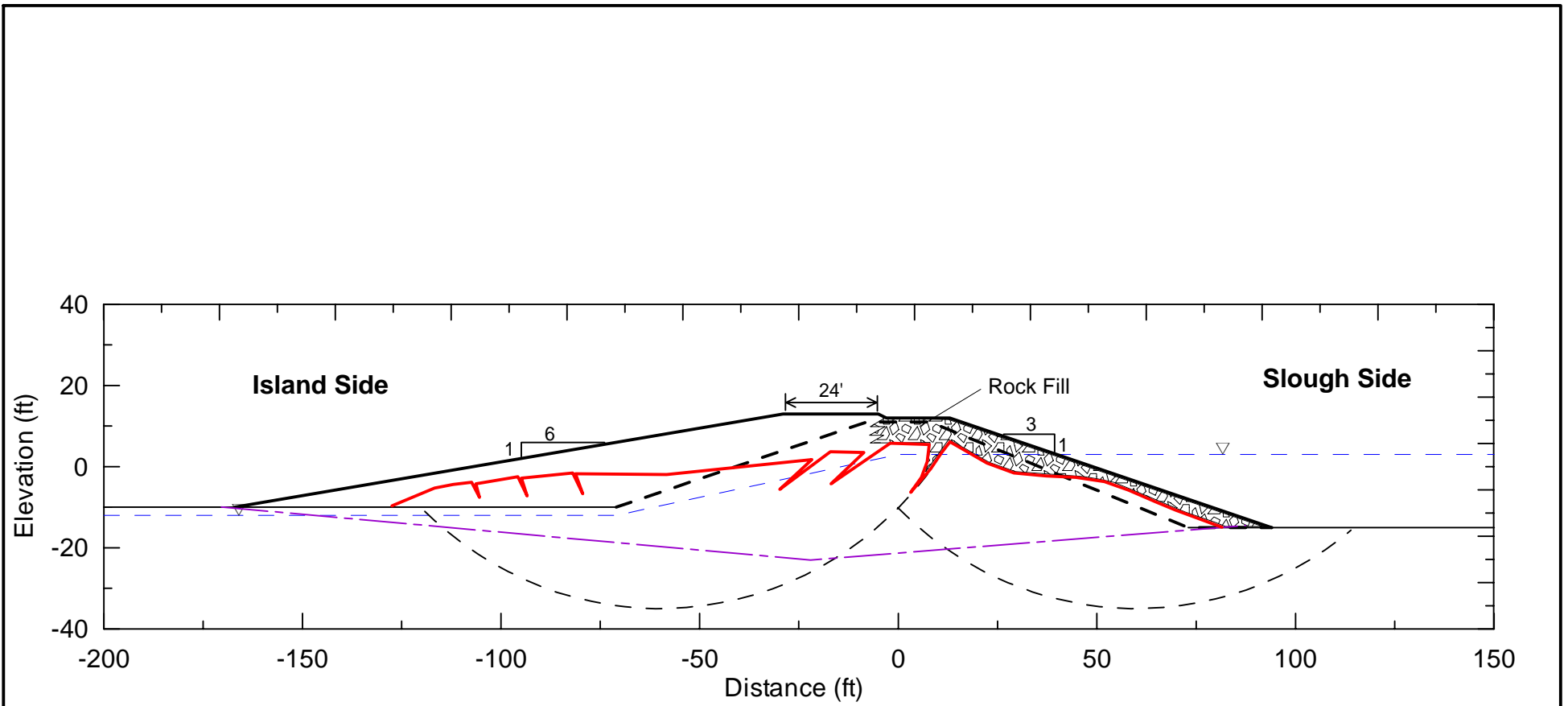
Delta Risk Management Strategy (DRMS)
Levee Fragility

URS

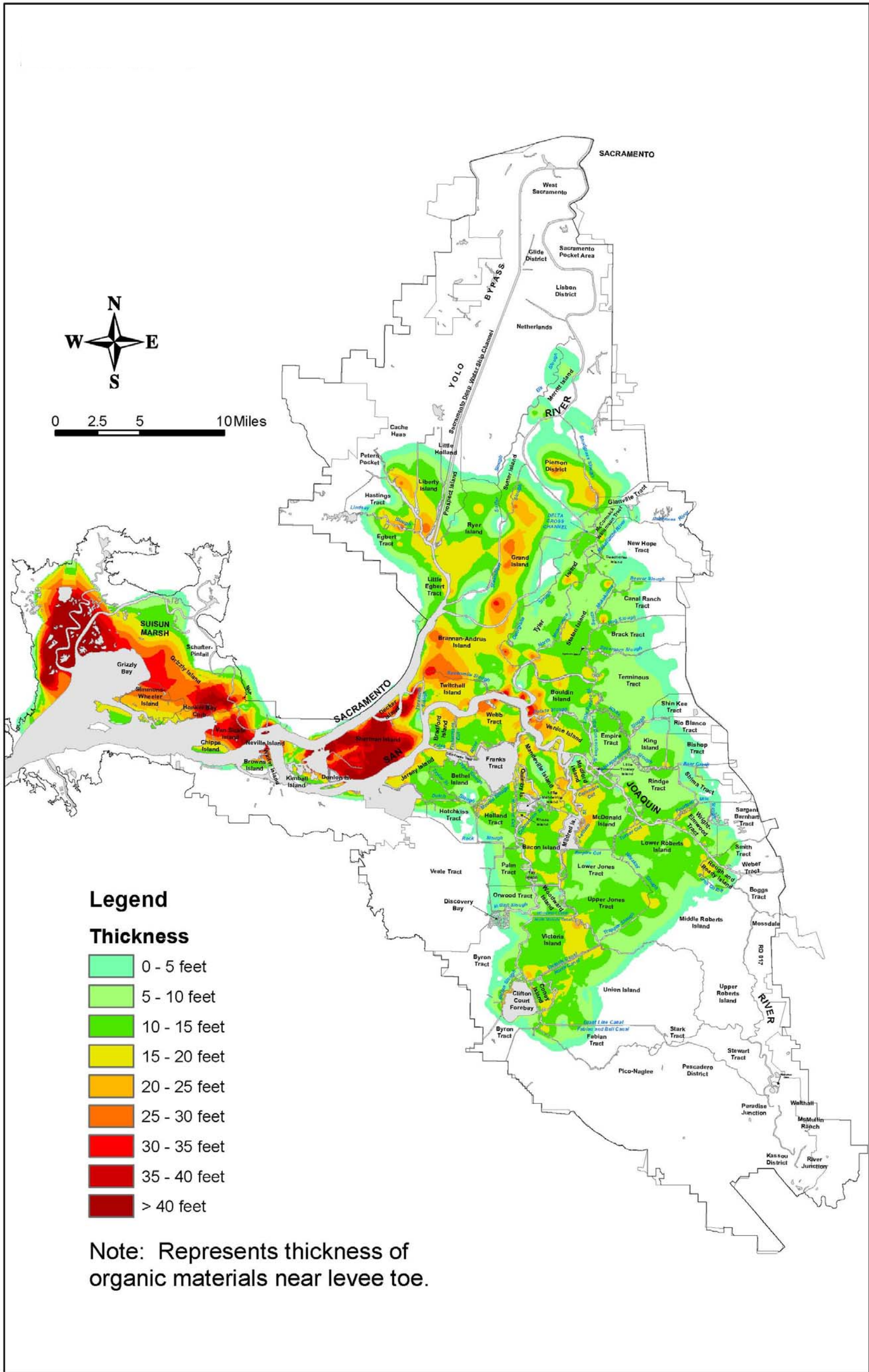
Project No. 26815621

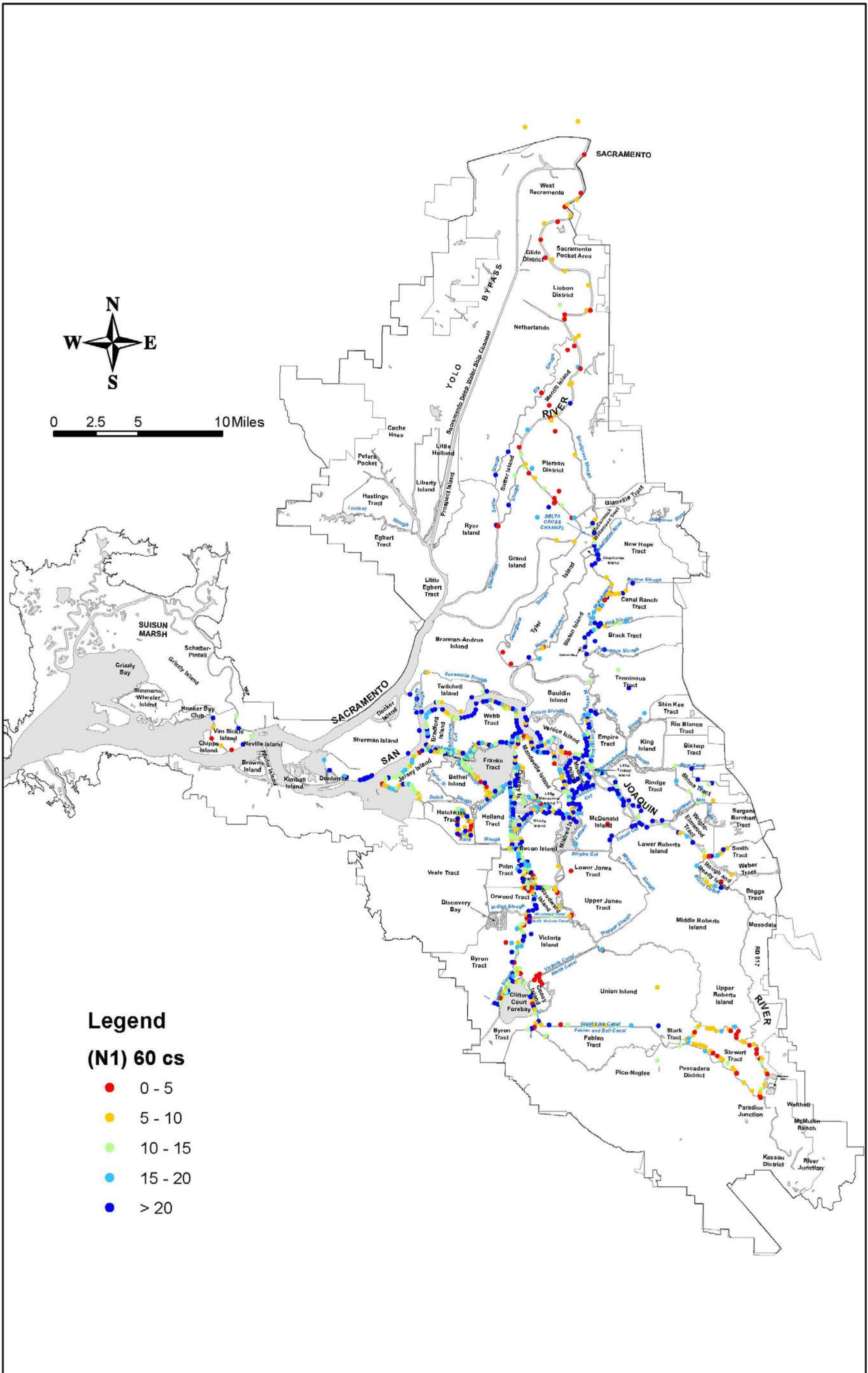
Dam Slumping Histories
Earthquake Damage
During February 11, 1971
San Fernando Earthquake
(Van Norman Dam)

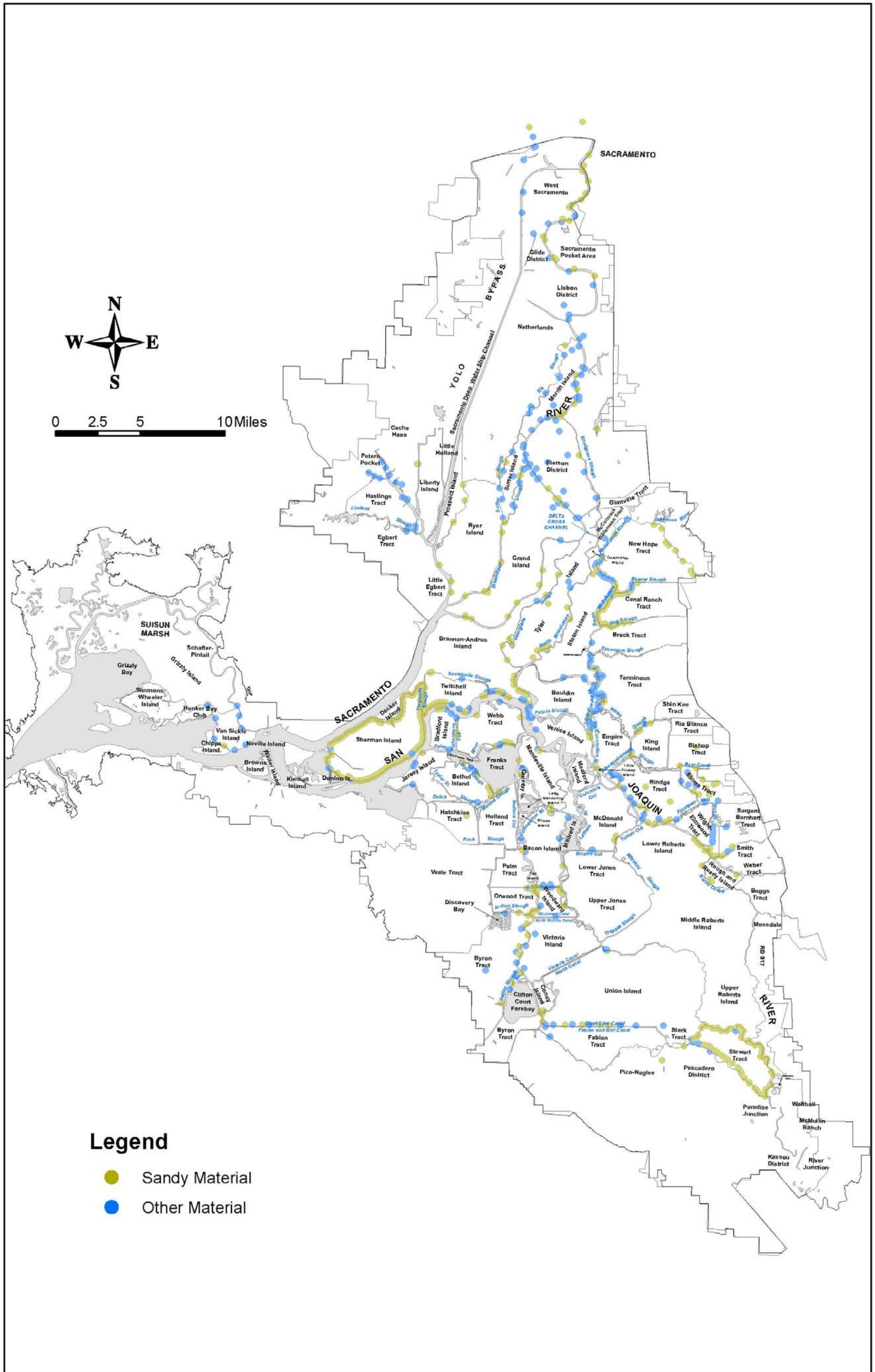
Figure
6-32

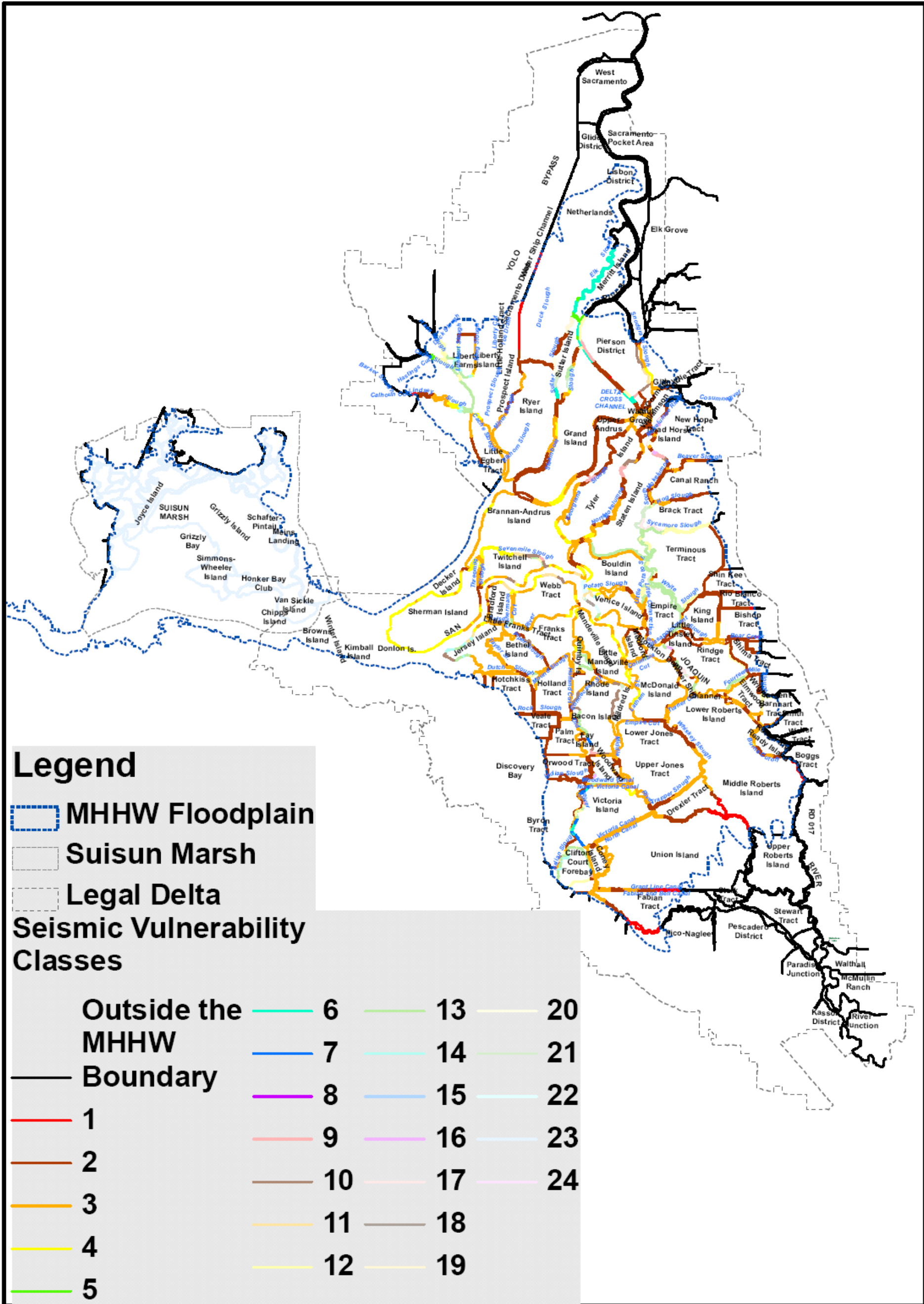


Delta Risk Management Strategy (DRMS) Levee Fragility		Schematic Diagram of Levee Slumping and Proposed Emergency Repair Method	Figure 6-33
URS	Project No. 26815621		









Legend

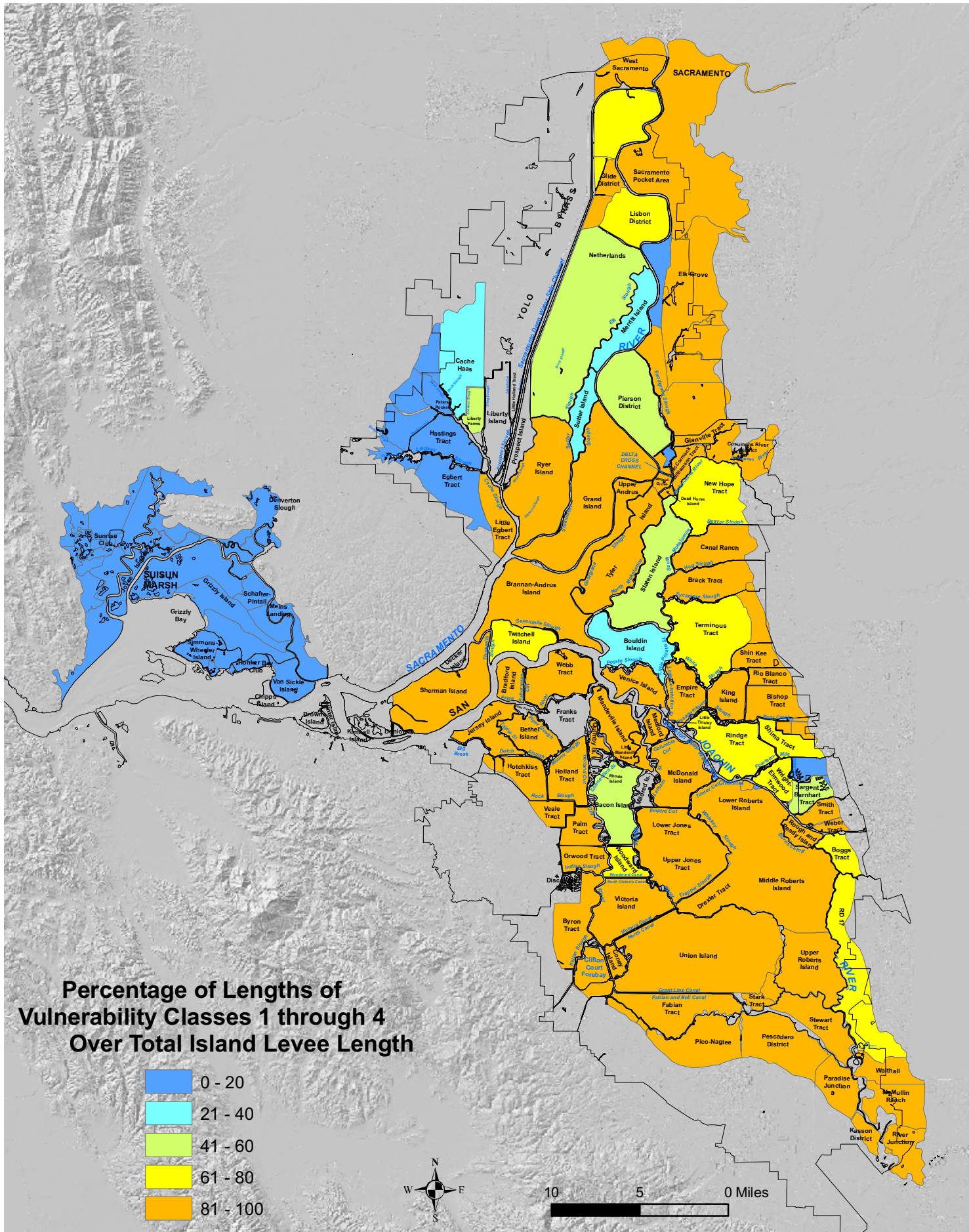
MHHW Floodplain

Suisun Marsh

Legal Delta

Seismic Vulnerability Classes

Outside the MHHW Boundary		6		13		20
		7		14		21
		8		15		22
1		9		16		23
2		10		17		24
3		11		18		
4		12		19		
5						

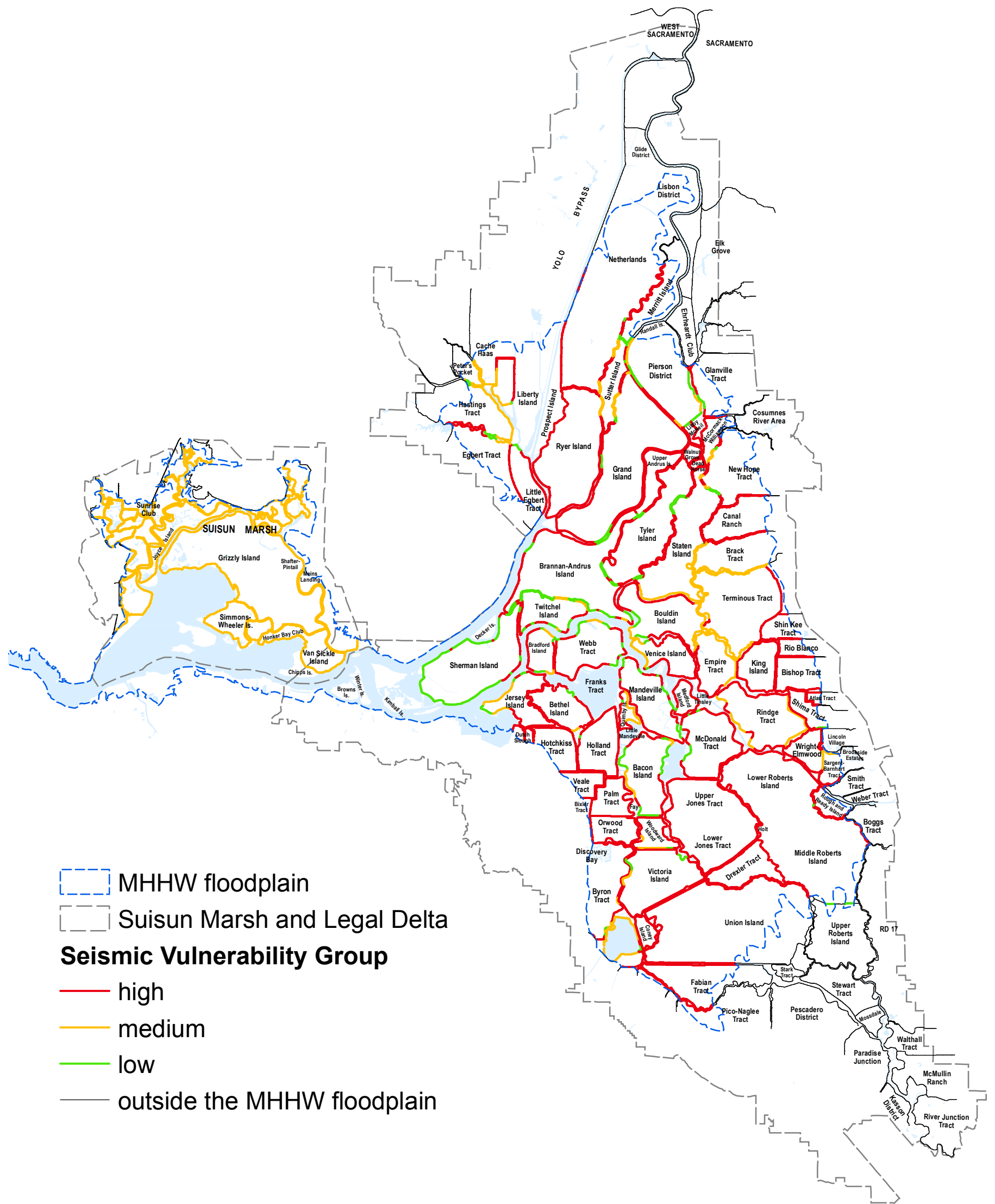


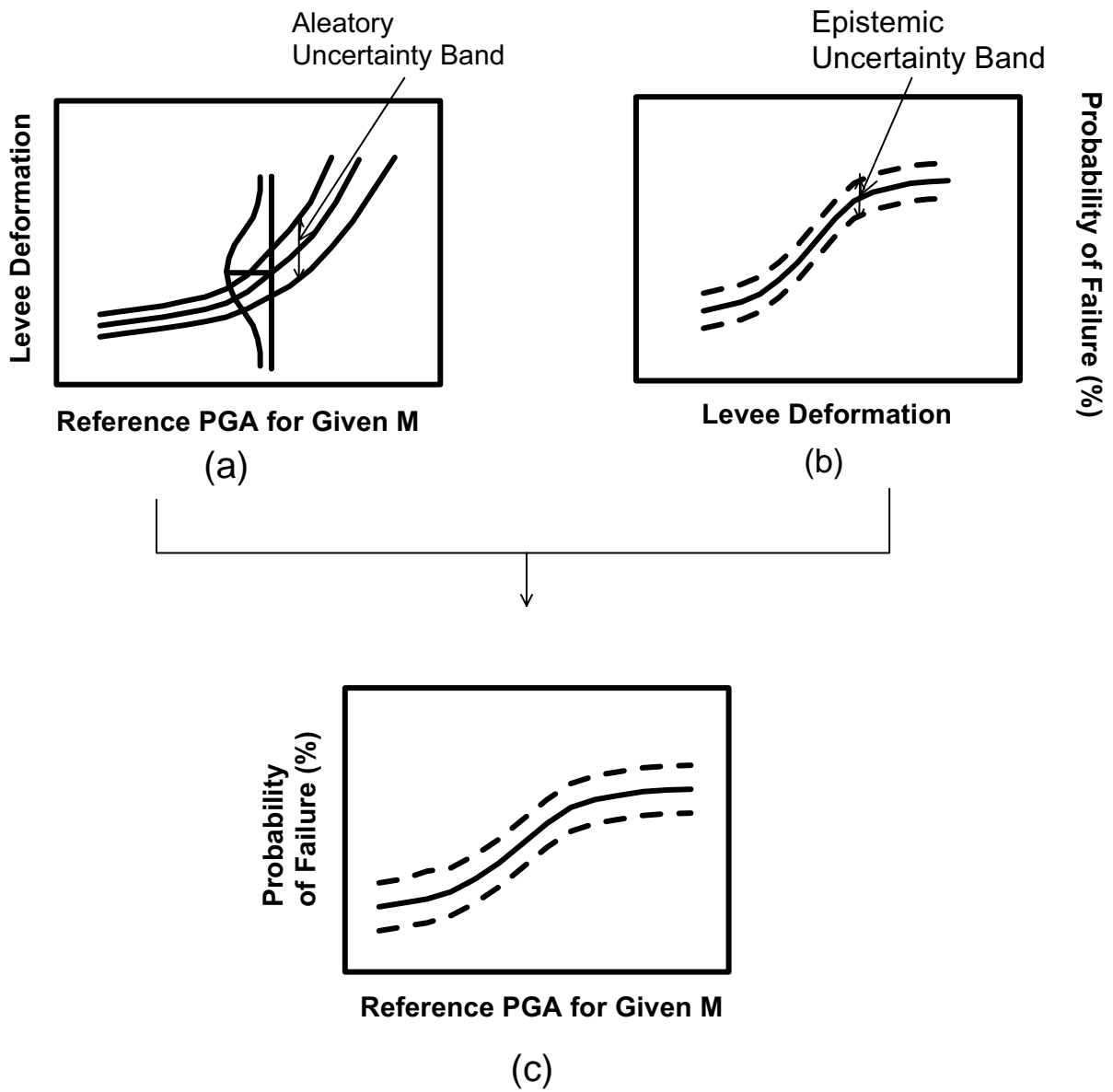
Delta Risk Management Strategy (DRMS)
Phase 2

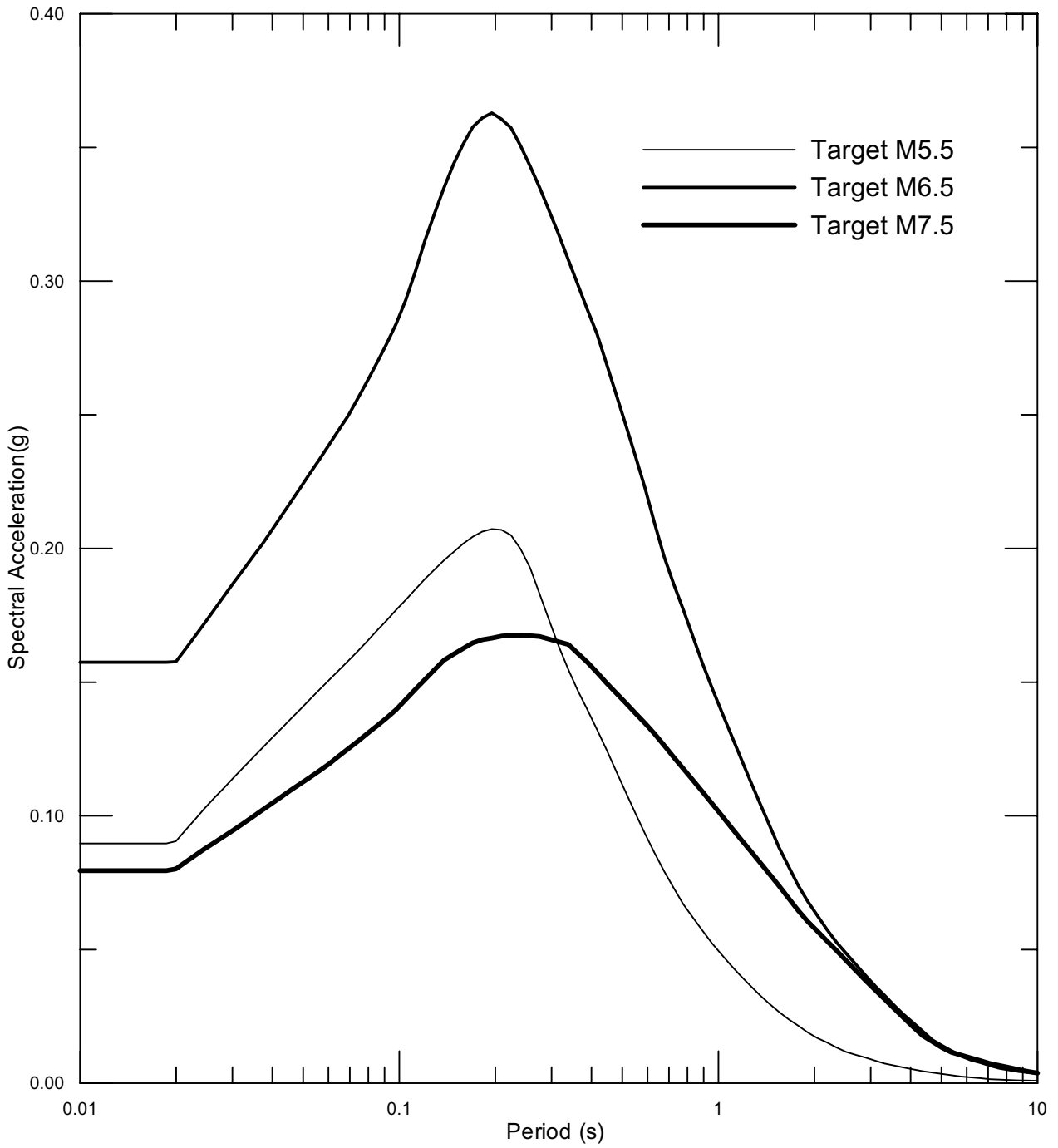
26815621.00019

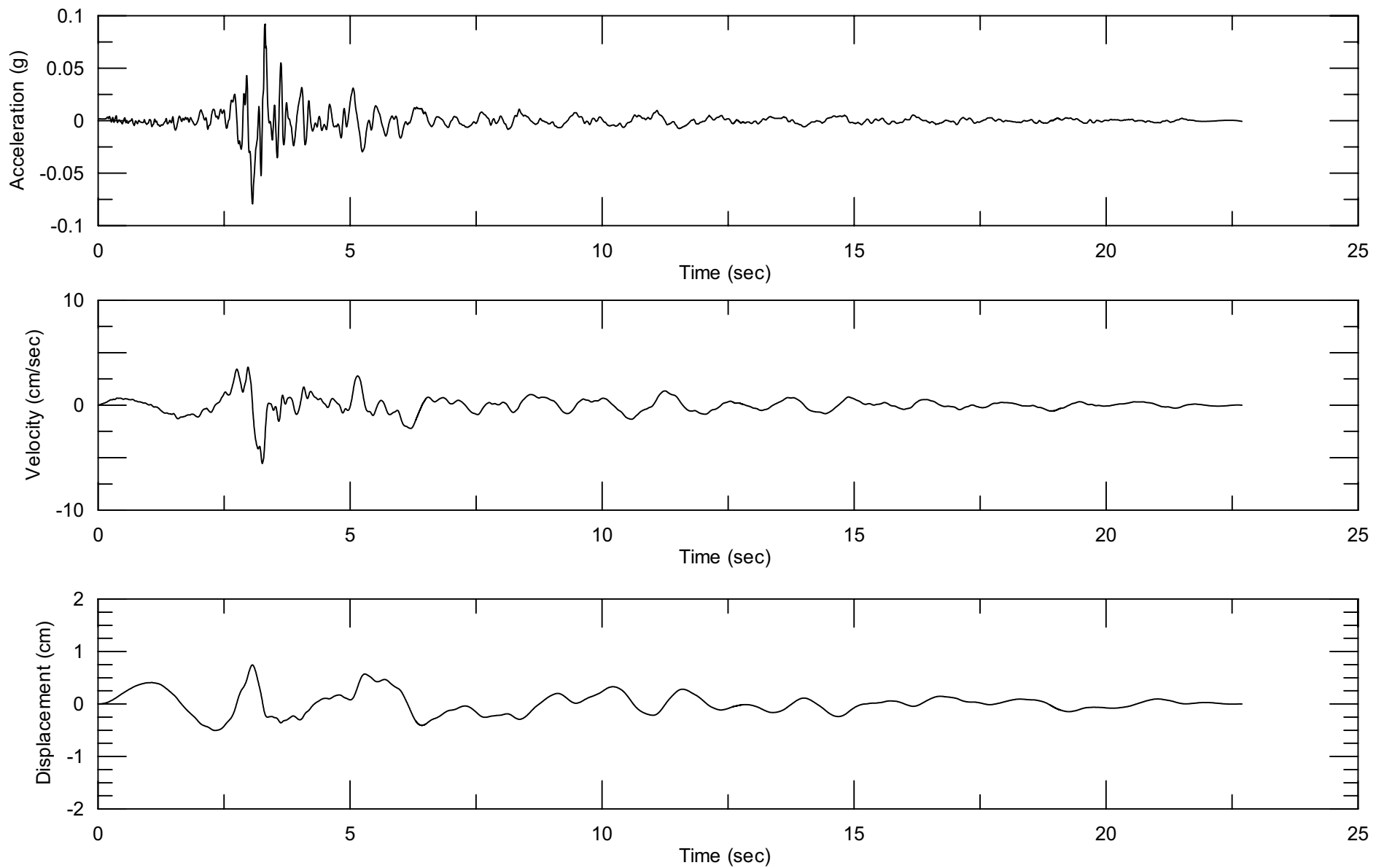
PERCENTAGE OF LEVEE LENGTH
WITH SEISMIC VULNERABILITY
CLASSES 1 THROUGH 4

Figure
6-37b









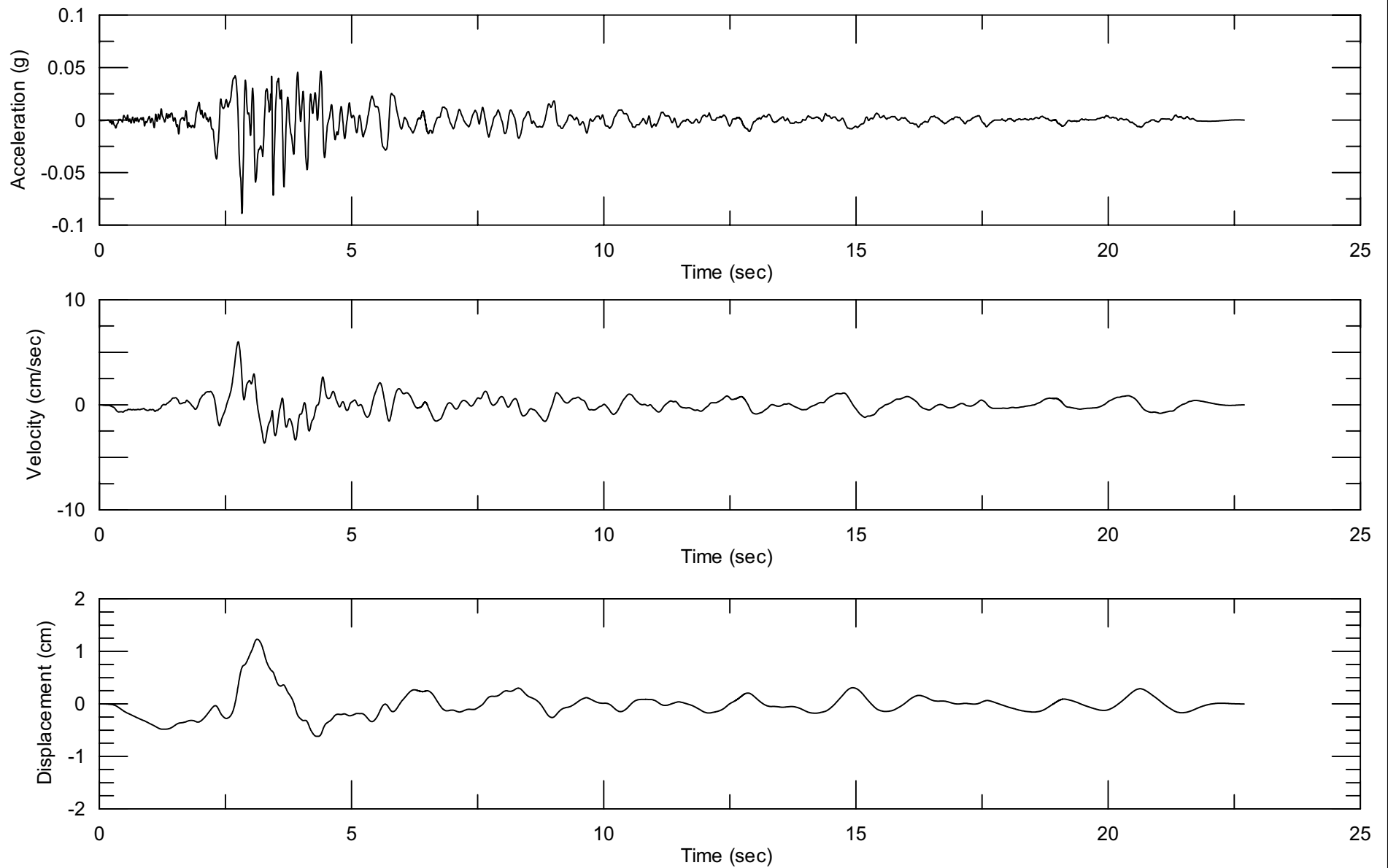
Delta Risk Management Strategy (DRMS)
Levee Fragility

URS

Project No. 26815621

Spectrally-Matched Time history for M 5.5 Event
for 1991 Sierra Madre Earthquake
at Station USGS 4734, 360 deg Component

Figure
6-40



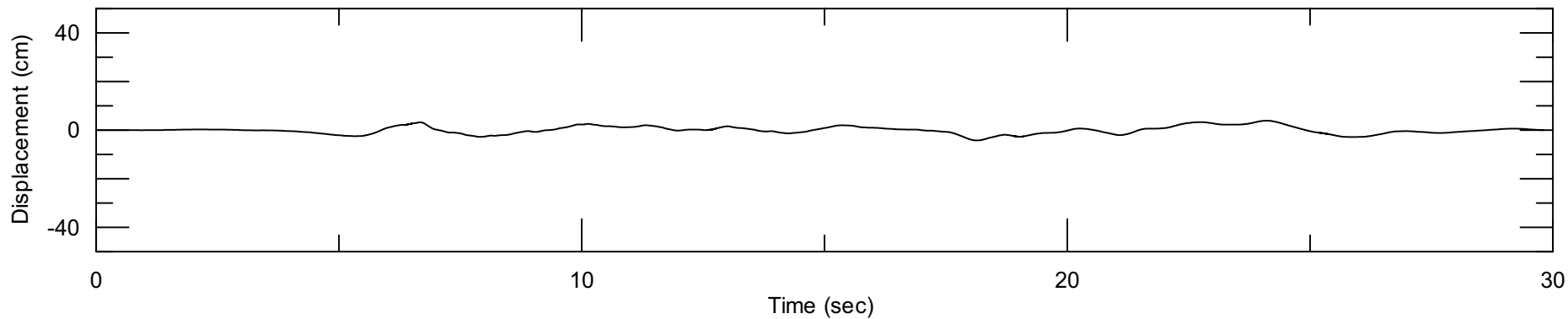
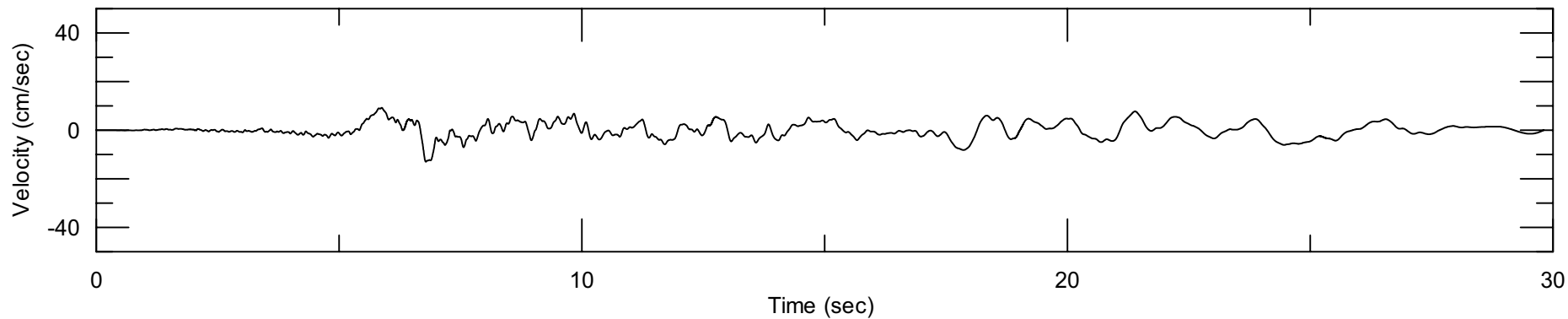
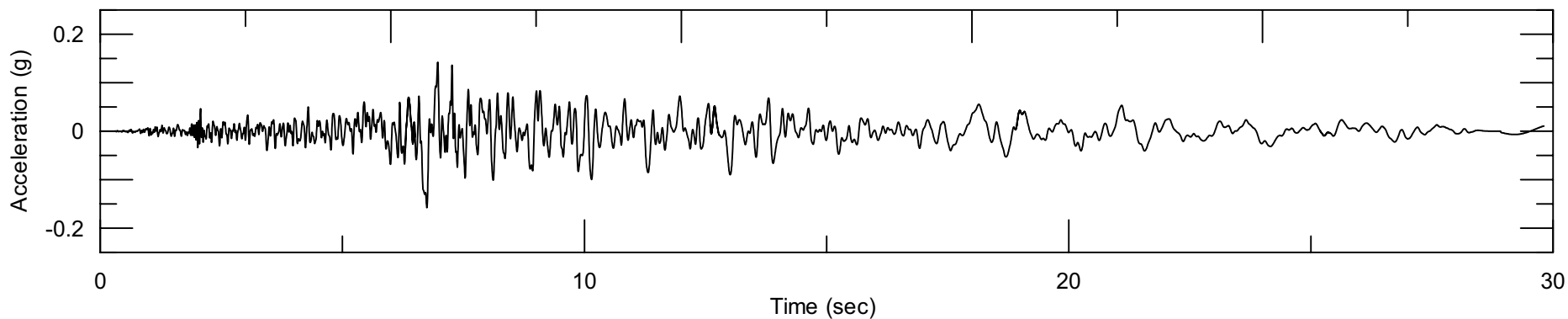
Delta Risk Management Strategy (DRMS)
Levee Fragility

URS

Project No. 26815621

Spectrally-Matched Time History for M 5.5 Event
for 1991 Sierra Madre Earthquake
at Station USGS 4734, 270 deg Component

Figure
6-41



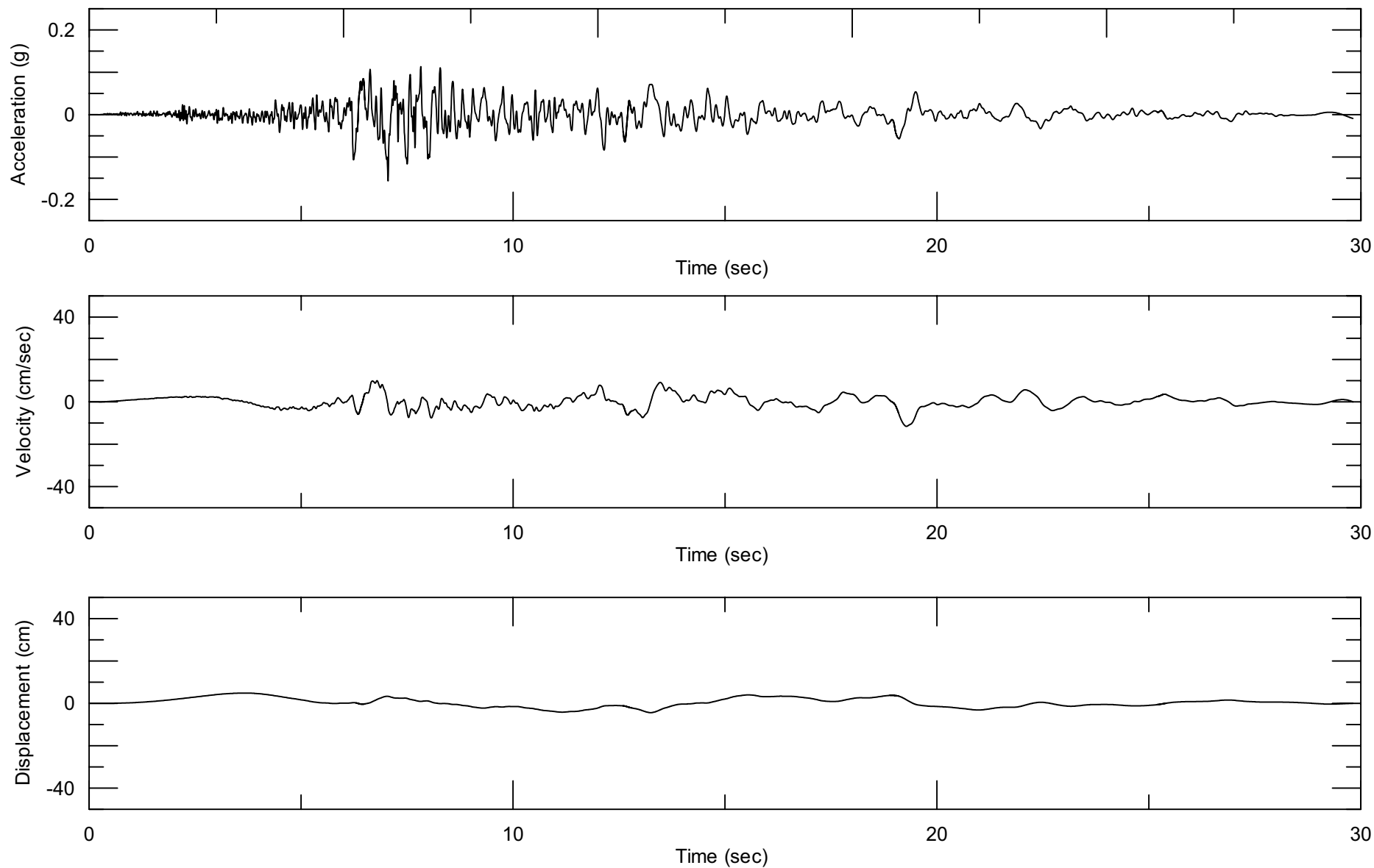
Delta Risk Management Strategy (DRMS)
Levee Fragility

URS

Project No. 26815621

Spectrally-Matched Time History for M 6.5 Event
for 1987 Superstition Hills Earthquake
at Station Wildlife Liquefaction Array,
090 deg Component

Figure
6-42



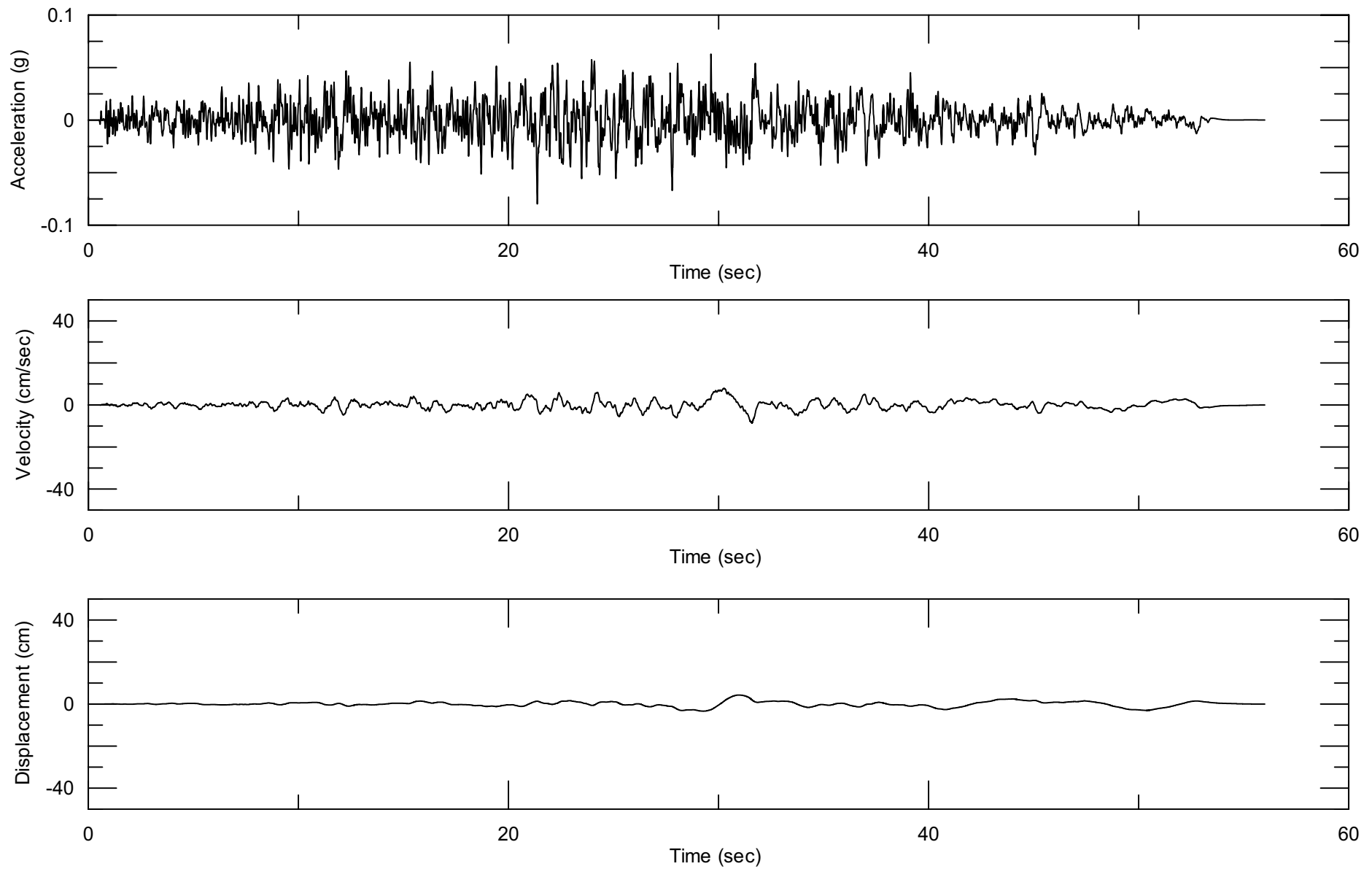
Delta Risk Management Strategy (DRMS)
Levee Fragility

URS

Project No. 26815621

Spectrally-Matched Time History for M 6.5 Event
for 1987 Superstition Hills Earthquake
at Station Wildlife Liquefaction Array,
360 deg Component

Figure
6-43



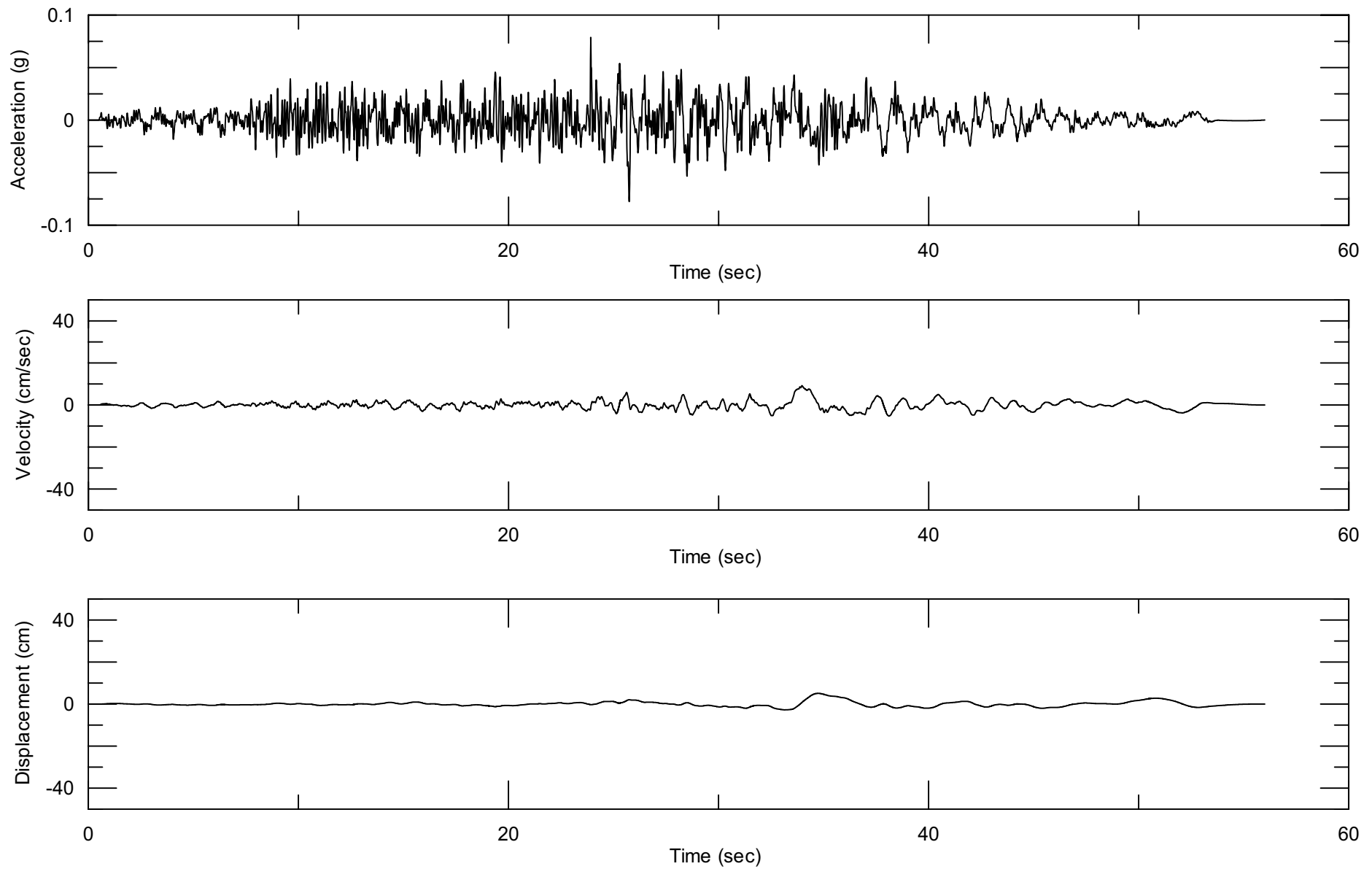
Delta Risk Management Strategy (DRMS)
Levee Fragility

URS

Project No. 26815621

Spectrally-Matched Time History for M 7.5 Event
for 1992 Landers Earthquake
at Station Hemet Fire Station,
000 deg Component

Figure
6-44



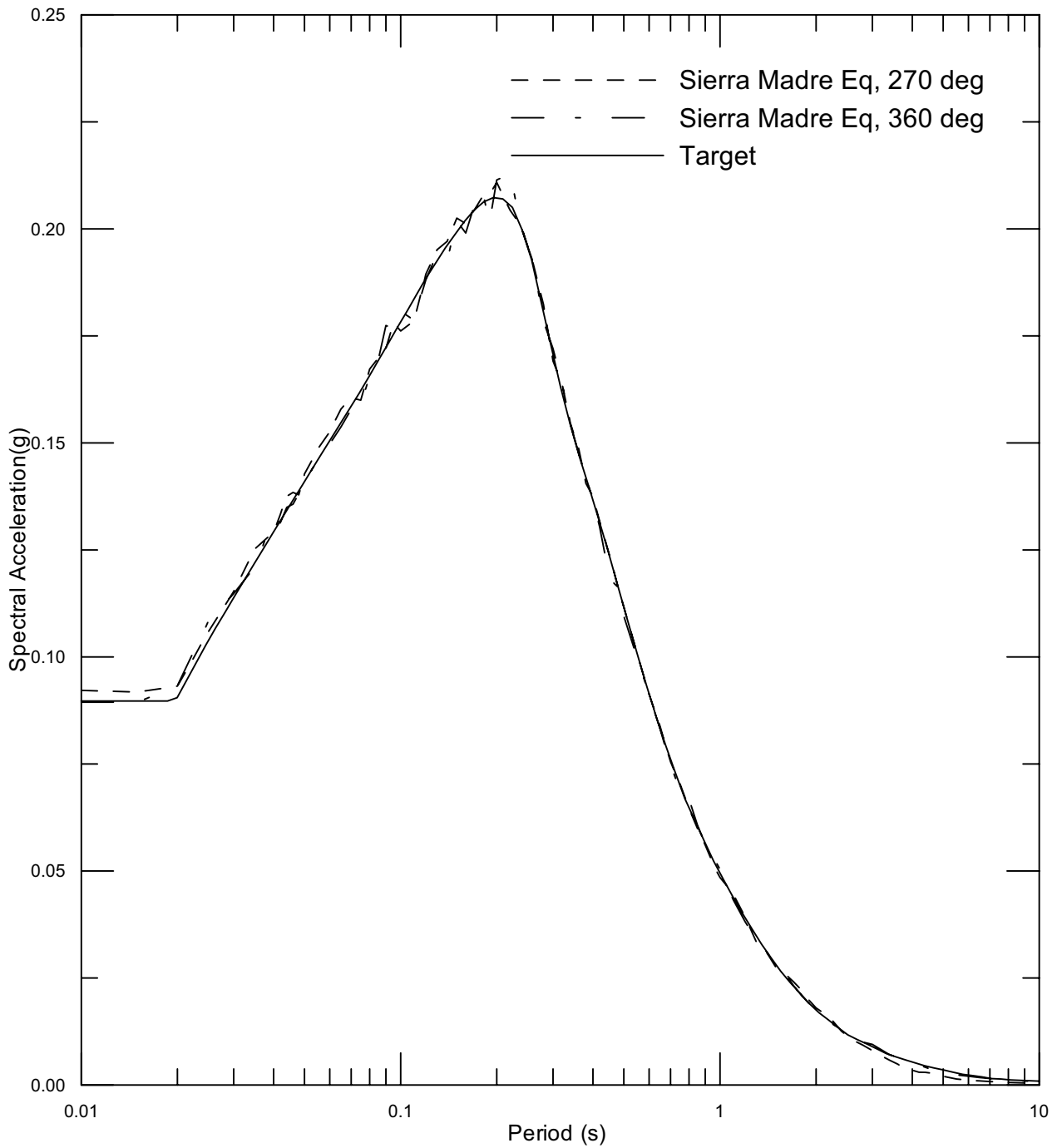
Delta Risk Management Strategy (DRMS)
Levee Fragility

URS

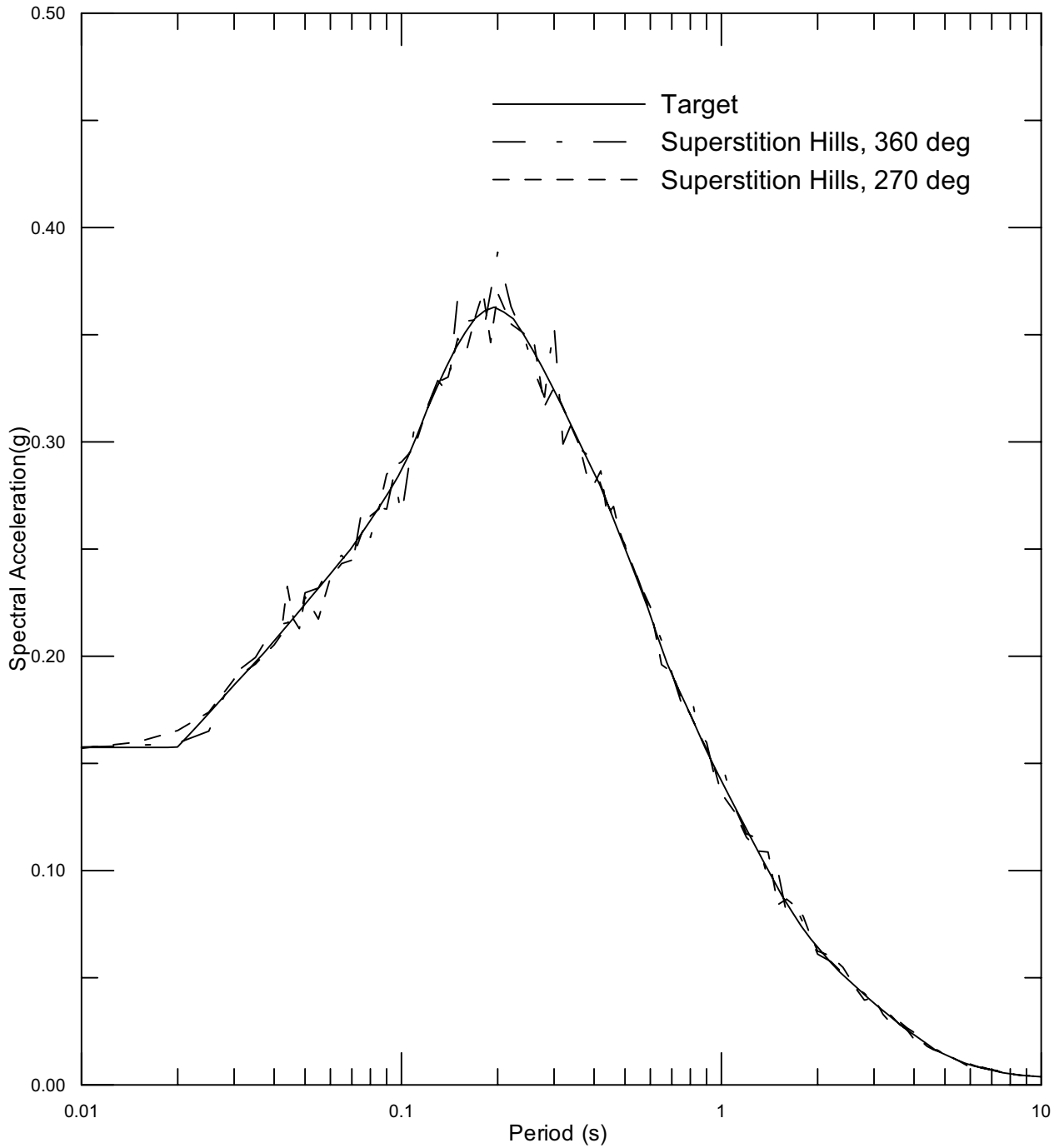
Project No. 26815621

Spectrally-Matched Time History for M 7.5 Event
for 1992 Landers Earthquake
at Station Hemet Fire Station,
090 deg Component

Figure
6-45



- Notes:
- 5% critical damping
 - Stiff soil outcrop target spectrum
 - Sierra Madre Earthquake (1991): M5.5; USGS 4734 station; Site D (stiff soil)



- Notes:
- 5% critical damping
 - Stiff soil outcrop target spectrum
 - Superstition Hills Earthquake (1987): M6.5; Wildlife station; Site D (stiff soil)

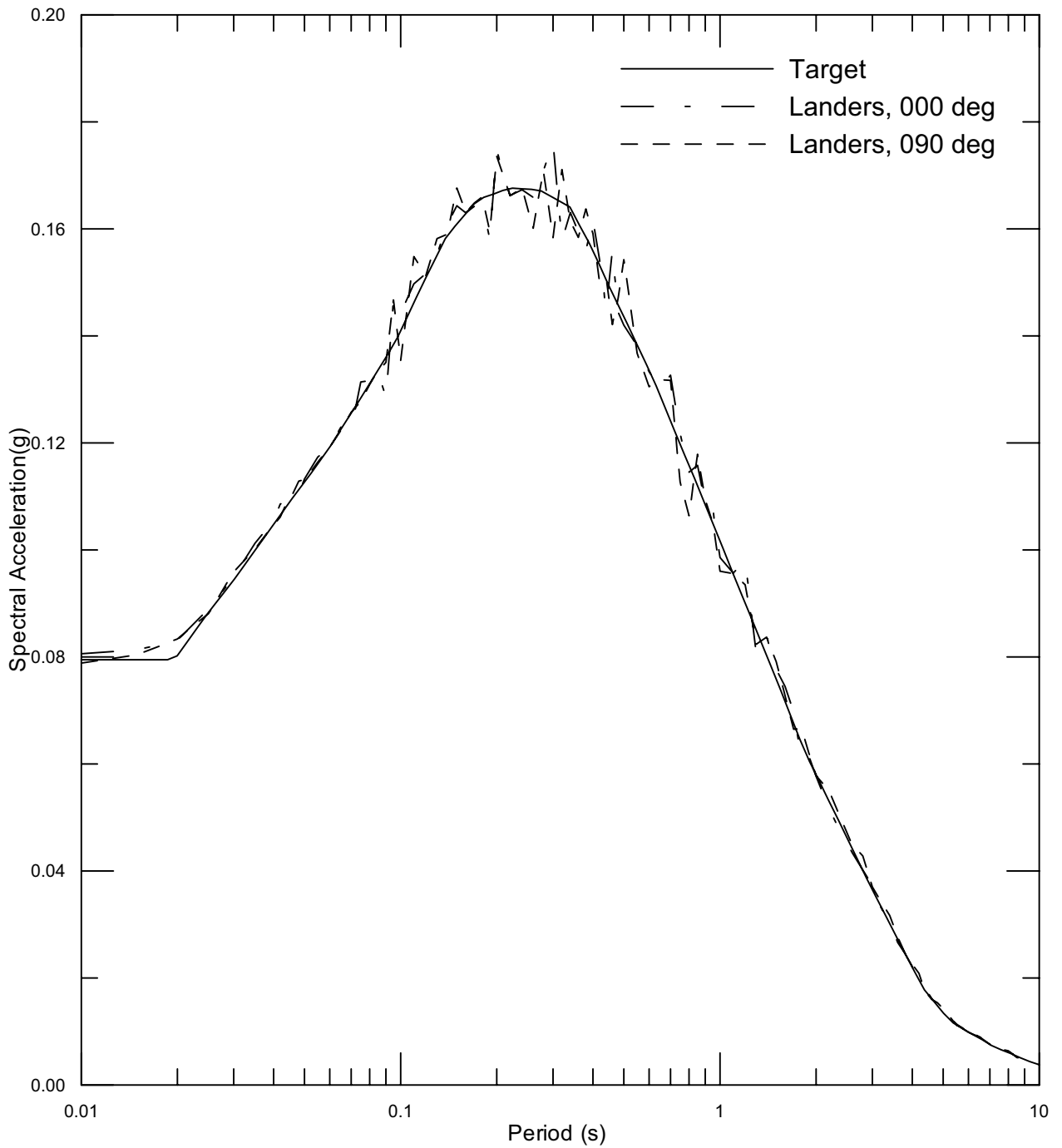
Delta Risk Management Strategy (DRMS)
Levee Fragility

URS

Project No. 26815621

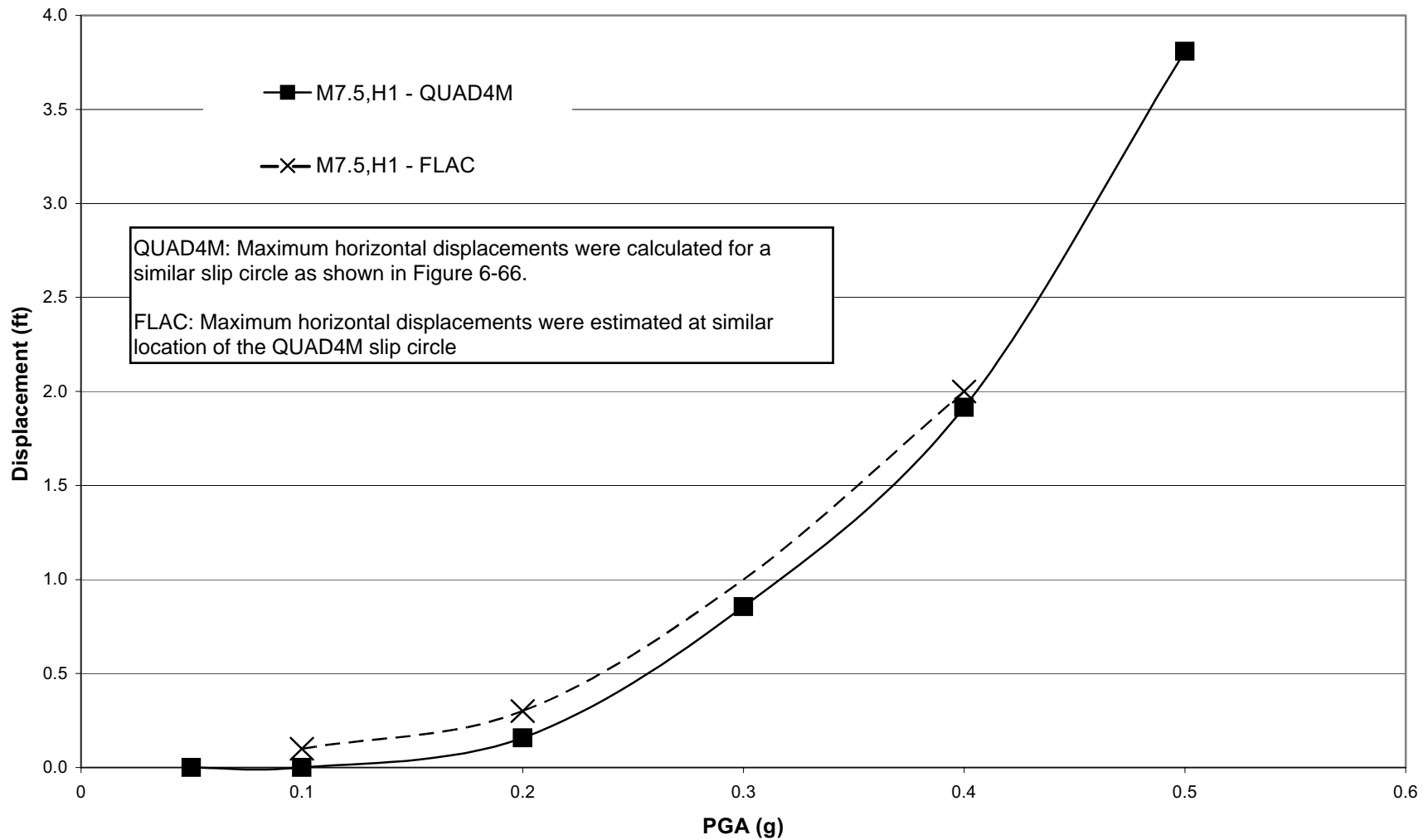
Comparison of Response Spectra
for M 6.5 Event

Figure
6-47



- Notes:
- 5% critical damping
 - Stiff soil outcrop target spectrum
 - Landers Earthquake (1992): M7.3; Hemet fire station; Site D (stiff soil)

Water Side Displacements - Steep Slope with 5 feet Peat

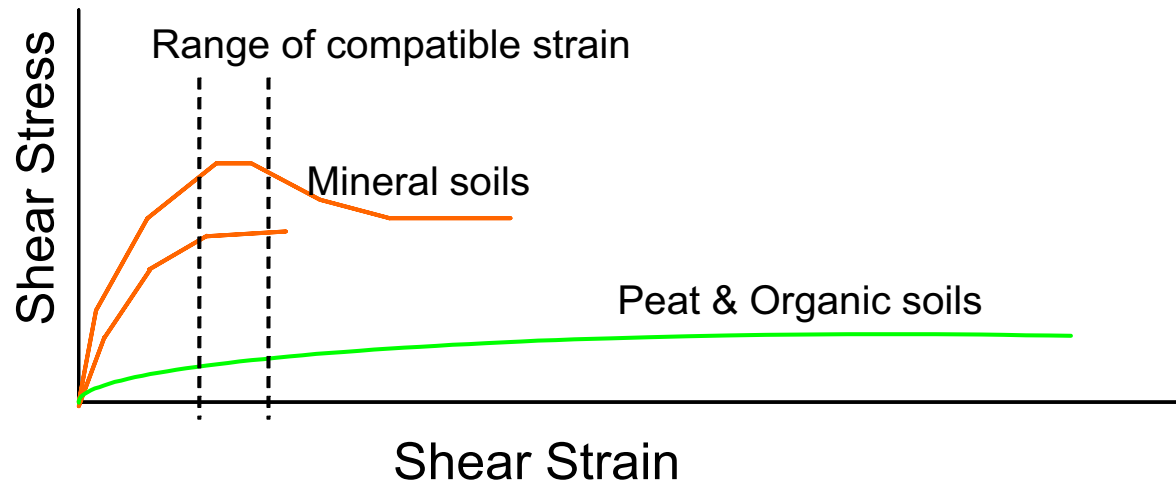
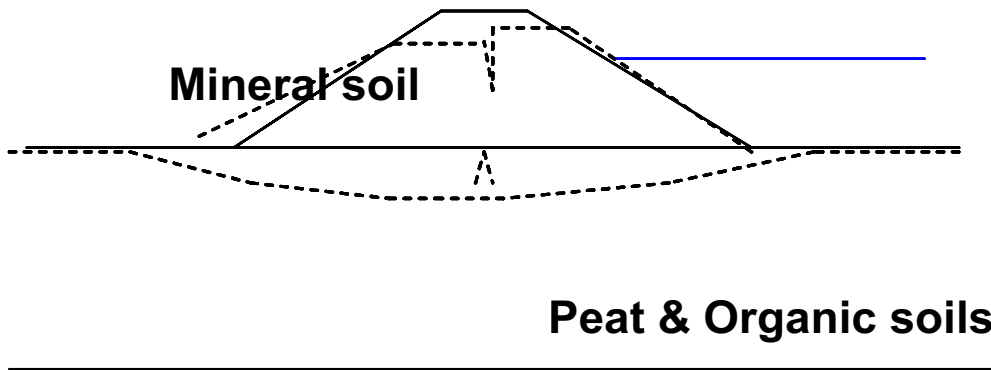


QUAD4M: Maximum horizontal displacements were calculated for a similar slip circle as shown in Figure 6-66.

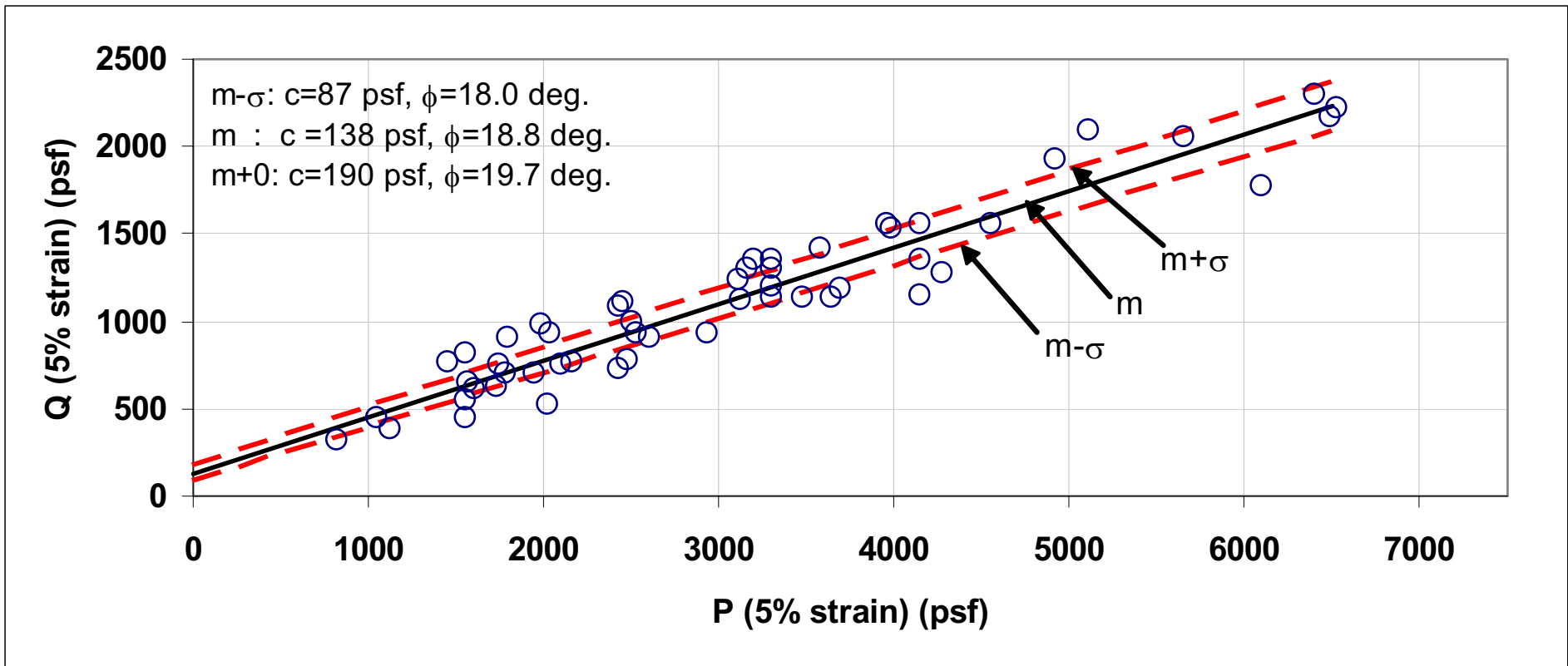
FLAC: Maximum horizontal displacements were estimated at similar location of the QUAD4M slip circle

Delta Risk Management Strategy (DRMS) Levee Fragility		Calculated Displacements for Validation QUAD4M vs FLAC Steep Slope Water Side Slope 5 Feet of Peat	Figure 6-49
URS	Project No. 26815621		

Deformed Levee Shape:

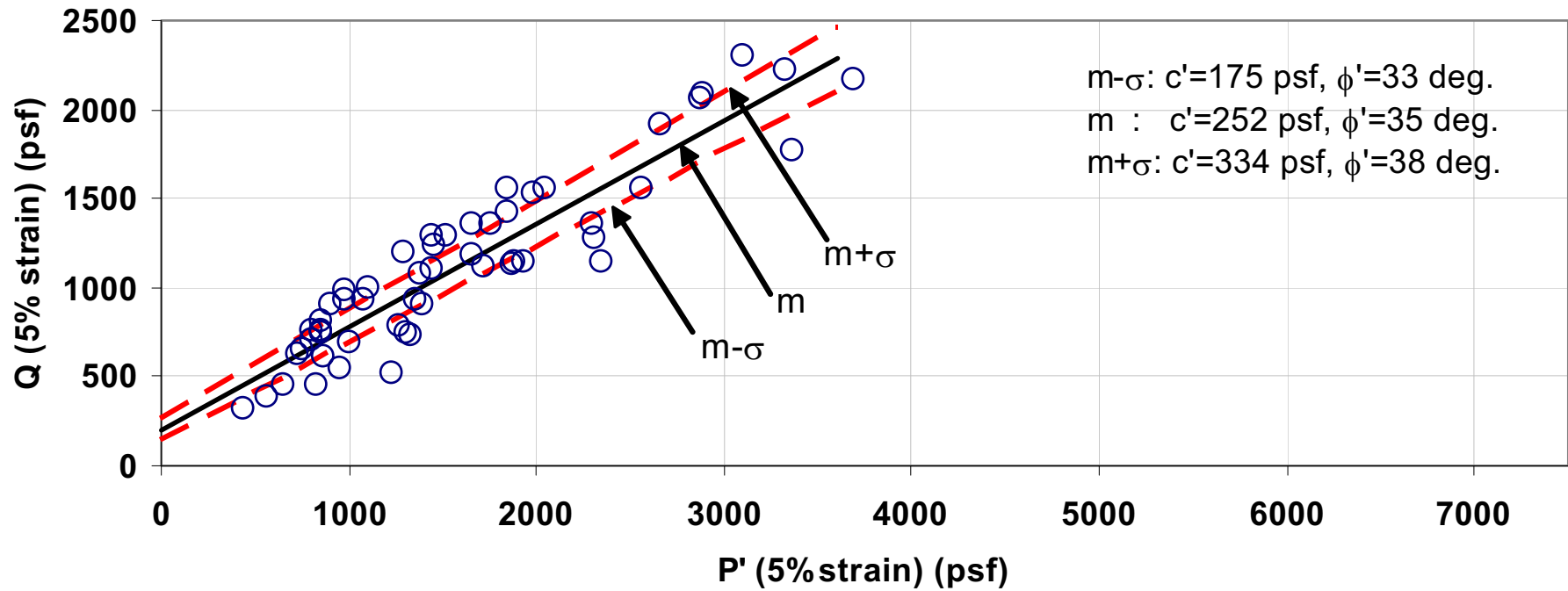


Delta Risk Management Strategy (DRMS) Levee Fragility		Strain Compatible Strength Peat vs Mineral Soil	Figure 6-50
URS	Project No. 26815621		



Data Source: Hultgren-Tellis Engineers, 2003

Delta Risk Management Strategy (DRMS) Levee Fragility		P-Q Plot at 5% Shear Strain for Peat Total Stress	Figure 6-51
URS	Project No. 26815621		



Data Source: Hultgren-Tellis Engineers, 2003

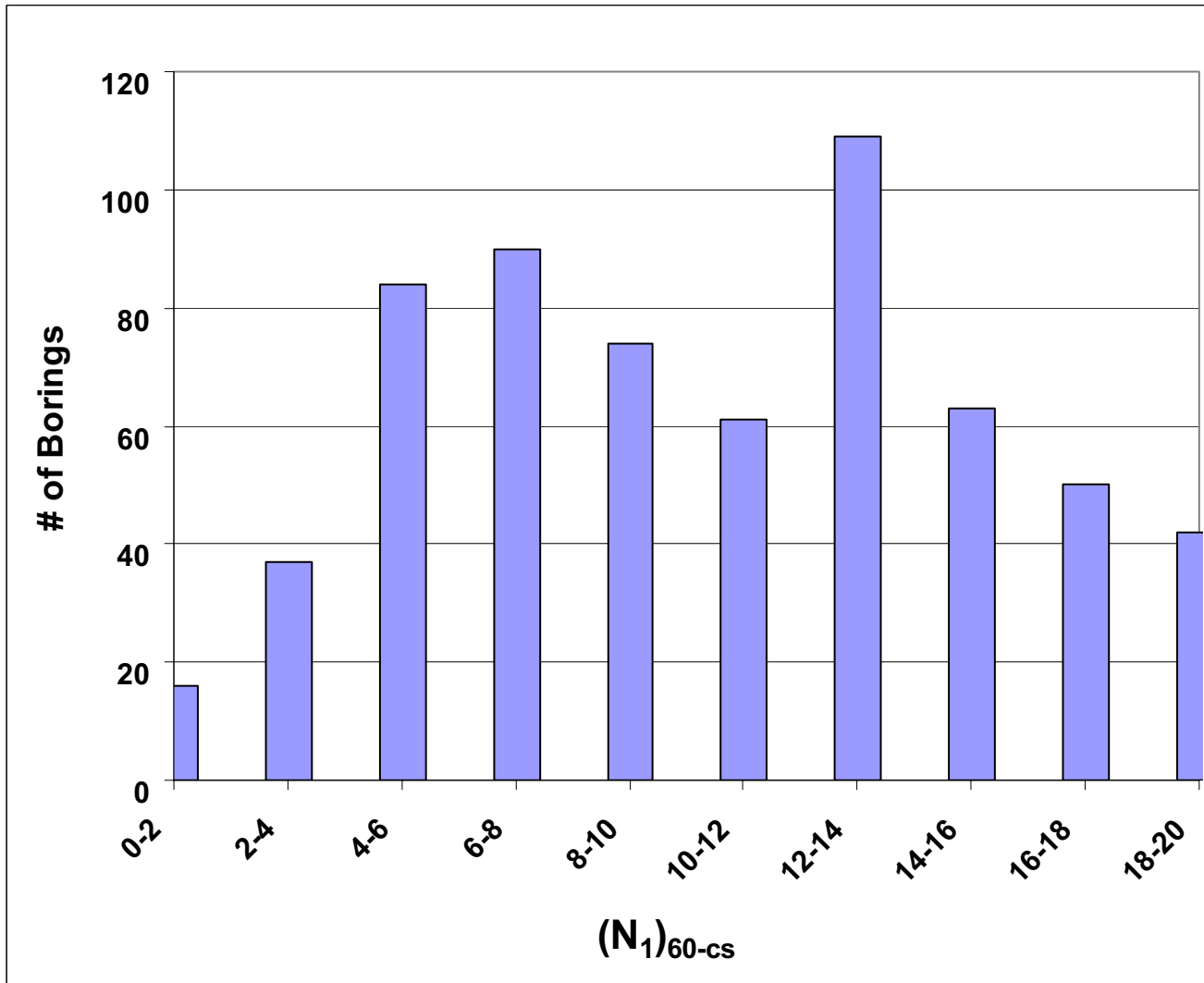
Delta Risk Management Strategy (DRMS)
Levee Fragility



Project No. 26815621

P'-Q Plot at 5% Shear Strain
for Peat
Effective Stress

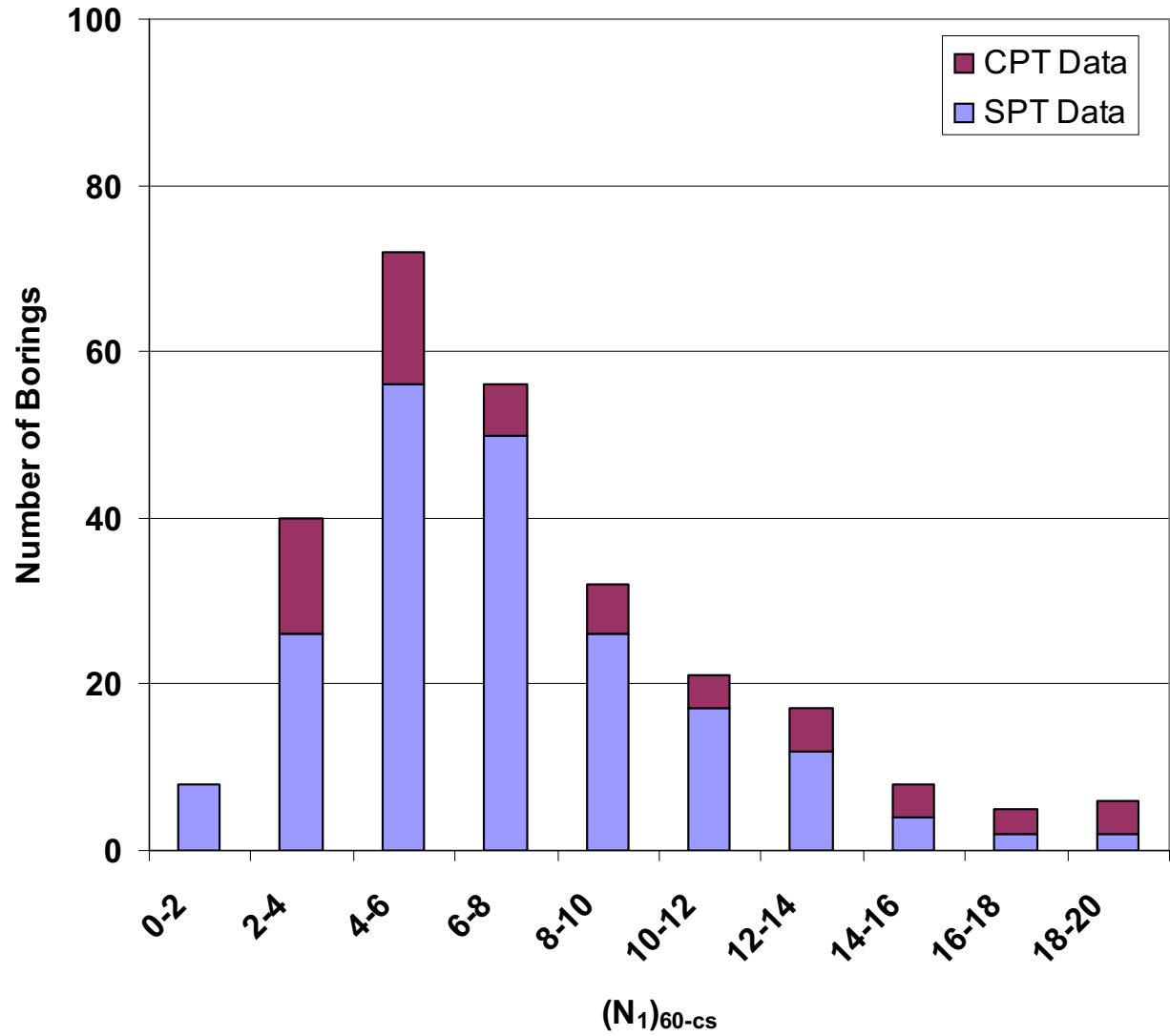
Figure
6-52



Mean = 11
 Mean + σ = 16
 Mean - σ = 6

Notes:
 Total number of SPT borings that showed,
 $(N_1)_{60-cs}$ of foundation sand <20 = 626
 $(N_1)_{60-cs}$ of foundation sand >20 = 310
 Data source: Various boring logs from past studies (see Table 2-1)

Delta Risk Management Strategy (DRMS) Levee Fragility		$(N_1)_{60-cs}$ Distribution for Foundation Sand with $(N_1)_{60-cs} < 20$	Figure 6-53
URS	Project No. 26815621		

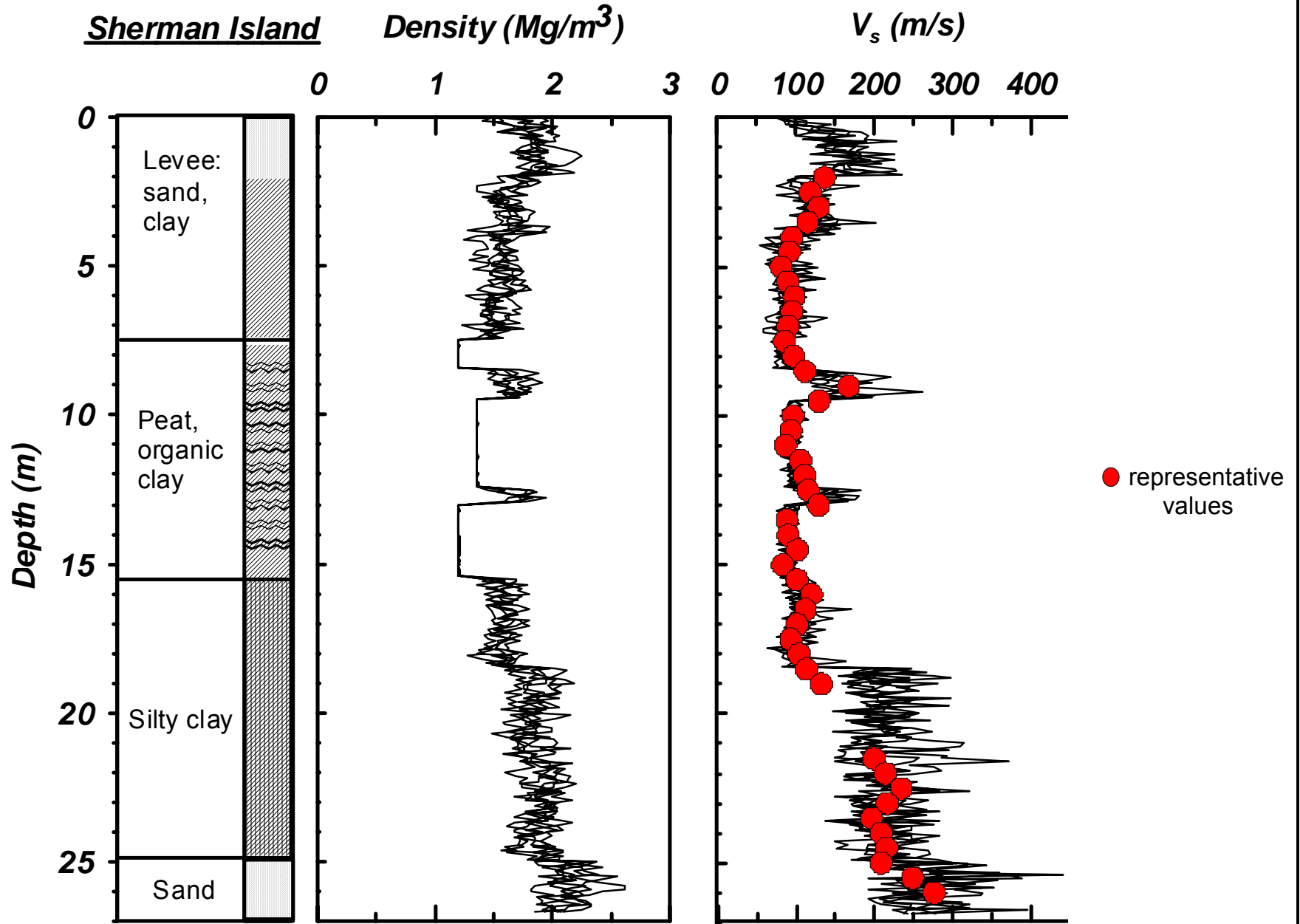


Mean = 8
 Mean + σ = 12
 Mean - σ = 4

Notes:
 Total number of SPT borings that showed $(N_1)_{60-cs}$ of sandy levee fill <20 = 203
 $(N_1)_{60-cs}$ of sandy levee fill >20 = 4
 Total number of CPT borings that showed $(N_1)_{60-cs}$ of sandy levee fill <20 = 62
 $(N_1)_{60-cs}$ of sandy levee fill >20 = 7

Data source: Various boring logs from past studies (see Table 2-1)

Delta Risk Management Strategy (DRMS) Levee Fragility		$(N_1)_{60-cs}$ Distribution for Levee Sand with $(N_1)_{60-cs} < 20$	Figure 6-54
URS	Project No. 26815621		



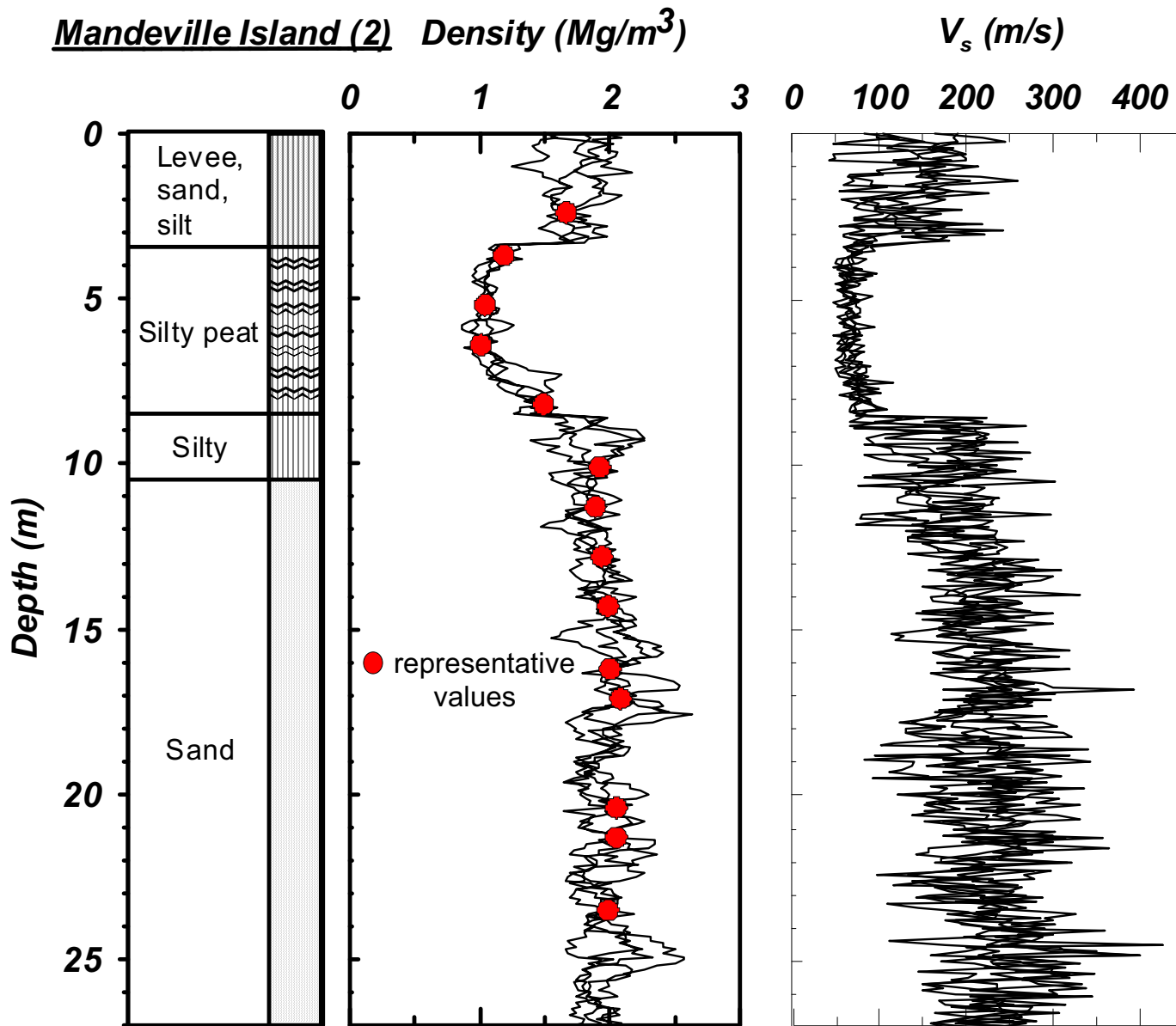
Delta Risk Management Strategy (DRMS)
Levee Fragility



Project No. 26815621

Typical V_s Profile
Sherman Island

Figure
6-55a



Source: Original data from DWR;
 Processed by Tadahiro et al. 2007

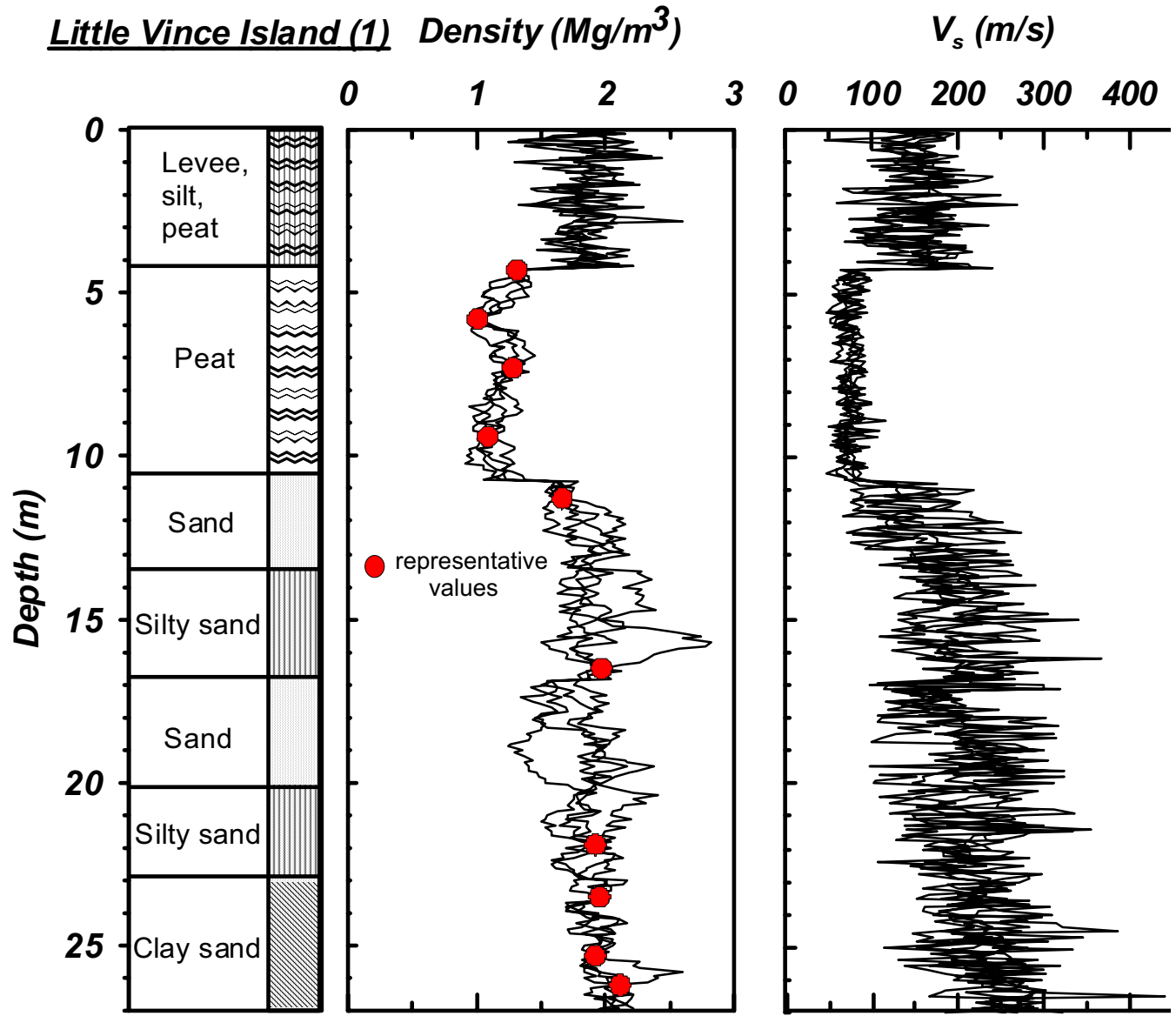
Delta Risk Management Strategy (DRMS)
 Levee Fragility

URS

Project No. 26815621

Typical V_s Profile
 Mandeville Island

Figure
 6-55b



Source: Original data from DWR;
 Processed by Tadahiro et al. 2007

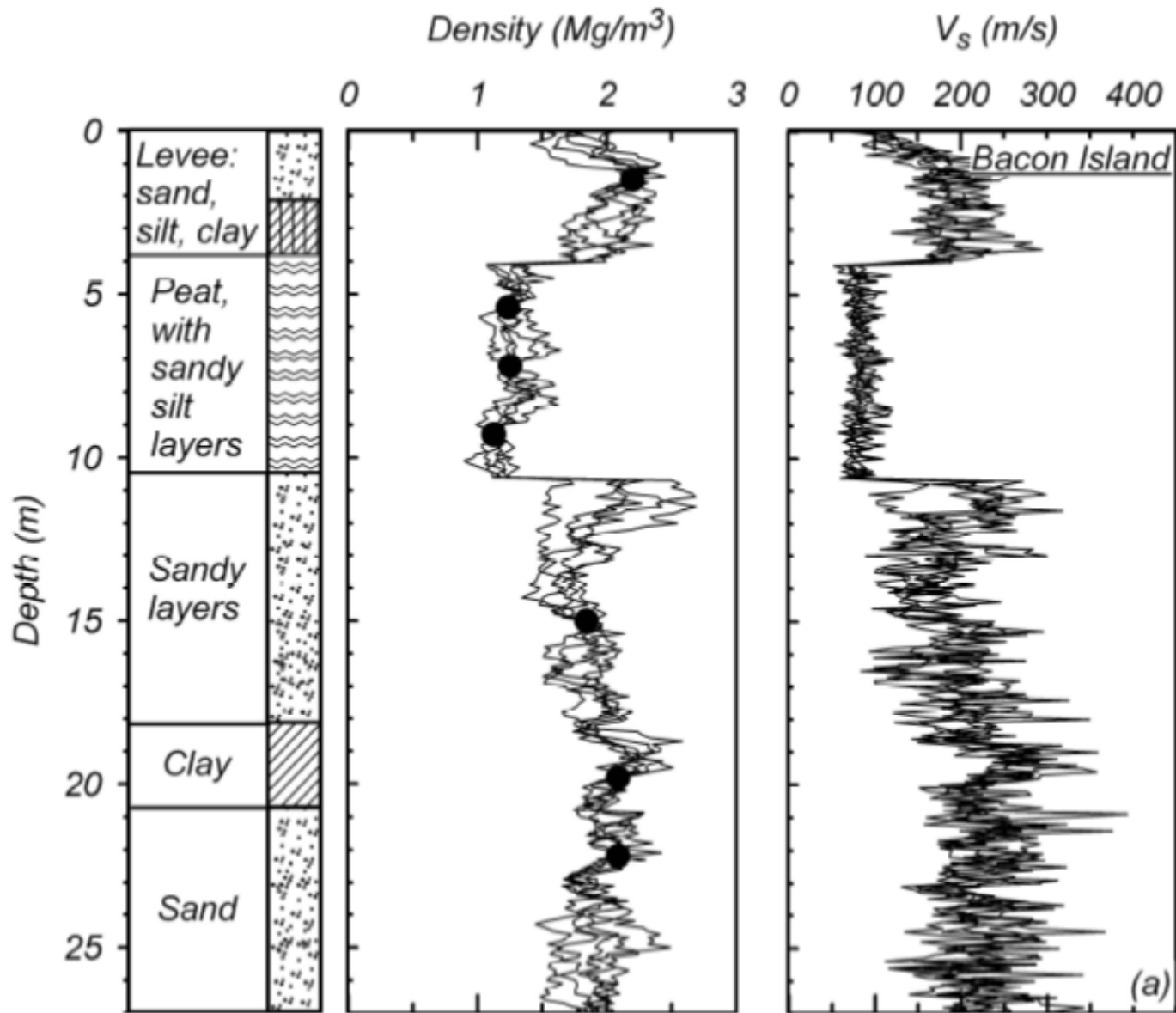
Delta Risk Management Strategy (DRMS)
 Levee Fragility



Project No. 26815621

Typical V_s Profile
 Little Vince Island

Figure
 6-55c



Source: Original data from DWR;
 Processed by Tadahiro et al. 2007

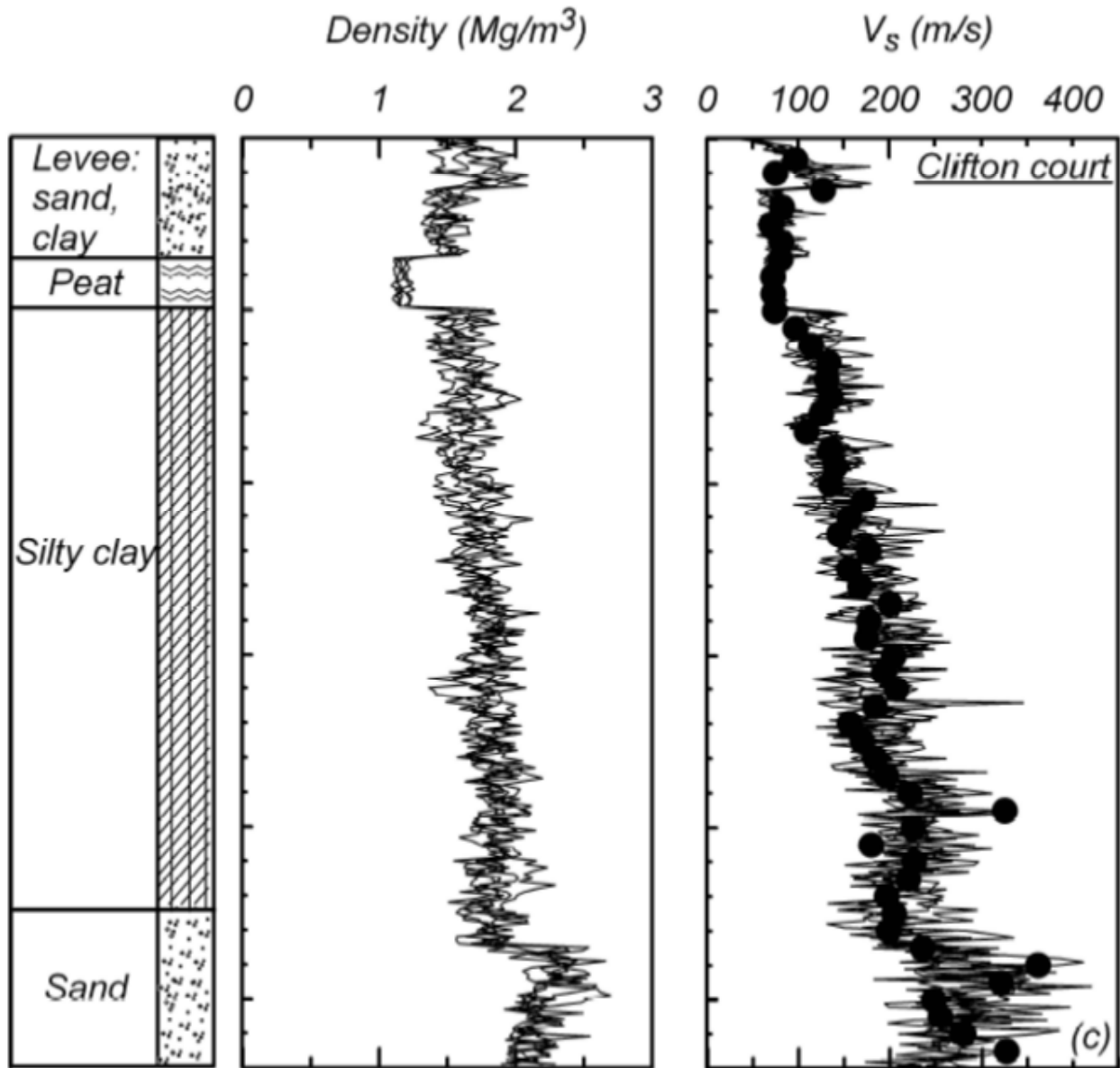
Delta Risk Management Strategy (DRMS)
 Levee Fragility

URS

Project No. 26815621

Typical V_s Profile
 Bacon Island

Figure
 6-55d



● representative values

Source: Original data from DWR;
Processed by Tadahiro et al. 2007

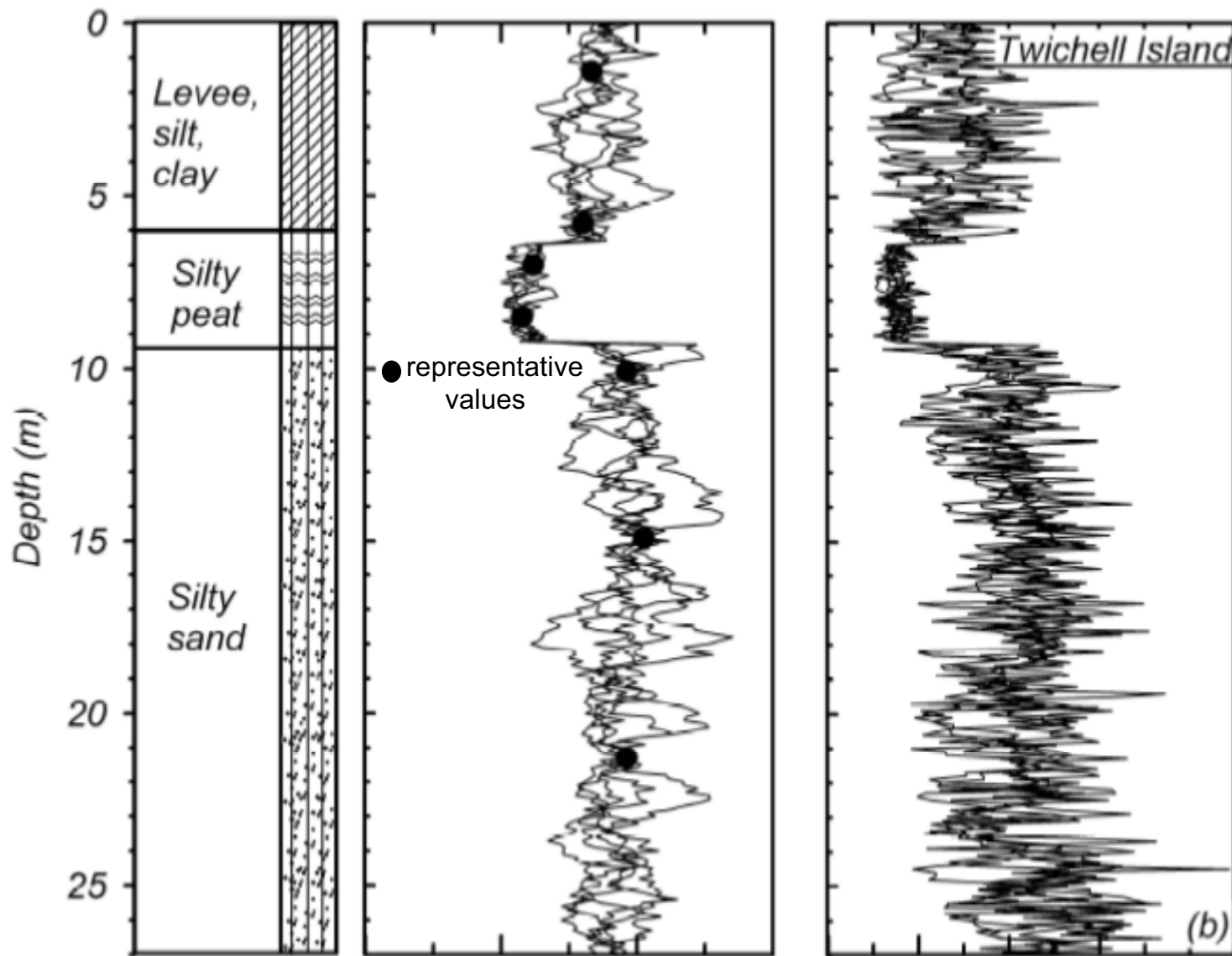
Delta Risk Management Strategy (DRMS)
Levee Fragility

URS

Project No. 26815621

Typical Vs Profile
Clifton Court

Figure
6-55e



Source: Original data from DWR;
 Processed by Tadaihiro et al. 2007

Delta Risk Management Strategy (DRMS)
 Levee Fragility

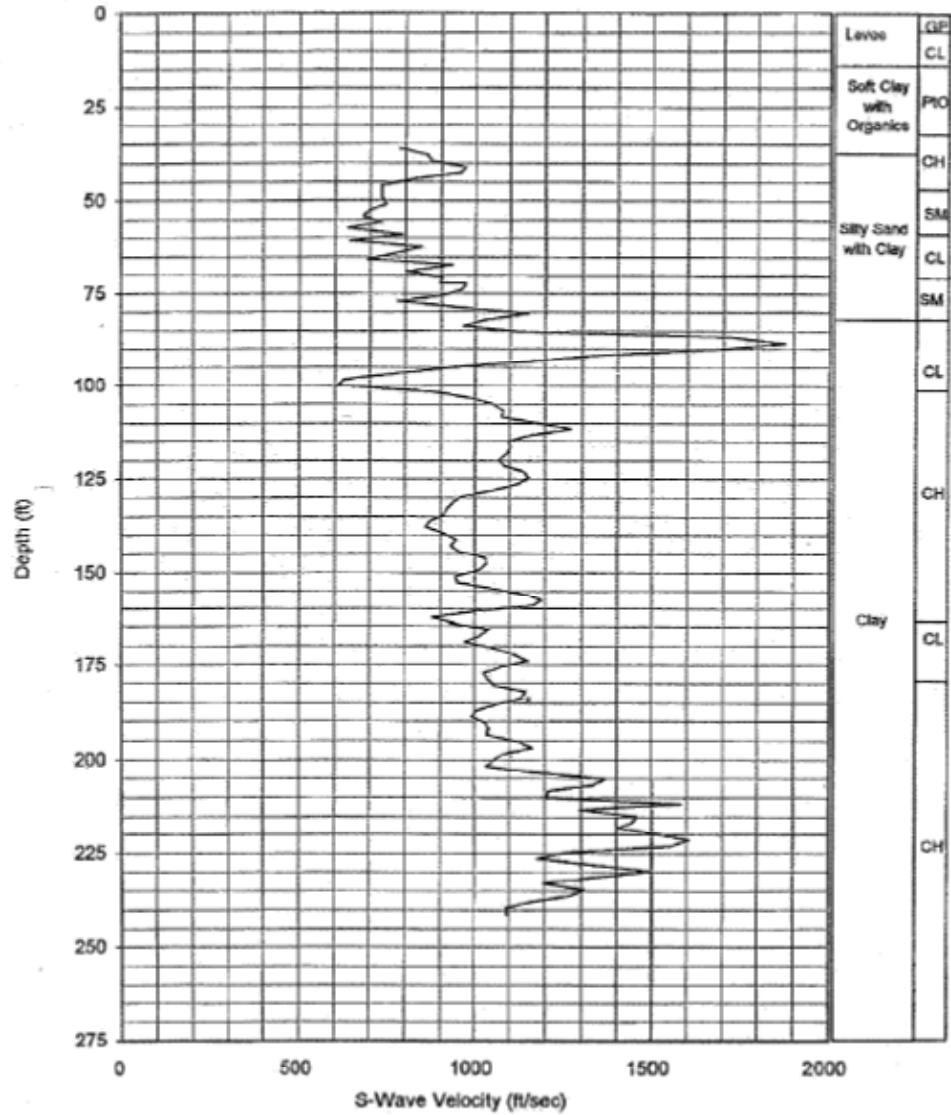
URS

Project No. 26815621

Typical V_s Profile
 Twitchell Island

Figure
 6-55f

MONTEZUMA SLOUGH DHP-4C
DEPTH vs. S-WAVE VELOCITY

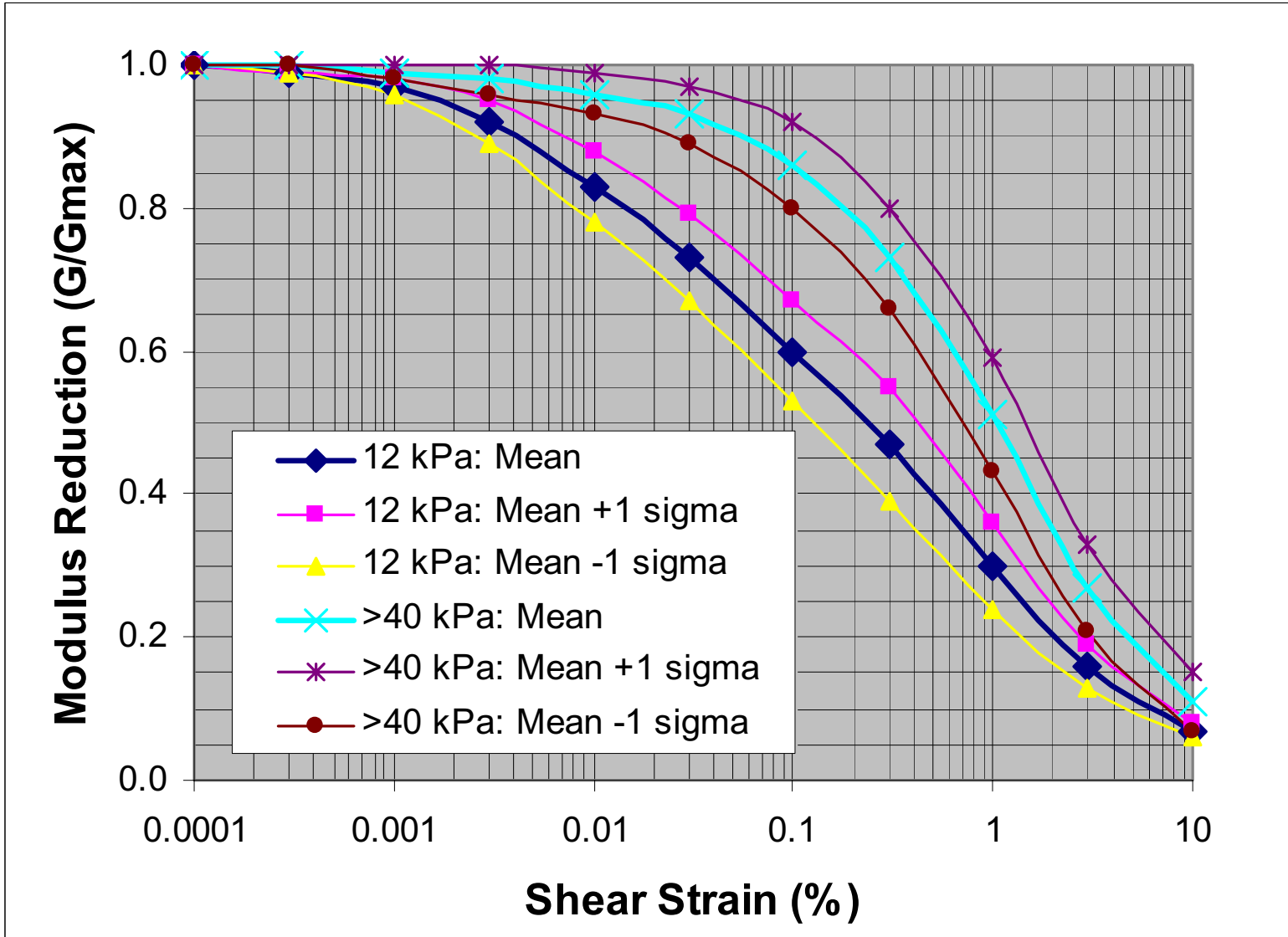


Source: Data from DWR

Delta Risk Management Strategy (DRMS) Levee Fragility	
URS	Project No. 26815621

Typical Vs Profile
Montezuma Slough

Figure
6-55g



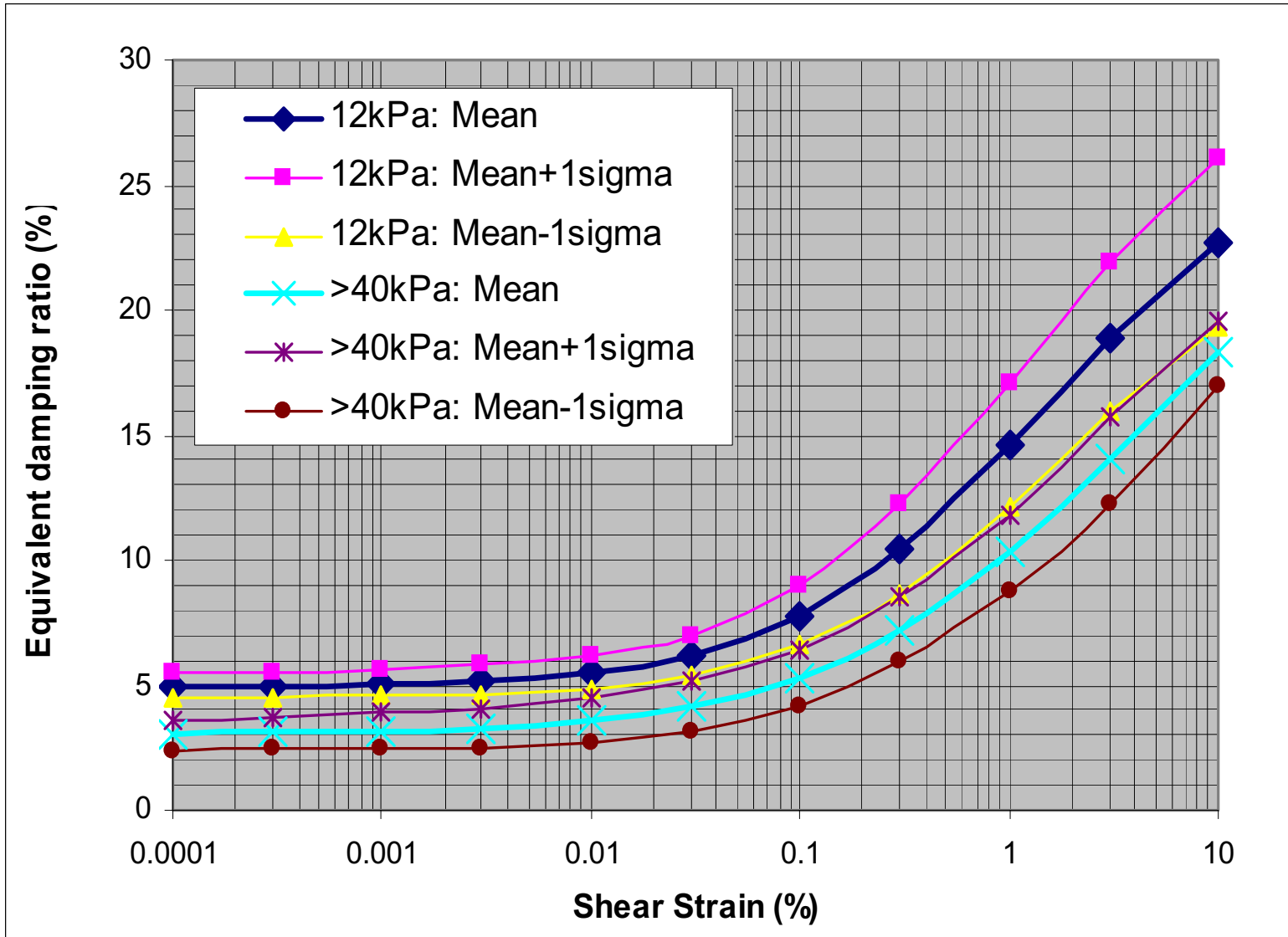
Delta Risk Management Strategy (DRMS)
Levee Fragility



Project No. 26815621

G/G_{max} Curves for
Peat
(Wehling et al., 2001)

Figure
6-56a



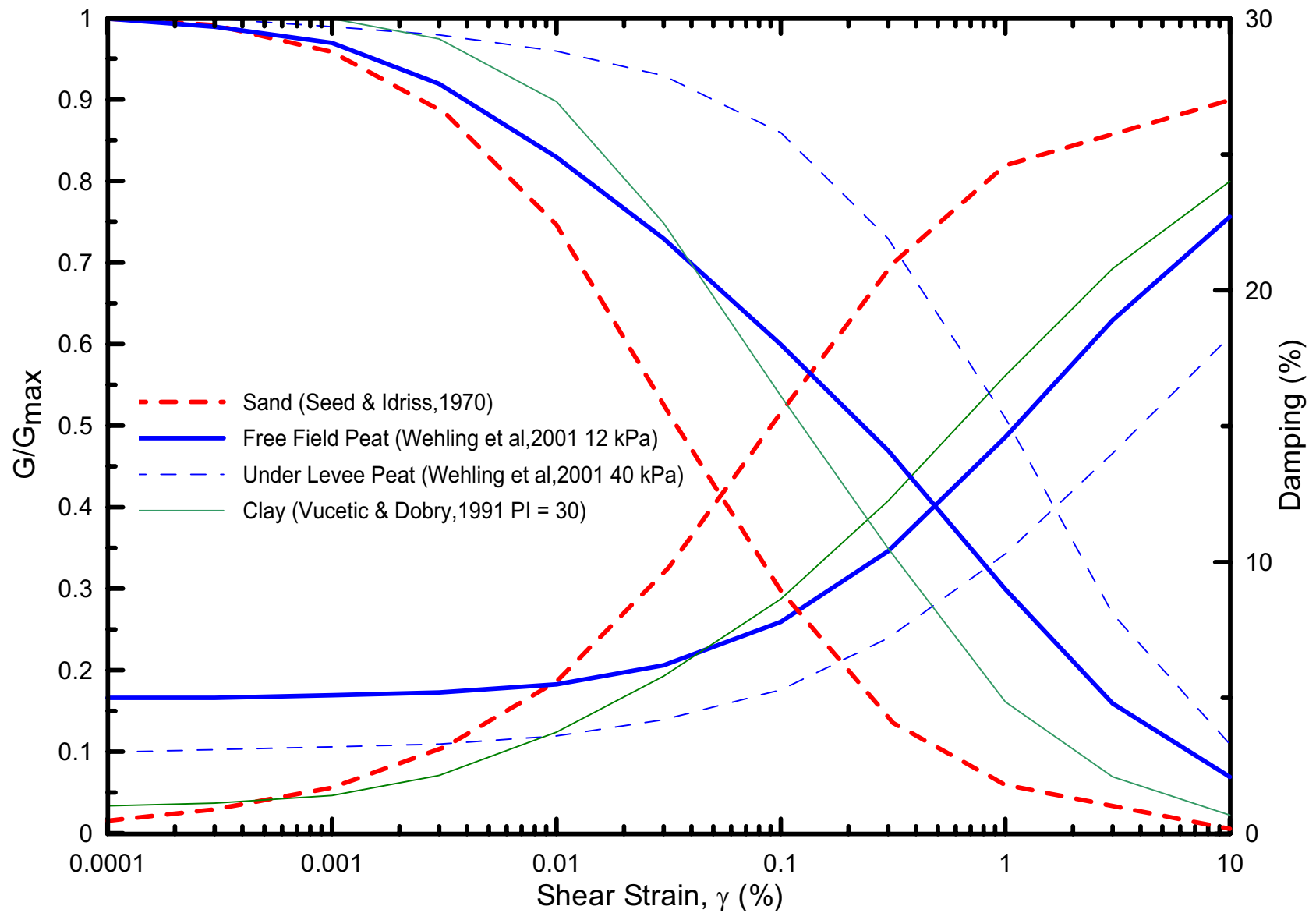
Delta Risk Management Strategy (DRMS)
Levee Fragility



Project No. 26815621

Damping Curves for
Peat
(Wehling et al., 2001)

Figure
6-56b



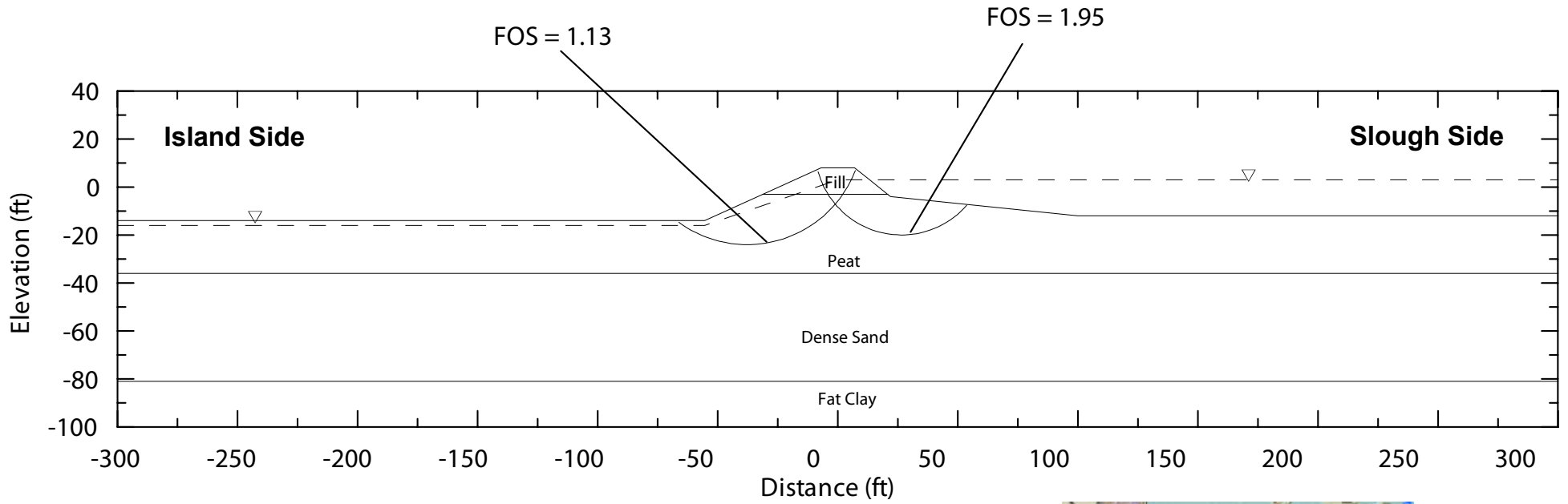
Delta Risk Management Strategy (DRMS)
Levee Fragility

URS

Project No. 26815621

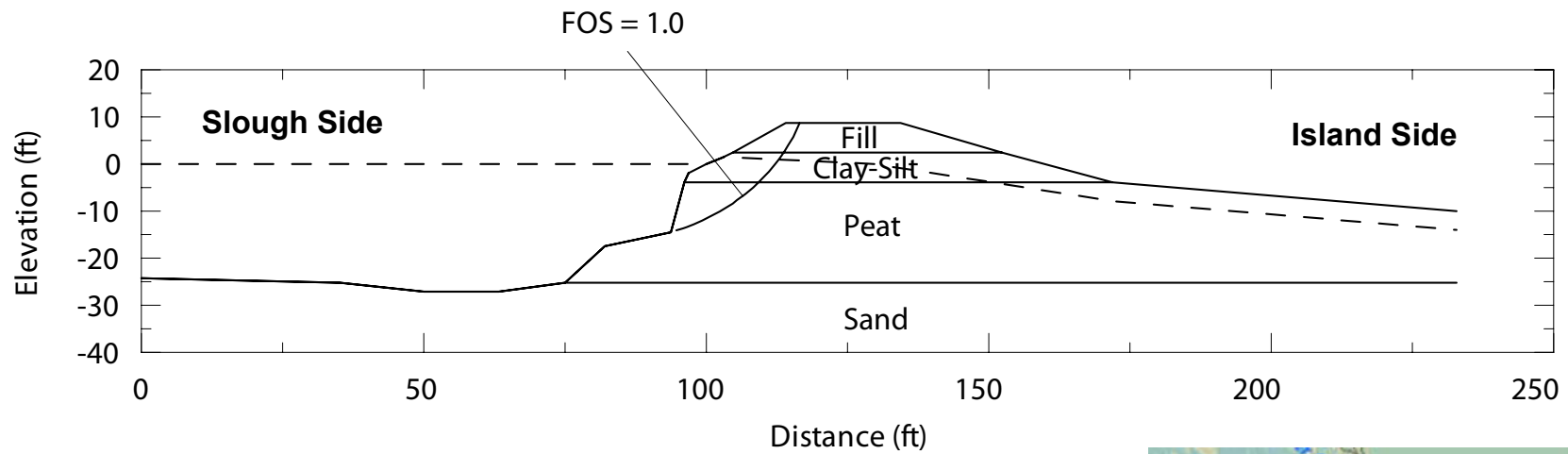
Modulus and Damping Curves used in
Dynamic Analysis

Figure
6-57



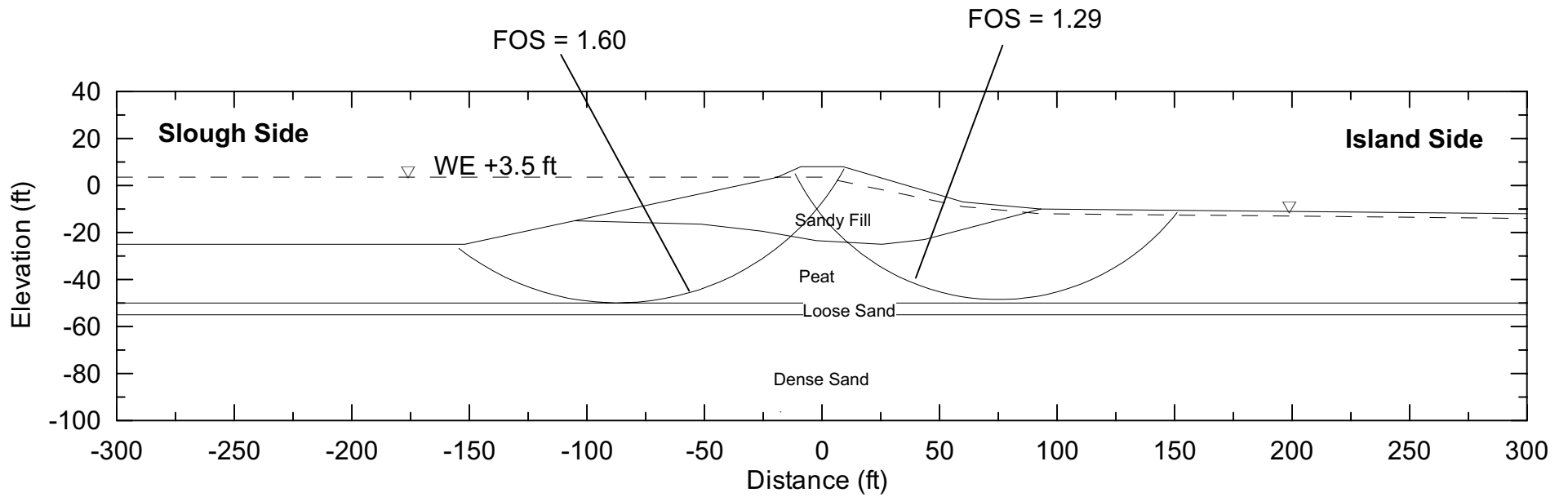
Type	Unit Weight (pcf)	ϕ'	c' (psf)
Fill	115	32	50
Peat	70	28	120
Dense Sand	125	38	0





Type	Unit Weight (pcf)	ϕ'	c' (psf)
Fill	115	35	50
Clay-Silt	90	32	100
Peat	70	28	120
Dense Sand	125	38	0

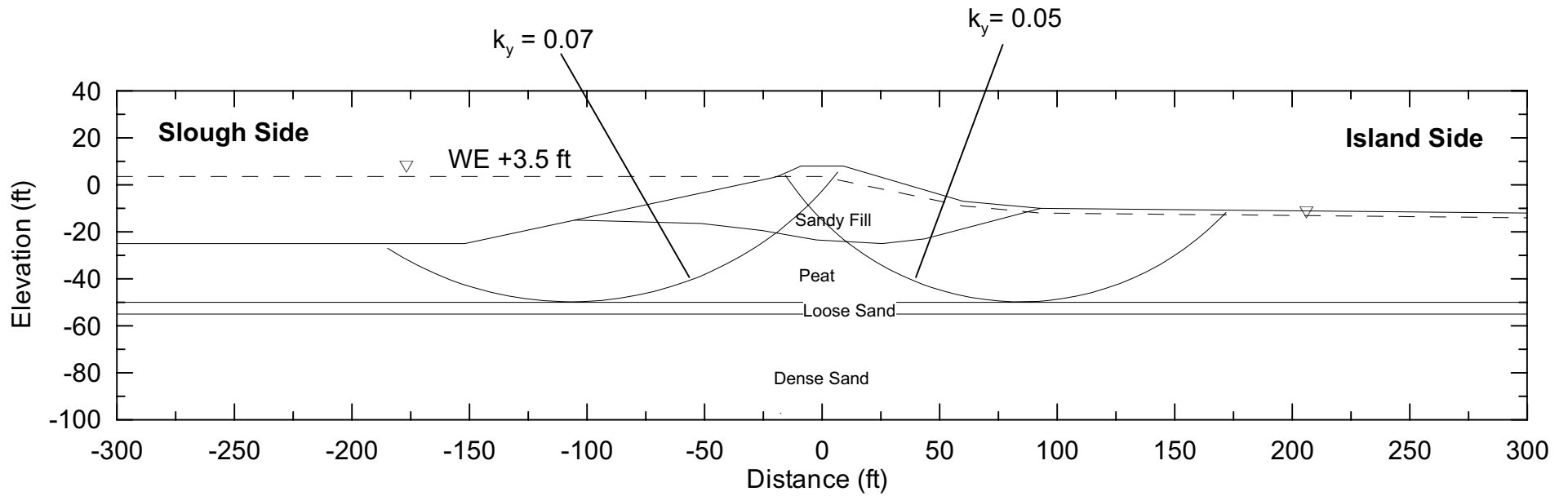




Type	Unit Weight (pcf)	ϕ'	c' (psf)	ϕ	c (psf)
Sandy Fill	115	30	0	-	-
Peat	70	28	120	18	140
Loose sand	125	32	0	-	-
Dense Sand	125	38	0	-	-

Note: See in-text table in Section 6.4.4.

Delta Risk Management Strategy (DRMS) Levee Fragility		Sherman Island - Station 650+00 Stability Analysis - Long Term	Figure 6-60a
URS	Project No. 26815621		



Type	Unit Weight (pcf)	ϕ'	c' (psf)	ϕ	c (psf)
Sandy Fill	115	30	0	-	-
Peat	70	28	120	18	140
Loose sand	125	32	0	-	-
Dense Sand	125	38	0	-	-

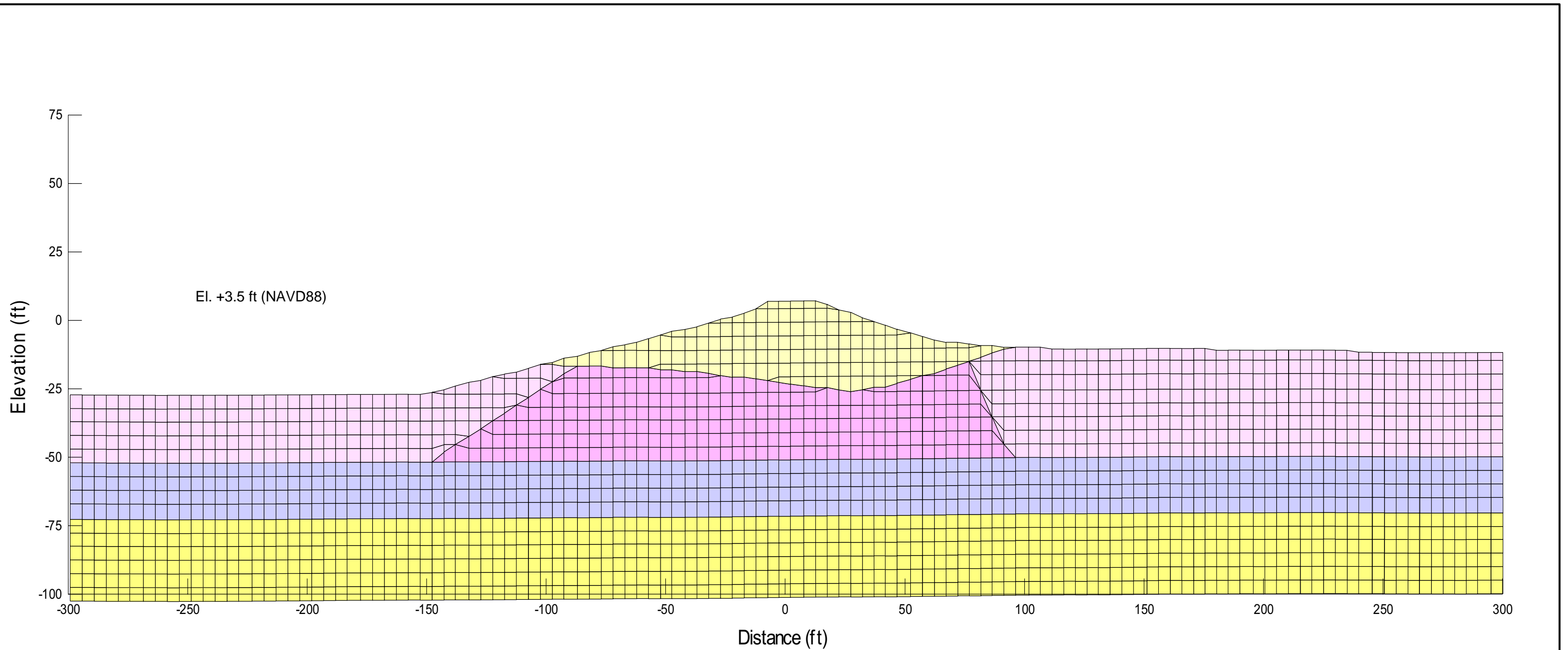
Delta Risk Management Strategy (DRMS)
Levee Fragility

URS

Project No. 26815621

Sherman Island - Station 650+00
Stability Analysis - Seismic

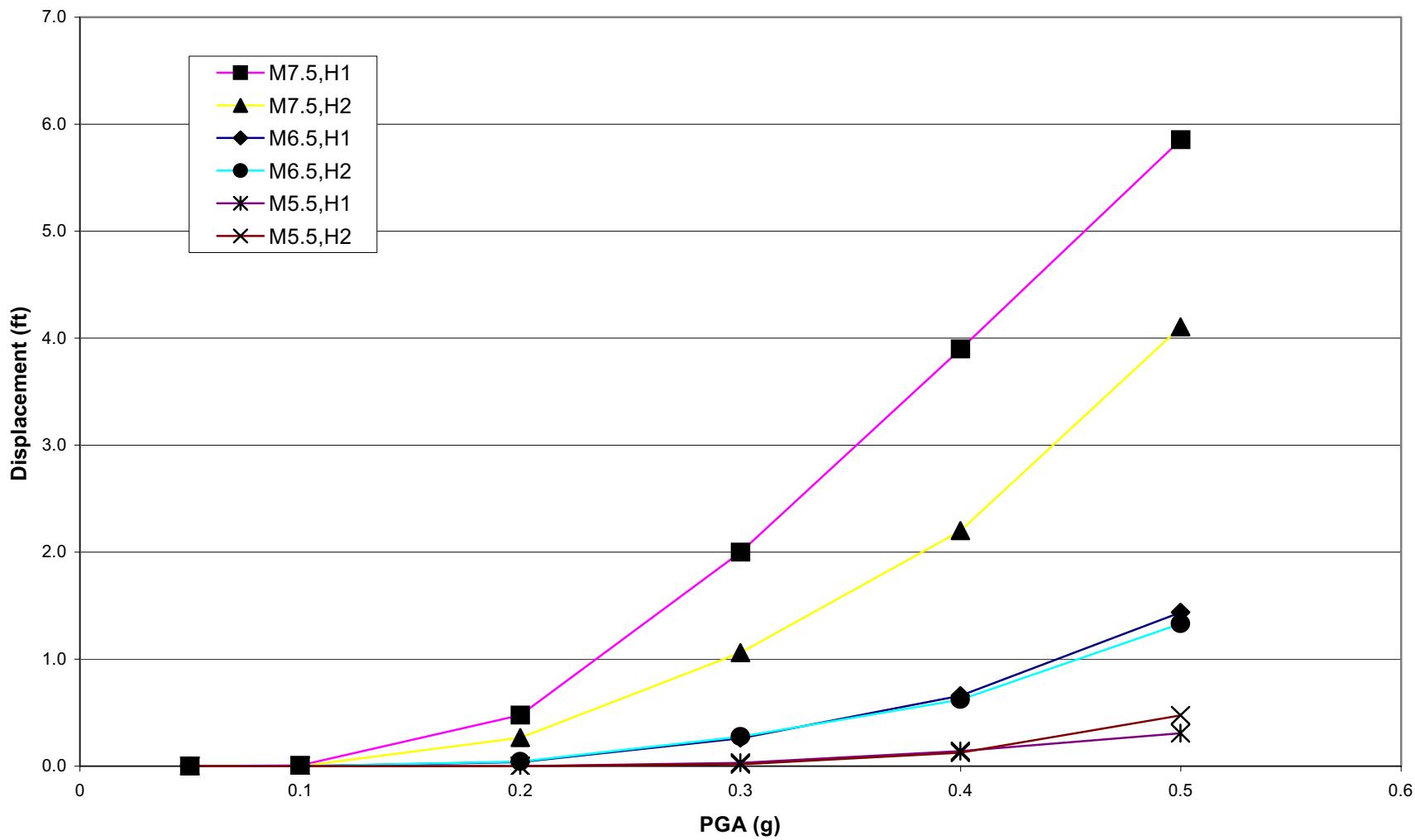
Figure
6-60b



Legend

- Levee Fill
- Free Field Peat
- Under Levee Peat
- Sand
- Dense Sand

Delta Risk Management Strategy (DRMS) Levee Fragility		Finite Element Model for Seismic Analysis Sherman Island - Station 650+00	Figure 6-61
URS	Project No. 26815621		



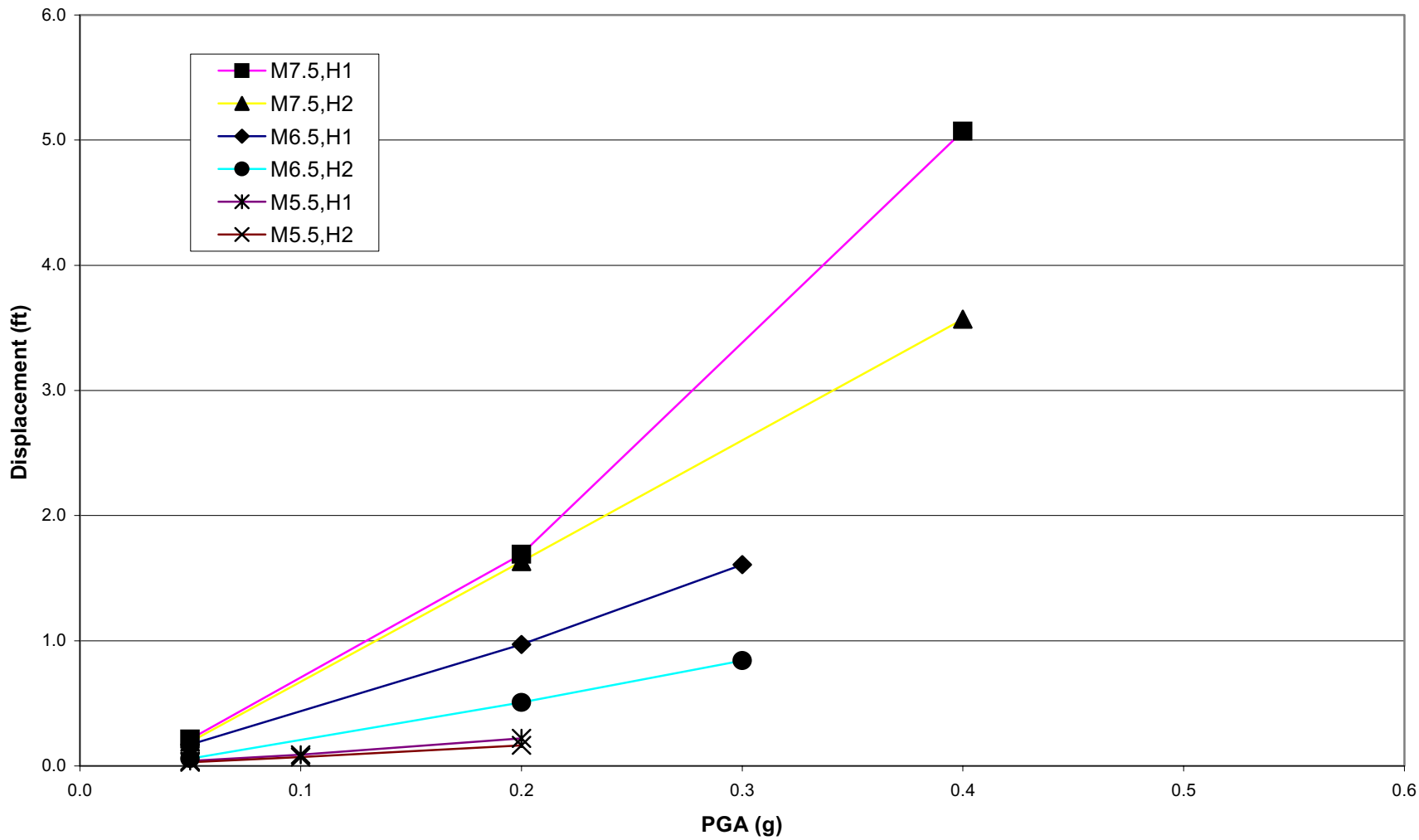
Delta Risk Management Strategy (DRMS)
Levee Fragility

URS

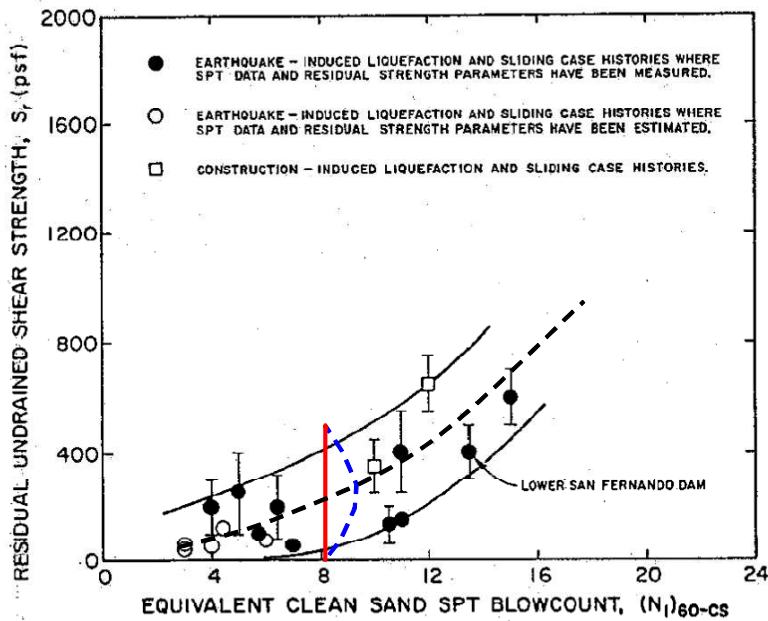
Project No. 26815621

Calculated Newmark Displacements
Sherman Island - Sta. 650+00
35 Feet of Peat

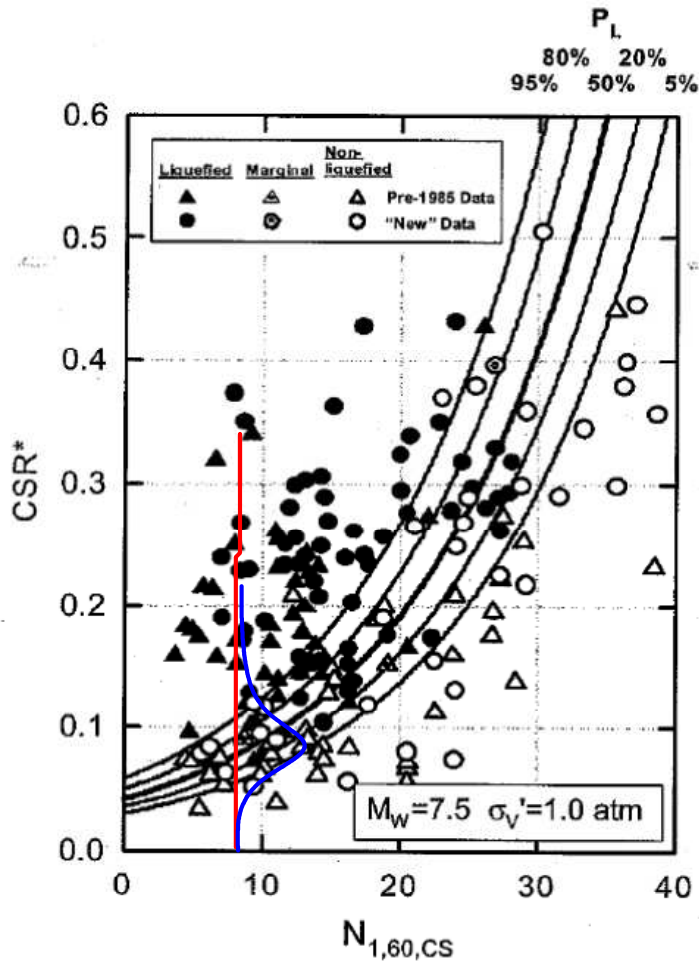
Figure
6-62



Delta Risk Management Strategy (DRMS) Levee Fragility		Calculated FLAC Displacements Sherman Island - Sta. 650+00 35 Feet of Peat	Figure 6-63
URS	Project No. 26815621		

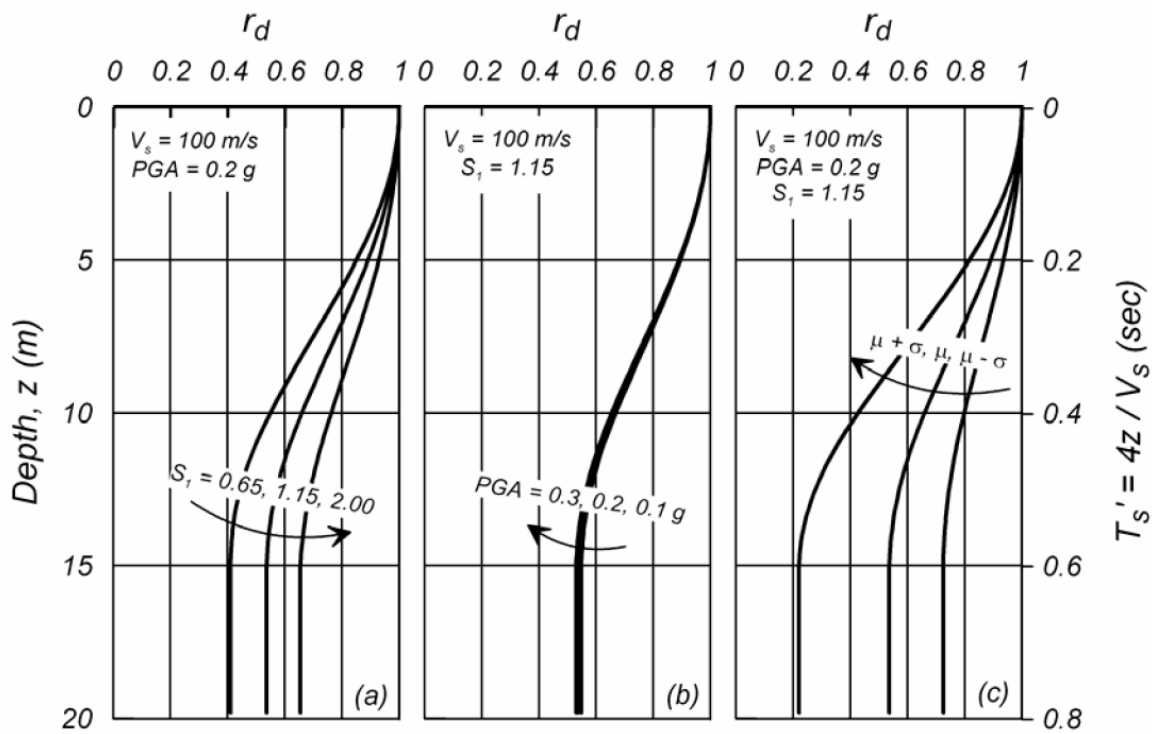


(1) Relationship Between $(N_1)_{60-CS}$ and Undrained Residual Shear Strength
 (Source: Seed and Harder 1990)

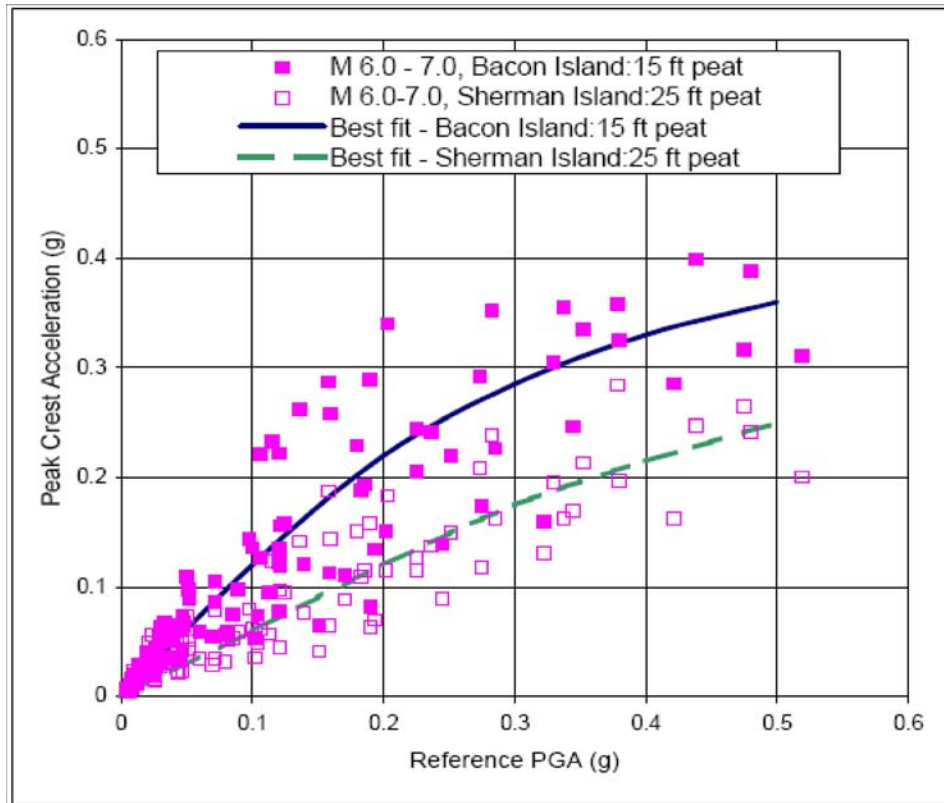


(2) Probabilistic SPT-Based Liquefaction Triggering Correlation
 (Source: Seed et al. 2003)

Delta Risk Management Strategy (DRMS) Levee Fragility		Undrained Residual Shear Strength and Probabilistic Liquefaction Triggering Correlation	Figure 6-64a
URS	Project No. 26815621		



(1) r_d vs Depth (Tadahiro et al. 2007)



(2) Reference PGA vs Peak Crest Acceleration

(Data from Tadahiro et al. 2007)

JOB TITLE : FLAC Mesh, No PEAT

(*10²)

FLAC (Version 5.00)

LEGEND

22-Jan-07 13:38
step 13052
-4.444E+02 <x< 4.444E+02
-4.889E+02 <y< 3.999E+02

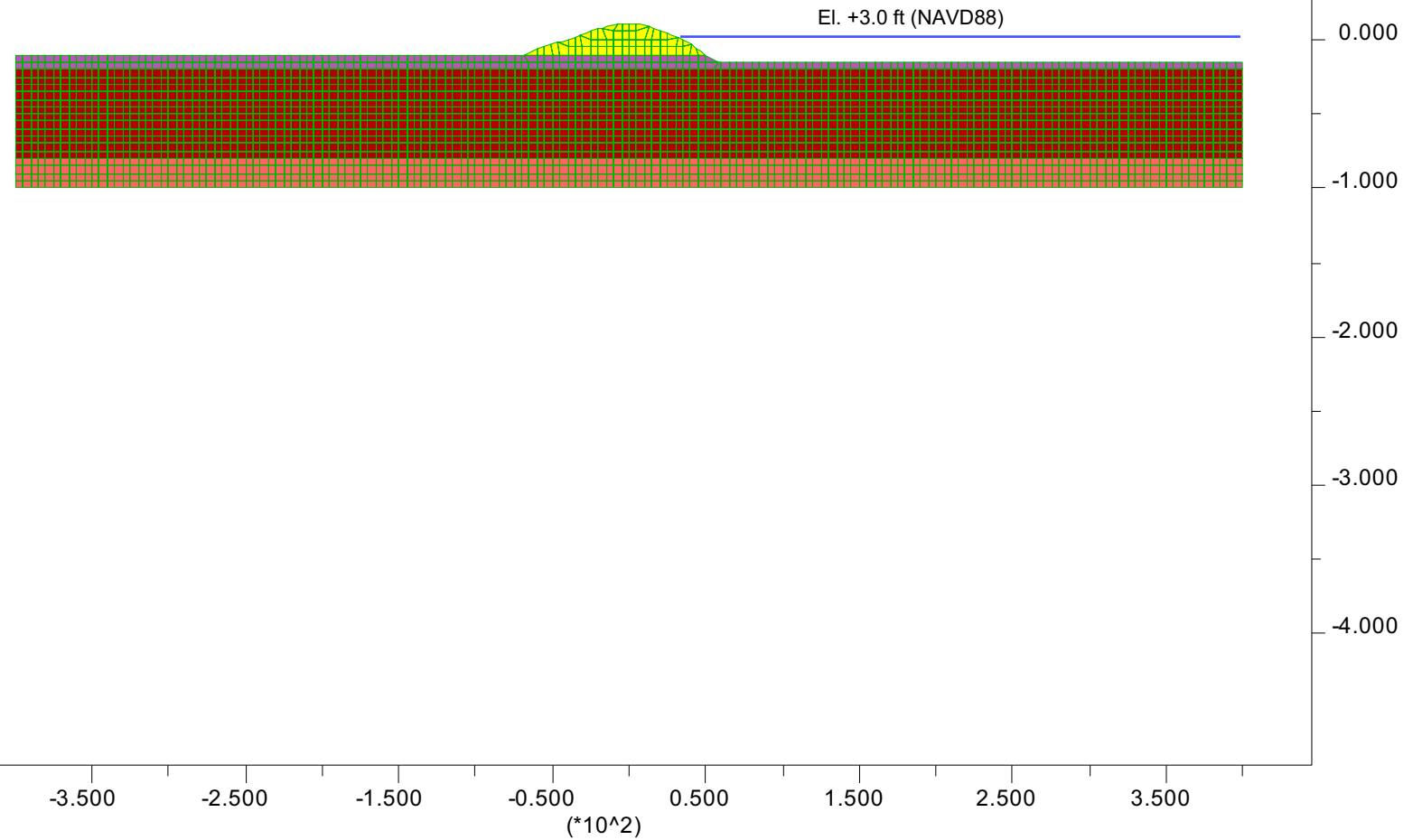
User-defined Groups

- CL
- SPSM2
- SPSM1
- FILL

Grid plot



1333 Broadway, Suite 800
Oakland, CA 94612



JOB TITLE : FLAC Mesh, 5 ft PEAT

(*10^2)

FLAC (Version 5.00)

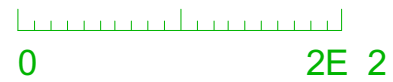
LEGEND

9-Dec-06 19:22
step 12048
-4.444E+02 <x< 4.444E+02
-4.889E+02 <y< 3.999E+02

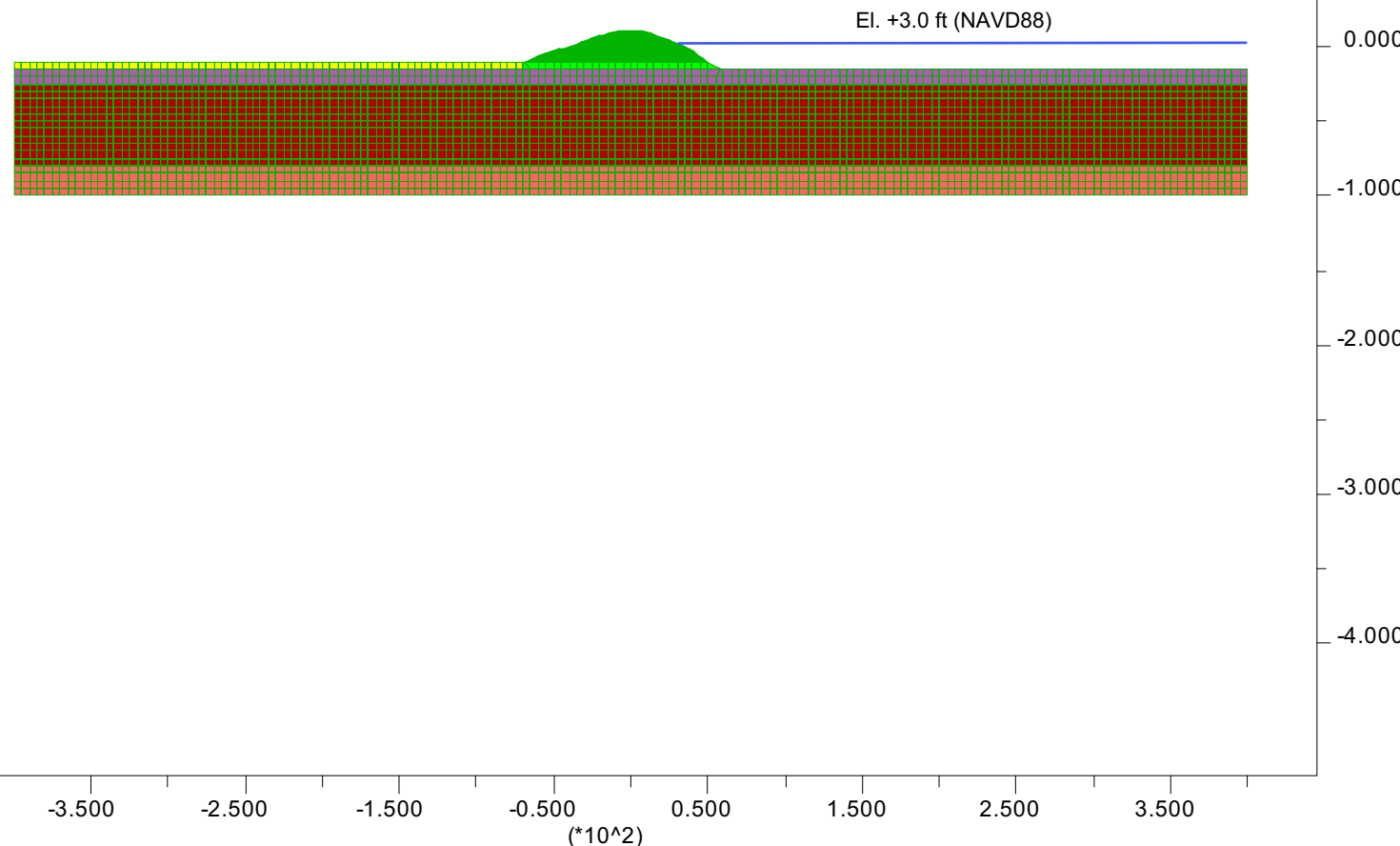
User-defined Groups

- CL
- SPSM2
- SPSM1
- PEAT
- ULPEAT
- FILL

Grid plot



1333 Broadway, Suite 800
Oakland, CA 94612



JOB TITLE : FLAC Mesh, 15 ft PEAT

(*10^2)

FLAC (Version 5.00)

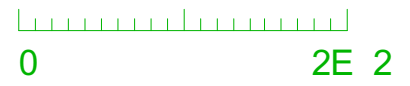
LEGEND

5-Dec-06 11:51
step 130350
Dynamic Time 5.6000E+01
-4.391E+02 <x< 4.391E+02
-4.836E+02 <y< 3.946E+02

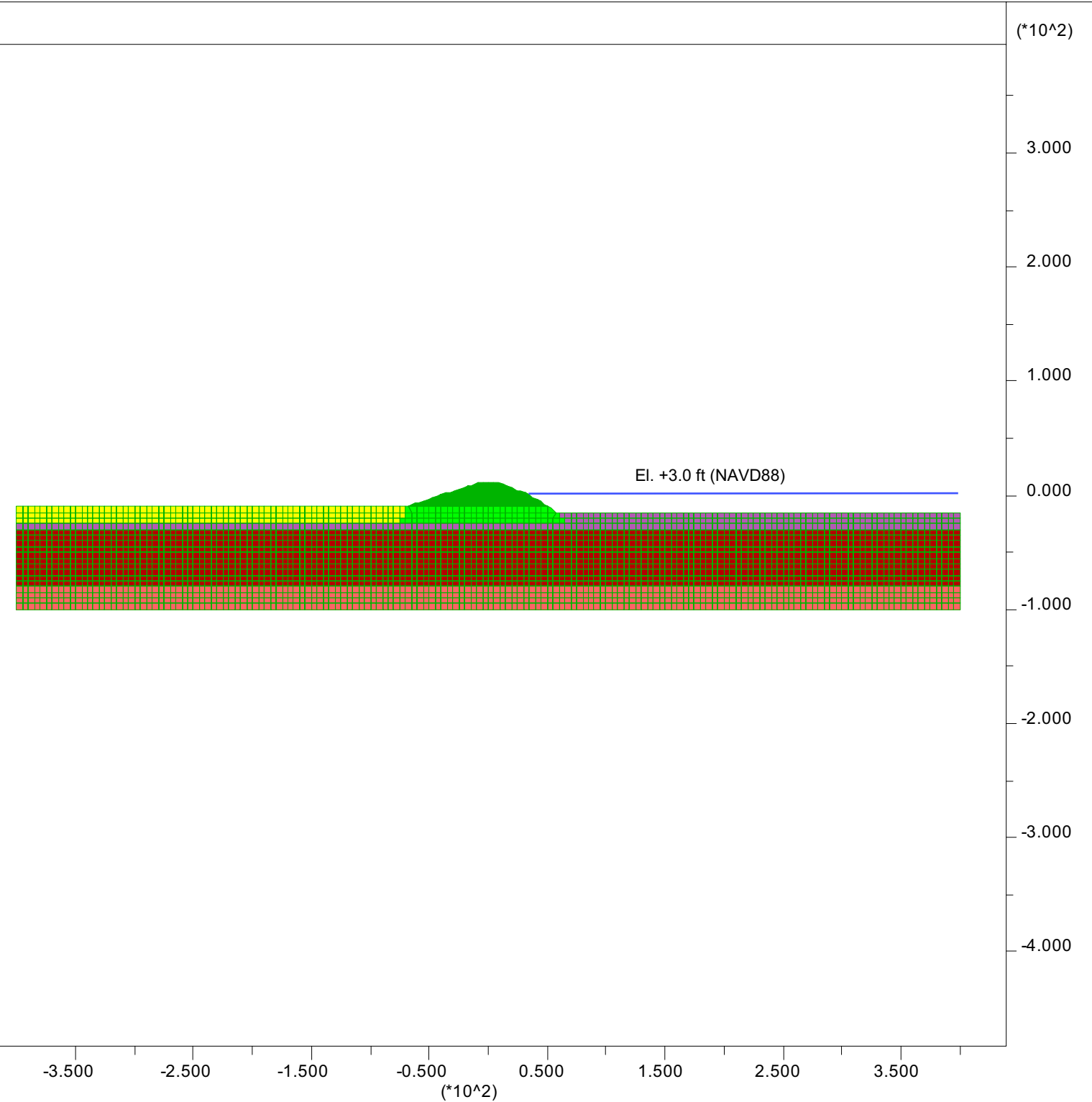
User-defined Groups

- CL
- SPSM2
- SPSM1
- PEAT
- ULPEAT
- FILL

Grid plot



1333 Broadway, Suite 800
Oakland, CA 94612



JOB TITLE : FLAC Mesh, 25 ft PEAT

(*10^2)

FLAC (Version 5.00)

LEGEND

9-Dec-06 18:58
step 11028
-4.444E+02 <x< 4.444E+02
-4.889E+02 <y< 3.999E+02

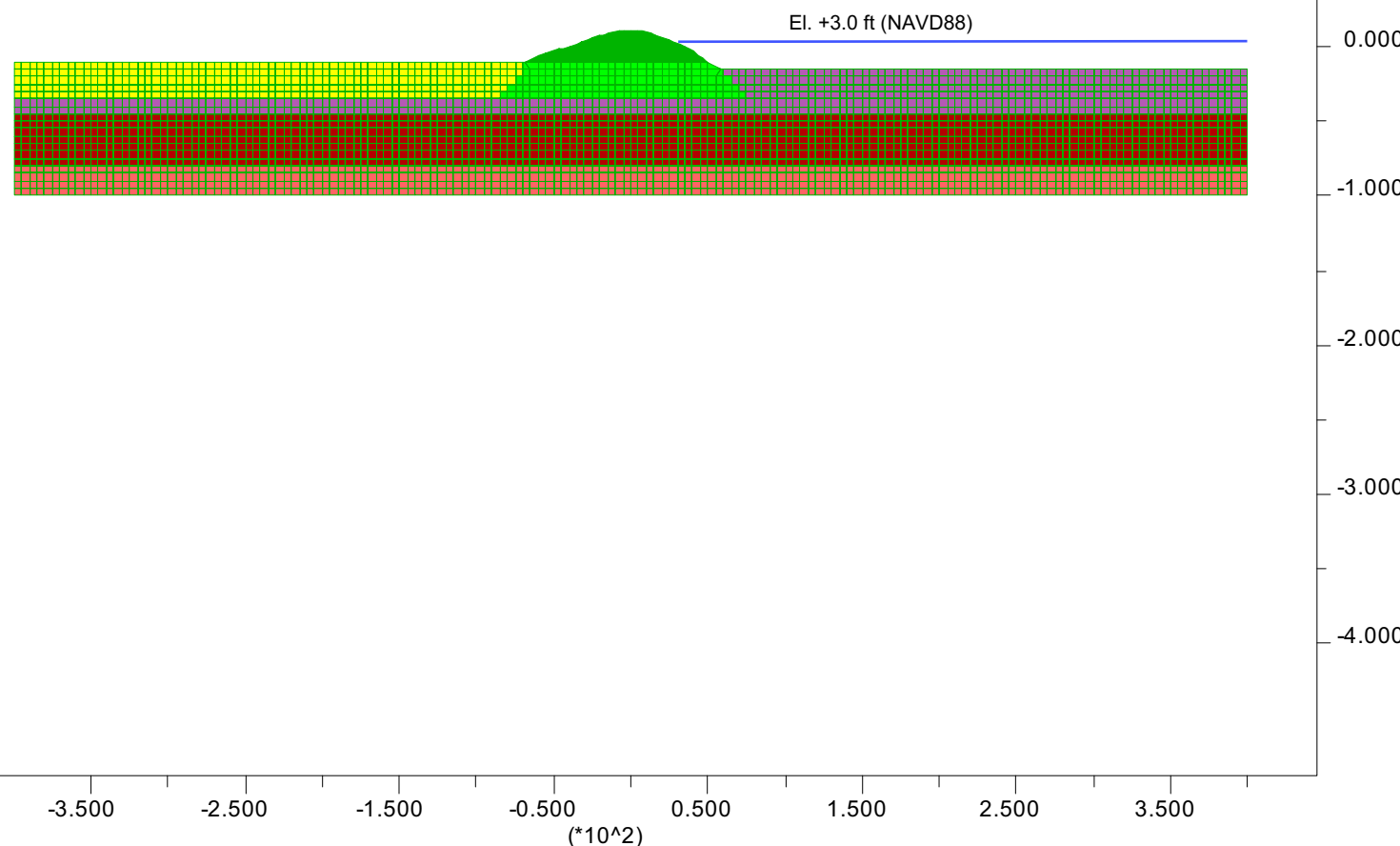
User-defined Groups

- CL
- SPSM2
- SPSM1
- PEAT
- ULPEAT
- FILL

Grid plot



1333 Broadway, Suite 800
Oakland, CA 94612



JOB TITLE : CSR Time History, Input Motion M5.5, H1 0.2g

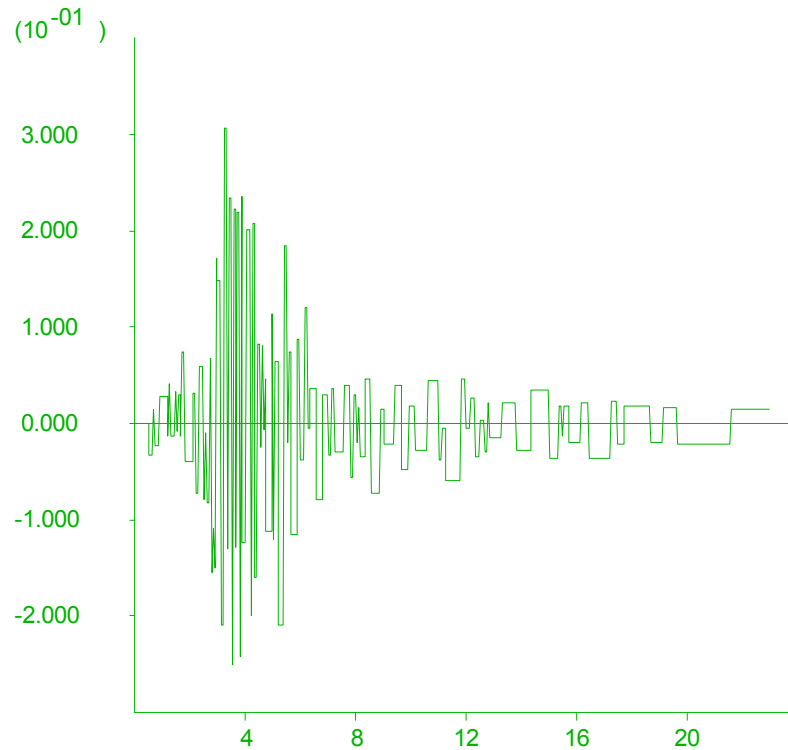
FLAC (Version 5.00)

LEGEND

9-Jan-07 18:42
step 62526
Dynamic Time 2.3000E+01

HISTORY PLOT

Y-axis :
68 sd_csr_zero (141, 17) PRP
X-axis :
1 Dynamic time



1333 Broadway, Suite 800
Oakland, CA 94612

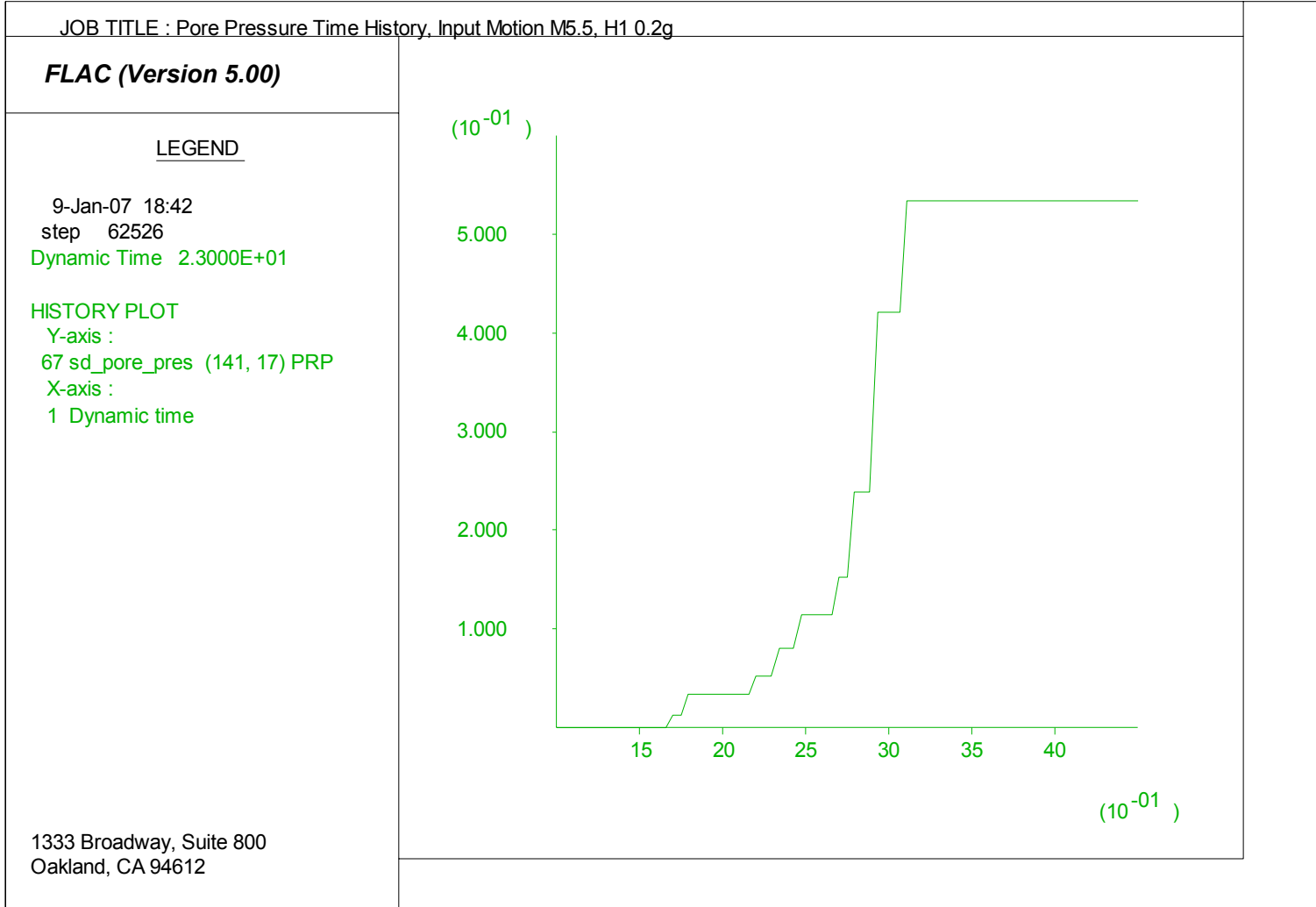
Delta Risk Management Strategy (DRMS)
Levee Fragility



Project No. 26815621

CSR Time History at Liquefiable
Sand Layer Under Levee Centerline
Idealized Section - 5 ft Peat
Input Motion M 5.5 H1, 0.2g

Figure
6-69



JOB TITLE : CSR Time History, Input Motion M6.5, H1 0.2g

FLAC (Version 5.00)

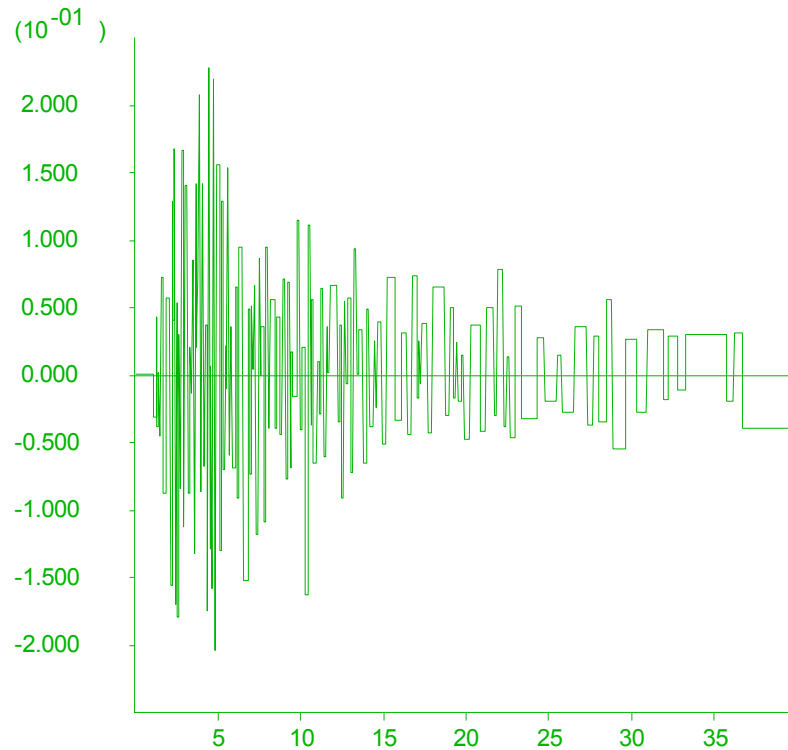
LEGEND

9-Jan-07 21:49
step 99815
Dynamic Time 4.0000E+01

HISTORY PLOT

Y-axis :
68 sd_csr_zero (141, 17) PRP
X-axis :
1 Dynamic time

1333 Broadway, Suite 800
Oakland, CA 94612



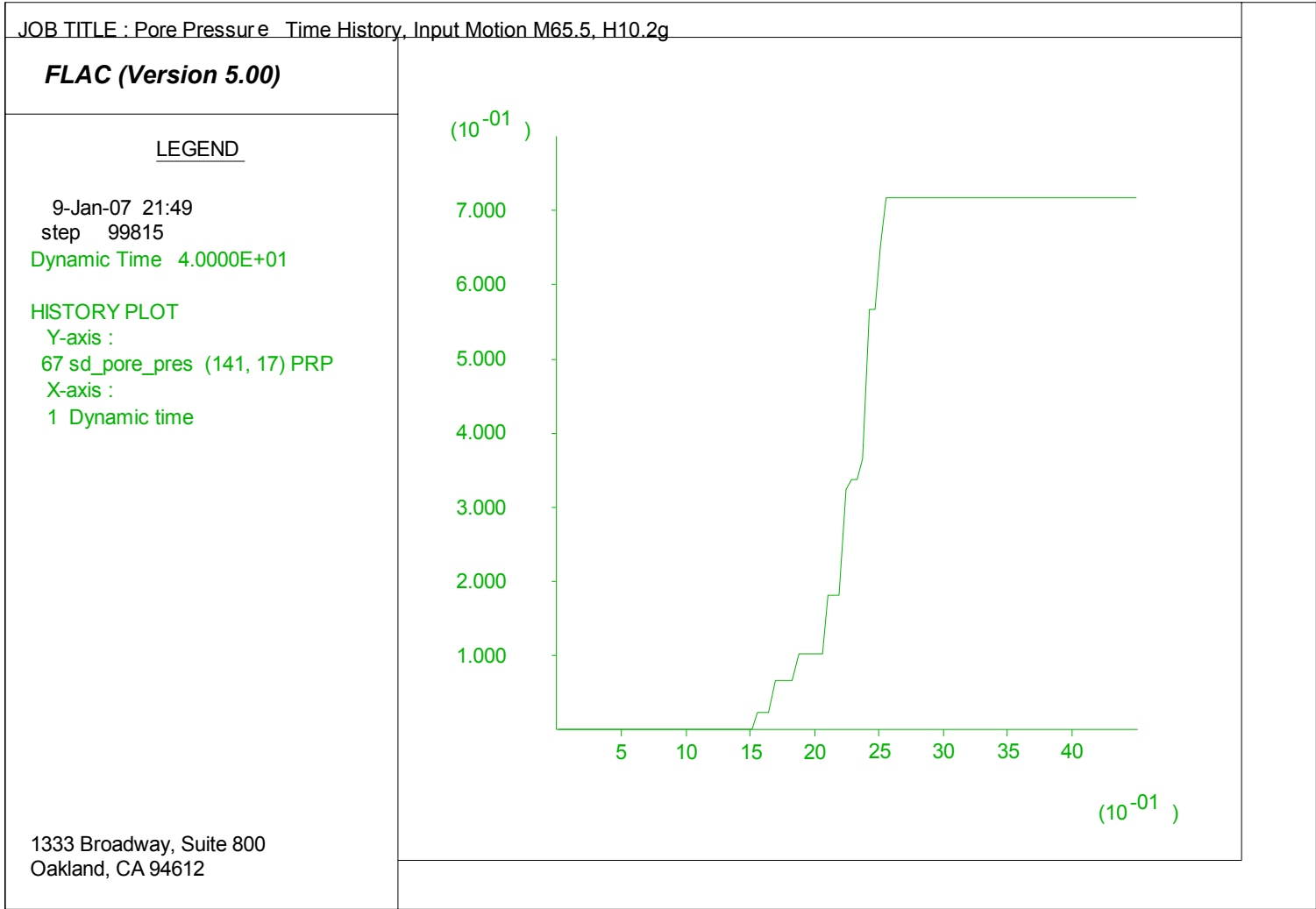
Delta Risk Management Strategy (DRMS)
Levee Fragility



Project No. 26815621

CSR Time History at Liquefiable
Sand Layer Under Levee Centerline
Idealized Section - 5 ft Peat
Input Motion M 6.5 H1, 0.2g

Figure
6-71



JOB TITLE : CSR Time History, Input Motion M7.5, H1 0.2g

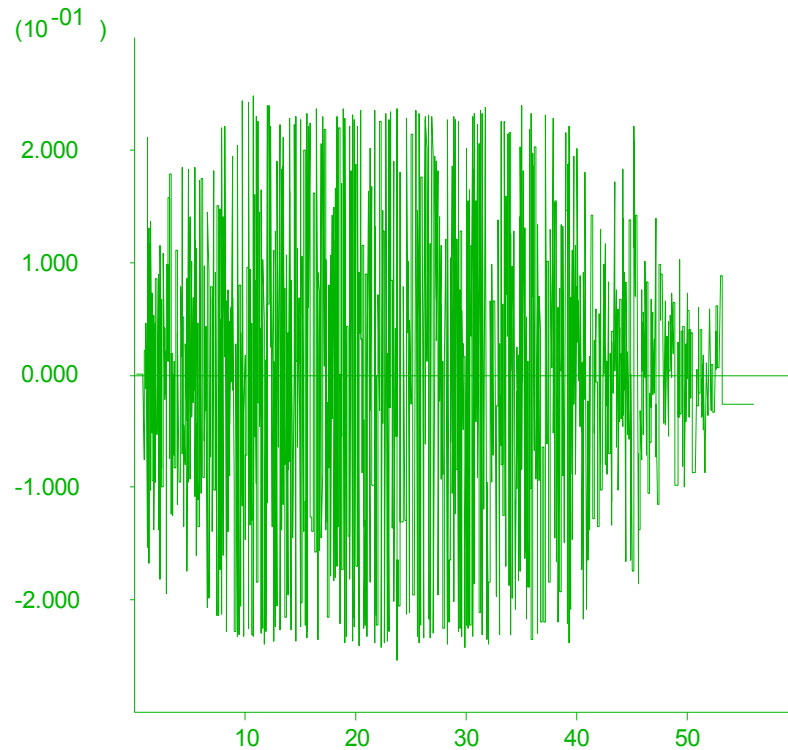
FLAC (Version 5.00)

LEGEND

10-Jan-07 2:35
step 134912
Dynamic Time 5.6000E+01

HISTORY PLOT

Y-axis :
68 sd_csr_zero (141, 17) PRP
X-axis :
1 Dynamic time



1333 Broadway, Suite 800
Oakland, CA 94612

Delta Risk Management Strategy (DRMS)
Levee Fragility

URS

Project No. 26815621

CSR Time History at Liquefiable
Sand Layer Under Levee Centerline
Idealized Section - 5 ft Peat
Input Motion M 7.5 H1, 0.2g

Figure
6-73

JOB TITLE : Pore Pressure Time History, Input Motion M7.5, H1 0.2g

FLAC (Version 5.00)

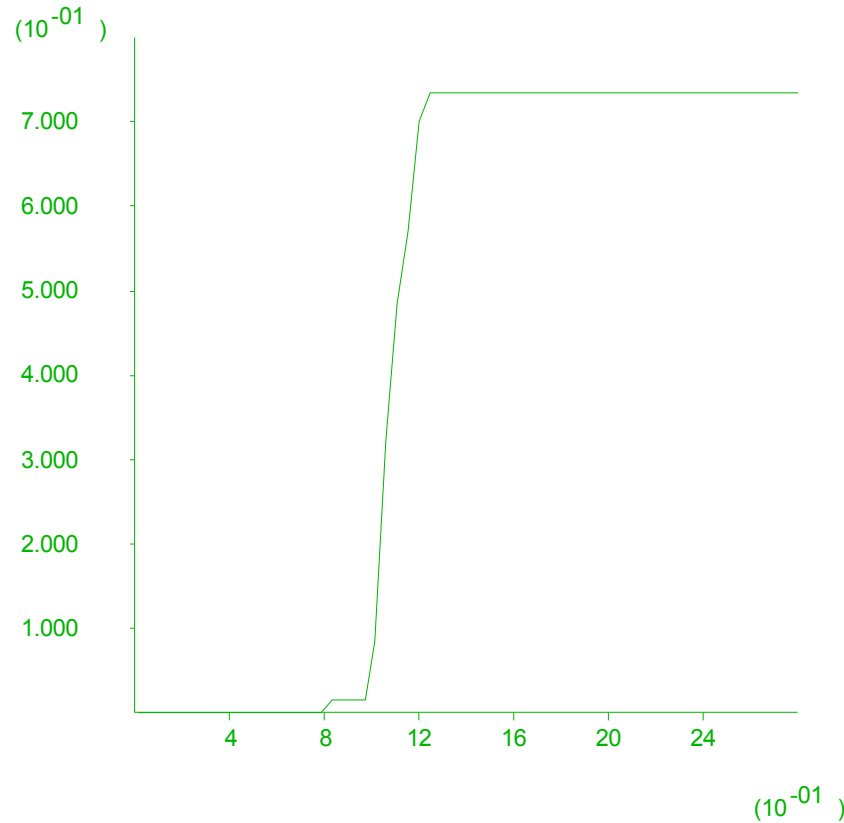
LEGEND

10-Jan-07 2:35
step 134912
Dynamic Time 5.6000E+01

HISTORY PLOT

Y-axis :
67 sd_pore_pres (141, 17) PRP
X-axis :
1 Dynamic time

1333 Broadway, Suite 800
Oakland, CA 94612



Delta Risk Management Strategy (DRMS)
Levee Fragility



Project No. 26815621

Pore Pressure Time History
at Liquefiable Sand Layer Under Levee Centerline
Idealized Section - 5 ft Peat
Input Motion M 7.5 H1, 0.2g

Figure
6-74

JOB TITLE : CSR Time History, Input Motion M5.5, H1 0.2g

FLAC (Version 5.00)

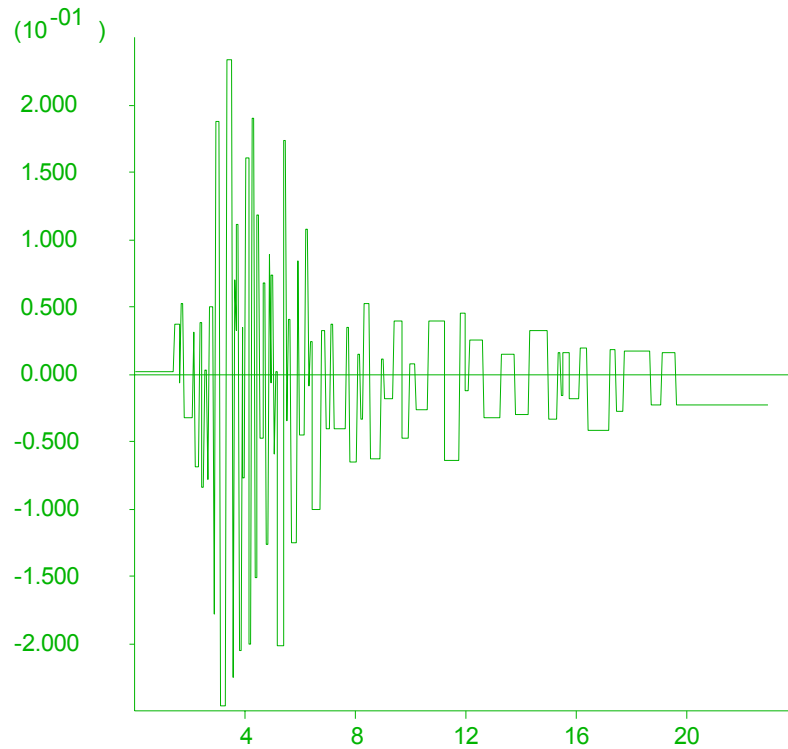
LEGEND

8-Jan-07 23:18
step 59332
Dynamic Time 2.3000E+01

HISTORY PLOT

Y-axis :
68 sd_csr_zero (141, 15) PRP
X-axis :
1 Dynamic time

1333 Broadway, Suite 800
Oakland, CA 94612



Delta Risk Management Strategy (DRMS)
Levee Fragility



Project No. 26815621

CSR Time History at Liquefiable
Sand Layer Under Levee Centerline
Idealized Section - 15 ft Peat
Input Motion M 5.5 H1, 0.2g

Figure
6-75

JOB TITLE : Pore Pressure Time History, Input Motion M5.5, H1 0.2g

FLAC (Version 5.00)

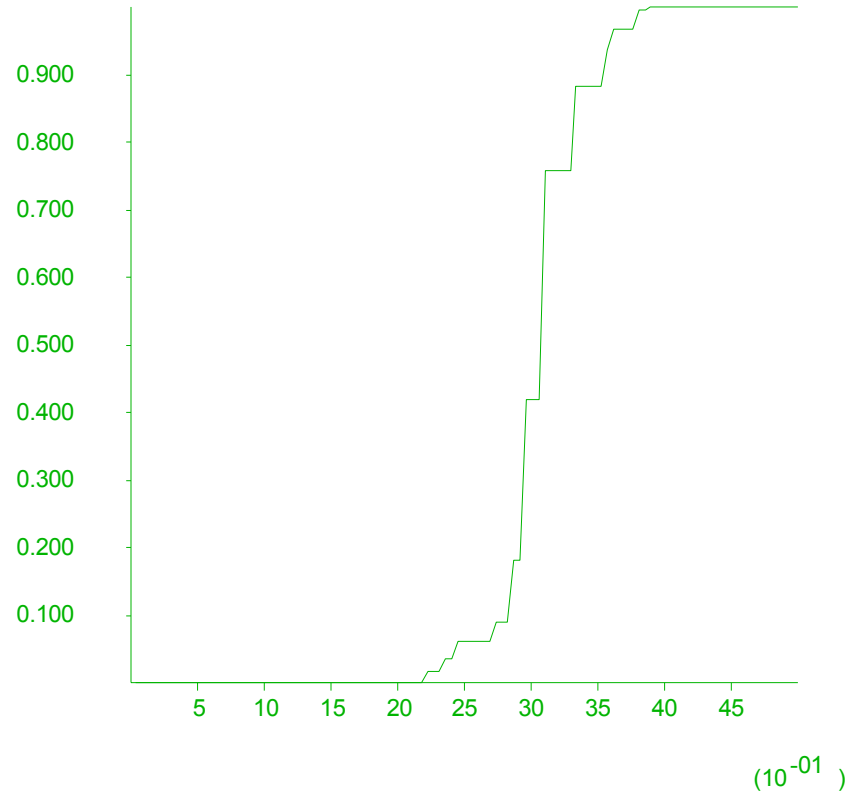
LEGEND

8-Jan-07 23:18
step 59332
Dynamic Time 2.3000E+01

HISTORY PLOT

Y-axis :
67 sd_pore_pres (141, 15) PRP
X-axis :
1 Dynamic time

1333 Broadway, Suite 800
Oakland, CA 94612



Delta Risk Management Strategy (DRMS)
Levee Fragility



Project No. 26815621

Pore Pressure Time History at Liquefiable
Sand Layer Under Levee Centerline
Idealized Section - 15 ft Peat
Input Motion M 5.5 H1, 0.2g

Figure
6-76

JOB TITLE : CSR Time History, Input Motion M6.5, H1 0.2g

FLAC (Version 5.00)

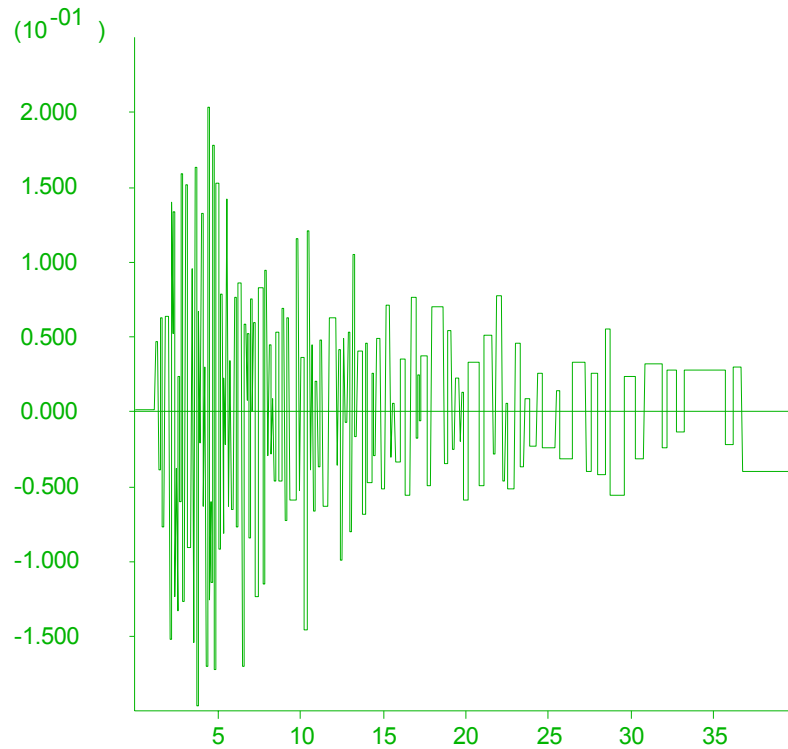
LEGEND

9-Jan-07 21:58
step 95763
Dynamic Time 4.0000E+01

HISTORY PLOT

Y-axis :
68 sd_csr_zero (141, 15) PRP
X-axis :
1 Dynamic time

1333 Broadway, Suite 800
Oakland, CA 94612



Delta Risk Management Strategy (DRMS)
Levee Fragility



Project No. 26815621

CSR Time History at Liquefiable
Sand Layer Under Levee Centerline
Idealized Section - 15 ft Peat
Input Motion M 6.5 H1, 0.2g

Figure
6-77

JOB TITLE : Pore Pressure Time History, Input Motion M6.5, H1 0.2g

FLAC (Version 5.00)

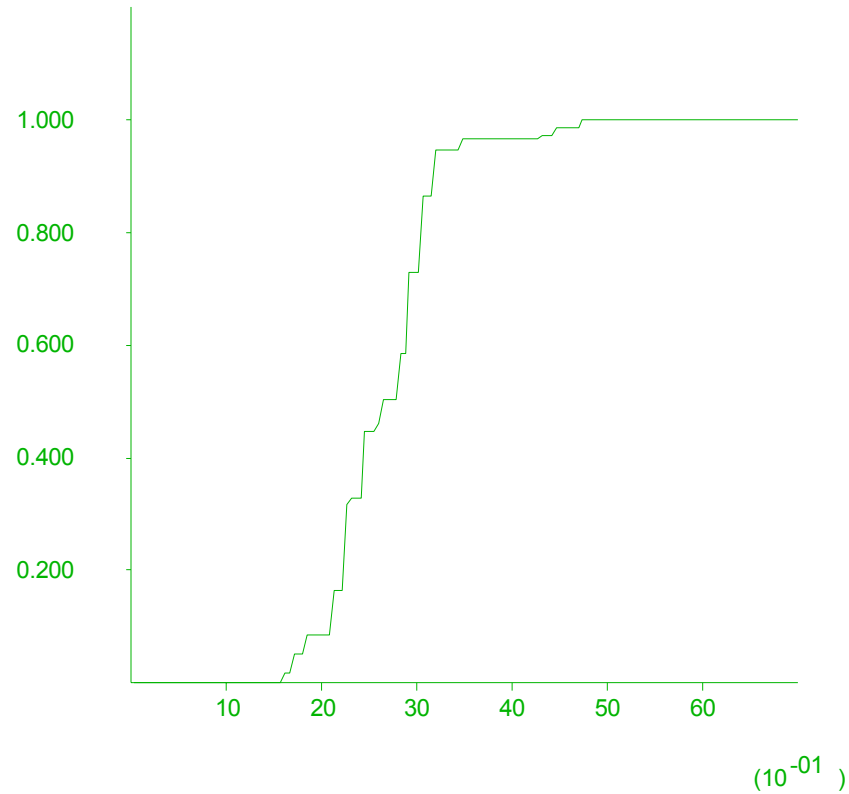
LEGEND

9-Jan-07 21:58
step 95763
Dynamic Time 4.0000E+01

HISTORY PLOT

Y-axis :
67 sd_pore_pres (141, 15) PRP
X-axis :
1 Dynamic time

1333 Broadway, Suite 800
Oakland, CA 94612



Delta Risk Management Strategy (DRMS)
Levee Fragility



Project No. 26815621

Pore Pressure Time History at Liquefiable
Sand Layer Under Levee Centerline
Idealized Section - 15 ft Peat
Input Motion M 6.5 H1, 0.2g

Figure
6-78

JOB TITLE : CSR Time History, Input Motion M7.5 H1 0.2g

FLAC (Version 5.00)

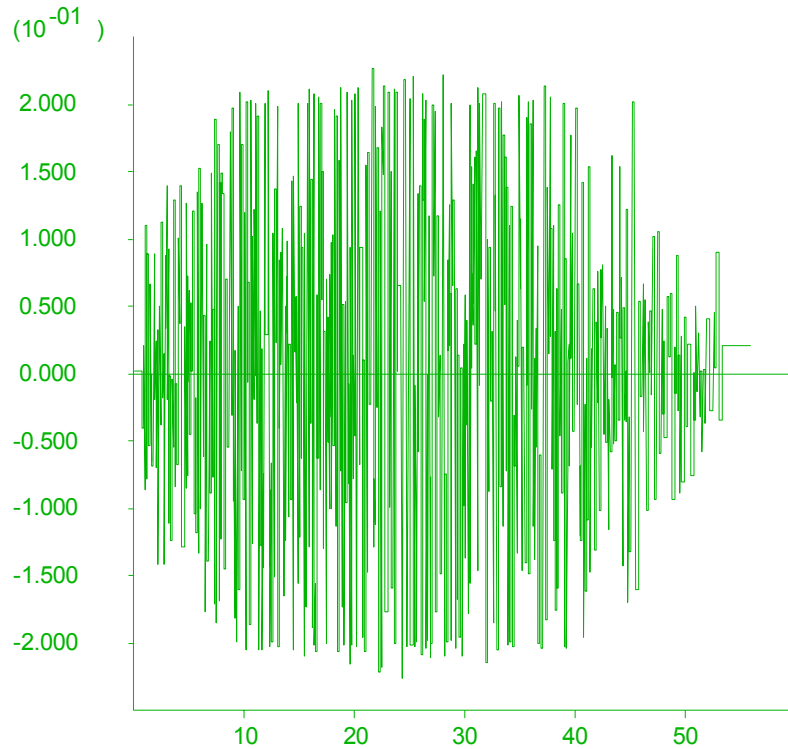
LEGEND

10-Jan-07 3:37
step 130051
Dynamic Time 5.6000E+01

HISTORY PLOT

Y-axis :
68 sd_csr_zero (141, 15) PRP
X-axis :
1 Dynamic time

1333 Broadway, Suite 800
Oakland, CA 94612



Delta Risk Management Strategy (DRMS)
Levee Fragility



Project No. 26815621

CSR Time History at Liquefiable
Sand Layer Under Levee Centerline
Idealized Section - 15 ft Peat
Input Motion M 7.5 H1, 0.2g

Figure
6-79

JOB TITLE : Pore Pressure Time History, Input Motion M6.5, H1 0.2g

FLAC (Version 5.00)

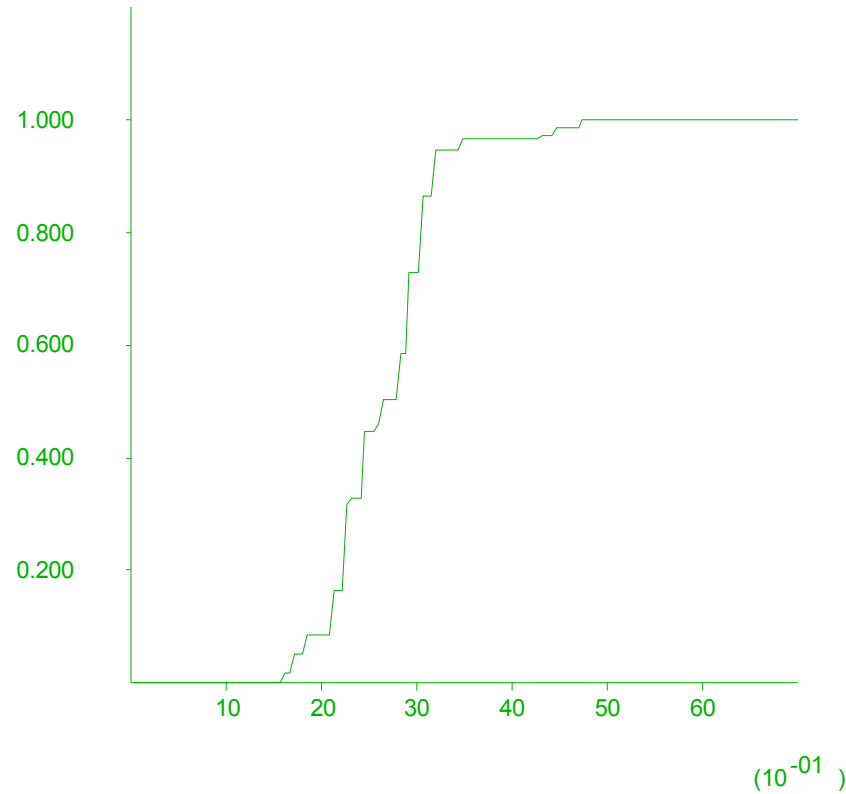
LEGEND

9-Jan-07 21:58
step 95763
Dynamic Time 4.0000E+01

HISTORY PLOT

Y-axis :
67 sd_pore_pres (141, 15) PRP
X-axis :
1 Dynamic time

1333 Broadway, Suite 800
Oakland, CA 94612



Delta Risk Management Strategy (DRMS)
Levee Fragility



Project No. 26815621

Pore Pressure Time History at Liquefiable
Sand Layer Under Levee Centerline
Idealized Section - 15 ft Peat
Input Motion M 7.5 H1, 0.2g

Figure
6-80

JOB TITLE : CSR Time History, Input Motion M5.5 H1, 0.2g

FLAC (Version 5.00)

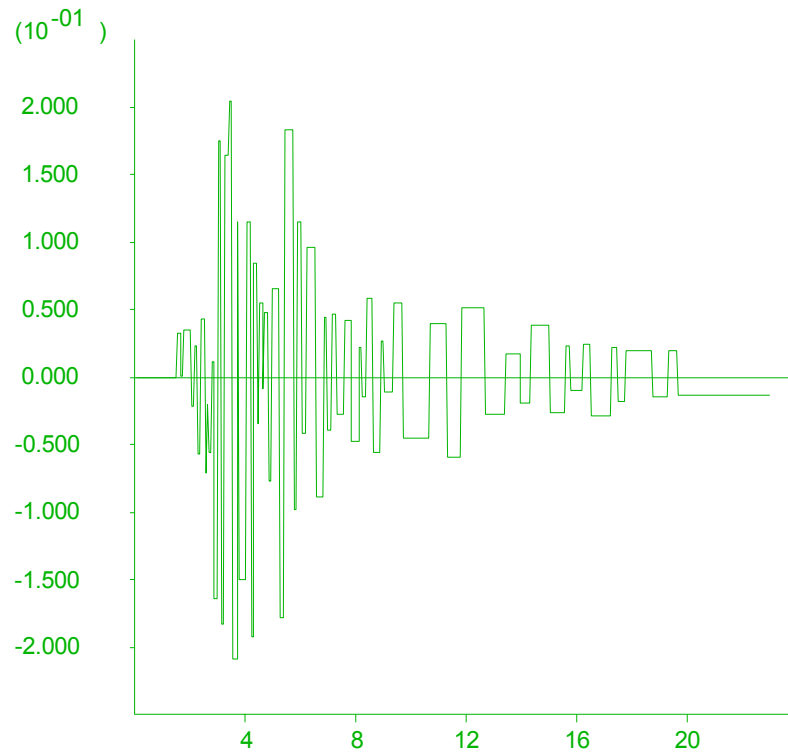
LEGEND

8-Jan-07 20:07
step 59058
Dynamic Time 2.3000E+01

HISTORY PLOT

Y-axis :
68 sd_csr_zero (141, 13) PRP
X-axis :
1 Dynamic time

1333 Broadway, Suite 800
Oakland, CA 94612



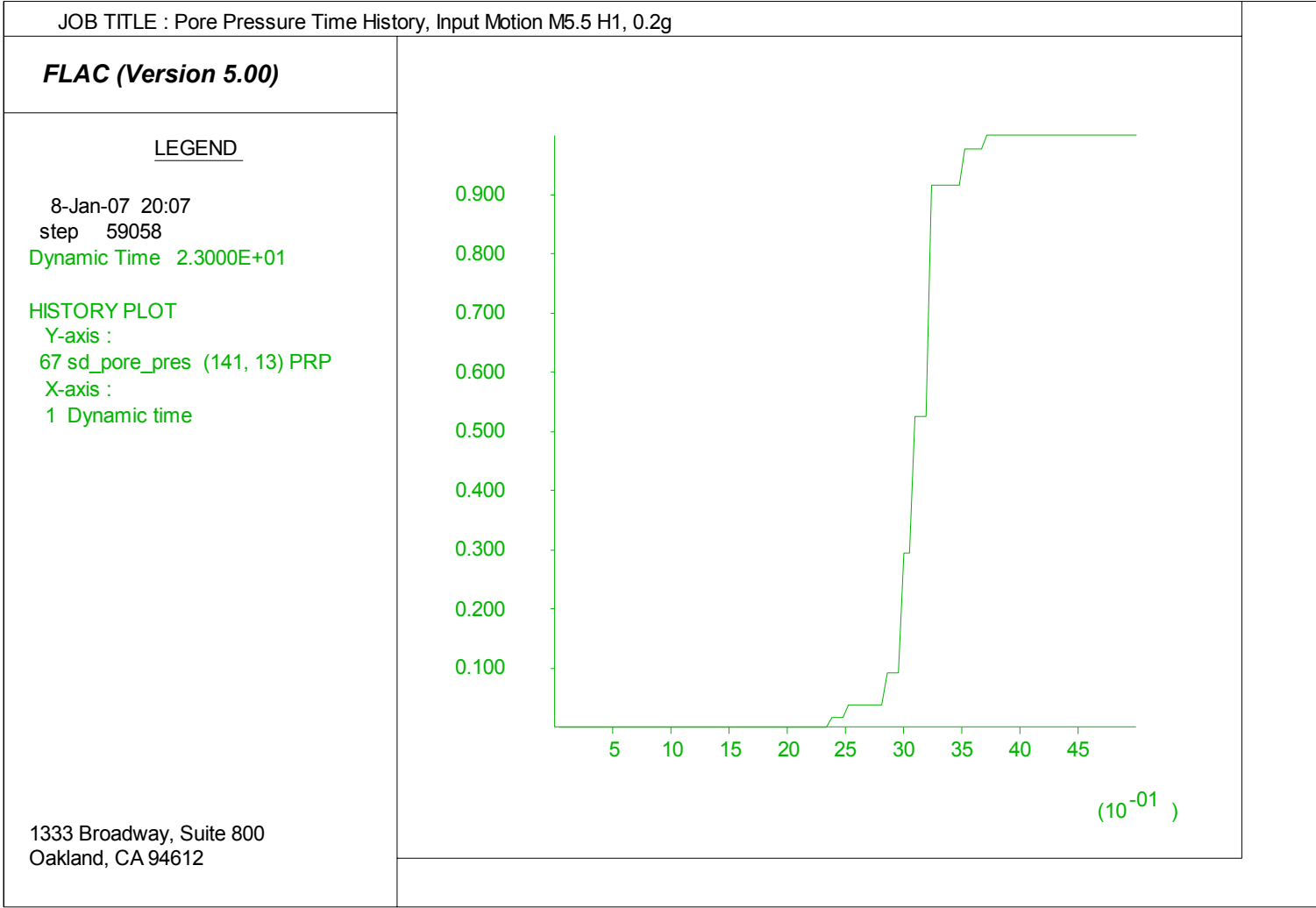
Delta Risk Management Strategy (DRMS)
Levee Fragility



Project No. 26815621

CSR Time History at Liquefiable
Sand Layer Under Levee Centerline
Idealized Section - 25 ft Peat
Input Motion M 5.5 H1, 0.2g

Figure
6-81



JOB TITLE : CSR Time History, Input Motion M6.5 H1, 0.2g

FLAC (Version 5.00)

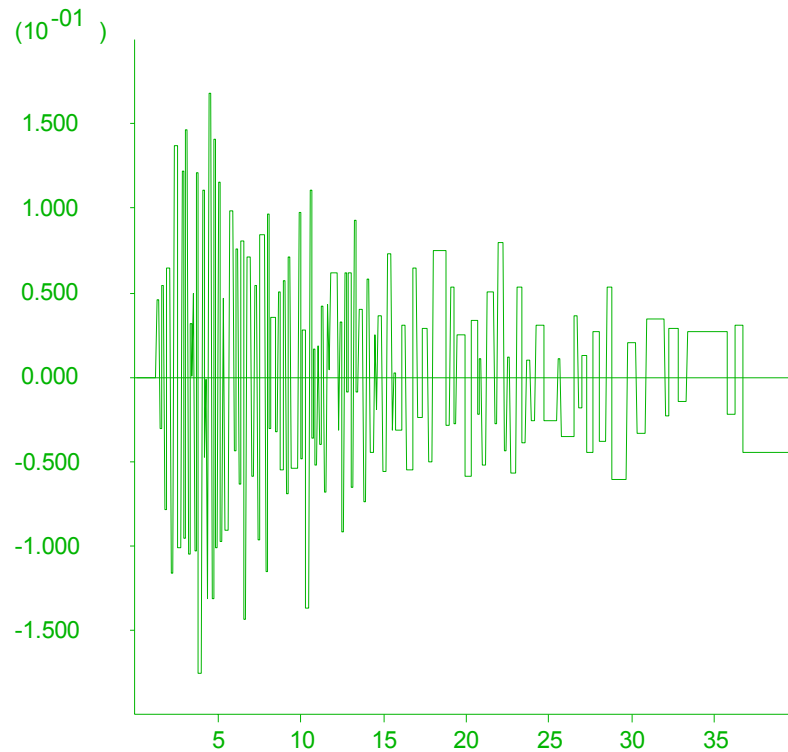
LEGEND

8-Jan-07 23:49
step 94557
Dynamic Time 4.0000E+01

HISTORY PLOT

Y-axis :
68 sd_csr_zero (141, 13) PRP
X-axis :
1 Dynamic time

1333 Broadway, Suite 800
Oakland, CA 94612



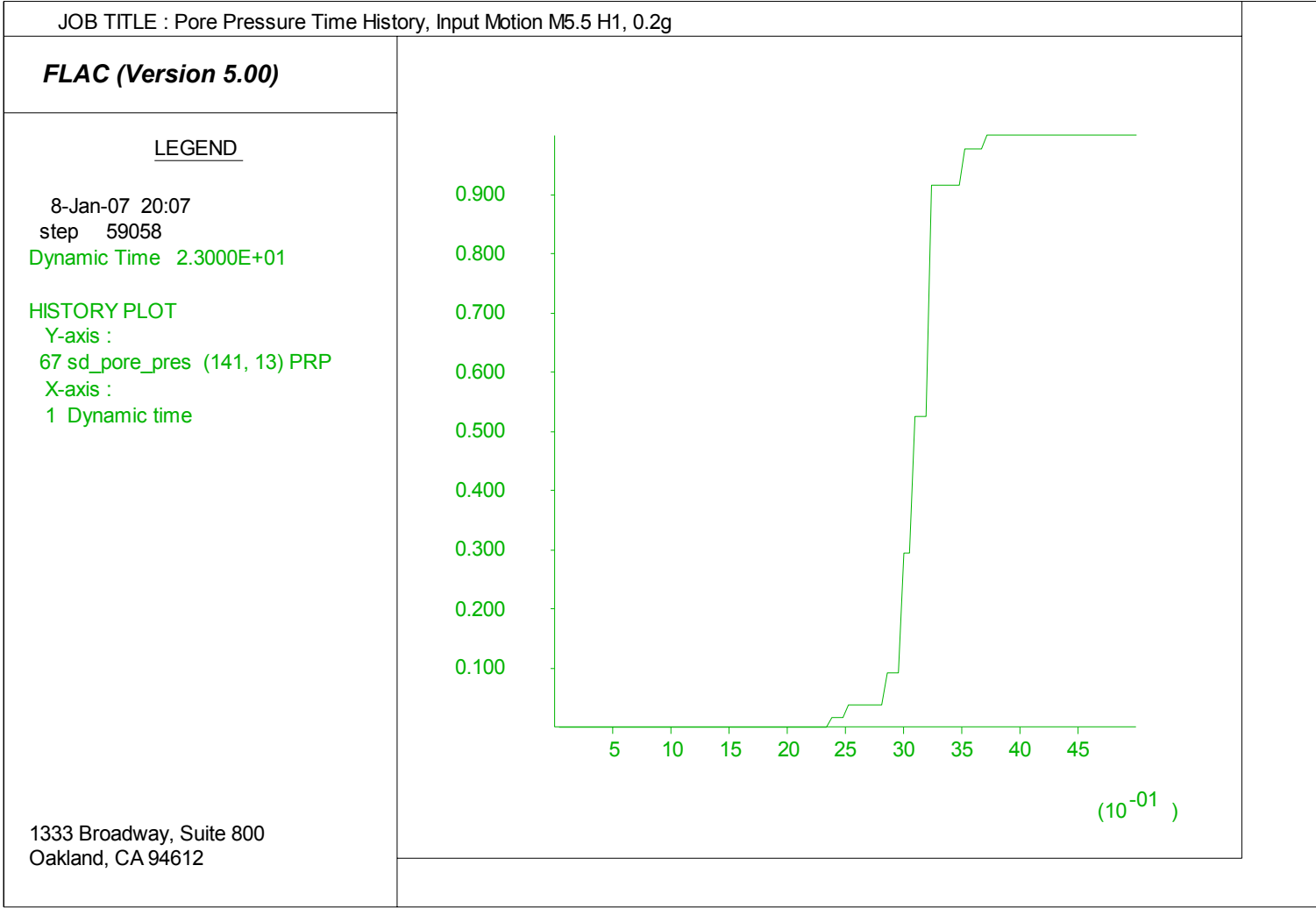
Delta Risk Management Strategy (DRMS)
Levee Fragility



Project No. 26815621

CSR Time History at Liquefiable
Sand Layer Under Levee Centerline
Idealized Section - 25 ft Peat
Input Motion M 6.5 H1, 0.2g

Figure
6-83



JOB TITLE : CSR Time History, Input Motion M7.5 H1, 0.2g

FLAC (Version 5.00)

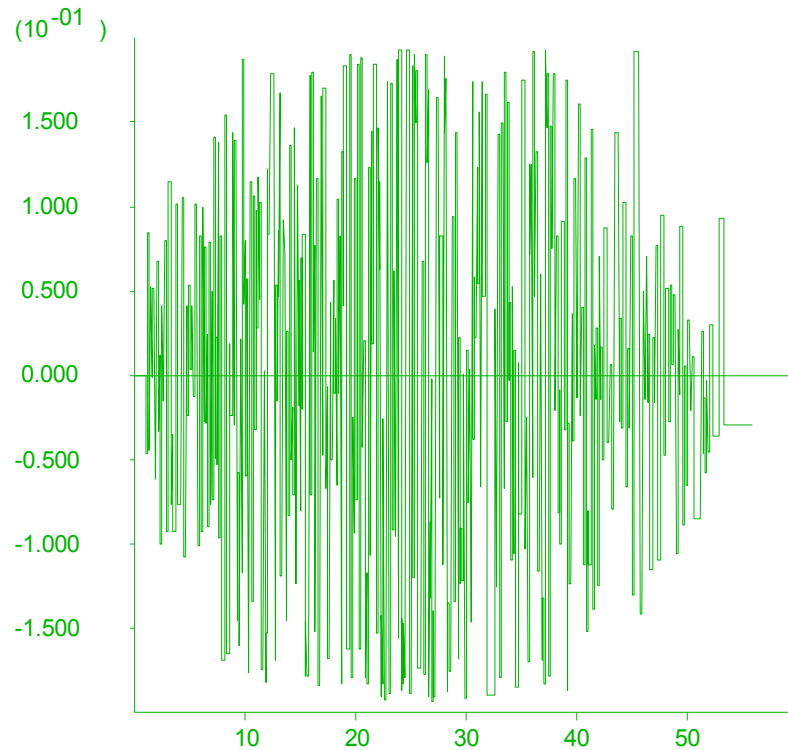
LEGEND

9-Jan-07 5:27
step 127967
Dynamic Time 5.6000E+01

HISTORY PLOT

Y-axis :
68 sd_csr_zero (141, 13) PRP
X-axis :
1 Dynamic time

1333 Broadway, Suite 800
Oakland, CA 94612



Delta Risk Management Strategy (DRMS)
Levee Fragility

URS

Project No. 26815621

CSR Time History at Liquefiable
Sand Layer Under Levee Centerline
Idealized Section - 25 ft Peat
Input Motion M 7.5 H1, 0.2g

Figure
6-85

JOB TITLE : Pore Pressure Time History, Input Motion M67; H1, 0.2g

FLAC (Version 5.00)

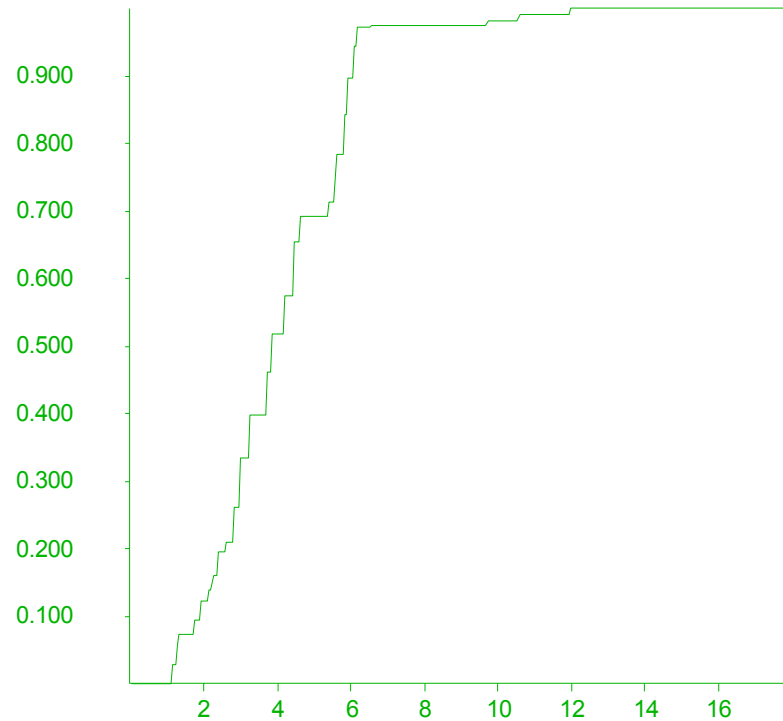
LEGEND

9-Jan-07 5:27
step 127967
Dynamic Time 5.6000E+01

HISTORY PLOT

Y-axis :
67 sd_pore_pres (141, 13) PRP
X-axis :
1 Dynamic time

1333 Broadway, Suite 800
Oakland, CA 94612



Delta Risk Management Strategy (DRMS)
Levee Fragility



Project No. 26815621

Pore Pressure Time History at Liquefiable
Sand Layer Under Levee Centerline
Idealized Section - 25 ft Peat
Input Motion M 7.5 H1, 0.2g

Figure
6-86

JOB TITLE : Horizontal Displacement Contours, Input Motion M5.5, H1 0.2g

FLAC (Version 5.00)

LEGEND

9-Jan-07 18:42

step 62526

Dynamic Time 2.3000E+01

-1.538E+02 <x< 1.540E+02

-1.988E+02 <y< 1.090E+02

X-displacement contours (feet)

-4.00E-01

-2.00E-01

0.00E+00

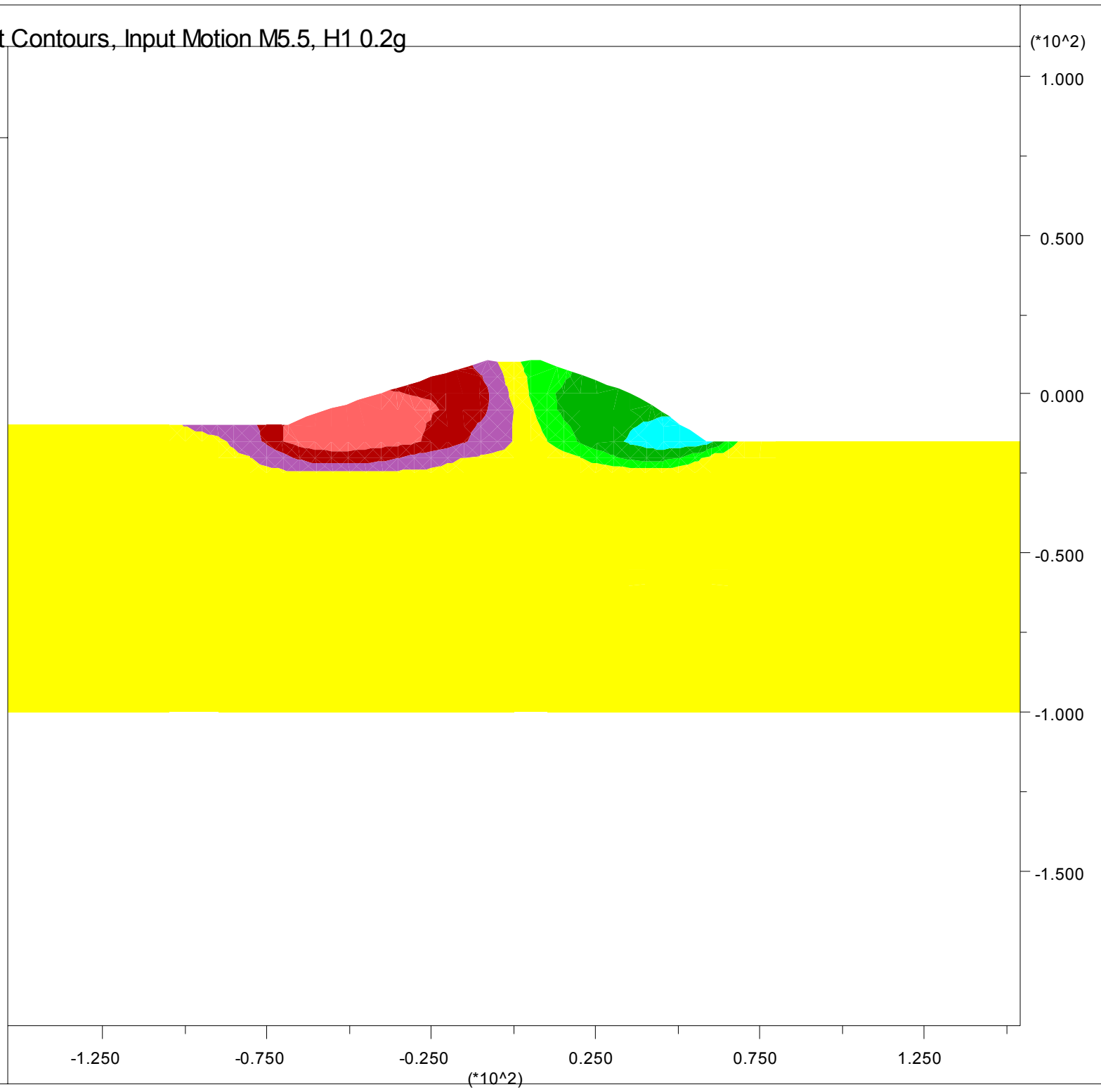
2.00E-01

4.00E-01

6.00E-01

Contour interval= 2.00E-01

1333 Broadway, Suite 800
Oakland, CA 94612



Delta Risk Management Strategy (DRMS) Levee Fragility		Horizontal Displacement Contours Idealized Section - 5 ft Peat Input Motion M 5.5 H1, 0.2g	Figure 6-87
URS	Project No. 26815621		

JOB TITLE : Horizontal Displacement Contours, Input Motion M6.5, H1 0.2g

FLAC (Version 5.00)

LEGEND

9-Jan-07 21:49

step 99815

Dynamic Time 4.0000E+01

-1.538E+02 <x< 1.540E+02

-1.988E+02 <y< 1.090E+02

X-displacement contours (feet)

-7.50E-01

-5.00E-01

-2.50E-01

0.00E+00

2.50E-01

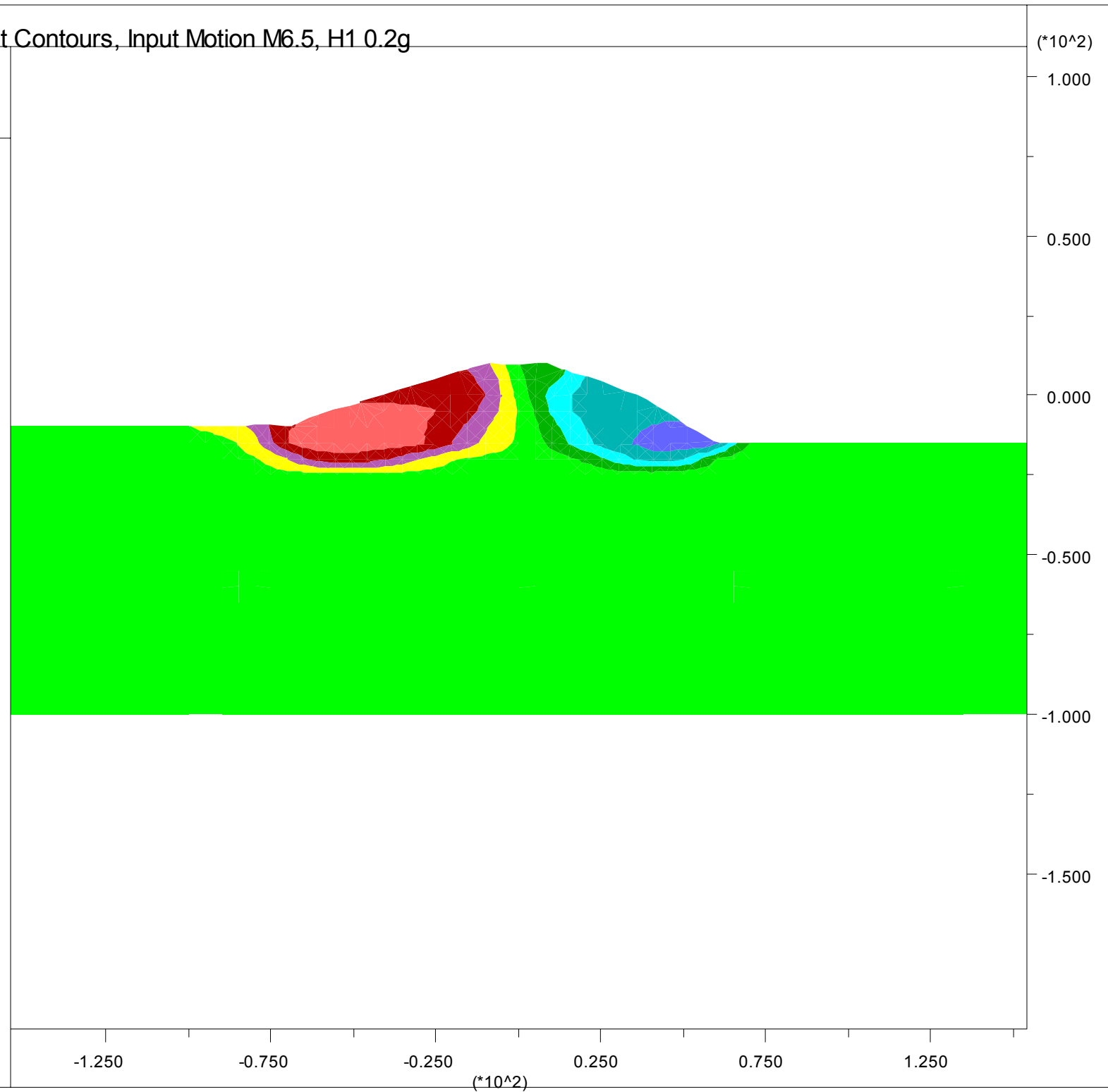
5.00E-01

7.50E-01

1.00E+00

Contour interval= 2.50E-01

1333 Broadway, Suite 800
Oakland, CA 94612



Delta Risk Management Strategy (DRMS)
Levee Fragility

URS

Project No. 26815621

Horizontal Displacement Contours
Idealized Section - 5 ft Peat
Input Motion M 6.5 H1, 0.2g

Figure
6-88

JOB TITLE : Horizontal Displacement Contours, Input Motion M7.5, H1 0.2g

(*10^2)

FLAC (Version 5.00)

LEGEND

10-Jan-07 2:35

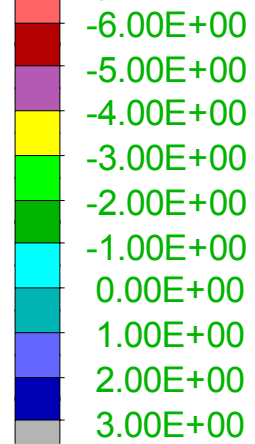
step 134912

Dynamic Time 5.6000E+01

-1.538E+02 <x< 1.540E+02

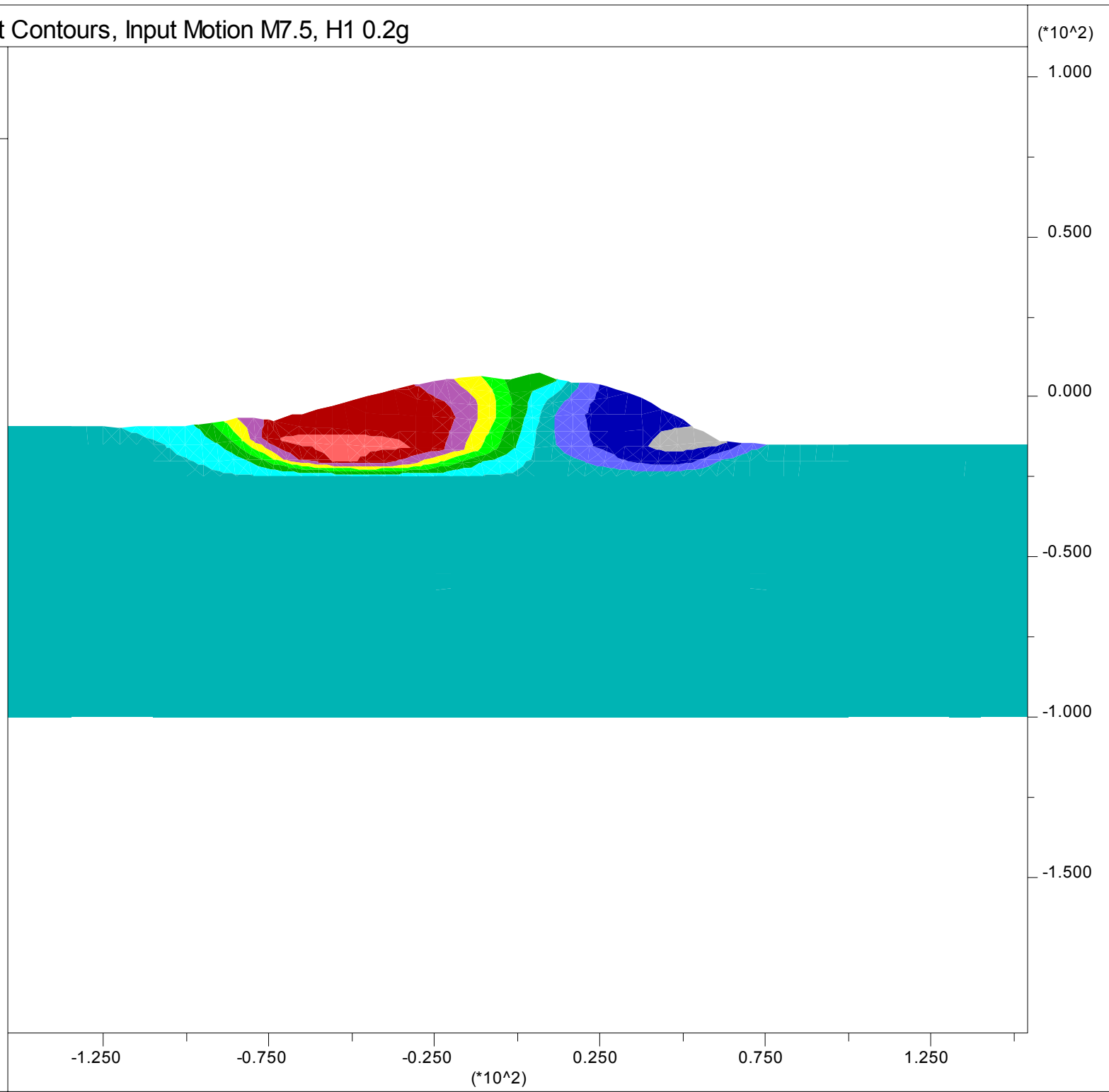
-1.988E+02 <y< 1.090E+02

X-displacement contours (feet)



Contour interval= 1.00E+00

1333 Broadway, Suite 800
Oakland, CA 94612



Delta Risk Management Strategy (DRMS) Levee Fragility		Horizontal Displacement Contours Idealized Section - 5 ft Peat Input Motion M 7.5 H1, 0.2g	Figure 6-89
URS	Project No. 26815621		

JOB TITLE : Displacement Contours, Input Motion M5.5, H1 0.2g

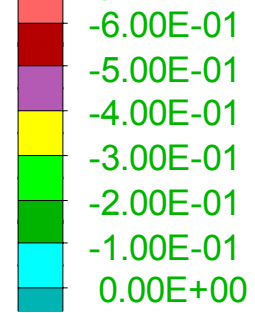
(*10^2)

FLAC (Version 5.00)

LEGEND

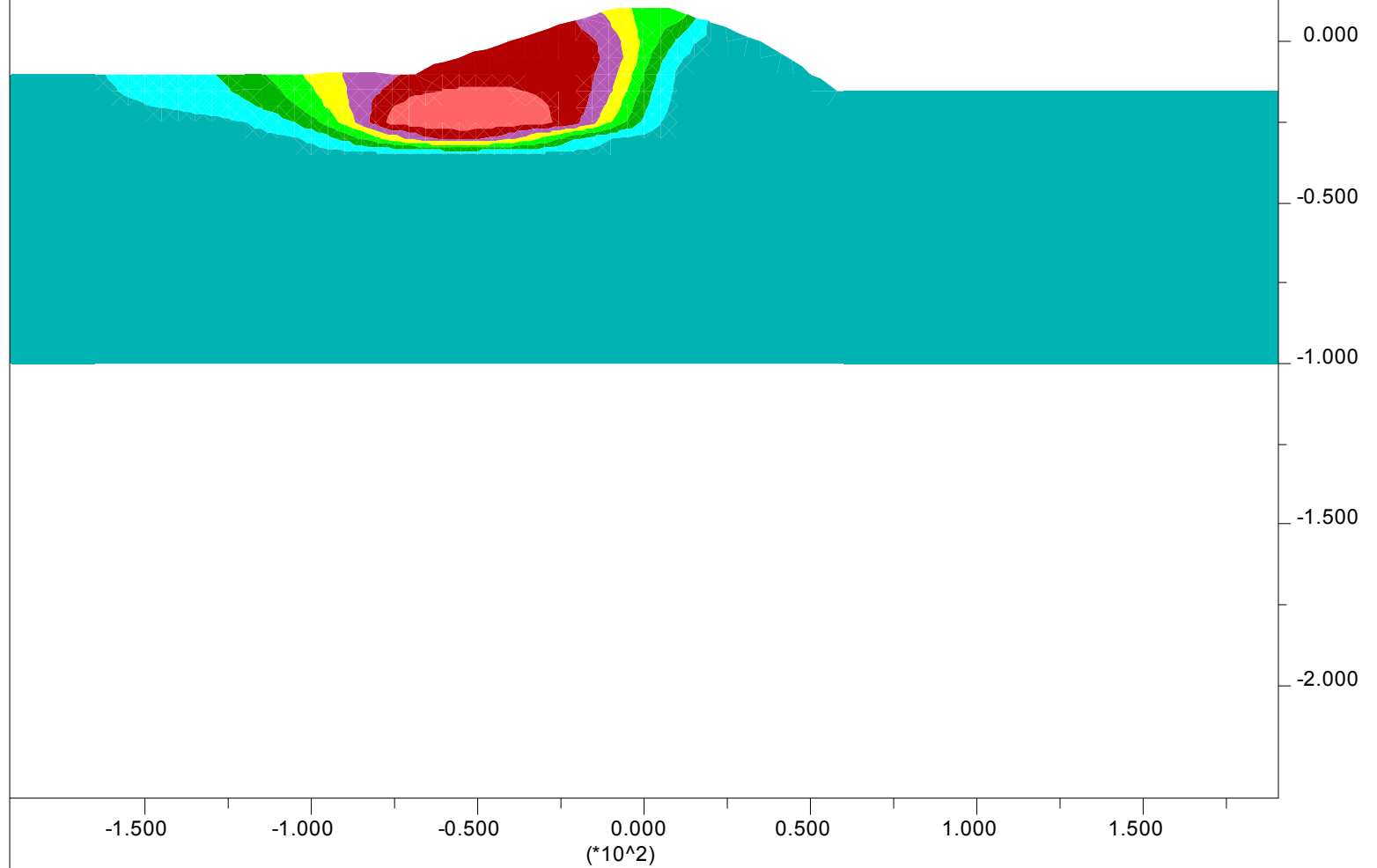
8-Jan-07 23:18
step 59332
Dynamic Time 2.3000E+01
-1.906E+02 <x< 1.907E+02
-2.353E+02 <y< 1.460E+02

X-displacement contours (feet)



Contour interval= 1.00E-01

1333 Broadway, Suite 800
Oakland, CA 94612



Delta Risk Management Strategy (DRMS) Levee Fragility		Horizontal Displacement Contours Idealized Section - 15 ft Peat Input Motion M 5.5 H1, 0.2g	Figure 6-90
URS	Project No. 26815621		

JOB TITLE : Displacement Contours, Input Motion M6.5, H1 0.2g

(*10^2)

FLAC (Version 5.00)

LEGEND

9-Jan-07 21:58

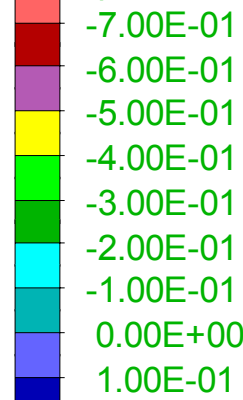
step 95763

Dynamic Time 4.0000E+01

-1.906E+02 <x< 1.907E+02

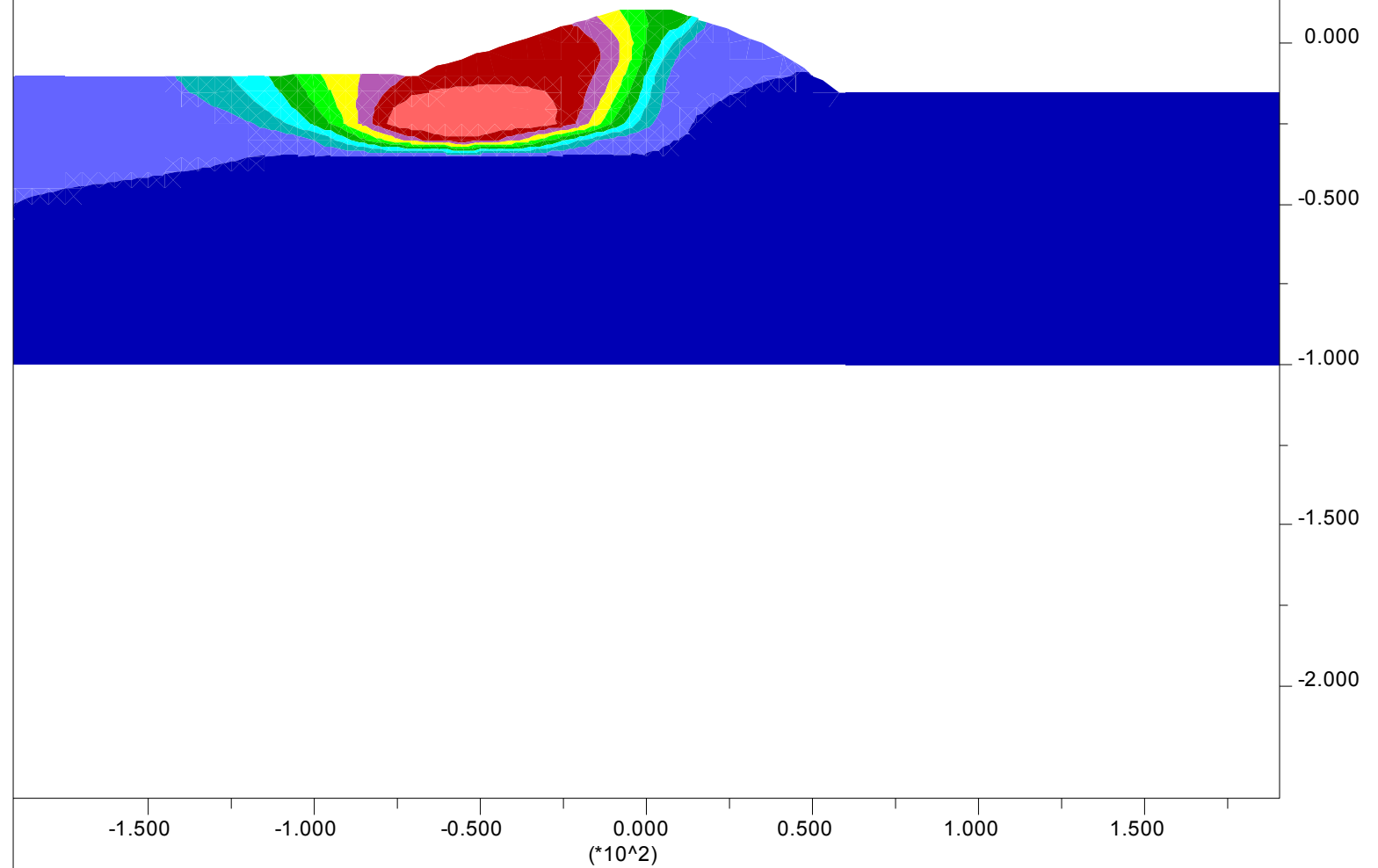
-2.353E+02 <y< 1.460E+02

X-displacement contours (feet)



Contour interval= 1.00E-01

1333 Broadway, Suite 800
Oakland, CA 94612



Delta Risk Management Strategy (DRMS)
Levee Fragility



Project No. 26815621

Horizontal Displacement Contours
Idealized Section - 15 ft Peat
Input Motion M 6.5 H1, 0.2g

Figure
6-91

JOB TITLE : Displacement Contours, Input Motion M7.5, H1 0.2g

(*10^2)

FLAC (Version 5.00)

LEGEND

10-Jan-07 3:37

step 130051

Dynamic Time 5.6000E+01

-1.906E+02 <x< 1.907E+02

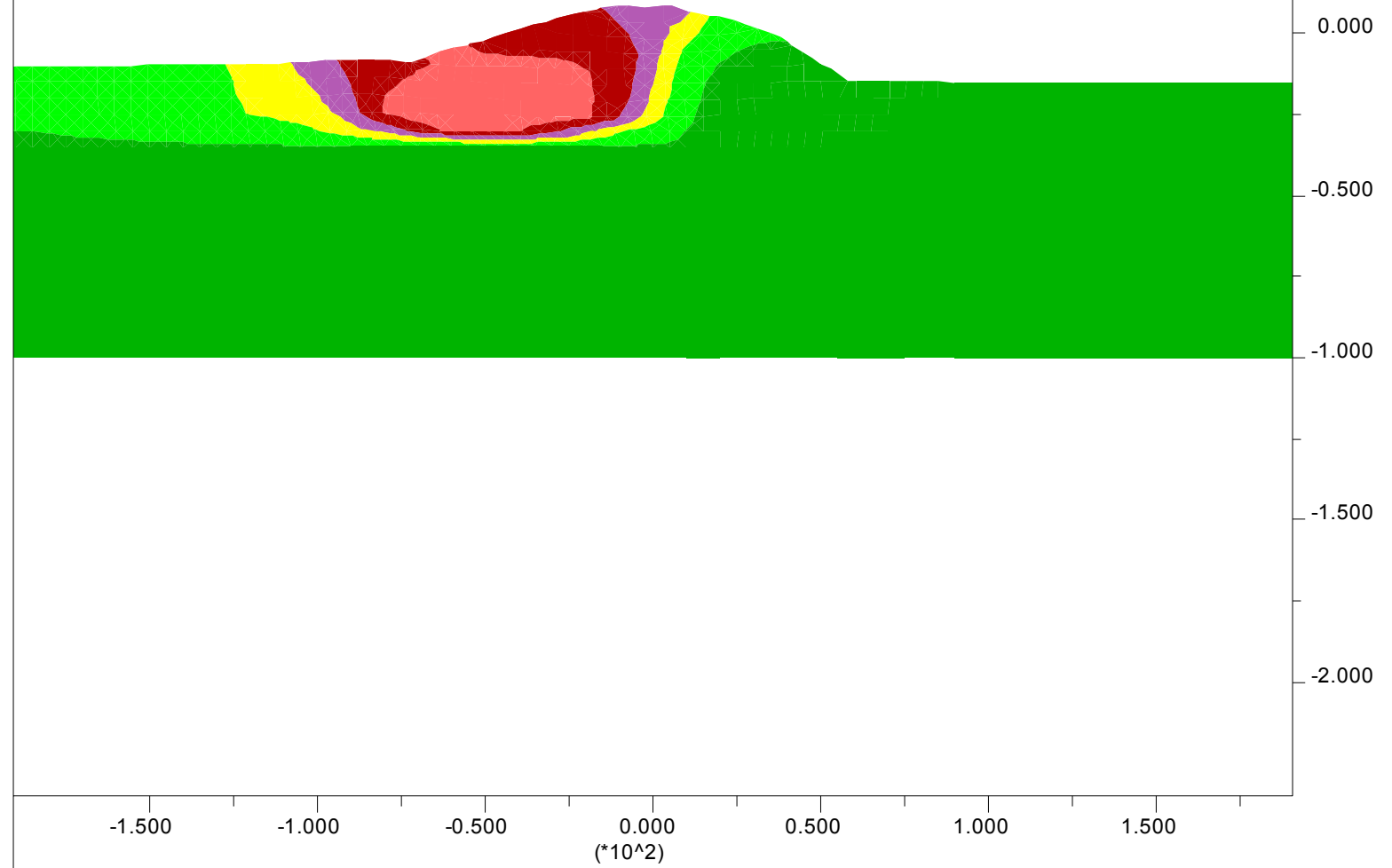
-2.353E+02 <y< 1.460E+02

X-displacement contours (feet)



Contour interval= 1.00E+00

1333 Broadway, Suite 800
Oakland, CA 94612



Delta Risk Management Strategy (DRMS)
Levee Fragility



Project No. 26815621

Horizontal Displacement Contours
Idealized Section - 15 ft Peat
Input Motion M 7.5 H1, 0.2g

Figure
6-92

JOB TITLE : Displacement Contours, Input Motion M5.5 H1, 0.2g

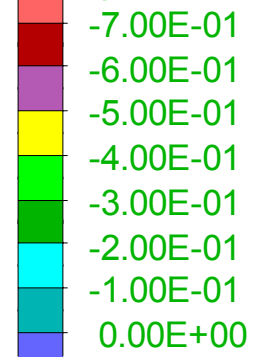
(*10^2)

FLAC (Version 5.00)

LEGEND

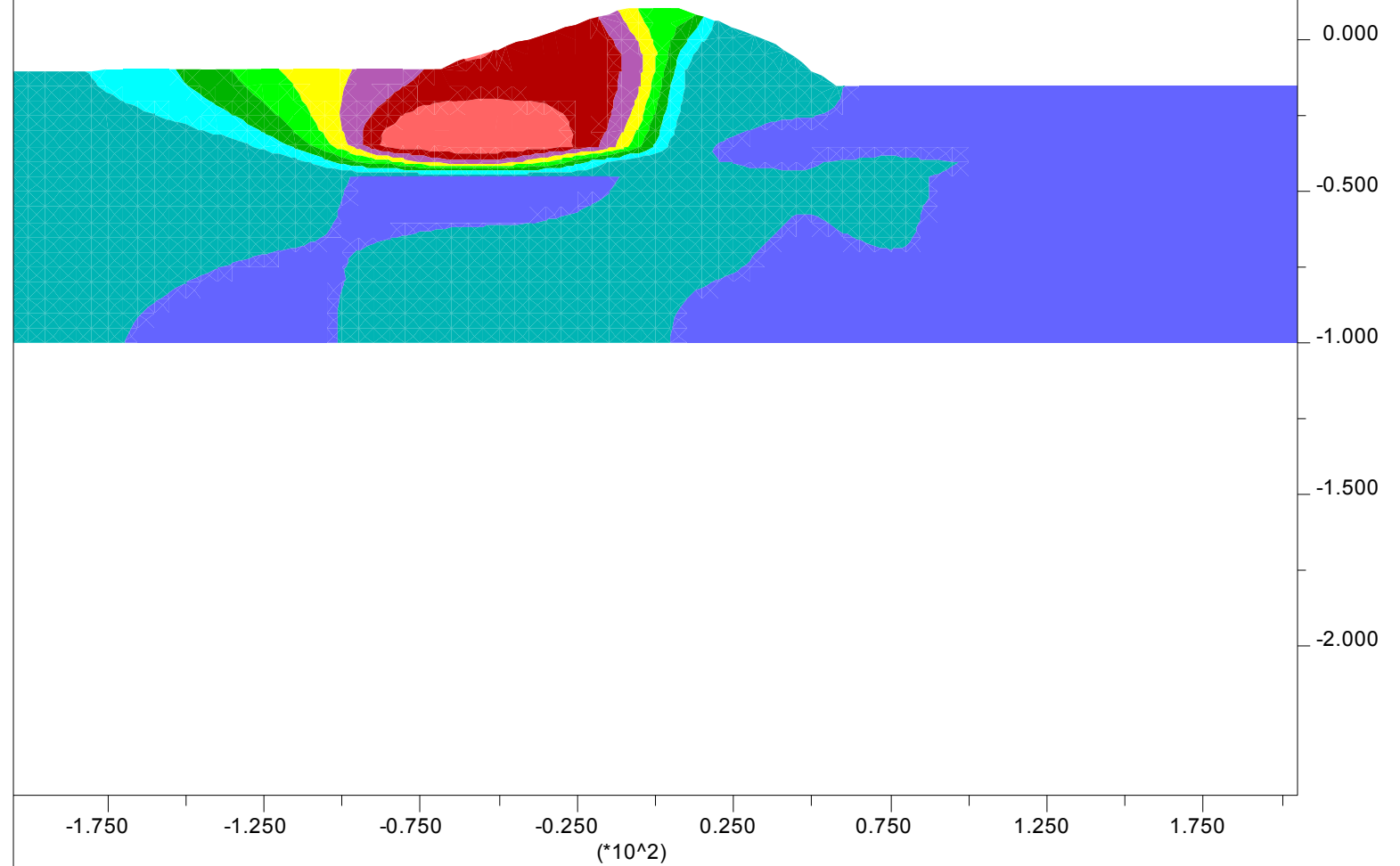
8-Jan-07 20:07
step 59058
Dynamic Time 2.3000E+01
-2.049E+02 <x< 2.049E+02
-2.495E+02 <y< 1.602E+02

X-displacement contours (feet)



Contour interval= 1.00E-01

1333 Broadway, Suite 800
Oakland, CA 94612



JOB TITLE : Displacement Contours, Input Motion M6.5 H1, 0.2g

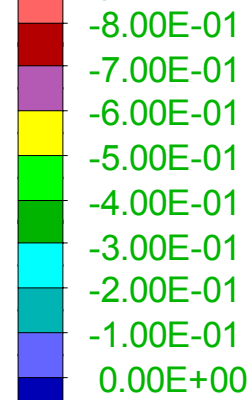
(*10^2)

FLAC (Version 5.00)

LEGEND

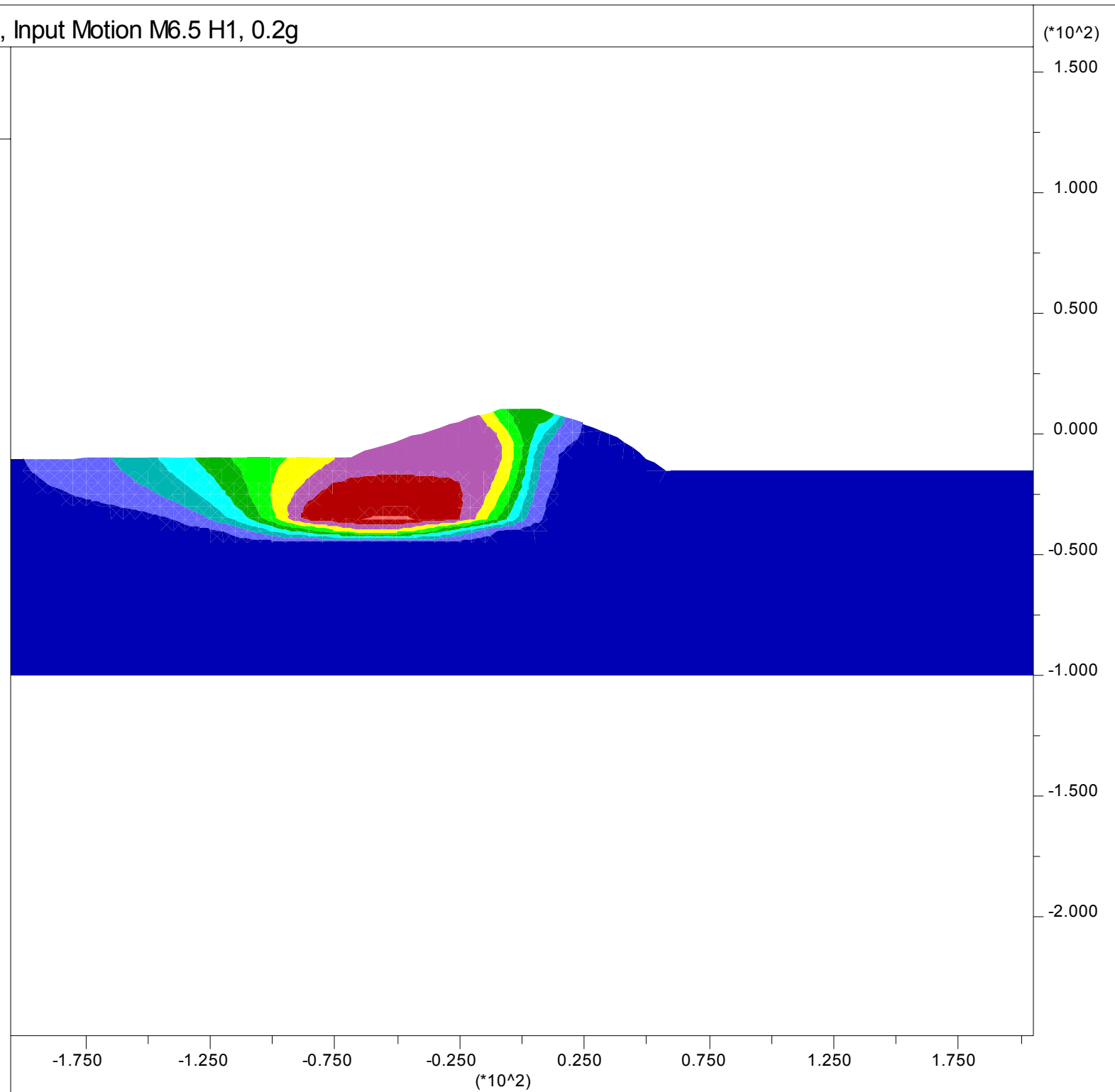
8-Jan-07 23:49
step 94557
Dynamic Time 4.0000E+01
-2.049E+02 <x< 2.049E+02
-2.495E+02 <y< 1.602E+02

X-displacement contours (feet)



Contour interval= 1.00E-01

1333 Broadway, Suite 800
Oakland, CA 94612



Delta Risk Management Strategy (DRMS) Levee Fragility		Horizontal Displacement Contours Idealized Section - 25 ft Peat Input Motion M 6.5 H1, 0.2g	Figure 6-94
URS	Project No. 26815621		

JOB TITLE : Displacement Contours, Input Motion M7.5 H1, 0.2g

(*10^2)

FLAC (Version 5.00)

LEGEND

9-Jan-07 5:27

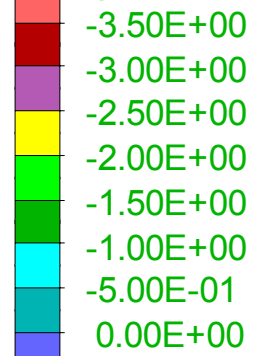
step 127967

Dynamic Time 5.6000E+01

-2.707E+02 <x< 1.391E+02

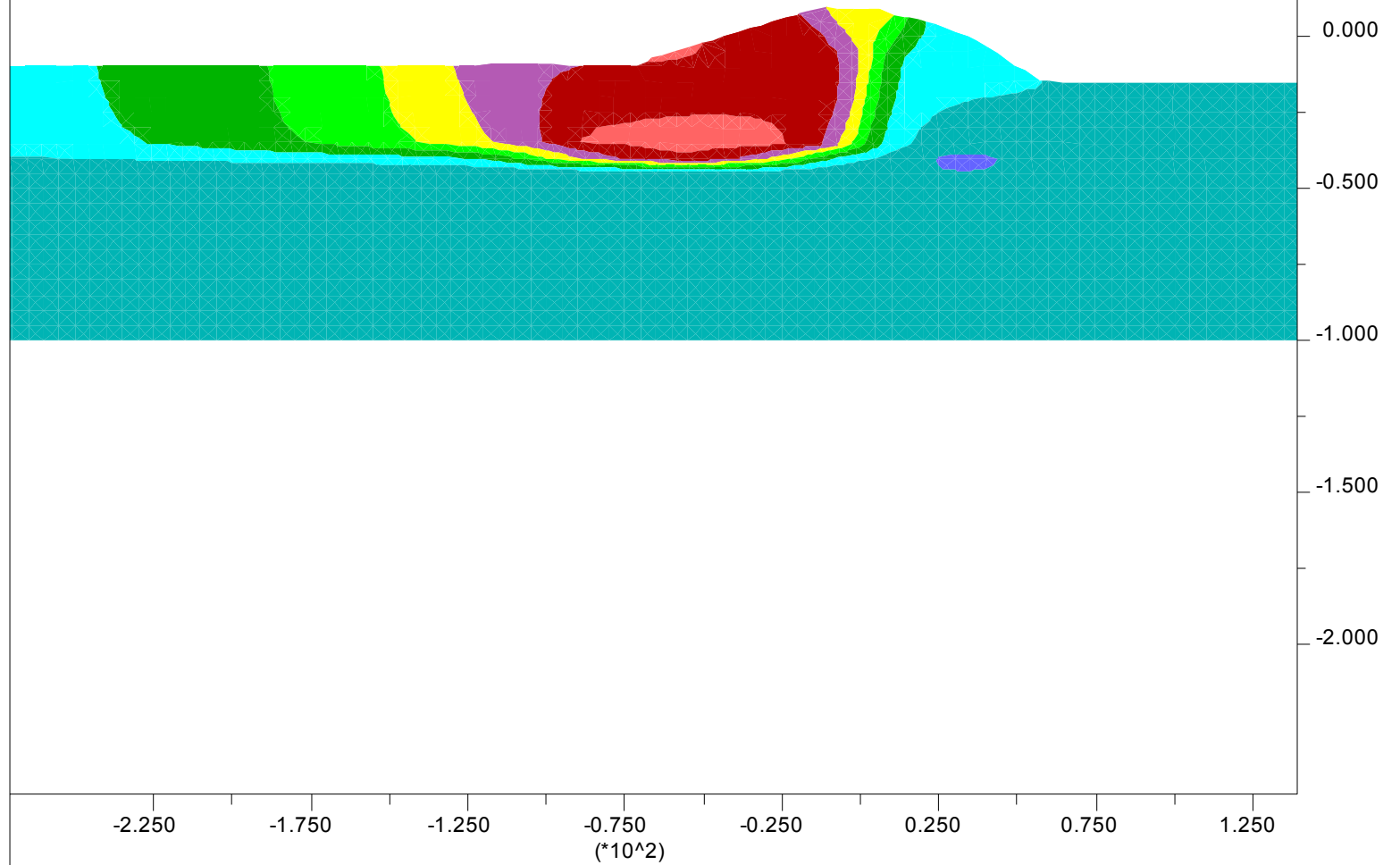
-2.495E+02 <y< 1.602E+02

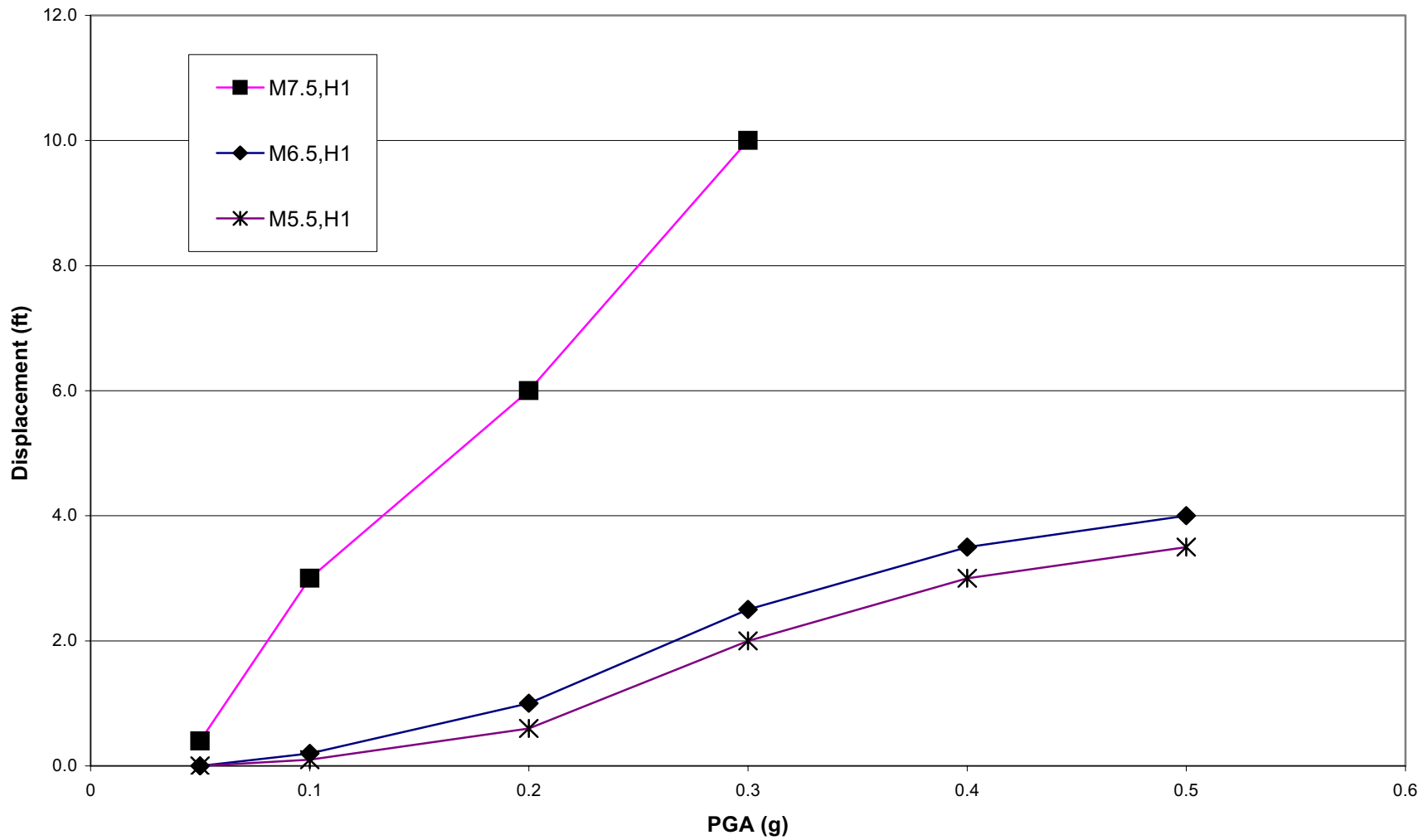
X-displacement contours (feet)



Contour interval= 5.00E-01

1333 Broadway, Suite 800
Oakland, CA 94612





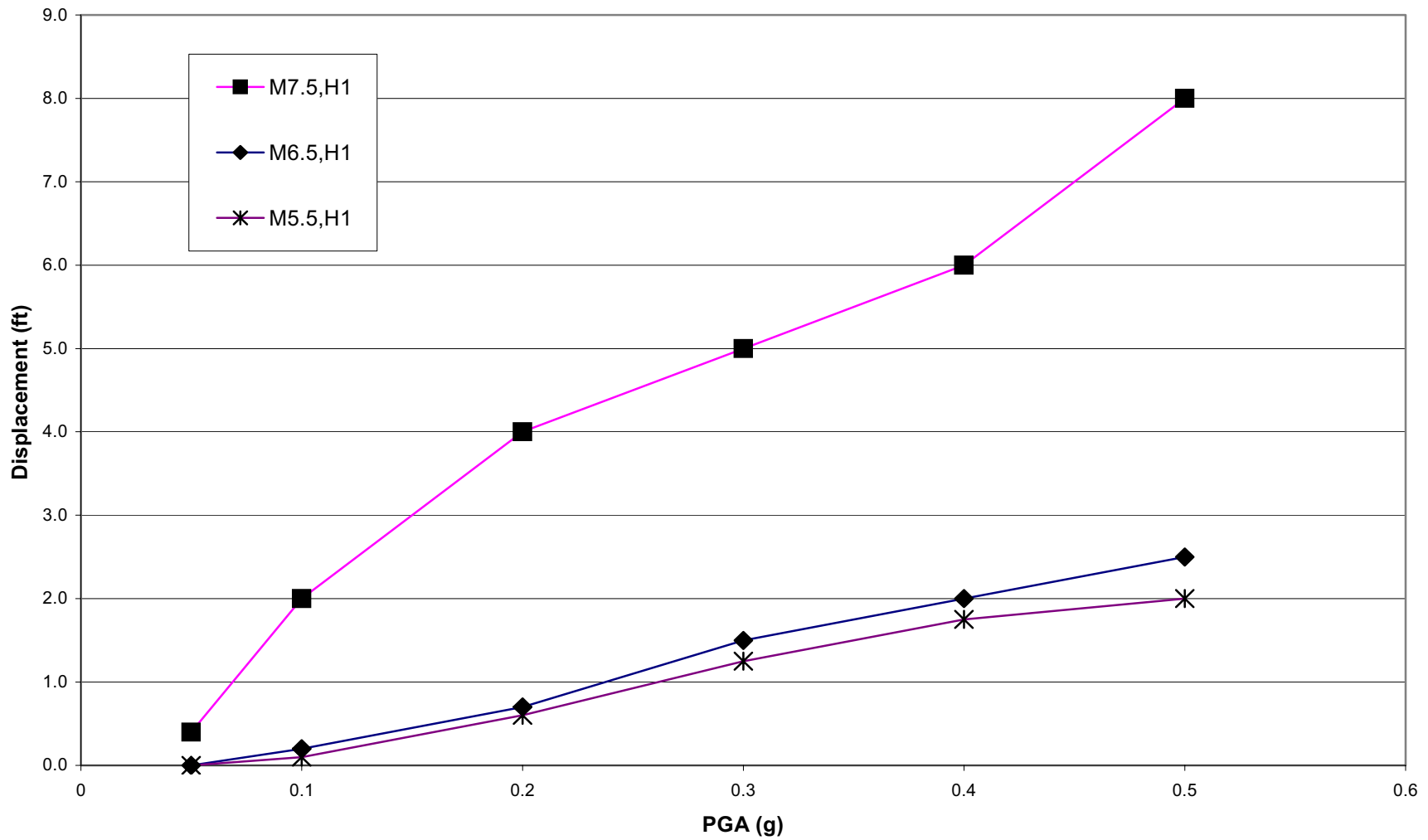
Delta Risk Management Strategy (DRMS)
Levee Fragility



Project No. 26815621

Calculated FLAC Displacements
Idealized Section with
Liquefiable Foundation Sand Layer
5 Feet of Peat

Figure
6-61



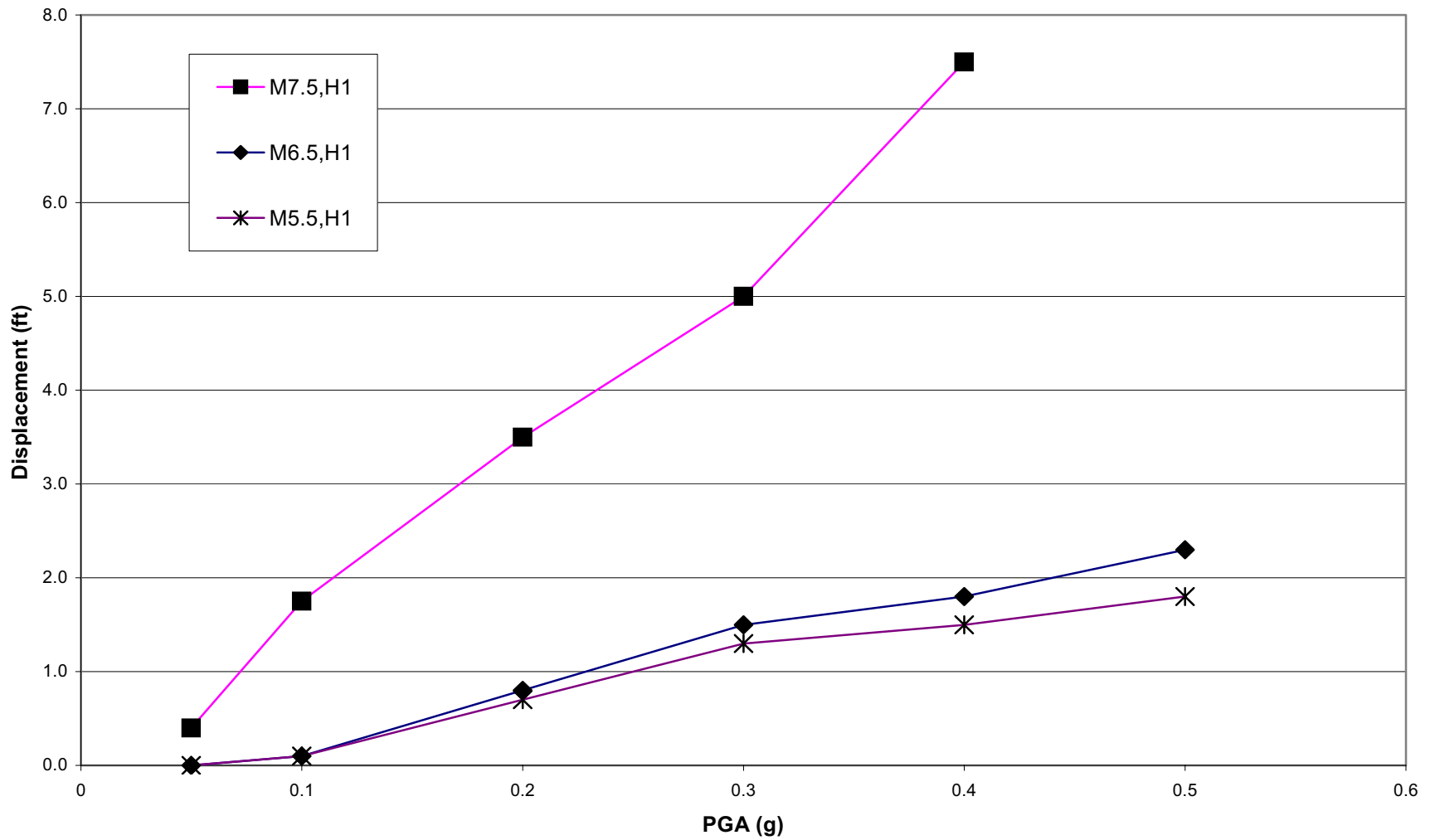
Delta Risk Management Strategy (DRMS)
Levee Fragility



Project No. 26815621

Calculated FLAC Displacements
Idealized Section with
Liquefiable Foundation Sand Layer
15 Feet of Peat

Figure
6-62



Delta Risk Management Strategy (DRMS)
Levee Fragility



Project No. 26815621

Calculated FLAC Displacements
Idealized Section with
Liquefiable Foundation Sand Layer
25 Feet of Peat

Figure
6-63

JOB TITLE : Deformed Mesh, Liquefied Fill, Su = 230 psf

(*10²)

FLAC (Version 5.00)

LEGEND

27-Nov-06 18:59
step 10365
-9.464E+01 <x< 9.464E+01
-1.391E+02 <y< 5.014E+01

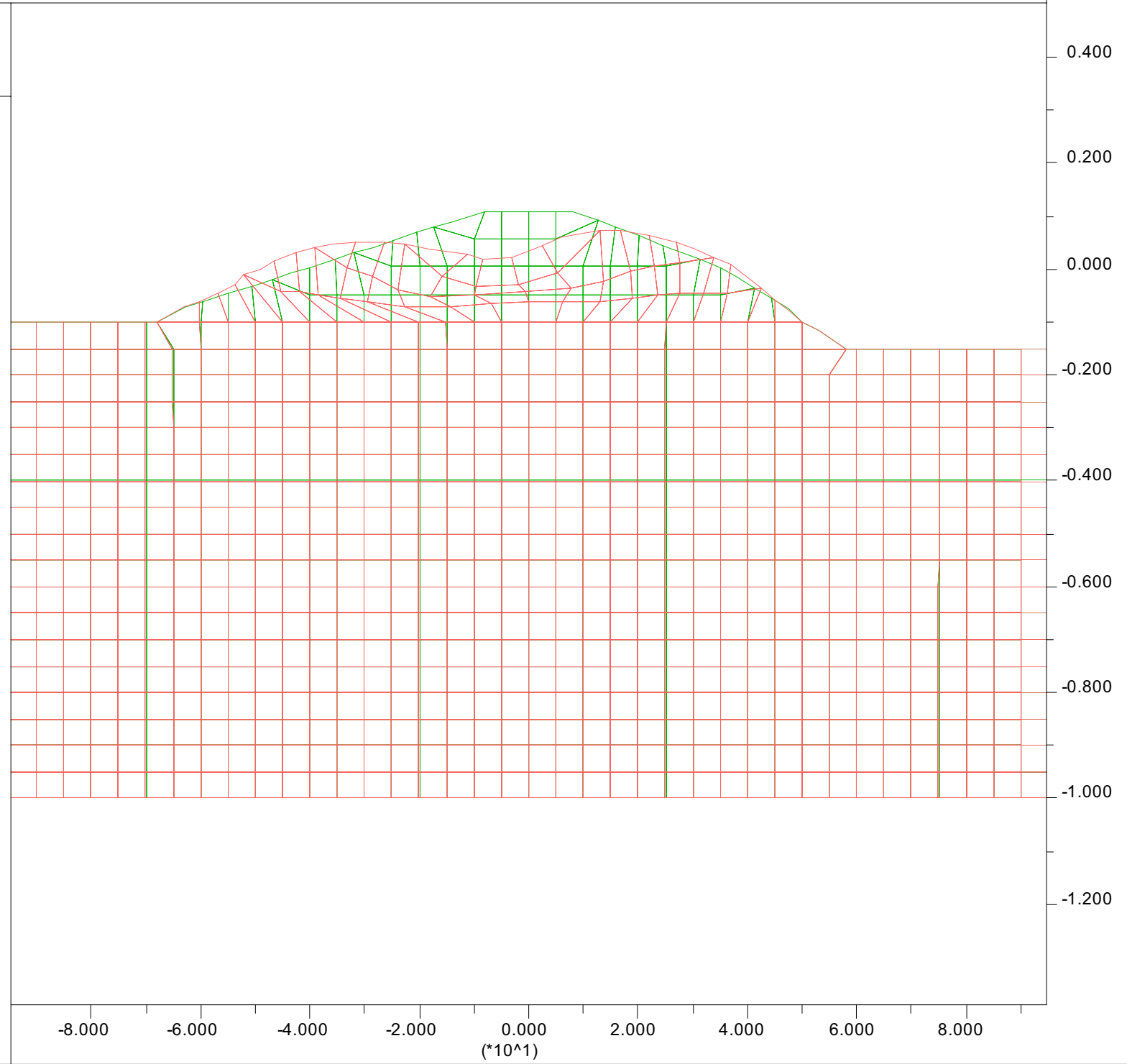
Grid plot

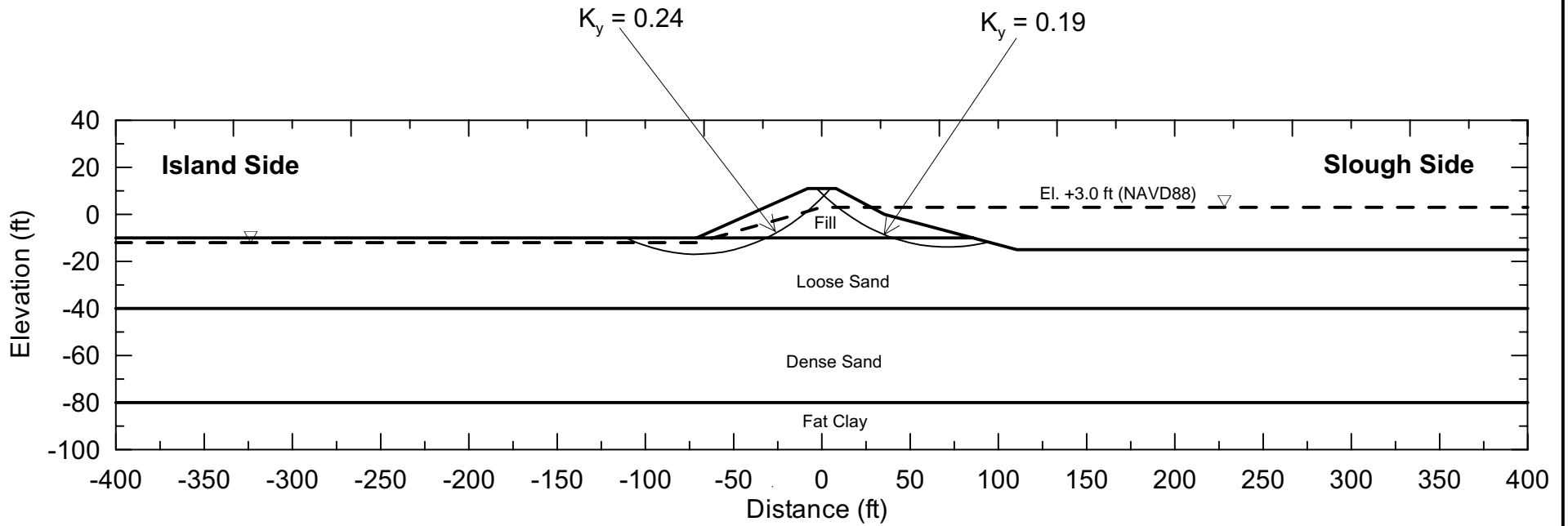


Exaggerated Grid Distortion

Magnification = 1.000E+00
Max Disp = 1.001E+01

1333 Broadway, Suite 800
Oakland, CA 94612





Type	Unit Weight (pcf)	ϕ'	c' (psf)	ϕ	c (psf)
Fill	115	30	50	-	-
Loose Sand	125	32	0	-	-
Dense Sand	125	38	0	-	-

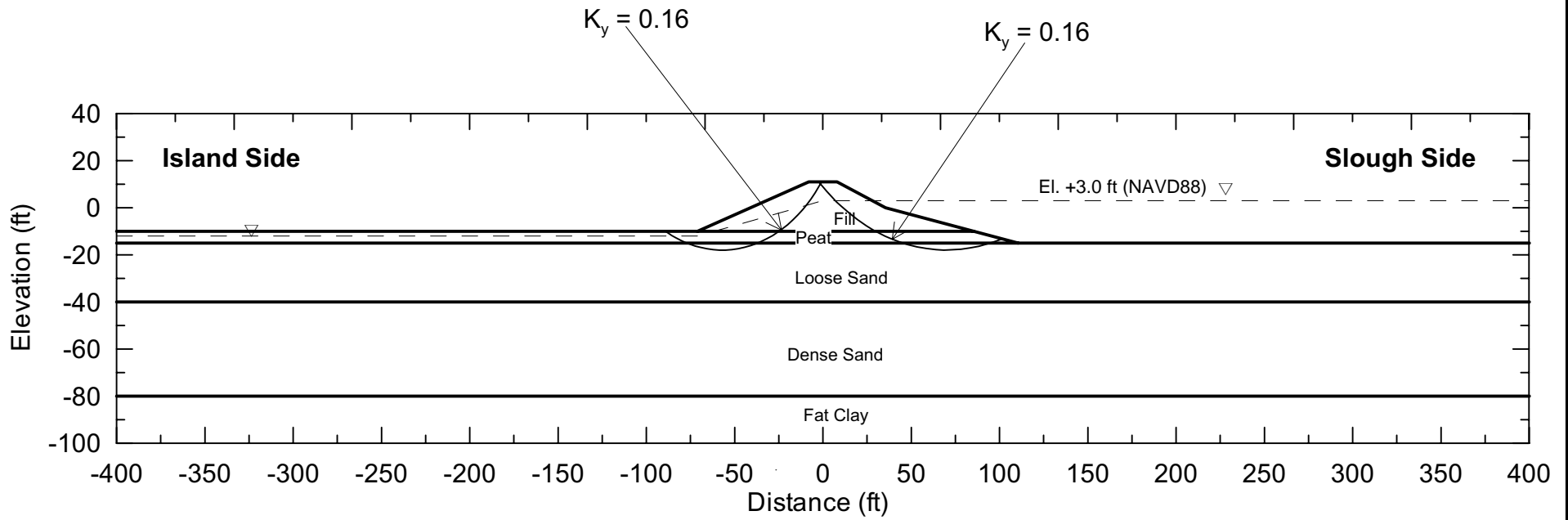
Delta Risk Management Strategy (DRMS)
Levee Fragility

URS

Project No. 26815621

Idealized Section
Stability Analysis - Seismic
No Peat

Figure
6-100



Type	Unit Weight (pcf)	ϕ'	c' (psf)	ϕ	c (psf)
Fill	115	30	50	-	-
Peat	70	28	120	18	140
Loose Sand	125	32	0	-	-
Dense Sand	125	38	0	-	-

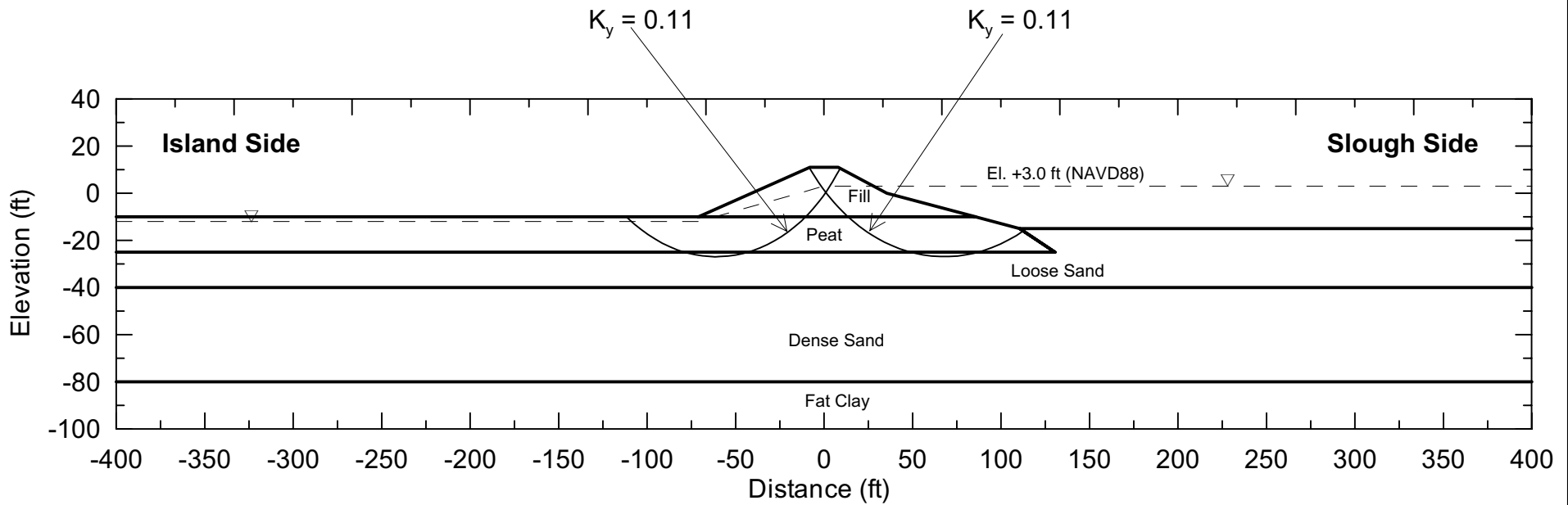
Delta Risk Management Strategy (DRMS)
Levee Fragility

URS

Project No. 26815621

Idealized Section
Stability Analysis - Seismic
5 Feet of Peat

Figure
6-101



Type	Unit Weight (pcf)	ϕ'	c' (psf)	ϕ	c (psf)
Fill	115	30	50	-	-
Peat	70	28	120	18	140
Loose Sand	125	32	0	-	-
Dense Sand	125	38	0	-	-

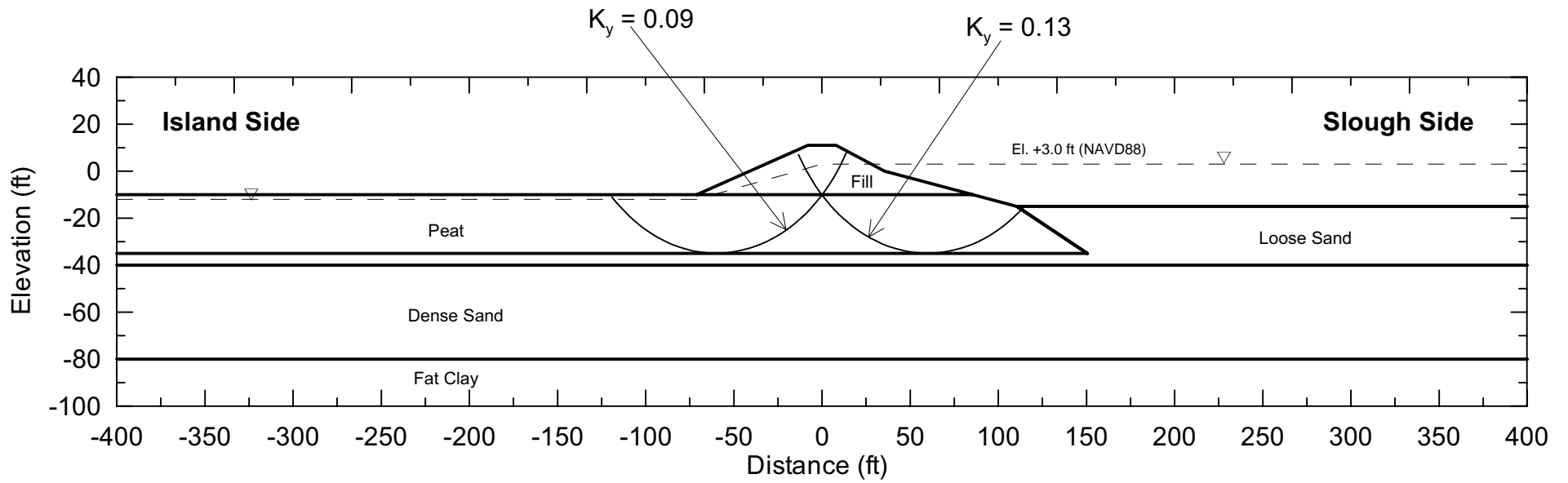
Delta Risk Management Strategy (DRMS)
Levee Fragility

URS

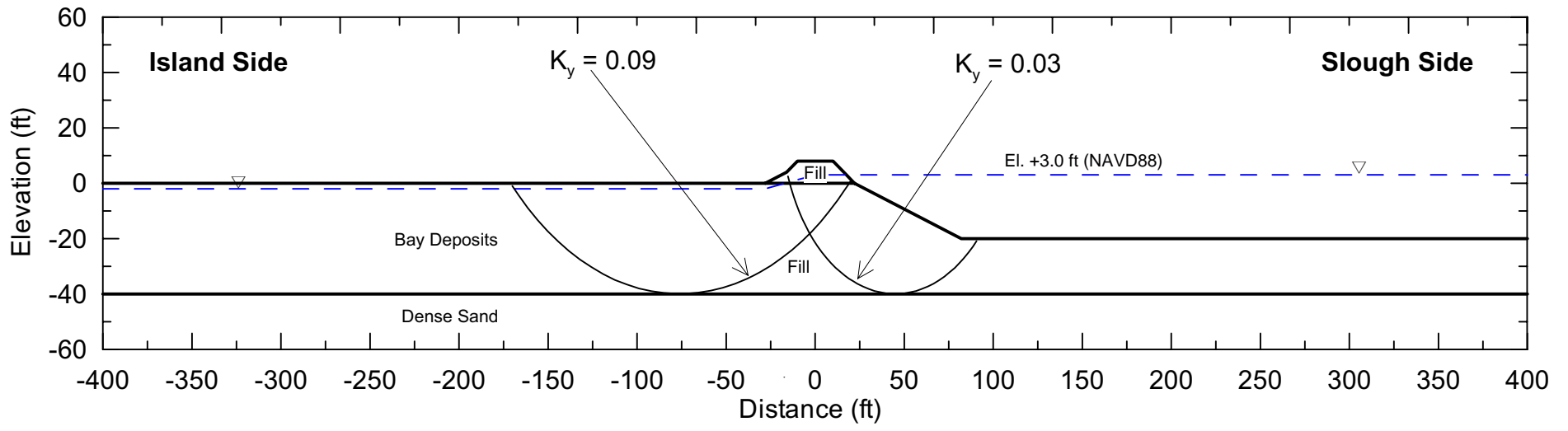
Project No. 26815621

Idealized Section
Stability Analysis - Seismic
15 Feet of Peat

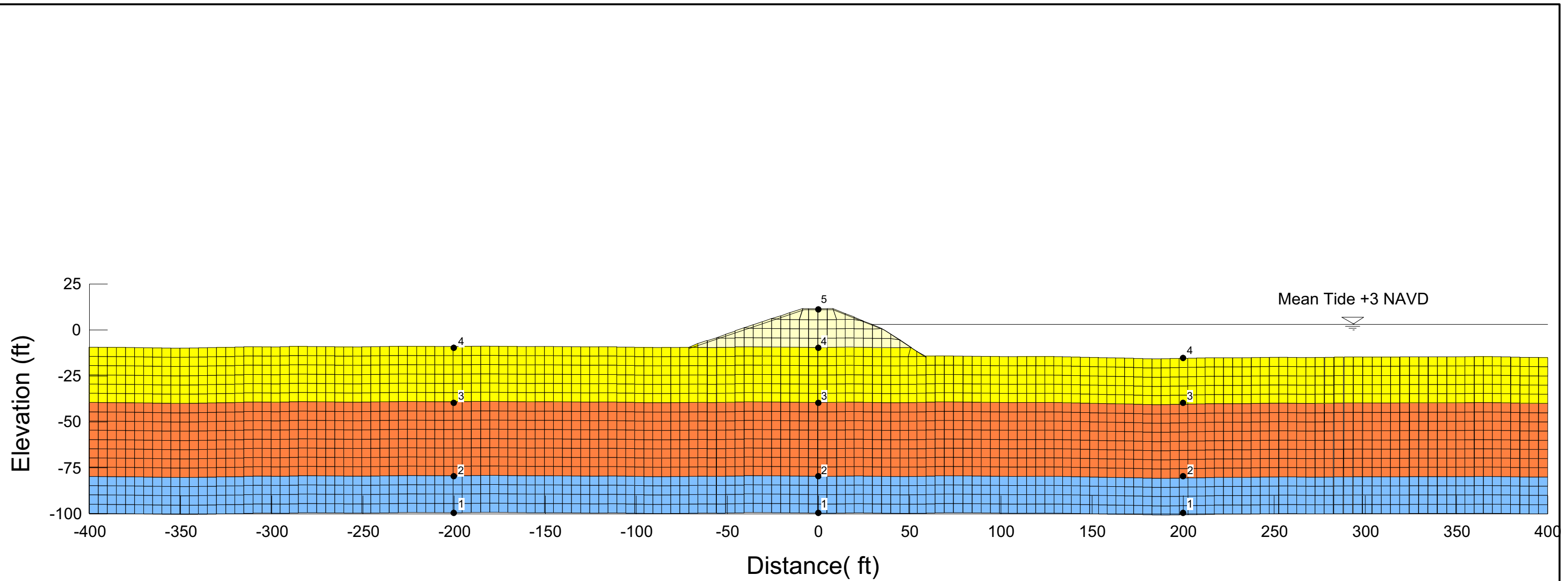
Figure
6-102



Type	Unit Weight (pcf)	ϕ'	c' (psf)	ϕ	c (psf)
Fill	115	30	50	-	-
Peat	70	28	120	18	140
Loose Sand	125	32	0	-	-
Dense Sand	125	38	0	-	-



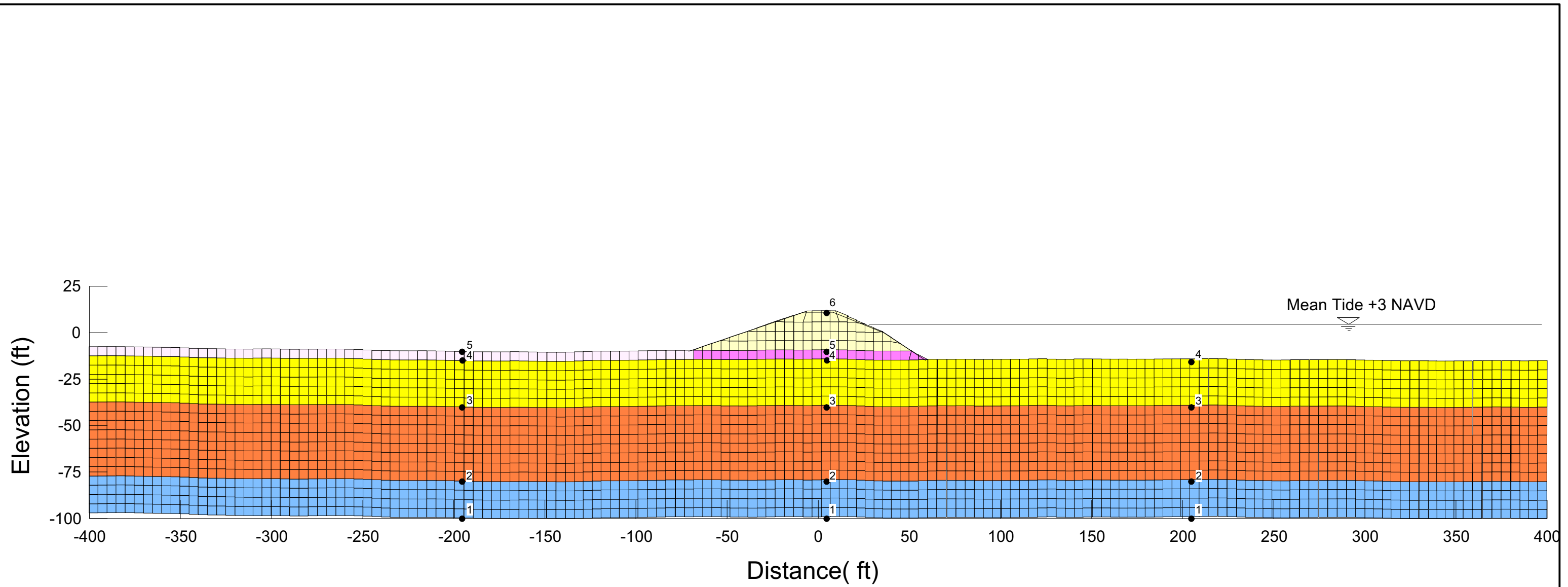
Type	Unit Weight (pcf)	ϕ'	c' (psf)	ϕ	c (psf)
Sandy Fill	115	30	50	-	-
Bay Deposit	110	0	300	0	300
Sand	125	38	0	-	-



Legend

- Levee Fill
- Sand
- Dense Sand
- Stiff Clay

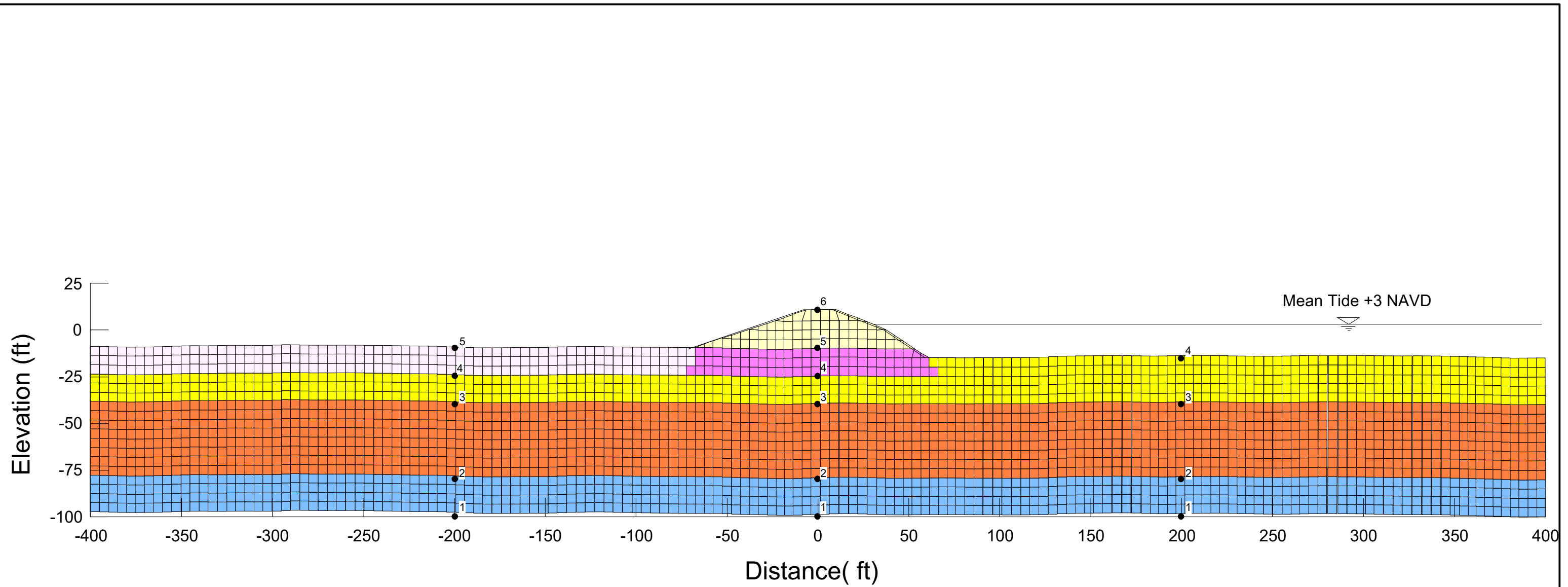
Delta Risk Management Strategy (DRMS) Levee Fragility		Finite Element Model for Seismic Analysis Idealized Section - No Peat	Figure 6-105
URS	Project No. 26815621		



Legend

- Levee Fill
- Free Field Peat
- Under Levee Peat
- Sand
- Dense Sand
- Stiff Clay

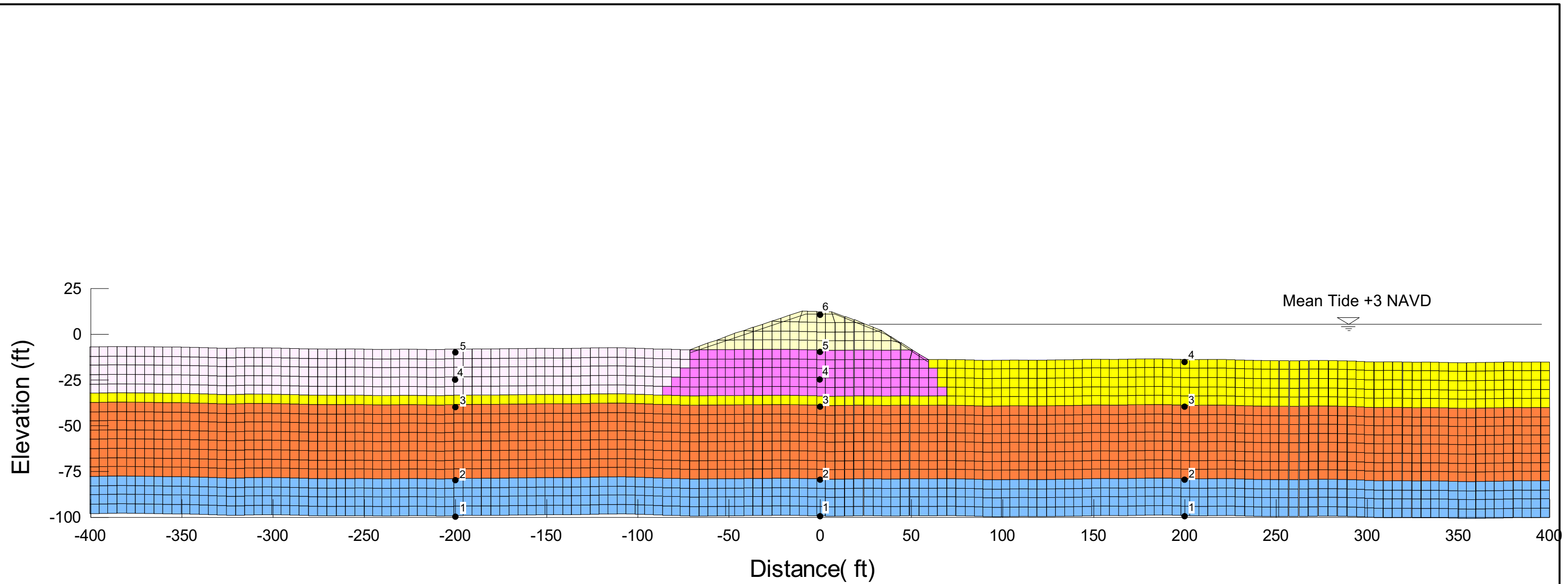
Delta Risk Management Strategy (DRMS) Levee Fragility		Finite Element Model for Seismic Analysis Idealized Section - 5 ft Peat	Figure 6-71
URS	Project No. 26815621		



Legend

- Levee Fill
- Free Field Peat
- Under Levee Peat
- Sand
- Dense Sand
- Stiff Clay

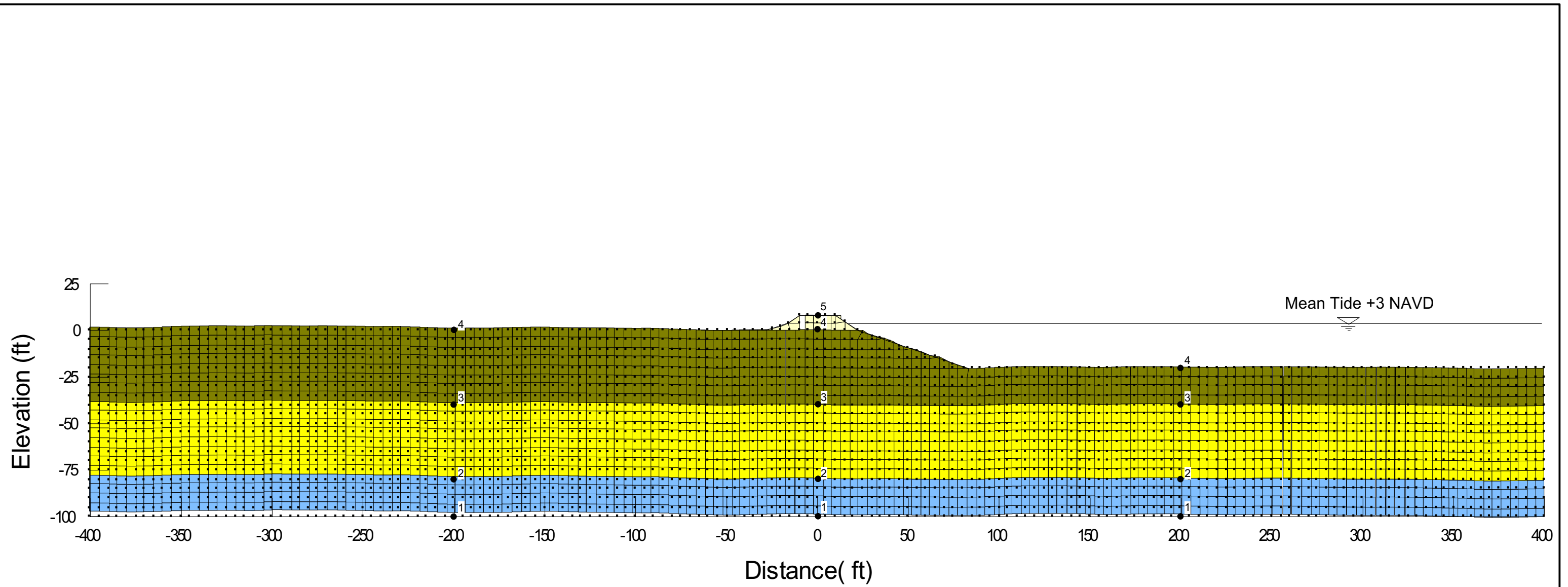
Delta Risk Management Strategy (DRMS) Levee Fragility		Finite Element Model for Seismic Analysis Idealized Section - 15 ft Peat	Figure 6-72
URS	Project No. 26815621		



Legend

- Levee Fill
- Free Field Peat
- Under Levee Peat
- Sand
- Dense Sand
- Stiff Clay

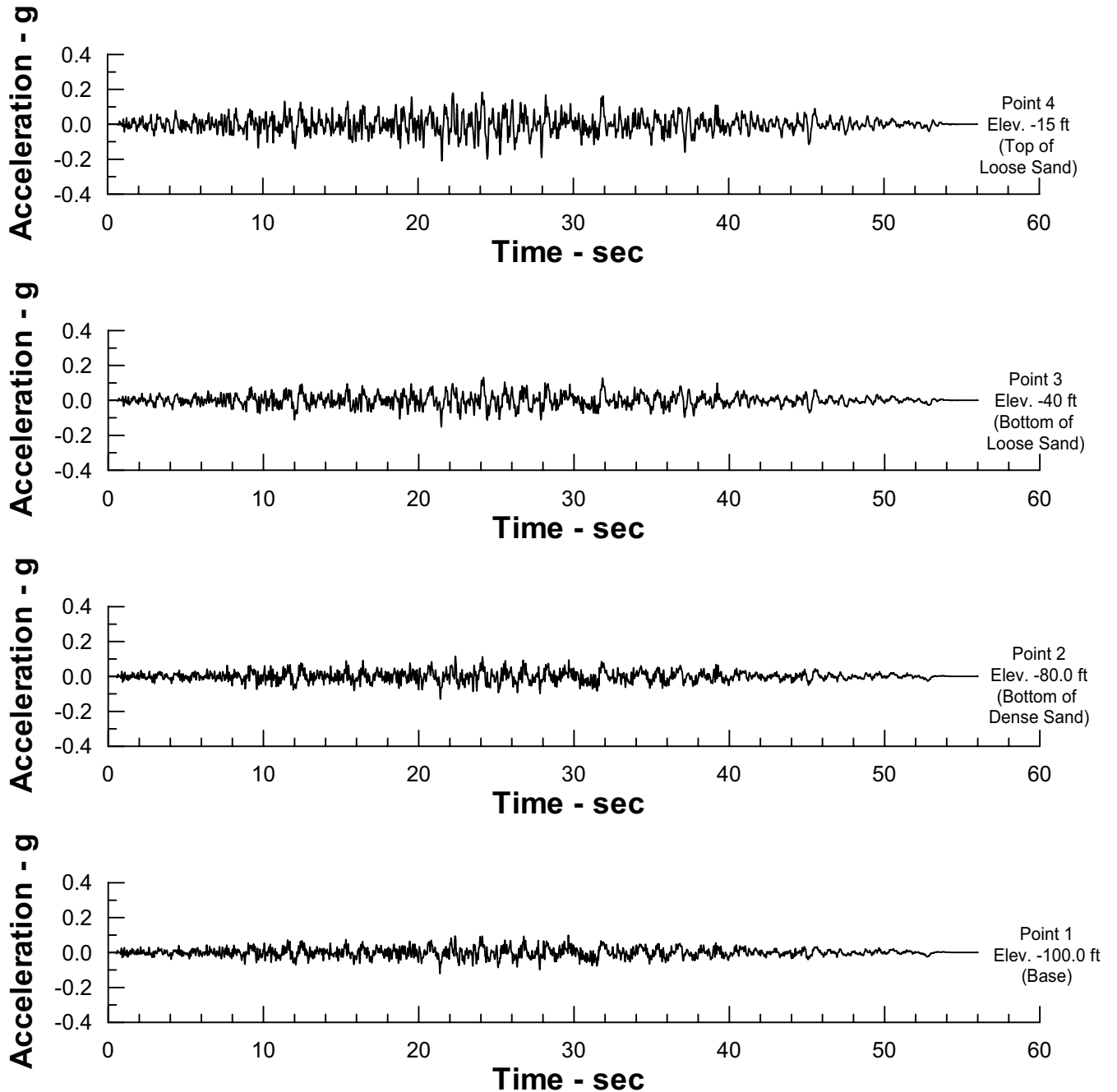
Delta Risk Management Strategy (DRMS) Levee Fragility		Finite Element Model for Seismic Analysis Idealized Section - 25 ft Peat	Figure 6-73
URS	Project No. 26815621		



Legend

- Levee Fill
- Bay Deposits
- Sand
- Stiff Clay

Delta Risk Management Strategy (DRMS) Levee Fragility		Finite Element Model for Seismic Analysis Suisun Marsh Section	Figure 6-109
URS	Project No. 26815621		



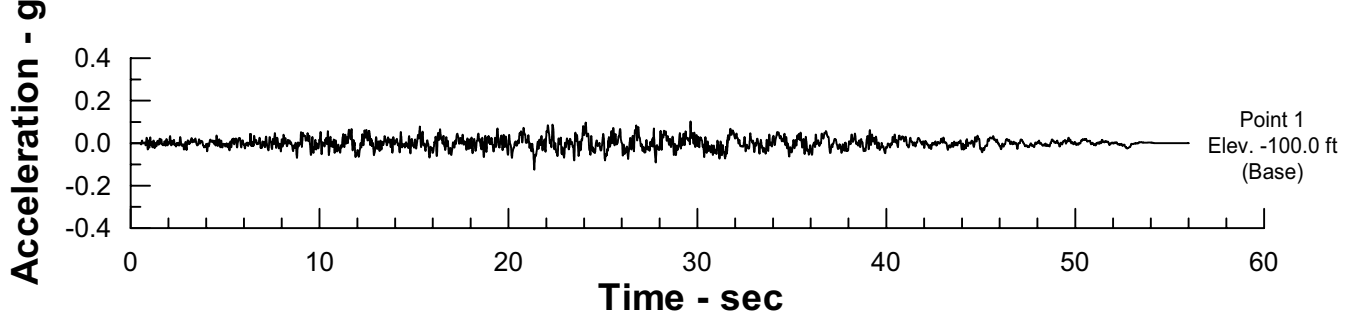
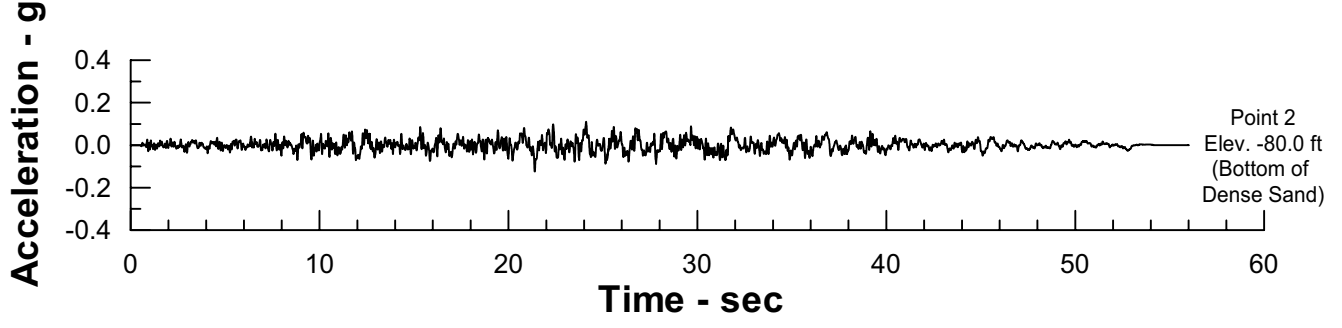
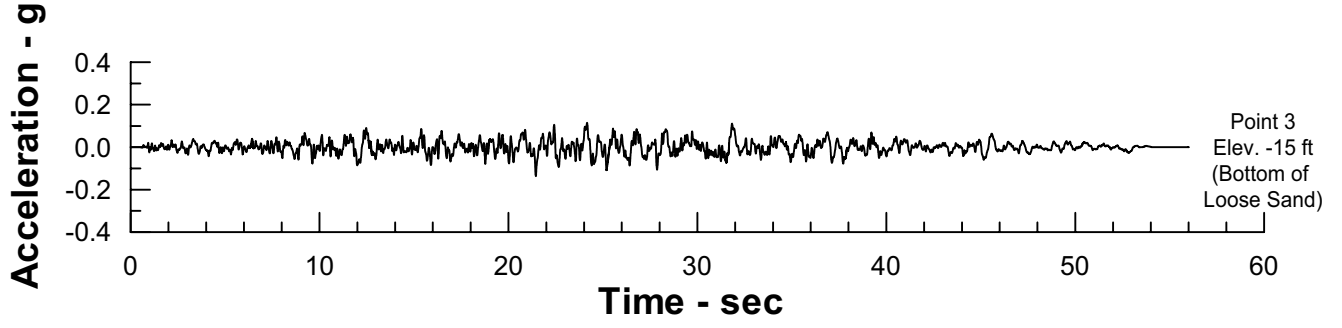
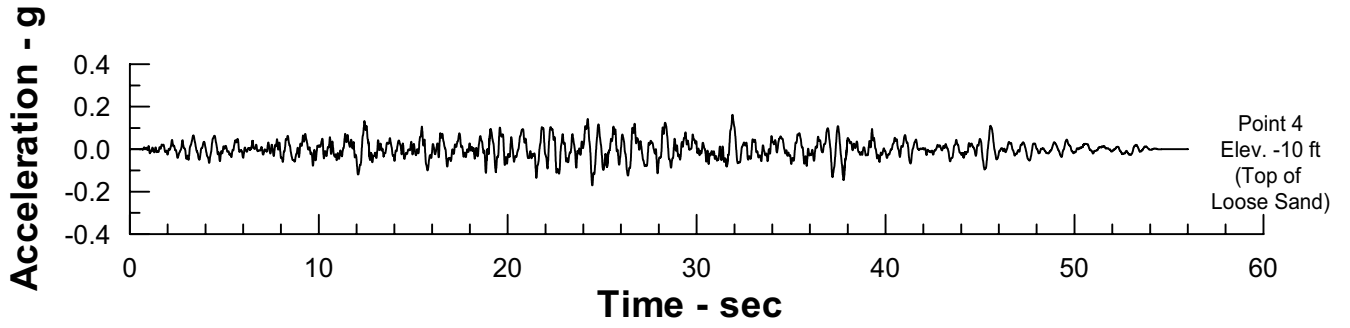
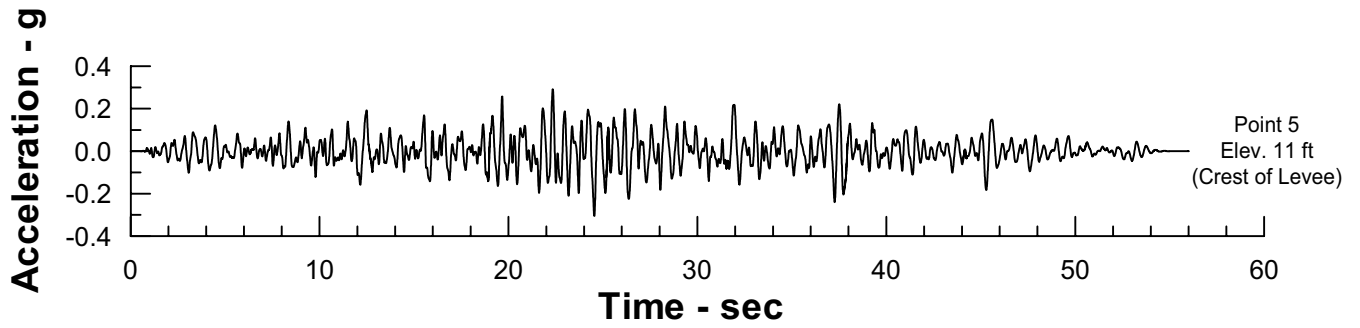
Delta Risk Management Strategy (DRMS)
Levee Fragility

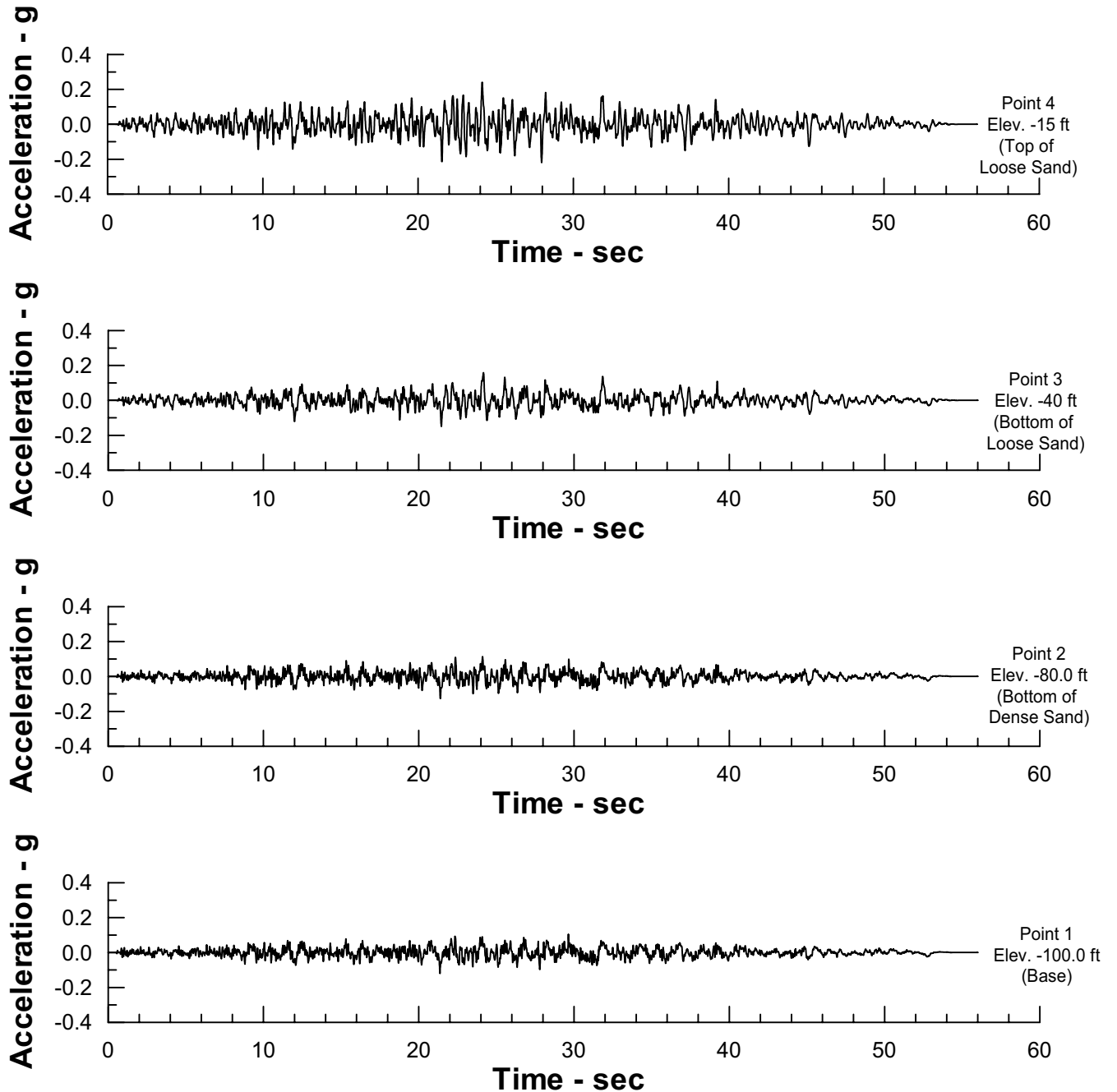


Project No. 26815621

Horizontal Acceleration
Time Histories Along Free Field Column: Island Side
(Input Motion: M 7.5 Horizontal-1 PGA 0.20g)
Idealized Section - No Peat

Figure
6-110





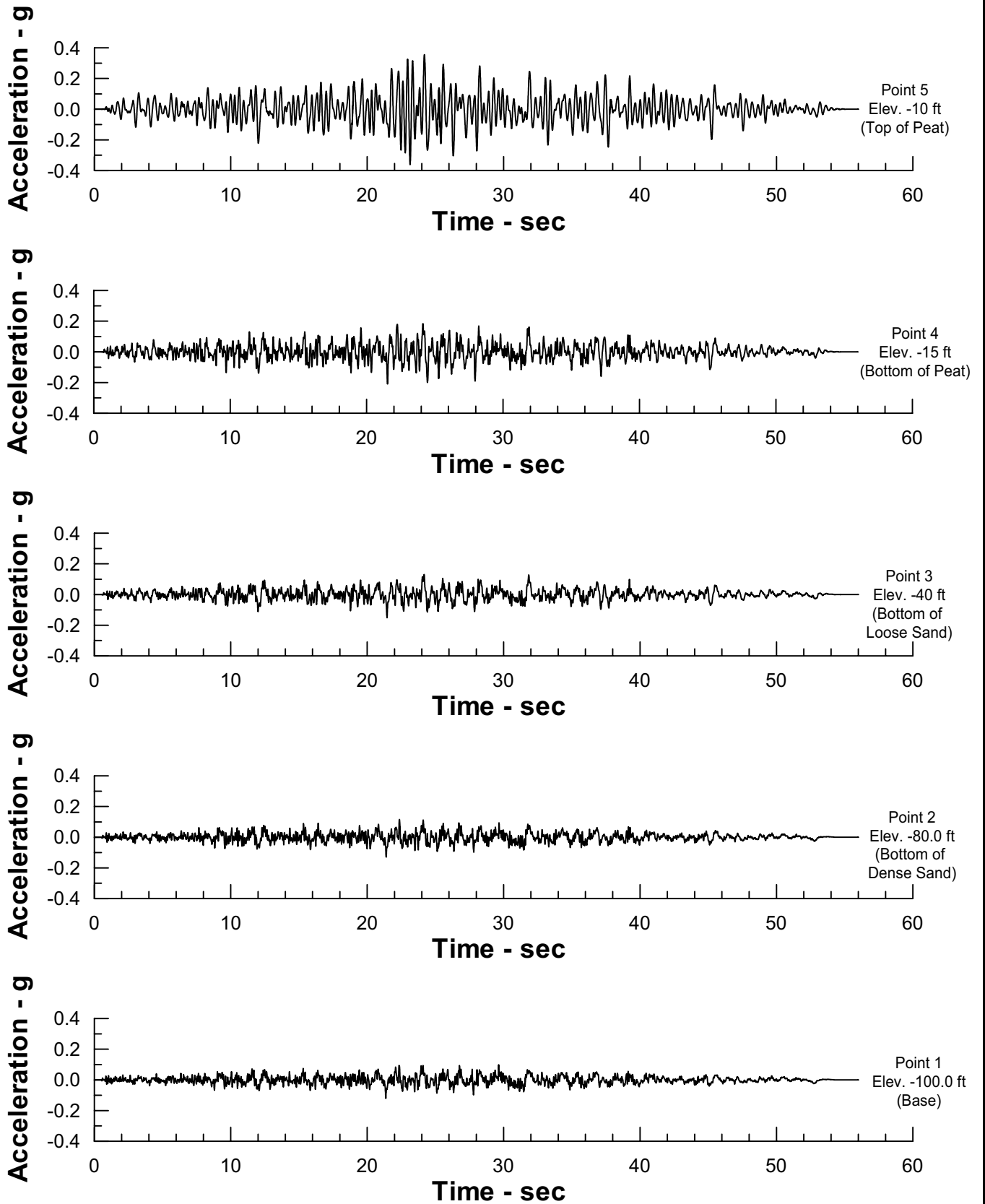
Delta Risk Management Strategy (DRMS)
Levee Fragility



Project No. 26815621

Horizontal Acceleration
Time Histories Along Free Field Column: Water Side
(Input Motion: M 7.5 Horizontal-1 PGA 0.20g)
Idealized Section - No Peat

Figure
6-112



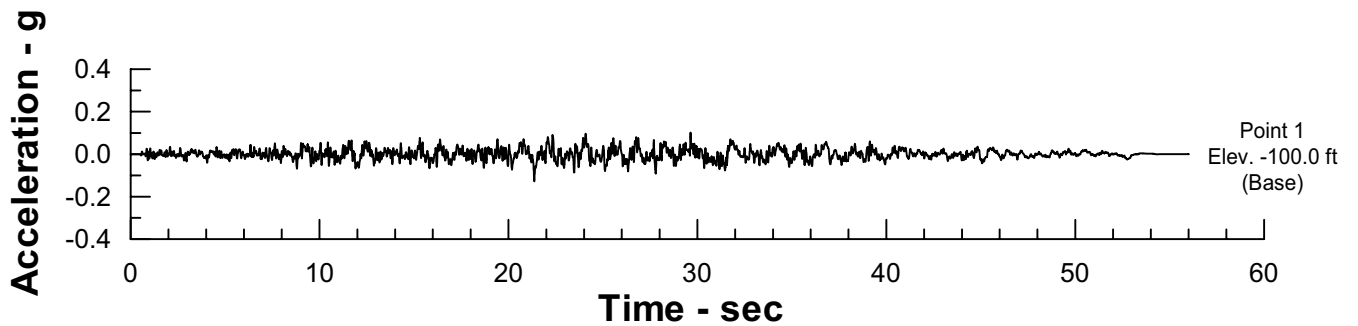
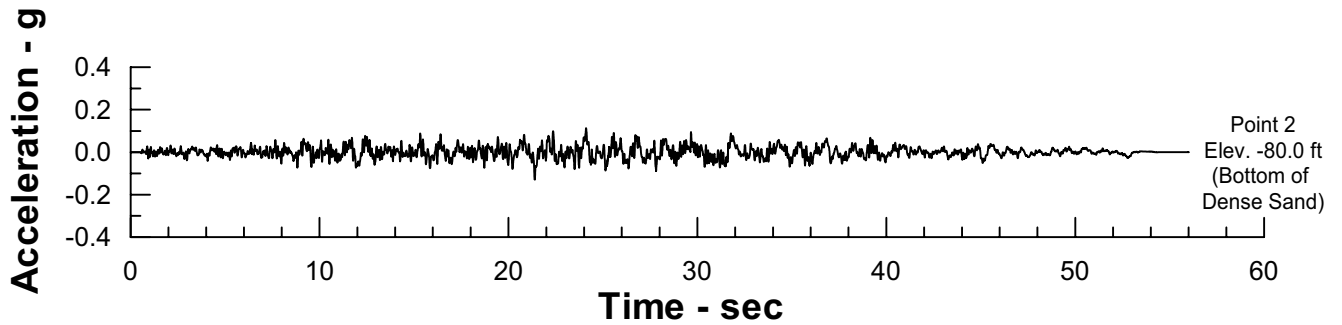
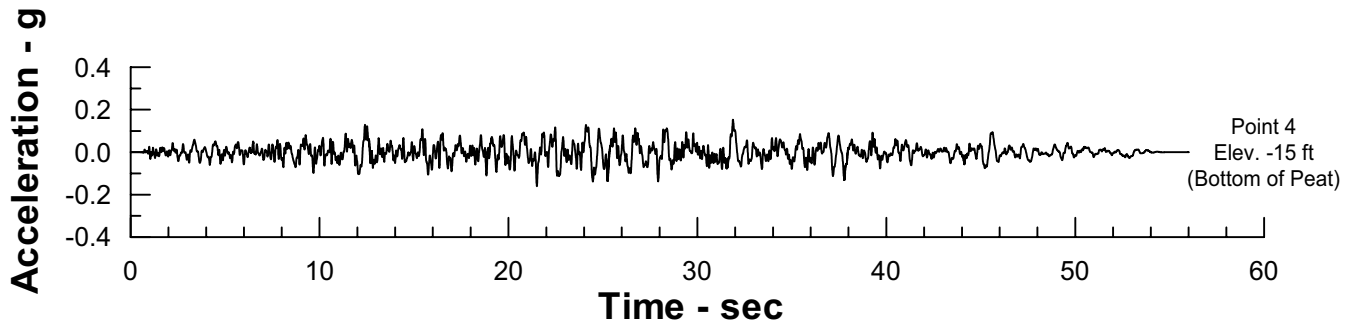
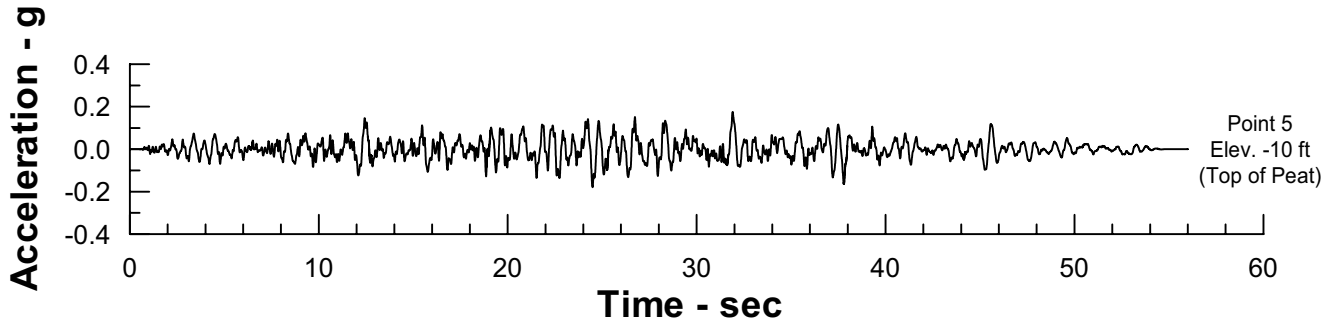
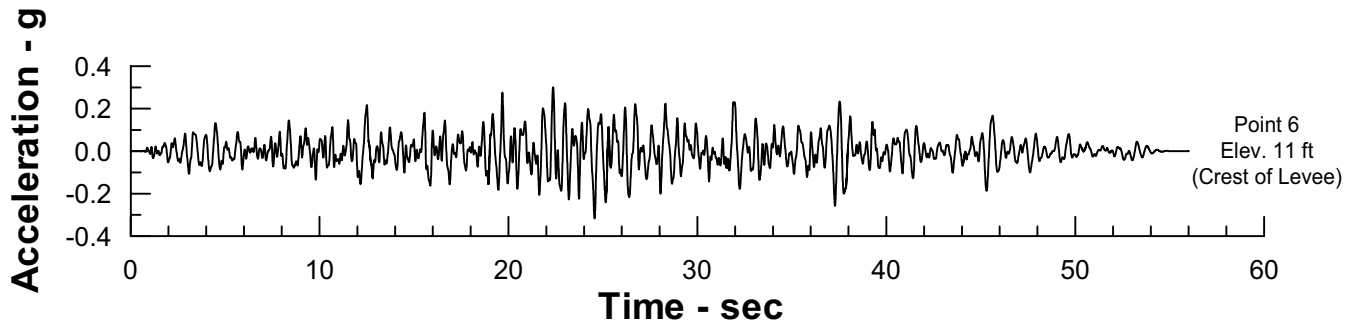
Delta Risk Management Strategy (DRMS)
Levee Fragility

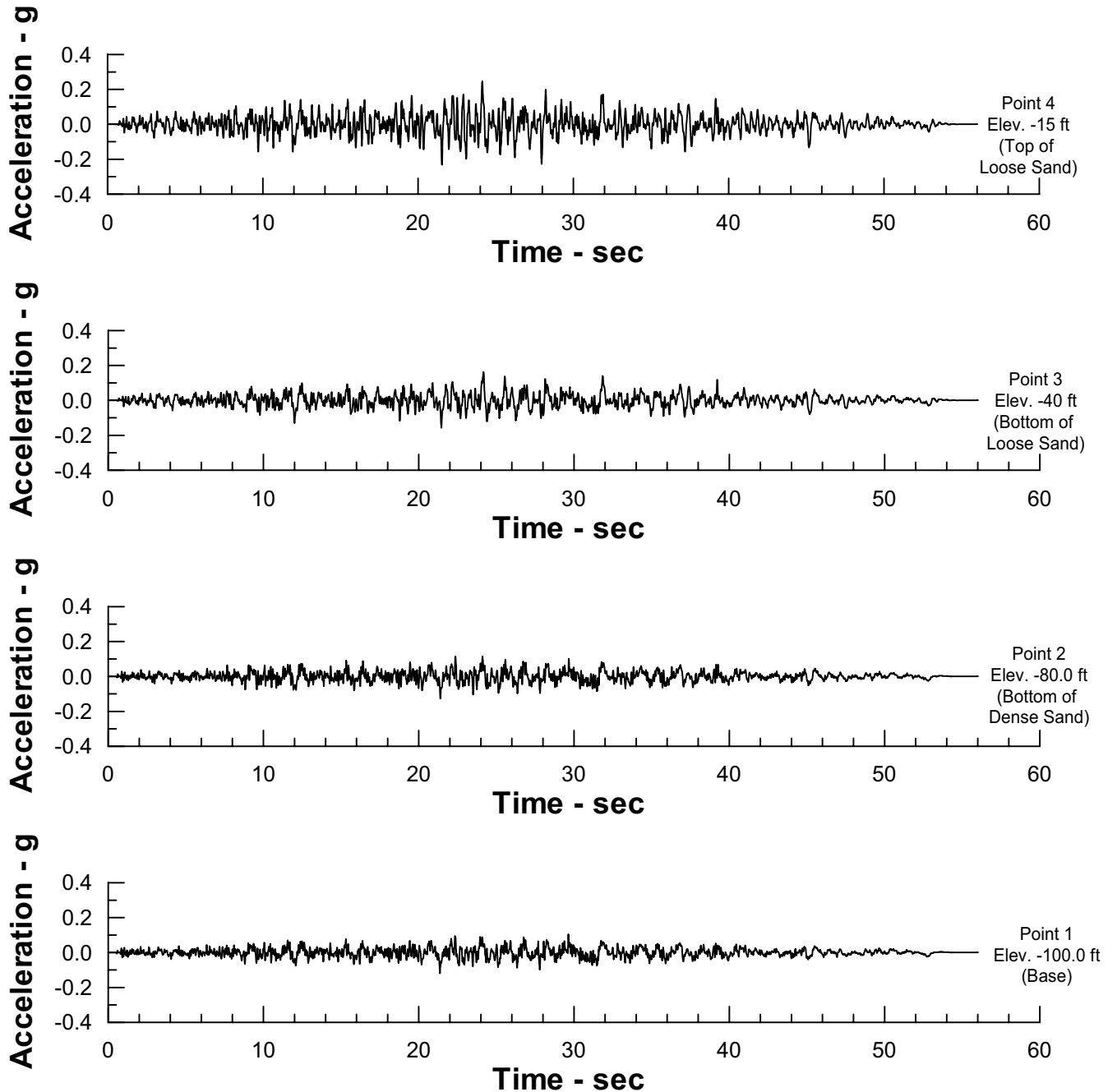


Project No. 26815621

Horizontal Acceleration
Time Histories Along Free Field Column: Island Side
(Input Motion: M 7.5 Horizontal-1 PGA 0.20g)
Idealized Section - 5 Feet of Peat

Figure
6-113





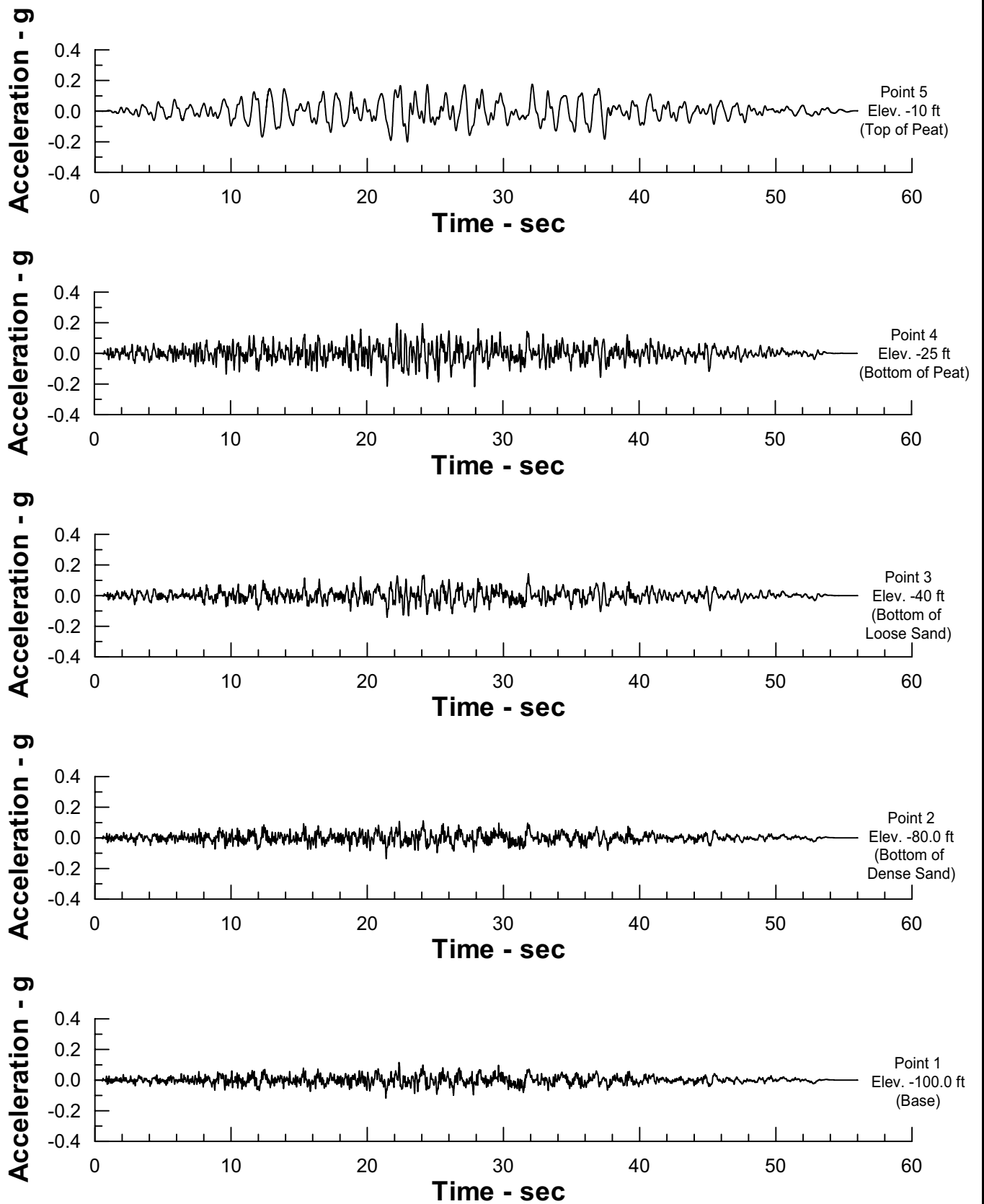
Delta Risk Management Strategy (DRMS)
Levee Fragility



Project No. 26815621

Horizontal Acceleration
Time Histories Along Free Field Column: Water Side
(Input Motion: M 7.5 Horizontal-1 PGA 0.20g)
Idealized Section - 15 Feet of Peat

Figure
6-115



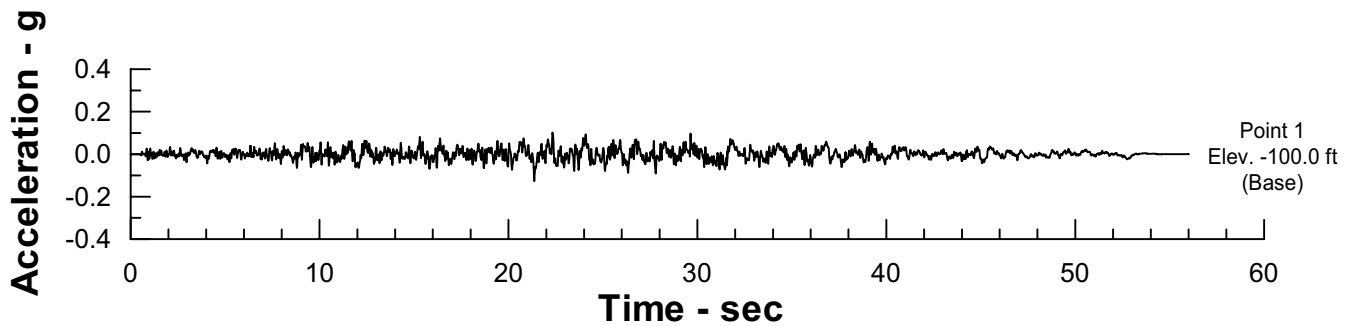
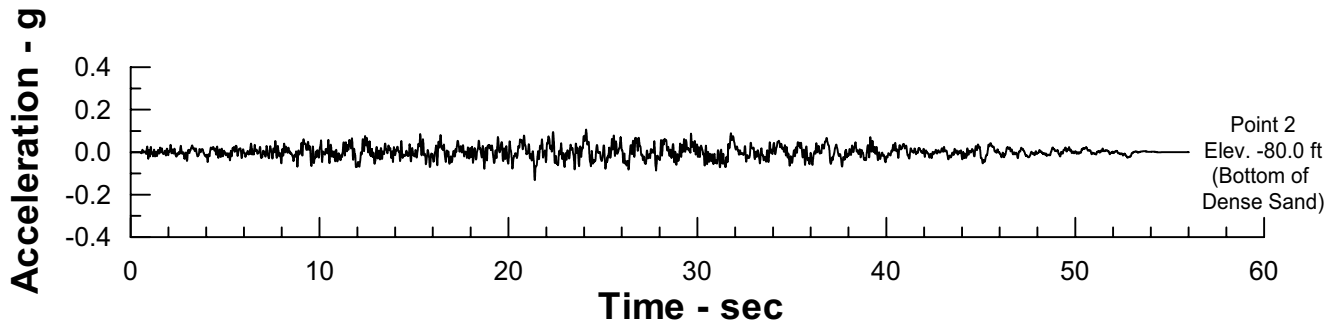
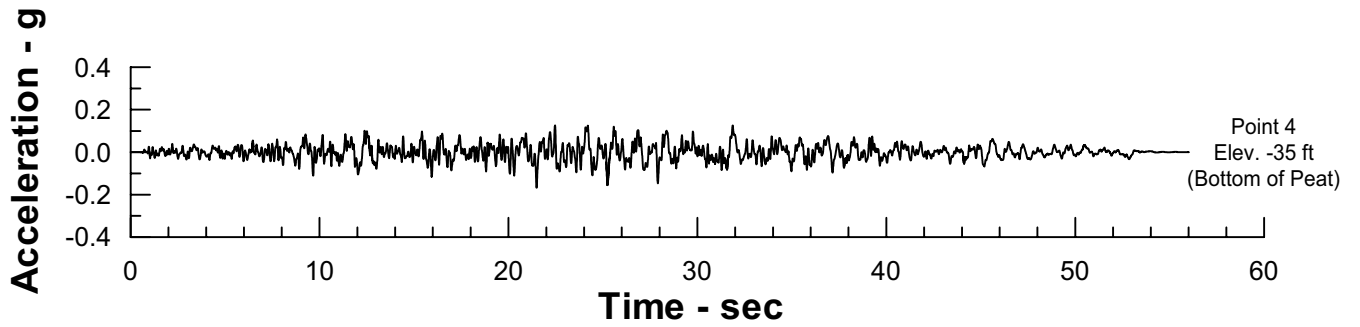
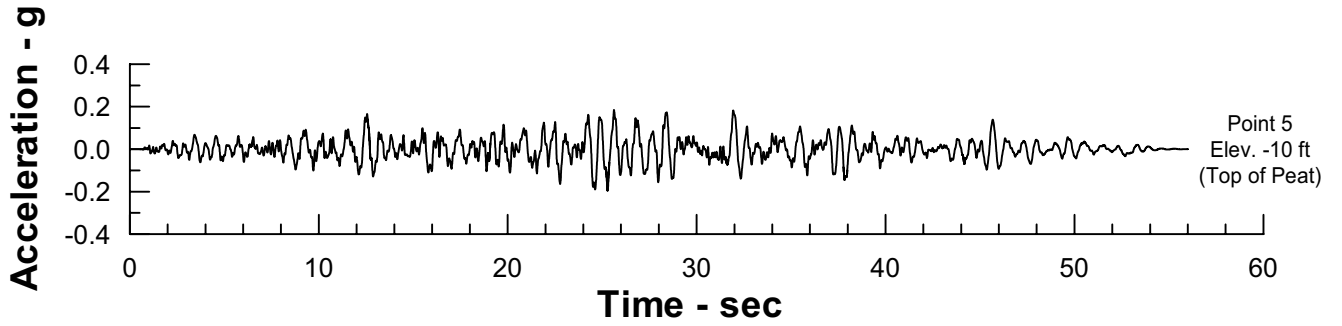
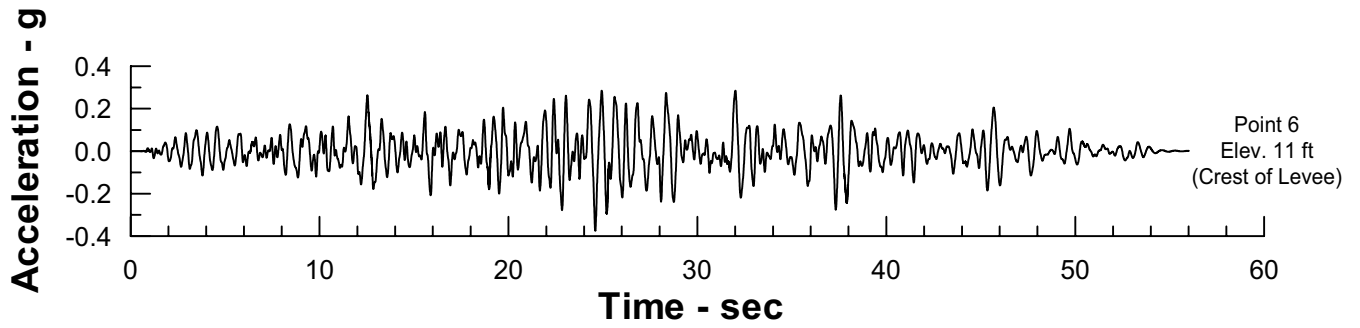
Delta Risk Management Strategy (DRMS)
Levee Fragility

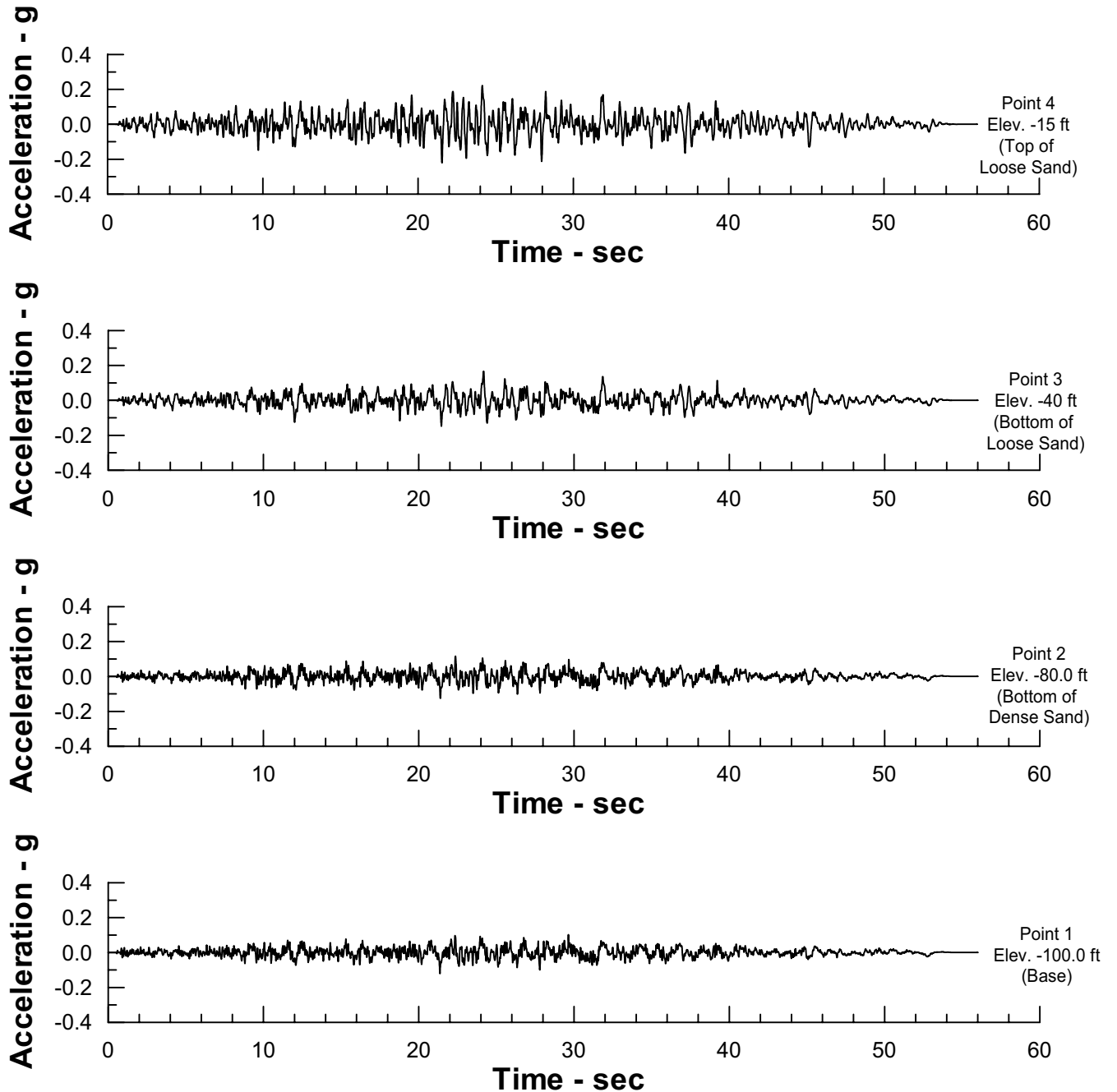


Project No. 26815621

Horizontal Acceleration
Time Histories Along Free Field Column: Island Side
(Input Motion: M 7.5 Horizontal-1 PGA 0.20g)
Idealized Section - 15 Feet of Peat

Figure
6-116





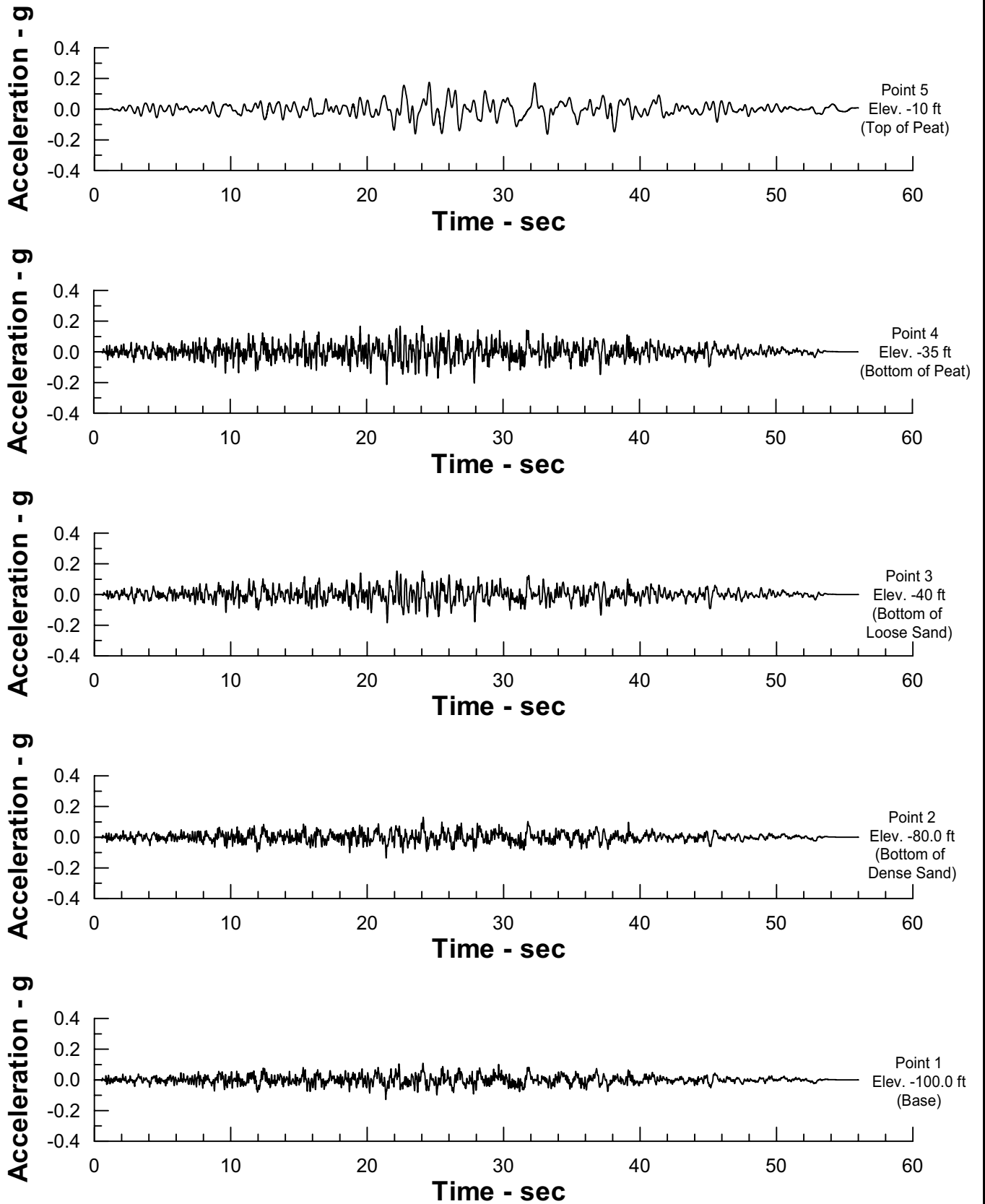
Delta Risk Management Strategy (DRMS)
Levee Fragility



Project No. 26815621

Horizontal Acceleration
Time Histories Along Free Field Column: Water Side
(Input Motion: M 7.5 Horizontal-1 PGA 0.20g)
Idealized Section - 15 Feet of Peat

Figure
6-118



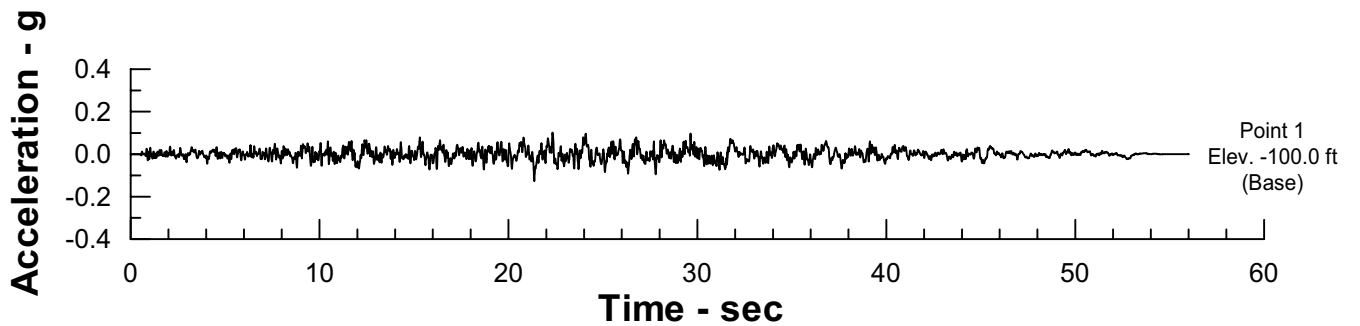
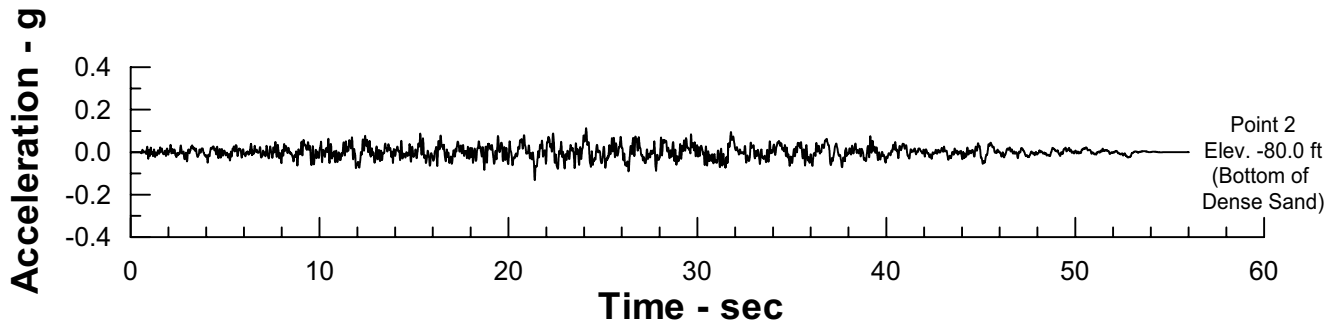
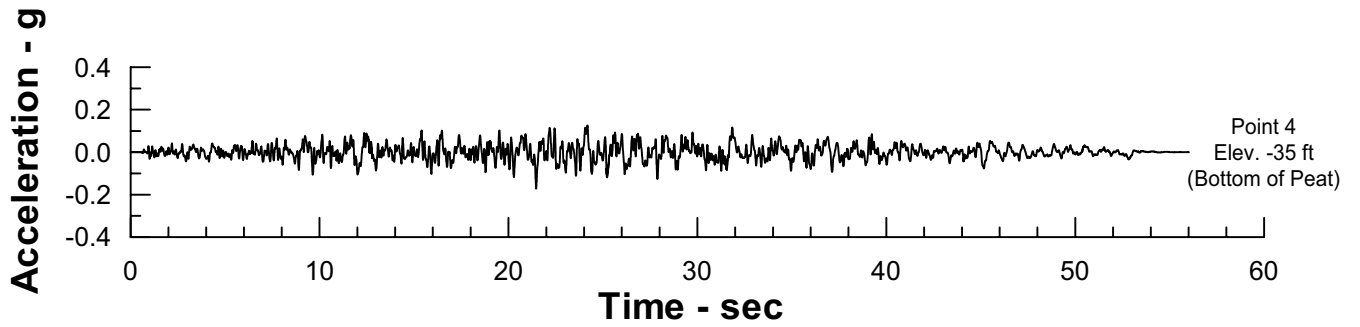
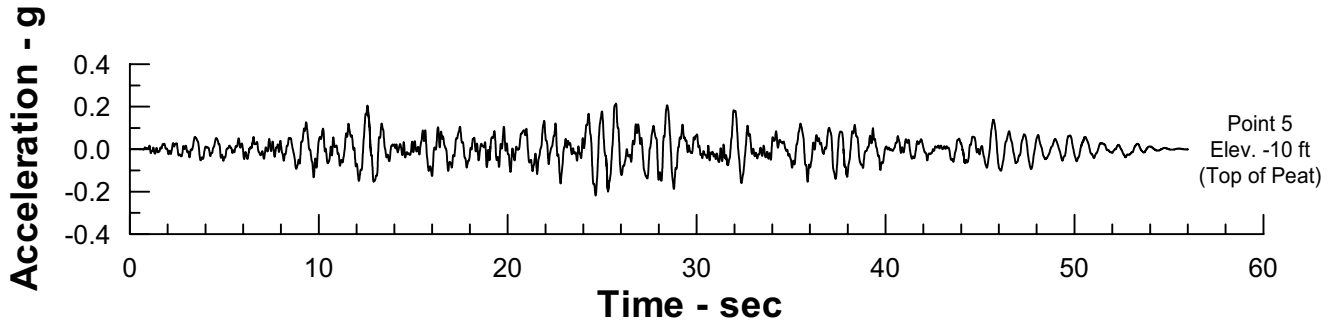
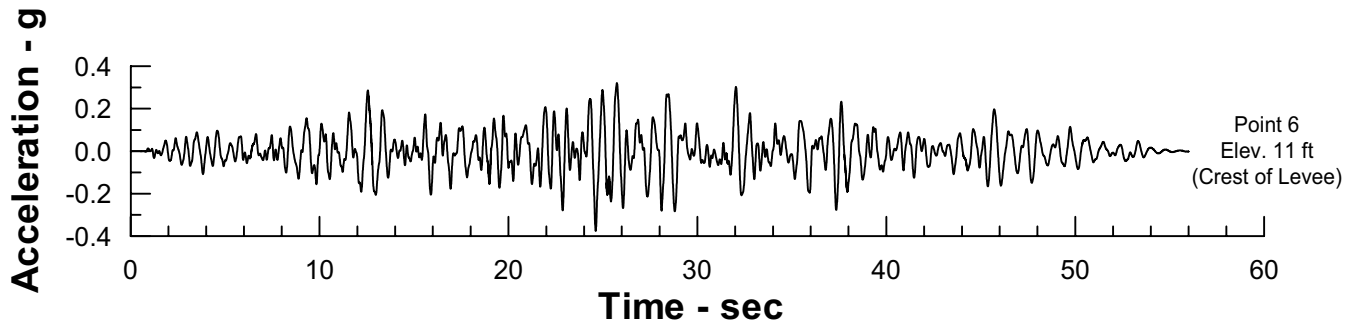
Delta Risk Management Strategy (DRMS)
Levee Fragility

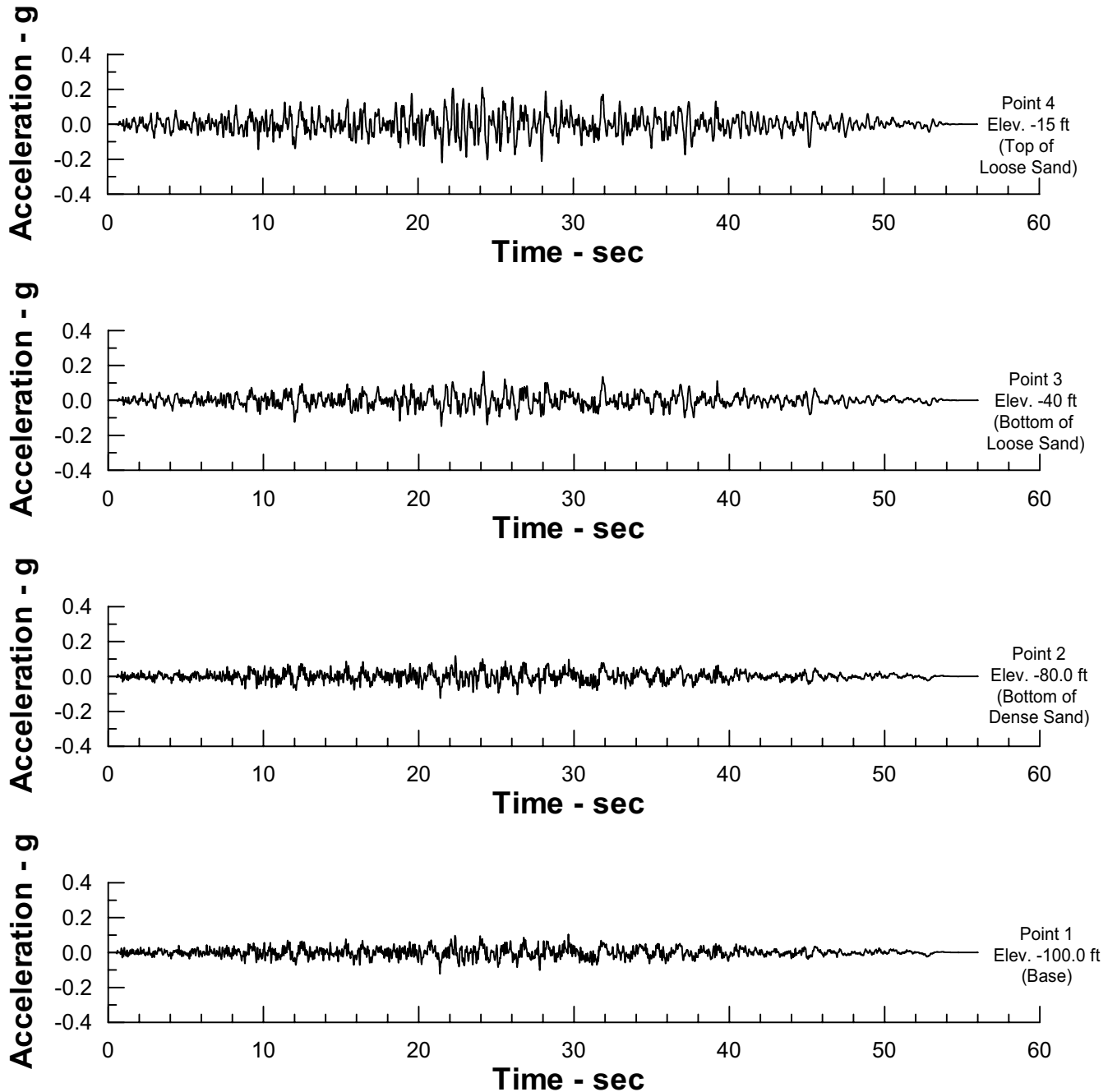


Project No. 26815621

Horizontal Acceleration
Time Histories Along Free Field Column: Island Side
(Input Motion: M 7.5 Horizontal-1 PGA 0.20g)
Idealized Section - 25 Feet of Peat

Figure
6-119





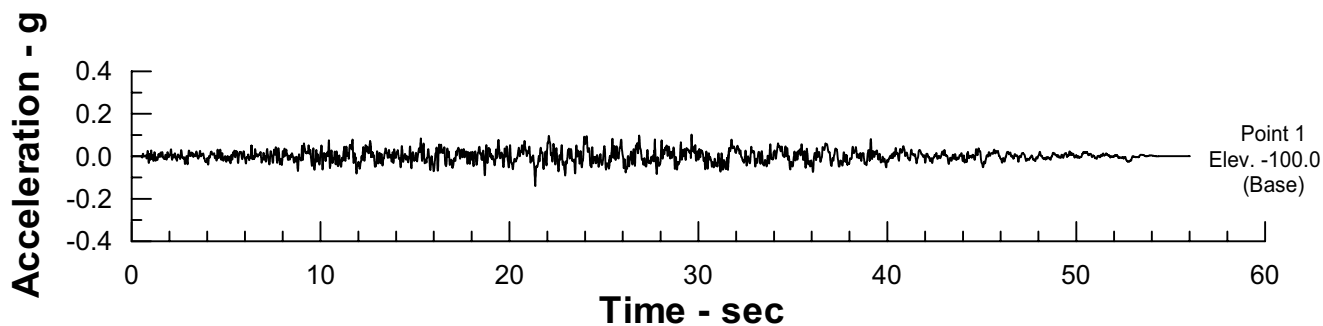
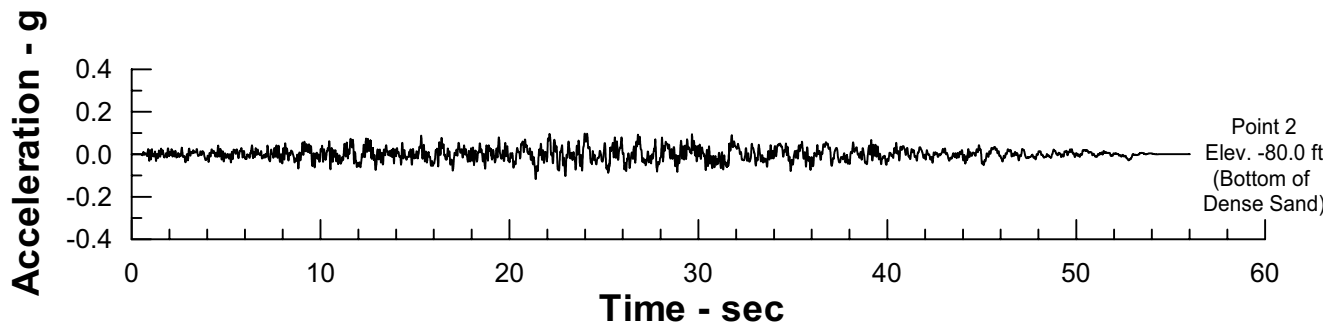
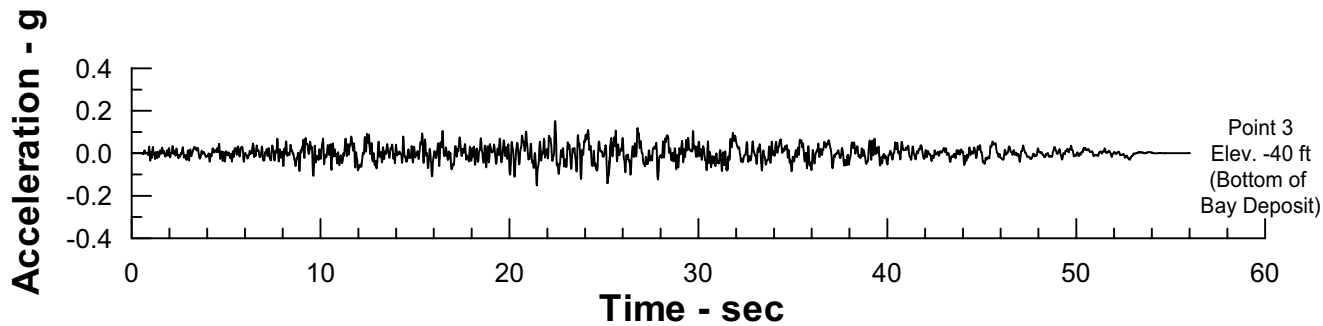
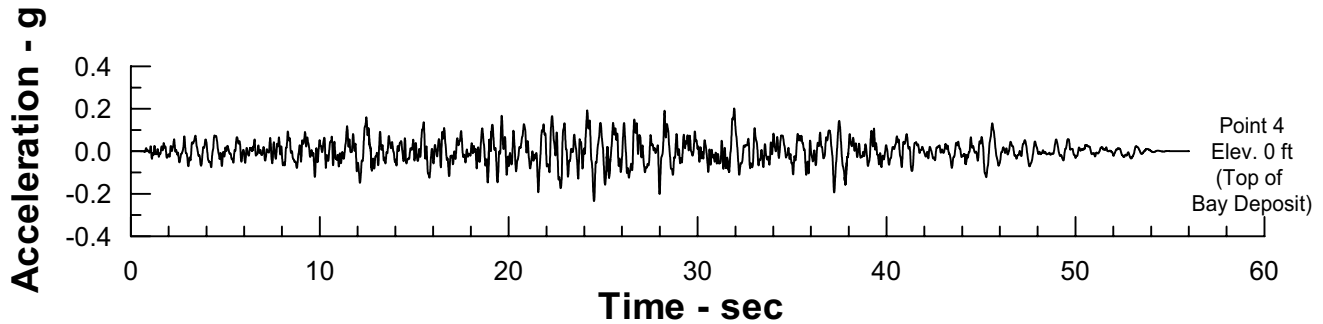
Delta Risk Management Strategy (DRMS)
Levee Fragility



Project No. 26815621

Horizontal Acceleration
Time Histories Along Free Field Column: Water Side
(Input Motion: M 7.5 Horizontal-1 PGA 0.20g)
Idealized Section - 25 Feet of Peat

Figure
6-121



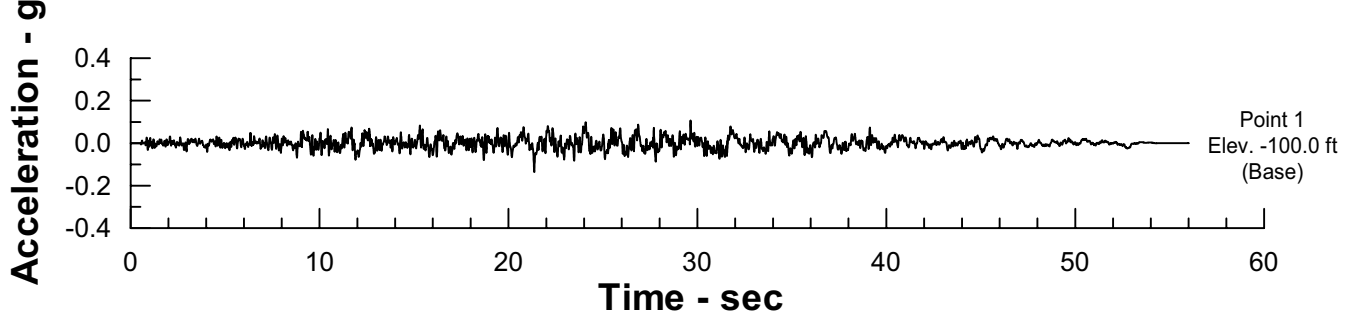
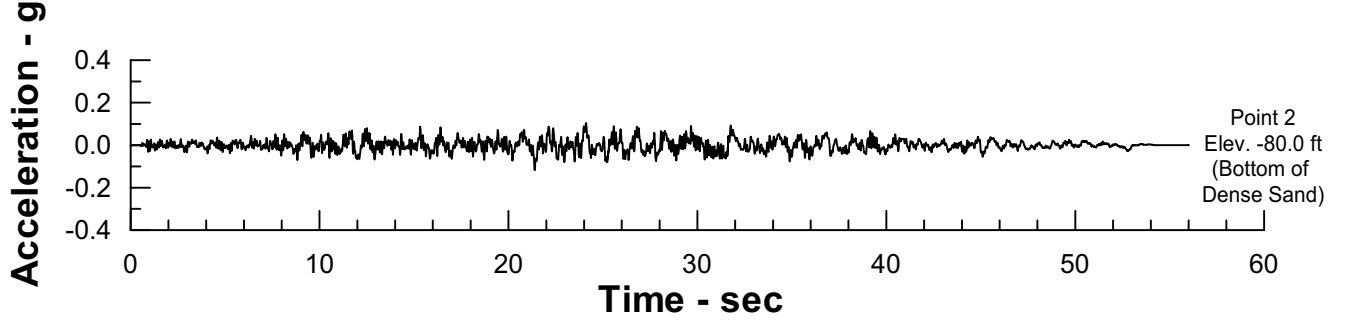
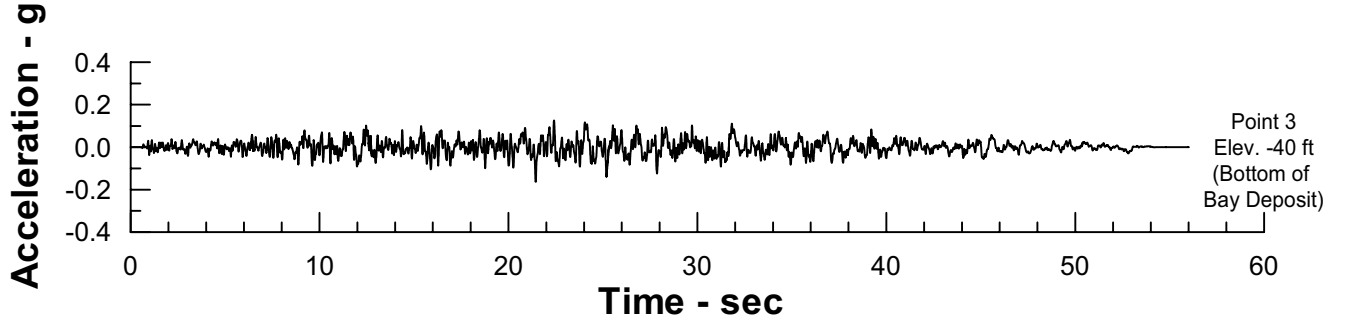
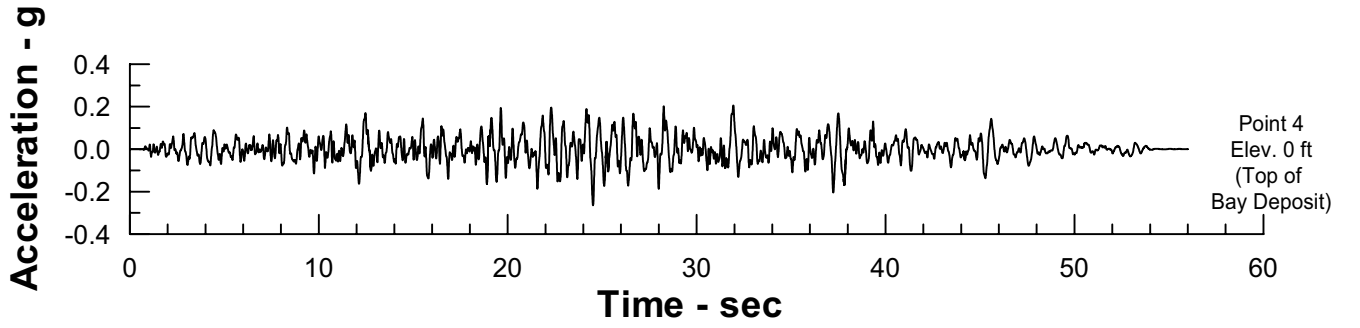
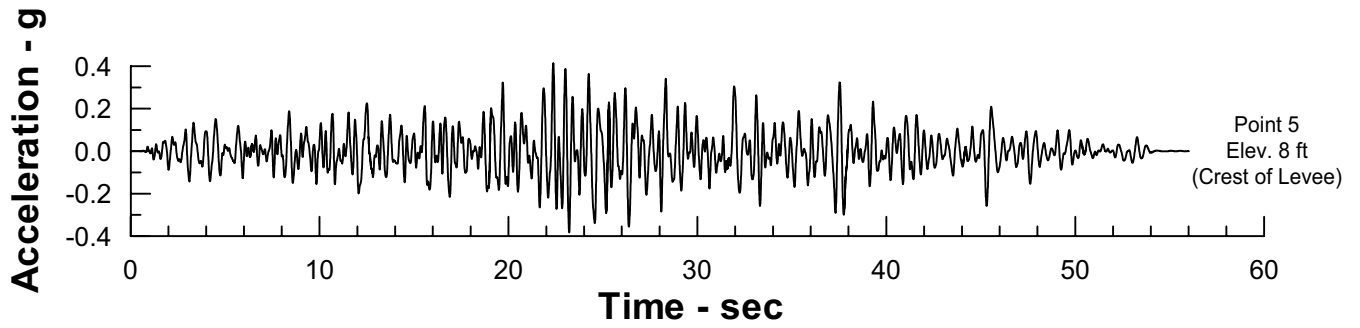
Delta Risk Management Strategy (DRMS)
Levee Fragility



Project No. 26815621

Horizontal Acceleration
Time Histories Along Free Field Column: Island Side
(Input Motion: M 7.5 Horizontal-1 PGA 0.20g)
Suisun Marsh Section

Figure
6-122



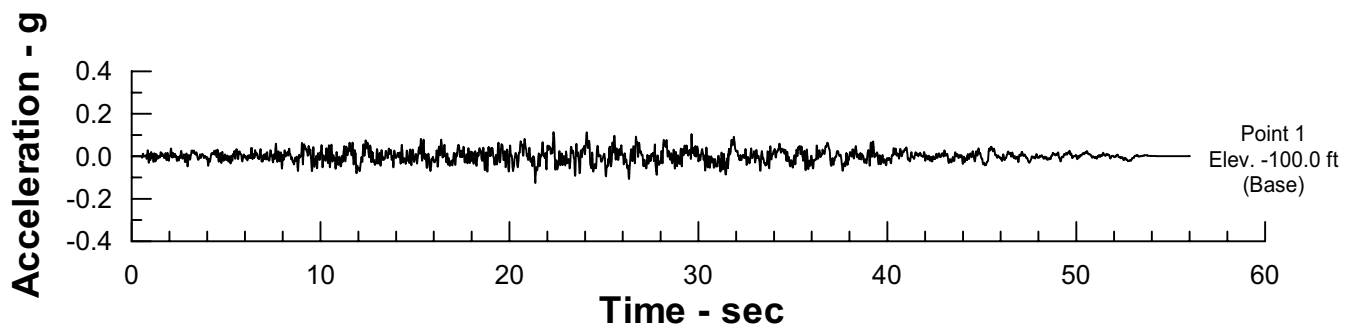
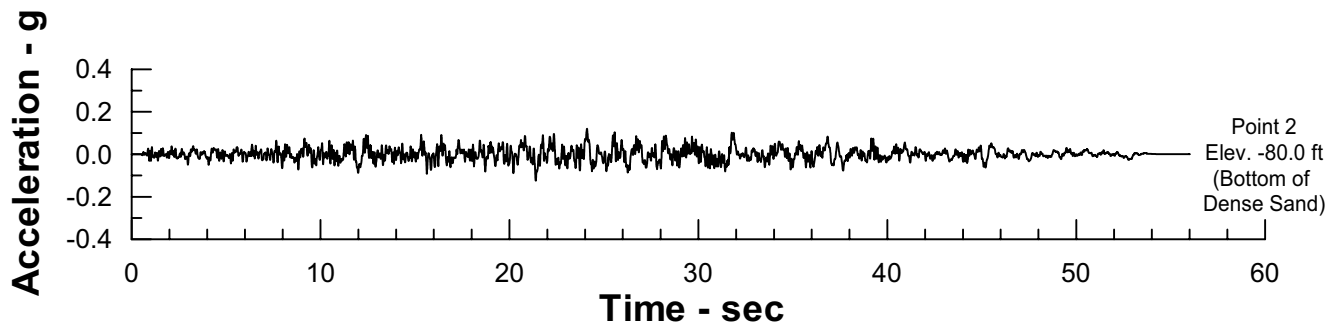
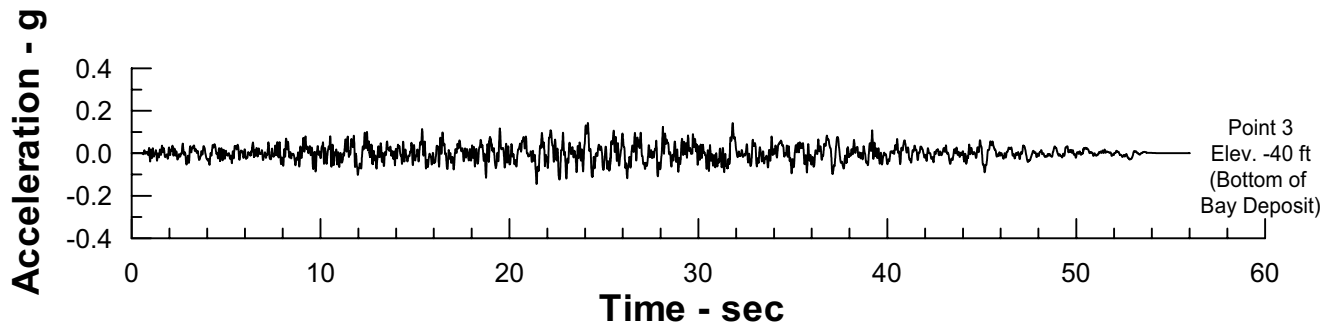
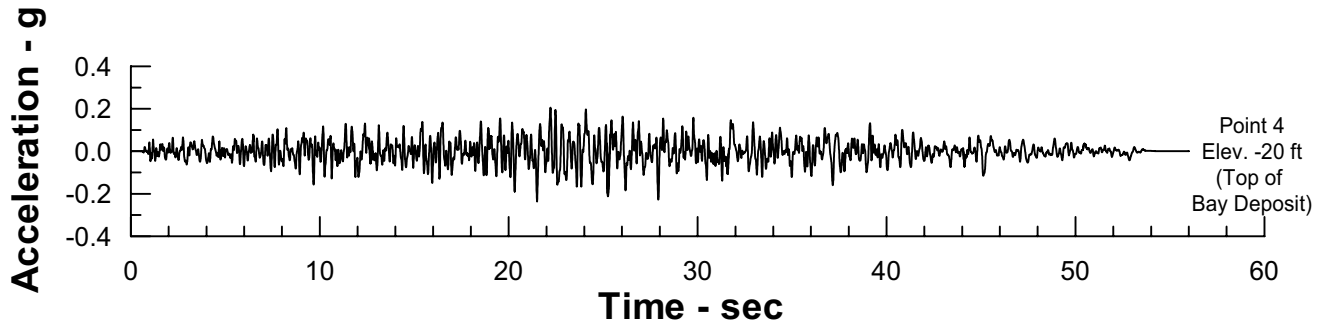
Delta Risk Management Strategy (DRMS)
Levee Fragility



Project No. 26815621

Horizontal Acceleration
Time Histories Along the Center Line of Levee
(M 7.5 Horizontal-1 PGA 0.20g)
Suisun Marsh Section

Figure
6-123



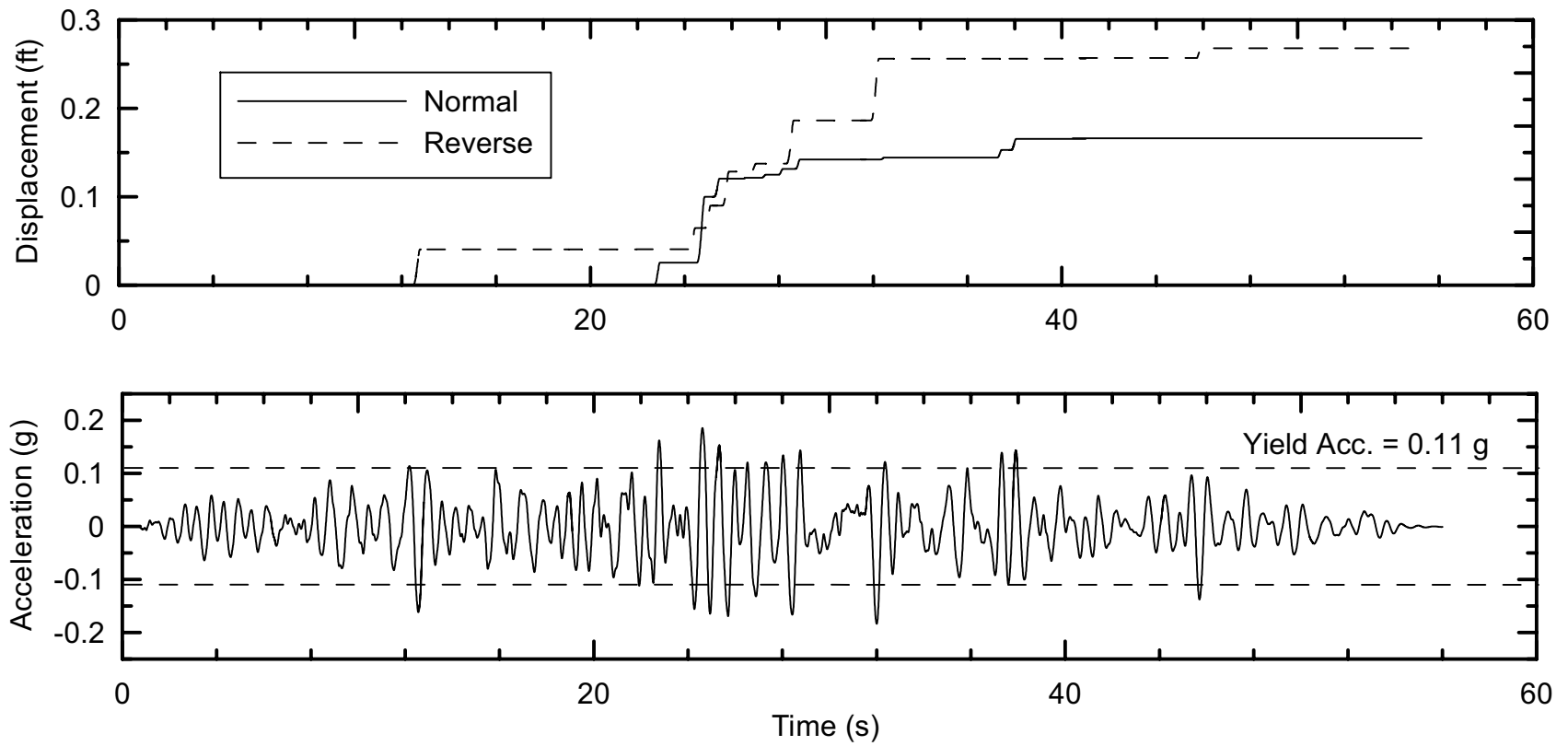
Delta Risk Management Strategy (DRMS)
Levee Fragility

URS

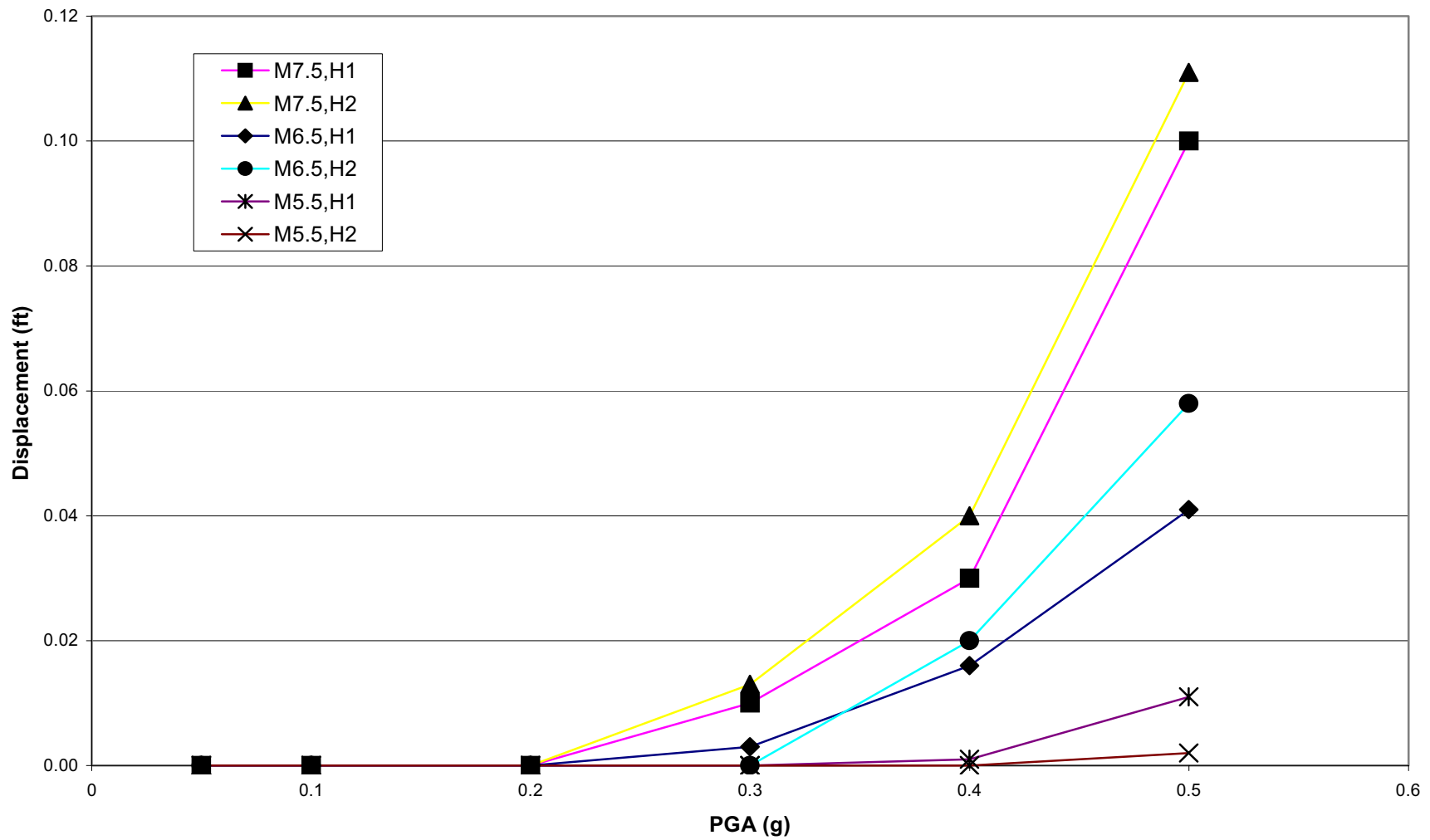
Project No. 26815621

Horizontal Acceleration
Time Histories Along Free Field Column: Water Side
(Input Motion: M 7.5 Horizontal-1 PGA 0.20g)
Suisun Marsh Section

Figure
6-124



Delta Risk Management Strategy (DRMS) Levee Fragility		Calculated Newmark Displacements M7.5 Horizontal #1 Time History, 0.2g PGA Idealized Section 15 Feet of Peat	Figure 6-125
URS	Project No. 26815621		



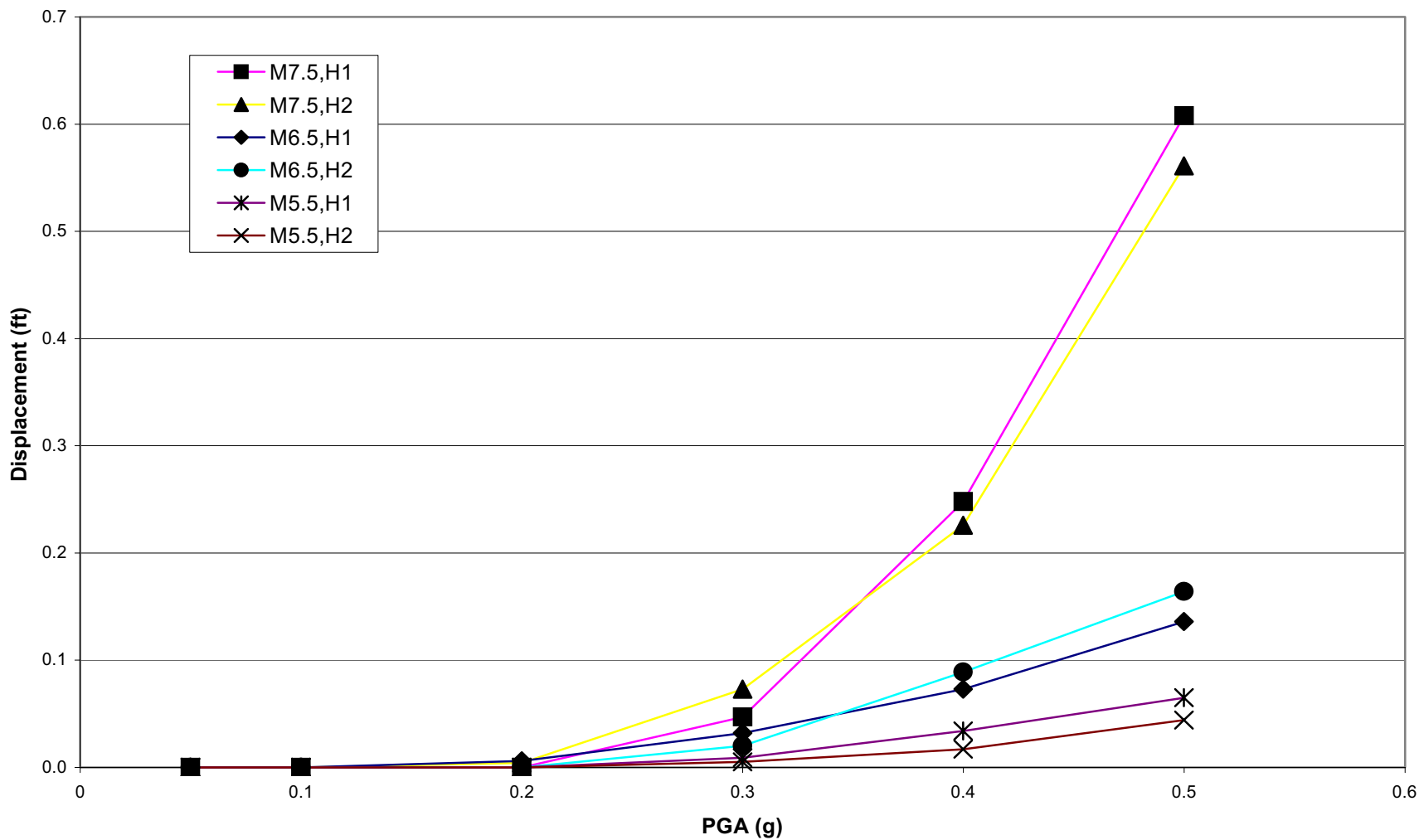
Delta Risk Management Strategy (DRMS)
Levee Fragility



Project No. 26815621

Calculated Newmark Displacements
Idealized Section
No Peat

Figure
6-126



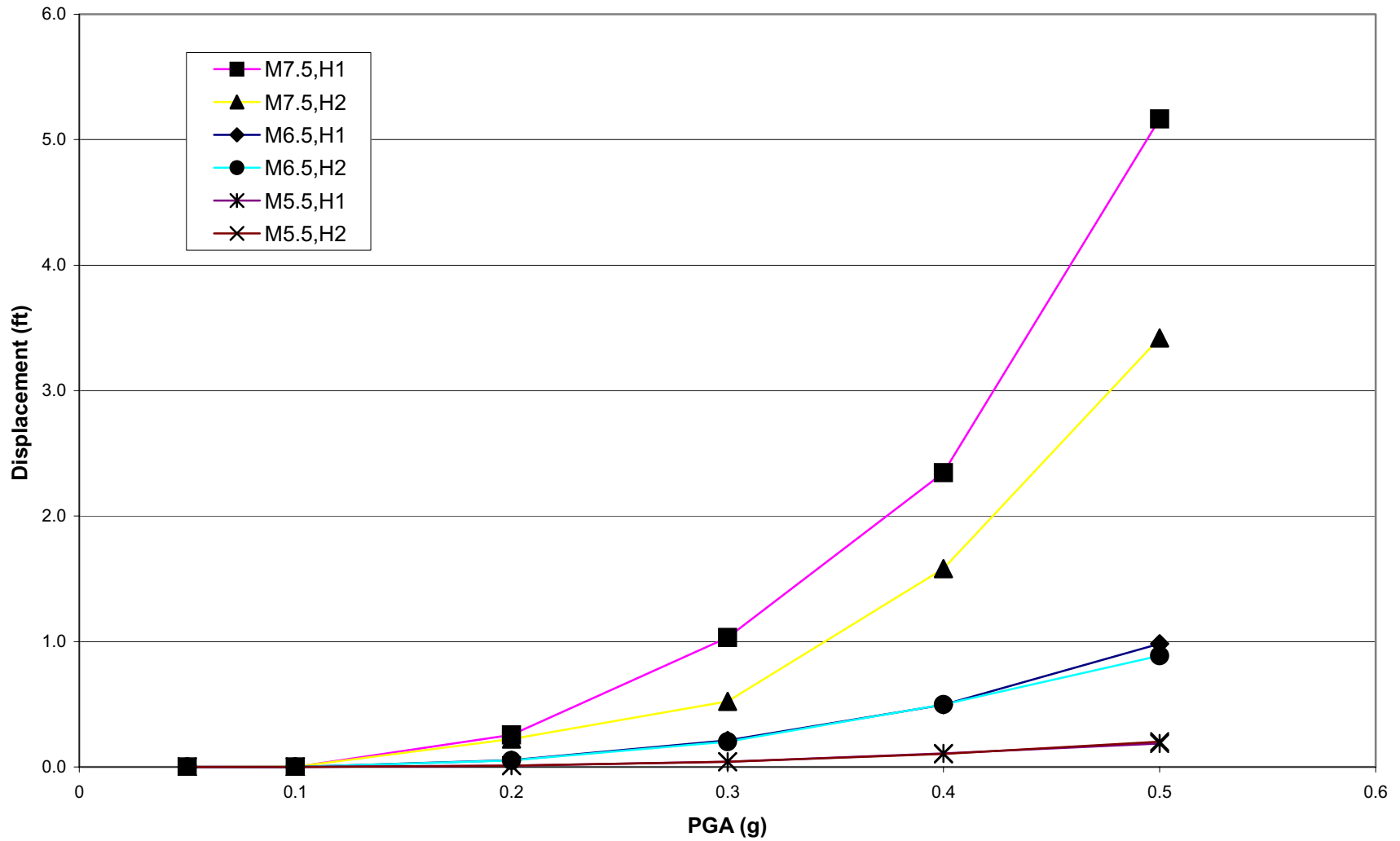
Delta Risk Management Strategy (DRMS)
Levee Fragility

URS

Project No. 26815621

Calculated Newmark Displacements
Idealized Section
5 Feet of Peat

Figure
6-127



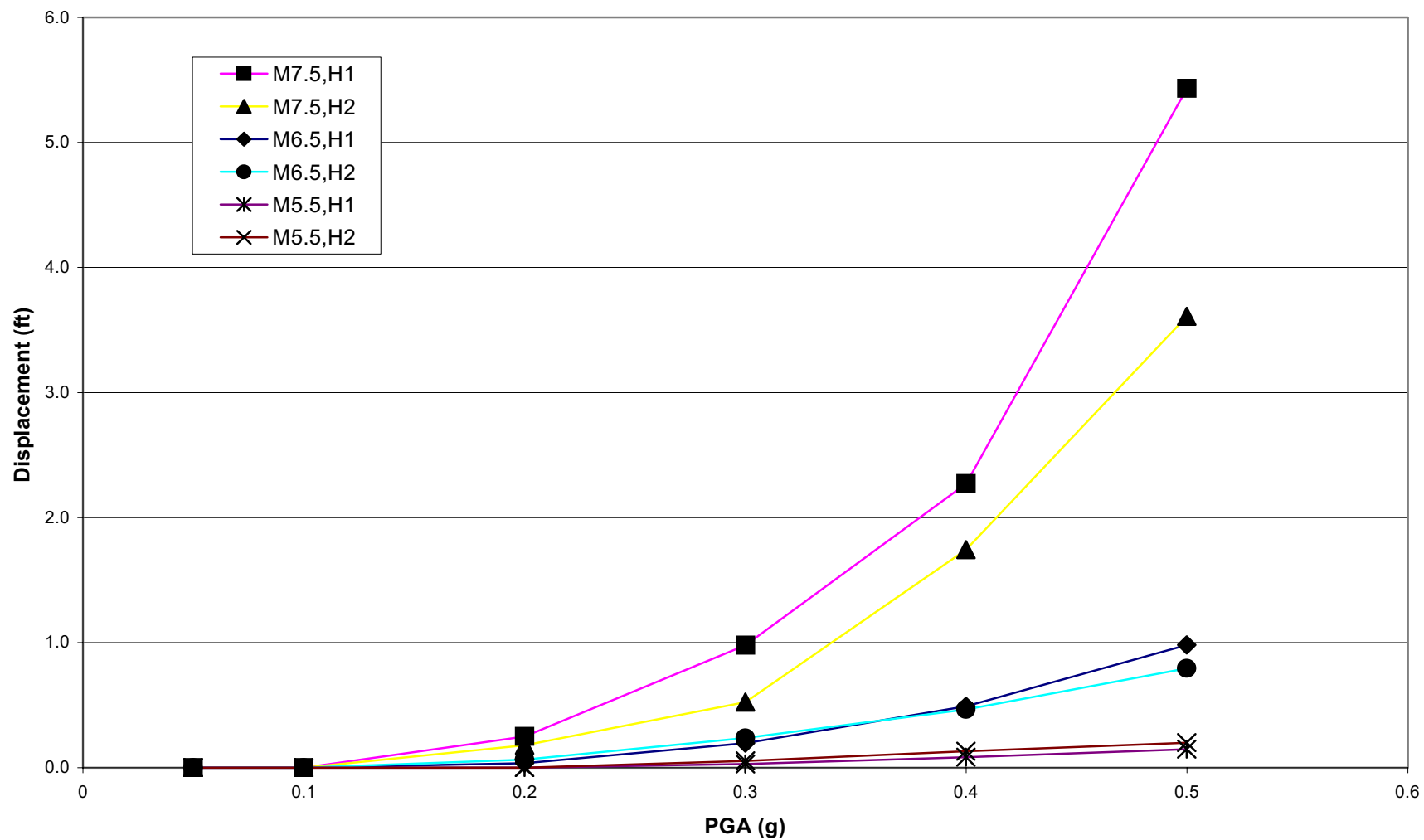
Delta Risk Management Strategy (DRMS)
Levee Fragility

URS

Project No. 26815621

Calculated Newmark Displacements
Idealized Section
15 Feet of Peat

Figure
6-128



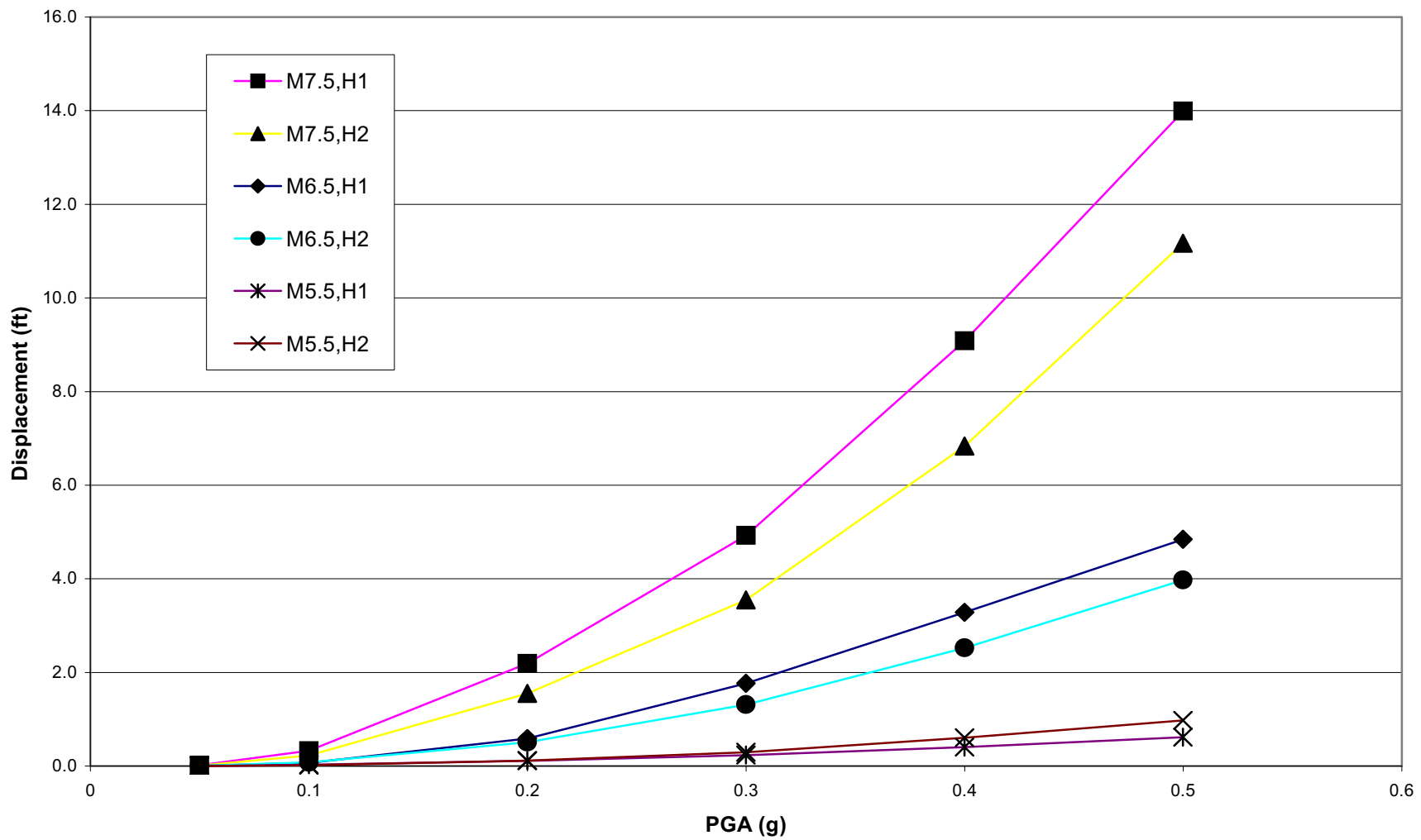
Delta Risk Management Strategy (DRMS)
Levee Fragility



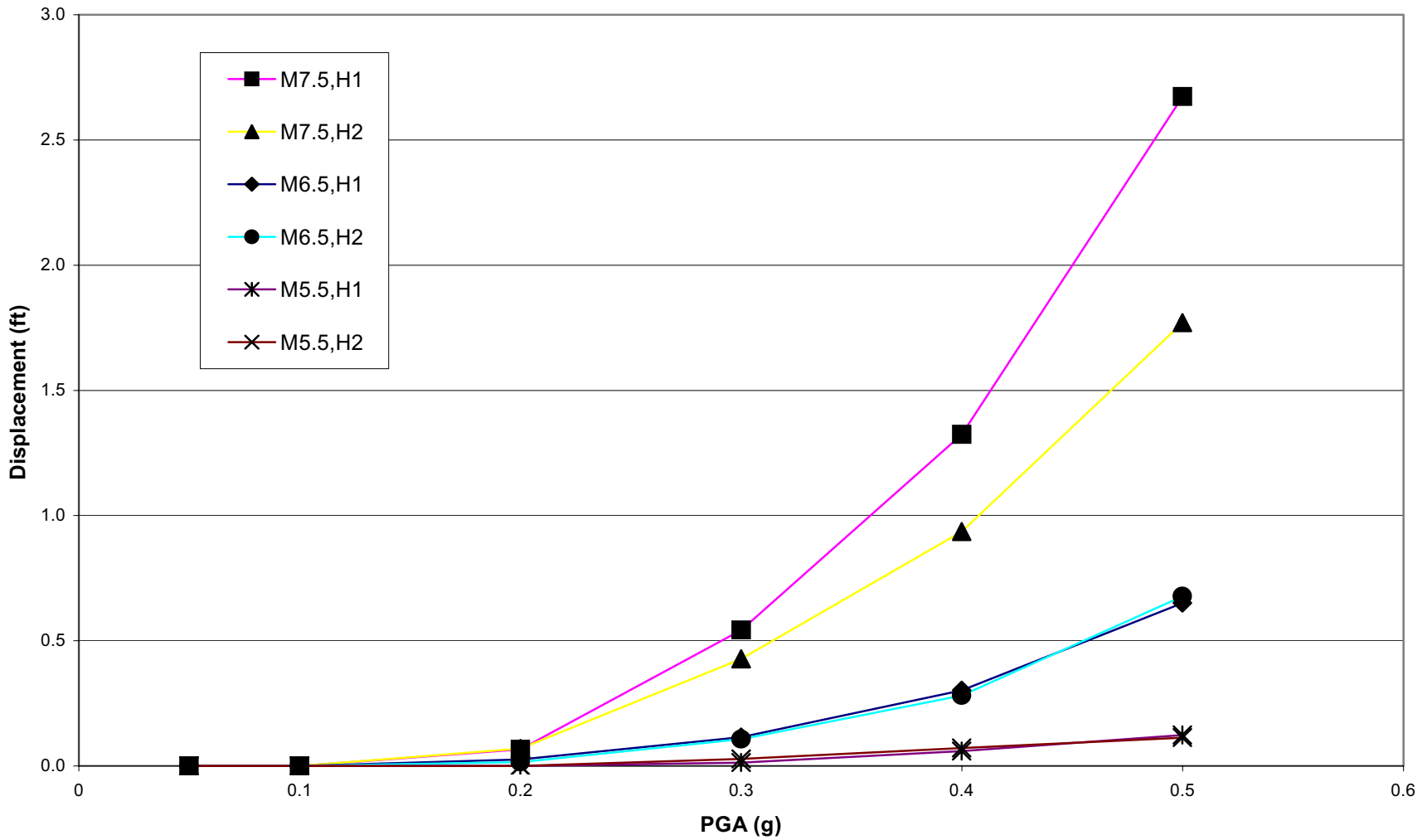
Project No. 26815621

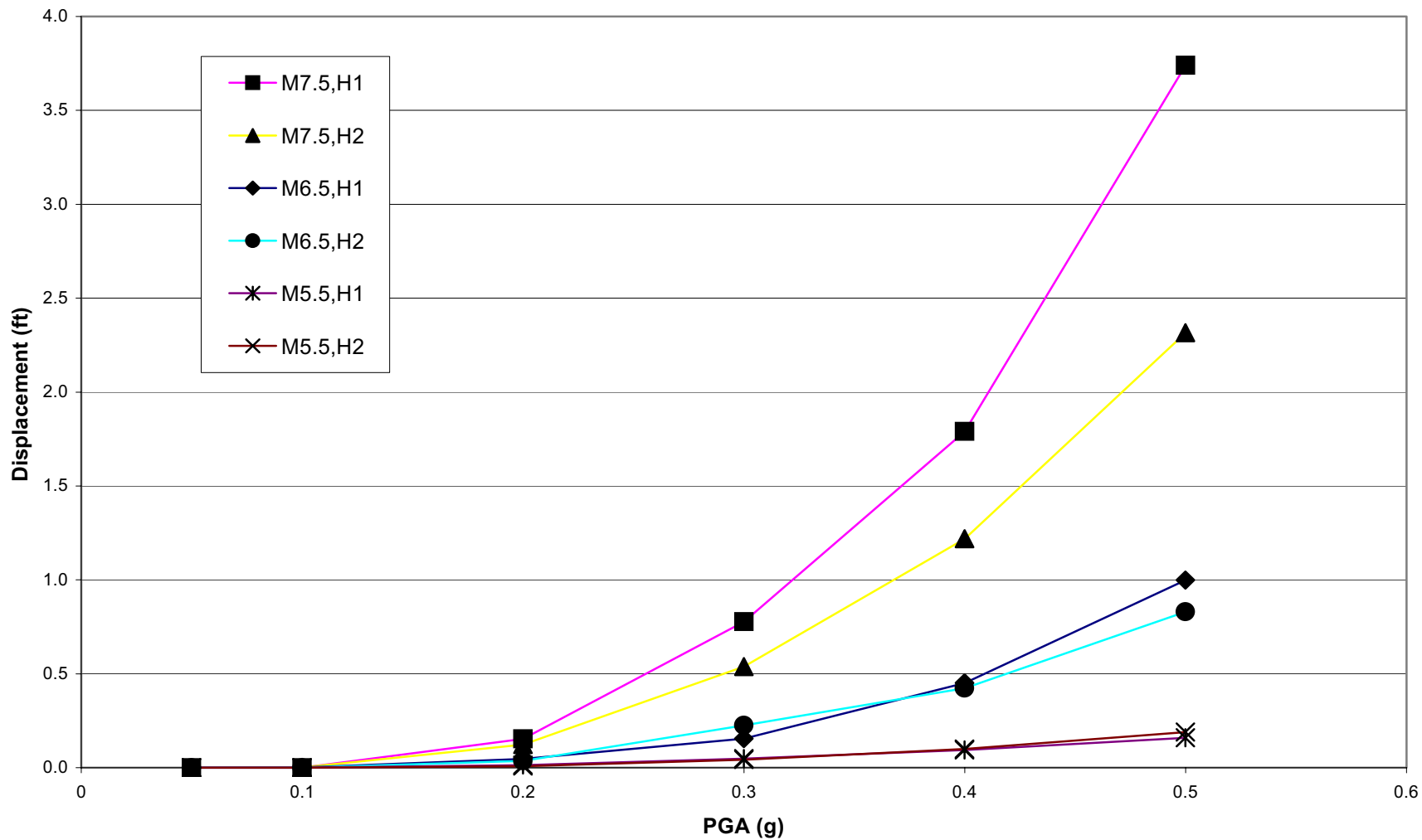
Calculated Newmark Displacements
Idealized Section
25 Feet of Peat

Figure
6-129



Delta Risk Management Strategy (DRMS) Levee Fragility		Calculated Newmark Displacements Idealized Section Suisun Marsh	Figure 6-130
URS	Project No. 26815621		





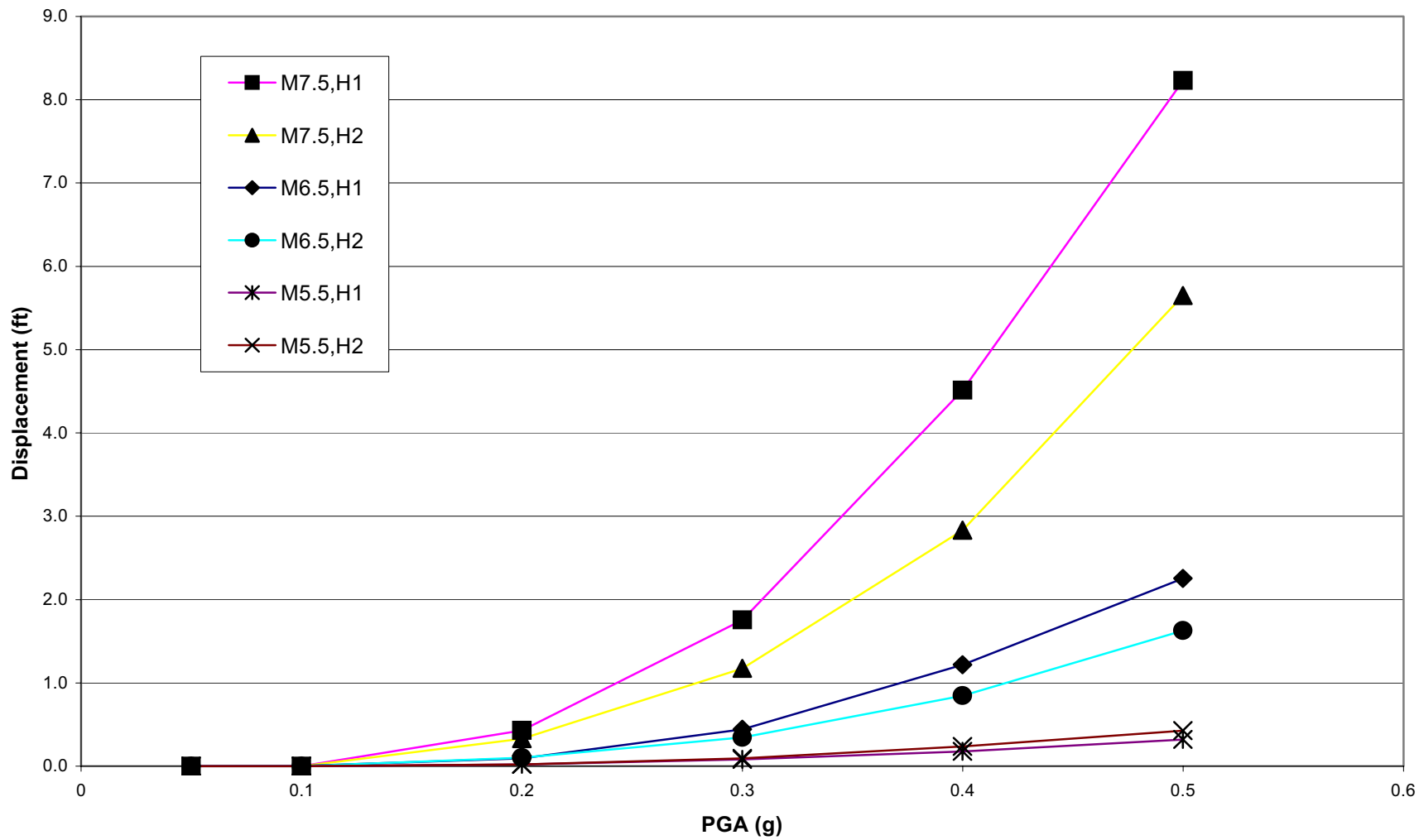
Delta Risk Management Strategy (DRMS)
Levee Fragility



Project No. 26815621

Calculated Newmark Displacements
Idealized Section with
Steep Water Side Slope
5 ft Peat

Figure
6-97



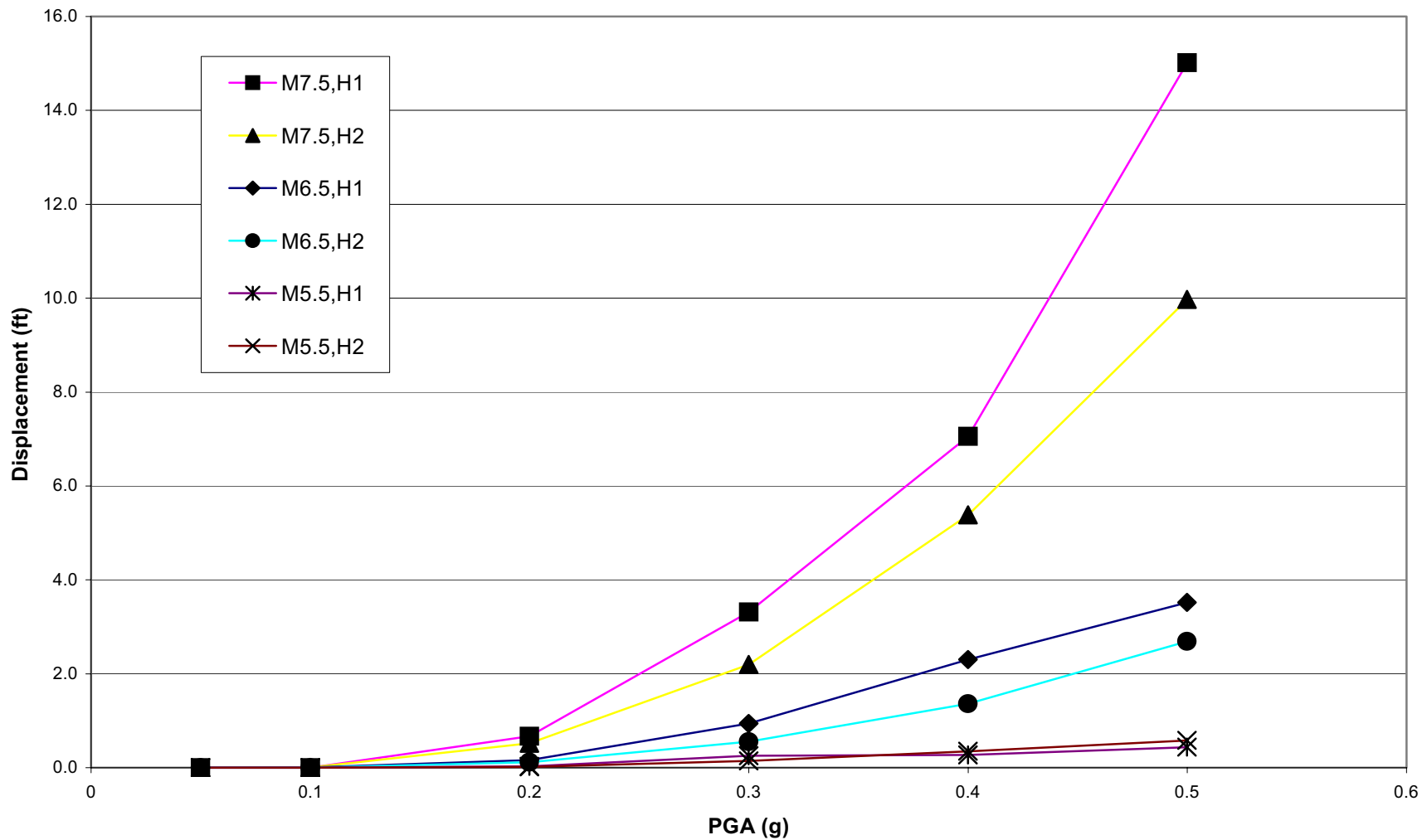
Delta Risk Management Strategy (DRMS)
Levee Fragility

URS

Project No. 26815621

Calculated Newmark Displacements
Idealized Section with
Steep Water Side Slope
15 ft Peat

Figure
6-98



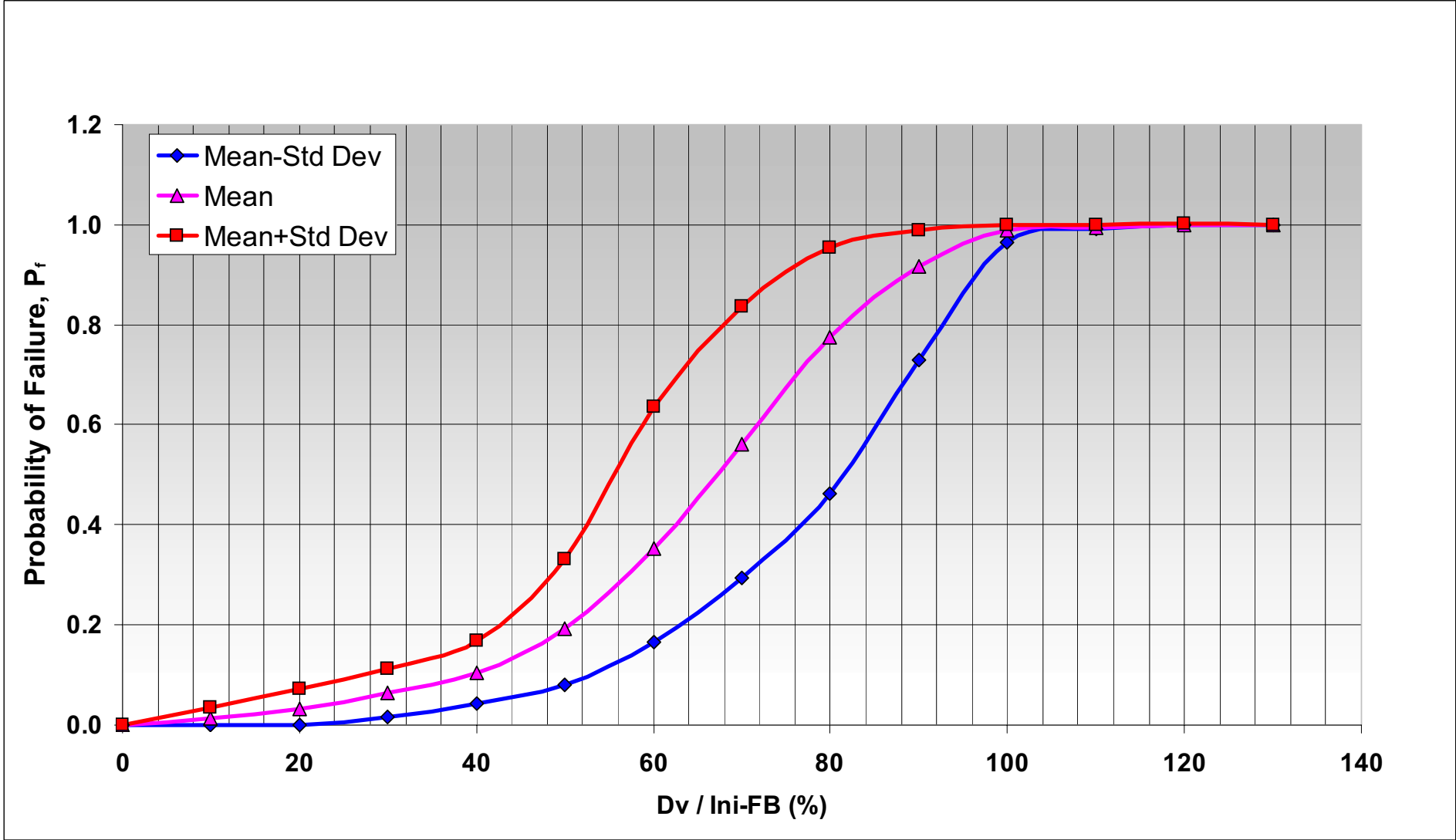
Delta Risk Management Strategy (DRMS)
Levee Fragility

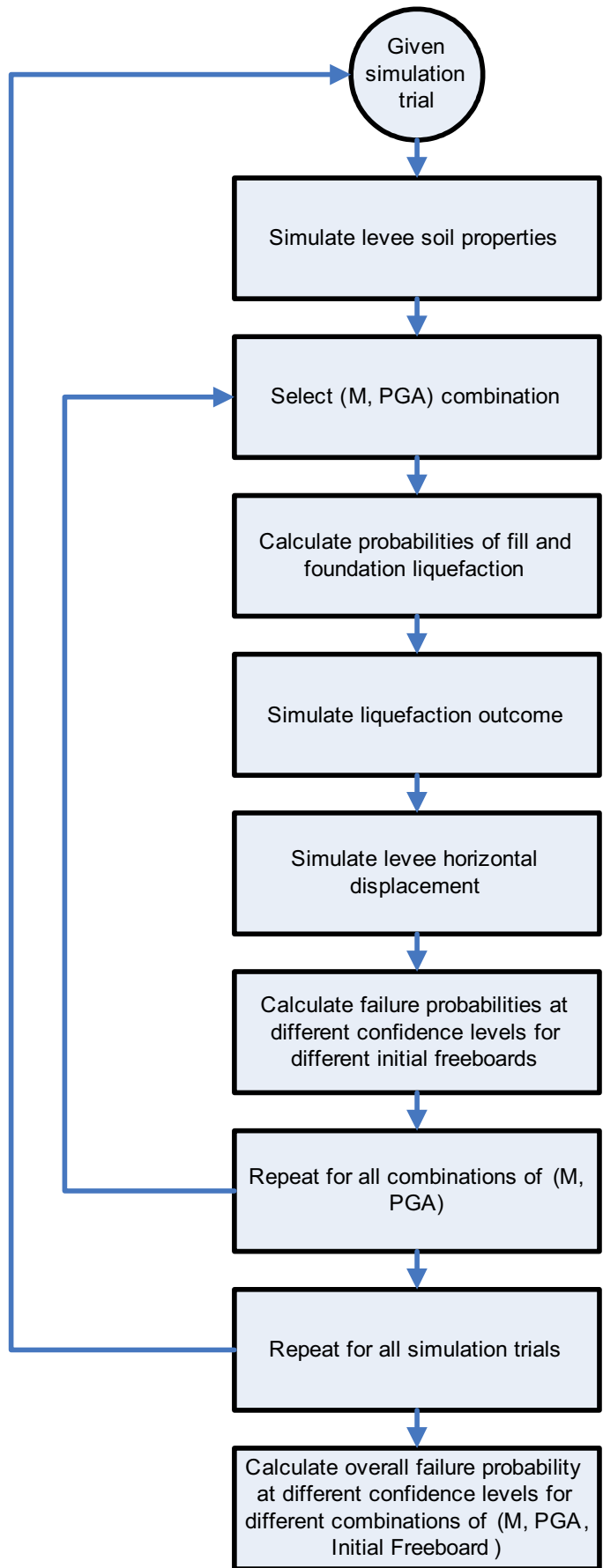


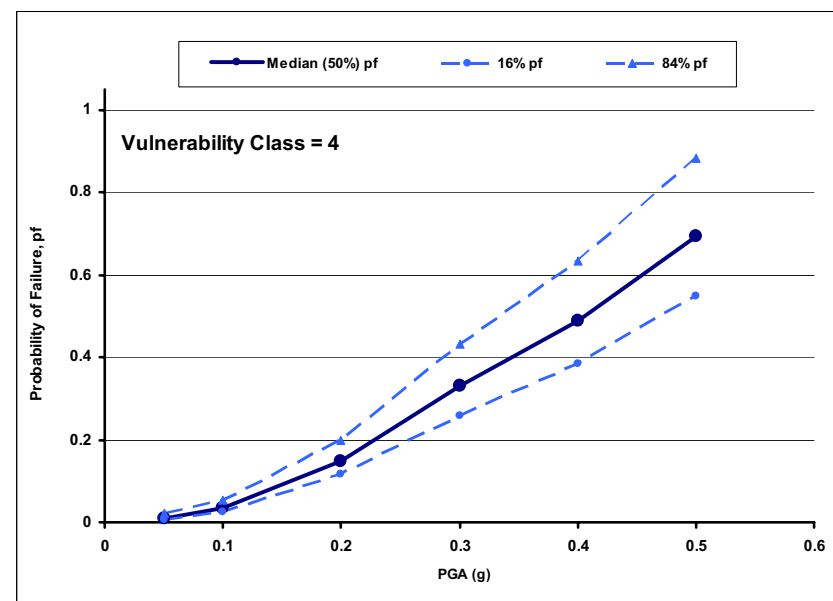
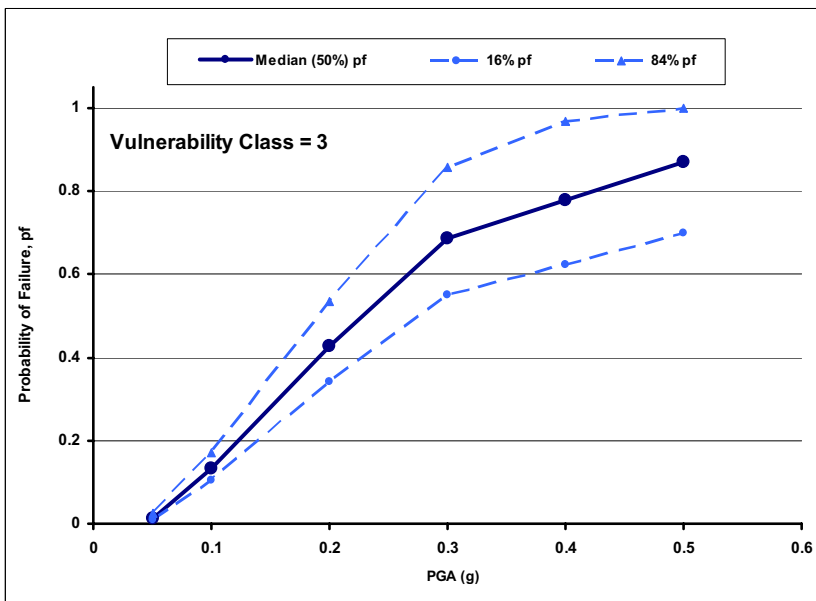
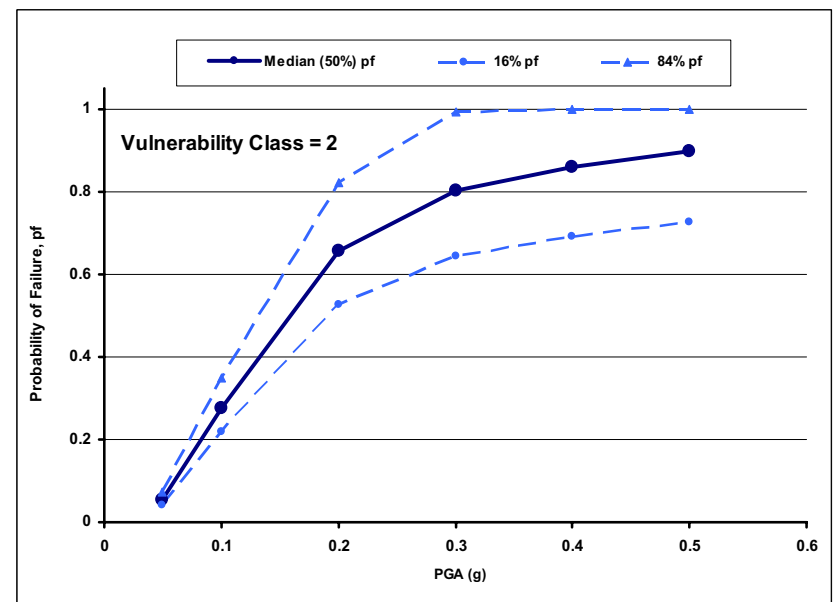
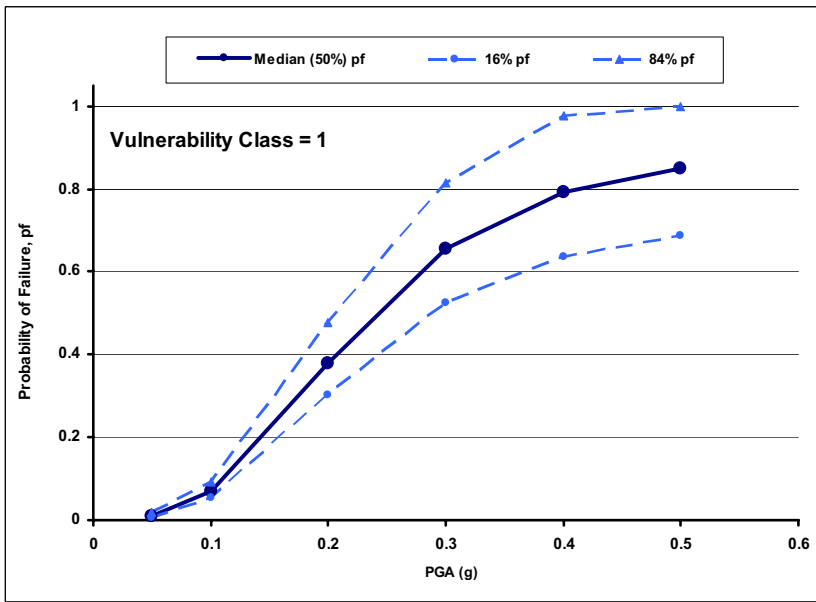
Project No. 26815621

Calculated Newmark Displacements
Idealized Section with
Steep Water Side Slope
25 ft Peat

Figure
6-99







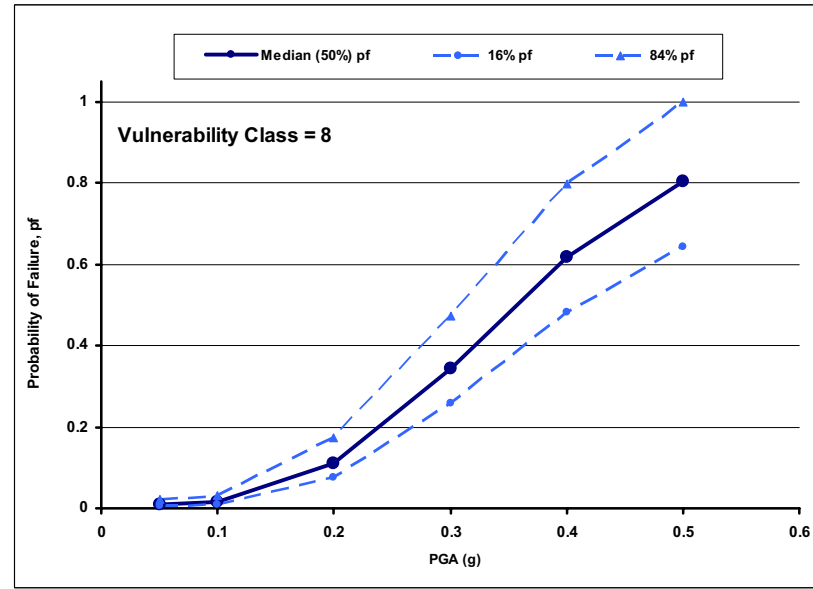
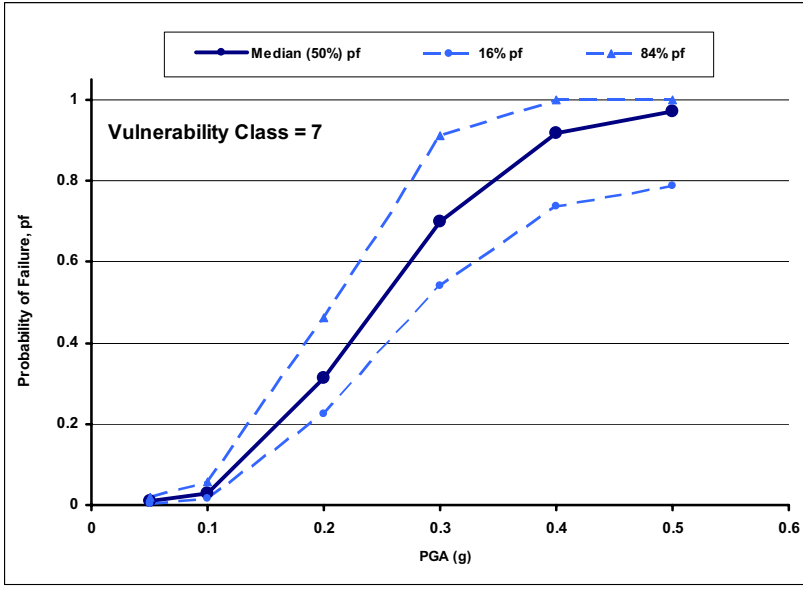
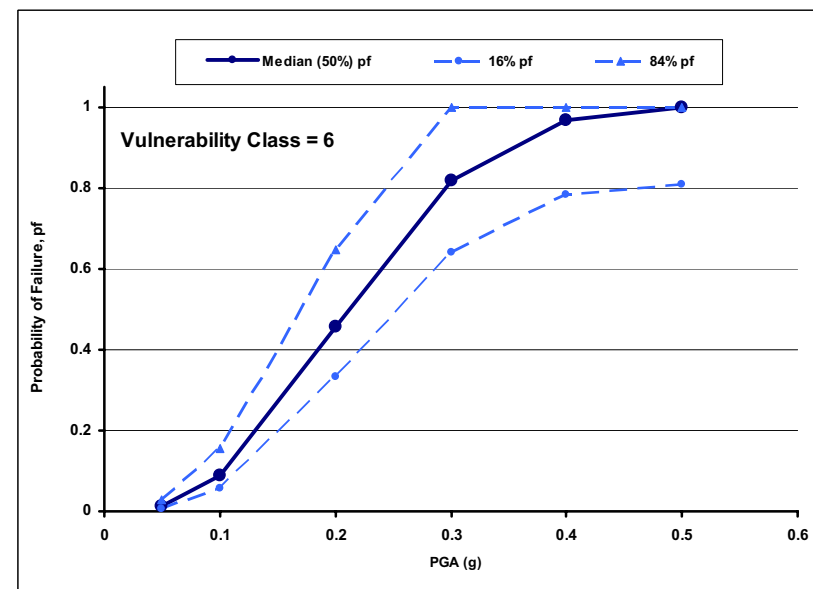
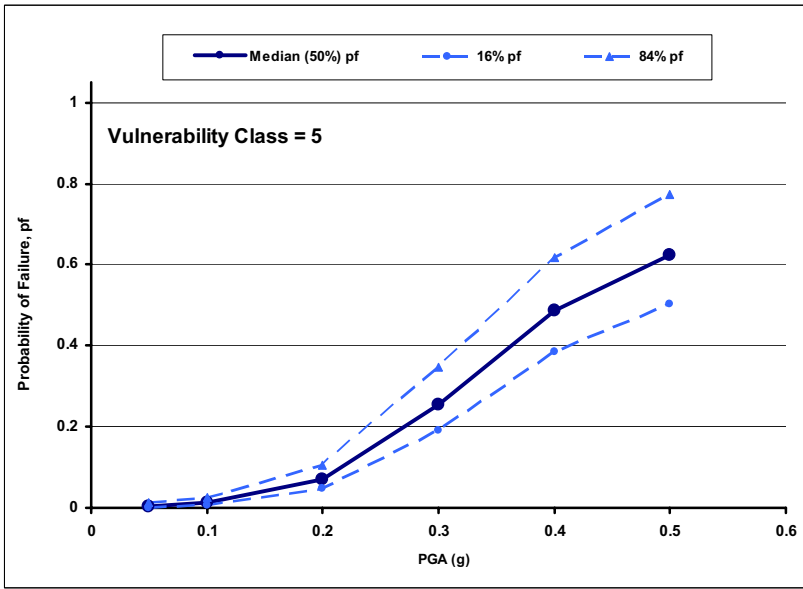
Delta Risk Management Strategy (DRMS)
Levee Fragility

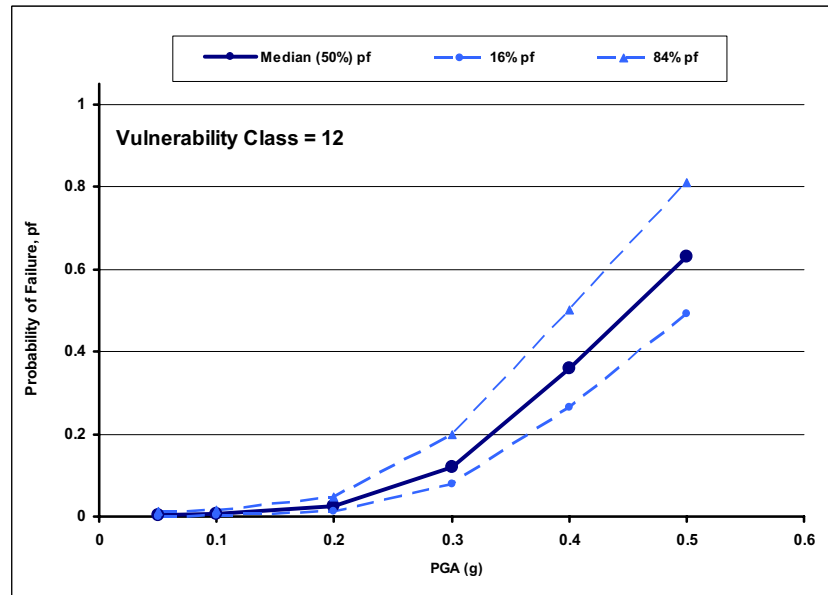
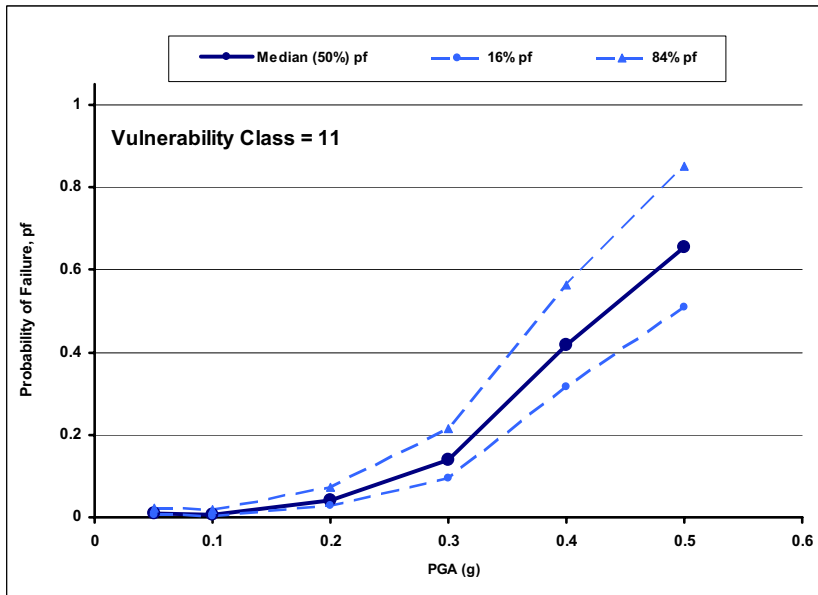
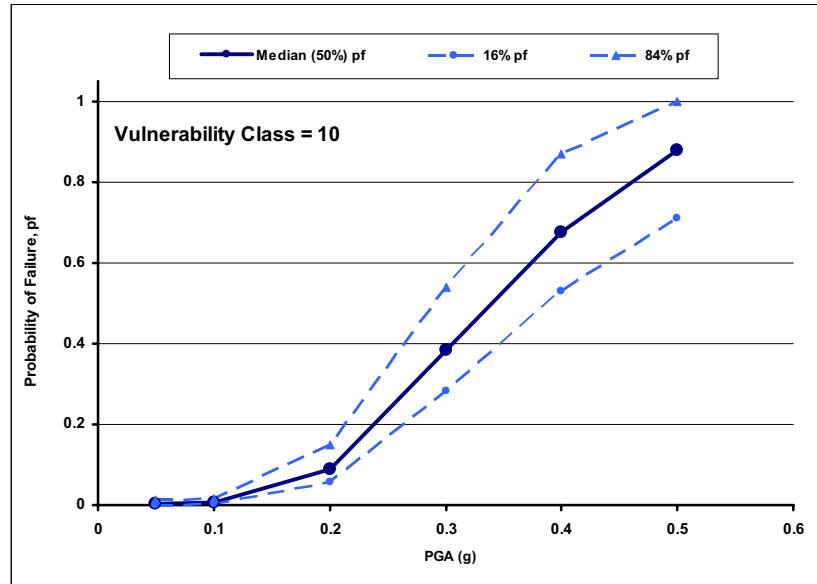
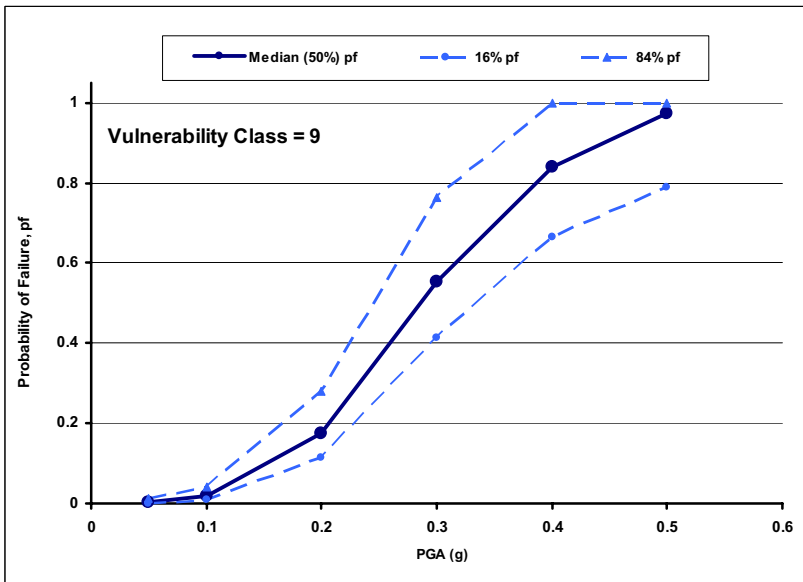
URS

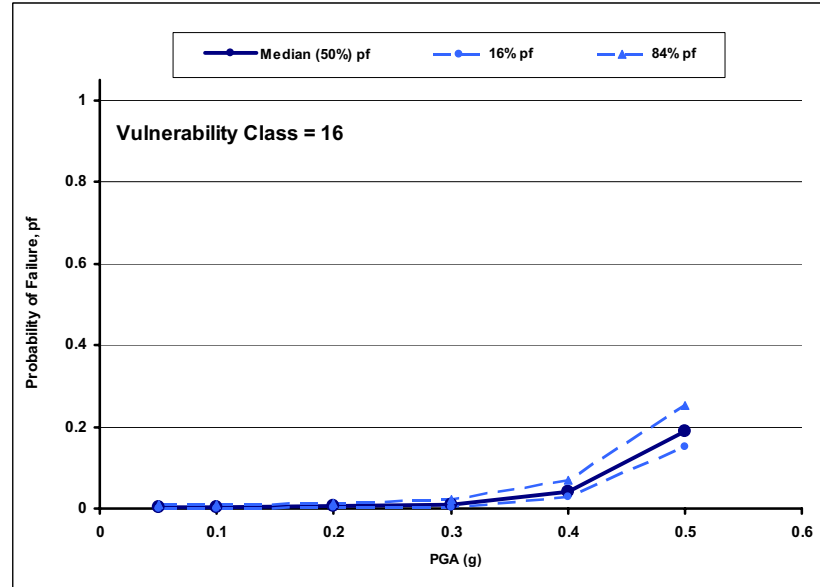
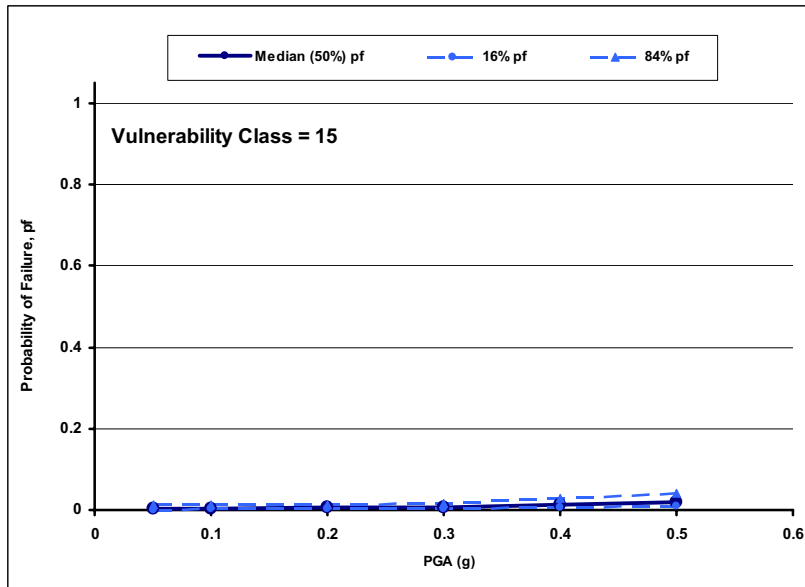
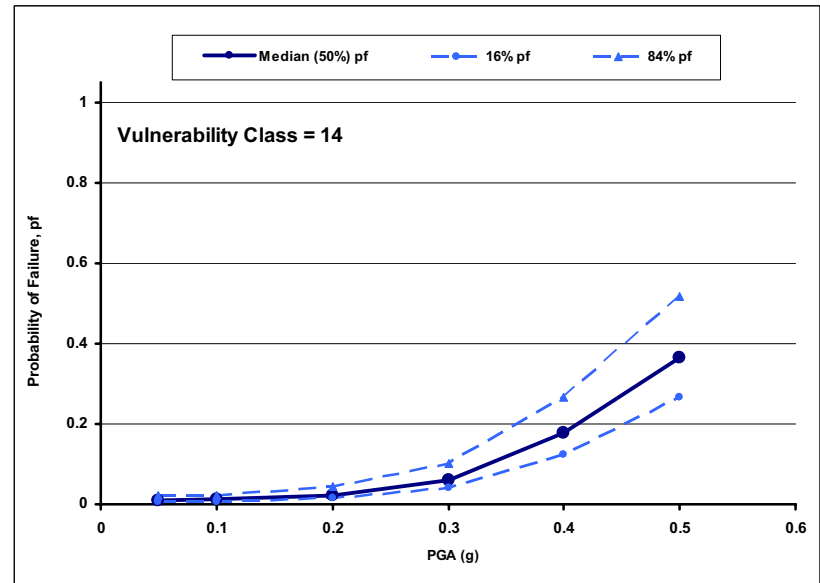
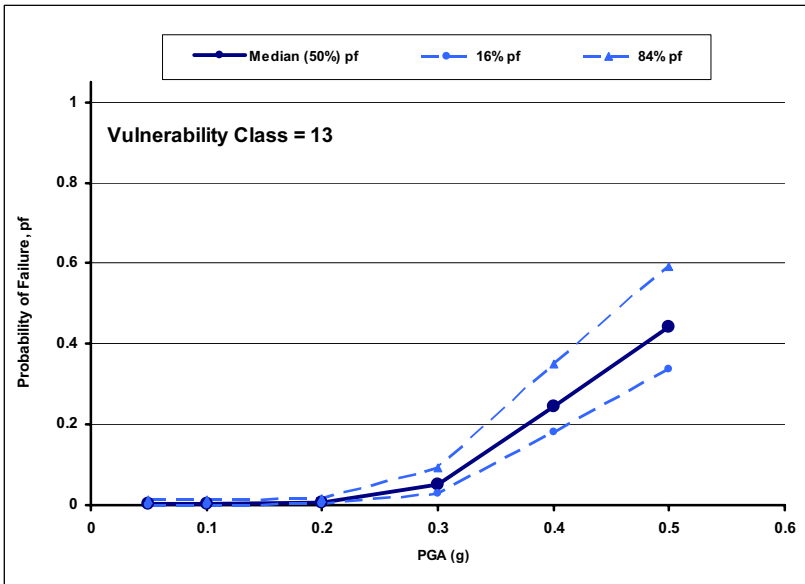
Project No. 26815621

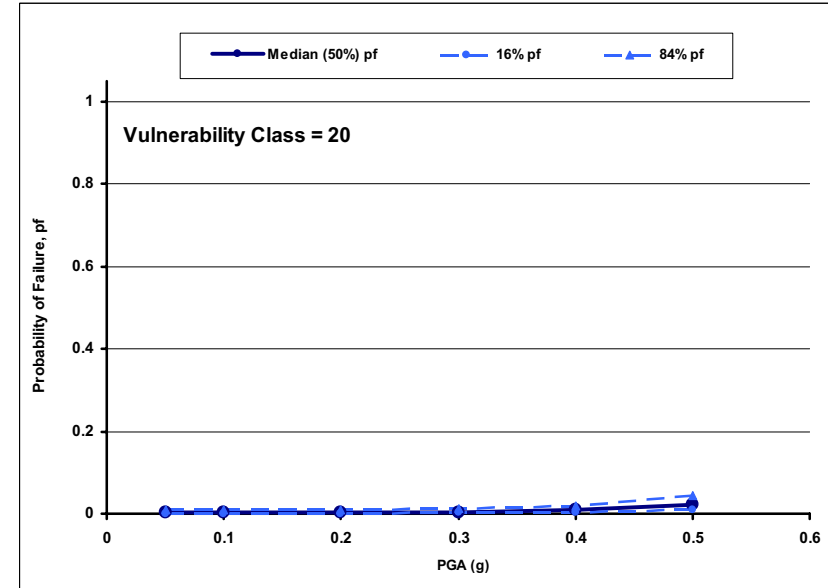
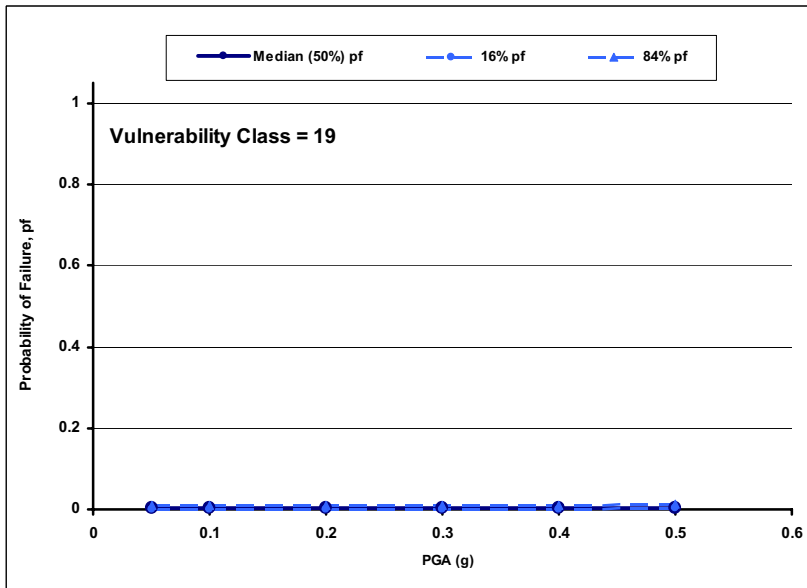
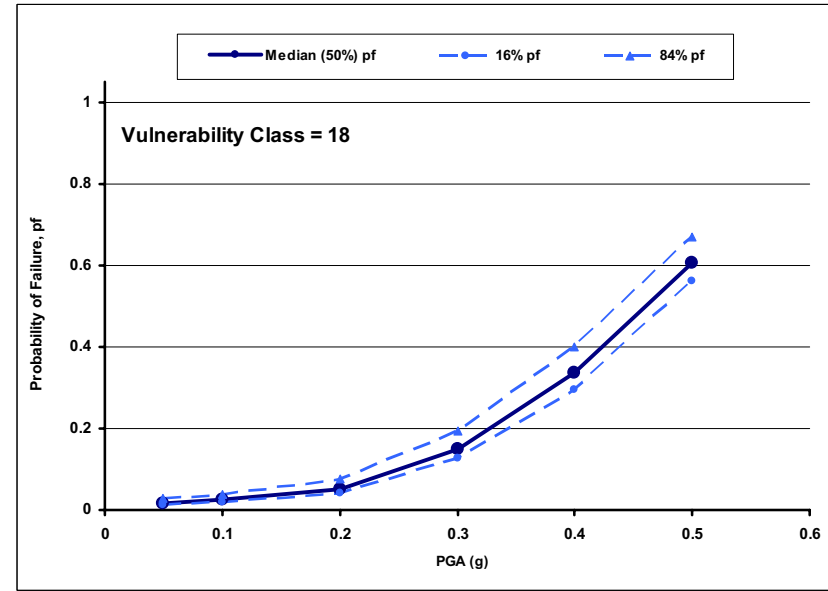
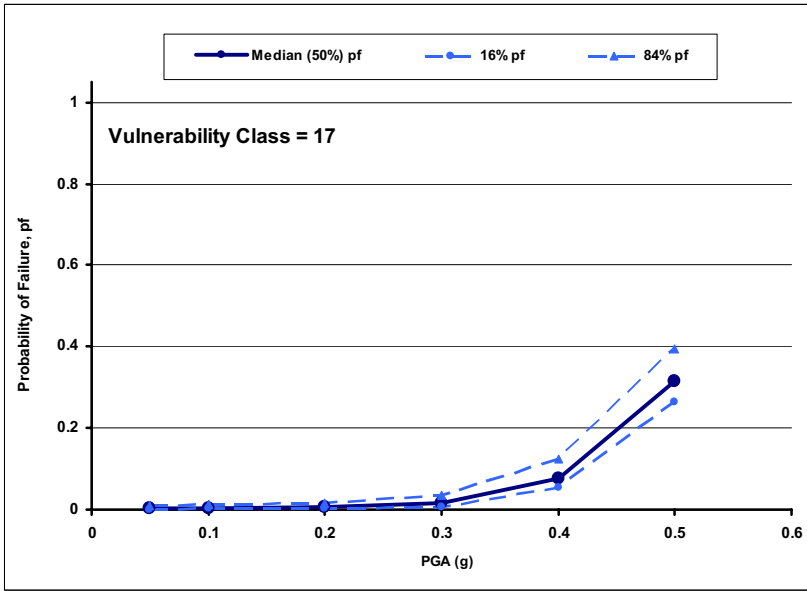
Estimated Failure Probability
at 16%, 50%, and 84% confidence levels
for M=6.5 and IFB=2 feet for
Vulnerability Classes 1, 2, 3 and 4

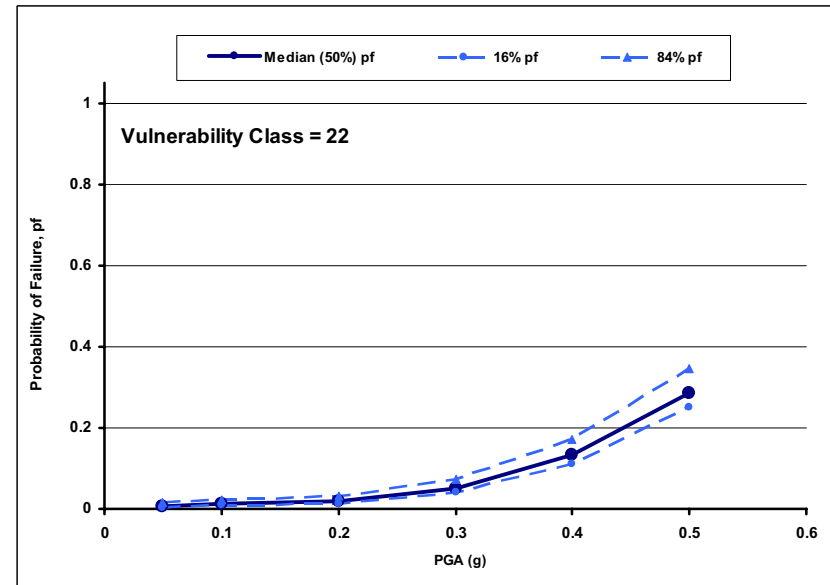
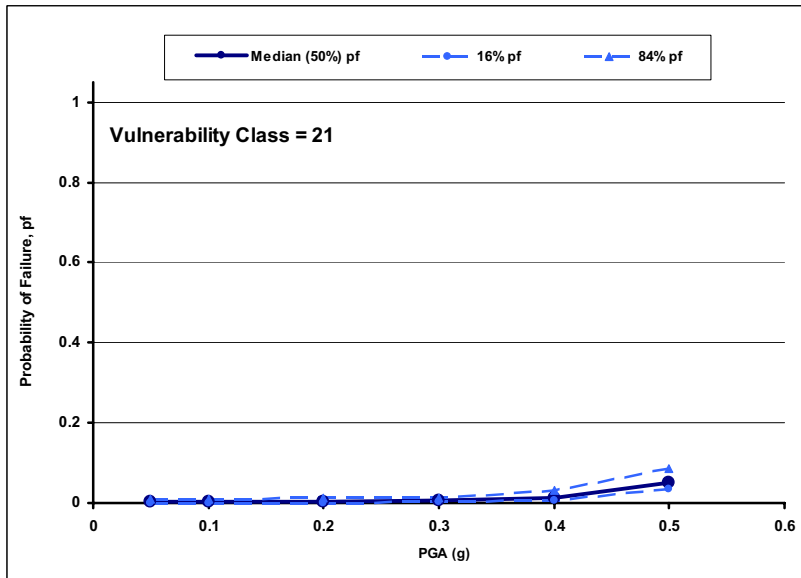
Figure
6-102a





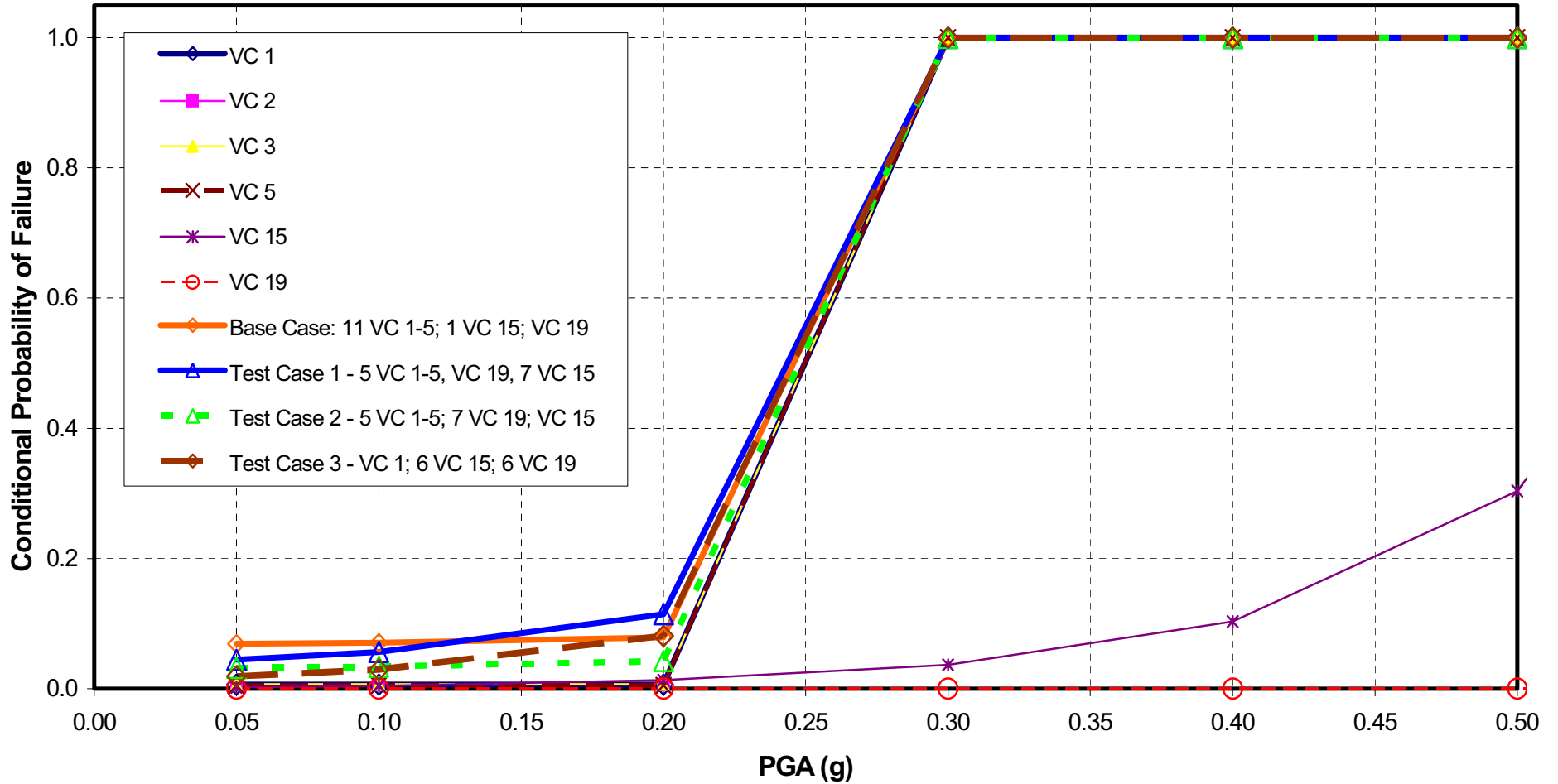






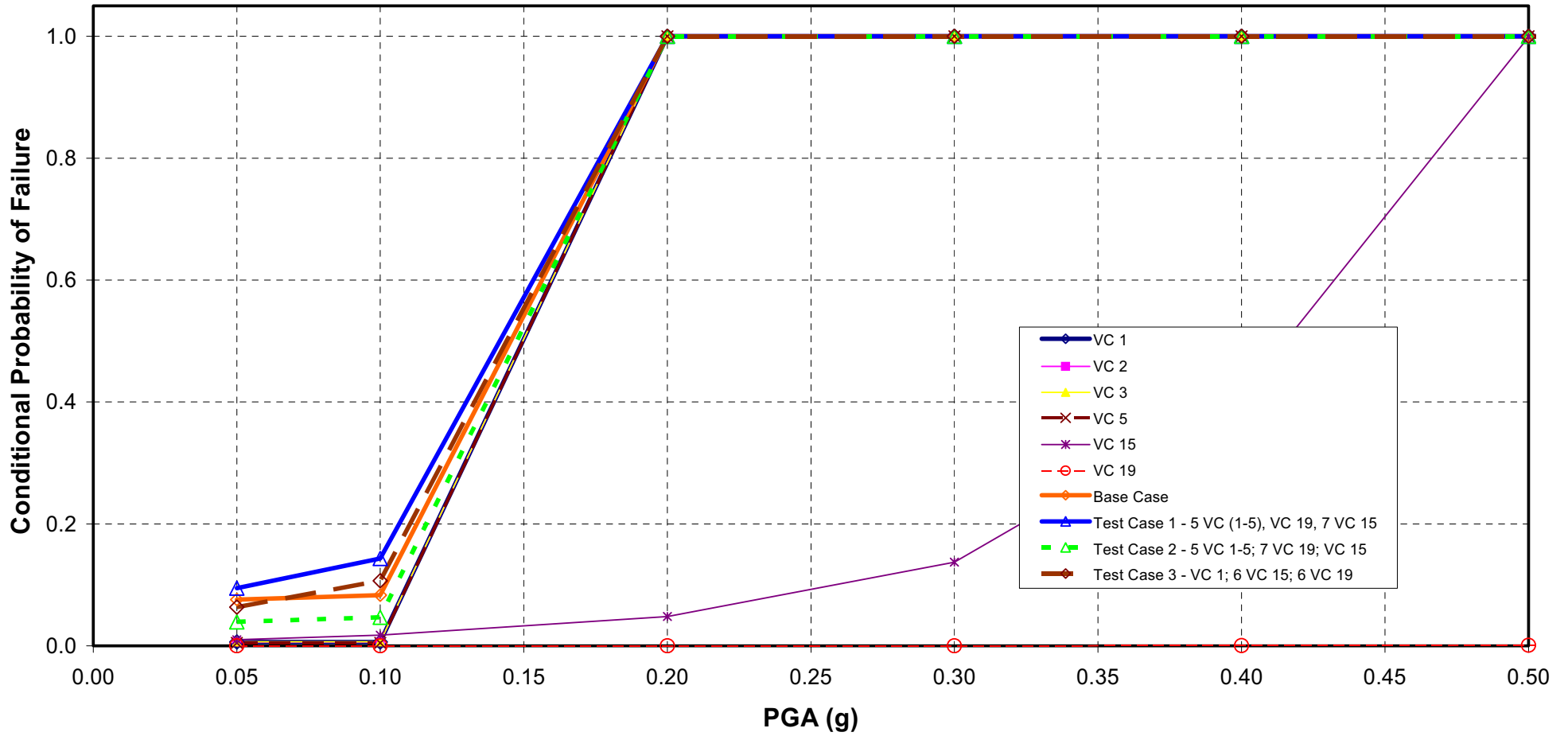
Delta Risk Management Strategy (DRMS) Levee Fragility		Estimated Failure Probability at 16%, 50%, and 84% confidence levels for M=6.5 and IFB=2 feet for Vulnerability Classes 21 and 22	Figure 6-102f
URS	Project No. 26815621		

Union Island - Base: M=5

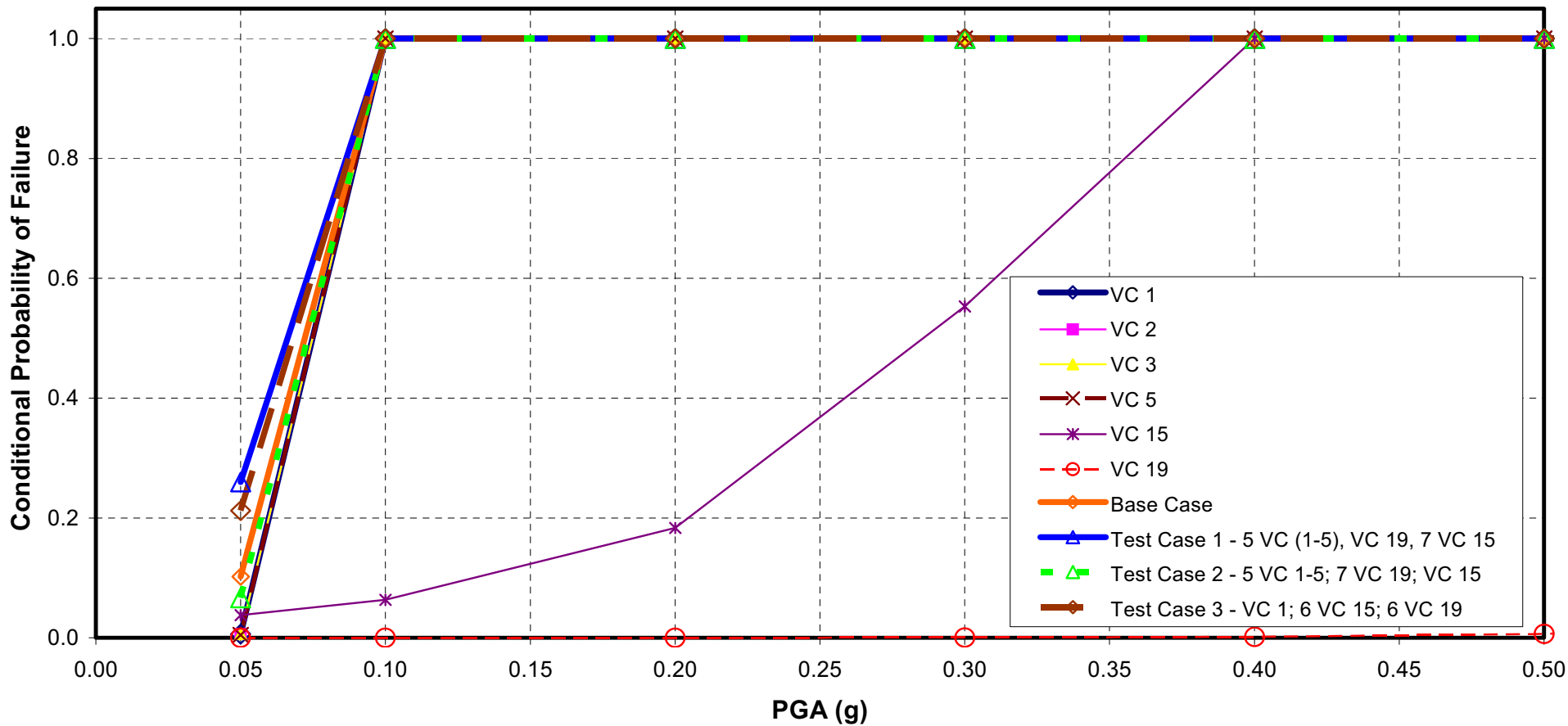


Delta Risk Management Strategy (DRMS) Levee Fragility		Sensitivity of Island Fragility Curve to the Vulnerability Class Assignment of Levee Reaches Union Island, M=5	Figure 6-103a
URS	Project No. 26815621		

Union Island - Base: M=6



Union Island - Base: M=7



Delta Risk Management Strategy (DRMS) Levee Fragility	
URS	Project No. 26815621

Sensitivity of Island Fragility Curve
to the Vulnerability Class Assignment
of Levee Reaches
Union Island, M=7

Figure
6-103c

Appendix 6A
Step-by-Step Hand Calculation
for a Selected Vulnerability Class (VC 10),
Magnitude (M 6.5), and Freeboard (2 feet)

Appendix 6A
Step-by-Step Hand Calculation
for a Selected Vulnerability Class (VC 10),
Magnitude (M 6.5), and Freeboard (2 feet)

6A1.0 Introduction

The consulting team conducted the following calculation steps to determine the best-estimate values for use in the hand calculation. However, at each step the required simulations to represent the contribution of the uncertainties around the mean are highlighted for the reader but not calculated by hand to avoid making this simple document too cumbersome.

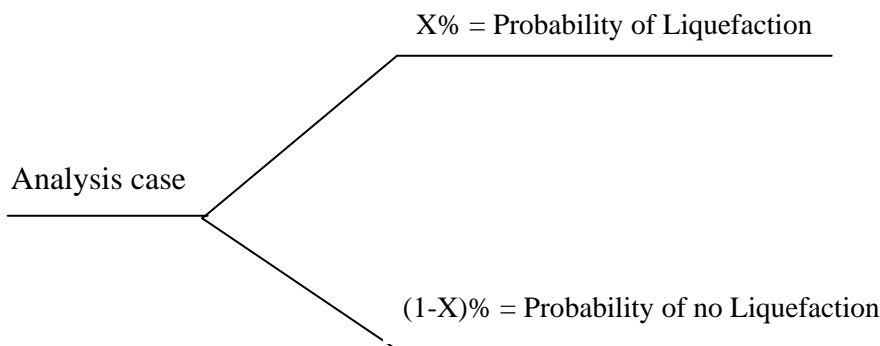
This example case represents the following conditions of Vulnerability Class 10 and loading values:

- Clayey levee fill (non liquefiable)
- Magnitude (M) 6.5
- 2 feet of freeboard
- Liquefiable foundation sand
- $N_{1-60-CS} = 5$ to 10
- Peat thickness = 10 feet to 20 feet
- Reference peak ground acceleration (PGA) used: 0.2g, 0.3g, and 0.4g

Table 6-1 of the Seismology Technical Memorandum (URS/JBA 2007a) defines the vulnerability classes.

This particular class represents a cross section on the west side of Bacon Island near the northern corner of Palm Track. The figures in Attachment 6A-1 (at the end of this appendix) show a site plan/cross section and a drawing prepared during the original investigation.

The following logic tree approach is adopted for each vulnerability class to allow the representation of the probability of liquefaction and the probability of no liquefaction.



The contribution from the two branches to the failure probability is calculated in the following manner:

$$P_i(\text{over all}) = X\% * P_i(\text{displacement for branch X}) + (1-X\%)* P_i(\text{displacement for branch (1-X)}) \quad (1)$$

Appendix 6A
Step-by-Step Hand Calculation
for a Selected Vulnerability Class (VC 10),
Magnitude (M 6.5), and Freeboard (2 feet)

6A1.1 Typical Cross Section

Figure 6A-1 shows a typical cross section.

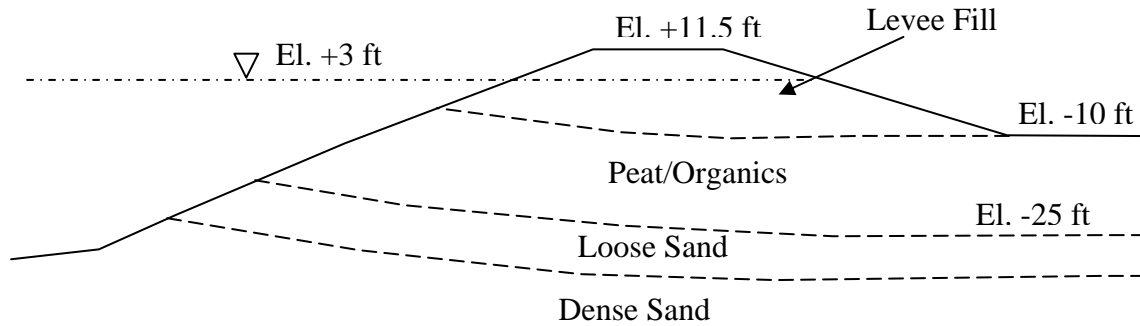


Figure 6A-1: Bacon Island – Cross Section No. 1

6A1.2 Basic Data

The crest and island floor elevations were corrected to account for subsidence and difference in datum from the original section shown in the attached site plan/cross section and site drawing.

- Crest elevation = 11.5 feet (North American Vertical Datum of 1988 [NAVD88])
- Landside toe elevation = -10 feet (NAVD88)
- Levee fill: Silty/sandy clay
- Peat/organic thickness: 15 feet
- **M:** 6.5
- Fines content of the foundation loose sand = 15%

Appendix 6A
Step-by-Step Hand Calculation
for a Selected Vulnerability Class (VC 10),
Magnitude (M 6.5), and Freeboard (2 feet)

6A2.0 Step-1: Estimate Probability and Distribution of $N_{1-60-CS}$

For this class, the range of $N_{1-60-CS}$ is between 5 and 10. For purposes of illustration, the consulting team chose the value of 8, as shown in Figure 6A-2, as being the closest to the best estimate. In the complete simulation, the range is fully sampled (100 points) for all $N_{1-60-CS}$ occurrences.

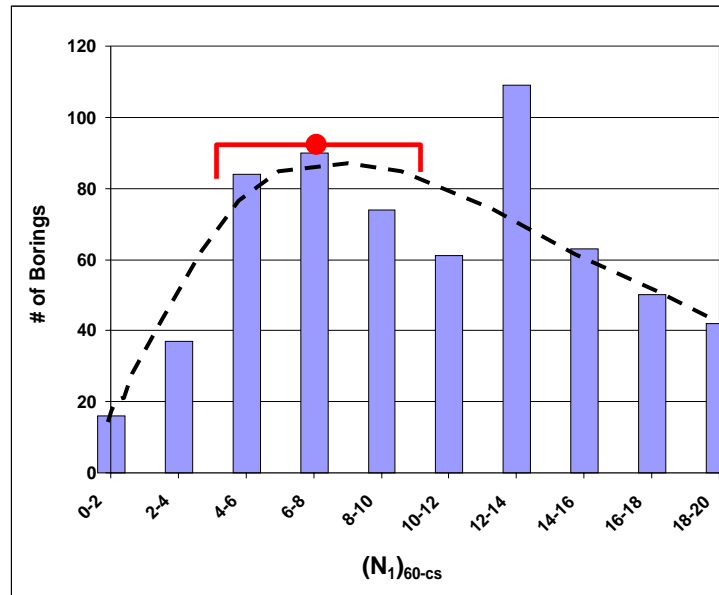


Figure 6A-2: $N_{1-60-CS}$ Distribution for Loose Foundation Sand with $N_{1-60-CS} < 20$

Appendix 6A
Step-by-Step Hand Calculation
for a Selected Vulnerability Class (VC 10),
Magnitude (M 6.5), and Freeboard (2 feet)

6A3.0 Step-2: Estimate Residual Shear Strengths (Sr)

The consulting team used the Seed and Harder (1990) relationship and estimated the range corresponding to the best estimate $N_{1-60-CS}$. For purposes of illustration, the team chose the best estimate value of S_r , which is 200 psf, as shown on Figure 6A-3. However, for the representation of the uncertainties, a range of S_r is used with FLAC to calculate the various deformation functions (deformation versus PGA).

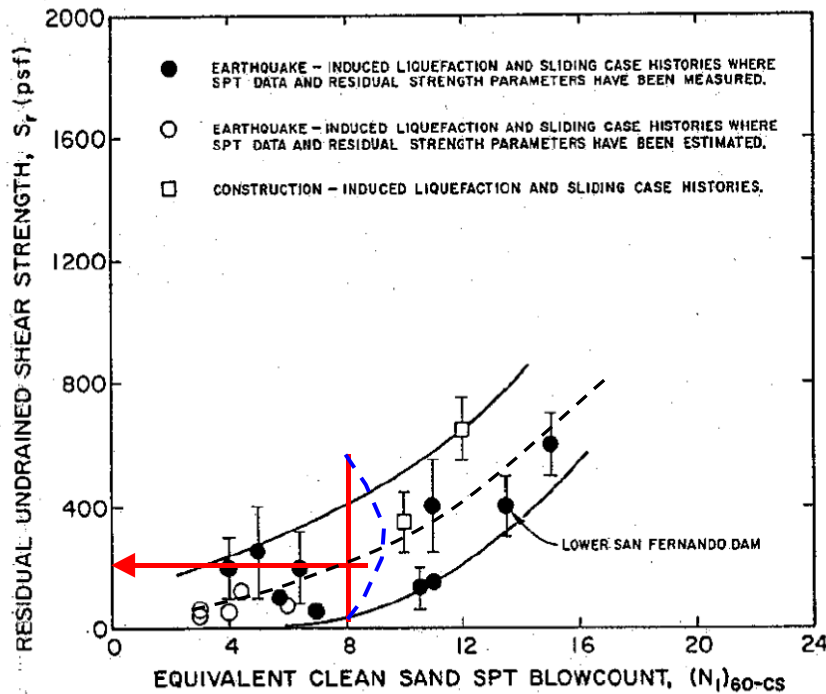


Figure 6A-3: Residual Shear Strength (S_r) VS ($N_{1-60-cs}$)
 (Seed and Harder 1990)

Appendix 6A
Step-by-Step Hand Calculation
for a Selected Vulnerability Class (VC 10),
Magnitude (M 6.5), and Freeboard (2 feet)

6A4.0 Step-3: Calculate Cyclic Stress Ratio (CSR)

The team calculated r_d from Figure 6A-4, as shown below. As shown on the figure, r_d is equal to 0.6.

From Figure 6A-5, the team calculated the best-estimate peak crest accelerations (PCA) from the reference PGA (0.2g, 0.3g, and 0.4g). The PCAs are 0.22g, 0.28g, 0.33g, respectively. However, during the full analysis, the simulation accounts for the full range around the mean values.

From Equation (2), below, the team calculated the cyclic stress ratio (CSR).

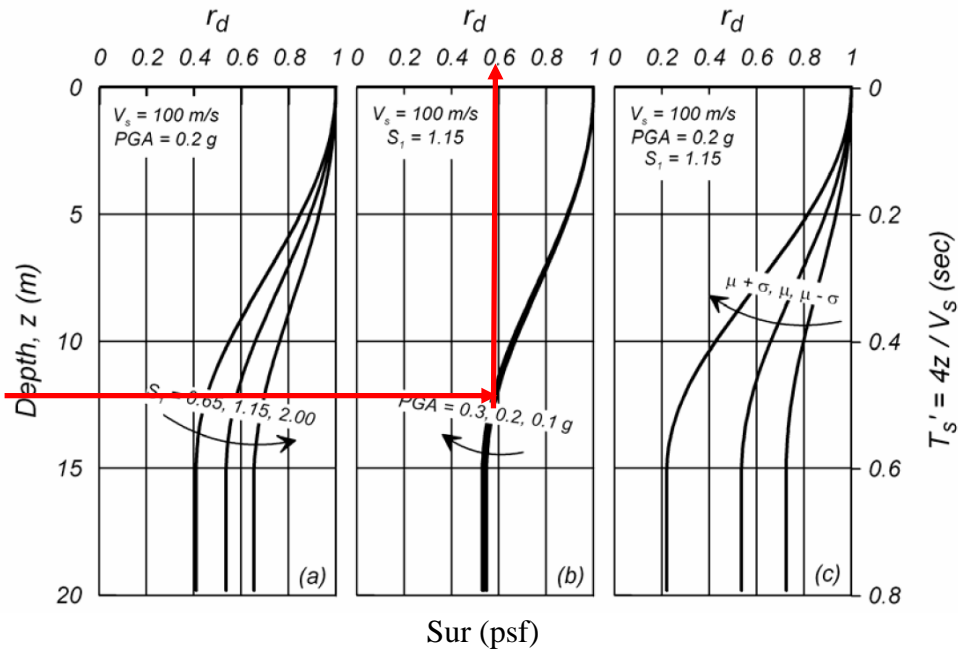


Figure 6A-4: r_d vs Depth
 (Tadahiro et al. 2007)

Appendix 6A
Step-by-Step Hand Calculation
for a Selected Vulnerability Class (VC 10),
Magnitude (M 6.5), and Freeboard (2 feet)

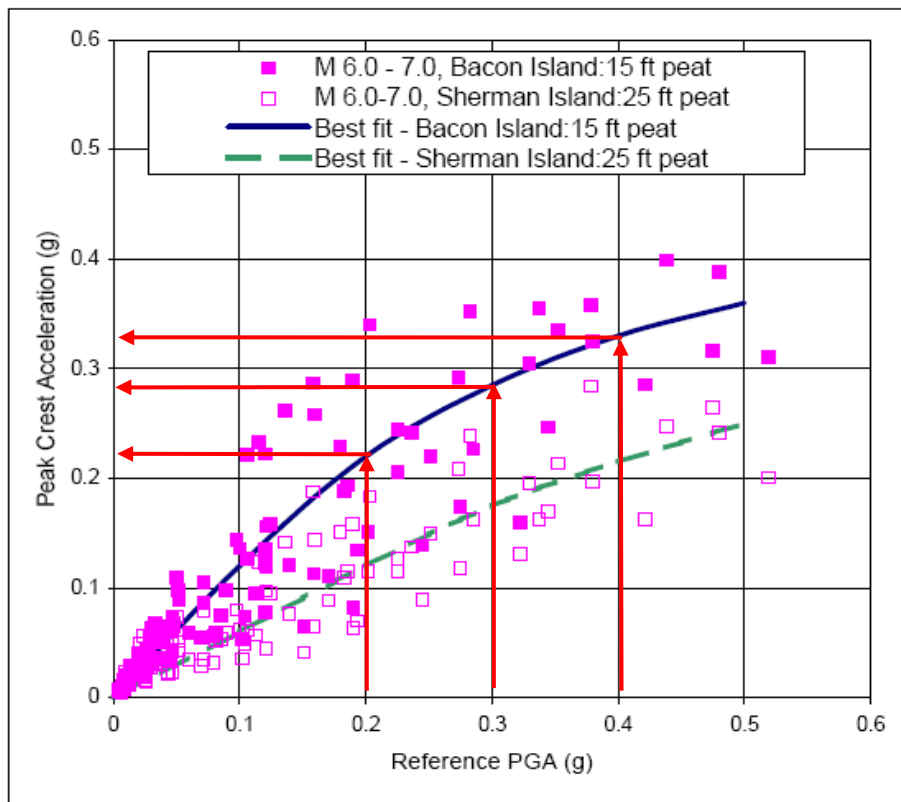


Figure 6A-5: Reference PGA versus Peak Crest Acceleration
(Data from Tadahiro et al. 2007)

Equation (3), below, of Section 6 of the Levee Vulnerability Technical Memorandum (URS/JBA 2008c) is not used for foundation CSR calculation; it is used for the liquefaction of the levee only. The conventional equation shown below is used to calculate the best estimate CSR for the three selected reference PGAs for liquefiable foundation sands.

$$\begin{aligned}
 \text{CSR} &= 0.65 r_d (a_{\text{max}}/g) \text{ (Vertical total stress/Vertical effective stress)} \\
 &= 0.65 * 0.6 * (a_{\text{max}}/g) * [(115 * 21.5 + 70 * 15 + 125 * 2.5) / (115 * 21.5 + 70 * 15 + 125 * 2.5 - 30.5 * 62.4)] \quad (2)
 \end{aligned}$$

$$\text{CSR (PCA-0.22)} = 0.16$$

$$\text{CSR (PCA-0.28)} = 0.22$$

$$\text{CSR (PCA-0.33)} = 0.26$$

6A5.0 Step-4: Calculate Probability of Foundation Liquefaction

Based on the values of CSR and the range of $N_{1-60-CS}$, the probability of liquefaction is estimated as shown in Figure 6A-6. The probability of liquefaction is automatically calculated from equation (3). For the three CSR values above, the probabilities of liquefaction are estimated to be 98 percent, 100 percent, and 100 percent for CSRs of 0.16, 0.22, and 0.26, respectively. Figure 6A-6 (for M 7.5) is provided only to illustrate the process of estimating the probability of liquefaction; Equation (3) is used instead.

After the probability of liquefaction is evaluated, the team went to logic diagram and applied values of X percent and (1 - X) percent for each CSR (or each PGA) value. In the current case, these values are:

X =98% and (1-X) =2%

X =100% and (1-X) =0%

X =100% and (1-X) =0%

For the case where the probability of no liquefaction is greater than zero, the team performed the same steps shown below and weight-averaged the probability of deformation contribution from both the 2 percent no liquefaction and the 98 percent liquefaction, as shown in Equation (1). For the no-liquefaction case, the team used corresponding deformation curves versus PGA, which are different from the liquefied foundation deformation curves.

As opposed to the best-estimate illustration provided here, the simulation will consider 500 point values distribution for each CSR and for the range of deformation.

$$P_L(N_{1,60}, CSR, M, \sigma'_v, FC) = \Phi \left[\frac{\left(N_{1,60} \cdot (1 + 0.004 \cdot FC) - 13.32 \cdot \ln(CSR) - 29.53 \cdot \ln(M) - 3.70 \cdot \ln(\sigma'_v) + 0.05 \cdot FC + 44.97 \right)}{2.70} \right] \quad (3)$$

where

P_L = the probability of liquefaction in decimals (i.e., 0.3, 0.4, etc.)

$N_{1,60}$ = foundation N_{1-60}

CSR = cyclic stress ratio

M = earthquake magnitude

σ'_v = effective overburden stress

FC = fine contents

Φ = the standard cumulative normal distribution

Appendix 6A
 Step-by-Step Hand Calculation
 for a Selected Vulnerability Class (VC 10),
 Magnitude (M 6.5), and Freeboard (2 feet)

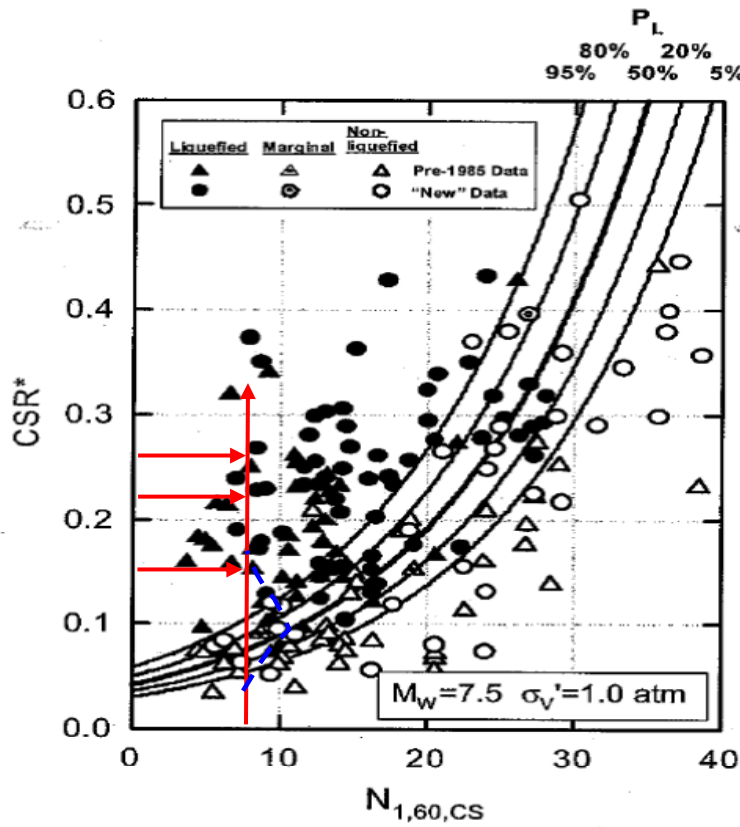


Figure 6A-6: Probabilistic SPT-Based Liquefaction Triggering Correlation
 (Source: Seed et al. 2003)

6A6.0 Step 5: Calculate Deformations

The consulting team calculated deformations given PGA. For the three illustrative reference PGAs (0.2g, 0.3g, and 0.4g), we calculated the deformation from Figure 6A-7 (deformation curves for liquefiable foundations; other curves for other cases). The horizontal deformation curve corresponding to $N_{1-60-CS} = 8$, shown in Figure 6A-7 is used. The calculated best-estimate deformations for each PGA are approximately: 1.3 feet, 2.5 feet, and 3.4 feet, respectively. However, the simulation will consider the entire range (500 points) of deformations for each PGA.

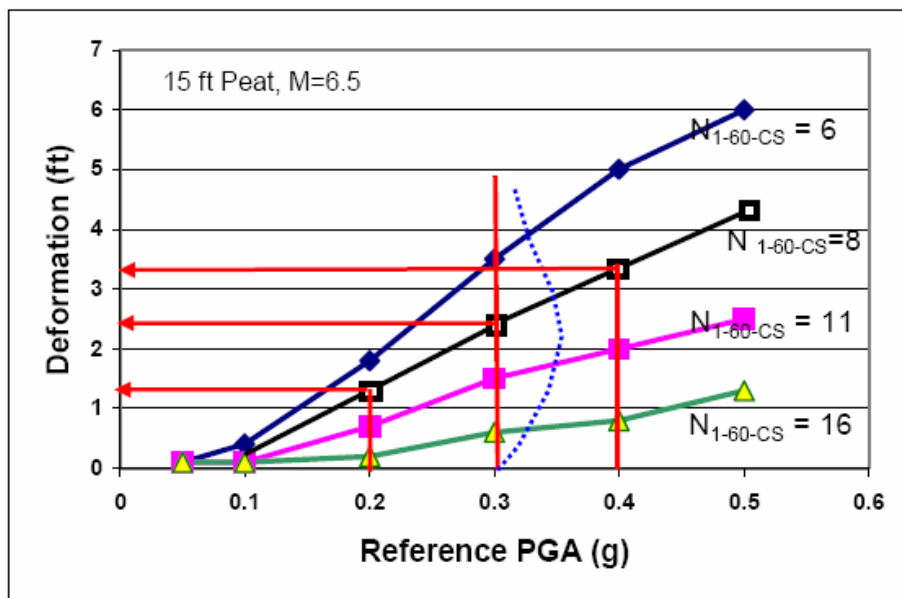


Figure 6A-7: Deformation versus Reference PGA for VC-10

Appendix 6A
Step-by-Step Hand Calculation
for a Selected Vulnerability Class (VC 10),
Magnitude (M 6.5), and Freeboard (2 feet)

6A7.0 Step 6: Calculate Probability of Levee Failure Given Deformation

For each deformation value, the team calculated the relative vertical deformation.

$Dv/In-FB = \frac{1}{2} \cdot Dh/In-FB$ (initial freeboard is 2 feet for this case)

For 1.3 feet \longrightarrow $Dv/In-FB = 0.325$ or 32.5%

For 2.5 feet \longrightarrow $Dv/In-FB = 0.625$ or 62.5%

For 3.4 feet \longrightarrow $Dv/In-FB = 0.85$ or 85.0%

The probability of failure was calculated for each relative deformation. For this case, the best estimate probability values are approximately: 8 percent, 40 percent, and 85 percent for PGAs of 0.2g, 0.3g, and 0.4g, respectively, as shown Figure 6A-8. However, for each value of deformation (Figure 6A-7) a simulation for the full range of probabilities (500 points) is performed. For this case, the team used the best-estimate values shown with red dots in Figure 6A-8. These were then plotted in Figure 6A-9. The hand-calculated values are well within the confidence bounds. The difference in the value at 0.4g could be the result of the skewed distribution of the failure probability density function where the mean is higher than the median.

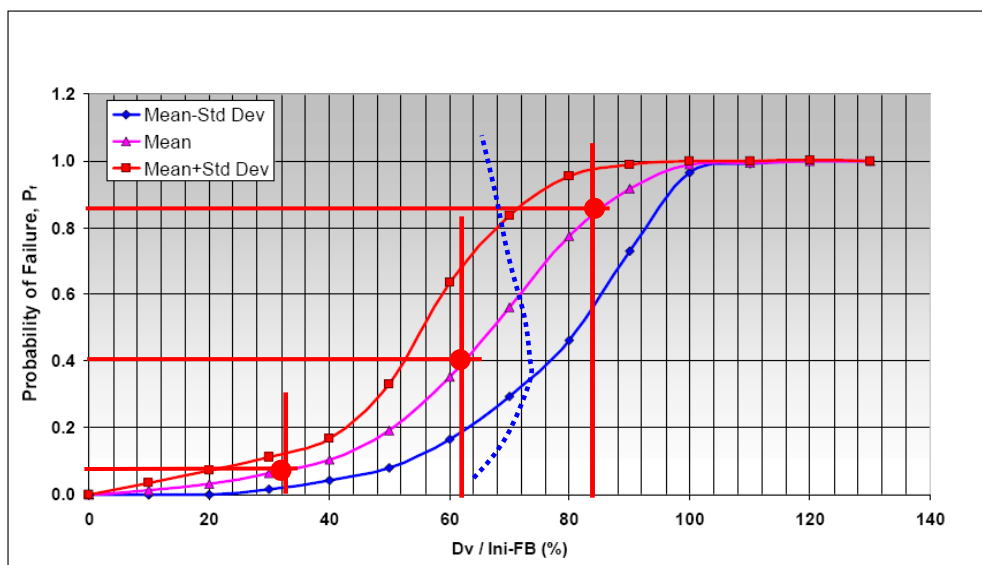


Figure 6A-8: Probability of Levee Failure versus Dv/Ini-FB

Appendix 6A
Step-by-Step Hand Calculation
for a Selected Vulnerability Class (VC 10),
Magnitude (M 6.5), and Freeboard (2 feet)

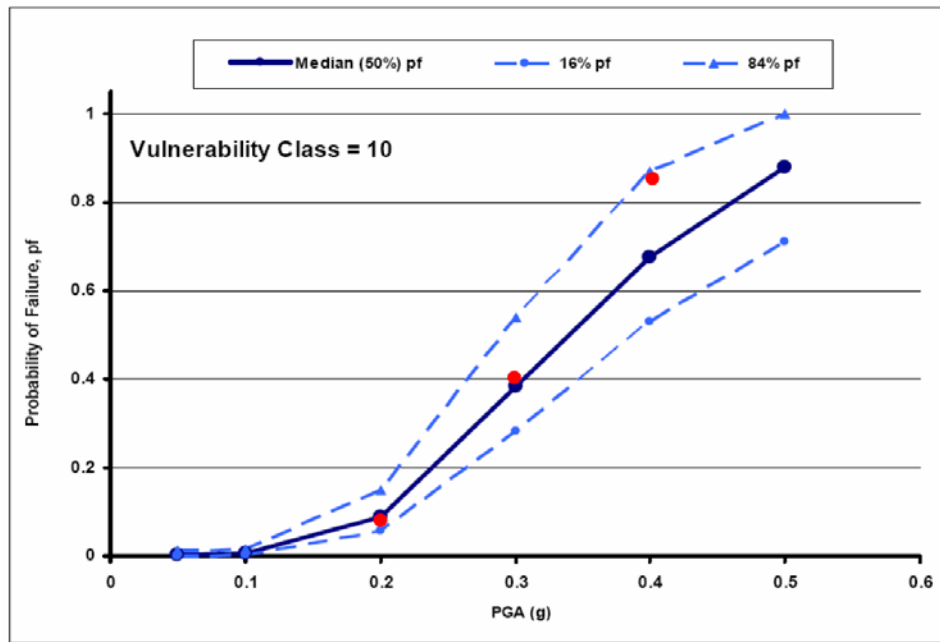
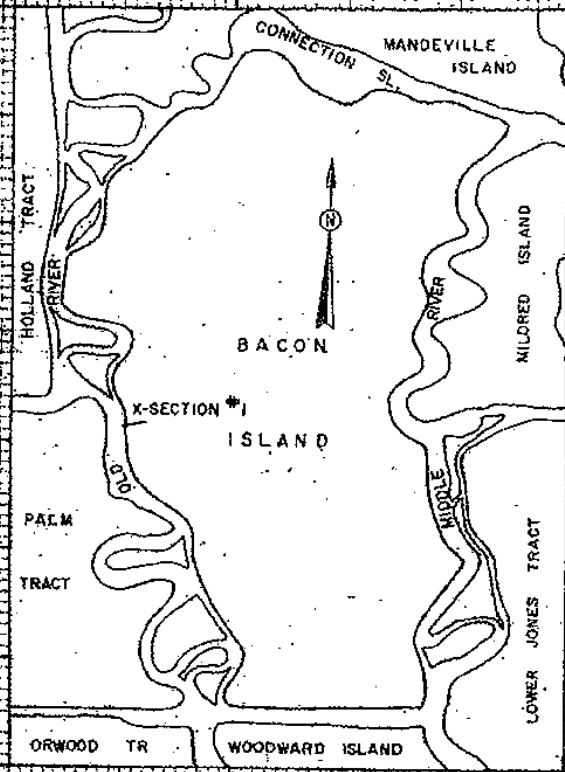


Figure 6A-9: Fragility Function for VC-10 and Best-Estimate Values

Attachment 6A-1
Site Plan/Cross Section No. 1 and Drawing

NOTES:
 BORING LOGS ARE BASED ON VISUAL CLASSIFICATION.
 ALL BORINGS ARE ONE INCH DIAMETER EXCEPT WHERE NOTED.
 HAMMER WEIGHT IS 14 LBS.
 DRILLING SPEEDS ARE 100 TO 175 RPM.
 DATES: MAY 1957 TO NOV. 1957
 AND NOV. 1957 TO DEC. 1957
 BARRE, HOLE # 1, 1958



LOCATION MAP

LEGEND

- BLOW COUNT PER FOOT (N) INDICATES PENETRATION INDICATES WASHED
- DRY DENSITY IN POUNDS PER CUBIC FOOT
- UNCONFINED COMPRESSIVE STRENGTH q_u IN TONS
- UNCONFINED COMPRESSIVE STRENGTH q_u IN TONS
- LIQUID LIMIT IN PERCENT
- PLASTICITY INDEX IN PERCENT
- SIEVE ANALYSIS: PERCENT PASSING NO. 200 SIEVE BY WEIGHT
- SPECIFIC GRAVITY
- SILT
- CLAY
- SAND
- ORGANIC SILT
- ORGANIC CLAY
- SILTY SILT
- SILTY CLAY
- SILTY SAND
- SAND WITH SILT LENSES

BACON ISLAND CROSS SECTION NO. 1

